NATIONAL AERONAUTICS AND SPACE ADMINISTRATION

SECOND ANNUAL EARTH RESOURCES AIRCRAFT PROGRAM STATUS REVIEW

VOLUME II

AGRICULTURE/FORESTRY, AND SENSOR STUDIES

Presented at the

NASA Manned Spacecraft Center
Houston, Texas

September 16 to 18, 1969

MANNED SPACECRAFT CENTER
HOUSTON, TEXAS

FOREWORD

On September 16, 17, and 18, a review of various aspects of the Earth Resources Program was held at the Manned Spacecraft Center, Houston, Texas. Particular emphasis was placed on the results of analysis of data obtained with the Manned Spacecraft Center and other aircraft which have contributed data to the program.

The review was arranged in conjunction with the Department of Interior, Department of Agriculture and the Department of the Navy. Attendees and participants at the meeting included program investigators, their immediate associates, and program representatives from the above named agencies and ESSA and NASA.

The review was divided into the disciplinary areas of Geology, Geography, Hydrology, Agriculture and Forestry, and Oceanography. An additional session was held on instrumentation. Program investigators presented the results of their work in each of these areas. The material presented is being published in three volumes:

Vol I – GEOLOGY AND GEOGRAPHY

Vol II – AGRICULTURE, FORESTRY, AND SENSOR STUDIES

Vol III – HYDROLOGY AND OCEANOGRAPHY

The review provided a current assessment of the program for both management and technical personnel. It is important to note that the material presented represented the current status on ongoing programs and consequently complete technical analyses will be available at a later date.

CONTENTS OF VOLUME I

CONTENTS OF VOLUME II

CONTENTS OF VOLUME III

TABLES

FIGURES

SECTION 18
THE INVENTORY OF VEGETATION RESOURCES-- USER REQUIREMENTS VS REMOTE SENSING CAPABILITIES

by

Robert N. Colwell
Forestry Remote Sensing Laboratory
University of California, Berkeley

INTRODUCTION

"Give a small boy a hammer and he soon discovers that everything needs pounding". Paraphrased, this is the message contained in an excellent book by Dr. A. A. Kaplan entitled, "The Conduct of Inquiry" (1964).

Those of use who profess to be remote sensing scientists should find much food for thought in this statement as we consider the possibility that each of us has a tendency to act like an enthusiatic boy who has been given an important new tool. In our instance the new tool is not a hammer, of course, but a highly sophisticated remote sensing system operable from either aircraft or spacecraft.

It is easy for either the boy or the remote sensing scientist to discover some exciting and even spectacular capabilities of the new tool. The difficult part is in learning how and where these capabilities might profitably be exercised in satisfying a genuine requirement. It may be with the greatest reluctance and only after several admonitions that the enthusiastic boy arrives at the following conclusion: "Of all the things that might be pounded with a hammer, the only things that need pounding are certain nails". When told, furthermore, that these certain nails must be pounded in strict conformity with requirements as to time, place and manner, most boys are likely to say "Forget it", (or something worse) and start looking for some tool more glamorous than a hammer to play with. Only a few can be expected to stay with the rigors of the trade and eventually enter into productive careers as "master carpenters".

Similarly, there is increasing evidence that many of today's remote sensing scientists, especially those who only recently were attracted to this glamorous field, are beginning to feel uncomfortably restricted by the admonition from Congressmen and budget makers that henceforth the remote sensing tool must be so used as to satisfy some legitimate user requirement and that there also must be some important restrictions as to time, place and manner of its use. As one of the top men in our field put it to me recently, "It looks as though all of the fun in this business is about over". Like small boys, such scientists are already losing interest and are looking for the next glamorous thing to play with. It will be interesting to note how many of them persevere under such admonitions and remain available for productive careers in this important field when the first earth resources technology satellites become operational.

Thus far, my comments have dwelt primarily on restrictions that need to be applied in order to prevent indiscriminate and unwise use of present-day remote sensing devices. But if a balanced presentation is to be given,

we must also emphasize the many legitimate and urgently needed applications for such devices. Therefore, it is primarily the applications that will be emphasized in the remainder of my paper and in each of the three papers that immediately follow mine on today's program.

But even before doing that, I must pause long enough to acknowledge that other workers have recently directed their attention to one aspect or another of the topic that I was asked to discuss here today.

Perhaps the most widely publicized of these recent reports seeking to relate user requirements to remote sensing capabilities is an article by Amrom Katz entitled, "Let Aircraft Make Earth-Resource Surveys", which appears in the June, 1969 issue of the magazine "Astronautics and Aeronautics". The subtitle for that article reads as follows: "What we need from Earth-resource surveys can be gained easier, better, sooner and cheaper using aircraft rather than spacecraft, and in a politically more palatable and manageable manner".

Coming from one with such prestige in the field as Katz enjoys, this forthright and all-encompassing statement would seem to resolve in one sentence all of the problems with which my present paper was about to deal. But perhaps before we adopthis latest pronouncement as the gospel we should consider an alternate possibility. Is this yet another example in which the philosophical expert starts with a false premise and then, through a series of unwarranted assumptions, plunges on to the grand but erroneous conclusion? Certainly his article is too thought-provoking, factually oriented and cleverly written for us to dismiss it so lightly. However, in my opinion, it contains sufficient evidence of each of these shortcomings to merit a closer analysis.

The false premise in Amrom's article is that we must use either aircraft or spacecraft. From the outset those of us who have been working on the NASA Earth Resources Survey Program have considered it probable that neither of these alternatives would provide the optimum solution. Consequently, much of our research has been designed toward developing a "multi-stage" sampling technique whereby the earth resource inventory would be performed using at least three data collecting systems: satellites, aircraft and ground observers, in that sequence. Each of these in turn would provide progressively closer looks at progressively smaller areas, but would provide progressively more detailed information about those areas. In fact, the major use of NASA aircraft that is being made by my group and by many others working in the Earth Resources Survey Program is in developing multi-stage sampling techniques that will employ such aircraft to maximum advantage in conjunction with spacecraft. An excellent example of this multi-stage sampling technique illustrating the great promise which it holds for the inventory of earth resources will be presented in the paper by Langley which immediately follows mine on today's program. That paper is entitled, "Multi-Stage Sampling of the Forest Resource Using Space Photography--an Apollo 9 Case Study".

As for unwarranted assumptions, it is probable that at least four major ones can be readily detected in Amrom's article by any one of us who actually works in the NASA Earth Resources Survey Program instead of merely

philosophizing about it. However, because of time and space limitations, my further comment on these assumptions must await another occasion. After all, this brief paper of mine is to be more than a mere critique of someone else's analysis of the subject.

The erroneous conclusion (or so I consider it to be) which automatically follows from Amrom's use of both a false premise and a series of unwarranted assumptions is the one expressed in the title of his article, "Let Aircraft Make Earth Resources Surveys", for he makes it abundantly clear that he finds no room for spacecraft in such a program.

It is not my custom to devote papers to the criticism of efforts on the part of my colleagues in the remote sensing field. However, in my opinion, there are three reasons why the brief criticism that has just been given constituted a valid exception: (1) because of the tremendous impact which the paper by Katz, marred though it is by significant errors, obviously has had upon the scientific community, (2) because he continues to gloat in print and elsewhere that those of us working in this field have offered "not a peep" in opposition to his learned pronouncements, and (3) because his paper, while dealing with exactly the same topic as I was asked to speak upon at this Houston seminar, arrives at a much different conclusion. The remainder of my paper will attempt to use a more positive approach,--one in which I will attempt to set forth a few facts as I see them, thereby exposing myself for a considerably larger amount of healthy criticism than that which Amrom's paper reportedly has received to date.

APPROACH TO THE PROBLEM

In seeking to relate remote sensing capabilities with user requirements, either of two approaches might be used.

In the first approach, remote sensing capabilities would be considered at the outset and, in the light of these capabilities, an exhaustive list would be compiled showing all the kinds of data that might be attained through the full exercise of these capabilities. Then due consideration would be given to each item on the list in order to determine whether that item might conceivably satisfy some user requirement.

In the second approach, a list of economically significant or otherwise important user requirements would be compiled. In the process of compiling the list, the investigator would take pains to determine the informational requirements of all the agencies and types of individuals who might conceivably be served. Once the list had been compiled, consideration would be given to the various remote sensing capabilities in an effort to determine which of these requirements might be met and by what remote sensing process.

If either of these two approaches were to be used, however, consideration would eventually need to be given to the best compromise between user requirements and remote sensing capabilities. For example if, under the second approach, it were found that one of the desired items of information could not be directly obtained by means of remote sensing, the investigator should consider whether the requirement might be so modified

as to make acceptable to the user some alternate kind of information which could indeed, be derived through the remote sensing process. (Examples of such solutions to the problem are given in a later section).

The following treatment uses the second of these two approaches in that user requirements are first listed and remote sensing capabilities are then considered. Primary emphasis is given to the vegetation resource.

USER REQUIREMENTS

As we begin a consideration of user requirements for information about the vegetation resource, Table 1 provides a useful point of departure.

Judging from that table there are only four main categories of vegetation for which information is sought, viz., agricultural crops, timber stands, rangeland vegetation and brushland vegetation. Starting with the left hand column of that table we see that, by and large, the users of agricultural crop data need only six categories of information, viz., crop type, crop vigor, crop-damaging agents, crop yield per acre by type, crop acreage by type, and total yield. Proceeding to the other three columns of Table 1 we note that essentially these same six categories of information likewise are the ones sought by the managers of timber lands, rangelands and brushlands, respectively.

Next, with the aid of Table 2, let us consider the many different agencies and groups desiring information about the vegetation resource. Perhaps our first observation, upon examining that table, is that we can logically list these many users under the same four column headings as were used in the previous table, viz., the agencies and groups concerned primarily with agricultural crops, timber stands, rangeland forage and brushland vegetation, respectively. This is, indeed, the case.

The array of users listed in Table 2 is truly a formidable one, yet that list is by no means a figment of the imagination. To the contrary each group or agency listed there presently uses a great deal of information about vegetation resources, although at present most of the information is not obtained from either aerial or space photography. These facts are documented in about 10,000 thoughtfully chosen words in the 1966 report by Sattinger and Polcyn entitled, "Peaceful Uses of Earth Observation Spacecraft".

The complexity of satisfying requirements for these many users is not so much attributable to the formidable length of the list appearing in Table 2 as it is to the fact that these many users want the information for different vegetation groupings, at different times and with differing levels of accuracy. In addition, they have differing requirements as to the speed with which vegetation information must be processed once the raw data have been collected, and also as to the frequency with which the information must be updated.

This latter consideration has led to our compiling a third and final table (Table 3) in our effort to document in concise, tabular form the various user requirements for vegetation resource data.

It is to be emphasized that, in this table as in the two which preceded it, the same headings can be used for the four vertical columns. At the risk of some oversimplification, this table lists six time intervals that are indicative of the frequency with which various kinds of information about the vegetation resource are needed (10-20 minutes; 10-20 hours; 10-20 days; 10-20 months; 10-20 years; and 20-100 years).

In considering relationships between the frequency with which earth resource data should be collected and the rapidity with which these collected data should be processed, the writer has found it useful to employ the term "half-life" in much the same way as it has been employed by radiologists and atomic physicists. The shorter the isotope's half-life, the more quickley a scientist must work with it once a supply of the isotope has been issued to him. One half-life after he has acquired the material only half of the original amount is still useful; two half-lifes after acquisition only one quarter of the original amount is still useful, etc.

By coincidence or otherwise, this half-life concept applies remarkably well to nearly every item listed in Table 3. Specifically, if the desired frequency of acquisition of any given type of information, as listed in that table, is divided by two, a figure is obtained indicating the time after data acquisition by which that particular item of information should have been extracted from the data. It is true that some value will accrue even if that item of information does not become known until somewhat later. But the rate at which the value of the information "decays" is in remarkably close conformity to the "half-life" concept.

Each item that is listed in Table 3 can be placed in one of the six categories of information listed in Table 1 and identified as a user requirement for one or more of the agencies listed in Table 2. Thus a certain unity can be found in these three tables. Consequently, by studying them, not just individually but in concert, we can better appreciate the true nature of the multifaceted user requirement that we seek to satisfy by the remote sensing of vegetation resources.

As previously indicated, there is a high degree of complexity in the user requirement for information on the vegetation resource. Consequently, the three tables which have just been given would probably be considered by many of these users to be a gross oversimplification. For example, many users think almost entirely in terms of protecting the vegetation resource from damaging agents and thus would view the problem somewhat more narrowly than we have viewed it here. On the other hand, there are those who think of the vegetation as only one of the many items which comprise the total "resource complex" in a given land area which they must manage. Almost certainly they would view the problem more broadly than we have in these tables, pointing out the importance of such non-vegetational components as soils, water, minerals, wildlife, and recreational potential.

An example of each of these two viewpoints will now be given, the first pertainining to agricultural resources and the second to forest resources.

Agriculturists recently were asked to list, crop-by-crop, the specific applications of remote sensing which might prove profitable in terms of cost/benefit ratios and total savings which might be effected. This resulted, not only in their listing the 6 categories of information appearing in Table 1, but also in their selecting the most important "candidate problems" in U. S. agriculture--all dealing with damage that is done each year to specific crops by specific insects or pathogens. These experts agreed that, if remote sensing would permit early detection of attacks by these insects or pathogens, effective control measures could be taken, thereby avoiding great economic loss. The most important items on this long list of agricultural "candidate problems" are as follows: (1) Control of Leaf and Stem Rust on Wheat and Oats, (2) Barberry Bush Eradication, (3) Cereal Leaf Beetle Eradication, (4) Imported Fire Ant Eradication, (5) Soybean Cyst Nematode Control, (6) Control of Burrowing Nematode Disease on Citrus, (7) Phony Peach and Peach Mosaic Eradication, (8) Control of Various Root Rot Conditions on Agricultural Crops and Timber Stands, (9) Control of Gypsy Moth Infestations on Pines, (10) Control of Wooly Aphid on Conifers, (11) Control of Pine Bark Beetles, (12) Control of Spruce Budworm Infestations, (13) Control of Conifer Limb and Stem Rust, (14) Control of Hardwood Dieback, and (15) Control of Dwarf Mistletoe on Conifers.

As for the previously mentioned "complexity", it results from the fact that each of these candidate problems poses its own remote sensing specifications in terms of sensors to be used, geographic areas to be sensed, optimum dates for sensing, signatures to be recognized, rapidity with which data must be analyzed and format in which data should be presented. Obviously a definitive study needs to be made soon to determine what the most suitable interaction should be between remote sensing personnel and these various users of remote sensing data. Only by this means can we properly match remote sensing capabilities to user requirements in the field of agriculture.

Foresters also have decided that they need essentially the same 6 categories of information as the agriculturists require, as seen in Table 1. Then, using a somewhat different approach, they have decided that remote sensing might be especially helpful to them by providing information on which to base "multiple use" decisions relative to each part of the forest. The multiple use concept is a complex one, and it is far more applicable in forestry than in agriculture. Some users of the forest would like to have all parts of the area managed primarily with a view to maximizing timber production. At the other extreme are those who want to preserve our forests as primeval museums to be enjoyed by posterity. In between are those who would condone each of these uses for specific parts of the forest so long as it didn't interfere with their objectives of using the forest primarily as a source of water for domestic use; or minerals for industrial use; or fish, game, boating, hiking, skiing, etc., for recreational use. The true complexity of the forester's decision-making problem, as he seeks to satisfy these many user requirements, is suggested merely from a reading of the forester's official definition of the term "multiple use":*

---

*Multiple Use Act, PL 86-517, HR 105-72, June 12, 1960.

> "The management of all the various renewable resources of the national forests so that they are utilized in the combination that will best meet the needs of the American people; making the most judicious use of the land for some or all of these resources or related services over areas large enough to provide sufficient latitude for periodic adjustments in use to conform to changing needs and conditions; that some land will be used for less than all the resources; and harmonious and coordinated management of the various resources, each with the other, without impairment of the productivity of the land, with consideration being given to the relative values of the various resources, and not necessarily the combination of uses that will give the greatest dollar return of the greatest unit output".

The above mentioned definition is sufficiently complex so that the concept of multiple use may easily escape the average reader. However, Draeger (1969) has rendered a service by providing the following more comprehensible statement of this concept:

> "The allocation of lands to various uses such that the combination of uses best meets the needs of those for whom the land is being managed, provided that in the process of developing this allocation, values and costs of each of the many possible patterns of exclusive uses and compatible co-uses are at least taken into consideration. In some instances, depending on the circumstances, several uses may be derived simultaneously from the same parcel of land, while in other cases a particular area may be allocated to only a single use but managed as a portion of a greater whole composed of many such exclusive-use parcels".

In terms of user requirements for information, each of these statements implies the following: Before an intelligent decision can be made regarding how best to use each part of the forest, information of two major types is needed (1) an accurate "in-place" delineation of both the forest vegetation and all associated resources (soils, water, minerals, topography, etc.) i.e., a complete "resource map", and (2) adequate sociological and technological data to know how, given this total resource complex, the forest as a whole, and each unit of it in particular, can be made to produce "the greatest good for the greatest number" (to use the words of Gifford Pinchot). Of these two complex and interrelated problems, the present Apollo 9 report deals only with the first.

As we conclude this discussion of User Requirements for Information about Vegetation Resources, three summarizing points seem worthy of emphasis: (1) Tables 1, 2 and 3 set forth most of these requirements, in terms of types of information desired, agencies and groups requiring the information, frequency with which the information is desired, and rapidity with which the data should be processed; (2) there are certain instances, as exemplified by the 15 candidate problems of agriculturists that we have listed, when we will

be told that our three tables may have set forth the user's requirements too broadly, since interest centers in only a few vegetation resource problems; and (3) there are certain other instances, as exemplified by the multiple use problems of foresters, when we will be told that our three tables may have set forth the user requirements too narrowly, since multiple use decisions depend not merely on vegetation resources but on the entire complex of earth resources (vegetation, soil, water, minerals, topography, etc.).

SOME EXAMPLES OF REMOTE SENSING CAPABILITIES FROM AIRCRAFT AND SPACECRAFT

The purpose of this section is to indicate the extent to which an analysis of multiband aerial and space photography will enable interpreters to satisfy the informational needs of various users.

As a basis for judging the remote sensing capabilities that are provided by aerial and space photographs I will cite specific findings of my group in efforts they have made to evaluate two kinds of photography: (1) multiband space photography that was taken of various earth resource test sites in the U. S. from an altitude of about 110 nautical miles by the Apollo 9 astronauts in March 1969, and (2) multiband aerial photography taken of these same sites from an altitude of approximately 70,000 feet, not only at the time of the Apollo 9 overflight in March, but also at monthly intervals since then. Both types of photography will first be described.

On the Apollo 9 mission, perhaps for the first time in history, simultaneous multiband photographs of the surface of the earth were obtained from space. We need clearly to recognize the potential usefulness of such photography (described in Table 4a) in the making of earth resource surveys.

Our ability to inventory earth resource features on multiband photography rests on the fact that every type of feature encountered on the surface of the earth tends to reflect and emit radiant energy in distinctive amounts at certain specific wavelengths. Consequently, when remote sensing is done simultaneously in each of several wavelength bands (a process variously known as "multiband sensing", "multispectral sensing" and "multiband spectral reconnaissance"), each type of feature theoretically becomes identifiable by virtue of its multiband "tone signature" or "spectral response pattern".

It was with this possibility in mind that a special Photographic Team, operating under auspices of the NASA Earth Resource Survey Program, held a series of meetings, extending over a period of more than two years, primarily for the purpose of selecting the three bands which would be most useful in a multiband space photography experiment.

Consistent with the recommendations of that team, the three bands used on the Apollo 9 mission in obtaining simultaneous black-and-white photographs from space were those exposing for the green, visible red and near infrared wavelengths of radiant energy, respectively. Also, consistent with the recommendations of that team, these same three wavelength bands are to be employed on ERTS-A, the first in a series of Earth Resources Technology Satellites, which is now scheduled for launch in early 1972.

Some investigators, on noting that a color film known as "Infrared

Ektachrome" contains three dyes which, in effect, are responsive to the green, red and infrared wavelength bands, respectively, have argued that this single color film would be able to provide all of the information obtainable from the corresponding three black-and-white photographs. In order to evaluate this argument, a fourth camera, containing Infrared Ektachrome film, was used on the Apollo 9 mission simultaneously with the three cameras that employed black-and-white films. This 4-camera package (consisting of 4 Hasselblad cameras having 80mm focal lengths and accommodating 70mm roll films) was designated by the NASA Photo Team as Scientific Experiment No. 065. Hereafter in this report, as elsewhere in the literature, this portion of the photography obtained on the Apollo 9 mission will be termed merely the "S065" photography. (See Figure 1).

Long before the launch of Apollo 9, it was recognized that certain earth resource features can best be inventoried through a comparative analysis of "sequential" space photography (i.e., that taken repetitively of the same area at suitable time intervals).* However, there appeared to be little likelihood that such photography could be obtained on future Apollo flights for at least two years. Consequently, NASA arranged for simulated space photography to be flown sequentially at monthly intervals throughout the 1969 growing season, from aircraft operating at very high altitudes (approximately 70,000 feet) using a 4-camera system that would accommodate essentially the same four film-filter combinations as were being used on the Apollo 9 - S065 experiment. At the time of this writing, such sequential "high-flight" photography has already been taken during the months of March, April, July and August, 1969, and plans call for continuation of this activity through the month of October. Several examples of that photography, and of the sequential interpretations made possible by it, appear in a report which our group is in the process of completing, entitled, "An Evaluation of Earth Resources Using Apollo 9 Photography". Hence, it will suffice here merely to include several photographic examples, most of which were taken either from the Apollo 9 spacecraft or from supporting high-altitude aircraft. A few additional examples are included, however, to illustrate more fully the remote sensing capabilities, either of aerial photography (Figures 1-5) or of imagery obtained with optical mechanical scanners (Fig. 6) or side-looking airborne radar devices (Fig. 7) . Also illustrated are opportunities for using various kinds of optical or electronic equipment to produce enhanced composite images by the additive color process. Such composite images have been profitably made in our studies either from multiband photographs taken at one time (Figs. 15,16) or on multidate photographs taken in one band (Fig.18)

Much has been said about opportunities for facilitating the photo interpreter's task, not just by using such image enhancement devices, but also by using automatic data processing equipment (e.g., computers) capable of identifying vegetation types and other earth resource features from their "tone signatures". Sometimes this will be possible on photography taken in only one band. However, even in such a simple case it may be necessary for the photo interpreter to interact properly with the computer at two or more stages in the development of the "recognition program". This is illustrated by a comparison of Figures 20 and 21.Thus, Figure 20 was made by computer techniques from Figure 19, a portion of the Imperial Valley Pan 25A "high-flight" photograph that was taken at the time of the Apollo 9 overflight. In order for this to be accomplished, a scanner was first used merely to scan

Figure 19 (in positive transparency form) resolution element-by-resolution element and scan line-by-scan line. Appropriate symbols (numbers, letters, etc.) were used to record up to 64 shades of grey. It will be noticed from an examination of Figure 20 that, in this first iteration, symbols happened to be assigned such that fallow ground (e.g., the cultivated field at "A") is characterized by numbers (primarily 2 through 8), while bare soil (e.g., the roads and ditch banks at "B" and "B'") is characterized by letters (primarily Q through V). In this initial coded printout, it will be noted that other features, being of different tones than fallow ground or bare soil, were coded to different symbols. Inspection of the results (i.e., a process which in this instance constitutes the second interaction between human and machine) suggests that an improved "program" might be written specifically if all of the above-mentioned numbers were printed as a single type of symbol (e.g., a dot) and all of the above-mentioned letters were printed as another single type of symbol (or perhaps better yet, might merely be made to register as blank spaces.) Then if the computer were so programmed that "everything else", by virtue of its having some other tone value or values than either of the above features, were made to printout as an "X", three categories of features would be automatically recognized. Upon inspecting this second printout (Fig. 21) and comparing it with "ground truth" or with the originally scanned photograph, the photo interpreter might decide that it would be desirable to achieve automatic recognition of still other features, among those currently lumped together in category "X". To do so might prove to be a more difficult programming task and probably would necessitate the use of photography taken either in additional wavelength bands, or on additional dates,--or perhaps both. At this point the task of optimizing the recognition code might become so complex as to warrant the use of computer techniques in the optimization process itself. Thus still another example of the necessity for interaction between human and machine is indicated.

The foregoing dissertation is not intended as a diversion from the central theme of this paper. Quite to the contrary, only through the use of such techniques can we hope to maximize the value of remote sensing capabilities in satisfying the informational requirements (with respect to both time and accuracy) of those who manage vegetation resources.

Automatic data processing based on tone or brightness values sometimes is done in a more direct fashion. Instead of scanning multiband photos, the terrain itself is scanned directly with an airborne multichannel "optical mechanical scanner" as the sensing vehicle flies along. Brightness values are thus obtained, as in the previous instance, resolution element-by-resolution element and scan line-by-scan line and they are recorded as signal strengths on magnetic tape, just as when photographs are scanned. From that point forward the process is identical with the one previously described. Furthermore, just as before, the human may find it desirable at successive stages to interact with both the computer printout and a continuous tone image (photograph). To obtain a photo-like image from scanner data one simply uses signal strengths, as recorded by the optical mechanical scanner to govern brightness values on a "glow tube" (e.g., a cathode ray tube such as the screen of a television set). Obviously, the brighter a spot was in the original scene, the greater the signal strength that was recorded by the scanner. Also, on "playback" of the magnetic tape record, the greater the signal strength for any given feature, the stronger the beam of electricity directed on a corresponding por-

tion of the glow tube and hence the brighter the glow. The resulting "visual display" on the tube can be viewed directly or photographed, as in Figure 22.

In concluding this section it is to be emphasized that Figures 9 through 23 all are remote sensing records of the same scene, either in original or enhanced form. Each form may be useful for one purpose or another as we seek to maximize the extent to which remote sensing techniques can satisfy user requirements. Aerial and space photos of other areas appear in Figures 24-28.

THE QUANTIFICATION OF REMOTE SENSING CAPABILITIES

As we seek in this paper to relate remote sensing capabilities to user requirements we must do more than merely present enhanced aerial and space photographs that the reader is likely to find aesthetically appealing. Quantitative tests should be made that are designed to (1) obtain statistically valid measures of interpreter performance when studying the different kinds of imagery; (2) measure this performance in terms of both time required and accuracy achieved when attempting to identify features that are meaningful to the user; and (3) measure performance as a function of the background of training and experience of the photo interpreter.

A part of the experiment presently to be described was based on the Imperial Valley Test Area and employed the various kinds of imagery appearing in Figures 12 through 16. Three other areas were also included in the experiment, viz. The Bucks Lake-Meadow Valley Area, the Davis Area, and the Dallas-Fort Worth Area. As will presently be seen this permitted an experimental design in which "familiarity with the area" (as acquired by a testee after studying the area on many kinds of imagery) could be minimized. By thus holding this factor and other factors as nearly constant as possible, when the interpretability of any given feature was being tested, the only variable remaining hopefully would be the imagery itself.

It was recognized that accuracy ratings should take into consideration not only the correct identifications that are made by a photo interpreter but also his errors of omission and commision.* In conducting our experiments, in any given area, such as the Imperial Valley Area, nine different kinds of imagery were employed. (Some of these were not enhanced while the others were enhanced by the various means previously discussed.) Each area was so selected that the interpretation of five categories would be both necessary and sufficient, by-and-large, for satisfying the most important informational requirements of the user. Thus, for example, in the Imperial Valley Area four discrete categories were to be recognized and a fifth category was included which would provide an additional meaningful grouping of the 4 categories.

The 9 image categories, and the corresponding abbreviations for them as used in Tables 4 through 9, were as follows: 25A = Panchromatic film with a 25A filter; 58 = Panchromatic film with a 58 filter; 89B = Black-and-white infrared film with an 89B filter; PF = Philco-Ford electronic combiner

---

*"Omission" is defined as the complement of "correct", i.e., % Omission = (100-%C). "Commission," on the other hand, is defined as the actual number of errors committed (e.g., calling a field "alfalfa" when in reality it is a barley field), expressed as a percent. Thus,

$$\% \text{ Commission} = \frac{\text{Total number of commission errors}}{\text{Total possible responses-total possible correct responses}} \times 100$$

image; CIR = color infrared, more commonly known as infrared ektachrome; IDECS = University of Kansas electronic combiner image; CIRID = A combined interpretation of color, infrared ektachrome and University of Kansas electronic combiner images; and Color = Ektachrome film with haze filter.

The four discrete categories used in the Imperial Valley Area were (1) Bare Soil (BS); (2) Cropland--a term used to include all land that was supporting agricultural vegetation (cultural crops) at the time of photography; (3) Alfalfa (A); and (4) Barley (B). The fifth category grouped all agricultural vegetation into a single unit and then required the photo interpreter simply to make the dichotomous choice, Bare Soil vs. Cropland. While other categories might have been established, they were encountered too infrequently to be of significance primarily because most crops grown in the Imperial Valley in any given year are not yet photogenic in March, the month when the Apollo 9 and supporting high flight photos were taken.

The use of the above 5 categories and 9 image types produced a 5 x 9 "array" in which there were 45 individual cells, each cell representing a unique combination of a particular category with a particular type of imagery. Statistically speaking, this required the use of a minimum of 45 interpreters in order to fill each cell with a suitable number of individual interpreters. Additional factors governing the selection of the number of interpreters were (1) the need for minimizing the problem of area familiarization and (2) the statistical desirability of having at least three replications per cell.

The 45 interpreters that were required for these tests were selected in such a way that they could be placed into three groups of 15 each according to their level of campetence--high, medium, low--based on background data sheets filled out by the interpreters. A "high" (highly skilled interpreter) was ranked as such if he had taken a remote sensing course and also had several years of work experience in the field; a "medium" was one who had taken a course in air photo interpretation or remote sensing but had little work experience in the field; and a "low" was one who had neither taken a course nor had obtained any work experience in the field. Each person was then randomly assigned to each of three cells such that each of the 45 cells contained a high, medium and low interpreter. This was accomplished in a manner such that no person would look at any one of the four test areas (the Imperial Valley Test Area, for example) more than three times. This arrangement kept the problem of area familiarization to a realistic minimum. It reduced the problem of interaction between the categories to be interpreted in a given area, and it also permitted three replications per cell for more valid statistical results. By establishing each cell as equivalent to any other cell in terms of level of competence, this test allowed meaningful comparisons to be made between cells (image types) by category.

For two reasons, administration of the actual interpreter tests was performed by the researchers: (1) to answer any questions which the interpreters might have about specific aspects of the test, and (2) to keep an accurate record of the time which each interpreter required to complete a particular test. At the outset, two methods of presenting images to the interpreter were tested, one employing prints and a second requiring projection of the images onto a viewing screen. One area was used as a control

and an equal number of skilled and unskilled interpreters were asked to interpret individual categories in the same manner. Statistically, no significant difference was noted between the interpretations accomplished using prints and those using projection techniques. Consequently, the researchers were able to choose what they considered to be the optimum method for presenting to the interpreter the test material for a given site. The actual tests were administered individually with a particular interpreter looking at one category on a discrete image type at one time.

When prints were employed, the interpreter was asked to identify particular categories in a prediction area based on information given in a training area on the same image. (See Figure 12) Information for the training samples was derived from available "ground truth" maps which our researchers had painstakingly compiled of the test area. The interpreters were required to record their identifications on a map where the prediction samples and training samples were delimited. An example of an interpretation of Bare Soil from IDECS enhanced Apollo imagery of the Imperial Valley will serve to explain the procedure. In this example a testee was given both the image and a map of the area on which only those fields of bare soil in the training area had been filled in. She then took 6 minutes to fill in what she considered to be the fields of bare soil on the rest of the image. A comparison with the "ground truth" map for the area was then made which showed that she correctly identified 16 fields, committed errors in 7 instances and omitted 6 fields which were in actuality bare soil.

When projection was employed, as in imagery of the Imperial Valley Test Area, answer sheets were sometimes used. In other instances, however, such as the Bucks Lake-Meadow Valley Test Area, an overlay containing the training and prediction areas was attached to a viewing screen and the image was then congruenced to the "ground truth" overlay. Here the interpreters were given numbered answer sheets on which to place letters that would signify how they had interpreted specific areas with the numbers on the sheet corresponding to those in the prediction area. These interpretation tests were carried out using projection techniques with the interpreters viewing images projected onto a screen in a darkened room. The resultant images measured approximately 18 x 13 inches and were viewed from a distance of approximately 12 feet, giving a scale on the Apollo imagery of the Imperial Valley of about 1:15,000; however, interpreters were encouraged to view the screen at what they considered the best distance. This ranged from a few feet up to 20 feet.

For the Imperial Valley Test Area results based on interpretations that were made of the Apollo 9 photography are summarized in Tables 4, 5 and 6 which deal, respectively, with "correct identifications", "commission errors" and "time requirements". Similarly, results based on interpretations that were made of the High Flight photography are summarized in Tables 7, 8 and 9.

For the other three test areas, (Bucks Lake-Meadow Valley, Davis, and Fort Worth-Dallas) results are presented in a similar fashion in our portion of the CRES report entitled 'Quantitative Evaluation of Multi Image Processors", which was prepared under auspic s of the Engineering Topographic Laboratories, U.S. Army, Fort Belvoir, Virginia. Although the Imperial Valley Test dealt almost entirely with cropland vegetation, our tests in the other areas also dealt with wildland vegetation and with certain other earth resource features

as well.

Table 10, which pertains to the Mesa, Arizona agricultural test site of 16-square miles, shows the results of photo interpretation testssimilar to those already described for the Imperial Valley area except that (1) more crop types and condition classes were included in the test and (2) not only multiband composites, but also multidate composites were included in the test. Abbreviations used in the second column of Table 10 (labelled "Image Type and Date") are sufficiently analogous to those used in Tables 4-9 to be self-explanatory.

Table 11 is based on interpretations which we have made, in similar fashion, of the Apollo 9 Infrared Ektachrome photographs shown in Figure 24 (but after these photographs had been suitably enlarged). The categories abbreviated in Table 11 have the following significance and reflect our desire to include some interpretation tests on space photography that would be even broader than those on which Tables 4-10 were based: D - Deciduous forest; P = Pine forest; M = Mixed deciduous and pine forest; C_V = Cultivated land that is vegetated; C_B = Cultivated land that is bare; C_F = Cultivated land that is fallow; W_O = Open bodies of water; W_R = Rivers and canals; R = Roads; and U = Urban and industrial areas. Notice, as explained in the caption to Table 11, that not only are correct answers by type indicated, but also errors of omission and commission, also by type.

In light of the examples that have just been given, we conclude this section by referring to Table 12, which is an effort to summarize in a quite different context, the present-day remote sensing capabilities in various parts of the electromagnetic spectrum. The following points indicated by that table seem worthy of emphasis: (1) there is a remote sensing capability in nearly every portion of the electromagnetic spectrum of interest to man; (2) the longer the wavelength, generally speaking, the larger the aggregations of matter for which properties are being sensed; (3) the highest spatial resolution is obtainable in the visible and solar infrared portions of the spectrum because (a) resolution in the shorter wavelengths is limited primarily by atmospheric scattering, and (b) resolution at longer wavelengths is limited by the aperture of the sensor used; (5) those wishing to study features on the surface of the earth are concerned with atmospheric penetrability as they look for "windows" of high atmospheric transmission, (6) those wishing to study properties of the atmosphere itself are concerned with atmospheric penetrabili ty as they look for spectral zones <u>other</u> than those occupied by the high transmission windows, and (7) in consequence of the last 2 points, there is some interest in exercising a remote sensing capability, for one purpose or another, in virtually every portion of the entire electromagnetic spectrum.

RELATING CAPABILITIES TO REQUIREMENTS

Of the three tables that we have presented to summarize "user requirements" we note that Table 1 deals with types of information desired about vegetation resources, Table 2 with the agencies and groups desiring that information, and Table 3 with how often and how rapidly they need it. In the interest of simplifying the analysis contained in the present section, we will deal with each of these tables separately. In so doing, we will draw, as necessary, on the quantitative indications of capabilities and limitations that are summarized in Tables 4 through 12.

Each of the six categories of information listed in Table 1 as being desired by those who manage agricultural crops, timber stands and forage and brush resources, respectively, will now be discussed in turn. In each instance needs of the agriculturist will be considered first, after which similar needs of those who manage timberlands, rangelands and brushlands, respectively, will be considered.

A. Species Identification

Agricultural Crop Species. It would be a poor farmer, indeed, who did not know what type of crop he was growing in each field that he was cultivating. However, this fact has proved to be of little help to the various federal agencies and other regionally or nationally oriented groups which need to know quickly, accurately and perhaps even discreetly, the acreages within vast areas that have been planted to various kinds of crops in a given year. Returns from questionnaires which these agencies send to farmers can be of value, but for compiling broad regional statistics these returns generally prove to be too meager, too late and on many occasions too inaccurate to satisfy agency needs. Consequently, each of these agencies has long been interested in obtaining such information from aerial photography and, more recently, from space photography.

Judging from the study which my colleagues and I have made of Apollo 9 photographs of the Phoenix and Imperial Valley areas, the overall accuracy with which crop types can be identified on multiband space photography ordinarily does not exceed 60%. While accuracies greater than 90% may be achieved for some crops (using the most favorable film-filter combinations), these seem to be offset by instances in which accuracies are as low as 30%. Far more encouraging results are indicated, however, when the same raw data as were used in obtaining these figures are examined more closely, bringing to light the following factors:

1. Inexperienced photo interpreters tend to make the most errors and thereby lower the overall average for accuracy of crop identification. To illustrate both the importance of this factor and at least a potential remedy to the problem posed by it, let us presume that we were to know, say in the year 1975, that 45 photo interpreters would be needed that year, periodically throughout the growing season, to study space photography and identify agricultural crops throughout the United States. Instead of training the first 45 people who happened to be available forthe task, we might (a) be more selective of trainees and (b) at the end of the training session retain only the top performers for use in the operational surveys. If by this process we found it necessary to train 150 candidates in order to have a sufficiently large population from which to select 45 top performers, this still might be the most efficient and economical procedure in the long run.

2. Even among the top performers, accuracy should improve with time on the job. On similar classification projects (but using aerial photos rather than space photos) the U. S. Forest Service has found that trainees require nearly 6 months of intensive, on-the-job training before they are able to achieve maximum performance.

3. When individual crop types cannot be identified on the photography, the mere identification of groups of crops may provide an adequate solution. The validity of this assertion is best documented by citing results of a recent research project which employed high-flight photography. A major objective of that project was to determine total wheat acreage in each of several very large areas. Those of us working on the project soon found that wheat could not be consistently identified on this photography because of the frequency with which it was confused with other "small grains" (oats, barley and rye) grown in the area. However, it was established (from an examination of records obtained by ground enumerators in each of several previous years) that the ratio of "wheat acreage" to "total small grain acreage" tended to be remarkably constant, year after year, in each of these areas. Consequently, the photo interpreters merely determined "total small grain acreage" and multiplied this figure by the proportionate "wheat acreage factor" to determine total wheat acreage. Subsequent ground truth data showed that the average error in estimating wheat acreages by districts was less than 5% and the maximum error was less than 10%.

4. The accuracy with which crop species might be identified can be significantly increased by the production of certain color image enhancements from multiband black-and-white photographs. As detailed in our previously mentioned Apollo 9 report, we made several such enhancements by means of additive color processes. Some of the enhancements were made optically and others electronically. It is probable that far more image enhancements could be profitably made from the Apollo 9 multiband photos than we have made to date. Most of the optical and electronic enhancements that were tested sought to enhance overall interpretability, thereby facilitating the identification of several different types of crops with merely one type of enhancement. Judging from results which our group previously has obtained when working with multiband aerial photography, a series of enhancements can be made quickly and easily, each of which, in turn, serves to differentiate some particular crop type from everything else. Thus, enhancement No. 1 may give a unique coloration for Crop A and thus permit it to be distinguished readily from everything else; then, merely by rotating the filter wheels of an optical combiner or the electronic control knobs of an IDECS or Philco-Ford device, enhancement No. 2 can be produced to give a unique coloration for Crop B vs. everything else; a third position gives enhancement No. 3, which facilitates differentiating Crop C from everything else, etc.

5. On operational surveys, few areas would exhibit the variety of crops, and hence the classification problems encountered in the Phoenix and Imperial Valley areas. Some of this nation's largest crop producing regions are devoted almost entirely to the production of two or three major crops (rice and sugar cane in one region, cotton and tobacco in a second region, corn and soybeans in a third region, etc.). Usually it is far easier for the photo interpreter to differentiate a particular crop from 2 or 3 other associated crops than from 8 or 10 (as in the Phoenix and Imperial Valley areas).

6. On operational surveys of agricultural areas, a month more favorable than March (when Apollo 9 flew) could be selected as the optimum time for photo acquisition. For example, three of the most prevalent crops in

the Phoenix and Imperial Valley Areas (sugar beets, barley and alfalfa) have very similar appearances on small scale photography during the month of March. These three crops are far more identifiable on photography taken later in the season. For example, we conducted crop identification tests on two sets of Infrared Ektachrome High Flight photographs of the Phoenix area taken in March and May, respectively. Whereas in March the three main crops, barley, mature alfalfa and sugar beets could only be identified to accuracies of 33%, 56% and 46% respectively, in May the corresponding accuracies were 90%, 83% and 40%.

Timber Species. Judging from our interpretation of Apollo 9 photographs of the Vicksburg, Mississippi area, it appears obvious that a photo interpreter would experience little difficulty in differentiating between forested areas and other areas even on black-and-white space photography of this quality.

On the Infrared Ektachrome space photography it also is possible to differentiate between the blue-gray coloration of bottomland hardwood stands and the purple-to-pink coloration of pine-hardwood stands. As documented by Langley, Heller and Aldrich, in their report entitled, "Multistage Sampling of the Forest Resource--An Apollo 9 Case Study", even this limited stratification of the timber resource greatly improves sampling efficiency. Furthermore, it is probable that by applying electronic image enhancements or microdensitometer traces to the multiband Apollo 9 photographs, still further stratification of timber types would be possible.

Just as sequential photography aids in the identification of agricultural crops, such photography also should facilitate the identification of timber species. However, in order to exploit that possibility the photo interpreter would need to develop a "calendar" of seasonal phenology for each tree species, analogous to the "crop calendars" used in identifying various agricultural crops on sequential photography.

An additional possibility for mapping timber types on space photography presents itself in areas having high topographic relief. Southern Arizona is one such area that was photographed by the Apollo 9 astronauts. In that area, south-facing slopes consistently provide a site where oaks can reach their highest elevational limits. North-facing slopes are protected and the snow remains longest in these areas with the result that they support pines and firs. It is on these slopes that conifers are able to occupy their lowest elevational positions. These relationships were found to hold very consistently on all of the areas of Arizona and New Mexico covered by the Apollo 9 photos.

Rangeland and Brushland Species. Virtually all of the rangelands and brushlands suitable for study on the Apollo 9 photographs are in arid desert lands of Arizona and New Mexico. A few alpine meadows which have excellent forage during the summer months also were photographed, but at the time of Apollo 9 overflights these areas were both snow covered and largely devoid of forage, thereby precluding the possibility of making a meaningful study of them.

Even in the arid desert lands herbaceous forage was so sparse, and

brush so nearly leafless when the Apollo 9 photos were taken, that it registered very poorly, if at all, on the space photography. However, in the very situation where vegetation is least conspicuous, landforms are most conspicuous. Consequently, an attempt was made, especially in the rangeland and brushland areas southwest of Phoenix, Arizona, to exploit the known correlation that exists between landform type and vegetation type. Results of that effort, while thus far somewhat superficial, have been highly encouraging. A similarly successful correlation was established in the vast desert area southeast of Tucson, Arizona, where the large shrubs and trees were confined primarily to large drainage channels, and the most xerophytic species to the interfluves, while species having intermediate drought resistance occupied intermediate environments between these two extremes.

Changes in pheonology with season often promise possibilities for the photo identification of rangeland and brushland species, just as they do for agricultural and timber species. For example, the following facts were found in our studies to apply to both the Sonoran Desert and the Chihuahan Desert regimes of southern Arizona:

(1) During the second week in March, when the Apollo 9 photographs were taken, only the coniferous forests and the evergreen species in the chaparral, oak and juniper-oak woodlands have green foliage and, therefore, register red on Infrared Ektachrome space photography.

(2) Species in the desert shrub area are leafed out in April. Hence, any additional area that appears red on April photography usually will be of this type.

(3) Grasslands leaf out in August, following the summer rainy season. Hence, any additional area that appears red on August photography usually will be of this type.

B. Determining the Vigor of Vegetation and the Identity of Plant-Damaging Agents

Agricultural Crops. If the objective is merely to detect areas in which there is sparse vegetation (attributable to a lack of crop vigor) space photography taken on a single date and with only one of several film-filter combinations probably will suffice. But if, in addition, a determination of the damaging agent is to be made, the photo interpreter's task is greatly facilitated by his having access to sequential photography taken with a multiband camera system at two or more dates during the growing season.

Of the many examples which might be given to illustrate this fact, only one will be offered here. In the Imperial Valley, at the time of this writing, there is a serious threat to the cotton crop attributable to a damaging agent known as "pink worm".* Heavy defoliation (and a consequent reduction in vegetation density) constitutes one of the manifestations of damage to the cotton plants by this organism and an associated defoliating insect.

---

* Strictly speaking, this damage is attributable to a combination of pink boll worm and certain leaf borers (defoliating insects).

Cotton fields having a low vegetation density are detectable even on space photography. Even so, if a cotton field were to be photographed on only one date "pink worm" damage might easily be confused with at least two other factors that can affect the density of vegetation in that field.

One of these factors, locally known as "cultivator blight" is attributable merely to poor traversing of a cultivator down the rows of cotton. Small deviations from the prescribed course will cause the cultivator tines to remove the developing cotton plants. The other factor is variable planting depth at the time the cotton seeds are being mechanically sown. The result is that in shallow-sown areas seedlings emerge from the soil and start vegetating the cotton field sooner than in deeply sown areas.

Given aerial or space photography that was taken on only one date during the development of plants in a cotton field, the photo interpreter may find it impossible to determine which of these three factors is responsible for the sparseness of vegetation. But if he is given photography taken on each of two dates, suitably spaced, he should be able to determine whether the area of sparse vegetation is increasing (indicating that "pink worms" are the damaging agent); remaining about the same size (attributable to "cultivator blight") or decreasing (because of late emergence of seedlings in deeply sown areas).

Our group will soon be submitting to NASA a special report dealing with our analysis of the March-October, 1969 high flight photography. In that report we hope to include sequential photographs that will illustrate the extent to which the above type of analysis can be made.

Timber Crop Vigor. In several reports which our group has submitted to the National Park Service and other sponsoring agencies, we have documented the feasibility of using aerial photographs to detect vigor loss in coniferous timber stands. In most instances the damaging agent was some species of bark beetle (e.g, Dendroctonus brevicomis, Scolytus ventralis). Several of our Forest Service colleagues, including Heller, Aldrich, Wear, Weber and Croxton, also have reported favorably on the feasibility of detecting insect attacks in timber stands, as well as fungus attacks that produce certain economically important disease (e.g., "Douglas fir Root Rot", "Ash Dieback", "Oak Wilt" and "Dutch Elm Disease".) Infrared-sensitive films often are best for detecting these maladies.

For the early detection of such phenomena the photo interpreter must be able to resolve individual tree crowns, or even portions of tree crowns. Space photography such as that obtained on the Apollo 9 mission does not provide sufficiently high spatial resolution to permit early detection of vigor loss on a tree-by-tree basis.

Once a sizable portion of the timber stand has become damaged, this fact should be determinable from a study of space photography of the Apollo 9 type. However, it was not possible to document this point in our present studies for two reasons: (1) To the best of our knowledge, such sizable infestations did not exist on any coniferous stands covered by Apollo 9 except for one area 50 miles north of Phoenix where a heavy snowfall still hung on the trees and obscured the foliage. (2) Even if such

infestations did exist on deciduous hardwood stands they would not have been detectable because the trees were in a nearly leafless condition in March.

The initial outbreaks of forest insect and disease infestations commonly occur in timber stands that occupy specific topographic sites. Such sites usually are detectable on space photography, and once detected could be aerially photographed periodically. This is yet another example, therefore, wherein the previously described process of "multistage sampling" might be used to good advantage.

Forage and Brush Vigor. In the rangelands northeast ofPhoenix, Arizona, some of the annual grasses, herbs and brush species were in a vigorously-growing state at the time of the Apollo 9 mission, especially at mid-elevation on the foothills. At lower elevations such vegetation tended to be growing less vigorously, mainly because of inadequate soil moisture. At higher elevations it also was growing less vigorously, mainly because cold air and soil temperatures (which characterize the winter and early spring months in this area) still prevailed. The more vigorously the vegetation is growing, the more infrared-reflective it is, and therefore the redder it appears as imaged on Infrared Ektachrome space photography. This characteristic is quite apparent on the Apollo 9 Infrared Ektachrome photos, the mid-elevation rangelands and brushlands being by far the reddest. As a corrolary to the above they are at the optimum state of "readiness" for grazing. Like other kinds of vegetation, grasses, herbs and shrubs can be damaged on occasion by insects and fungi. When this occurs, the same principles governing damage-detection on aerial or space photographs will apply as were described in the previous section dealing with timber stands.

C. Yield Estimation

Agricultural Crops. To the extent that it is possible for the interpreter of space photographs to distinguish crop types, estimate crop vigor and identify crop damaging agents (as discussed in preceding sections) it also is possible for him to estimate crop yields. However, it first is necessary for him to "calibrate" various photographic images of crops in terms of crop yields. When such calibrations are being developed, the dimension of time must be taken into consideration, which again points to the desirability of obtaining sequential photographs on properly selected dates. For example, in previous aerial photo interpretation studies on yield of wheat our group found that fields which, three weeks before first heading, exhibit 80% severity of a disease known as "black stem rust", will produce a yield that is only 10% of normal, whereas fields which do not exhibit 80% severity until one week before first heading, will produce a yield that is 90% of normal.

Until such calibrations have been developed, crop-by-crop, meaningful estimates of yield cannot be made from aerial or space photography. Our limited work in this area, using both Apollo 9 and sequential high flight photography, suggests that a great deal of this type of research might profitably be conducted in the near future. We are further drawn to this conclusion upon noting the emphasis given by U. S. Department of Agriculture personnel to various "candidate problems" (as previously listed) every one of which stems from a concern about the yield reduction imposed

on some particular crop by some particular damaging agent.

Timber Stand Yields. Foresters measure potential yields by determining volumes of merchantable timber by species in each part of the forest. Until about 1940 such information was obtained entirely by on-the-ground measurements known as "timber cruises". Then it was found that a study of aerial photos would permit the forest to be stratified into nearly homogeneous units, thereby reducing by 90 percent or more the amount of ground measurement required. Consequently, most timber volume estimates of the past 2 or 3 decades, both in the United States and in most other parts of the world, have been made with the aid of aerial photos.

Photographs obtained on the Apollo 9 mission permitted foresters, for the first time, to make a realistic test of the extent to which space photography might still further facilitate the task of acquiring forest yield data (i.e., estimates of timber volume by species). Mention already has been made of the Apollo 9 case study performed by Langley et al. As indicated in that study and confirmed by our own photo interpretation tests of the Vicksburg, Mississippi area, space photography can be used to excellent advantage as the first element of a multistage sampling system. As previously indicated, even the crude stratification of timber stands that is done on space photography can improve sampling efficiency by approximately 60 percent when the objective is to determine potential yields of timber stands throughout the forest.

Forage and Browse Yields. "Animal-carrying capacity" is perhaps the most common measure of yield employed by those who manage rangelands and brushlands. Such capacity is commonly expressed in "animal months per unit area per year", thereby indicating the number of adult animals of a specified type which can profitably be grazed on a specified area. As with many of the other applications discussed in this paper, only very crude estimates of animal carrying capacity could be made from space photography of the Apollo 9 type unless some prior "calibration" had been made on representative space photographs. The closest approach to this task that has been performed to date will be found in the joint report of Poulton, Driscoll and Schrumpf, entitled, "Range Resources Inventory from Space and High Altitude Photography".

In most rangeland areas, whether forage is consumed in the green state or after it has dried, yield is directly proportional to the total amount of healthy vegetation that was present in the area at the peak of the growing season. In such areas, space photography may provide the means by which a very useful stratification of rangeland forage by yield categories can be made. This relationship may be less useful, of course, in areas where unpalatable or poisonous species comprise a variable and unknown proportion of the total vegetation.

D. Area Measurement

Agricultural Areas. The solution of this problem is greatly facilitated if the land has been surveyed into sections (640 acres), quarter sections (160 acres) and 40-acre blocks. In that event, the net acreage in each field usually can be obtained merely by deducting from gross acreage the land occupied by roads, canals and buildings. In areas of rolling to steep topography, fields may assume highly irregular shapes and may be intermingled with swamp-

lands, brushlands and timberlands. In such areas, methods described below may provide the most satisfactory solution.

Acreage Determination in Timber, Forage and Brushland Areas. A method commonly known as "dot apportioning" can be used in conjunction with aerial or space photos in areas where land use classes can be recognized on the photos but where the exact boundaries are difficult to discern, just as on many parts of the Apollo 9 photography. That method makes use of a dot grid that has been printed on a piece of transparent cellulose acetate. The acetate is placed over the photo (either randomly or systematically, depending on the sampling design). Then, for each dot a determination of the land use class (timber type, forage type, brush type, etc.) represented by the photo image directly beneath the dot is made and recorded. Once an adequate sampling for area has been obtained by this means, the acreage comprising the total area is apportioned to land use classes in accordance with dot counts.

Space photos are superior to aerial photos for making such determinations on sloping ground. Relief displacements, on vertical aerial photos, cause areas to appear too small if they slope away from the camera station and too large if they slope toward it. On vertical space photos, however, this problem usually can be ignored. Relief displacements are so minimal that any such photo can be treated as a map without danger of introducing significant errors in area determinations.

E. Determination of Total Yield

This determination is merely a mathematical problem once the space photos have provided information as previously discussed on vegetation type, crop yield and acreage. Hence, no further discussion of this item is deemed necessary in this paper.

II. Capabilities in Relation to Table 2.

Table 2 lists the major agencies desiring information of the types listed in Table 1. As explained in the report by Sattinger and Polcyn on "Peaceful Uses of Observation Satellites" (1966), each agency has its own preferences as to format in which the information should be presented. Most of them, however, merely are trying to get a true "picture" (to use their own words) of the resources they are seeking to manage. Alternately stated, they wish to know, in terms of the resources they seek to manage, "how much of what is where". Since we therefore are considering with reference to Table 2 merely different ways in which information might be presented to each user, no remote sensing breakthrough in this respect is required. Therefore, as we conclude our brief consideration of Table 2 and proceed to a consideration of Table 3, it is at least helpful to reflect on the remarkable extent to which an annotated enlargement of a space photograph of the Apollo 9 type might give each of these many users the desired resource "picture"--both literally and figuratively.

III. Capabilities in Relation to Table 3.

It is indicated in Table 3 that some types of information pertaining to the vegetation resource are desired at intervals as frequent as 10 to 20 minutes, at least during certain critical periods and in certain geographic areas. Also, the table indicates that for most of the benefit to be realized, such information must be extracted and disseminated to those seeking it within 5 to 10 minutes (i.e., within about one "half-life" after data acquisition).

While the results of our Apollo 9 test may justify optimism in satisfying some informational requirements, there are several reasons why such optimism does not appear to be justified with respect to these particular emergency or "early warning" types of requirements:

(1) Since a single satellite orbiting the earth at an altitude of a few hundred miles is within data-collecting range of a given area only for about 3 minutes every 3 or 4 days, a prohibitively large number of these vehicles, operating in tandem, obviously would be required in order to provide the frequency of surveillance desired.

(2) Presumably it is as important to be able to acquire this kind of information at night as in the daytime, and no night-time photographic capability from space is currently envisaged.

(3) Even if a vehicle were over the proper area at the proper time of day, the chances are extremely poor in many areas that conditions would be sufficiently cloud-free to permit reconnaissance by means of photography. (One recent study, for example, indicated that during the crop-growing season only one pass out of 28 would be cloud-free for a 1000-square mile agricultural area in Indiana).

(4) Automatic data processing techniques probably would be required in order to process the acquired data quickly enough to permit timely delivery of the desired information to the user.

Fortunately, most of the information desired relative to vegetation resources is not needed so frequently nor so promptly as that just discussed. While weather will constitute a serious deterrent in many areas, we find that the further we proceed down the lists in Table 3 the less troublesome that factor becomes (since we have more opportunities for cloud-free weather while in orbit over the area of interest).

CONCLUSIONS

From our studies of the Apollo 9 photography, and of the supporting high flight photography that was obtained both at the same time and on subsequent dates at roughly one-month intervals, we conclude the following:

1. Although the nominal resolution of the Apollo 9 photography is only about 300 to 400 feet, based on low contrast targets, (see Table 4) some features such as roads and canals having a least dimension of only 20

to 30 feet are clearly discernible.

2. The nominal resolution of the supporting high flight photography is approximately one order of magnitude better than that obtained on the Apollo 9 mission.

3. The accurate discrimination of some important earth resource features (e.g., timbered vs. agricultural lands; vegetated vs. fallow fields) is possible even on individual black-and-white space photos.

4. A great many more earth resource features are identifiable on Infrared Ektachrome space photos (e.g., bottomland hardwood stands, pine- hardwood stands, and certain individual crop types).

5. The interpretability of some of these features is still further increased through the use of optical or electronic equipment to form color composite images from two or more wavelength bands of black-and-white photography.

6. High flight photography, despite its much higher spatial resolution, and even though taken with the same film-filter combinations as were used on the Apollo 9 mission, provided very little improvement in the interpretability of specific earth resource features that were subjected to quantitative evaluation tests as described below:

7. Detailed studies were made in several geographic areas in order to arrive at a quantitative determination of the interpretability of the Apollo 9 photographs and of the associated high flight photography. In these tests the photography was studied both in its original state, either as opaque prints or as positive transparencies, and after being electronically or optically enhanced by various means. One set of studies dealt with agricultural crops near Phoenix, Arizona and also in the Imperial Valley of California. These quantitative studies led us to the following conclusions:

a. When the only photography made available to the photo interpreters is that which was taken by the Apollo 9 astronauts (in March, 1969--a less-than-optimum time of year for this purpose) the accuracy with which they are able to identify crop types and field conditions rarely exceeds 60%. Those who wish to use this kind of agricultural information ordinarily require a much higher order of accuracy, e.g., 90 to 95 percent.

b. If, in addition, the photo interpreters are given access to the high flight photography that was taken on the same date but at much higher spatial resolution, the quantitative data show that, for the particular earth resource features being investigated, there was no statistically significant improvement in image interpretability. Given sequential high flight photography taken at later dates, however, the accuracy was substantially improved.

c. On both the space photography and the high flight photography, Infrared Ektachrome was significantly more interpretable than any of the matching frames of multiband black-and-white photography.

d. When the matching frames of black-and-white photography were com-

bined and enhanced either optically or electronically, interpretability was improved to where the information derivable was roughly equivalent to (but only rarely better than) that obtained from the Infrared Ektachrome photography. It is to be emphasized, however, that our studies to date on this particular project have not permitted us to adequately investigate the full possibilities of multiband image enhancement. Primarily because of time limitations, the enhancements that we have studied thus far are those which were made with a view to improving the overall interpretability of the multiband black-and-white photography, as indeed they did. The next step will be that of using optical and electronic image enhancements of this multiband black-and-white photography to make an entire series of color enhancements, one of which is designed to distinguish one earth resource feature from everything else, a second enhancement to distinguish a second earth resource feature from everything else, etc. Some of our earlier studies, although dealing only with aerial photography, have shown that through the making of such a series of enhancements, results superior to those provided by Infrared Ektachrome photography are quite commonly obtained.

e. In any operational system designed to exploit the broad synoptic view of space photography, it would be highly desirable to achieve high spatial resolution on the entire frame instead of merely on small sections of it as in this report. Before this could be done, however, an optical combiner providing far better means for effecting registration than the one available to us would need to be developed; and for electronic combiners the additional need would exist for increasing the number of scan lines on the raster.

8. A system such as the ones which we and our associates have developed for classifying range resources, timber stands and other land use classes on space photography can greatly improve the efficiency of a multistage sampling system that is based on space photography, aerial photography and field observation. In the Vicksburg, Mississippi area, for example, quantitative tests showed that photo interpreters could achieve an accuracy of 80 to 90 percent in making such stratifications from Apollo 9 photography.

9. The various kinds of earth resource data dealt with in this report correspond quite closely to the informational requirements of those who seek to manage earth resources. Hence our findings would appear to be not only of scientific interest, but also of great potential practical importance.

10. While, on the one hand, there are strong proponents for using aircraft rather than spacecraft for the making of earth resource surveys and, on the other hand, those who advocate using spacecraft rather than aircraft, our findings are for the most part in support of a third view, viz., that operational earth resource surveys of the future might best be made by means of a multistage sampling technique which employs spacecraft, aircraft and ground observations.

11. Because of the importance of obtaining sequential photographic coverage to aid in the inventorying of earth resources from aerial and space photography, and because cloud cover makes very difficult the obtaining of sequential coverage in many geographic areas of interest, we must reiterate one important conclusion of our earlier reports: Cloud cover is likely to be the most serious deterrent to the making of operational resource surveys on photography taken from either aircraft or spacecraft.

From our studies of image examples other than those directly tied to the Apollo 9 mission but included in this paper, we conclude the following:

1. Without question there are instances in which vegetation types and early evidence of vigor loss might be detected better by means of black-and-white photography taken from aircraft or spacecraft with the proper film-filter combination than by direct on-the-ground observation (see, for example, Fig. 1).

2. When the visible spectrum is recorded on a color film containing three dyes, some features become discernible that could not have been discerned by recording the same wavelengths on a single panchromatic frame (see, for example, the top half of Fig. 2).

3. When both Ektachrome and IR Ektachrome photos are taken of a vegetated area, more species may be identified than if only one photo or the other were available (see, for example the bottom half of Fig. 2).

4. When both a K-band radar image and a conventional photograph are available of the same vegetated area, more information can be derived than if only one image or the other were available (see Fig. 7).

5. Thermal images, like conventional photographs, yield more information when multiband sequential records are obtained than when the imagery is obtained in only one band or on only one date.

In concluding this paper I will make a final reference to the analogy that was used in beginning it. We must recognize that it is not all bad that the enthusiastic small boy with the hammer seems to think that everything needs pounding; nor it it all bad that some enthusiastic users of remote sensing tools seem to think that everything needs sensing. In both instances, experience is the best teacher and disciplinarian, and enthusiasm on the part of the user is one of the most treasured qualities to be preserved. We still have much to learn about how to use these powerful new tools of the remote sensing trade, yet many a taxpayer and his congressman are hoping for operational benefits soon after launch of the first Earth Resources Technology Satellite. Here's hoping that we can continue to conduct the research and gain the experience that will make us the equivalent of master carpenters when ERTS-A flies.

LITERATURE REFERENCES

Alexander, R. H. 1964. Geographical data from space. The Professional Geographer 16(6):1-5.

American Society of Photogrammetry. 1960. Manual of Photographic Interpretation. George Banta Co. Menasha, Wisconsin 868 p.

Badgley, P. C. 1966. Orbital remote sensing and natural resources. Photogrammetric Engineering 32(5):780-790.

Badgley, P. C. and L. F. Childs. 1967. Earth resources survey from space. Presented at the Ocean From Space Symposium of American Society of Oceanography.

Carneggie, D. M., W. C. Draeger and D. T. Lauer. 1966. The use of high altitude color and spectrozonal imagery for the inventory of wildland resources, Vol. I of III: The Timber Resource. Annual Progress Report to NASA by Forestry Remote Sensing Laboratory, University of California, Berkeley. 41 p. Illus.

Colwell, R. N. 1966. Uses and limitations of multispectral remote sensing. Proceedings of Fourth Symposium on Remote Sensing. University of Michigan 71-100 p.

Colwell, R. N. 1969. An evaluation of earth resources using Apollo 9 photography. Final Report for NASA Earth Resources Survey Program by Forestry Remote Sensing Laboratory, University of California, Berkeley. Two volumes, illustrated.

Ellermeier, R. D. and D. S. Simonett. 1965. Imaging radars on spacecraft as a tool for studying the earth. International Symposium on Electromagnetic Sensing of the Earth from Satellites. Miami Beach, Florida. Nov. 22-24.

Fischer, W. A. 1966. Orbital surveys of the earth. Proceedings of Symposium on Peaceful Uses of Space. Stanford, California. Unpubl.

Fischer, W. A. and C. J. Robinove. 1968. A rationale for a general purpose earth resources observation satellite. In Proceedings of University of Washington Remote Sensing Symposium. Feb. 15-16.

Gawarecki, S. J., R. J. P. Lyon and W. Nordberg. 1965. Infrared spectral returns and imagery of the earth from space and their application to geologic problems. American Astronautical Society Vol. 4:13-33.

Heller, R. C., J. L. Bean and J. W. Marsh. 1952. Aerial survey of spruce budworm damage in Maine in 1950. Journal of Forestry Vol. 50(1):8-11.

Hoffer, R. M. 1967. Interpretation of remote multispectral imagery of agricultural crops. Purdue University, Agricultural Research Bulletin No. 831-33 p.

Holter, M. R. 1967. Infrared and multispectral sensing. Bioscience, 17(6):376-383.

Katz, A. H. 1960. Observation satellites: problems and prospects. Astronautics, Vol. 2.

Katz, A. H. 1967. Reflections on satellites for earth resource surveys. Rand Corporation P-3753 28 p.

Langley, P. G. 1965. Automating aerial photo interpretation in forestry--how it works and what it will do for you. Proceedings, Society of American Foresters. 172-177 p.

Lauer, D. T. 1967. The feasibility of identifying forest species and delineating major timber types in California by means of high-altitude multispectral imagery. Annual Progress Report to NASA on Remote Sensing Applications in Forestry. 95 p.

Lent, J. D. 1966. Cloud cover interference with remote sensing of forested areas from earth-orbital and lower altitudes. Report to NASA on Remote Sensing Applications in Forestry by Forestry Remote Sensing Laboratory, University of California, Berkeley. 55p.

Lowe, D. S., J. Braithwaite and V. L. Larrowe. 1966. An investigative study of a spectrum-matching system. Final Report under NASA Contract 8-21000. 105 p.

Lowman, P. D., Jr. and Te Lou Chang. 1964. Hyperaltitude photography and its applications. Proceedings of Symposium on Remote Sensing of Environment, University of Michigan. 153-169 p.

Lyons, E. H. 1967. Forest sampling with 70mm fixed air-base photography from helicopters. Photogrammetria 22(6):213-231. September.

Meyers, V. I., C. L. Wiegand, M. D. Heilman and J. R. Thomas. 1966. Remote sensing in soil and water conservation research. Proceedings, 4th Symposium on Remote Sensing of Environment, University of Michigan.

Moore, R. K. 1966. Radar as a remote sensor. CRES Report No. 61-7. Center for Research in Engineering Science, University of Kansas, Lawrence.

Olson, C. E., Jr. 1960. Elements of photographic interpretation common to several sensors. Photogrammetric Engineering 26(3):630-637.

Pecora, W. T. 1967. Surveying the earth's resources from space. Proceedings of 27th Annual Meeting, Congress on Surveying and Mapping.

Pettinger, L. R. 1969. Multiple resource inventory on space and high altitude photography. In Proceedings of 2nd Aircraft Symposium, NASA, MSC, Houston, Texas. In press. 18 p. Illus.

Risley,E. M. 1967. Satellites for earth survey. Earth Sciences Newsletter No. 2.

Robinove, C. J. 1966. A preliminary evaluation of airborne and spaceborne remote sensing data for hydrologic uses. U.S.G.S. Technical Letter NASA-50.

Sattinger, I. J. and F. C. Polcyn. 1966. Peaceful uses of earth-observation spacecraft. Vol. II. Survey of Applications and Benefits. Report No. 7219-1-F(II):159 p. Institute of Science and Technology, University of Michigan.

Simonett, D. S. and S. A. Morain. 1965. Remote sensing from spacecraft as a tool for investigating arctic environments. CRES, University of Kansas. Report No. 61-5.

Wear, J. F. 1966. The development of spectro-signature indicators of root disease on large forest areas. Pacific Southwest Forest & Range Experiment Station Annual Report to NASA. 30 Sept.

Wilson, R. C. 1967. Space photography for forestry. Photogrammetric Engineering 23(5):483-490.

Yost, E. F. and S. Wenderoth. 1967. Multispectral color aerial photography. Photogrammetric Engineering 33(9):1020-1033.

USER REQUIREMENTS FOR VEGETATION RESOURCE DATA

Table 1: Type of Information Desired

For Agricultural Crops	*For Timber Stands*	*For Rangeland Forage*	*For Brushland Vegetation (mainly shrubs)*
Crop Type (Species & variety)	Timber Type (Species composition)	Forage Type (Species composition)	Vegetation Type (Species composition)
Present crop vigor and state of maturity	Present tree and stand vigor by species and size class	Present "Range Readiness" (for grazing by domestic or wild animals)	Vegetation density
Prevalence of crop-damaging agents by type	Prevalence of tree-damaging agents by type	Prevalence of forage-damaging agents (weeds, rodents, diseases, etc.) by type	Other types of information desired will depend upon primary importance of the vegetation (whether for watershed protection, game habitat, aesthetics, etc.)
Prediction of time of maturity and eventual crop yield per acre by crop type and vigor class	Present volume and prediction of probable future volume per acre by species and size *class in each stand*	Present animal-carrying capacity and probable future capacity per acre by species and range con*dition class in each for*age type	
Total acreage within each crop type and vigor class	Total acreage within each stand type and vigor class	Total acreage within each forage type and condition class	Same as above
Total present yield by crop type	Total present and probable future yield by species and size class	Total present and probable future animal carrying capacity	Same as above

USER REQUIREMENTS FOR VEGETATION RESOURCE DATA

Table 2: Agencies and Groups Desiring the Information

Agricultural Crops	Timber Stands	Rangeland Forage	Brushland Vegetation
Federal Agencies:Agricultural Stabilization and Conservation Service; Cropland Conservation Program; Conservation Reserve Program; Agr. Conservation Program; Emergency Conservation Measures Program;Commodity Credit Corp.;Agri. Marketing Service;Statistical Reporting Service;Economic Research Service; Soil Conservation Service;Federal Crop Insurance Corp.;Farmers Home Adm.; Rural Community Development Service;Foreign Agri.Service; Famine Relief Program;Foreign Economic Assistance Program Dept.of Commerce Agri. Census Program.	Federal Agencies: U. S. Forest Service Bureau of Land Mgt. plus many federal agencies listed in column 1	Federal Agencies: U.S.Forest Service Bureau of Land Mgt plus many federal agencies listed in column 1	Federal Agencies: Primarily U.S.Forest and Bureau of Land Mgt.
State and County Agencies Agri. Extension Service State Tax Authority	State and County Agencies: Division of Forestry; Forest Extension Service;State Tax Authority	State and County Agencies: Livestock Reporting Service; Range Extension Service; State Tax Authority	State and County Agencies: Division of Forestry; Division of Beaches and Parks ; Water Resource Agency; State Tax Authority
Private Agencies: Producers of Fertilizers and Pesticides; Crop harvesting Industry; Food Processing and Packing Industry; Transportation Industry; Food and Fiber Advertising and Marketing Industry	Private Agencies: Producers of Fertilizers and Pesticides; Logging Industry Wood Processing Industry; Transportation Industry;Wood & Wood Products Advertising and Marketing Industry.	Private Agencies: Producers of Fertilizers and Pesticides; Meat Packing Industry; Tanning Industry; Transportation Industry;	Private Agencies: Hunting and Fishing Clubs Public Utilities Commissions; Local Irrigation Dist.

USER REQUIREMENTS FOR VEGETATION RESOURCE DATA

Table 3 : Frequency With Which the Information is Needed (Examples Only)
To Convert This Table to "Rapidity With Which Informationis Needed", Use "Half-Life" Concept (See Text)

For Agricultural Crops	For Timber Stands	For Rangeland Forage	For Other Vegetation (mainly shrubs)
10-20 minutes - Observe the advancing waterline in croplands during disastrous floods. Observe the start of locust flights in agricultural areas	10-20 minutes - Detect the start of forest fires during periods when there is a high "Fire Danger Rating"	10-20 minutes - Detect the start of rangeland fires during periods when there is a high "Fire Danger Rating"	10-20 minutes - Detect the start of brushfield fires during periods when there is a high "Fire Danger Rating"
10-20 hours - Map perimeter of on-going floods and locust flight. Monitor the Wheat Belt for outbreaks of Black Stem Rust due to spore showers	10-20 hours - Map perimeter of on-going forest fires	10-20 hours - Map perimeter of on-going rangeland fires	10-20 hours - Map perimeter of on-going brushfield fires
10-20 days - Map progress of crops as an aid to crop identification using "crop calendars" and to estimating date to begin harvesting operations	10-20 days - Detect start of insect outbreaks in timber stands	10-20 days - Update information on "Range Readiness" for grazing	10-20 days - Update information on times of flowering and pollen production in relation to the bee industry and to hay fever problems
10-20 months - Facilitate annual inspection of crop rotation and of compliance with federal requirements for benefit payments	10-20 months - Facilitate annual inspection of fire-breaks	10-20 months - Facilitate annual inspection of fire-breaks	10-20 months - Facilitate inspection of fire-breaks
10-20 years - Observe growth and mortality rates in orchards	10-20 years - Observe growth and mortality rates in timber stands	10-20 years - Observe signs of range deterioration and study the spread of noxious weeds	10-20 years - Observe changes in "Edge Effect" of brushfields that affect suitability as wildlife habitat
20-100 years - Observe shifting cultivation patterns	20-100 years Observe plant succession trends in the forest	20-100 years - Observe plant succession trends on rangelands	20-100 years - Observe plant succession trends in brushfields

Table 4a.

Focal Settings and Camera Resolution Characteristics of the S065 System

Camera Designation	Film-Filter Combination Used	Focal Setting	AWAR*	GRD**
AA	IR Ektachrome, Wratten 15	50 ft.	33.4	470'
BB	Panatomic X, Wratten 58	Infinity	59.2	280'
CC	Infrared B&W, Wratten 89B	33 ft.	32.2	470'
DD	Panatomic X, Wratten 25A	Infinity	43.1	370'

*AWAR is the abbreviation for "area weighted average resolution" and in this instance applies to a high contrast target. It is expressed in this table in line pairs per millimeter for each camera and for the focal setting at which that camera was operated on the Apollo 9 mission.

**GRD is the abbreviation for "ground resolved distance" and in this instance applies to a low contrast target. Figures given are for distance on the ground, in feet, encompassed by one line pair. For linear features of moderately high contrast the effective GRD values may be better than the nominal GRD values listed here by a factor of 10 or more. For example, one lane roads extending across the desert are frequently discernible on the Apollo 9 S065 photography, even though the width of the entire roadway clearing is no greater than 20 to 30 feet. These GRD values assume a flight altitude of 200 kilometers (108 nautical miles).

Table 4a. Information relative to the spatial resolution capabilities of lenses used on Apollo 9 in the 4-camera S065 experiment. For a discussion of the significance of these values in relation to the findings of our report, see text. The above AWAR values were taken from University of Arizona, Optical Sciences Center, Technical Memorandum No. 1 by P. B. Keenan and P. N. Slater, entitled "Preliminary Postflight Calibration Report on Apollo 9 Multiband Photography Experiment S065", September, 1969. The above GRD values will appear in a final report of the same title by Keenan and Slater and are included here by permission of the authors.

	IMAGERY*	25A			58			89B			PF			FRSL			CIR			IDECS			CIR, COLOR & IDECS			COLOR		
CATEGORY	SKILL	PC	AC	%C	PC	AC	%C	PC	AC	%C	PC	AC	%C	PC	AC	%C	PC	AC	%C	PC	AC	%C	PC	AC	%C	PC	AC	%C
BARE SOIL	HIGH	22	10	45	22	18	82	22	12	56	22	16	73	22	11	50	22	14	64	22	17	77	22	15	68	22	10	45
	MEDIUM	22	17	77	22	16	73	22	11	50	22	15	68	22	10	45	22	13	60	22	13	59	22	12	55	22	11	50
	LOW	22	10	45	22	13	59	22	13	59	22	18	82	22	11	50	22	13	60	22	8	36	22	10	45	22	12	55
CROPLAND	HIGH	80	77	96	80	52	65	80	78	98	80	63	79	80	79	99	80	80	100	80	71	89	80	79	99	80	78	98
	MEDIUM	80	77	96	80	15	19	80	80	100	80	11	14	80	75	94	80	78	98	80	71	89	80	72	90	80	75	94
	LOW	80	64	80	80	58	73	80	79	99	80	48	60	80	80	100	80	70	88	80	71	89	80	71	89	80	62	78
ALFALFA	HIGH	34	3	9	34	7	21	34	25	74	34	5	15	34	33	97	34	7	21	34	5	15	34	2	6	34	28	82
	MEDIUM	34	17	50	34	15	44	34	7	21	34	10	29	34	22	65	34	10	29	34	7	21	34	1	3	34	3	9
	LOW	34	10	29	34	12	35	34	10	29	34	13	38	34	10	29	34	7	21	34	12	35	34	4	12	34	11	32
BARLEY	HIGH	30	26	87	30	25	83	30	19	63	30	21	70	30	5	17	30	22	73	30	19	63	30	19	63	30	21	70
	MEDIUM	30	8	27	30	11	37	30	15	50	30	11	37	30	19	63	30	22	73	30	12	40	30	11	37	30	19	63
	LOW	30	7	23	30	21	70	30	12	40	30	24	80	30	13	43	30	6	20	30	17	57	30	14	47	30	20	67
BARE SOIL VS CROPLAND	HIGH	102	92	90	102	59	58	102	92	90	102	95	93	102	91	89	102	93	91	102	93	91	102	95	93	102	89	87
	MEDIUM	102	89	87	102	87	85	102	46	45	102	86	84	102	91	89	102	94	92	102	90	88	102	92	90	102	89	87
	LOW	102	86	84	102	70	69	102	80	78	102	91	89	102	87	85	102	86	84	102	65	64	102	90	88	102	81	79

*For key to the 9 types of imagery, see text.

PC = Total possible correct responses
AC = Actual number of correct responses by interpreters on this test
%C = Percent correct responses on this test

H = Highly skilled interpreter
M = Medium level interpreter
L = Unskilled interpreter

Table 4 AVERAGE "CORRECT IDENTIFICATIONS" ON APOLLO 9 PHOTOGRAPHY OF THE IMPERIAL VALLEY TEST SITE AS MADE BY 45 PHOTO INTERPRETERS

	IMAGERY*	25A			58			89B			PF			FRSL			CIR			IDECS			CIR, COLOR & IDECS			COLOR		
CATEGORY	SKILL	PE	AE	%E	PE	AE	%E	PE	AE	%E	PE	AE	%E	PE	AE	%E	PE	AE	%E	PE	AE	%E	PE	AE	%E	PE	AE	%E
BARE SOIL	HIGH	80	2	2	80	5	6	80	0	0	80	12	15	80	3	3	80	1	1	80	3	3	80	2	2	80	2	2
	MEDIUM	80	8	10	80	23	28	80	1	1	80	18	22	80	1	1	80	1	1	80	2	2	80	2	2	80	1	1
	LOW	80	3	3	80	18	22	80	0	0	80	7	8	80	2	2	80	0	0	80	2	2	80	2	2	80	4	5
CROPLAND	HIGH	22	7	31	22	6	27	22	12	54	22	7	31	22	8	36	22	9	40	22	4	18	22	7	31	22	11	50
	MEDIUM	22	7	31	22	15	68	22	9	40	22	8	36	22	9	40	22	8	36	22	9	40	22	8	36	22	8	36
	LOW	22	1	4	22	6	27	22	8	36	22	4	18	22	8	36	22	7	31	22	4	18	22	6	27	22	8	36
ALFALFA	HIGH	68	16	23	68	8	11	68	46	67	68	6	8	68	52	76	68	9	13	68	16	23	68	7	10	68	30	44
	MEDIUM	68	17	25	68	19	27	68	16	23	68	11	16	68	21	30	68	18	26	68	5	7	68	9	13	68	12	17
	LOW	68	25	36	68	21	30	68	16	23	68	28	41	68	18	26	68	21	30	68	25	36	68	8	11	68	13	19
BARLEY	HIGH	72	35	48	72	31	43	72	12	16	72	23	31	72	10	13	72	5	6	72	12	16	72	10	13	72	23	31
	MEDIUM	72	22	30	72	11	15	72	20	27	72	17	23	72	31	43	72	9	12	72	9	12	72	17	23	72	13	18
	LOW	72	13	18	72	31	43	72	12	16	72	31	43	72	12	16	72	6	8	72	18	25	72	6	8	72	19	26
BARE SOIL VS CROPLAND	HIGH	102	10	10	102	43	42	102	10	10	102	7	7	102	11	11	102	9	9	102	9	9	102	7	7	102	13	13
	MEDIUM	102	13	13	102	15	15	102	56	55	102	16	16	102	11	11	102	8	8	102	12	12	102	10	10	102	13	13
	LOW	102	16	16	102	32	31	102	22	22	102	11	11	102	15	15	102	16	16	102	37	36	102	12	12	102	21	21

*For key to the 9 types of imagery see text.

PE = Total possible commission errors on this test
AE = Actual number of commission errors made by the interpreters on this test
%E = Percent commission error on this test

H = Highly skilled interpreter
M = Medium level interpreter
L = Unskilled interpreter

Table 5 AVERAGE "COMMISSION ERRORS" MADE BY 45 PHOTO INTERPRETERS ON APOLLO 9 PHOTOGRAPHY OF THE IMPERIAL VALLEY TEST SITE.

	IMAGERY*	25A			58			89B			PF			FRSL			CIR			IDECS			CIR, COLOR &IDECS			COLOR		
CATEGORY	SKILL	Pt	At	%t	Pt	At	%t	Pt	At	%t	Pt	At	%t	Pt	At	%t	Pt	At	%t	Pt	At	%t	Pt	At	%t	Pt	At	%t
BARE SOIL	HIGH	50	6	12	50	4	8	50	6	12	50	6	12	50	11	22	50	3	6	50	8	16	50	3	6	50	11	22
	MEDIUM	50	6	12	50	7	14	50	4	8	50	8	16	50	5	10	50	4	8	50	2	4	50	4	8	50	8	16
	LOW	50	8	16	50	9	18	50	2	4	50	4	8	50	4	8	50	6	12	50	2	4	50	5	10	50	4	8
CROPLAND	HIGH	50	7	14	50	10	20	50	5	10	50	11	22	50	11	22	50	3	6	50	9	18	50	3	6	50	6	12
	MEDIUM	50	12	24	50	5	10	50	15	30	50	5	10	50	8	16	50	20	40	50	3	6	50	7	14	50	8	16
	LOW	50	11	22	50	8	16	50	10	20	50	13	26	50	8	16	50	7	14	50	7	14	50	13	26	50	8	16
ALFALFA	HIGH	50	3	6	50	10	20	50	5	10	50	19	38	50	9	18	50	9	18	50	10	20	50	6	12	50	3	6
	MEDIUM	50	4	8	50	7	14	50	10	20	50	5	10	50	15	30	50	15	30	50	9	18	50	15	30	50	5	10
	LOW	50	21	42	50	8	16	50	6	12	50	20	40	50	11	22	50	13	26	50	10	20	50	9	18	50	3	6
BARLEY	HIGH	50	13	26	50	11	22	50	5	10	50	11	22	50	8	16	50	4	8	50	2	4	50	3	6	50	10	20
	MEDIUM	50	6	12	50	7	14	50	7	14	50	5	10	50	4	8	50	35	70	50	5	10	50	4	8	50	7	14
	LOW	50	8	16	50	10	20	50	12	24	50	35	70	50	7	14	50	17	34	50	8	16	50	6	12	50	10	20
BARE SOIL VS CROPLAND	HIGH	50	11	22	50	8	16	50	9	18	50	7	14	50	7	14	50	3	6	50	5	10	50	2	4	50	4	8
	MEDIUM	50	11	22	50	10	20	50	21	42	50	9	18	50	4	8	50	3	6	50	5	10	50	2	4	50	11	22
	LOW	50	11	22	50	13	26	50	11	22	50	15	30	50	7	14	50	13	26	50	8	16	50	6	12	50	12	24

*For key to the 9 types of imagery, see text.

Pt = 50 minutes time limit to complete test
At = Actual time required to complete test
%t = Percent time on this test

H = Highly skilled interpreter
M = Medium level interpreter
L = Unskilled interpreter

Table 6 AVERAGE "TIME REQUIREMENTS" FOR THE INTERPRETATION OF APOLLO 9 PHOTOGRAPHY OF THE IMPERIAL VALLEY TEST SITE BASED ON THE WORK OF 45 PHOTO INTERPRETERS

	IMAGERY*	25A			58			89B			PF			FRSL			CIR			IDECS			CIR, COLOR & IDECS		
CATEGORY	SKILL	PC	AC	%C	PC	AC	%C	PC	AC	%C	PC	AC	%C	PC	AC	%C	PC	AC	%C	PC	AC	%C	PC	AC	%C
BARE SOIL	HIGH	22	15	68	22	18	81	22	12	55	22	6	27	22	15	68	22	14	64	22	14	64	22	14	64
	MEDIUM	22	19	86	22	21	95	22	12	55	22	5	23	22	15	68	22	13	59	22	12	55	22	13	59
	LOW	22	13	59	22	12	55	22	13	59	22	10	45	22	11	50	22	12	55	22	13	59	22	13	59
CROPLAND	HIGH	80	79	99	80	79	99	80	68	85	80	73	91	80	67	84	80	77	96	80	79	99	80	79	99
	MEDIUM	80	72	90	80	61	76	80	62	78	80	59	74	80	78	98	80	72	90	80	79	99	80	73	91
	LOW	80	53	66	80	79	99	80	55	69	80	59	74	80	77	96	80	78	98	80	71	89	80	77	96
ALFALFA	HIGH	34	16	47	34	32	94	34	11	32	34	17	50	34	4	12	34	23	68	34	19	56	34	3	9
	MEDIUM	34	6	18	34	10	29	34	24	71	34	10	29	34	7	21	34	8	24	34	12	35	34	3	9
	LOW	34	3	9	34	4	12	34	5	15	34	6	18	34	3	9	34	5	15	34	2	6	34	7	21
BARLEY	HIGH	30	16	53	30	19	63	30	18	60	30	14	47	30	23	77	30	12	40	30	24	80	30	20	67
	MEDIUM	30	17	57	30	16	53	30	10	33	30	5	17	30	28	93	30	18	60	30	23	77	30	18	60
	LOW	30	13	43	30	7	23	30	10	33	30	14	14	30	13	43	30	7	23	30	22	73	30	14	47
BARE SOIL VS CROPLAND	HIGH	102	95	93	102	100	98	102	81	79	102	85	83	102	97	95	102	96	94	102	18	18	102	94	92
	MEDIUM	102	95	93	102	91	89	102	89	87	102	78	76	102	88	86	102	94	92	102	89	87	102	94	92
	LOW	102	95	93	102	86	84	102	75	74	102	76	75	102	94	92	102	93	91	102	89	87	102	99	97

*For key to the 9 types of imagery, see text.

H = Highly skilled interpreter
M = Medium level interpreter
L = Unskilled interpreter
PC = Total possible correct responses
AC = Actual number of correct responses by interpreters on this test
%C = Percent correct responses on this test

Table 7. AVERAGE "CORRECT IDENTIFICATIONS" ON MARCH, 1969 HIGH FLIGHT PHOTOGRAPHY OF THE IMPERIAL VALLEY TEST SITE AS MADE BY 45 PHOTO INTERPRETERS

	IMAGERY*	25A			58			89B			PF			FRSL			CIR			IDECS			CIR, COLOR & IDECS		
CATEGORY	SKILL	PE	AE	%E	PE	AE	%E	PE	AE	%E	PE	AE	%E	PE	AE	%E	PE	AE	%E	PE	AE	%E	PE	AE	%E
BARE SOIL	HIGH	80	2	3	80	26	33	80	8	10	80	5	6	80	0	0	80	0	0	80	2	3	80	0	0
	MEDIUM	80	2	3	80	8	10	80	8	10	80	6	8	80	0	0	80	1	1	80	0	0	80	5	6
	LOW	80	1	1	80	10	13	80	5	6	80	10	10	80	0	0	80	4	5	80	1	1	80	3	4
CROPLAND	HIGH	22	8	36	22	10	45	22	8	36	22	8	36	22	7	32	22	8	36	22	3	14	22	7	32
	MEDIUM	22	1	5	22	5	23	22	7	32	22	6	27	22	6	27	22	3	14	22	10	45	22	2	9
	LOW	22	22	100	22	7	32	22	8	36	22	1	5	22	4	18	22	7	32	22	12	55	22	4	18
ALFALFA	HIGH	68	23	34	68	57	84	68	15	22	68	20	29	68	12	18	68	32	47	68	9	13	68	6	9
	MEDIUM	68	12	18	68	24	35	68	13	19	68	13	19	68	13	19	68	9	13	68	15	22	68	7	10
	LOW	68	17	25	68	10	15	68	24	35	68	16	24	68	13	19	68	11	16	68	5	7	68	5	7
BARLEY	HIGH	72	15	21	72	29	40	72	36	50	72	29	40	72	22	31	72	13	18	72	18	25	72	12	17
	MEDIUM	72	20	28	72	18	25	72	15	21	72	12	17	72	27	38	72	10	14	72	20	28	72	10	14
	LOW	72	20	28	72	24	38	72	3	4	72	24	38	72	18	25	72	3	4	72	16	22	72	4	6
BARE SOIL VS CROPLAND	HIGH	102	7	7	102	2	2	102	21	21	102	17	17	102	5	5	102	6	6	102	1	1	102	8	8
	MEDIUM	102	7	7	102	11	11	102	13	13	102	24	24	102	14	14	102	8	8	102	13	13	102	8	8
	LOW	102	7	7	102	16	16	102	27	26	102	26	25	102	8	8	102	9	9	102	13	13	102	43	3

*For key to the 9 types of imagery, see text.

PE = Total possible commission errors on this test
AE = Actual number of commission errors made by the interpreter on this test
%E = Percent commission error on this test

H = Highly skilled interpreter
M = Medium level interpreter
L = Unskilled interpreter

Table 8 AVERAGE "COMMISSION ERRORS" MADE BY 45 PHOTO INTERPRETERS ON MARCH, 1969 HIGH-FLIGHT PHOTOGRAPHY OF THE IMPERIAL VALLEY TEST SITE

	IMAGERY*	25A			58			89B			PF			FRSL			CIR			IDECS			CIR, COLOR & IDECS		
CATEGORY	SKILL	Pt	At	%t	Pt	At	%t	Pt	At	%t	Pt	At	%t	Pt	At	%t	Pt	At	%t	Pt	At	%t	Pt	At	%t
BARE SOIL	HIGH	50	4	8	50	9	18	50	8	16	50	6	12	50	2	4	50	7	14	50	4	8	50	6	12
	MEDIUM	50	10	20	50	8	16	50	7	14	50	9	18	50	3	6	50	4	8	50	6	12	50	4	8
	LOW	50	10	20	50	7	14	50	9	18	50	8	16	50	4	8	50	3	6	50	4	8	50	10	20
CROPLAND	HIGH	50	6	12	50	8	16	50	17	34	50	2	4	50	13	26	50	4	8	50	5	10	50	7	14
	MEDIUM	50	15	30	50	12	24	50	12	24	50	4	8	50	7	14	50	7	14	50	3	6	50	9	18
	LOW	50	8	16	50	11	22	50	12	24	50	10	20	50	6	12	50	7	14	50	5	10	50	9	18
ALFALFA	HIGH	50	12	24	50	12	24	50	8	16	50	7	14	50	5	10	50	10	20	50	4	8	50	8	16
	MEDIUM	50	15	30	50	8	16	50	12	24	50	7	14	50	4	8	50	10	20	50	22	44	50	9	18
	LOW	50	2	4	50	12	24	50	17	34	50	15	30	50	8	16	50	3	6	50	10	20	50	10	20
BARLEY	HIGH	50	13	26	50	4	8	50	15	30	50	14	28	50	5	10	50	4	8	50	6	12	50	14	28
	MEDIUM	50	11	22	50	8	16	50	5	10	50	8	16	50	3	6	50	6	12	50	13	26	50	10	20
	LOW	50	7	14	50	3	6	50	5	10	50	15	30	50	8	16	50	3	6	50	11	22	50	8	16
BARE SOIL VS CROPLAND	HIGH	50	9	18	50	4	8	50	12	24	50	13	26	50	3	6	50	7	14	50	5	10	50	7	14
	MEDIUM	50	17	34	50	8	16	50	10	20	50	16	32	50	5	10	50	6	12	50	6	12	50	9	18
	LOW	50	12	24	50	9	18	50	9	18	50	10	20	50	6	12	50	5	10	50	6	12	50	12	24

*For key to the 9 types of imagery, see text.

Pt = 50 minutes time limit to complete test
At = Actual time required to complete test
%t = Percent time on this test

H = Highly skilled interpreter
M = Medium level interpreter
L = Unskilled interpreter

Table 9 AVERAGE 'TIME REQUIREMENTS" FOR THE INTERPRETATION OF HIGH-FLIGHT PHOTOGRAPHY OF THE IMPERIAL VALLEY TEST SITE BASED ON THE WORK OF 45 PHOTO INTERPRETERS

Test #	Imagery Type and date	Total % cor.	Barley	Mature Alfalfa	Cut Alfalfa	Alfalfa	Sugar Beets	Wheat	Bare Soil Moist	Bare Soil Dry	Bare Soil	Cereal
			%cor / %com	%cor / %com	%cor / %com	%cor / %com	%cor / %com	%cor / %com	%cor / %com	%cor / %com	%cor / %com	%cor / %com
1	25A-Apollo 9 March	43	34 / 37	53 / 68	40 / 53	56 / 53	16 / 86	0 / 100	63 / 62	54 / 31	83 / 29	39 / 33
2	89B-Apollo 9 March	47	27 / 35	48 / 65	59 / 52	71 / 48	43 / 74	0 / 100	42 / 35	82 / 41	89 / 17	42 / 27
3	25A-High Flight March	47	34 / 38	55 / 60	40 / 46	53 / 47	43 / 79	0 / 100	42 / 58	87 / 41	88 / 30	40 / 31
4	58-High Flight March	41	30 / 47	44 / 58	57 / 65	61 / 50	0 / 100	25 / 88	21 / 68	75 / 32	62 / 31	35 / 41
5	89B-High Flight March	45	33 / 42	53 / 65	41 / 45	57 / 46	25 / 89	0 / 100	76 / 31	57 / 40	86 / 15	40 / 41
6	CIR-Apollo 9 March	65	50 / 28	52 / 54	91 / 33	80 / 34	25 / 62	50 / 83	83 / 25	75 / 20	98 / 3	83 / 27
7	CIR-High Flight March	64	33 / 34	56 / 56	80 / 34	76 / 38	46 / 74	0 / 100	75 / 0	100 / 26	100 / 7	36 / 30
8	CIR-High Flight April	60	57 / 24	47 / 64	38 / 47	75 / 22	33 / 79	0 / 100	- / -	- / -	96 / 10	66 / 22
9	CIR-High Flight May	72	90 / 6	83 / 37	44 / 35	72 / 21	40 / 79	0 / 100	- / -	- / -	81 / 20	87 / 9
10	FRSL Color Comp.-H.F. March	58	36 / 19	80 / 62	62 / 37	81 / 43	22 / 64	0 / 100	75 / 37	84 / 23	100 / 11	37 / 19
11	FRSL Color Comp.-A9 March	50	39 / 24	53 / 59	63 / 44	72 / 39	21 / 89	0 / 100	58 / 41	63 / 48	97 / 14	43 / 19
12	P.F. Color Comp.-H.F. March	46	23 / 21	66 / 58	47 / 51	62 / 35	8 / 93	25 / 92	69 / 60	68 / 39	98 / 29	29 / 22
13	P.F. Color Comp.-A9 March	33	24 / 57	39 / 55	28 / 74	44 / 55	33 / 91	50 / 67	23 / 74	56 / 42	42 / 54	27 / 54
14	Multidate 25A-High Fl. Composite March and May	76	86 / 3	- / -	- / -	74 / 29	0 / 100	0 / 100	- / -	- / -	88 / 26	86 / 33
15	Concurrent 3 Date, CIR March, April, May	81	82 / 4	78 / 37	75 / 17	83 / 21	35 / 72	25 / 50	- / -	- / -	98 / 8	81 / 3

TABLE 10. Summary table indicating the percent-correct (and percent commission error) identifications for individual and overall crop types on each of the various space photos, sequentially obtained aerial photos, and corresponding color composites examined in an interpretation test of the Mesa agricultural test site.

PHOTO INTERPRETER'S RESULTS	GROUND TRUTH									
	D	P	M	C_V	C_B	C_F	W_O	W_R	R	U
D	**49**		7				2			
P	1	**27**	13	4			1			
M	5	2	**28**				1			
C_V				**74**						5
C_B		1		2	**20**					3
C_F						**18**				1
W_O	1						**36**			1
W_R								**18**	6	
R								2	**34**	
U	4		2			2				**20**
TOTAL ITEMS	60	30	50	80	20	20	40	20	40	30
NUMBER INCORRECT	11	3	22	6	0	2	4	2	6	10
PERCENT CORRECT	81	90	56	92	100	90	90	90	85	67
PERCENT COMMISSION	15	41	22	6	23	5	5	25	5	28

Table 11. Quantitative expression of interpretation accuracy achieved from a study of vegetation and other earth resources on the Apollo 9 Infrared Ektachrome photos of the Louisiana-Mississippi area appearing in Figure 24. For legend to the categories listed in this table, see text. Numbers in bold-faced diagonal boxes indicate number of areas in each category that were correctly identified, on the average, by 10 photo interpreters. Numbers to left and right of them indicate commission errors, by type, and numbers above and below them indicate omission errors, by type.

TABLE 12. A TABULAR SUMMARY OF REMOTE SENSING CAPABILITIES IN VARIOUS PARTS OF THE ELECTROMAGNETIC SPECTRUM

Wavelength in Microns	10^{-6}	10^{-4}	10^{-2}	10^{0}	10^{2}	10^{4}
Spectral Region	Gamma Ray	X-Ray	UV	Visible / Solar IR	Thermal IR	Microwave
Properties Sensed	Sub-Atomic and Atomic Dissociations and Electron Shifts			Molecular Effects* (3 types, see below)	Macromolecular Effects (texture, dielectric reflectivity of radar pulses, thermal emissivity)	
Detectors Used	Ionization Detectors (e.g., gamma ray spectrometers and phosphors)			Photographic Films / Quantum Detectors (e.g., optical mechanical scanners, thermal radiometers)	Antennae & Circuits (e.g., radar and passive sensors)	
Atmospheric Penetrability**	C	C	C,H	C,H / C,H	C,H,S	C,H,S,F
Spatial Resolution Attainable in Milliradians	500	500	.01 to .1	.01 to .001 / .01 to .1	1.0	10

Resolution in these short wavelengths is limited primarily by atmospheric scattering

$$S = k_1 \cdot \frac{1}{\lambda^4}$$

where S = scattering
λ = wavelength

Resolution in these long wavelengths is limited primarily by aperture of the sensor

$$R = k_2 \cdot \frac{\lambda}{D}$$

where R = resolution
D = diameter of the "collecting optics"

* Primarily the effects which are governed by (1) electron shifts in the bonding of atoms; (2) energy changes in the vibrations of atoms within the molecule; and (3) changes in rotational energy of the molecule as a whole.

** C = clear weather only, CH = clear or hazy, CHS = clear, hazy or smoky, CHSF = clear, hazy, smoky or foggy.

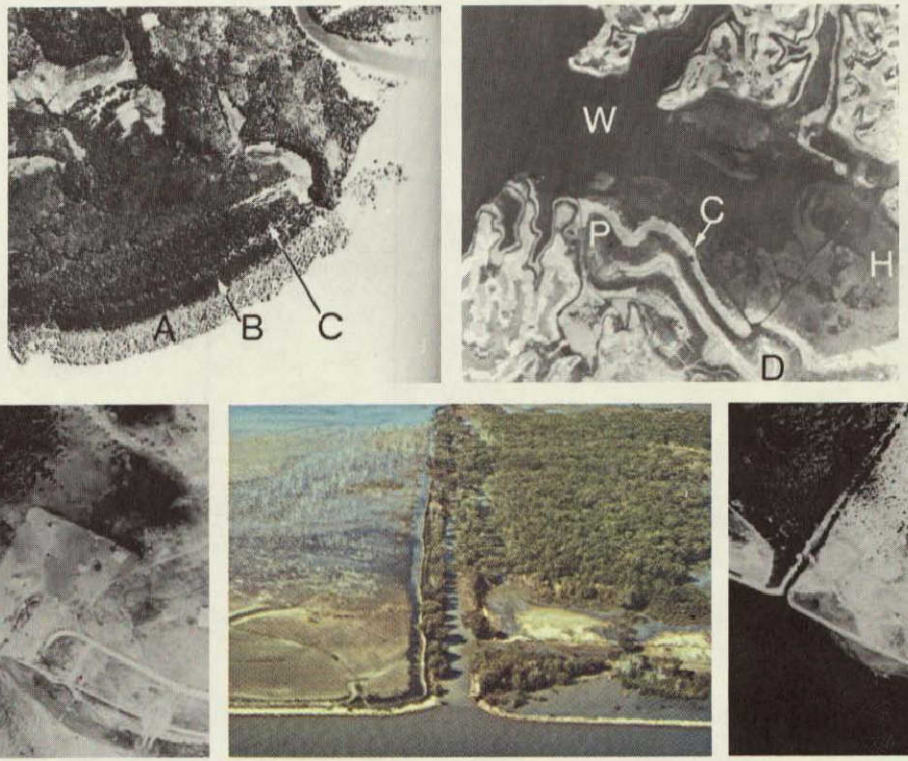

Figure 1. These aerial photos illustrate the importance of photographic tone (a characteristic that also is readily discerned on space photos) as an aid in the inventory of vegetation resources. Top left: A mangrove swamp in which Avicennia (A) is readily differentiated from the very dark-toned Rhizophora (R) and the moderately dark-toned Brugiera (B). Top right: An agricultural area in China emphasizing the close relation between vegetation type (as identified by photographic tone) and topographic site. The first vegetation "contour" inland from the dark-toned water (W) is water hyacinth(H), followed by cord grass (C), paddy crops (P) (very dark-toned) and dry land crops (D) along the ridge. Bottom left and right: Timberlands in Australia which exhibit essentially the same tone to left and right of the levee on the panchromatic photo (left) but much different tones on the infrared photo. These multiband "tone signatures" indicate that trees on the left of the levee are unhealthy hardwoods while those on the right are healthy. The center photo taken by the writer one year later confirms the accuracy of this prediction. Bottom left and right photos courtesy of Australian Department of National Development

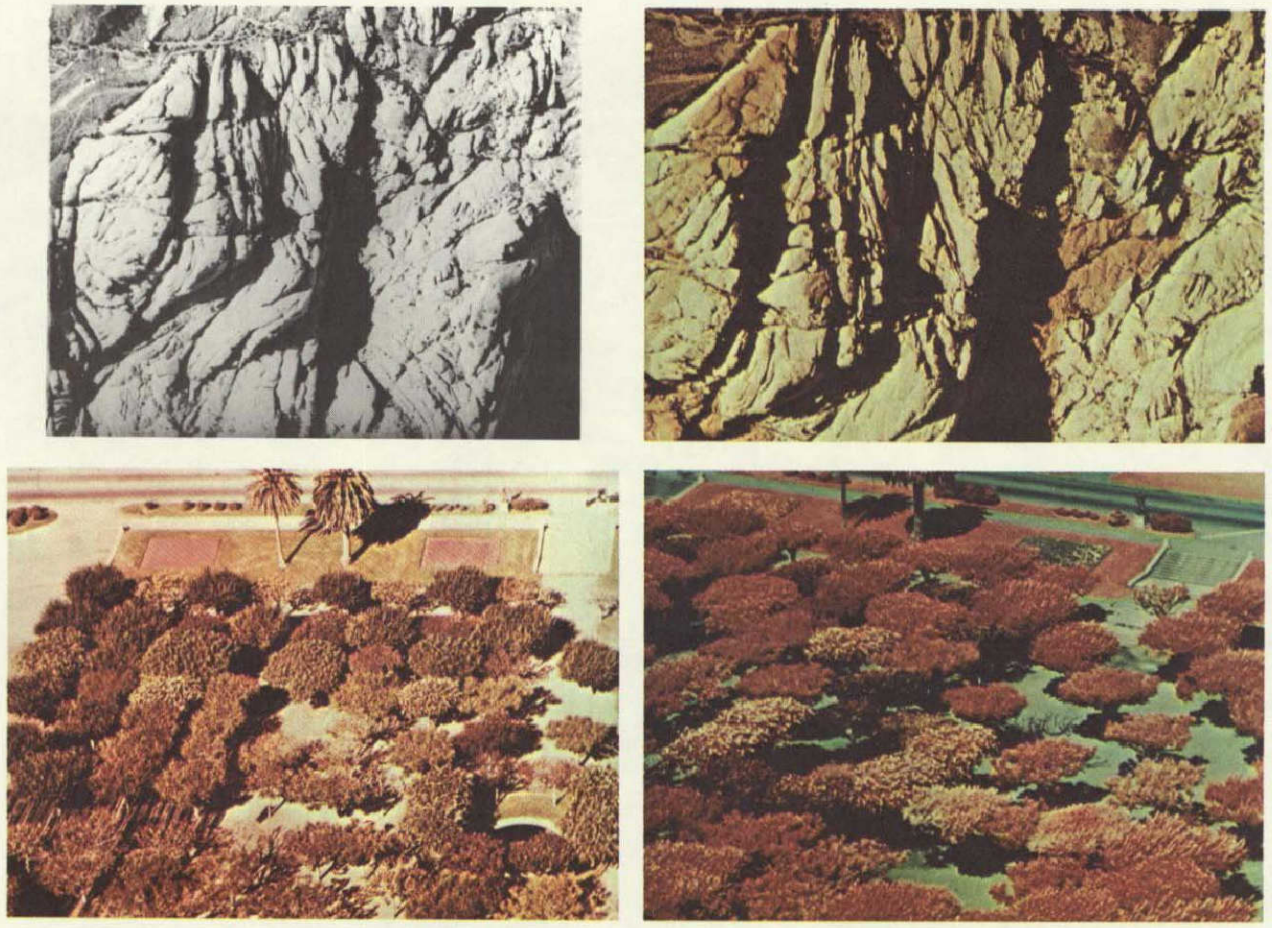

Figure 2. These aerial photos illustrate the importance of photographic color as an aid to the inventory of earth resources. Exactly the same wavelengths of energy were used in taking the two photos comprising the top pair. The two types of Navajo sandstone exhibit the same tone on the panchromatic photo (left) but decidedly different colors on the Ektachrome photo. In the bottom pair tree species farthest from the camera station are best identified on the Ektachrome photo (left) while tree species nearest the camera station are best identified on the Infrared Ektachrome photo.

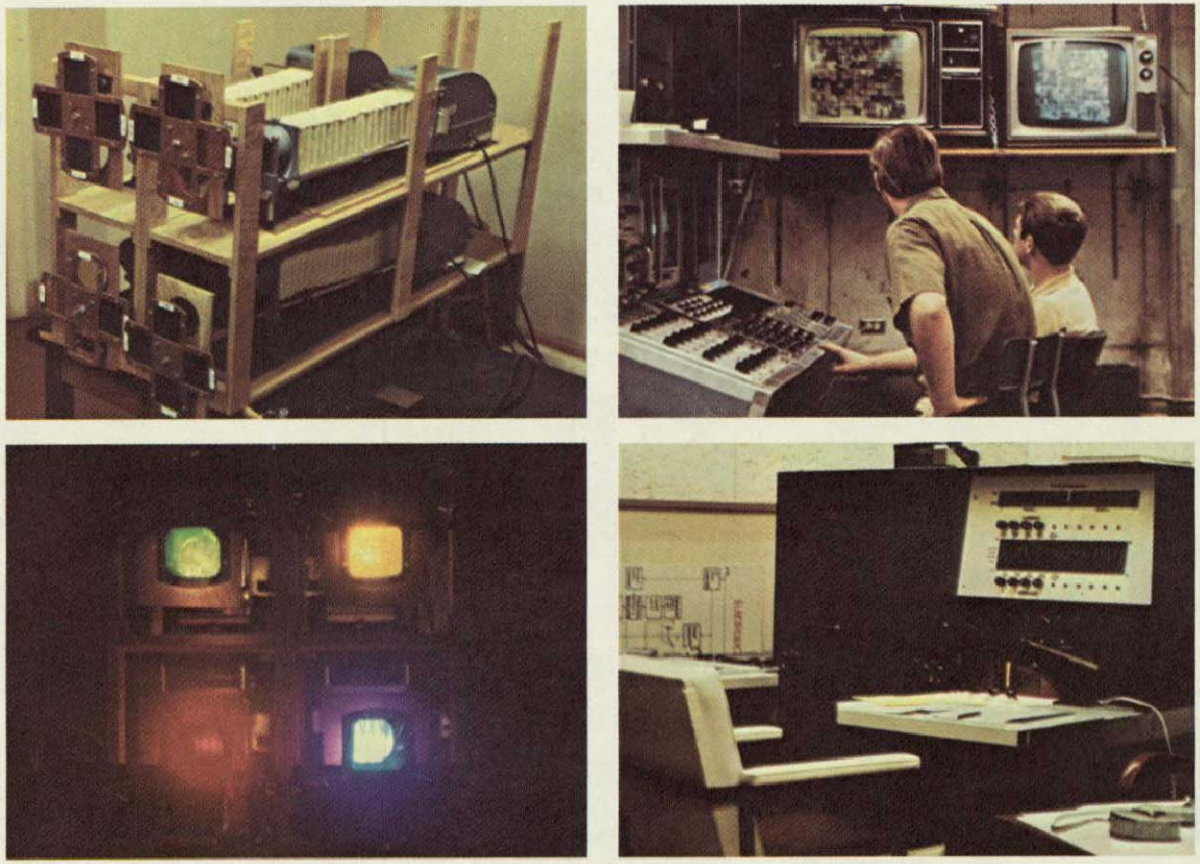

Figure 3. Shown here are the three devices used in forming the enhanced images appearing in Figures 4 through 6 and 16 through 18. All three of the devices shown here use additive color techniques to combine multiple black-and-white images either optically or electronically. Left pair: The FRSL (Forestry Remote Sensing Laboratory) Optical Color Combiner, showing the manner in which a wheel of colored filters is placed in the optical path of each of the four projectors. Top right: The Kansas University electronic enhancement device known as IDECS (for Image Discrimination Enhancement Combination and Sampling). Bottom right: The Philco-Ford electronic enhancement device or "Image-Tone Enhancement System". Not clearly visible here is the viewing aperture (approximately 5" x 7") located in the dark area to the left of the console controls.

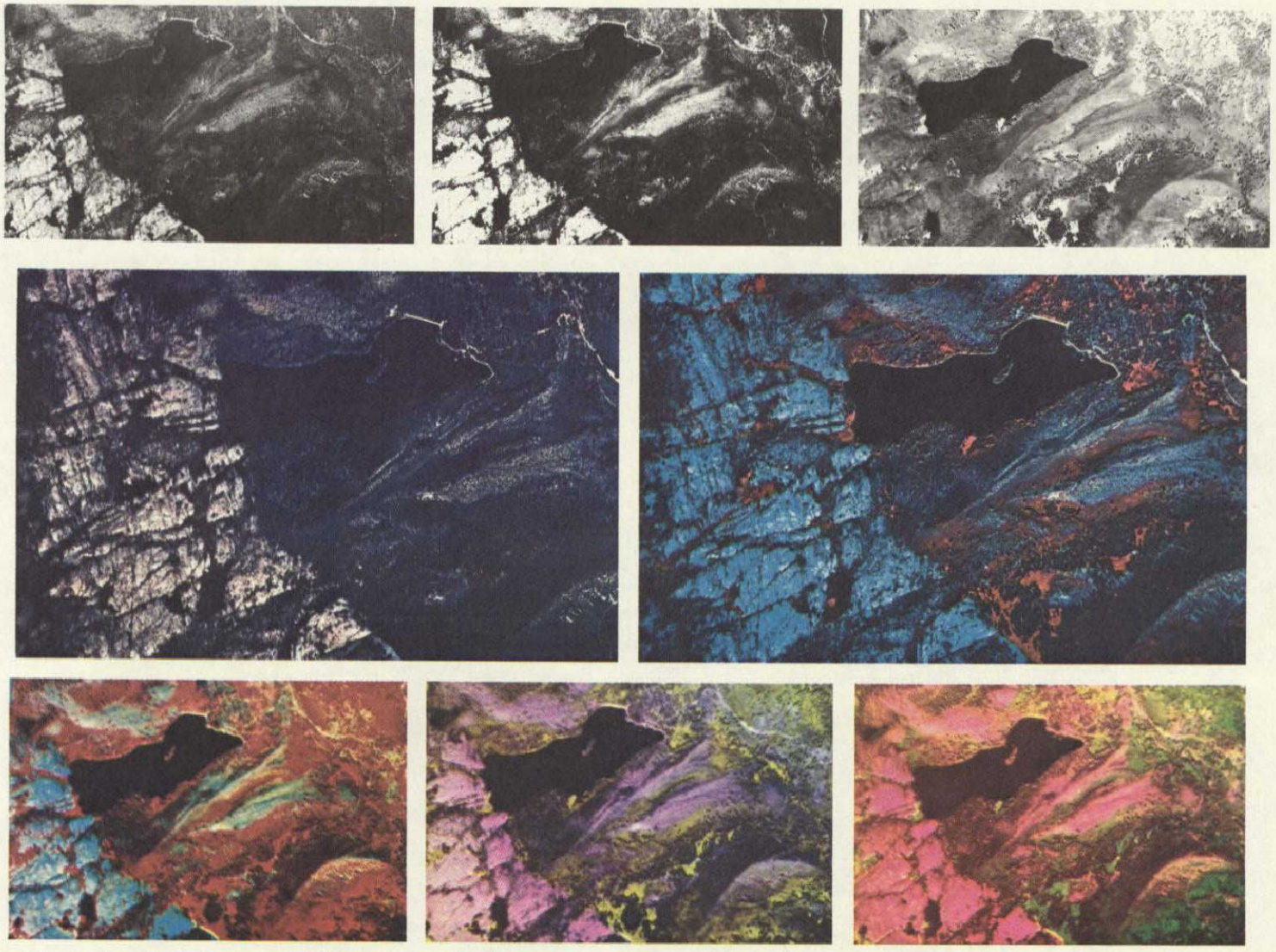

Figure 4. NASA Bucks Lake Test Site. See text for analysis of these color enhancements.

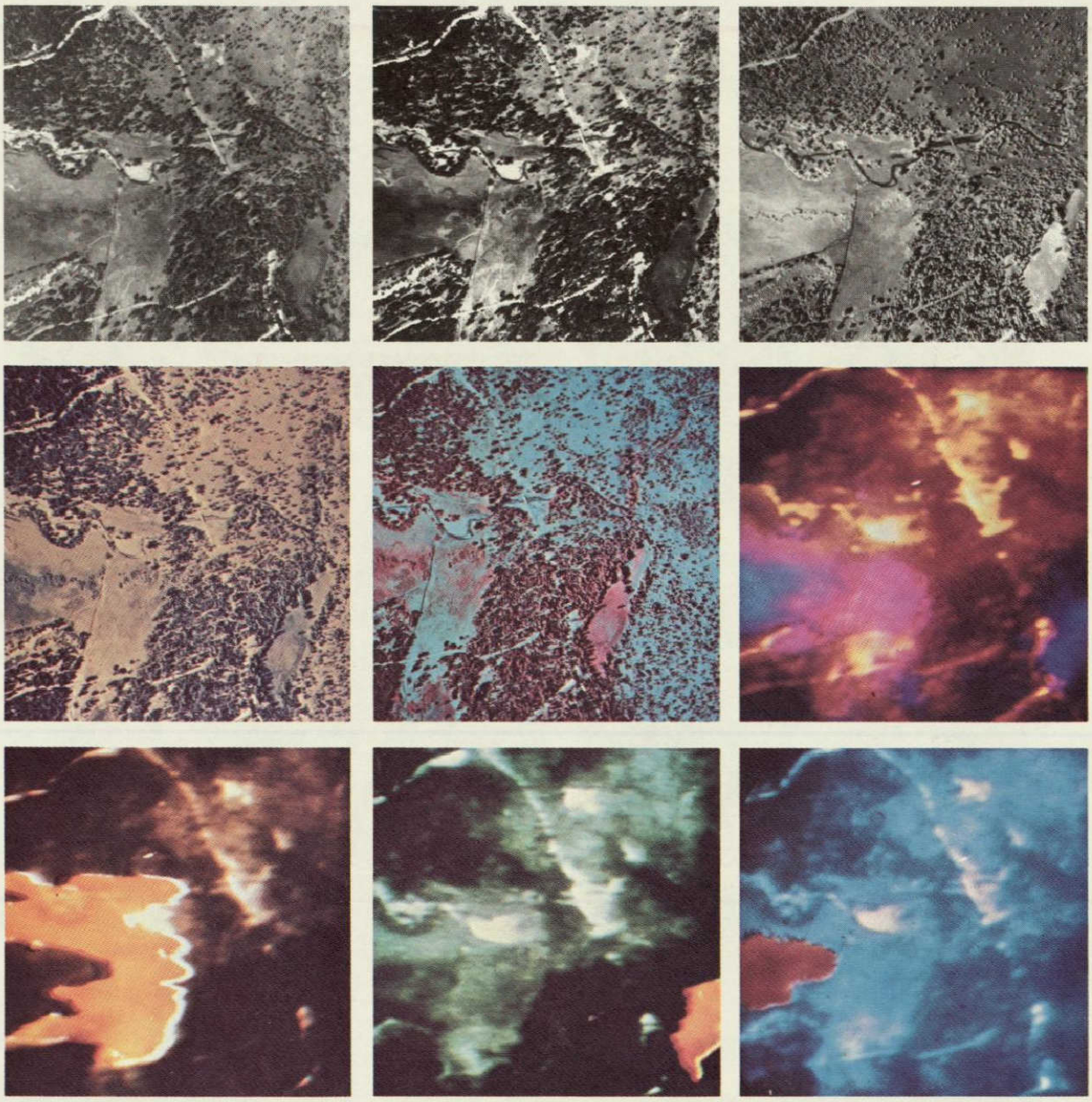

Figure 5. Multiband and enhanced photography of a portion of the NASA Bucks Lake Test Site. This example illustrates that certain kinds of information pertaining to vegetation and other earth resources can be discerned on suitably enhanced imagery, even though not discernible on high quality Ektachrome or Infrared Ektachrome photos that recorded essentially the same wavelengths of energy. The top 3 photos were obtained simultaneously with Pan-58, Pan-25A and Infrared-89B film-filter combinations, respectively. In the middle row the left photo was taken with Ektachrome film and the middle photo with Infrared Ektachrome. The remaining photos are various enhancements made with the IDECS equipment that appears in Figure 3, using as input the three black-and-white photos of the top row. For example, the bottom right photo differentiates bunch grass and willow vegetation (red coloration) from "everything else", and the bottom center photo differentiates sedge and rush vegetation (yellow coloration) from everything else. Similarly, the bottom left photo differentiates annual grasses (yellow) from "everything else". The right photo in the middle row is best for overall interpretability.

IDECS photos courtesy of CRES, University of Kansas and Dr. John Estes

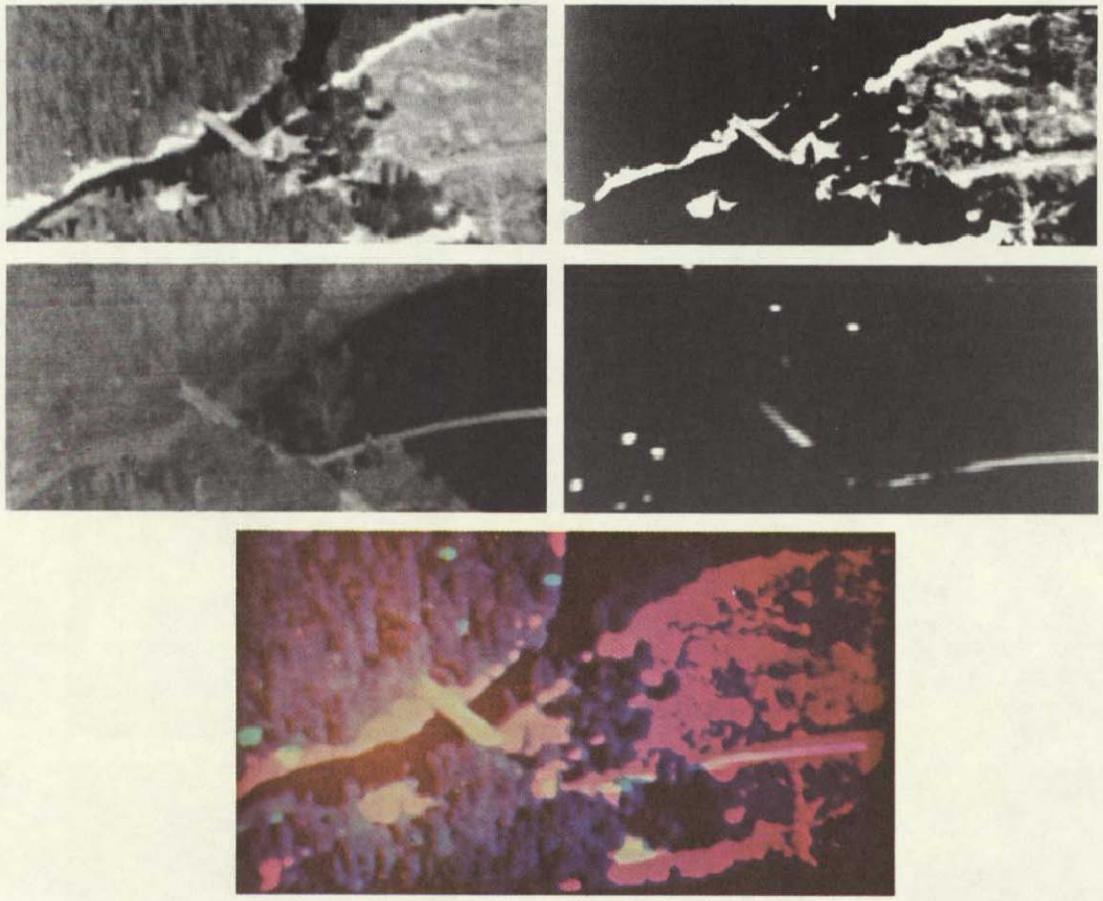

Figure 6. Thermograms of a portion of Yosemite Valley, as photographed from Glacier Point, more than 3,000 feet above the floor of the Valley. The wavelength bands used were so selected as to exploit the fact that the power peak of features at room temperature is at about 9 to 10 microns and that of fires is at about 5 microns. The top left thermogram (taken in the 8-14 micron band at 1030 a.m.) shows good detail in the timbered areas; the top right thermogram,(also taken in the 8-14 micron band but at 0830 a.m.) shows good detail in the grassland areas; the bottom left photo (taken in the 8-14 micron band at 0015 a.m.) accentuates the road and bridge; and the bottom right photo (taken in the 3.5 to 5.5 micron band) accentuates camp fires. The color composite at the bottom of this figure was formed with the 4 projectors shown in Figure 3 and employed all 4 of the thermograms shown above. Consequently, details of all 4 types of features mentioned above are seen in this single composite presentation.

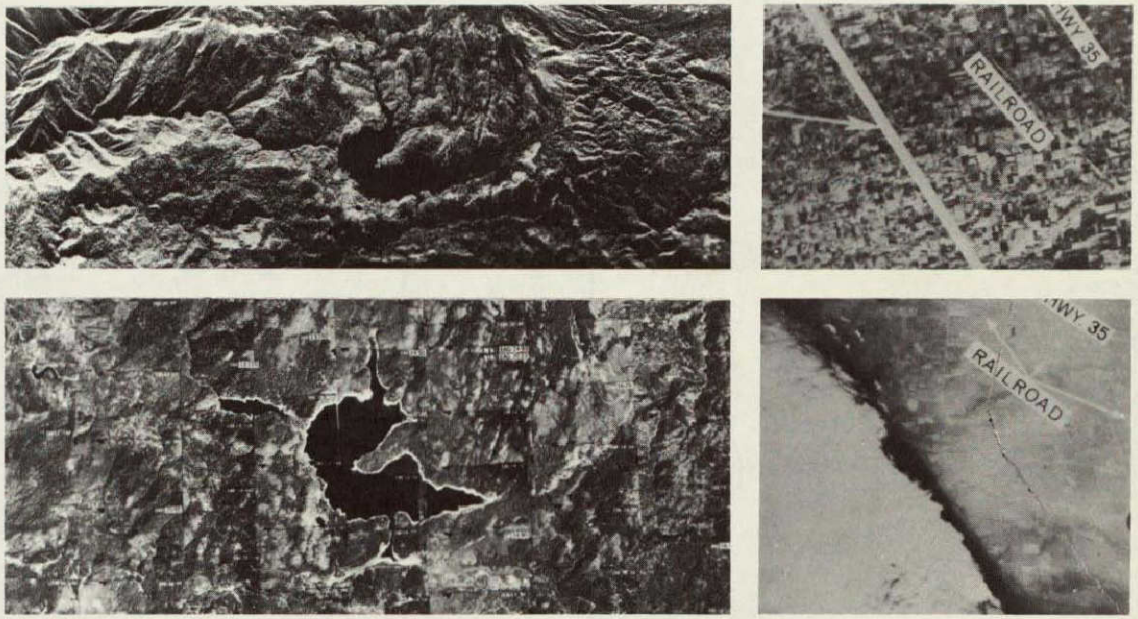

Figure 7. K-Band radar imagery as an aid to vegetation mapping. Left: "HH" radar imagery (top) and matching panchromatic minus blue aerial photography of NASA Bucks Lake Test Site. The identification of certain vegetation types on this radar imagery is facilitated not only by their tone values but also by their texture characteristics and by their association with certain topographic features that are better seen on radar imagery than on conventional photography. Right: Matching radar (top) and panchromatic imagery taken simultaneously of an area over which a cloud front is drifting. Note that areas beneath the clouds are imaged as clearly on the radar imagery (but not on other kinds of imagery) as those that are cloud-free). As summarized in Table 4, this "all weather capability" is of great advantage in areas which usually are covered with clouds and hence cannot be imaged with other sensing devices. Radar images courtesy of CRES, University of Kansas and Westinghouse Electric Corporation

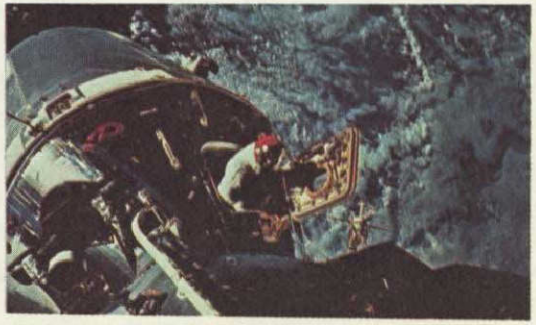

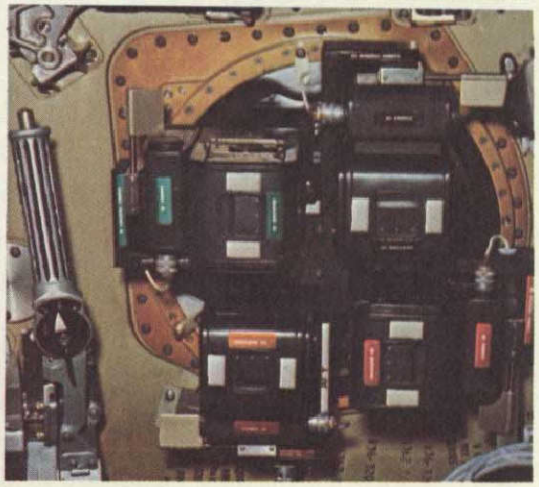

Figure 8. Left: The four Hasselblad cameras (80mm focal length and 70mm film width) used by the Apollo 9 astronauts in performing the "S065" photographic experiment. Film-filter combinations employed by the 4 cameras (beginning with the top left camera and proceeding clockwise) were as follows: Infrared Aerographic (SO-246) with a Wratten 89B (dark red) filter; Panatomic X (3400) with a Wratten 58 (green) filter; Infrared Ektachrome (SO-180) with a Wratten 15 (orange) filter; and Panatomic X (3400) with a Wratten 25A (light red) filter. In addition, the Apollo 9 astronauts operated hand-held Hasselblad cameras loaded with Ektachrome film to obtain matching frames of photography of selected NASA test sites, as illustrated in Figures 10 and 22. Top right: The open hatch of the Apollo 9 spacecraft is clearly seen. Note that earth features shown here exhibit essentially the same image coloration when photographed through the window as when photographed through unobstructed space. This is an important consideration because the window shown here is the one through which all the S065 space photographs were taken and it therefore was important that it exhibit no abnormal light transmission characteristics. Bottom right: The 4-camera S065 system after it has been installed over the hatch window of the spacecraft.

Photos courtesy of Allen Grandfield, NASA MSC, Houston.

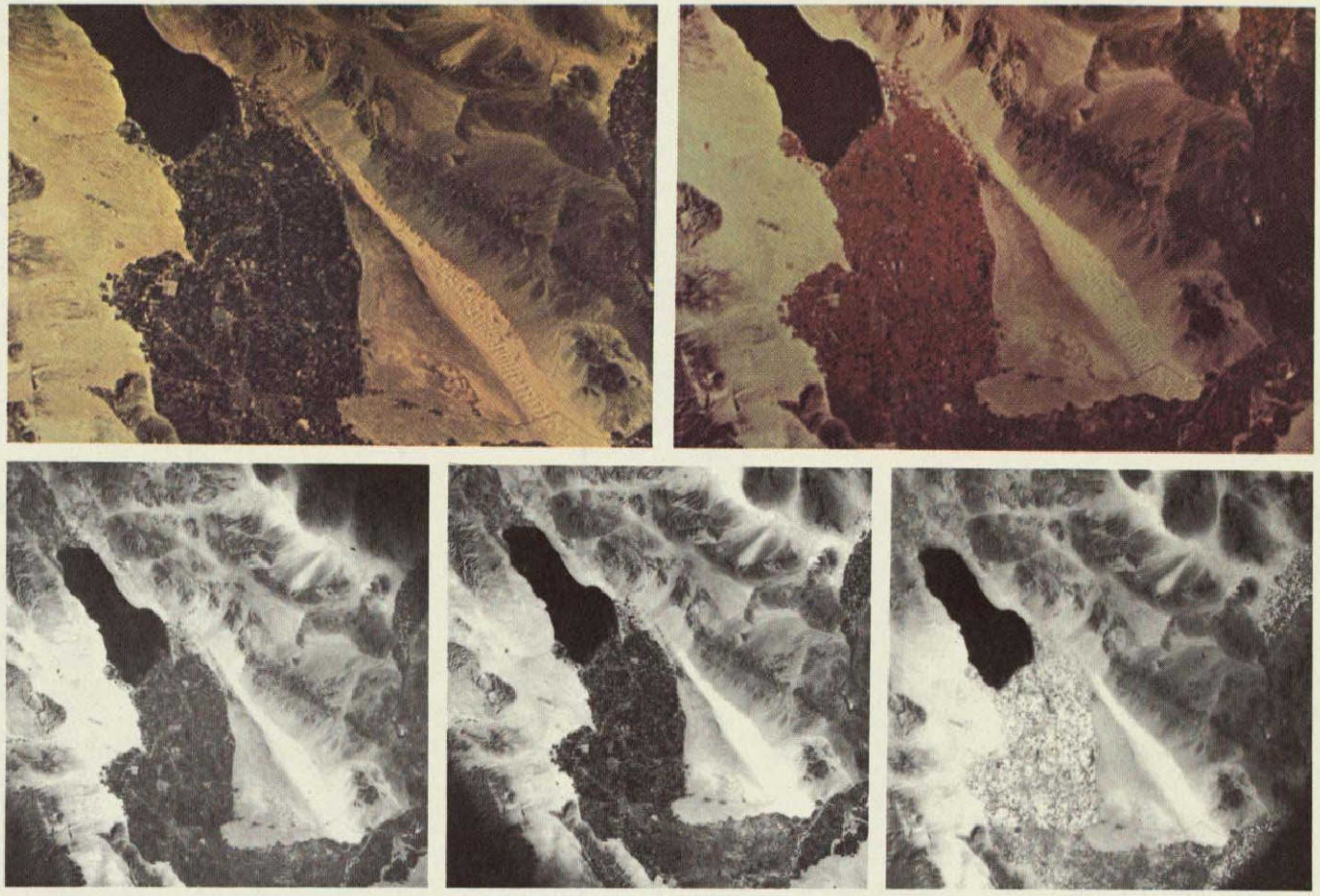

Figure 9. Imperial Valley Test Area as photographed by the Apollo 9 astronauts with 5 different cameras from an altitude of approximately 130 statute miles. The top left photo was taken with a hand-held Hasselblad camera loaded with Ektachrome film. The other four photos were taken simultaneously with the four Hasselblad cameras of the S065 system. (The two color photos have been enlarged here more than the three black-and-white photos). Portions of this area, still further enlarged and in some instances enhanced, appear in Figures 13 through 18.

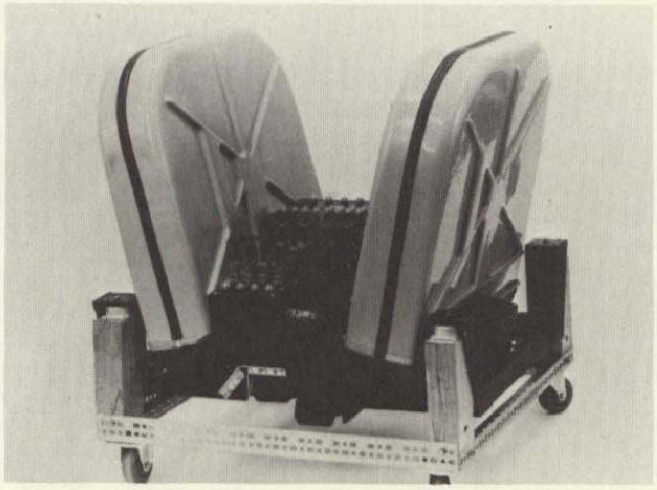

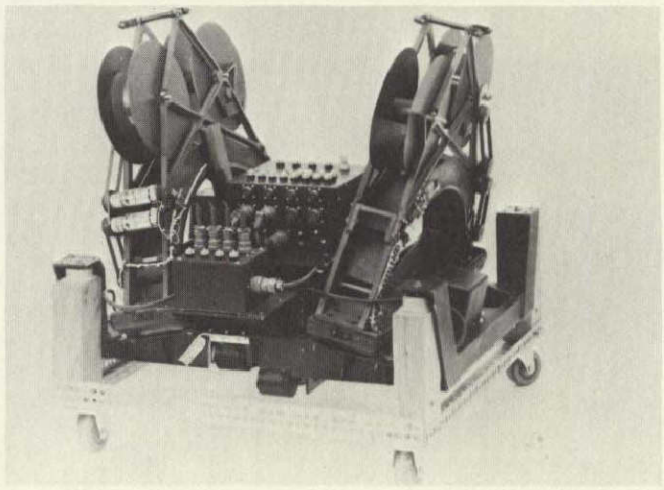

Figure 10. These two views show the 6-camera configuration used in obtaining sequential "high-flight" photography in support of the Apollo 9 S065 experiment. The left photo shows (on its left and right edges) the two HyAc 12-inch focal length panoramic cameras, with light-tight covers in place. The film width for these cameras is 70mm. In the right photo the HyAc camera covers have been removed to show the supply and take-up spools, drive mechanism and arcuate film platens. Normal film load in each of these two cameras is 1000 feet, although 1400 feet of thin-base film can be accommodated. The cameras are, of necessity, mounted in convergent mode, each inclined 13° from the vertical. The two small black cylinders in bottom foreground of this assembly are film drive spools for two of the four Nikon 35mm (21mm focal length) cameras. Normal film load for each of the four Nikon cameras is 250 exposures. On a typical NASA-sponsored high-flight, the film-filter combinations used in the two HyAc cameras are Pan plus X (2402) with Wratten 25A filter and Infrared Ektachrome (8443) with Wratten 15 filter. Film-filter combinations used in the four Nikon cameras are Panatomic X (3400) with Wratten 25A filter; Panatomic X (3400) with Wratten 58 filter; Infrared Xerographic (2424) with Wratten 89B filter; and Infrared Ektachrome (8443) with Wratten 15 filter, respectively. Numerous examples of sequential photography taken with this system appear in succeeding chapters of this report and in Figures 1.5 and 1.6. The large black box midway between the two HyAc cameras is the standard control box for these cameras. It provides pulses of the proper voltage and duration for taking successive exposures and for recycling the cameras between exposures. The smaller black box in the foreground serves a similar function for the four 35mm Nikon cameras. (Photos courtesy of Mark Systems, Inc.)

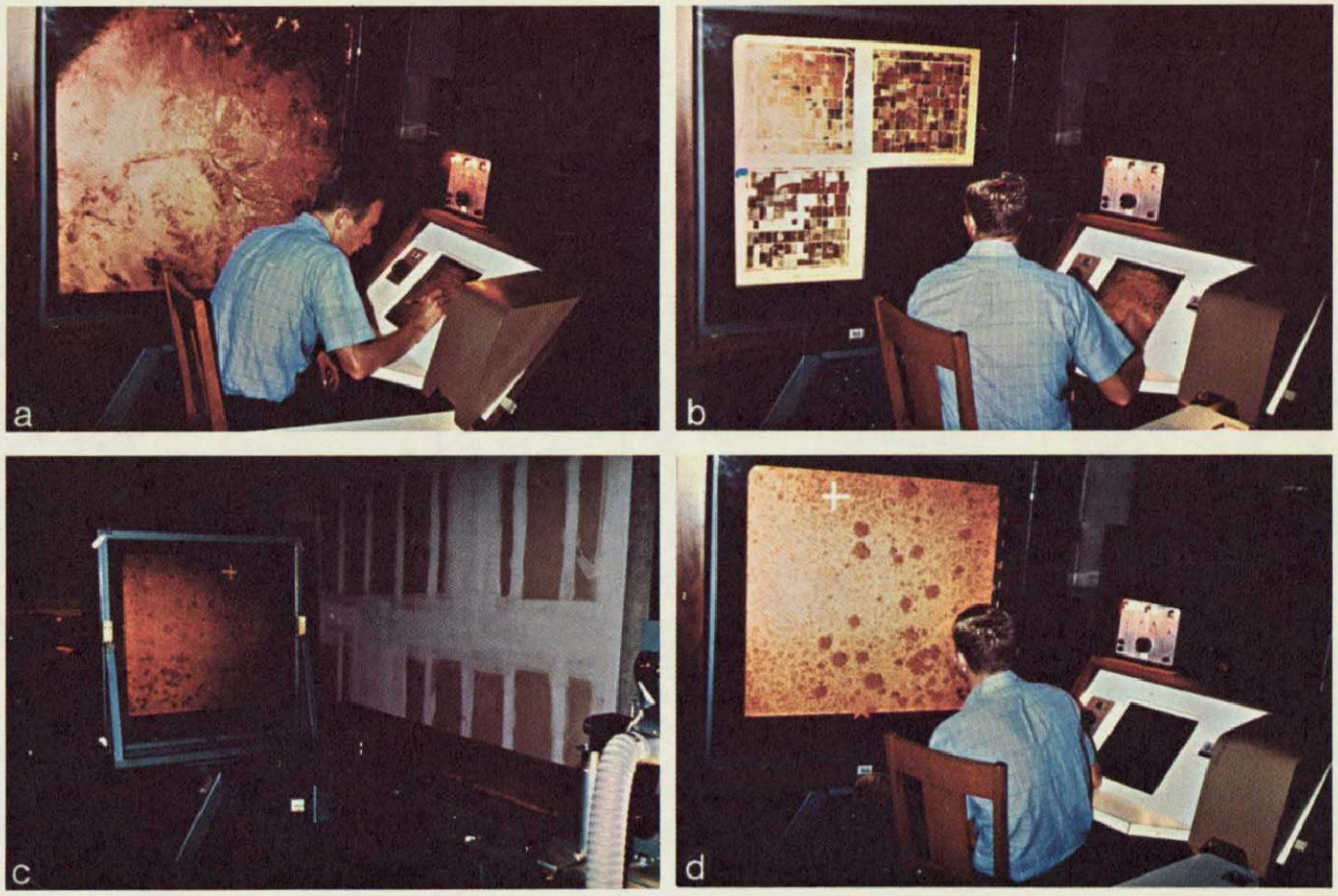

Figure 11. Shown here are 4 scenes of the Itek rear projection viewing equipment that is being used to examine 70mm photographs obtained on the Apollo 9 mission. The equipment also is used to view the sequential photography from each "high-flight" mission that is being flown as a follow-on to the Apollo 9 "S065" photographic experiment. Magnifications up to 20 diameters can be profitably exploited in viewing such photography. The large screen immediately to the left of the operator in 3 of the above views displays (a) a frame of Apollo 9 Infrared Ektachrome photography, (b) 3 frames of Philco Ford enhanced imagery, and (d) a very large scale Infrared Ektachrome aerial photo that is being used in our tests of multistage sampling techniques. As shown in (a), the operator can display a second photo of the same area, for comparative purposes, on a smaller viewing screen directly in front of him. To facilitate the making of image comparisons it is possible to display both images at the same scale or, as in this instance, at different scales. The automatic focussing capability and automatic film drive mechanism of this rear-projection equipment greatly facilitate its use.

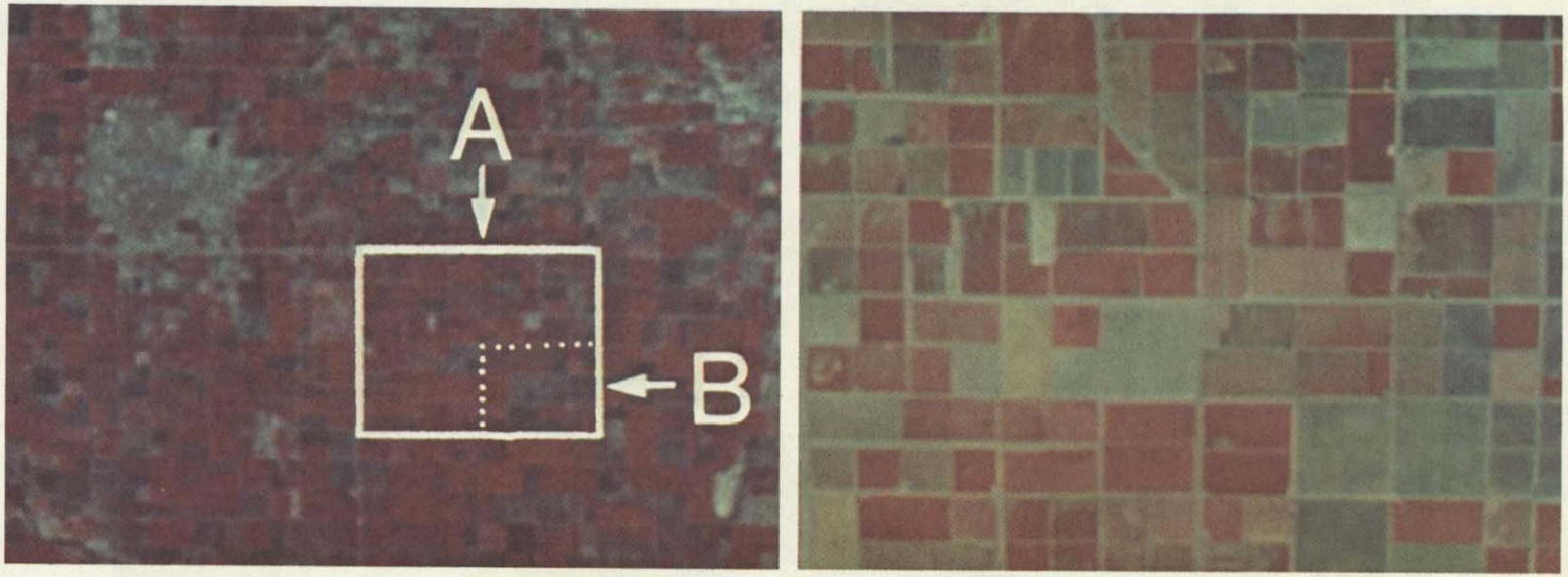

Figure 12. Imperial Valley Test Area. Left: 5X enlargement of part of the Infrared Ektachrome space photo shown in Figure 10. The largest grey area appearing in the upper left corner of this photo is the town of El Centro. Right: Enlargement of part of the Infrared Ektachrome High Flight photo taken on the same date from an altitude of approximately 70,000 feet. A record of "ground truth" for the area outlined on this photo appears in Figure 14. Additional imagery of this same area appears in Figures 15 through 17.

IMPERIAL VALLEY GROUND TRUTH

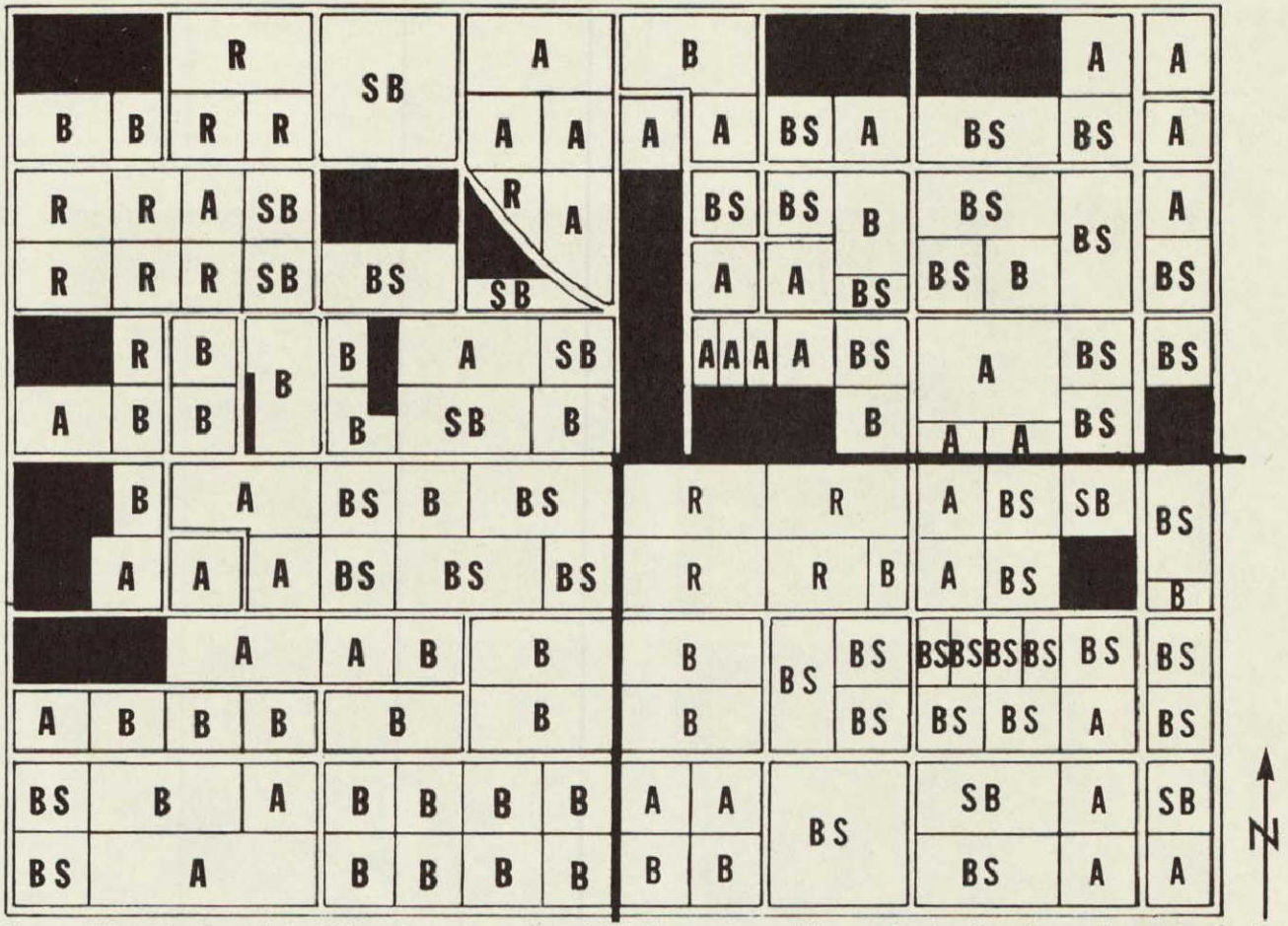

Figure 13. The Imperial Valley Test Area for which "ground truth" was obtained both at the time of the Apollo 9 overflight and at the time of each subsequent supporting "high flight" that was made at an altitude of approximately 70,000 feet. The lower right quadrant was used as a "training" area and the remainder as a "testing" or "prediction" area in order to obtain the results shown in Tables 4 through 9, as described in the text. For legend to above symbols, see text.

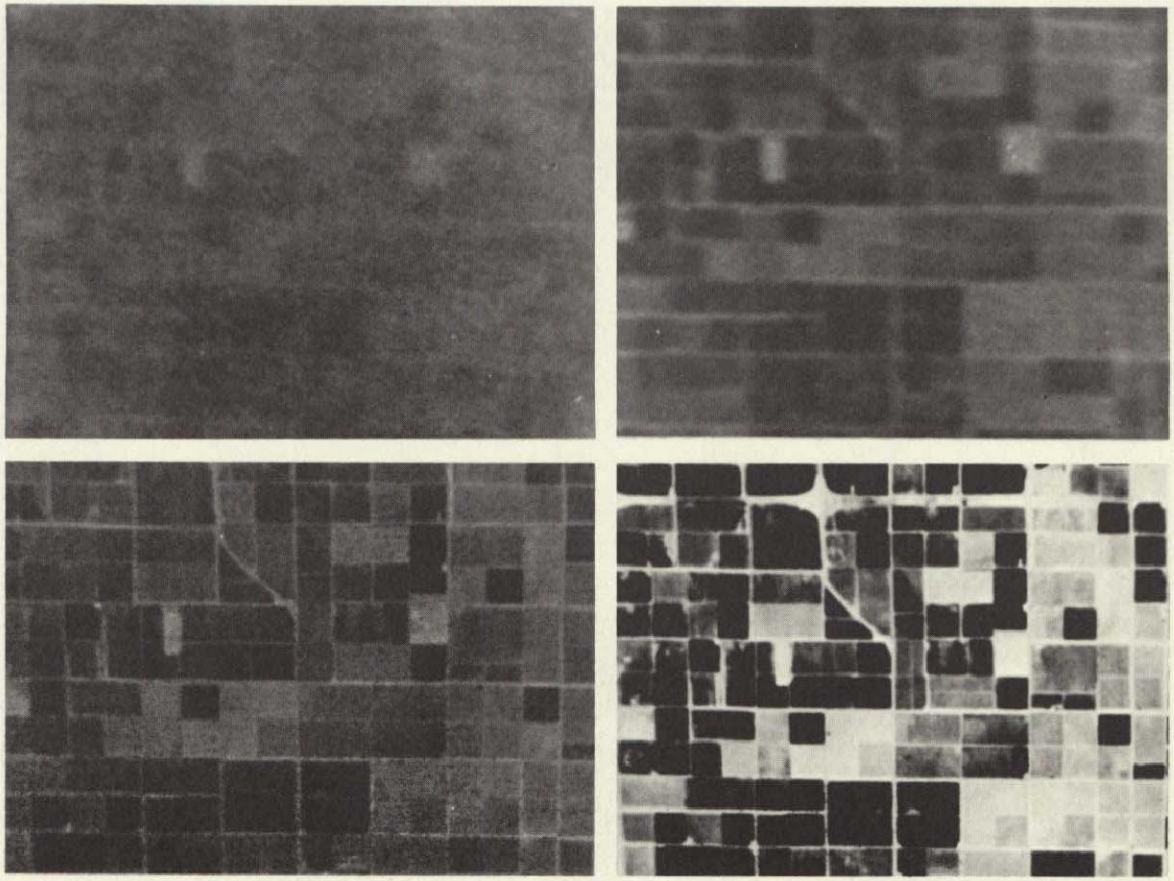

Figure 14. Imperial Valley Test Area. Left pair: Apollo 9 space photo (top) and High Flight aerial photo, both taken with panchromatic film and a Wratten 58 filter to expose for the green band. Right pair: Apollo 9 space photo (top) and High Flight aerial photo, both taken with panchromatic film and a Wratten 25A filter to expose for the red band. All photos have been enlarged to a common scale of approximately 1/200,000.

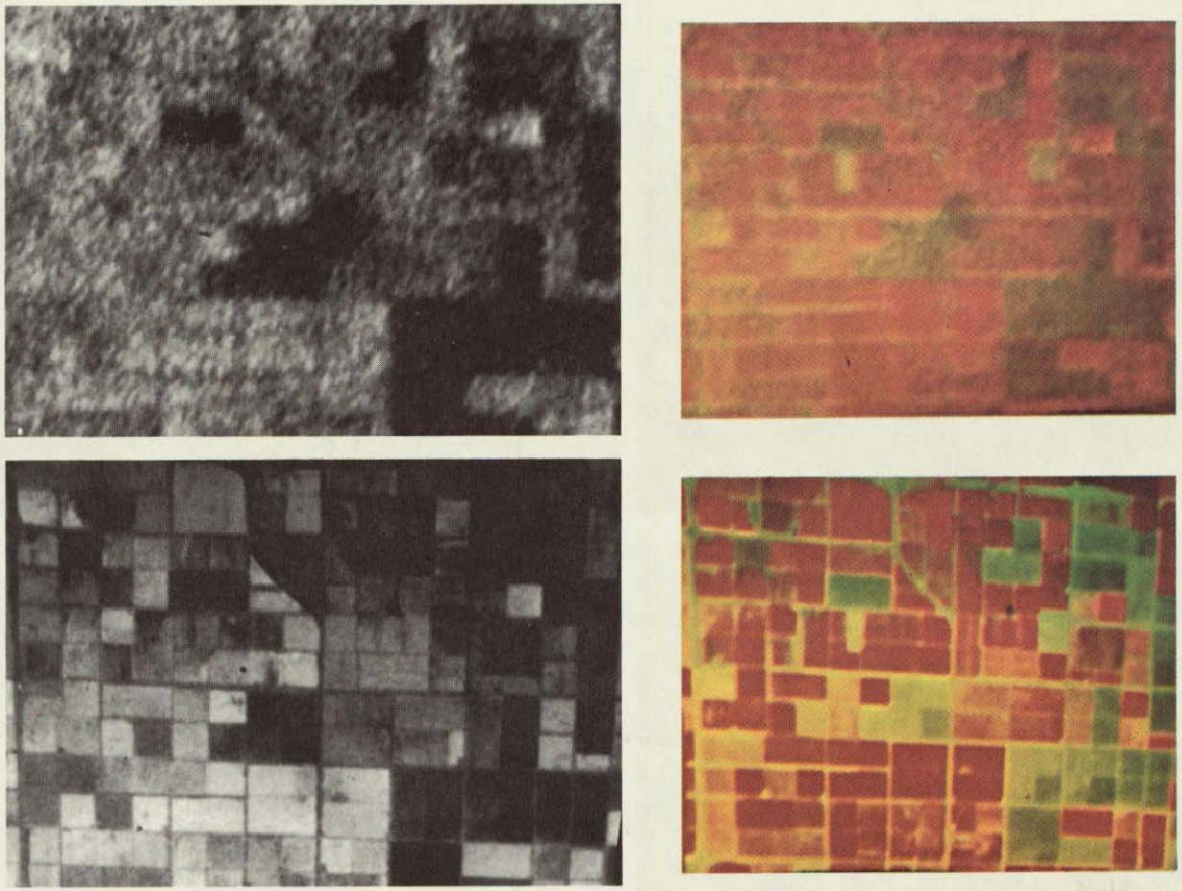

Figure 15. Imperial Valley Test Area. Left pair: Apollo 9 space photo (top) and High Flight aerial photo, both taken with Infrared film and a Wratten 89B filter to expose for the near infrared band. Right pair: FRSL optically combined images made from the red and infrared bands of space photography (top) and from the green; red and infrared bands of High Flight aerial photography.

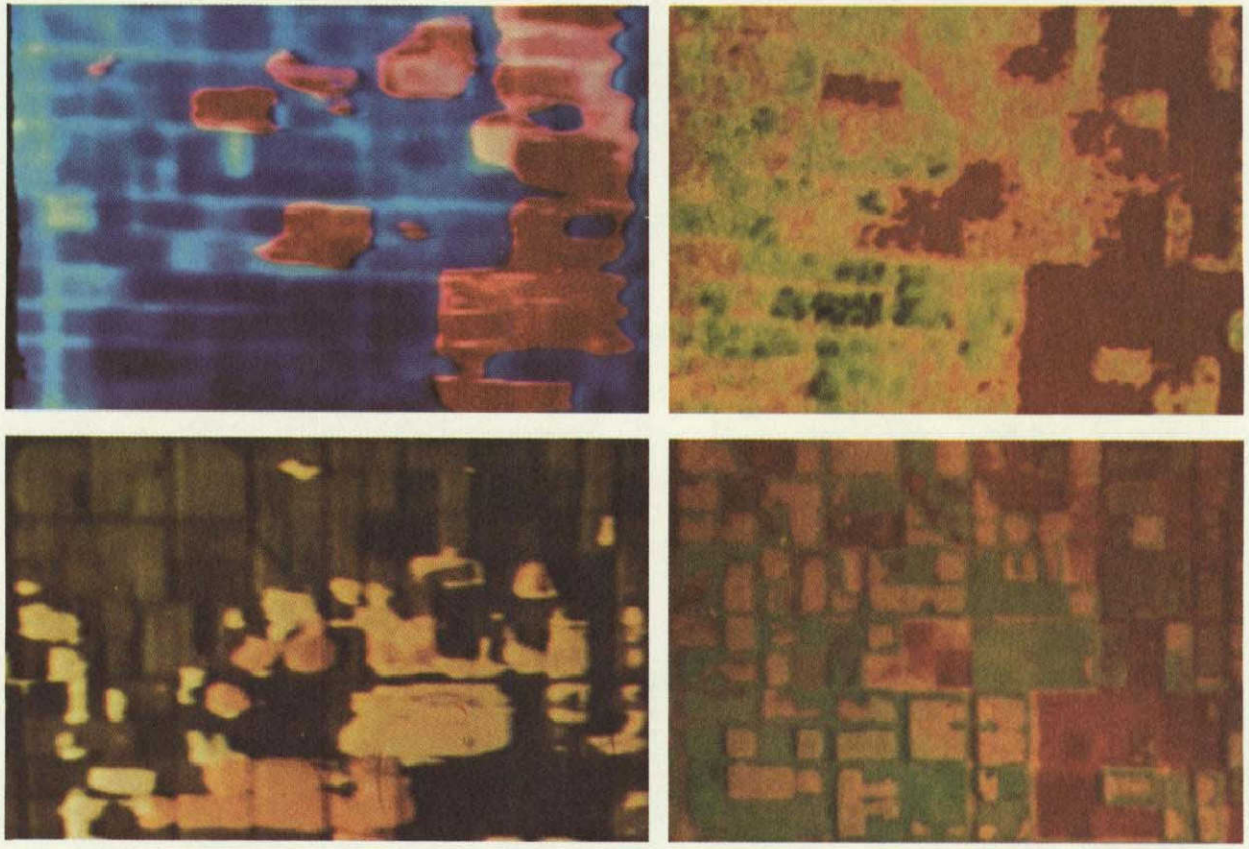

Figure 16. Imperial Valley Test Area. Left pair: IDECS electronically combined images made from the red and infrared bands of Apollo 9 space photography (top) and from the green, red and infrared bands of High Flight aerial photography. Right pair: Philco-Ford electronically combined images made from the red and infrared bands of Apollo 9 space photography (top) and from the green red and infrared bands of High Flight aerial photography.

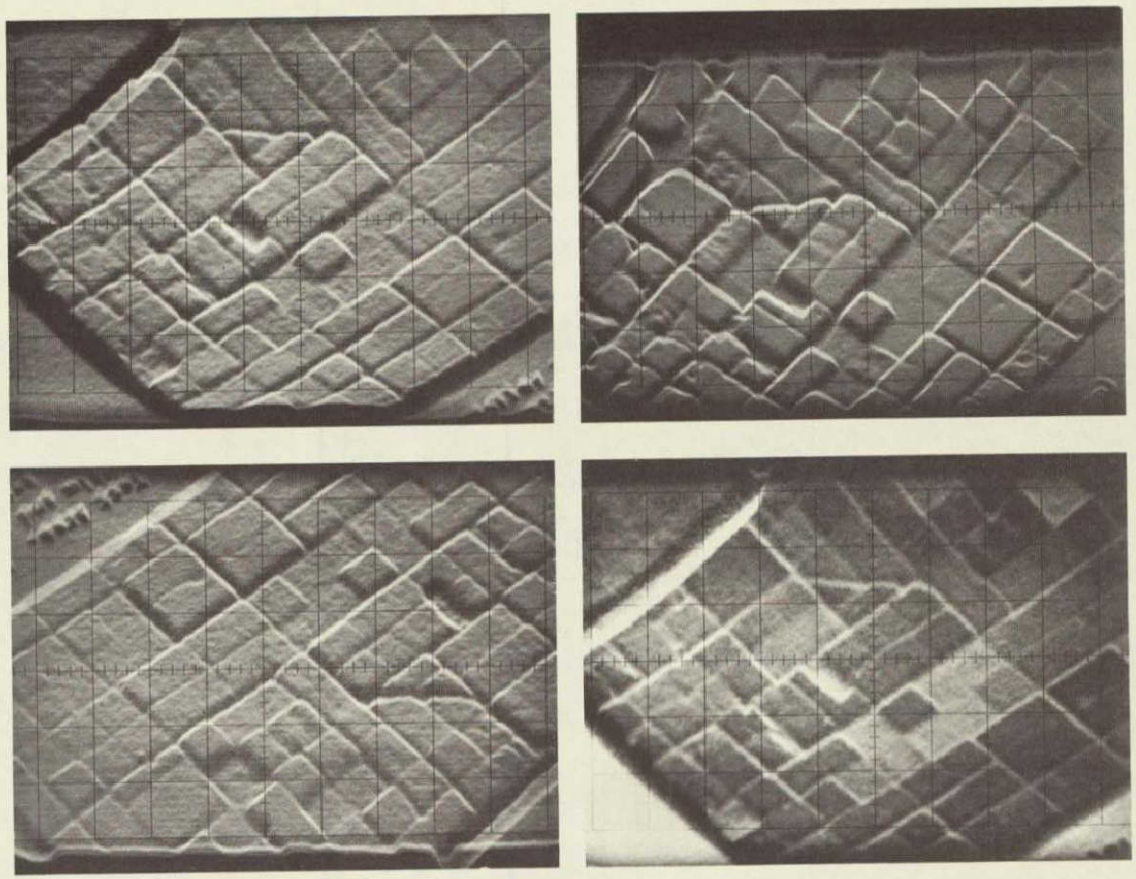

Figure 17. Line Scan Modulation Displays of a portion of the Imperial Valley Test Area. In the top pair deflection modulations based on tone or brightness are downward, causing fields which contain crops to appear to stand up above the fallow fields, much as in the original scene. These displays were made by scanning the Pan-58 and Pan-25A high flight photos, respectively. (See Fig. 15). In the bottom left photo, the same portion of the Pan-58 high flight photo has been scanned, but deflection modulations are upward, causing a pseudoscopic effect which facilitates the interpretation of roads, levees and fallow fields. In the bottom right photo, the deflection modulations are again downward and in addition tone differences discernible in the original Pan-25A high flight photo of Fig. 15 have been preserved. For further description of this process, see publication by Dalke, Estes, Moore and Colwell entitled "Multi-Image Correlation Systems Study," Univ. of Kansas, 1968. The above photos are courtesy of Mr. Richard Webber, Department of Physiological Optics, Univ. of Calif.

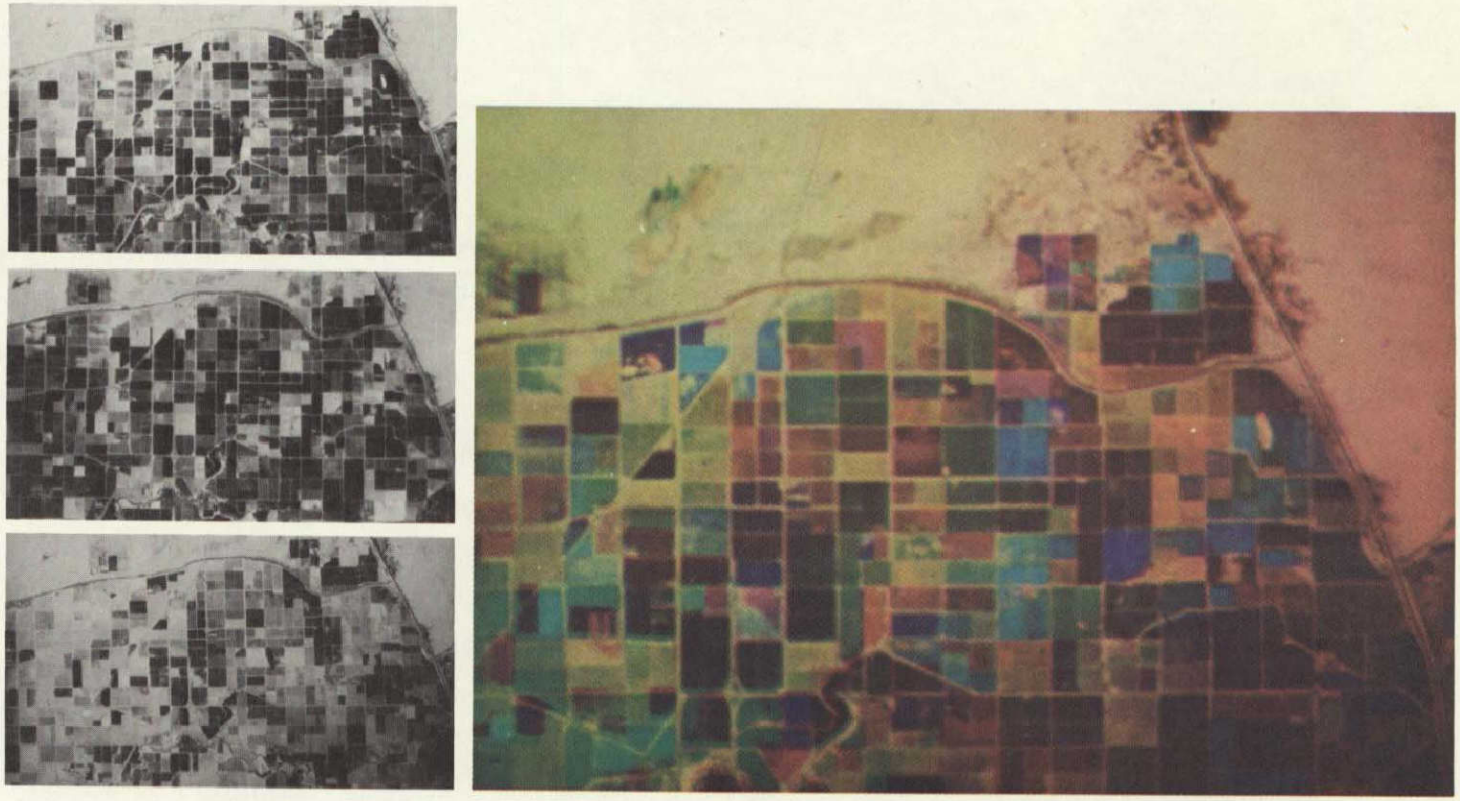

Figure 18. Imperial Valley Test Area. Left column: Three sequential black-and-white (Pan 25A) aerial photos, taken on High Flight missions in March, May and August, respectively. Right photo: FRSL optically combined photo made by simultaneously projecting these three black-and-white photos through red, blue and green filters, respectively. In this color composite, red-orange fields are row crops (mainly lettuce) which have been harvested at some time during this period; green-blue fields are continuous cover crops (mainly alfalfa) which have been mowed at intervals during this period; yellow-chartreuse fields are bare and have been bare (fallow) throughout this period; and black fields are mainly sugar beets which have provided a vegetation cover continuously throughout this period. Enhanced photo courtesy of Jerry D. Lent, Forestry Remote Sensing Laboratory Univ. of Calif.

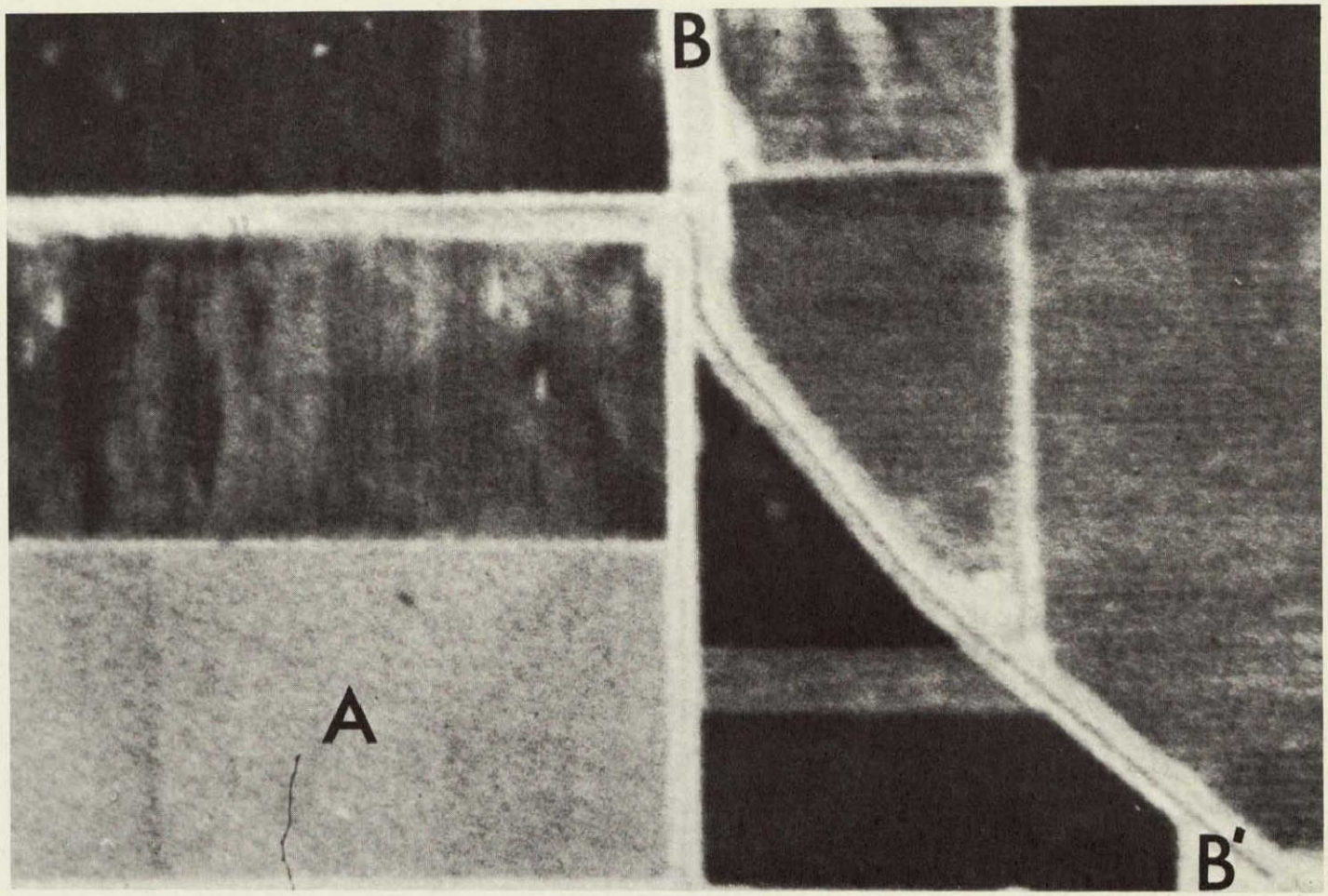

Figure 19. Imperial Valley Test Site. Enlargement of part of the Pan-25A high flight photo shown in Figure 14. Compare with the "print-out" appearing in Figures 20 and 21 which were made by (1) scanning a transparency of this photo with a scanning microdensitometer; (2) recording in analogue form on magnetic tape the brightness values thus obtained, scan line-by-scan line and resolution element-by-resolution element; (3) developing a simple "computer program" which would govern the print-out symbol for each brightness value; and (4) running the magnetic tape through the computer thus programmed.

Figure 20. Computer print-out that was initially obtained by the process described in the caption to Figure 19. Interaction between the human and the machine, as described in the text, permits a more suitable coding of brightness values than the above. A second print-out, obtained after such interaction appears in Figure 21.

Courtesy of Jerry D. Lent, FRSL, U.C. Berkeley, Calif.

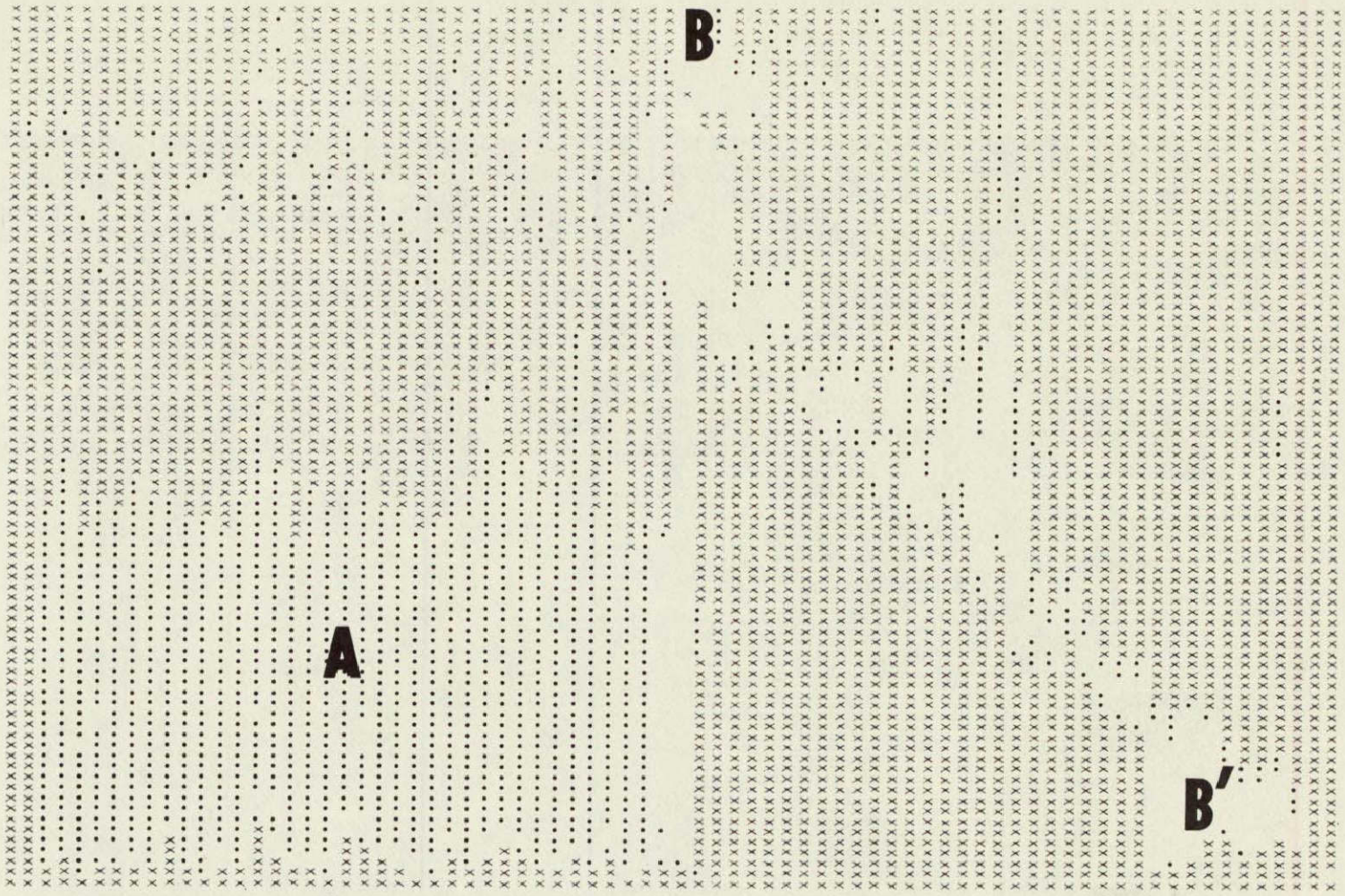

Figure 21. Computer print-out that was obtained after inspection of Figure 20 and the drafting of a new computer program that would cause all portions of a fallow field, such as "A" to be registered as dots; all bare soil as blanks; and "everything else" with the symbol "X". The large symbols "A", "B" and "B'" appearing on this print-out, and also on Figure 20 have been added to facilitate tie-in with the similarly annotated spots on Figure 19.

Courtesy of Jerry D. Lent, FRSL, U.C. Berkeley, Calif.

Figure 22. Thermal infrared imagery of the Imperial Valley Test Site. This record was obtained through use of an optical mechanical scanner that was flown over the test site in March, 1969 at the time of the Apollo 9 overflight. For some crop types and field conditions a more complete and reliable "tone signature" is obtained by using this imagery in conjunction with multiband photography such as that shown in Figures 14-15. (Imagery courtesy of Infrared and Optical Sciences Laboratory, University of Michigan.)

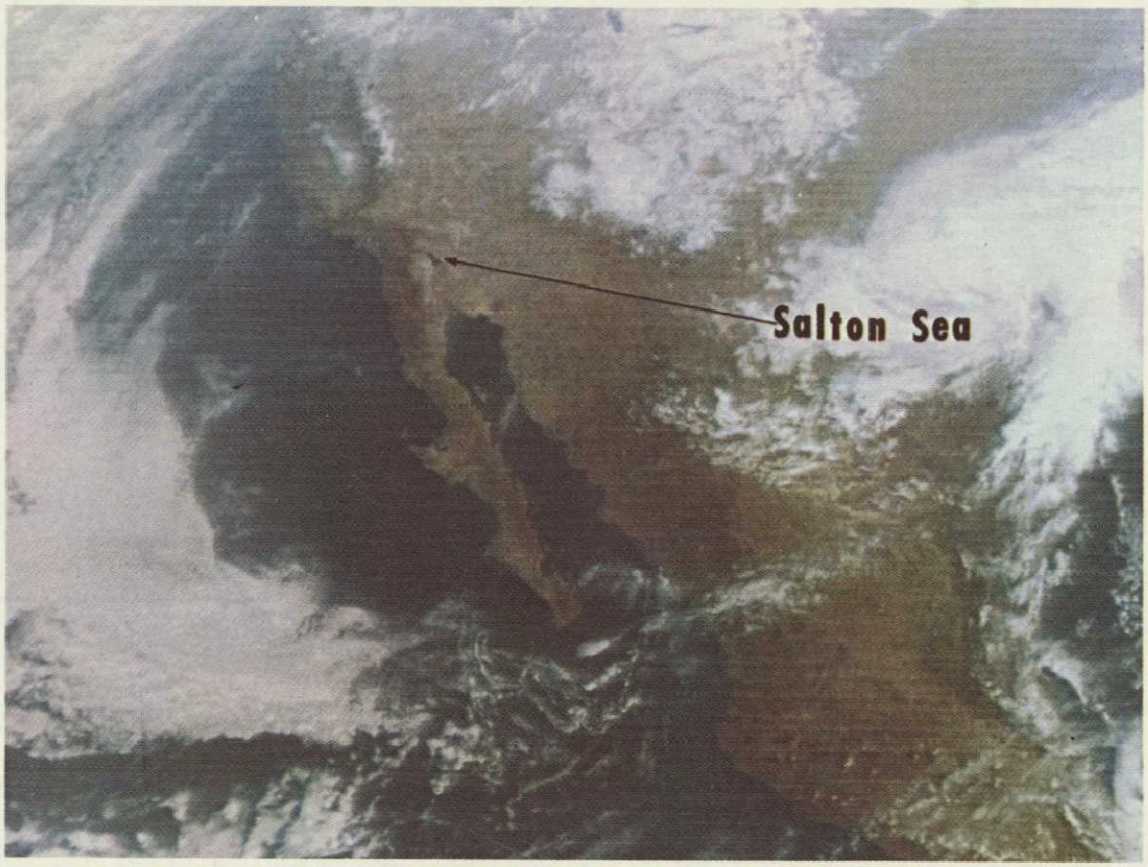

Figure 23. Imperial Valley-Salton Sea Area as imaged from an earth-synchronous (geostationary) satellite from an altitude of approximately 22,300 statute miles, while looking obliquely through two atmospheres at an angle of approximately 50 degrees from the vertical. From the black-and-white multiband record televised back to earth it was possible to construct a color composite by an "additive color" process similar to that used in the optical combiner of Figure 3. While such a system in its present form is resolution-limited (a 15" focal-length, 5" aperture spin camera is used) this limitation is being overcome through construction of long focal length, high resolution systems. Because of the geostationary orbit and gyrostabilized mount, image-motion compensations at the instant of exposure will not be required even in the higher resolution system. A "squadron" of such vehicles, properly deployed, could provide continuous year-round stereoscopic full color, multiband coverage during daylight hours (weather permitting) of those portions of the globe in which most of the world's vegetation resource grows and human population resides. As one element in a multiband, multidate, multistage sampling system this type of coverage could be of tremendous value to those who need quick, accurate vegetation inventories periodically in order to manage the world's vegetation resources more intelligently. If the vehicles were placed in an "ecliptic orbit" (i.e. in a plane angled at 23.5 degrees with respect to the equator, instead of in a true geostationary (equatorial) orbit, virtually all of the advantages mentioned above would still pertain and the area brought under surveillance during the summer growing season in the northern hemisphere could be greatly increased, and likewise (6 months later) in the southern hemisphere. Photo courtesy of NASA and U.S. Geologic Survey. For further details about the capabilities of geosynchronous satellites see an article by Alden P. Colvocoresses entitled "Surveying the Earth from the Air" soon to be published in the magazine "Image Technology."

Figure 24. Louisiana-Mississippi Test Area. Infrared Ektachrome photo mosaic made by assembling two overlapping Apollo 9 space photographs that were taken in March 1969 from an altitude of 150 statute miles. The areas outlined are imaged in aerial photos on succeeding pages to indicate the benefits of multistage sampling when making earth resource inventories. Even moderate cloud cover (such as the 10 to 20% found east of the Mississippi River in this mosaic) can greatly reduce the suitability of this photography for resource inventory purposes.

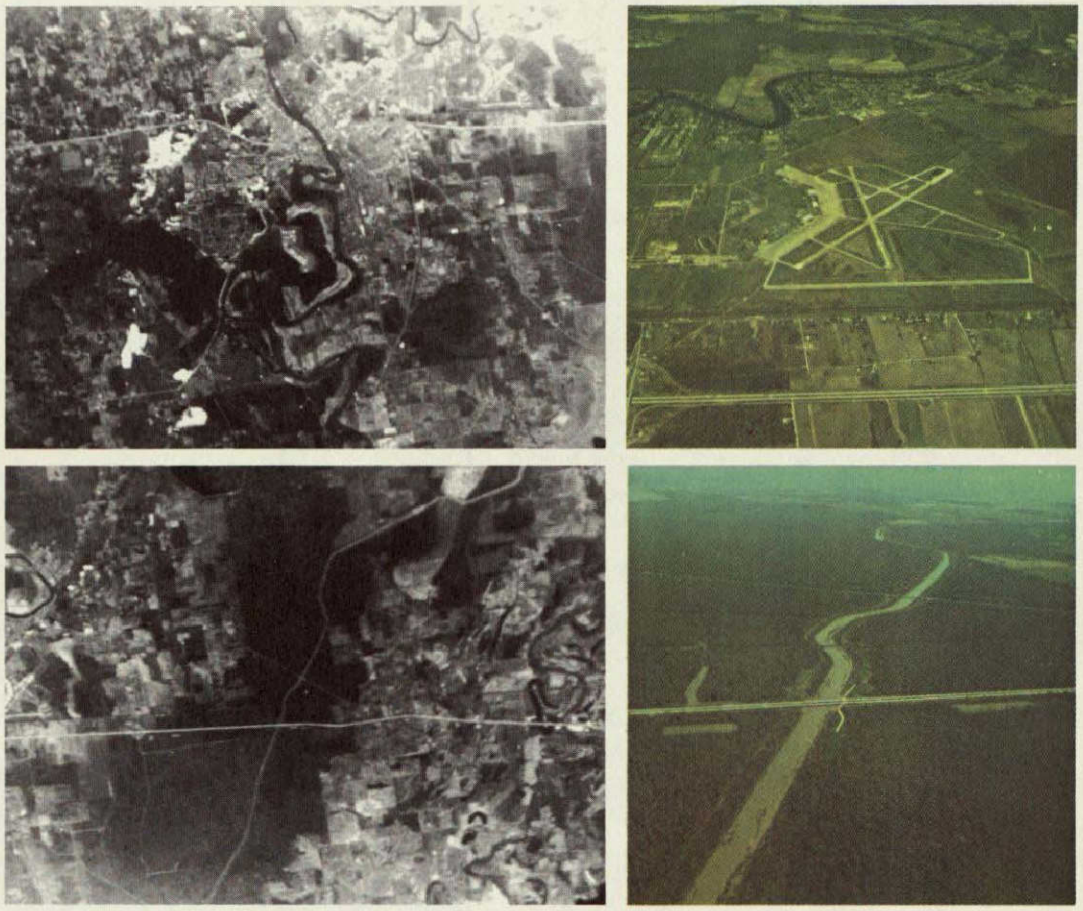

Figure 25. Louisiana-Mississippi Test Area. Top pair: The Pan-25A Apollo 9 space photo on the left is an additional 5X enlargement of the area near Monroe, Louisiana (outlined at "A" in Figure 19). The area comprising the upper right portion of this photo also is imaged in the oblique Ektachrome photo on the right which was taken from the camera station indicated by an arrow. Bottom pair: The Pan-25A Apollo 9 space photo on the left is an additional 5X enlargement of the area east of Monroe, Louisiana, outlined at "B" in Figure 19. The central part of this photo also is imaged in the oblique Infrared Ektachrome photo on the right which was taken from the camera station indicated by an arrow. Note, by comparing these matching photos, how readily one can distinguish roads, airfields, rivers, canals and urban features on space photography and differentiate between agricultural and timberlands as the first "stratification" in a multistage sampling process.

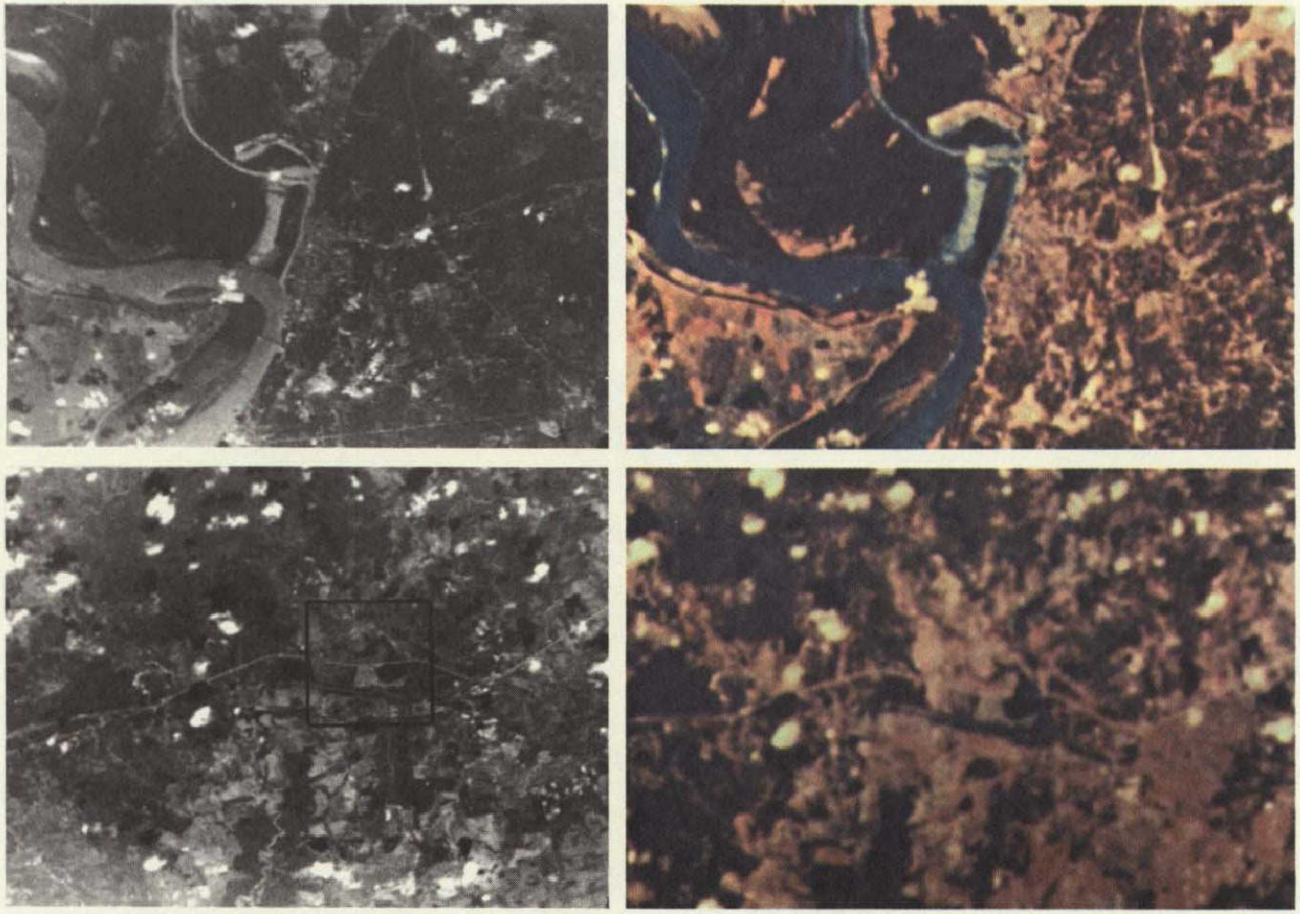

Figure 26. Louisiana-Mississippi Test Area. Top pair: These Pan-25A (left) and Infrared Ektachrome space photos are additional 5X enlargements of the area centered around Vicksburg, Mississippi (outlined at "C" in Figure 19). Note superiority of the Infrared Ektachrome photo for differentiating timberlands from non-timbered areas, despite higher spatial resolution of the Pan-25A photo. Bottom pair: Another matched pair of Pan-25A and Infrared Ektachrome space photos taken by the Apollo 9 astronauts. These photos are additional 5X enlargements of the area east of Vicksburg, Mississippi (outlined at "D" in Figure 19). The square outlined on the left photo is imaged on a large scale aerial photo in Figure 22. The accuracy with which vegetation types and other land use categories could be identified on the space photos shown in Figures 19 through 21 will be found in Table 7.

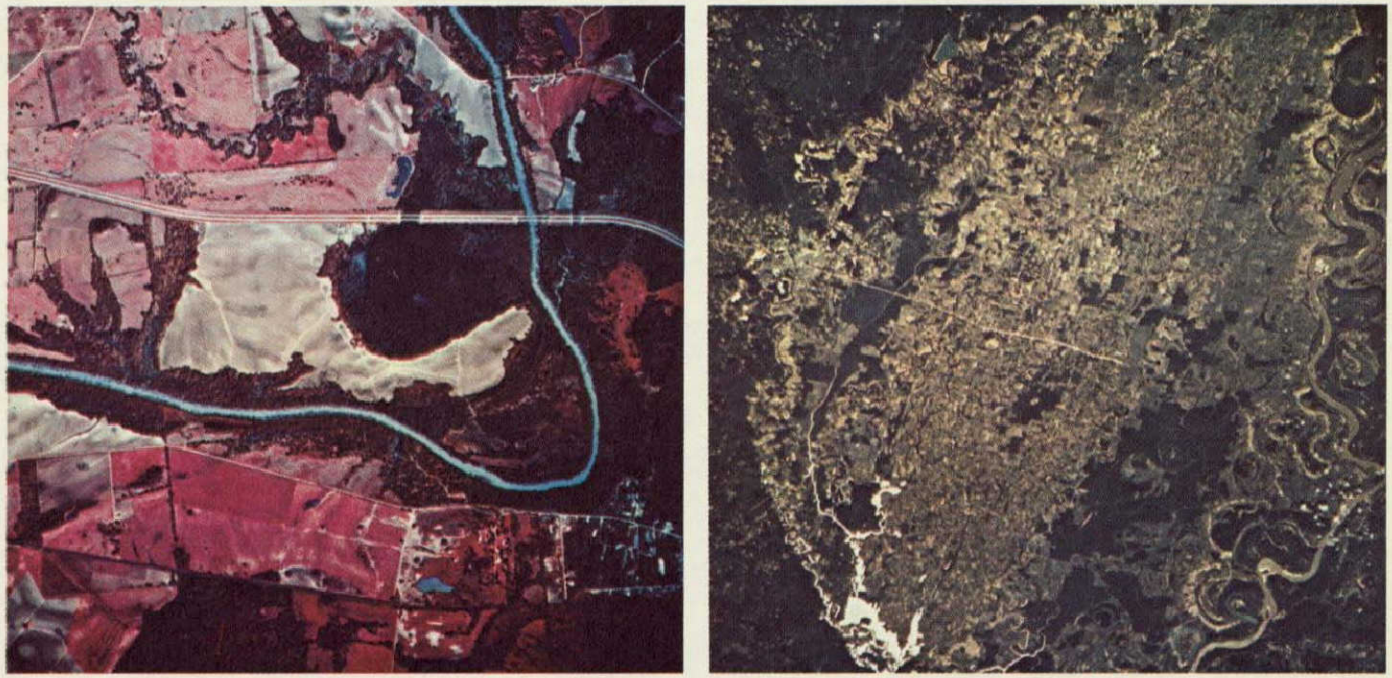

Figure 27. Louisiana-Mississippi Test Area. Left photo: This Infrared Ektachrome aerial photo was taken in March, 1969, approximately at the time of the Apollo 9 overflight and shows the area outlined on the bottom left space photo of Figure 21. In taking this aerial photo, personnel of the NASA-USDA Forestry Remote Sensing Laboratory operated a K-17 camera with 12" focal length at an altitude of 20,000 feet, thereby obtaining a photo scale on the original 9" x 9" transparency of 1/20,000. In the above photo the transparency has been reduced to a scale of 1/40,000. In the area shown here a deciduous forest of bottomland hardwoods is seen to be intermixed with pastures and cultivated lands. The ability to discern individual trees on this photo and identify some of them by species makes such photography complementary to space photography in a multi-stage sampling system as described in the text. Right photo: Ektachrome space photo taken with a hand-held Hasselblad camera by the Apollo 9 astronauts of part of the Louisiana-Mississippi Test Area. (Compare with left half of Figure 19).

Figure 28. Possibilities for detecting loss of vigor in plants, even on photography taken from an earth orbiting spacecraft, are suggested from a study of this conventional panchromatic aerial photograph (scale approximately 1/16,000) of a forested area in Oregon. The nearly circular areas in which vegetation is sparse have diameters up to 700 feet. The pattern suggests infestations of a root-rot fungus, Poria weirii, and field checking has shown the presence of that fungus in the infested areas. However, as in many other situations, a combination of topographic and biotic factors probably accounts for the pattern of low-vigor, low-density timber shown here. (Photo courtesy of John Wear, Remote Sensing Project, U. S. Forest Service).

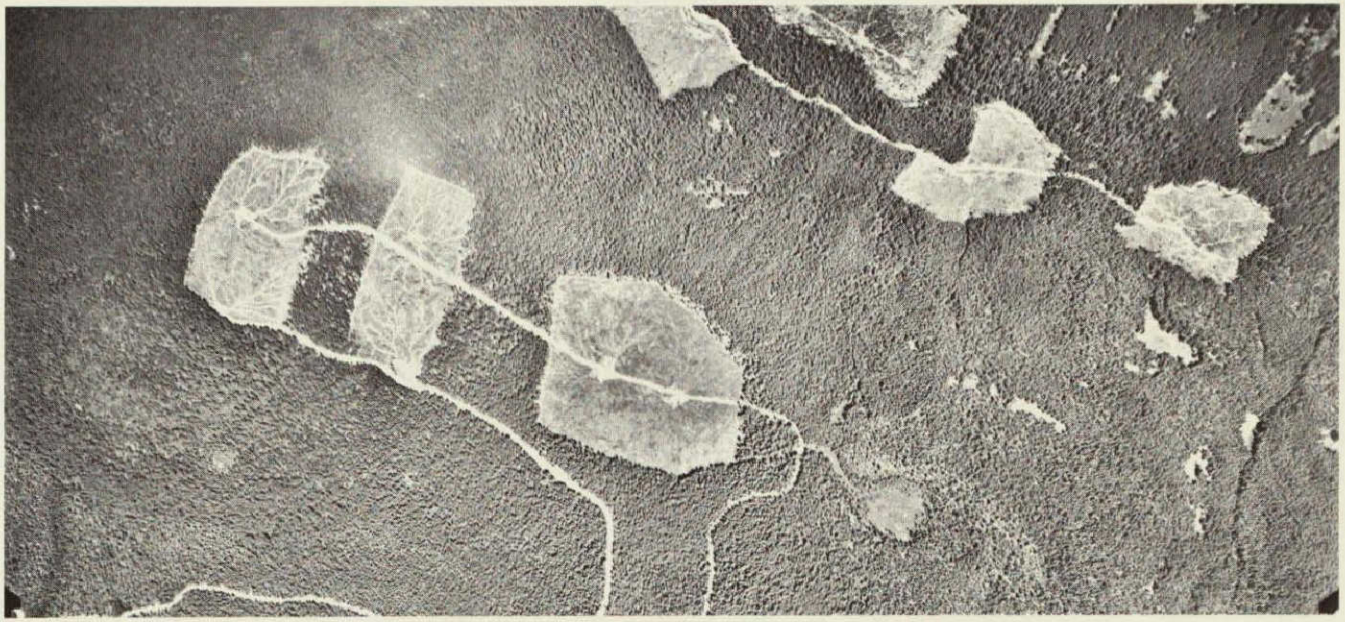

Figure 29. Possibilities for detecting significant changes in vegetation on repetitive photography taken from an earth orbiting spacecraft are suggest from a study of this conventional panchromatic aerial photograph (scale approximately 1/16,000) of a forested area in Oregon. The conspicuous light-toned areas are those in which clear-cutting of the timber has recently taken place. If a space photo revealed only the location and approximate dimensions of such clear-cut areas, the remote sensing information needed to calculate volume of timber, by species, that had been removed probably would thereby have been provided, since recent timber cruises would be available indicating volume by species, just prior to logging, area-by-area, throughout this forest. (Photo courtesy of John Wear, Remote Sensing Project, U. S. Forest Service).

N71-11978
SECTION 19

MULTI-STAGE SAMPLING OF FOREST RESOURCES BY USING SPACE PHOTOGRAPHY

... An Apollo 9 Case Study

Philip G. Langley[1/] Robert C. Aldrich[2/] Robert C. Heller[3/]

Pacific Southwest Forest and Range Experiment Station
Forest Service, U. S. Department of Agriculture
Berkeley, California

Abstract:

The exploration of earth resources from space can lead to the development of a dynamic forest resources information system based on imagery obtained from remote sensors and newly developed sampling techniques. With this in mind, we conducted a pilot timber inventory on 10 million acres of land in Arkansas, Georgia, Louisiana, and Mississippi by using photography taken from the Apollo 9 spacecraft. To increase sampling efficiency, the space photos were used with 1/60,000 scale Polaroid, 1/12,000 scale 70mm, and 1/2,000 scale 70mm color aerial photos in a stratified five-stage probability sampling design. This design yields unbiased estimates that are independent of the quality of the imagery. Sampling errors are, however, inversely related to the quality of the photo data. The best results were obtained on 5 million acres in the Mississippi Valley area, where a 58 percent reduction in sampling error was attributed to information obtained from the Apollo 9 photography. The sampling design can be used to survey agricultural as well as forestry resources from space.

1/ In charge of forest measurement techniques research.

2/ Principal research forester, remote sensing research.

3/ In charge of remote sensing research.

Introduction:

One of the great potential benefits of remote sensing from space is increased ability to inventory and evaluate earth resources. In forestry this potential can be expressed as an opportunity to develop a dynamic resource inventory and information system to provide current statistics needed in formulating forest policy and management plans.

But a resource information system based solely on remote sensing and holding complete, detailed, accurate data for every acre of land over vast areas is not now feasible for several reasons. First, earth resource data obtained from remote sensors do not correlate perfectly with ground conditions, thereby introducing errors into the system. Second, certain detailed resource data can be obtained only on the ground, for example, bole and growth measurements on forest trees. And third, even if complete data were available, not enough computers or storage banks are available in the country to handle this information easily. Therefore, the only feasible method of obtaining detailed resource information, applicable to large land areas, is by means of sample estimates--even when remote sensors are used from space.

The national Forest Survey[4/], conducted by the Forest Service of the U. S. Department of Agriculture already has a continuing inventory program in operation (1). It provides timber volume, growth, and harvest statistics to local and national planners and to Congress. However, the survey is geared to provide estimates on a 5- to 10-year cycle, whereas inventory data are collected on different specified units each year. Hence, when reports are issued they are based on partially outdated information--some by as much as 9 years. At the same time, the increased pace of wood utilization, coupled with the increased pressure on available forest land from other user groups, is making it increasingly difficult just to keep up with the changes in the forest resource picture.

What is needed to ease this situation is a resource inventory and information system based on space-age technology. The system should be able to provide up-to-date estimates at any time quickly and efficiently on a national as well as local basis. Such a system can be structured on sample estimates obtained by means of remote sensing and ground measurements. Each new sample survey should improve some aspect of the information system and, as the information improves, each new survey should become more efficient.

There is no "standard" sampling procedure applicable to all forest inventories using space photographs. The design used in a particular situation should take into account the kinds of population parameters being estimated, the distribution of the population variables used to estimate the parameters, existing information relating to the variables,

[4/] Forest Survey is a branch in the Division of Forest Economics and Marketing Research, Forest Service, U. S. Department of Agriculture, Washington, D. C.. The Forest Survey was authorized by the McSweeney-McNary Forest Research Act of May 22, 1928.

and the optimal allocation of funds available for the survey. In forest sampling, however, even a cursory inspection of space photographs strongly suggests that their use in an inventory calls for some form of multi-stage sample design. If feasible, the design should take advantage of additional information that may become available at each stage.

Two years ago, we began developing new multi-stage sampling theories, using the additional information available at each stage, in conjunction with timber mortality surveys using remote sensing[5/]. During these surveys, it became increasingly obvious that some combination of small-scale and large-scale imagery would be the ideal solution to several kinds of forest surveys, from intensive management plan inventories to extensive forest surveys. What finally evolved was the application of a theory developed for the mortality surveys to general forest surveys involving more than one photo scale.

The general design developed was multi-stage sampling with arbitrary probabilities of selection at every stage. The sampling probabilities are formulated from the additional information available at each stage by virtue of the increasingly finer resolution of remote sensory imagery. At the last stage, measurements are obtained on the ground. These ground measurements are entered in the sampling formula to obtain estimates applicable to the entire area of interest. Usually, the sampling probabilities are proportional to predictions made by interpreting the imagery unit by unit. It is hoped that these predictions are highly correlated to the variables of interest. For example, tree height and crown diameter as measured on photographs are highly correlated to tree volume as measured on the ground. However, the prediction could relate as well to number of trees or to area of commercial forest land. In agricultural surveys, the predictions could relate to such things as bushels of wheat or acres of alfalfa.

In probability sampling, the estimates are unbiased no matter what the degree of correlation is between the predictions and the variables. However, zero correlation is analagous to sampling with equal probabilities, and negative correlation results in unreliable estimates. That is, the estimates have a high sampling error--even though they are unbiased. High positive correlation, on the other hand, leads to very precise estimates--even with small sample sizes. In fact, perfect predictions made from remote sensor data lead to a sampling error of zero, and only one ground observation is needed to establish the level of the estimate. Of course, this utopia is never the case, and several ground observations are needed to obtain reliable estimates. The trick is to design the sampling formula to fit all the conditions of the problem at hand to obtain precise estimates at minimum cost.

5/ Langley, P. G. 1968. Multi-stage variable probability sampling--theory with applications in estimating tree mortality. (unpublished manuscript)

The Apollo 9 Forest Inventory Study:

The Apollo 9 multi-spectral photography mission (SO 65) provided the opportunity to try out our multi-stage sampling theory using space photography. In this study, we were not interested in what was discernible here and there on the space photos. Instead, we were interested in determining the potential usefulness of space photos in an operational environment where the observations were drawn at random. The main question we set out to answer was, "What contribution can the information obtainable from the space photos make toward reducing the sampling error of a timber inventory?" A secondary question was, "What is an effective mechanism for utilizing support aerial photography in controlling the variation within relatively large primary sampling units delineated on space photos?"

The remainder of this paper describes a pilot timber inventory conducted by the authors with the cooperation of field personnel from the Southern and Southeastern Forest Experiment Station, U. S. Forest Service. The survey area encompassed 10 million acres of land in Louisiana, Mississippi, Arkansas, and Georgia photographed from the Apollo 9 spacecraft.

The Apollo 9 Photography:

On April 3, 1969, film copies of the Apollo 9 photography mission (SO 65) were obtained from the NASA Manned Spacecraft Center (MSC) at Houston. It was not feasible to utilize all the film-filter combinations provided by the multi-band photography because doing so would require techniques for which no adequate data were available for use in this study. Therefore, we decided to concentrate on the infrared color imagery which we considered to be the best for our purpose. Fortunately, one of us, (R. C. Aldrich, who interpreted the space imagery) had extensive experience with forestry applications of infrared color photography with forest surveys in the Southeastern United States.

The first step in the inventory was to determine the broad characteristics of the forest population by examining the space photos. By referring to Apollo 9 frame No. 3740 (fig. 1) of the Mississippi Valley area, we can see a sharp line of demarkation between areas containing upland pine and hardwood and those containing bottomland and upland hardwood, but with no significant amounts of pine. This distinction suggests that stratifying by these two categories may significantly lower the sampling error.

Next, we considered the spatial distribution of the forest population as viewed from space. In the upland pine stratum, we have a fairly homogeneous mass of forested area. In the bottomland and upland hardwood stratum, there exists a more clustered distribution of relatively small woodlots. These two different patterns suggest a different sampling approach for each. However, since we knew little about the distribution of trees within the forested areas, we decided to partition the entire photograph into squares approximately 4 miles on a side, each square containing about 10, 240 acres; then attempt to minimize the within-unit variation with subsequent aerial photointerpretation. These 4- by 4-mile

squares constituted the population from which our primary sampling units were selected. With units this large, we were able to satisfy three objectives: (1) the units were readily identifiable from an aircraft for rephotographing at a larger scale; (2) they were large enough so that a meaningful prediction could be made as to the relative amount of timber volume contained in each unit if, indeed, such a prediction could be made given our limited information base; and (3) they were large enough that the between-unit variation in average timber volume per acre of forest land could be relatively low within strata. The success of the study depended on these three objectives being met.

After delineating the population units on the space photos, each square was examined through a Bausch and Lomb Zoom 70 stereoscope under 7.5 x magnification (fig. 2). From this examination, the interpreter estimated the proportion of each square occupied by forest land (fig. 3). This proportion was used to predict the relative timber volume in the square. The contention was that, on areas of this size, forest area and timber volume were highly correlated.

After predictions were made on all the squares, a primary sample was drawn at random with probability proportional to the prediction. Five squares were selected in the Mississippi Valley area and five in the Georgia area.

The Support Aerial Photography:

Between April 15 and April 24, 1969 the authors, in an Aero Commander 500B assigned to the Remote Sensing Research Project at the Pacific Southwest Forest and Range Experiment Station, Berkeley, California, obtained needed support photography on each of the 10 primary sampling units selected for the inventory. The camera package consisted of a Crown Graphic camera with a Polaroid back and two Maurer KB-8 70mm cameras mounted in a single frame (fig. 4).

The first aircraft imagery obtained over the primary sample units consisted of 1/60,000 scale photographs taken on Polaroid film through a Wratten 15 filter (fig. 5). The purpose of using Polaroid was to obtain and interpret the imagery while still airborne. The scale was chosen so that the entire sample square would be covered by the 5-inch film format in one pass. After obtaining the Polaroid photography but while still airborne, we prepared an aerial mosaic of the area and superimposed a strip grid partitioning the entire 4- by 4-mile square into sub-sampling units (fig. 6). The strip subunits were of such a dimension that selected ones could be rephotographed in one pass at a scale of 1/12,000 with 70mm photography.

Immediately after the Polaroid mosaic was prepared, each strip was examined and a new prediction was made as to the relative quantity of timber contained in each. The forest information contained on the 1/60,000 scale photos was sufficiently detailed as to allow the prediction of timber volumes needed in selecting a sample of strips for the following stage. At the same time, the photos were not so detailed as to hinder

the interpreter in his rapid appraisal of the imagery. The new information was used to determine sampling probabilities by which 2 strips were selected in each square. A hand-operated adding machine and a table of random numbers were all that were needed to make the selections with probability proportional to our predicted timber volumes.

The selected strips were marked on the Polaroid mosaic, which was then given to the pilot to use as a flight map for the next stage. The two selected strips were rephotographed with the two 70mm cameras. One camera, equipped with a 1-1/2-inch lens, covered the entire strip at a scale of 1/12,000. The other camera, equipped with a 9-inch lens, provided a sample of 1/2,000 scale color photographs simultaneously (fig. 7). The 1/2,000 scale photos consisted of a systematic sample with a random start taken down the center of the strip.

The white square in figure 6 indicates the position of one of the 1/12,000 scale 70mm photographs (fig. 8). The black square on the 1/12,000 scale photo indicates the location of a sample 1/2,000 scale color photograph (fig. 9).

Back in the laboratory, the strip boundaries were delineated on a mosaic of the 1/12,000 scale photographs. Then, the photo coordinates of these boundaries were digitized at 0.01-inch intervals using a Bendix datagrid digitizer (fig. 10). From these data, the strip areas were computed. The proportion of the strip covered by the 1/2,000 scale photos was computed from the number of 1/2,000 scale photographs obtained in a strip and the area of the strip. The inverse of this proportion was used to expand the timber volume estimates from the cluster to the strip level.

The 1/2,000 scale clusters of color photographs constituted stage three in our survey design. They were obtained in triplets so as to provide stereoscopic coverage of the center frame. The number of triplets ranged from 13 to 20 per strip, and 337 triplets were obtained on all sample strips.

The center photograph of each triplet was partitioned into four square plots, each plot being about 0.6 acre in the Mississippi Valley area and 0.8 acre in the Georgia area (fig. 9). These size plots are convenient for locating and measuring on the ground.

The Ground Plots:

Each of these large scale photoplots was examined stereoscopically and estimates were made as to stand height determined by means of a parallax wedge described by Wert and Myhre (3), crown coverage determined by counting dots on a grid, and crown diameter. Separate estimates were made for pine and hardwood. From these estimates, timber volumes were predicted on all plots by using an aerial photo volume table (2). At this resolution level, it was easy to eliminate from further consideration those plots which fell on non-forest land or which contained no timber volume. From this information, one plot per strip was selected for

measurement on the ground. Again, the selection probabilities were proportional to predicted timber volumes at that level.

For each plot drawn, a packet of photographs was made up containing each scale of photography covering the plot. This packet was given to the field crew to aid in locating the plots on the ground. Little difficulty was encountered in locating the field plots.

After a field plot was located and laid out on the ground, each tree's diameter was measured and recorded along with species. The diameters were used to predict each tree's volume from a volume table but modified by the timber cruiser's ability to adjust for defects and deformities in the tree. By using these predictions, four to six trees were selected on which bole measurements were obtained by means of a precision optical dendrometer (fig. 11). The wood volumes of these sample trees were later computed from the dendrometer measurements.

The Sampling Formula:

To obtain timber volume estimates applicable to the entire survey area, the measured tree volumes are expanded back through the sampling formula. In the Apollo 9 study, the estimated timber volume in each stratum was

$$v = \frac{1}{m}\sum^{m}\frac{1}{p_I n_i}\sum^{n_i}\frac{1}{p_j}\frac{A_j}{a_c}\frac{1}{p_p t_p}\sum^{t_p}\frac{v_k}{p_k}$$

in which

v_k is the measured volume of the k^{th} sample tree on a selected ground plot,
p_k is the probability of selecting the k^{th} sample tree
p_p is the probability of selecting the p^{th} plot from the cluster of plots delineated on the 1/2,000 scale 70mm photos in a strip,
p_j is the probability of selecting the j^{th} sample strip in a sample 4- by 4-mile square area,
p_I is the probability of selecting the i^{th} sample square,
a_c is the area covered by the cluster of 1/2,000 scale 70mm photographs within a strip,
A_j is the total area of the j^{th} sample strip,
t_p is the number of sample trees measured on the p^{th} plot,
n_i is the number of sample strips in the i^{th} 4- by 4-mile square, and
m is the number of 4- by 4-mile squares included in the primary sample.

Results:

The best results were obtained on 5 million acres covered by the Apollo 9 photographs in Louisiana, Mississippi, and Arkansas. With only ten ground plots, constituting a sampling fraction one to .8 million in terms of area, we obtained an estimate of 2.225 billion gross cubic feet

of timber, with an estimated sampling error of only 13.0%. Half of this error was attributable to inadequate tree volume tables we used on the ground to correlate with the dendrometer measurements.

The gain in the sampling error we achieved by using information from the space photos was quite substantial. If we had used the same sampling plan--but with equal probabilities at the first stage and without the benefit of stratification--we would have incurred a sampling error of 30.7%. Stratifying on the space photos brought the error down to 22.5%. Then, by using probability sampling in selecting the primary sample, the error came down to 13%. Hence, a 58% reduction in the sampling error (from 30.7 to 13.0) was directly attributable to the information gleaned from the Apollo 9 photos.

In the Georgia area, we were less fortunate. So far, we have been unable to show a gain in the sampling error as a result of information on the space photos. This is due to low correlation between our predicted volumes on the primary sample units and our estimated volumes on corresponding units obtained by subsampling on the ground. However, now that we have some ground data, we can attempt to determine the cause of the problem and improve our prediction techniques.

Discussion and a Look to the ERTS:

While we may not have formulated the optimal sample design for the Apollo 9 study, we felt we successfully perceived and dealt with the majority of the problems that might have arisen operationally as well as statistically. As techniques are developed for extracting better information from multi-spectral data, by either manual or automatic methods, we will be able to better inventory vast forested areas from space rapidly with a minimum of ground work.

Looking ahead to the time when the Earth Resources Technology Satellite will be launched, we would like to suggest the following modus operandi for a first forestry and agriculture resource information system based on remote sensing from space:

1. Multi-spectral data telemetered to earth from the satellite is processed by computer and immediately converted into condensed tables of predictions relating to variables of interest to national and local management planners. These predictions could be associated with land units of some arbitrary, but not necessarily equal, size. This information base is continually updated as the satellite obtains new data over a given area.

2. When specific information is needed about certain resources, a decision is made as to the allowable error of the estimates to be obtained.

3. Using the information stored in the system, a sample of primary units is drawn according to an appropriate set of selection

probabilities. The sample size is determined by the allowable error and the quality of the information currently in the system that relates to the variables of interest. The information on some variables will be more reliable than on others.

4. An aircraft, bearing a full complement of remote sensors, or simple cameras, is dispatched to the sample areas and new, higher resolution data are obtained. This could be done in one or more stages. If more than one stage is needed, an on-board image analyzer and computer could be programmed to determine the sub-sampling probabilities from the imagery just obtained and select the sample for the next stage.

5. At the last aerial stage, a small sample of ground plots is selected for ground measurements.

6. The ground observations are entered into the sampling formula to obtain the needed estimates applicable to the area of interest.

7. These final estimates serve to improve the statistical models used in assigning the original resource predictions from satellite data. At the same time, the data base relating to the parameters for which new estimates have just been obtained is improved.

Taking this approach, a workable resource information system for forestry and agriculture could be made ready to utilize information immediately upon its receipt from the Earth Resources Technology Satellite and begin supplying needed answers to questions concerning the status of the resource base. In time, the data base will improve in precision to the point where a minimum of aircraft and ground data are needed to answer specific questions asked by management planners and policy makers. When that point is reached, the system could be queried and answers returned almost instantaneously as to the quantity and distribution of agricultural and forest resources in any part of the country.

Finally, there are other advantages to an approach of this kind to a resources information system. One that should be mentioned is that information about specific variables is improved as the need arises. Hence, an exact definition of the make-up and accuracy of the data base is not essential in the beginning. The data base will be improved as the system is used operationally. Another feature that should be mentioned is that various users have the opportunity to participate at a level of sophistication that suits them. They can obtain subsamples using multi-channel scanners or simple cameras. Furthermore, they can carry out their own field work and handle their own data processing for the aerial and ground stages of their surveys. These qualities should appeal to other countries who wish to share in the ERTS program.

LITERATURE CITED

1. Aldrich, R.C. 1968. Remote sensing and the forest survey--present applications, research, and a look at the future. Proc. Fifth Symp. on Remote Sensing of Environ. Univ. Mich 968:357-372, Illus.

2. Avery, Gene 1958. Composite aerial volume table for southern pine and hardwoods. J. Forestry 56:741-745.

3. Wert, S.L., and Myhre, R.J. 1967. Wedge measures parallax separations on large-scale 70mm aerial photographs. U.S. Forest Serv. Res. Note PSW-142, Illus. Pacific SW. Forest & Range Exp. Sta., Berkeley, Calif.

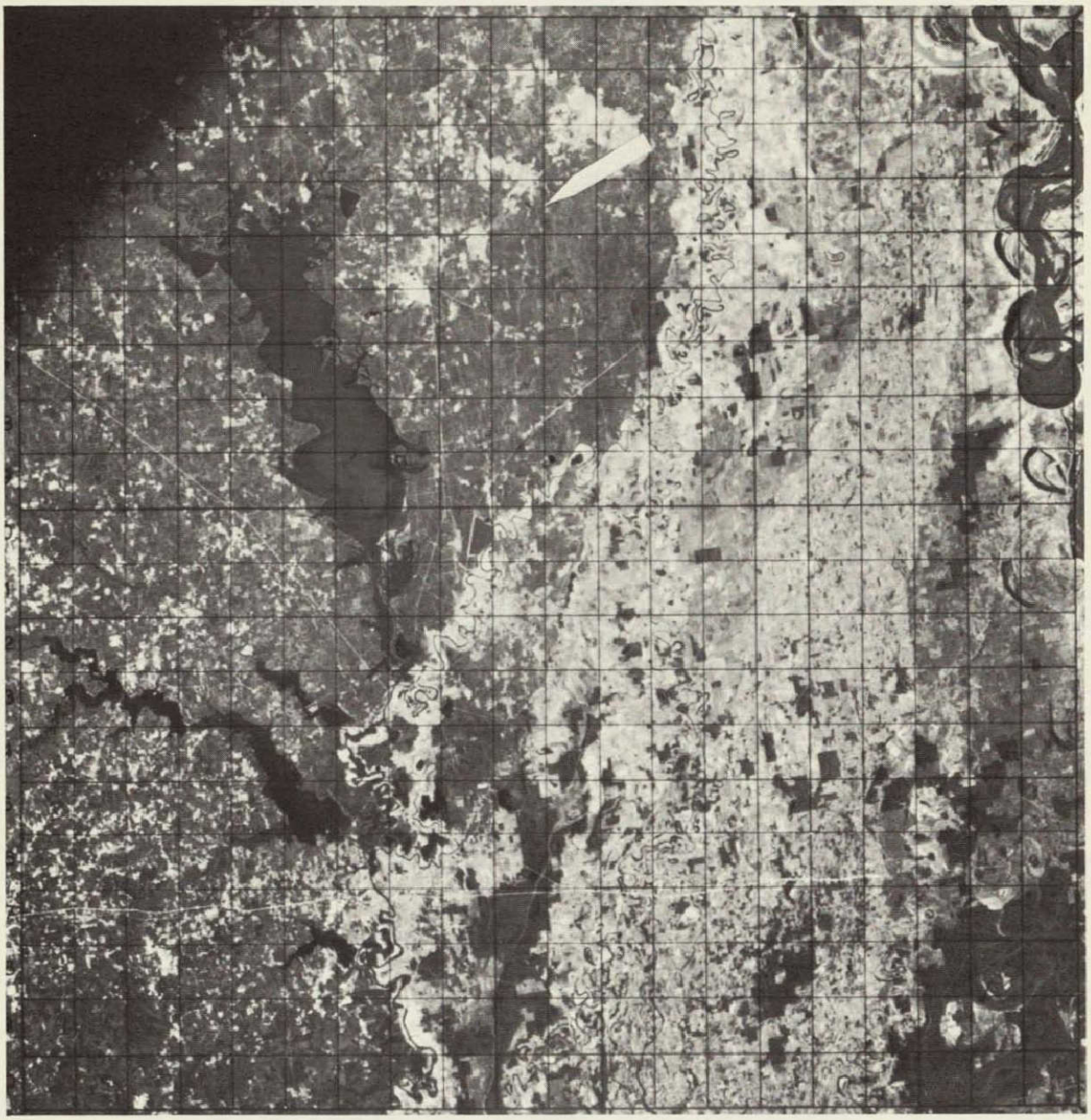

Figure 19-1.- A reproduction made from Apollo 9 infrared color frame 3740 enlarged approximately 2-1/2 times. The grid of 400 four- by four-mile squares was used to predict timber volumes for the first level of inventory information.

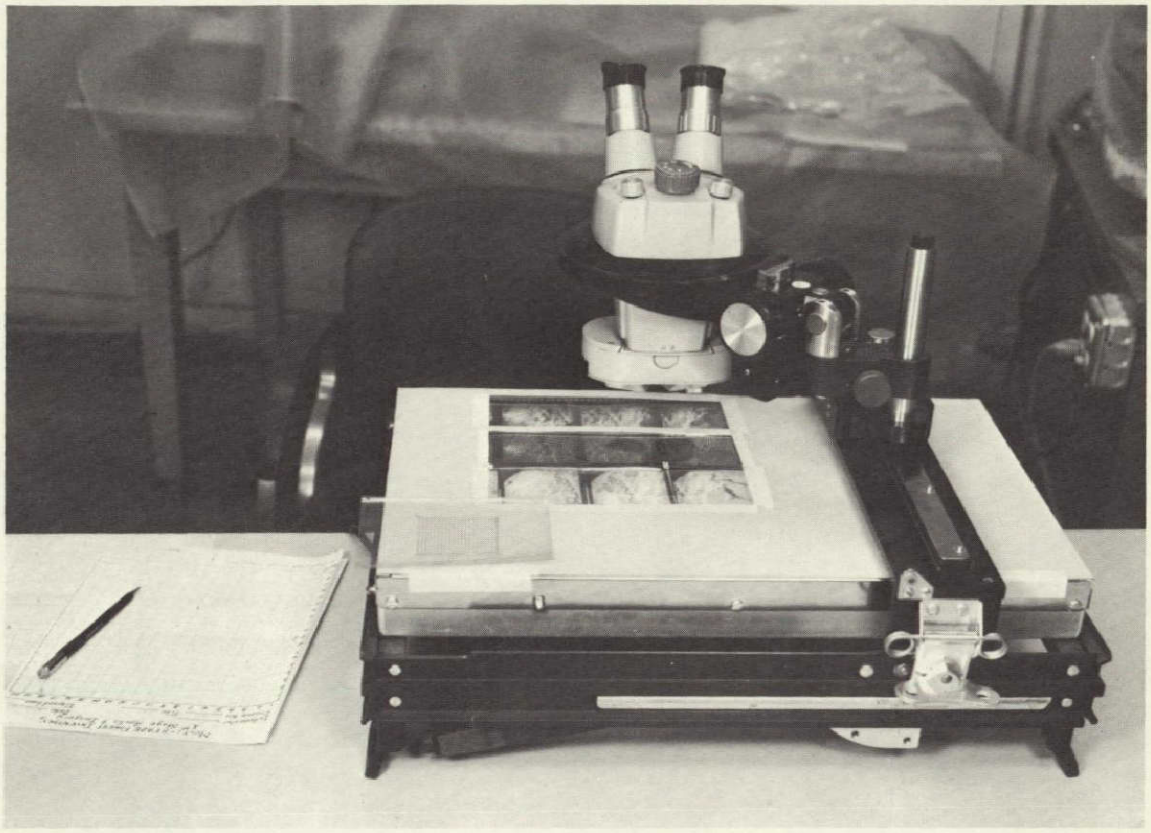

Figure 19-2.- Apollo 9 infrared color photographs were interpreted with the aid of a Bausch and Lomb Zoom 70 Stereoscope with 7.5 x magnification. Apollo 9 infrared Aerographic (89B filter) and Panchromatic (25A filter) films were also used to aid in separating forest from other land uses.

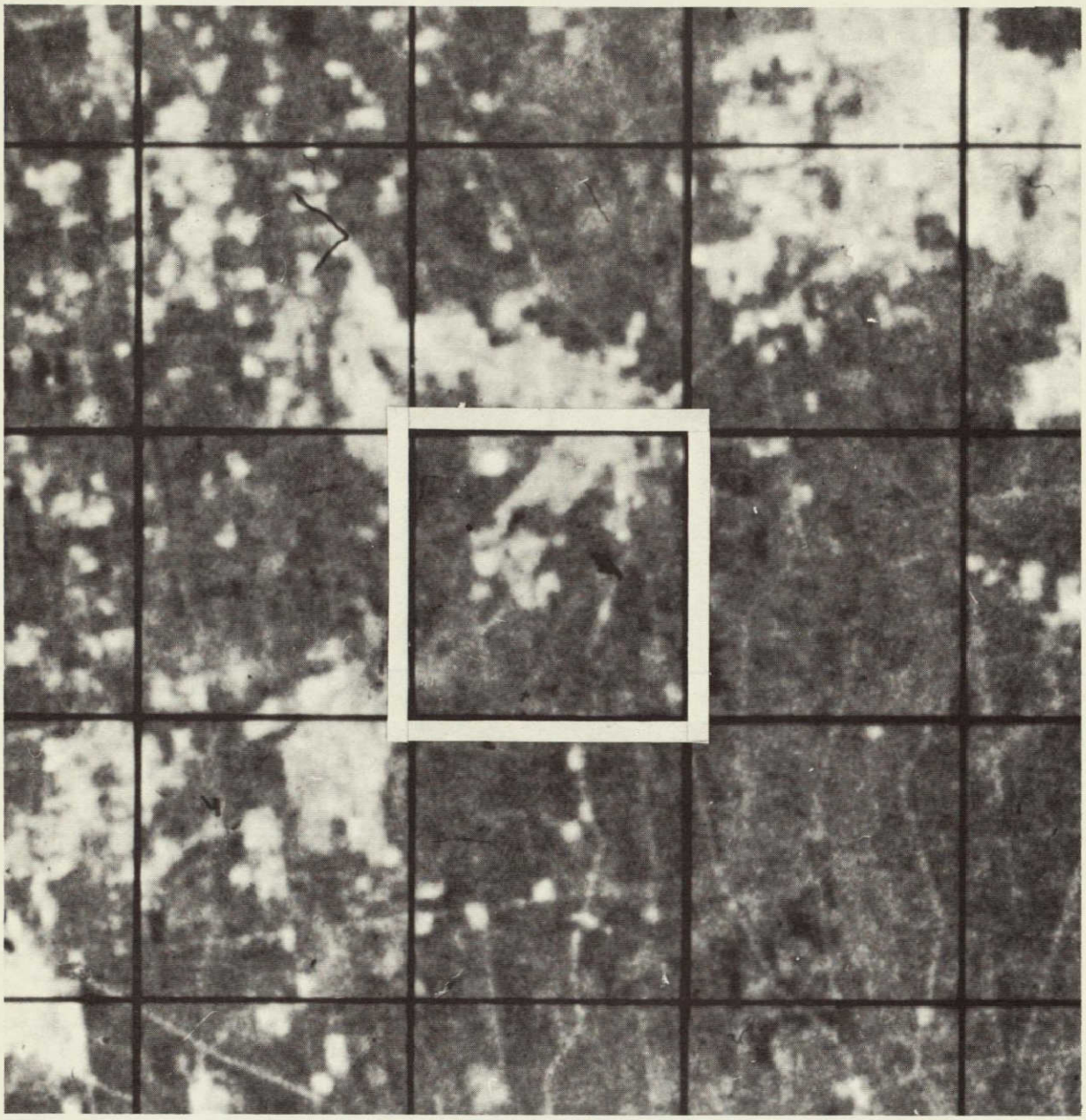

Figure 19-3.- Each 4- by 4-mile square within the Apollo 9 frame was examined and the proportion of the area occupied by forest land was estimated.

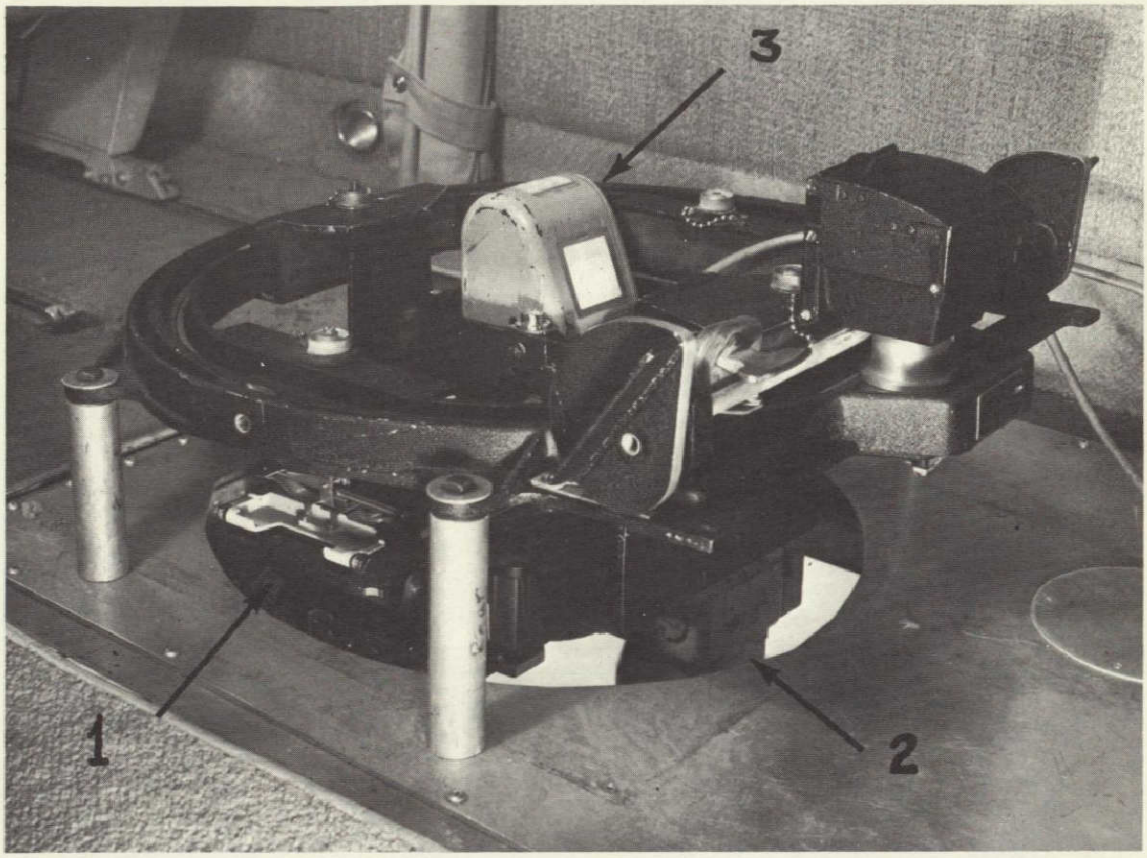

Figure 19-4.- This aerial camera set-up was used to obtain support photography for primary sampling units selected from the space photograph. Included is a (1) Crown Graphic with Polaroid back, (2) a J. A. Maurer KB-8 70mm camera with a 1-1/2 inch lens and (3) a J. A. Maurer KB-8 with a 9-inch lens.

Figure 19-5.- Polaroid photography (1/60,000) was taken over each primary sampling unit selected for the first stage in the multi-stage sample. The mosaic shown is for the 4- by 4-mile square indicated by the arrow on the space photo in fig. 1.

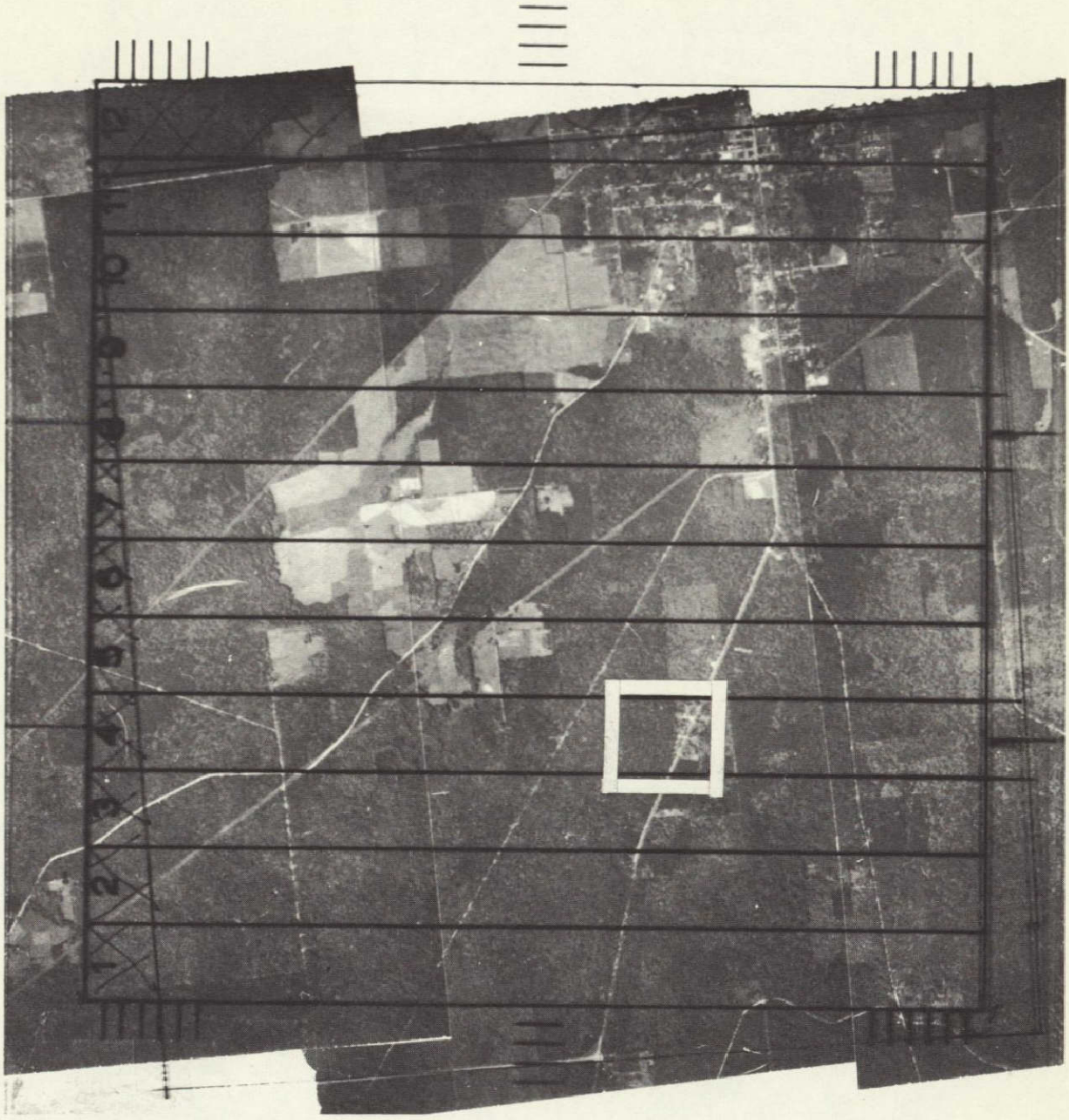

Figure 19-6.- The 4- by 4-mile primary sample covered by the Polaroid mosaic was divided into sub-sampling units by using a transparent strip grid. The area outlined in white indicates the position of the 1/12,000 scale photograph shown in figure 8.

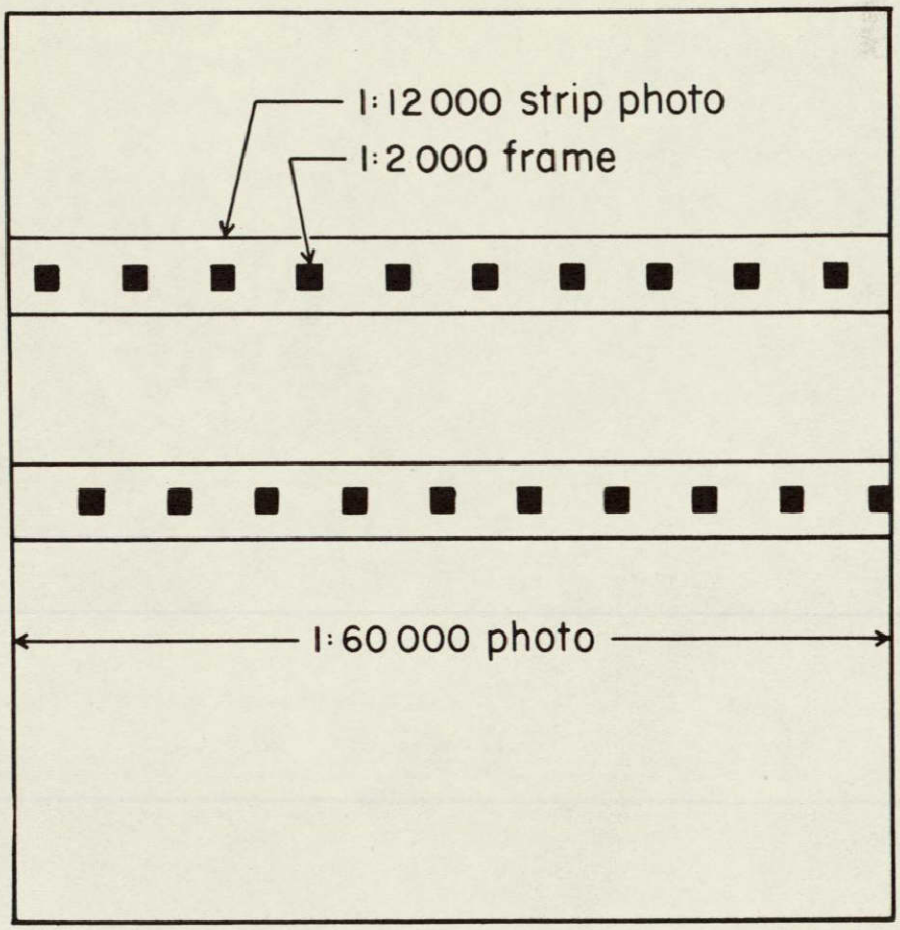

Figure 19-7.- The scaled diagram shows how the two 1/12,000 scale 70-mm photo sample strips and 1/2,000 scale 70-mm color samples are related to each other and to the 1/60,000 scale Polaroid photograph.

Figure 19-8.- An enlarged 1/12,000 scale photograph of the area outlined by the white square in figure 6. The area outlined in black corresponds to the coverage of the 1/2,000 scale photograph in figure 9.

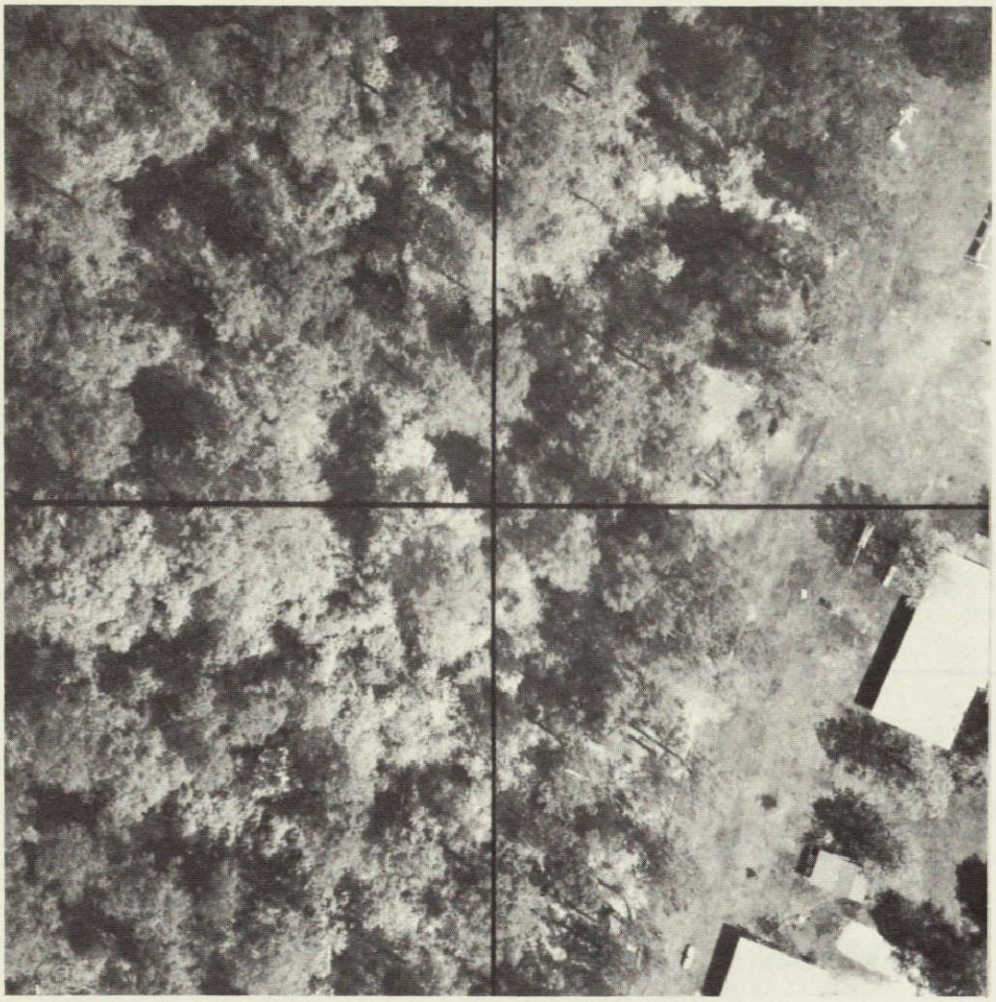

Figure 19-9.- A 1/2,000 scale photograph corresponding to the area outlined in black on the 1/12,000 scale photograph in figure 8. The grid divides the photograph into four sample plots approximately 0.625 acre in size.

Figure 19-10.- Photo coordinates of sample strip boundaries outlined on the 1/12,000 scale photo mosaic were digitized at 0.01 inch-intervals using this Bendix datagrid digitizer.

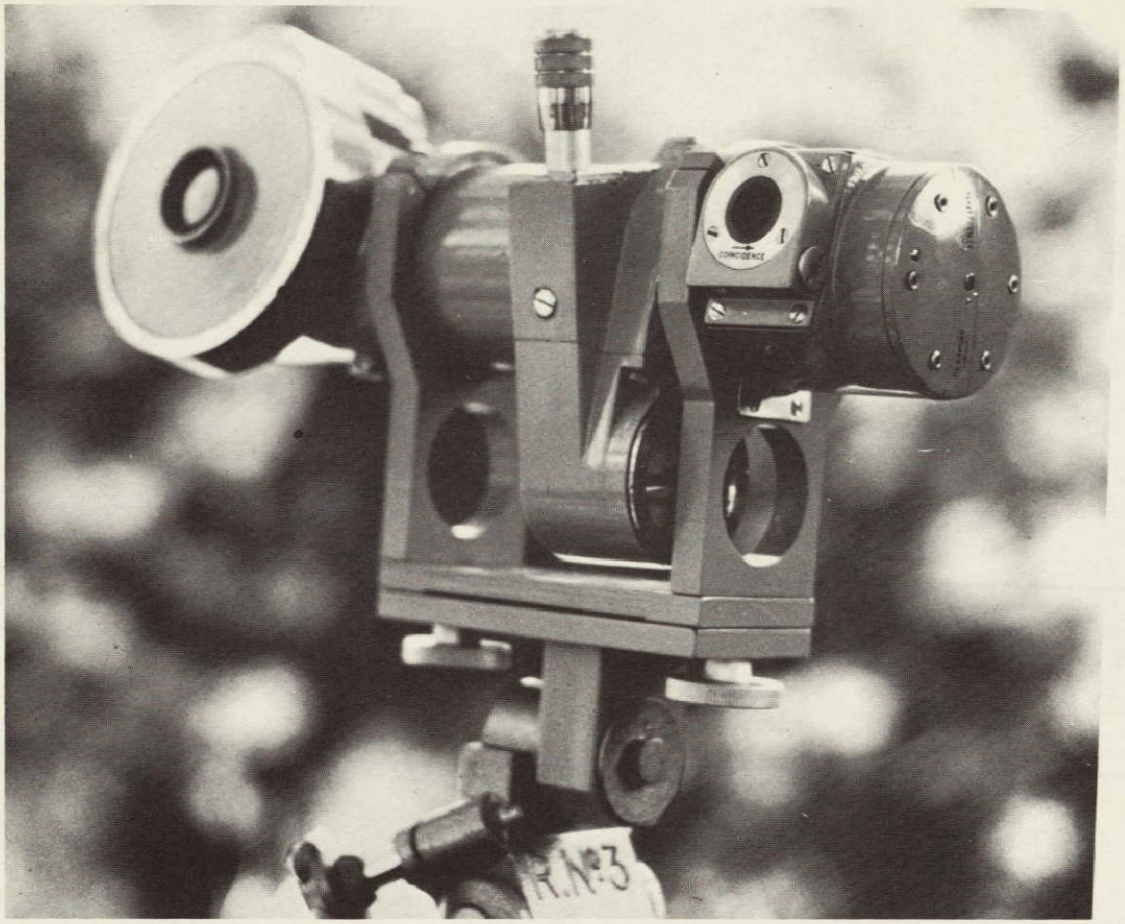

Figure 19-11.- An optical dendrometer was used to make bole measurements on four to six trees on each ground plot.

SECTION 20

RANGE RESOURCE INVENTORY FROM SPACE AND SUPPORTING AIRCRAFT PHOTOGRAPHY

By Charles E. Poulton, Professor of Range Ecology
Richard S. Driscoll, Project Leader
and Barry J. Schrumpf, Graduate Research Assistant
Oregon State University, Corvallis; USDA, USFS, Rocky Mountain Forest and Range Experiment Station, Ft. Collins, Colorado; and Oregon State University, Corvallis; respectively.

INTRODUCTION

In land use and resource management, there are two areas where remote sensing technology and applications are of particular importance. These are in resource inventory and analysis and in the monitoring of responses of the resource to man's manipulation. Indicative of the first of these, a Joint USDA-SAES Task Force on Research Program recently identified and placed in high priority the updating of a national inventory of rangeland resources. They explained in depth the research requirements to develop an operational program for this inventory.[1] This program is particularly compatible with the use of multistage photography whereby refinement of data and informational detail is possible as photo scale becomes larger.

The second application area, resource monitoring, also derives unique potential benefits from each of these stages of remote sensing. The solution of these problems in the measurement and interpretation of vegetation, especially herbland and shrubland vegetation, requires that facts be secured about the population within a sufficiently narrow time span to avoid the natural seasonal changes which always occur as a result of normal vegetational development. Repetitive seasonal coverage is, however, a frequent requirement for ideal data acquisition. This requirement is becoming more specifically defined and more feasible to attain as a result of recent progress and conceptual developments in the Earth Resources Program. Heretofore, nearly all of our measurement techniques

---

[1] A Joint Task Force of the U.S. Department of Agriculture and the State Universities and Land Grant Colleges. 1968. A National Program of Research for Forage, Range and Pasture. Research Program Development and Evaluation Staff, USDA, Washington, D. C. 91 p.

have been based on ground systems which usually require extended time periods for completion. These periods frequently span an interval during which the relative makeup or characteristics of the plant community change. Consequently, a false picture may be presented or the interpretation of data complicated.

Space and aerial photography, as well as other kinds of remotely procured imagery, have a unique characteristic which we in vegetational resource management have only begun to exploit. It captures and preserves a scene at a moment in time by recording the facts about the landscape which no other data gathering system can provide. These facts include such things as distribution, kinds, and amounts of vegetation. Such data are needed for decisions in the use of individual resources and for the integrated management of a number of interrelated resource uses.

Space photographs provide a superior synoptic base upon which, generally, broad-level vegetational classifications and pre-stratification can be made. Such classifications are considered the starting poing for any range resource inventory program. However, due to the combined effect of original photo scales and ground resolution of presently available space photography, these classifications will almost always consist of groupings (sets) of individual ecosystems[1/], each of which requires more detailed analysis than can be handled from space photos alone. Consequently, underflights with aircraft are required to provide photographs from which supporting and more detailed data can be obtained as additional refinement is needed for resource inventory and monitoring.

The purpose of this paper is to review interim results and progress on the use of space and aircraft photography for range resource inventories. Preliminary guidelines on vegetational mapping and a legend concept by which the information can be conveyed to the user are presented. A multistage sampling procedure to obtain data needed for detailed interpretation of space photography is explained. The same procedure enables one to explain the makeup of the vegetational units interpreted from space photography. The potential contribution of multiseasonal photography in photo interpretation is discussed.

The work reported herein was done under Amendment No. 5 to NASA Contract No. R-09-038-002. That done in connection with mapping techniques and development was carried out in the Tucson, Arizona, area by Dr. C. E. Poulton, Principal Investigator, and his associates. Work done on sampling was carried out in the Roswell, New Mexico, area, Dr. R. S. Driscoll, Principal Investigator. Work drawn upon to illustrate the multiseasonal

---

[1] In this discussion, an ecosystem is defined as a unique and fundamental unit of landscapes having analogous environment. Each is defined and characterized by the specific plant community that occupies the areas representing the ecosystem.

photography concept was carried out in the Tucson area by Barry J. Schrumpf and in Colorado by Driscoll.

Others contributing to this research include Robert C. Heller and colleagues of the Forest Remote Sensing Project, Pacific Southwest Forest and Range Experiment Station, who provided various scale aircraft photographs of the Roswell, New Mexico, area. Edmundo Garcia-Moya, working under Poulton's direction, contributed especially to the legend development.

NATIVE VEGETATION MAPPING AND SYMBOLIC LEGENDS

The obvious output to the user of remotely sensed resource data analysis is a map, statistical tables, a narrative report, or a combination of these. Five things are important in realizing full effectiveness in the use of these data:

1) Both the remote sensing system and the interpretive output must be oriented to a specific problem and/or information need statement from a user.

2) Ground truth or image-subject relationships must be understood with meaningful clarity, and interpretation skills must be developed--whether by man, machine, or a combination.

3) Legends must be developed from research into the plant community components and the ecological characteristics and classes represented in the area sensed.

4) All possible information must be interpreted, appropriately confirmed, and labeled with the proper legend symbols.

5) The relevance of the information to practical objectives must be explained and the data appropriately summarized to meet user needs.

Before we consider mapping legend details, it is important to understand one remote sensing principle and three cartographic principles:

Remote Sensing Principle:

> The image or signature of a subject, in our case a vegetational community or an ecosystem, is not a function of ground-truth fact alone but also of both the sensor system and the way it is used.

Depending on scale, resolution, and the characteristics of an imaging system, different ground subjects may not be sensed as individual entities. Their signatures may be integrated and appear to represent a single subject when they, in fact, do not. On the other hand, the system may sense real

differences that are irrelevant to the subject or problem at hand--that is, the system may see too much; and the interpreter then has to develop the skill of overlooking these items and discriminating when it is appropriate to do so and when it is not.

Cartographic Principles:

1) Maps may be drawn of individual, pure image classes (SIMPLE MAPPING UNITS) or of mixtures of image classes (COMPLEX MAPPING UNITS).

2) For Complex Mapping Units, the legend symbolization must denote each component of the delineation (each ecosystem in the set), NOT an average of the characteristics of the set.

3) The legend must convey facts and present characteristics of the thing sensed, not human interpretations of these characteristics.

In expansion of the latter principle, the process of identifying and expressing facts must be carefully separated from explanations or interpretations of the meaning and significance of these facts. Otherwise, the resource inventory data-base will be confounded with current human opinion--only to change as knowledge grows and thus to outdate what would otherwise have been a permanent data-base for decision-making about native vegetation and related resource problems.

Symbolic legends for vegetation and related resource mapping are especially important and useful for: (1) labeling map delineations in a concise and meaningful way; (2) conveying information quickly and easily to users of the maps; (3) providing a reference to the longer descriptive and interpretive or narrative legend that is a part of any completed resource analysis; (4) providing a simple way to relate similar mapping units as it becomes necessary to generalize detailed mapping or to provide cartographic representations of only part of the legend detail on any one map; and (5) providing a concise way to enter large amounts of information into computer storage or summary tables.

A legend for use in photo interpretation of the ecology of naturally vegetated landscapes should provide for: (1) simple correction as more is learned about the ecosystems described by the initial legend units, and (2) the refinement of information conveyed by the symbolic legend without discarding either the legend system or previously annotated maps. A symbolic legend in which notations of the general to the specific progresses from left to right through the symbol seems to meet the above criteria. Such arrangement also permits the photo interpreter to cut off the notation at the point where strong doubts begin to arise about his interpretation statements. As these doubts are erased by experience, new knowledge, or further ground work, the annotation may be extended and the maps easily maintained to convey up-to-date information. This legend format is illustrated in Figure 1. The system provides for numeric and/or alphabetic

notations that treat both vegetation and key environmental features. The broadest and most easily photo interpreted items are symbolized in the left-hand digits; the items that are more detailed or more difficult to identify are noted to the right. About the only disadvantage of this legend system is that it is non-connotative--except as the symbols are individually memorized. This is compensated by the ease of computerization of data and the small space required for expression of large amounts of information.

A Vegetation Legend:

The vegetational legend is derived from an understanding of the plant geography, vegetational growth forms, and phytosociology or plant community structure of the region. We have developed a decimal notation system keyed to ecological plant geography, the broad vegetational classes, and to the plant communities that are either identified in the literature of this region or have been provisionally worked out from our own ground truth research. The primary classes are shown in Table I, and one class, the 03.0 Steppe or "Desert Grassland", is expanded as an illustration of legend detail, organization, and technique in Table II.

Note that digits to the left of the decimal point identify major geographic types (Table I). The first two digits to the right of the decimal point usually connote uniformity in the dominant species occupying the area. Each succeeding digit indicates further subdivision to specific plant community or ecosystem level. We have found that highly specific kinds of plant communities--the indicators of specific ecosystems--can be symbolized within a region or major ecological province by not more than four digits to the right of the decimal. A "zero" (0) class is always a general, indeterminant, or non-specific class for use where further detail is either unknown or unavailable.

Legends based on this concept may be set up on a world-wide, national, regional, county, or local management unit basis. With very little modification, the broad classes used here could be adapted for world-wide and national application; but the detail appearing to the right of the decimal point will nearly always have to be handled on a regional or local basis. Our present legend is local in scope--fitting reasonably well the area specified. Interestingly, however, all but one of the primary categories and twelve out of twenty-eight of the secondary categories apply to the Roswell, New Mexico, area. We have mapped extensive areas using these legend units on both space and supporting aircraft photography. Currently, we have a man field checking interpretations to see how well he can identify delineations with this legend. He is also obtaining more ground data on ecosystems for refined explanations of what the photo images mean.

In any kind of remote sensing interpretation, it is relatively easy to put lines around images that are different and that may have significant meaning. In some instances, it is not easy to determine the relevance of these differences with certainty. They may be highly relevant for one

problem or purpose, and for another of no significance at all. Furthermore, it is not always possible at the outset of a resource inventory and analysis to determine the criteria for relevancy, so some things may become important after they are recognized. In any case, the interpreter must provide an identification for all delineations as the second step in his activity. This is where the real difficulty arises; for even the most capable interpreters, ground checking is often necessary for positive identification--especially when detail is added to the legend at specific ecosystem or plant community level. There are three important requirements that greatly aid identification decisions by a photo interpreter--regardless of the kind, scale, or resolution of the imagery:

1) Know where the imaged area is located.

2) Know the gross climatic, geologic, and soils characteristics or features of the region.

3) Be enough of a resource ecologist to know what to expect.

This information and ability greatly narrows the alternatives facing the photo interpreter as he begins to put meaningful labels on what he has mapped or to adjust his mapping accordingly.

An important aid to the identification of vegetational images comes from the classification of macrorelief--a task perhaps more easily and rapidly done from space photography than any other kind of photographic imagery. We choose to call the highest order or broadest category of land surface features MACRORELIEF (Table III). For a given region, each macrorelief class tends to support its own unique set of ecosystems (Table IV). It should be obvious that this information narrows the alternative choices of legend units once macrorelief is classified. These classes are easily applied to space and small-scale high-flight photography (Figure 2), especially when it is available in excellent stereo coverage as from Apollo 6. The vegetation interpreter--whether machine-aided or not--must draw heavily on this and other kinds of convergent and associated evidence in reaching image-identification decisions. In addition to macrorelief, drainage pattern is also useful when making vegetation interpretations from space photography. More specific landform classes are helpful as associated evidence in vegetation interpretations, but many of these are not appropriate to use with space photography because of image scale. In addition, unsolved problems have been encountered in our work in Arizona, Oregon, and Nevada because of redundancy in accepted landform names. Many landform classes important to the student of geomorphology are not individually relevant to the ecology of the Earth's surface. We are currently studying groupings of landform classes that will provide this relevance.

With all the above kinds of observations as background, delineations can be identified from photography to the limits imposed by the photography itself, by the subject, and by the knowledge and skill of the interpreter.

Whether vegetational resources are identified by interpretation or by ground checking, they can easily be symbolized in a meaningful way with the legend we have presented (Figure 3). It will be seen that most of these delineations from space photography represent complex mapping units--that is, different vegetational classes occurring together within the same delineation. Where these differences are not strongly contrasting (at the appropriate classification level), they may be covered by a single legend entry; where they are strongly contrasting, by multiple entries. In space photography we are normally dealing with image areas that represent the more broadly generalized levels of vegetation classification or complex sets of ecosystems rather than single, unique systems. Multistage sampling is an essential technique to statistically document the variations between and within these resource delineations and to quantify characteristics of the resource.

MULTISTAGE SAMPLING

Frame No. AS9-26A-3806 from the Apollo 9 mission was selected as the primary base for this work. The selection of the color infrared photograph was based on past experience with this imaging medium. Discrimination among vegetation types and even plant species is generally better with color infrared photography than with conventional color or black and white.

This photo was taken on March 12, 1969, at 9:30 a.m., Mountain Standard Time, from an elevation of 120 nautical miles. The original photo scale was approximately 1:2.8 million, and there was no cloud cover. Good stereo coverage was not available since there was only 7-10% overlap with adjacent photos.

The coverage included approximately 9300 square miles in the vicinity of Roswell, New Mexico, extending north to south from Fort Sumner to Lake Arthur and west to east from Fort Stranton to the Mescalero Ridge (Figure 4). The main drainage of the area is the Pecos River. The elevation, excluding the mountains on the west, ranges from approximately 3400 feet to 5000 feet. The generalized vegetation types in the area included: (A) grama/galleta grasslands, (B) grama/tobosa shrubsteppe, (C) creosote bush/tarbush shrub, and (D) mesquite/shinery oak shrub. Agriculture--primarily cotton, alfalfa hay, and small grains--has been developed south of Roswell.

Unfortunately, the native vegetation in the area was in winter dormancy at the time of the Apollo 9 overpass. Consequently, the characteristic reddish color of green, growing vegetation as imaged by color infrared photography was not present in the imagery as an interpretation aid. Therefore, preliminary reconnaissance and ground mapping, using prints of this photo as a base, were delayed until late April and early May, when the deciduous shrubs had developed new foliage. This provided a valuable aid to vegetation interpretation since it was then possible to

use other interpretable features, such as landform, prominent landmarks, and macrorelief, to more precisely delineate the major vegetation type boundaries.

Five locations representing generalized vegetation complexes were selected for further study by multistaged sampling. In addition to exposure 3806, exposure 3449 from the AS9 mission on conventional aerial Ecktachrome film was used to ascertain the locations of these sampling units. This photo was taken on March 9 at 11:05 a.m. Mountain Standard Time. Sixty to seventy percent of the soil surface was exposed through the vegetative cover at the time of the satellite overpass, and this bare soil imaged more distinctly on the color film than on the color infrared film, therefore providing more distinct image discrimination.

On June 5, sampling photographs at three scales, 1:80,000, 1:20,000, and 1:2400, were made along one flight line across each of these five test locations. Color infrared and Anscochrome D/200 film were exposed simultaneously. This was done with a Forest Service airplane using twin mounted 70 mm. Maurer KB-8A cameras. The delay in obtaining the sampling photos was necessary to coincide with growth of most plant species and to provide more precise image interpretations.

Ground sampling was confined to positive identification of individual plant species, determination of relative composition of plant communities, and notations on soil surface color, relative amounts of exposed soil, and stoniness.

Of the five sample areas, one was selected for use in this discussion as an example of the multistage sampling procedure. It is located half-way between C and E in Figure 4. Basically, the design is a subsampling system in which large-scale photos were used successively to sample the next smaller scale photos. The sampling photography, as well as ground examination, revealed four primary ecosystems within the designated area on the AS9 photo (Figure 5). These included (A) sink holes in a limestone-gypsum overburden vegetated with pure stands of galleta grass--these areas lined with dune mesquite, (B) creosote bush/fluffgrass hills, (C) creosote bush hills on which very minor amounts of other vegetation occurred--approximately 70 percent of the soil surface was exposed and was covered with light-colored gravels and pebbles, and (D) alkali sacaton swales with nearly pure stands of the species. The swale areas are usually lined with dune mesquite, salt bush, and salt cedar.

The 1:2400 scale color infrared photos were used in sampling the 1:20,000 photos to estimate the number of shrubs within the shrub types (Figure 6). Stereo triplets, systematically exposed along the total length of the flight line, were used as the sampling photos. On this basis, there were eight principal sampling units within the shrub types, each sampling unit consisting of a 4-acre area. Each sampling unit was divided into sixteen ¼-acre subsampling units. Four subsamples were then randomly selected from each

sample unit to determine shrub numbers by photo interpretation.

Based on the statistics, there was an indicated average of 37 shrub plants per ¼-acre area in the shrub types, with a standard error of 15 (Table V-A). This large standard error was due to unusually high shrub density in two of the sampling units. This indicates we would need to either (1) increase sample size to reduce this standard error to an acceptable level, or (2) stratify vegetation into more meaningful units. The two sampling units with large shrub counts could conceivably represent different range condition classes within a single ecosystem in which shrubs had increased due to excessive grazing or other catastrophy, or they could actually represent different ecosystems.

The 1:20,000 scale photos (Figure 7) were used to sample the area covered by the 1:80,000 photos in determining the areal extent of the four previously described primary ecosystems. Continuous strip coverage was made along the flight line. This provided four primary sampling units, each consisting of 256 acres. A template was placed over the center of each stereo pair so that area within the template included the 256 acres. This area was then subdivided into 16 equal parts or subsample units, each of these units representing 16 acres. Eight of these subunits were randomly selected for ecosystem sampling, and a dot-grid was placed over the template so that each dot represented one acre.

The area of each ecosystem within each subsampling unit was determined by interpreting the ecological category covered by each dot. On the basis of the statistics, approximately 1% of the total area sampled was classified as sink-holes (Table V-B). Sampling error was not determined for this statistic. It represented such a small portion of the total area that greatly increased sample size would be required to provide a reliable estimate of the amount of this ecosystem.

The type area estimated for the other three ecosystems in the sample included 5.7, 6.5, and 3.6 acres per 16-acre subsample unit for the creosote bush/fluffgrass hills, creosote bush hills, and alkali sacaton swales, respectively, with respective sampling errors of 1.4, 0.9, and 0.8 acres. These errors may or may not be acceptable levels of accuracy, depending on the needs of a particular range inventory. If objectives are to determine the animal grazing capacity of an area, increased sample size may be desirable to more precisely determine this parameter. If only general knowledge of the areal extent of each ecosystem is required, these sampling errors would probably be acceptable.

The 1:80,000 photos were then used to sample the extent of the ecosystems included in the total area covered by the types designated in the original AS9 frame (Figure 8). Continuous strip coverage was again used along the total length of the flight line, and this represented approximately 42% of the total area included in the AS9 photo.

Three primary sample units, each consisting of 1,024 acres, were used for the sampling base. A similar dot-grid/template system was used for this part of the problem. In this case, however, each dot represented 64 acres and the area under each dot was interpreted as to one of the four primary ecosystems. Eight subsamples were randomly selected from each primary sample.

The sink-hole area was estimated at 1% of the total area, similar to the estimate derived from the 1:20,000 photos. There were so many zeros in the data, however, that sampling error was not computed. Again, sample size would have to be greatly increased or much larger scale photography would have to be used to compute a reasonable estimate of the area covered by this unit.

The interpreted area of the creosote bush hills was approximately 42% of the total area. This corresponds very closely to the results obtained using the 1:20,000 scale photos. Therefore, based on these data, the 1:80,000 scale photos would provide an acceptable subsampling level to determine the area of creosote bush hills designated in photos similar to that obtained by the AS9 mission.

Such good relationships did not exist for the other ecosystems in the type. The area of the two units was estimated at 57% of the total area delineated in the AS9 base as compared to 59% estimated by the 1:20,000 photos for the 1:80,000 base. However, the area of the members of each set was quite different; 12% creosote bush/fluffgrass hills versus 36%, and 45% alkali sacaton swales versus 23%. These discrepancies are primarily due to interpretation errors between the two ecosystems at the 1:80,000 scale. The image differences between these two units become more subtle as photo scale decreased, thus providing greater chances of making incorrect interpretation decisions from a single season of photographic coverage.

As management demands become more exacting and require more specific facts about the absolute makeup of the vegetational component, multiseasonal photography becomes an important consideration in avoiding interpretation errors.

REPETITIVE SEASONAL PHOTOGRAPHY

Inventorying vegetational features of range and forested lands can be facilitated by using repetitive or multiseasonal photography. The fact that plants having healthy, green leaves are red on properly exposed color infrared film provides the basis for interpreting these photographic images in terms of vegetation.

The appearance of plants as they respond to changes in moisture, temperature, and insolation conditions throughout the year provides criteria for vegetational typing and individual species identification. This opportunity exists because the periodic biological changes characteristic of one

plant species or group of similar species can be regionally unique due to differing rates and times of change. Throughout a year, these changes define a plant's phenology. An example of this phenomenon is exhibited by deciduous shrubs. The usual phenological steps involved may begin with current annual stem growth and new leaves. As the leaves mature, flowers develop, which in turn may provide fruit. After the fruit ripens and the seeds are dispersed, the leaves are dropped and the plant becomes dormant. Each stage of development tends to produce its unique color infrared image.

By considering the time of year when plants are either dormant or have leaves, the plants of southern Arizona can be assigned to three generalized groups: (1) evergreens, which possess leaves throughout the year; (2) cool-season deciduous plants, which respond to the winter rains and the warming spring temperatures; and (3) warm-season deciduous plants, which leaf out after the summer rains.

The plant species involved in the woodland, chaparral, and montane forest types commonly represent group 1 - the evergreens. Many of the desert shrubs belong to group 2, and at least one shrub, whitethorn (Acacia constricta), and most of the perennial grasses are in group 3.

Photographic images can be classed as representing vegetational types belonging to group 1, 2 or 3. After noting the date of photography, some interpretation decisions may be made by merely detecting the presence of red color in the photographic image. It seems very plausable that this color determination could be done automatically. A vegetational type consisting of plants having similar phenologies, e.g. a steppe dominated by perennial grasses, would be represented by a shade of red in the photographic image when the new growth over-topped the old dried material from the year before. Where one plant species clearly predominates in a vegetational unit, the appearance of that plant will have a controlling influence on the photographic image of the unit. In this way, single species identification is not only possible, on the proper photographic scale, but also the identification of an ecosystem that might be very heterogeneous in terms of plant species, phenologies, and growth forms.

An application of this technique could be as follows. Color infrared photography taken in March would show only the evergreens as red, and the appropriate delineations and identifications could be easily made. In April and May the ecosystems that include many of the desert shrubs would be most obvious and could be located on photography taken at that time (Figure 9). The steppes would be more apparent on late August photography. Also from August photography, one might detect those previously identified areas of desert shrub which support a dense understory of perennial grasses, in contrast to those lacking such an understory. Group 1 vegetation - the evergreens - is especially detectable on S065 and March high-flight photography. We are awaiting duplication of subsequent high-flight photography, especially HyAc panoramic, color infrared photography, in order to further develop and illustrate this technique.

SUMMARY AND CONCLUSIONS

As more detailed quantitative information is required about the ecosystems represented in the mapping units on space photography, multiscaled photos are required to provide the subsampling basis for obtaining the added detail. Photos at scales of 1:80,000 appear satisfactory for determining the areal extent of strongly contrasting ecosystems whose image characteristics are markedly different from adjacent units. However, as the differences between ecosystems become more subtle, so will their image characteristics; and the difficulty of interpretation increases as photo scale decreases. As the image differences become more subtle among phenologically different vegetations, the place of multiseasonal photography becomes more apparent. It appears from our work to date that multiseasonal photography may hold the best key to the correct identification of a maximum number of vegetational delineations on aerial or space photography. This is especially true where the seasonal development of the different vegetations is well known as a basis for interpretation.

Since resource management decisions require detailed information, scales of 1:20,000 or larger may be required to provide acceptable quantitative data for this information. Extremely large-scale photography will provide important additional information about the resource. Such things as range plant species density and dispersion can be measured by using photography of 1:2400 and larger scales. This kind of information is required for monitoring changes in vegetation over time and for determining the actual makeup of the plant community. It is recognized that not all species in the ecosystem will be detectable and identifiable. However, measurement of the larger and perhaps most characteristic species of the community is possible. These often reflect the effects of man's use and manipulation.

As we continue to develop the capability of examining vegetational and related resources through space and aerial photography, it is important to keep in mind some of the interrelationships between the three major resource management functions, Policy and Broad Planning, Land-Use Decisions, and Resource Management, as well as the requirements of the separate activities within each of these functions. These are graphically portrayed in the chart of Figure 10. It is very important to realize that present space imaging capability with which we have all been working is not well suited to the needs of day-to-day vegetational resource management. It best serves the needs of broad policy and planning. There are, however, many interrelationships between these various functions and activity levels. Depending on the specific nature of the problem, valid exception may be taken to this statement and to the generalities represented by the italicized indications of image applicability to the various jobs charted in Figure 10. Perhaps the greatest factor interacting with photo scale to determine usability is image resolution. Obviously, small-scale photography with exceptional resolution may be superior to low-resolution intermediate-scale photos when one considers enlargement capability. Based on the range of scales with which we have been working, Figure 10 presents our current

assessment of the minimum requirements of each functional and activity level for imagery of natural resources to meet the varied needs of the resource user and management decision-maker. Depending on the function and level being monitored, the requirements for resource monitoring are also suggested by the italicized symbols in Figure 10.

Table I: Primary legend classes and symbols for the annotation of vegetational resource maps in the Tucson-Willcox-Ft. Huachuca area of southwestern Arizona.

SYMBOLIC LEGEND	*NAME OF CLASS*
01.0	Sonoran Desert
02.0	Chihuahuan Desert
03.0	Steppe
04.0	Oak/Juniper Savanna
05.0	Woodland and/or Chaparral
06.0	Montane Forests
09.0	Barren Land
10.0	Cultivated Land
11.0	Urban, Industrial and Transportation
12.0	Water Resources

Table II: Part of the detailed vegetation legend for the Tucson-Willcox-Ft. Huachuca area of southeastern Arizona.

SYMBOLIC LEGEND	*DESCRIPTION OF VEGETATION*
03.0	STEPPE
*03.1	Bunch/Sodgrass steppe (pure grass uplands)
03.2	Soaptree Yucca grassland
03.21	Soaptree Yucca/Sotol grassland
03.22	Soaptree Yucca/Sotol/Zinnia/Coldenia grassland
03.3	Mesquite grasslands (convex uplands)
03.31	Mesquite/Grama (uplands)
03.32	Mesquite/Tobosa grass (bottomlands)
03.4	Mesquite/Burroweed grassland
03.41	Mesquite/Burroweed with grasses
03.42	Mesquite/Burroweed/Creosote Bush without grasses
03.5	Creosote Bush/Whitethorn/Ocotillo grassland
03.6	Nolina grassland
03.7	Creosote Bush grassland (bottomlands)
*03.8	Pure grass bottomlands
*03.81	Tobosa grassland
*03.82	Sacaton grassland

*These categories fit the Roswell, New Mexico, area. Categories of other secondary classes (to the 1/10th decimal notation) are also closely related to the vegetation types in the Roswell area.

Table III: Macrorelief classes particularly appropriate for mapping from space photography. These classes are ecologically relevant and aid photo interpretation.

SYMBOLIC LEGEND	*NAME AND ABBREVIATED DESCRIPTION OF CLASS*
1	Flat Land, less than 5% slope, or if smooth on a generally tilted substratum, the tilt is less than 10%.
2	Undulating to Rolling Land, slopes within the system greater than 5% but contours blend smoothly.
3	Hilly Land, simple drainage systems, contours generally tend to blend smoothly, usually a simple main and secondary ridge system. Elevational change usually restricted to one or two vegetational zones.
4	Mountainous Land, complex superimposed drainage systems, slopes tend not to blend smoothly, ridge and valley systems complex and tend to rise upon one another to greater heights than hilly lands. Usually represent more than two vegetational zones.

Table IV: A decision on macrorelief and landform aids in vegetation interpretation from space and/or high altitude imagery. Note that unique kinds of vegetation tend to be associated with these macrorelief and/or landform classes.

MACRORELIEF CLASS	*MOST LIKELY VEGETATION OR GROUND FEATURE (LEGEND SYMBOL)*
Flatlands	
Bajadas, Fans or Terraces	01.1, 01.2, 01.3, 2.1, 2.2
Bottomlands	02.3, 03.7, 03.81, 03.82, 09.1, 10.0, 12.0
Hilly Lands	01.4, 04.0, 05.0
Mountains	04.0, 05.0, 06.0

Table V: Preliminary multistage sampling results.

(A)

SAMPLE ITEM (Per Unit)	*ESTIMATES OF PARAMETERS AT PHOTO SCALES USED*	
	1:2400	*1:20,000*
	Sample Data	Predictions
Number of Shrubs	37 per ¼ acre	148 per acre
$S\bar{y}$	± 15	± 60

(B)

SAMPLE ITEM (Per Unit)	*ESTIMATES OF PARAMETERS AT PHOTO SCALES USED*			
		Total Area Sampled		
		3867 Acres		9091 Acres
	1:20,000	*1:80,000*		*1:2,790,000*
	Sample Data	Predictions	Sample Data	Predictions
Creosote Bush/Fluffgrass				
% of area	36%[1/]		12%	
Acres ± $S\bar{y}$	5.7 ± 1.4	1392 ± 334	8.0 ± 5.3	1091 ± 720
Alkali Sacaton				
% of area	23%		45%	
Acres ± $S\bar{y}$	3.6 ± .8	889 ± 195	28.7 ± 5.9	4092 ± 818
Creosote Bush				
% of area	40%		42%	
Acres ± $S\bar{y}$	6.5 ± .9	1548 ± 201	26.7 ± 4.7	3818 ± 687
Sink Holes				
% of area	1%		1%	
Acres	.16	38	.7	90

[1/] Percentage based on 16 acre sample area for 1:20,000 and 64 acres for 1:80,000.

Figure 1: Ecosystem legend for range resource analysis from space and supporting aircraft imagery.

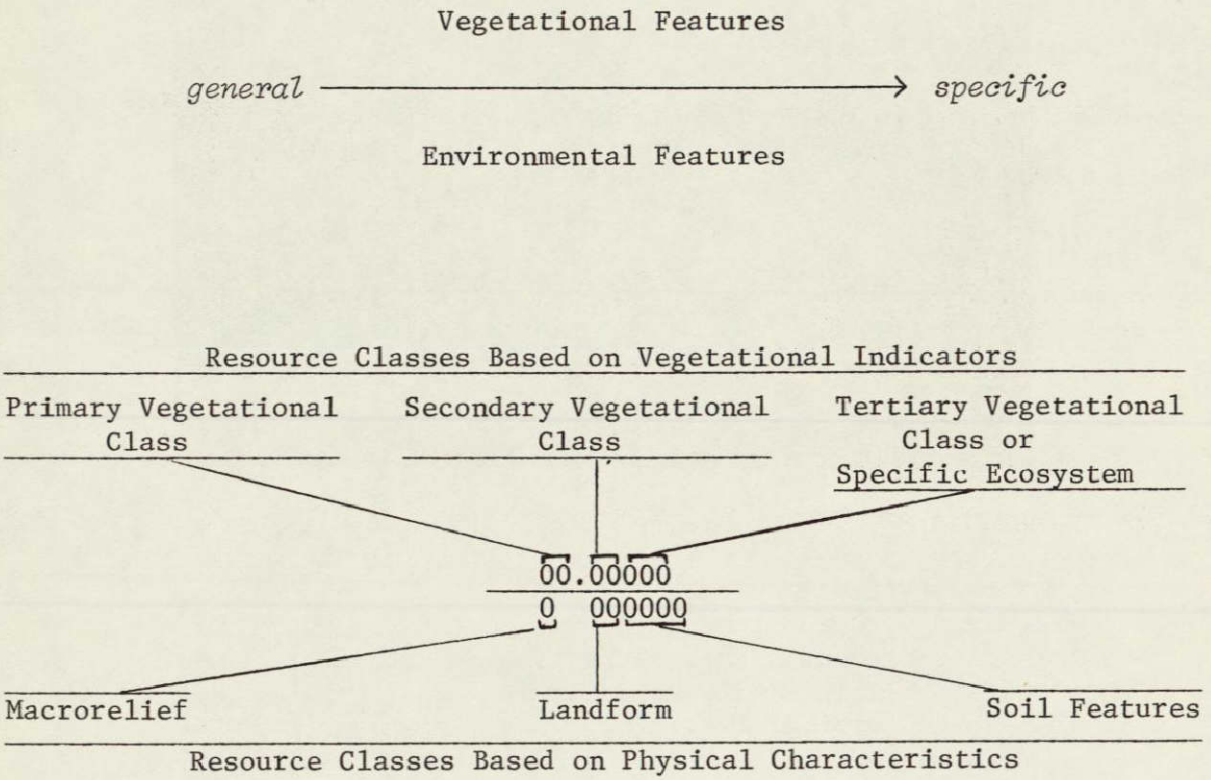

Figure 20-1.- Ecosystem legend for range resource analysis from space supporting aircraft imagery.

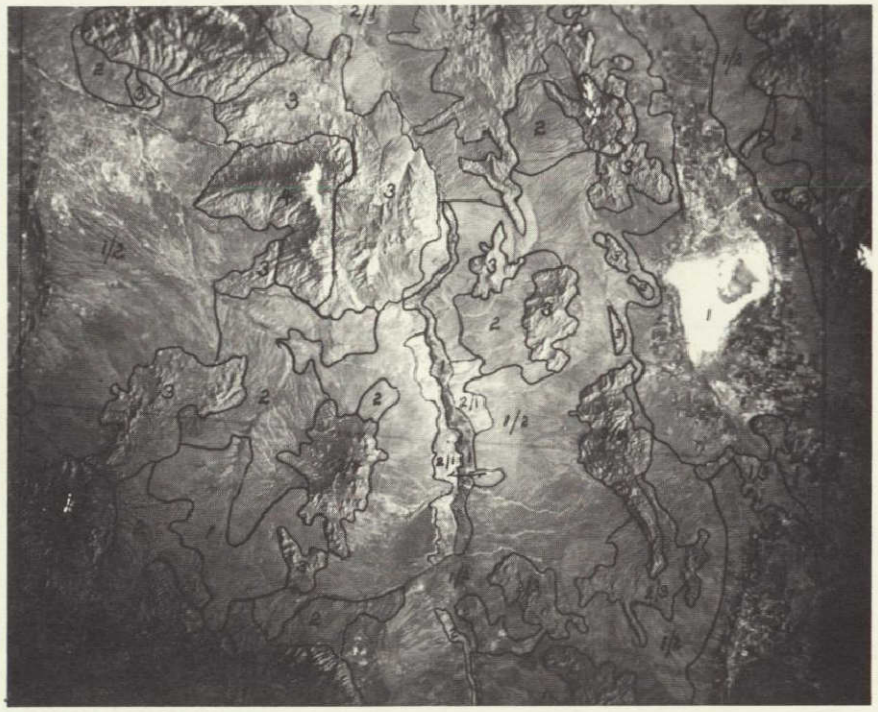

Figure 20-2.- Macrorelief mapping from space photography (AS6-2-1142) aids in the interpretation of vegetational resources and is relevant to regional land-use planning and policy decisions. Complexes of different classes that are impractical to separate within single delineations are indicated by a double symbol, e.g., 2/1. The first symbol indicates the predominant class. 1 = Flat Land; 2 = Undulating to Rolling Land; 3 = Hilly Land; and 4 = Mountainous Land. The excellent stereo coverage of Apollo 6 greatly facilitates resource mapping at this level.

Figure 20-3.- Mapping and legend symbolization of vegetational resources illustrated on space photography (AS6-2-1442). Only the part of the legend appropriate to mapping from space photography is used (see Figure 1). Note that most delineations are treated as complex mapping units. For partial identification of legend examples consult Tables I, II, and III.

Figure 20-4.- The Roswell, New Mexico, area from space (AS9-26A-3806). Generalized vegetative types include: (A) Grama/galleta steppe, (B) Grama/tobosa shrub-steppe, (C) Creosote bush/tar bush shrub, (D) Mesquite/shinery oak shrub. Agricultural lands (E) occur primarily south of Roswell. The native vegetation, except for evergreen species, was in winter dormancy at the time the photo was taken. Therefore, the characteristic reddish image color of green growing vegetation was not available as an interpretive aid. Five locations representing similar ecosystem sets were selected on this frame for multistaged sampling. One of the locations, half way between C and E, was used to illustrate the procedure and explain results.

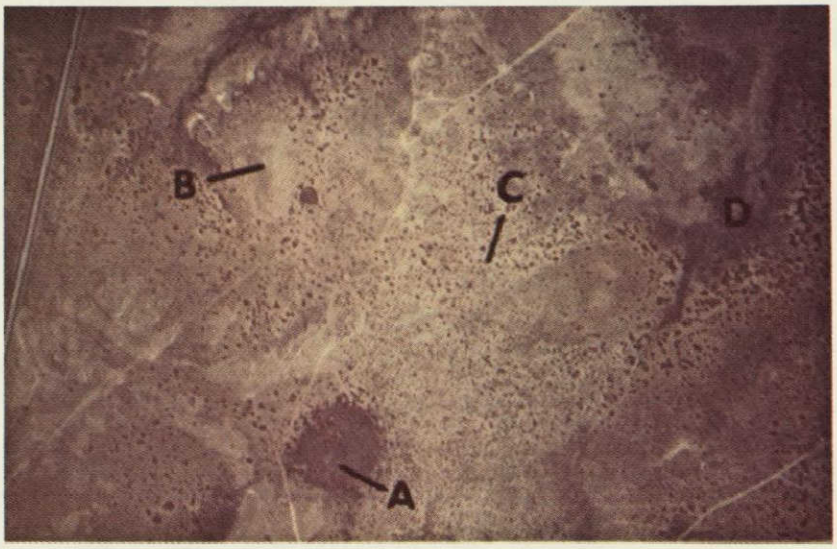

Figure 20-5.- Ground examination and photo interpretation using 1:20,000 scale photos revealed 4 primary ecosystems within the ecosystem set as identified on the space photograph: (A) sink holes with pure stands of galleta grass, (B) Creosote bush/fluffgrass hills, (C) Creosote bush hills with little other vegetation, (C) Alkali sacaton swales.

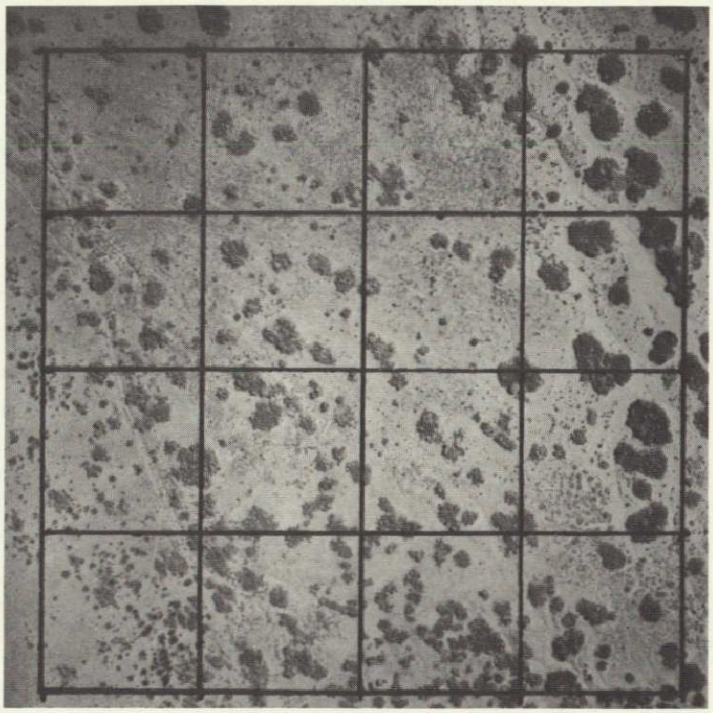

Figure 21-1 Black and white copy of a 1:2400 scale color infrared photo used to determine number of shrubs per unit area when sampling 1:20,000 photos. In addition to quantifying amount of shrubby vegetation at a single point in time, this kind of photography will be useful for monitoring specific changes in vegetation by evaluating such parameters as change in dispersion and density caused by events such as grazing, fire, or insect and disease depredations.

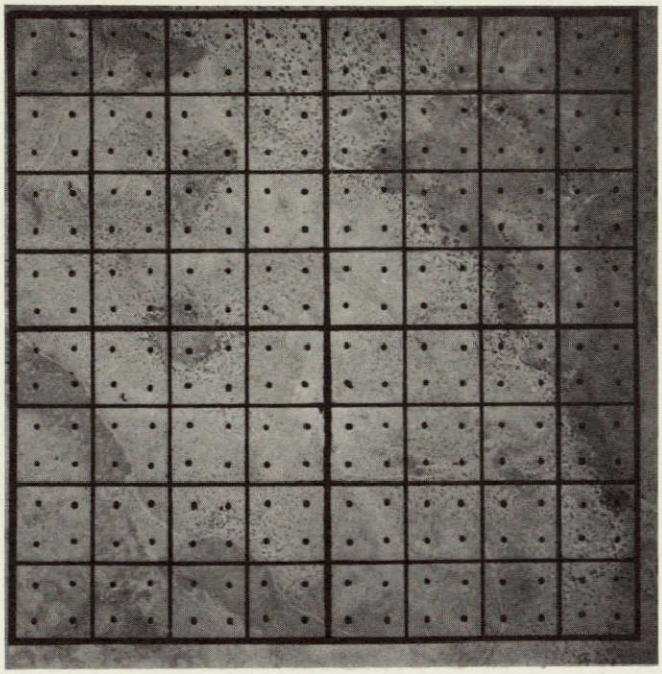

Figure 20-7.- Black and white copy of a 1:20,000 scale color infrared photograph was used to sample 1:80,000 scale photographs to determine the areal extent of each of the four ecosystems represented in the designated area of the space photograph. Each dot in the template overlay represents 1 acre.

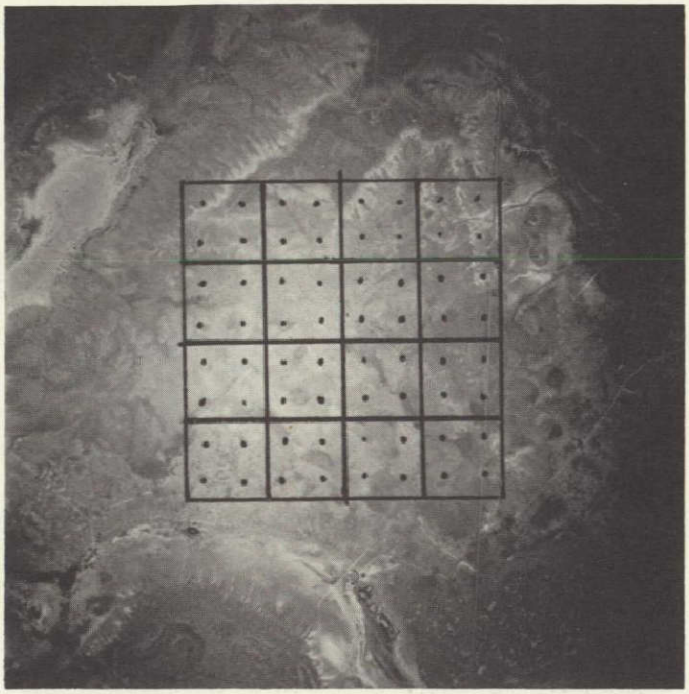

Figure 20-8.- Black and white copy of a 1:80,000 scale color infrared photo used to provide a final sample estimate of the extent of each of the four ecosystems represented in the designated area on the space photograph. Subtle image differences between the junction of Creosote bush/fluffgrass hills and Alkali sacaton swale ecosystems resulted in interpretation errors. This photo scale would likely be unusable for complete subsampling of space photographs except for those ecosystems with image boundaries markedly different from adjacent units. This is represented by the sharp demarcation between the Creosote bush hills and Alkali sacaton swales.

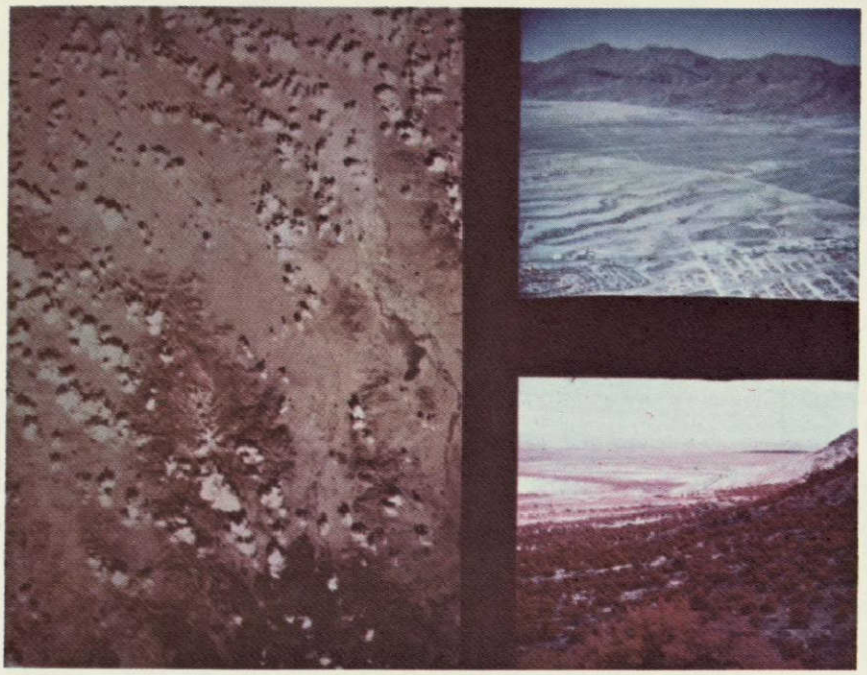

Figure 20-9.- The three color infrared photographs in this plate are Frame AS9-26A-3753 (left) a 35 mm. aerial oblique (upper right), and a 35 mm. ground photograph (lower left). The space photograph was taken in March and shows the location of the evergreen species in the mountains. In the aerial oblique photograph the evergreen species are seen to extend nearly to the base of the mountain front. This photography, taken in May, also indicates the presence of cold season deciduous desert shrubs in the runnels on the bajada. These plants also appear red. The ground photograph (lower left) taken in July shows a continuum for evergreens in the foreground to cold season deciduous desert shrubs in the background. Comparisons of this photograph with one taken in March and showing a similar scene, would serve to distinguish the two vegetation types and their extent — a distinction not as easily accomplished on photography from a single date.

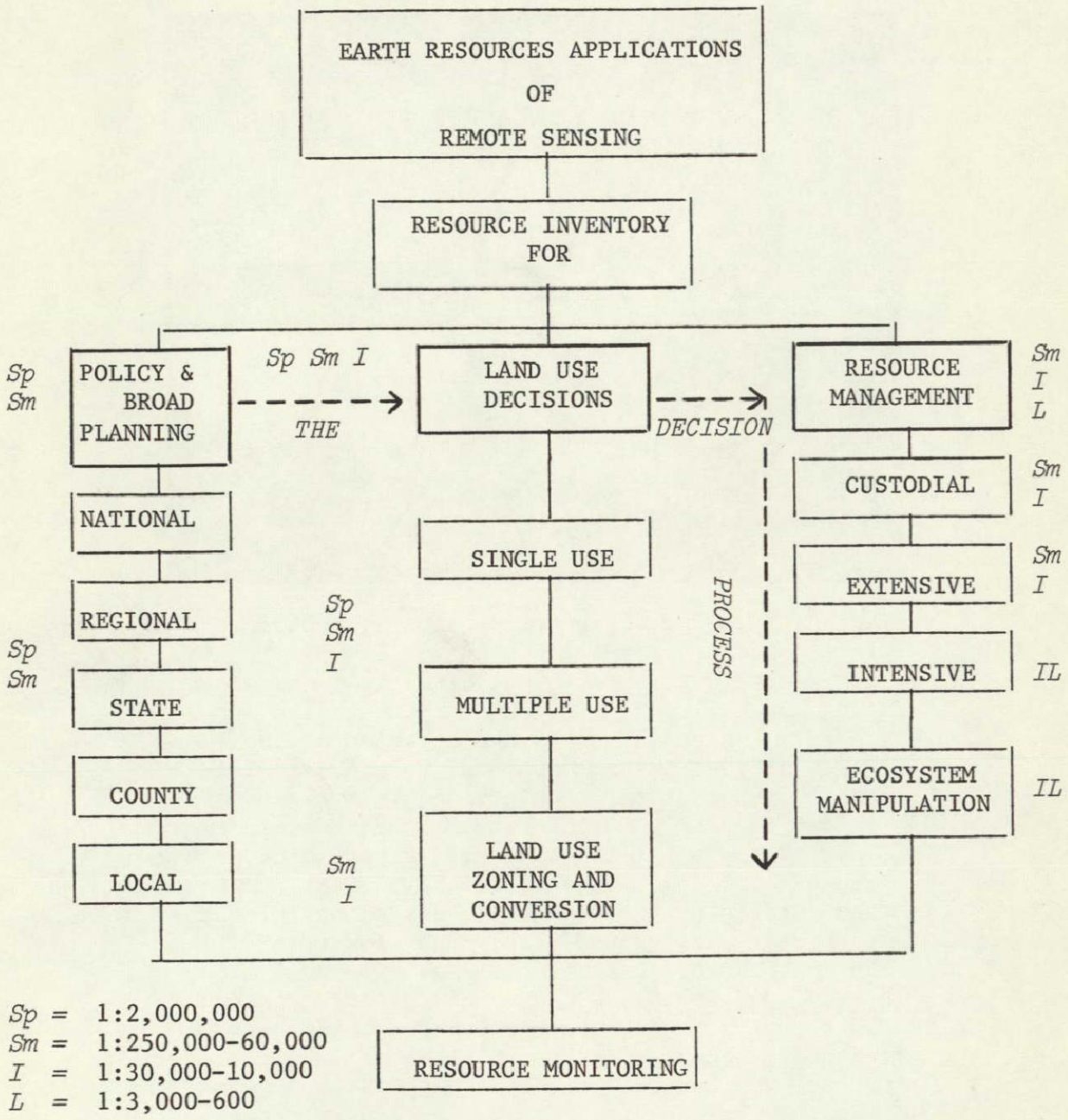

Figure 20-10.- Suggested photo scales required to provide resource data in the decision-making process for land use planning and management. The heavy broken line indicates the sequence in the decision process.

SECTION 21
MULTIPLE RESOURCE INVENTORY ON SPACE AND HIGH-ALTITUDE PHOTOGRAPHY

by

Lawrence R. Pettinger
School of Forestry and Conservation
University of California, Berkeley

INTRODUCTION

Studies of space photography have frequently centered on the analysis of a single resource. However, where the impact of large numbers of people on the land is significant, the evaluation of several valuable resources within a single geographic area is necessary for sound resource management. Phoenix, Arizona, is located in such an area where the demands of a growing urban population are being made on lands managed for agriculture, grazing, and mineral resources, as well as wildlands not currently managed to provide economic returns (Figure 1). Studies of Apollo 9 photography and high altitude NASA photography obtained monthly since the Apollo 9 flight permit these resources to be evaluated on a sequential we well as multispectral basis.

While the Phoenix area is only one of several which the Forestry Remote Sensing Laboratory at Berkeley has been studying, it serves very well as an example of the possibility for making multiple resource inventories on space photography. Consequently, my presentation will deal entirely with work which our group has been doing in that area.

IMAGERY OBTAINED

Two types of imagery have provided the basis for our work. Multispectral black-and-white and Infrared Ektachrome photographs were obtained for the Phoenix area in March of this year from the photographic experiment carried out by the Apollo 9 spacecraft. Simultaneously with the Apollo mission, high altitude photography was obtained along selected flight lines from an altitude of 65,000 feet. From this aircraft, 70mm photographs of the same film types as obtained by Apollo 9 were procured, as well as HyAc panoramic photographs of two types, Infrared Ektachrome and Pan-25A.

Since the high altitude imagery closely simulates the type and quality to be expected from space on a sequential basis within a few years, conclusions based upon the study of such photography can hopefully be used to predict the benefits which will be derived from space photography obtained in the future.

LAND USE MAPPING

One of the most basic kinds of information about the resources of an area can be derived from a broad land use map prepared from a space photograph. This has been done for the Phoenix area (Figure 2) by making photo delineations based on limited ground survey work. The following proportions of land were found in each category:

Land Use Category	Percent Land Area
Urban	5
Agricultural cropland	20
Rangeland	43
Upland and mountains	24
Watercourses	8

A small scale map of the type shown in Figure 2 gives an indication of the relative location of the resources associated with each land use category. If prepared over a period of several years, such maps will indicate how land use patterns change over time.

When large areas have been stratified in this manner, subsampling designs can be formulated to derive more detailed information for each land use category. Separate sampling designs can then be used which take into consideration the frequency, variability and relative importance of the components of each class of resources.

AGRICULTURE RESOURCE

Agricultural crops in the Phoenix area constitute one of Arizona's most valuable resources. The position of much agricultural land in a "buffer zone" surrounding urban areas (see Figure 1) is important since urban expansion must be made at the expense of land currently under cultivation. Studies of urban growth will necessarily entail some consideration of the agricultural resource.

Inventories of crop type and determination of crop acreages are two of the most important tasks which must be undertaken for the preparation of an agricultural census. It is evident from an examination of Figure 3 that, even on space photos, individual fields can be readily discerned. Since the average field size is usually 40 acres or some multiple thereof, it is a relatively simple matter to determine the total acreage of all crop categories by determining acreages of the individual fields. In addition, total land area under cultivation can be determined by using an area calculating device on a photo which contains broad delineations of agricultural cropland (such as in Figure 2). An appropriate reduction in area under cultivation can be made for roads and structures.

Determination of crop type is a more complex problem. From orbital spacecraft or jet aircraft altitudes, many of the subtle patterns that aid in crop identification on photographs of larger scale are not discernible. Detection of plant spacing, height and width of each plant, and other indicators, such as presence or absence of hay bales, is not possible. Photographic tone becomes the most important image characteristic for crop identification.

It is important at this point to recognize that the optimum time or times of year must be selected for maximum discrimination of crop types. The Apollo 9 and high flight imagery obtained in March has been rated poor for

overall crop identification. At this time of year we note that barley, alfalfa and sugar beet fields are all covered completely by healthy green foliage. The variability of tones are as great within a single crop type as between crop types, and interpreters had difficulty in making identifications on imagery obtained at this time of year (Figure 3). To aid in the identification of crop type, high altitude photographic missions have been flown to obtain sequential photography. Examples of this imagery appear in Figure 4.

A sixteen square-mile area was chosen near Mesa, Arizona, for a detailed evaluation of the ability of interpreters to identify crop type. This area was chosen because it was contiguous (easy for collection of ground truth), contained all the major crop types, and included enough individual fields for a meaningful test (over 120 fields in the area). Detailed ground truth was obtained for this area on each flight date. A sample of the type of information collected is presented in Figure 5.

From a field-by-field tabulation, for each date that sequential photos were obtained, it was determined that the pattern of crop development for a given field could be classified as belonging to one of four distinct sequences. These are depicted in four bands of a "crop calendar" in Figure 6. Once a calendar of this type has been prepared, it can be used in two ways. First, crop identification for each field can be made by studying the appearance of the field on photographs taken on different dates. For each date the interpreter can judge whether or not the field in question is vegetated, is reaching maturity (whether foliage is green or dry), and, if the field is not vegetated, whether or not it has been recently irrigated. Then reference can be made to determine which sequence on the crop calendar most closely resembles the sequence observed on the photograph.

Secondly, the crop calendar can be used to select the optimum date(s) for obtaining photography of agricultural cropland. For the Mesa area, one would suggest that mid-May is the optimum date for identifying cereal grains from all other crops by their unique signature (Figure 4). Similarly, since it is known that nearly all fields containing bare soil in March were planted to cotton later that year, one can predict, on the basis of the evaluation of March imagery alone, the quantity and distribution of the cotton crop for that year.

Various types of color composite images were prepared with the objective of enhancing either (a) the overall interpretability of several features (e.g., crop types) or (b) the interpretability of a single feature. Optical enhancements have been made using the optical combiner at the Forestry Remote Sensing Laboratory. Electronic enhancements have been made using two devices: the Philco-Ford Image-Tone Enhancement system and the University of Kansas Electronic Processing system (Figure 7).

Interpretation tests have been designed to determine the relative interpretability of each image type available. The following images are included in the test: Pan-25A, IR 89B and Infrared Ektachrome photos from both the Apollo 9 and high altitude aircraft flights (March 12); Infrared Ektachrome high altitude photographs taken on April 23 and May 21 (interpreted singly and in concert with the March Infrared Ektachrome image); and color composites

made using the FRSL system and Philco-Ford systems. The training and test map (Figure 5b) was used for administering the test for each image. Its preparation and use are described in that figure. Test results are not complete at this time. However, completed analysis of the data will appear in a report entitled, "An Evaluation of Earth Resources Using Apollo 9 Photography", by the Forestry Remote Sensing Laboratory in October, 1969.

Initial evaluation of the imagery indicates that the greatest improvement in interpretability for crop type will result from the analysis of sequential photographs since these images will exploit the unique seasonal changes which each of the crop types undergoes. Another FRSL special report to be published later this year will deal solely with these sequential aspects.

RANGE RESOURCE

One of the major uses of much of the wildland surrounding Phoenix, Arizona, is for grazing by domestic and wild animals. Since the production of meat on this rangeland depends on the quantity and quality of the herbage and the time of year when it is taken by livestock, it becomes important to monitor changes in the vegetation. By so doing, grazing can be manipulated so as to provide greatest animal development consistent with maintenance of high quality range condition.

Two major communities of range plants are found in the area being studied. The semi-desert shrub type is found on alluvial plains to the north and southwest of Phoenix. Rainfall is low and temperatures are high in these areas, and forage production is poor. Since the shrubs which dominate these areas are quite woody and have low forage value, the best grazing is to be expected in the spring when annual grasses and weeds are vigorous and green. The second range community is the chaparral type, found at higher elevation in the mountains north of Phoenix. More rainfall is available to this type, more palatable plant species are present, and forage value is consequently higher.

A broad vegetation map showing these vegetation categories is being prepared. Apollo 9 photography is quite useful for this type of mapping. However, certain types of information which are necessary for a range resource inventory, such as species composition, amount of plant cover and amount of forage present, cannot be ascertained directly from a space photograph.

There are two alternatives which seem to hold definite merit as solutions to this problem. First, large scale conventional aerial photos can be obtained for representative areas using a subsampling system. Estimates of vegetation parameters made on these photographs can be expanded for each type.

Similar information can be derived directly from orbital photography using a second technique. It is known that plant communities tend to be associated with unique landforms, climatic conditions, specific soil types and soil moisture regimes. These associations tend to be rather clear-cut

in semi-desert regions. As a result, the photo interpreter can learn to make inferences, even about vegetation he cannot see directly, from a careful study of landforms and topographic features which are quite evident. An example of this technique is illustrated in Figure 8 and 9 for the semi-desert shrub type. Here, for example, upland mountains are quite apparent. Soils in these areas will be shallow and rocky, with no subsurface moisture. Vegetation is sparse and unpalatable. Bajadas are detectable as coalesced alluvial fans on the lower slopes of upland areas. They contain more well-developed soils and vegetation, and thus better forage potential. Bottomland areas are easily identifiable on space photographs; they are known to contain surface and subsurface moisture, a relative profusion of vegetation, and fine-textured soils. Recognition of these characteristic landforms by a trained interpreter permits him to use the "convergence of evidence" principle to make inferences about vegetation parameters and soil conditions which he cannot detect directly from the photographs.

GEOLOGIC RESOURCE

The major responsibility for evaluating geologic resources on space photography lies with a number of other NASA-financed investigators. However, since geologic resources constitute an important part of the total resource endowment of the Phoenix area, our team engaged in limited studies of geologic resources of that area.

Three different sites were selected from Apollo 9 photography (Figure 10). The first area, near Gila Bend, was chosen as a familiarization area (Figure 11). A geologic overlay was prepared for the Gila Bend area by making reference to the Arizona Bureau of Mines Geologic Map of Maricopa Co. Subsequent study of the tonal and textural signatures associated with various geologic features helped prepare our geologist for the follow-on studies.

The objective of the study was to test the feasibility of mapping geologic resources at a scale of 1/250,000 from the four film-filter combinations used in the Apollo 9 experiment. Two test areas were chosen in which the interpreter had had no prior experience. The Roosevelt-San Carlos Reservoir area appeared to have a wide variety of discernible geologic features, and usable non-stereo coverage in all four film-filter combinations was available. Although its geology appears to be less varied, the Yuma site was included to evaluate the benefit which stereo coverage might provide.

Mapping units were delineated on each film type using a combination of tonal, textural and topographic features. The success of such delineations rests in part on the success of the initial familiarization process as well as on the amount of photogeology experience which the interpreter has.

After the delineation was completed, a legend was prepared with each category area being fully described in terms of image characteristics. Securing of ground data from selected sample points is now planned so that category areas can be identified and map boundaries adjusted where necessary. The accuracy with which the interpretation has been done can then be assessed through comparison with existing geologic maps.

HYDROLOGIC RESOURCE

In regions where increasing demands for water are made by industry, agriculture and households, it often becomes necessary to monitor the supplies of water very closely so that all requirements can be satisfied. In large areas where an inadequate inventory of water resources exists and funds for snow and hydrologic surveys are scarce, there is some possibility that orbital and high altitude photography could provide the basis for making a usable estimate of water yields.

The perimeter of the snow pack can be delineated with ease on space photographs and, when ground measurements of snow depth and water content are made at representative locations, the amount of snow accumulation and snow melt can be estimated. Sequential photography could be used to best advantage in monitoring these changes throughout the year.

In addition to monitoring the snowpack from orbital photography, there exists some potential for accurately determining the amount of snowmelt to be received by each watershed or reservoir system. In the Phoenix area, Roosevelt Lake and the other lakes along the Salt River provide water for irrigation, industry and household use, as well as for recreation and water sports. More efficient planning for water storage and release is possible if one can determine the exact amount of each snowpack that will be received by each reservoir catchment system.

With this objective in mind, the snowpack of the Four Peaks area was sectioned off according to the drainage system which would receive each part of the water from melting snow. This delineation was made without the benefit of topographic maps or stereo coverage, yet the results are quite promising when compared to the same delineations made on a topographic map of the same area (Figure 12). In both cases the hatched areas indicate which parts of the drainage basins will receive no runoff from the snowpack.

The added input of stereo coverage is being investigated to determine how this technique might be improved. There appears to be great promise for making rapid, accurate water resource studies of this kind for large watershed areas at low cost on an operational basis.

CONCLUSION

The potential for making broad land use maps and earth resource surveys has been evaluated using Apollo 9 space photographs, and small scale photographs obtained by high altitude aircraft. This paper demonstrates that several different photo interpretation procedures can be integrated to extract information from space and aerial photographs regarding several resources within a single geographic area.

Specific techniques were discussed for the inventory of agricultural, range, geologic and hydrologic resources. In each case, a particular set of interpretation procedures were chosen depending upon the nature of the resource. For example, the seasonal changes which characterize agricultural crops and native vegetation suggest that sequential photography obtained at

the optimum times of the year would provide the best opportunity for identifying each of the important features. In contrast, geologic features change very slowly over time and a single set of photography would be adequate for mapping geologic features.

Color composite images, both optical and electrical types, were prepared to enhance differences between crop types. Interpretation tests were described that are being used to evaluate how well crop types can be identified on the various space and sequential high altitude photographs, as well as color composite images made from these photographs.

REFERENCE CITED

1. Benson, L. and R. A. Darrow. 1954. The trees and shrubs of the southwestern deserts. University of Arizona, Tucson.

Figure 21-1.- This mosaic of Apollo 9 Infrared Ektachrome photographs (AS-26-3801 and AS-26-3802) shows the area in which multiple resource inventory studies were undertaken. Note the relationship between urban Phoenix (center of left photograph) and the agricultural land which surrounds it. Also of importance to the land manager is the vast area of wildland surrounding Phoenix. Some of this land is usable for grazing while much of it is not currently managed to produce economic returns.

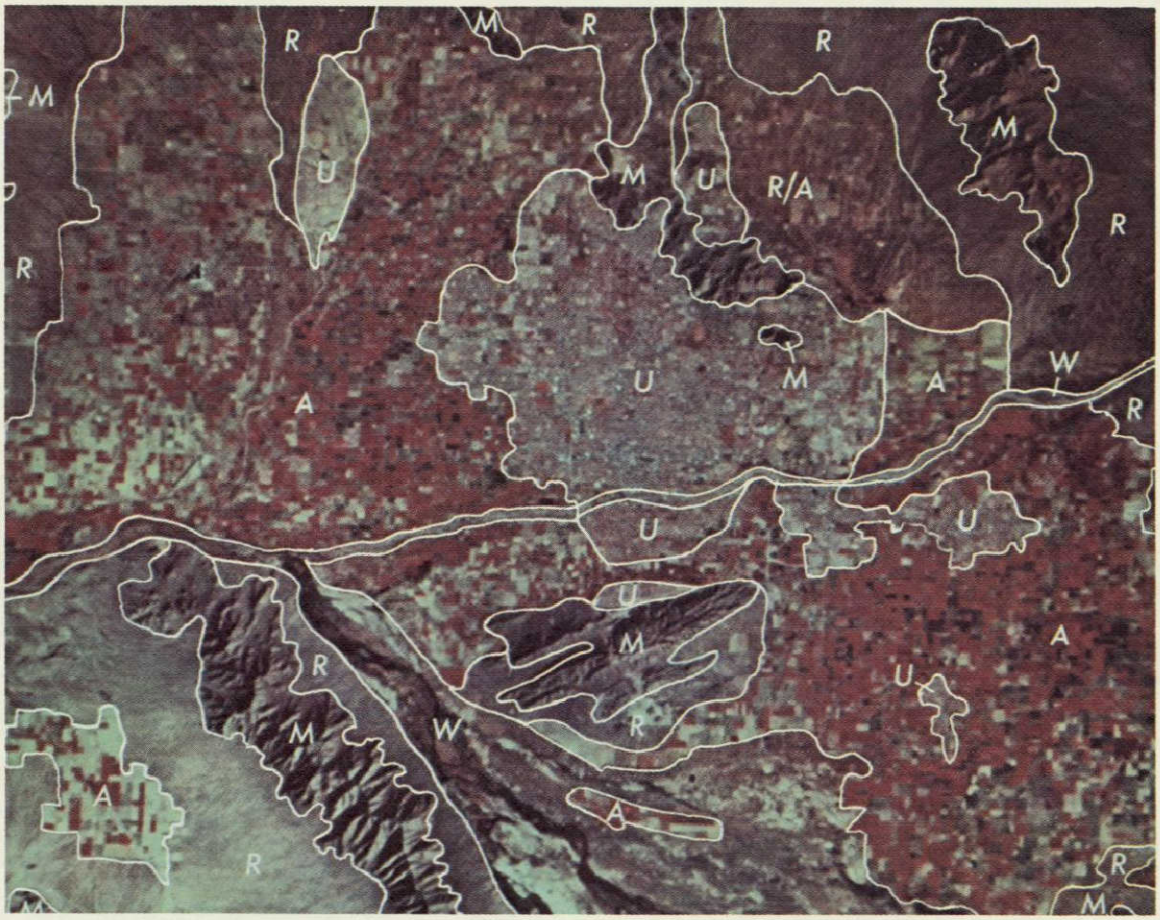

Figure 21-2.- A portion of the Phoenix, Arizona, area as it appears on the Apollo 9 Infrared Ektachrome space photograph. The following broad land use categories have been delineated: urban(U), agricultural cropland(A), rangeland(R), uplands and mountains(M) and watercourses(W). Once these initial stratifications have been made, sampling designs can be formulated for obtaining more detailed information about each type of resource.

(a) Panchromatic 25A-Apollo 9, scale 1/240,000.

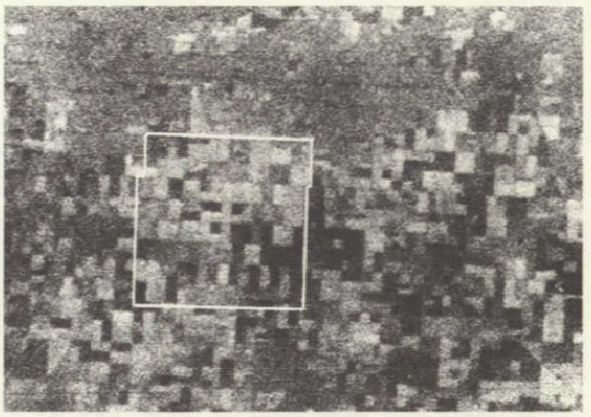

(b) Panchromatic 58-Apollo 9, scale 1/240,000.

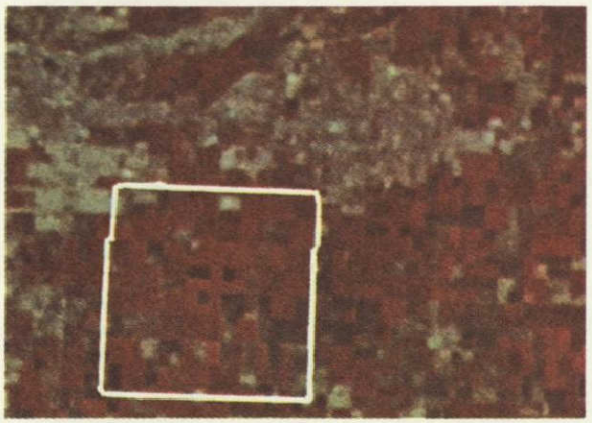

(c) Infrared Ektachrome-Apollo 9, scale 1/240,000.

(d) Infrared Ektachrome-High altitude flight, scale 1/110,000.

Figure 21-3.- Two kinds of small scale imagery have been employed in this study. Apollo 9 space photographs (a, b, c) and high altitude aerial photos (d) were obtained in March, 1969, and are reproduced above at the scales indicated. The area outlined is a sixteen square-mile area in which detailed ground data regarding crop type and condition have been gathered on the date of each high altitude flight. Even though the high altitude aerial photograph is of higher resolution than the space photograph, preliminary interpretation results indicate that crop type can be distinguished with essentially the same success on both space and high altitude photographs.

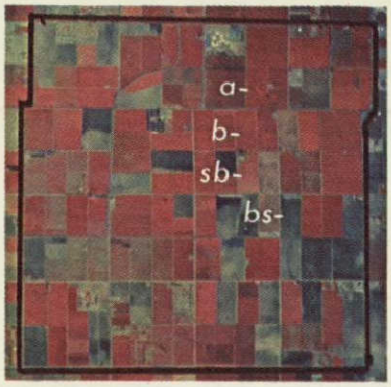

(a) March 12, 1969.

(b) April 23, 1969.

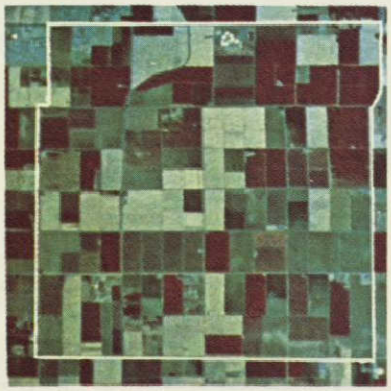

(c) May 21, 1969.

(d) August 5, 1969.

Figure 21-4.- These high altitude photographs of the Mesa test site were obtained during the 1969 growing season on the dates indicated. Changes in tone can be correlated with stage of crop development as indicated in the crop calendar (Figure 6). For example, the barley field (b) on the March photo cannot be distinguished from the alfalfa field (a) or the sugar beet field (sb) adjacent to it. However, in May the barley field has matured and can be distinguished from alfalfa and sugar beets. In August the sugar beet field has been harvested and can be distinguished from the alfalfa field. Note also how fields that contained bare soil in March (one such field is labeled bs) supported a continuous cover of cotton in August. In general, the analysis of sequential photographs for crop identification produces better results than if only photographs taken on one date is studied. The barley sequence is found in band no. 1 of the crop calendar, bare soil appears in band no. 2, sugar beets in band no. 3 and alfalfa is in band no. 4.

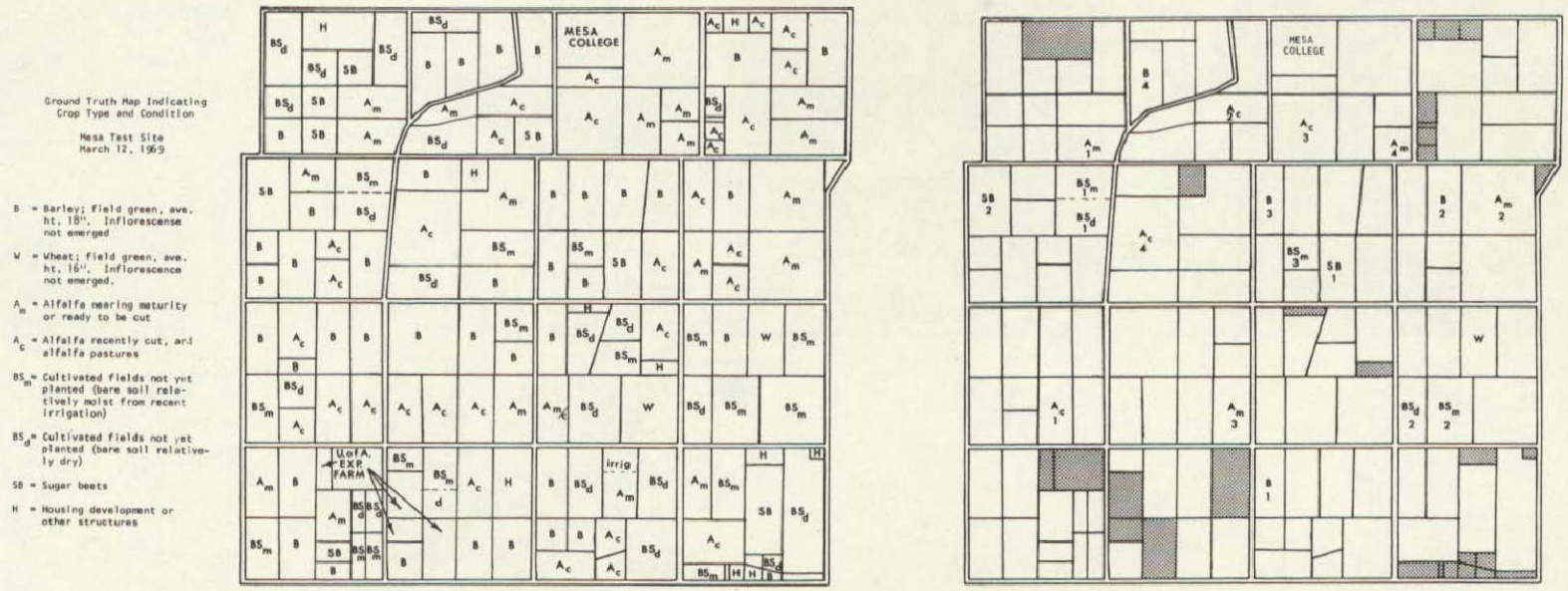

Figure 21-5.- The map on the left (a) contains ground truth information for the sixteen square-mile Mesa test site on March 12, 1969. Repetitive collection of these data is necessary to make optimum use of the sequential photography. The map on the right (b) was prepared for use in the interpretation test for crop identification. The annotated fields are training examples which were selected to represent the variability of signature for each crop type. Shaded areas are areas not containing crops (i.e., housing developments, feedlots, etc.). After studying the training fields on the test image, the interpreters were asked to identify the remaining fields in the test site.

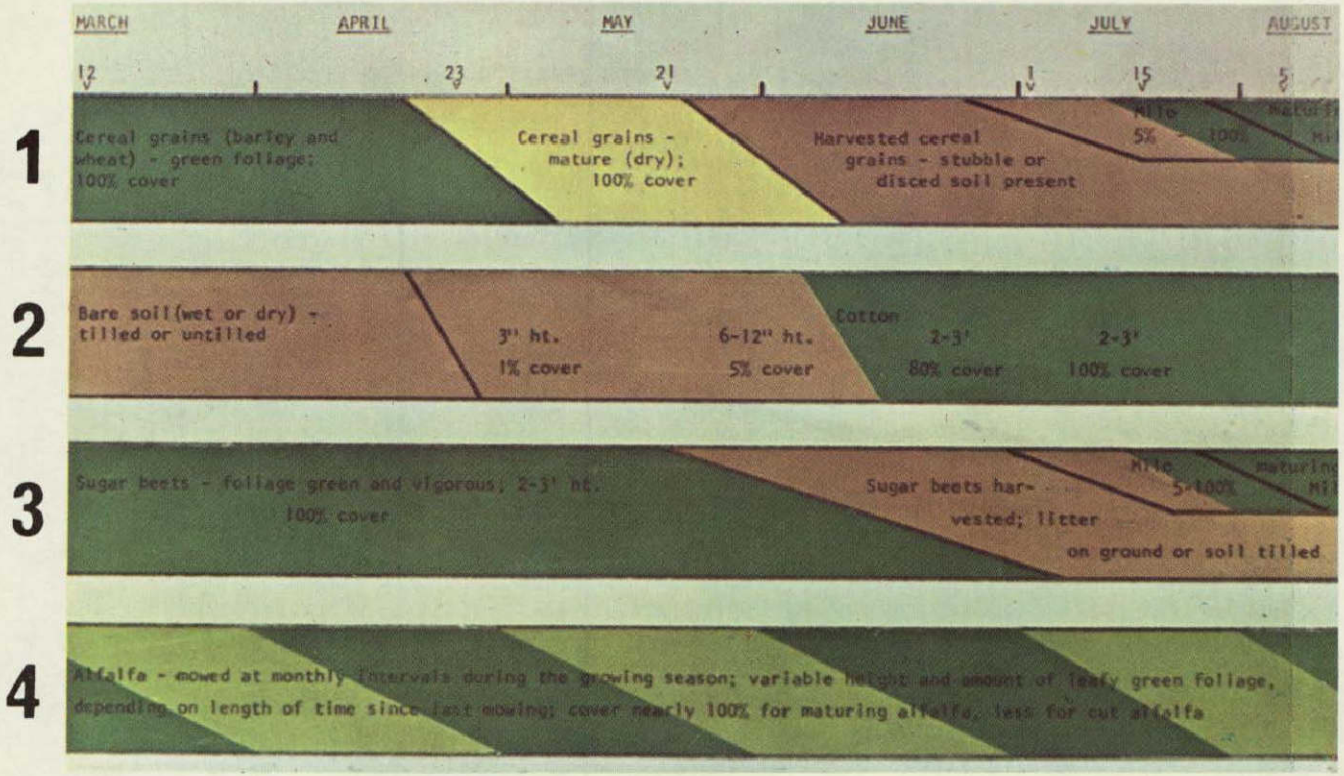

Figure 21-6.- This crop calendar summarizes four distinct patterns of crop development which have been identified in the Mesa agricultural test site during the 1969 growing season. The descriptions in each band indicate the crop type and general condition of each crop for the corresponding time period. The slope of the diagonal lines separating one condition from another is representative of the rate at which changes occur. For example, most cotton planting occurs at the same time (steep slope) while sugar beet fields are harvested over a period of several weeks (gradual slope). Dates at the top of the calendar indicate when ground truth data were collected.

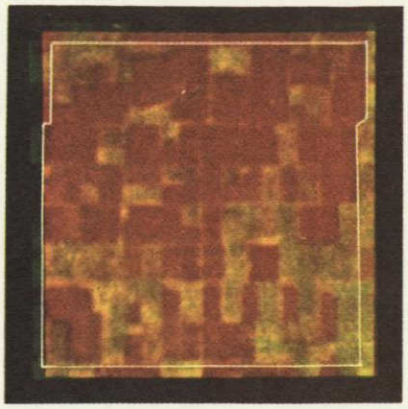

(a) FRSL color composite made from Pan-25A, Pan-58 and IR-89B Apollo 9 space photographs.

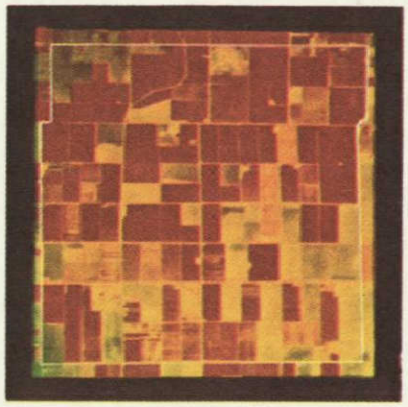

(b) FRSL color composite made from Pan-25A, Pan-58 and IR-89B high altitude photographs.

(c) Philco-Ford color composite made from Pan-25A and IR-89B high altitude photographs.

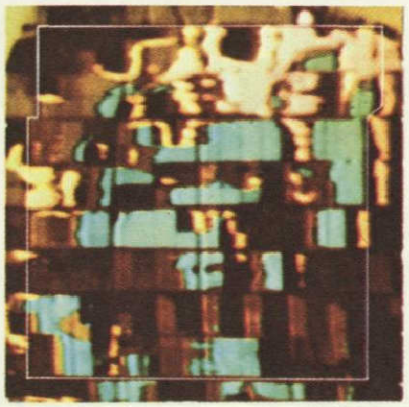

(d) IDECS color composite made from Pan-25A, Pan-58 and IR-89B high altitude photographs.

Figure 21-7.- Examples of various color composite images of the Mesa agricultural test site. Images (a), (b), and (c) were prepared to enhance the overall interpretability of the image, while image (d) was prepared so as to enhance barley (green) and alfalfa (yellow) from all other crops. Images (a) and (b) were both prepared using the same colored filters and, except for differences in resolution, produce similar color signatures for the fields on the images.

(a) Infrared Ektachrome oblique photograph of range transect.

(b) Enlargement of Infrared Ektachrome Apollo 9 photograph.

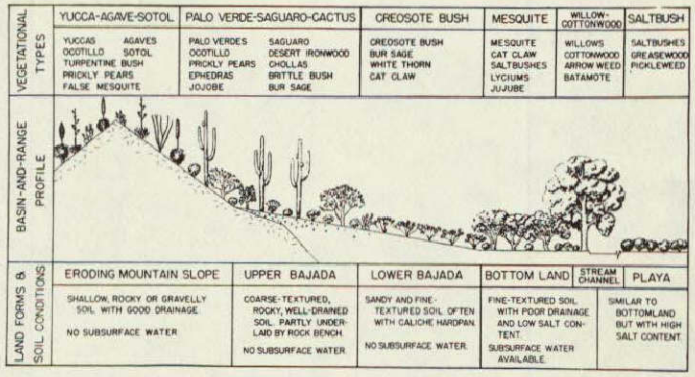

(c) Idealized profile showing relationship between land surfaces and vegetation-soil types.

(d) Reduction of portion of 70mm HyAc panoramic Infrared Ektachrome photograph.

Figure 21-8.- A transect across the semidesert shrub type in an area southwest of Phoenix, Arizona, is shown here. Neither of the small scale images (b or d) provides directly the detailed information regarding vegetation type and condition, soil type and moisture availability that is needed by the range manager. If the relationship between vegetation types and landforms depicted in (c) (from Benson, L. and R. S. Darrow, "The Trees and Shrubs of the Southwestern Deserts," Univ. of Arizona Press, 1954) is understood, the interpreter can make valid inferences between vegetation and landforms. Field work along a line from the salt playa to the mountains, as seen on (a), (b) or (d) above, has documented that these relationships do exist (see Figure 20-9).

(a) Upper bajada.

(b) Lower bajada.

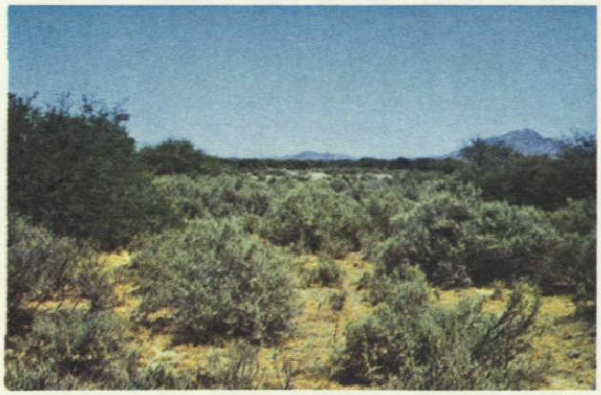

Figure 21-9.- These ground photographs show the general appearance of the plant species which occupy various portions of the range transect of Figure 8. Field checking in each zone has confirmed the relationship between species and landforms and soil conditions. The upper bajada (a) contains palo verde, creosote and saquaro cactus. The lower bajada (b) is covered with creosote. Mesquite and saltbush dominate the bottomland (c). The playa (d) supports only sparse stands of salt-tolerant herbs and grasses. Once these relationships have been confirmed, it is possible to infer the presence of vegetational types from the recognition of characteristic landforms.

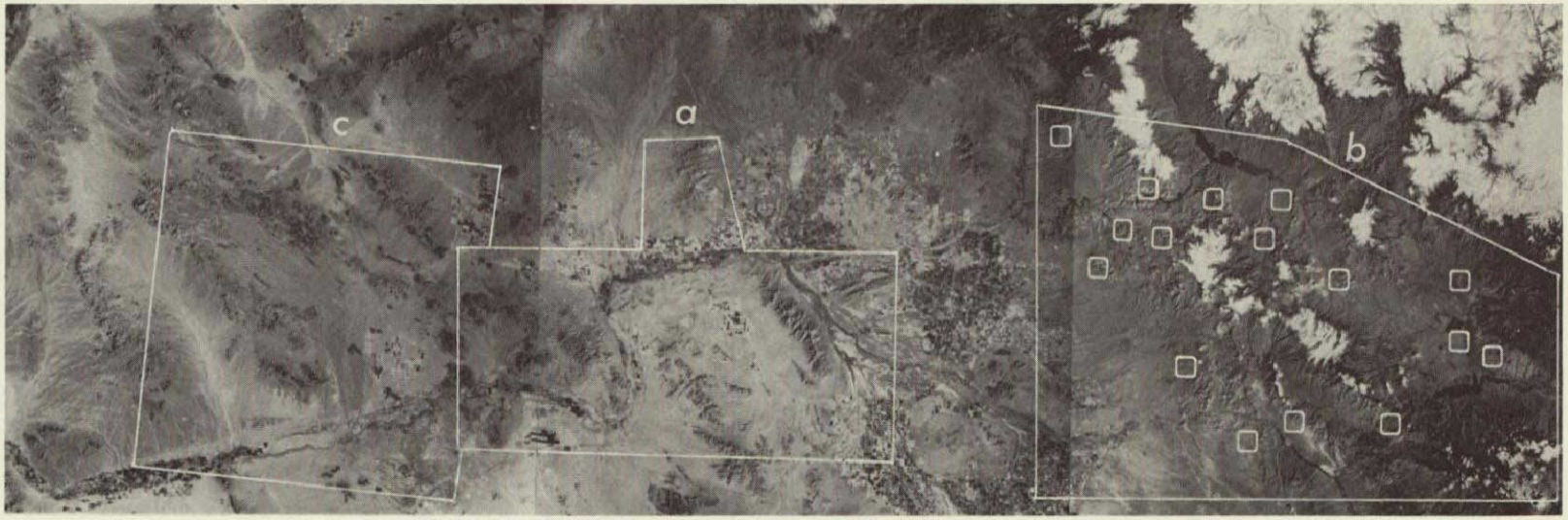

Figure 21-10.- Photo mosaic of the area from Yuma to Roosevelt Lake prepared from Infrared Ektachrome Apollo 9 photographs. Outlined here are the three geology study areas: (a) the familiarization area at Gila Bend, (b) the main study area around Roosevelt Lake and San Carlos Reservoir (non-stereo coverage), and (c) the test area east of Yuma (stereo coverage). Small squares in the main test area represent locations where ground survey work will be undertaken.

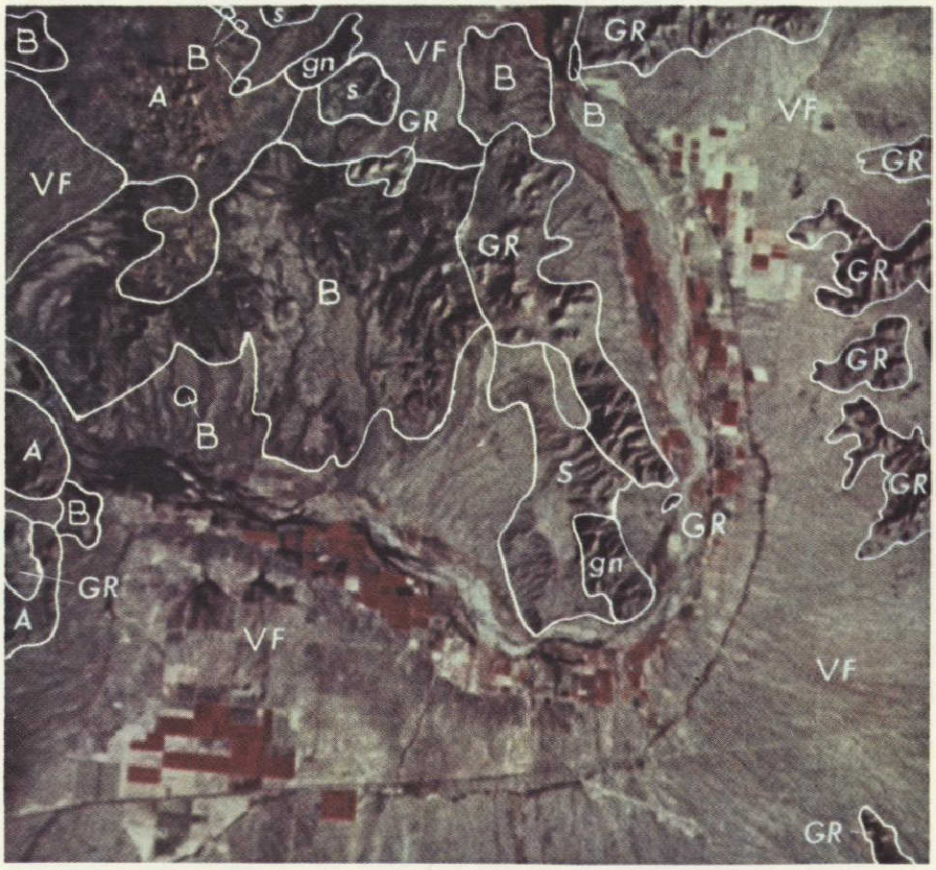

Figure 21-11.- Geologic overlay of the Gila Bend, Arizona, area, prepared with reference to the Arizona Bureau of Mines Geologic Map of Maricopa county. This overlay was used to help the interpreter become familiar with the image characteristics of geologic features on orbital photography. Many rock types are present: Igneous - Andesite = A, Basalt = B, Granite = GR; Metamorphic - Granite gneiss = gn, Schist = s; Sedimentary = S; Unconsolidated valley fill = VF.

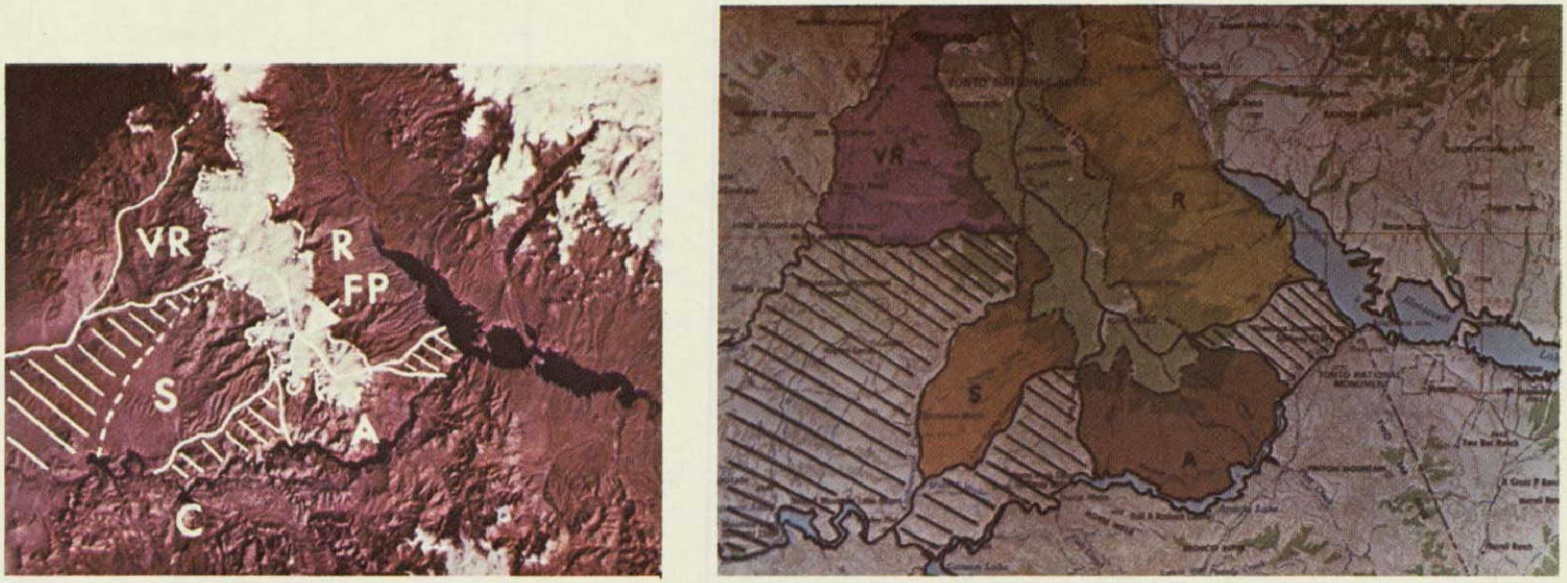

Figure 21-12.- Sectioning of the annual snowpack on Apollo 9 photography has been tested using the Four Peaks area of the Mazatzal Mountains east of Phoenix, Arizona. On the left photo (enlargement of Apollo 9 Infrared Ektachrome frame AS-26-3802), the snow pack has been delineated according to the drainage basin which will receive each portion of the snowmelt. Dotted lines represent questionable delineations. The right photo is a portion of a topographic map where the same delineations have been made. Shaded areas denote where no melt water will flow. Close agreement between the two delineations indicates some promise for this technique to be used operationally. Place names are denoted above as follows: A = Apache Lake, R = Roosevelt Lake, S = Saguaro Lake, VR = Verde River, FP = Four Peaks, C = Canyon Lake.

SECTION 22

INTERACTION OF ELECTROMAGNETIC ENERGY WITH AGRICULTURAL CROPS [1]

Craig L. Wiegand, Harold W. Gausman, William A. Allen, and Ross W. Leamer [2]

ABSTRACT

The remote sensing research program at Weslaco is studying (a) the interaction of electromagnetic radiation with plants, soils, and water and (b) wavelengths and procedures for discriminating agricultural crops. Some results are:

1. Absolute spectrophotometric data indicate that over the wavelength interval 500 to 1400 nm (nanometers), leaf signature is mainly a function of leaf pigments and structure; and, growth stress conditions cause a rounding of the reflectance plateau in the wavelength interval 750 to 900 nm.

2. The discrimination of crop species based on infinite reflectance (R_∞) was very successful for the wavelength interval 1300 to 2200 nm. R_∞ can be measured remotely and the useful wavelengths occur in atmospheric windows.

3. Two pattern recognition techniques, the "Minimum Distance to the Mean" (MDM) and the "Statistical Pattern Recognition" (SPR), were investigated. MDM schemes are deemed adequate and involve considerably fewer formula steps and less computer time than SPR procedures.

4. Advances in photographic transparency quantitization and analysis a: illustrated using Apollo 9 SO-65 Experiment and aircraft imagery. The techniques involve use of optical density differences among densities measured with different bandpass filters in the light beam and no filter in the light beam. The procedures have been computerized for crop and soil condition discrimination.

---

[1] Contribution from the Soil and Water Conservation Research Division, Agricultural Research Service, USDA. Research reported done in cooperation with Texas A&M University and supported in part by NASA Contract No. R-09-038-002, Current Code No. 160-75-01-07-10.

[2] Research Soil Scientist, Research Plant Physiologist, Research Physicist, and Research Soil Scientist, respectively, USDA, Weslaco, Texas.

INTRODUCTION

Aims of the remote sensing research program at Weslaco (site No. 32) are: (a) understanding the interaction of electromagnetic radiation with plants, soils, and water; (b) advancing analytical procedures for discriminating agricultural crops and growth stress conditions; and (c) recommending useful wavelengths for incorporation into operational systems. Both laboratory and field investigations are conducted. Irrigated agricultural crops and soil conditions, and reliable supporting ground truth are emphasized. The presentation today consists of a cross section of results from the 1969 Annual Report (1). The illustrations are chosen to give you a general view of the nature and the scope of our investigations. Aircraft and spacecraft data received, and plans for the coming year are also described.

AIRCRAFT AND SPACECRAFT DATA

Aircraft and spacecraft data obtained at our request or used by us this past year are indicated below.

Mission 75 was flown July 8, 1968 with the Convair 926. The resulting data (AAS-5, RC-8 camera, Reconofax IV, 13.3 GHz scatterometer) are only fair for the following objectives: identification of crop types and conditions; identification of soil types; relation of plant temperature to soil moisture conditions; detection of brown soft scale (Coccus hesperidum L) infestation of citrus trees; and relation of altitude to remote sensor imagery.

The Apollo 9 spacecraft did not cover test site 32 as we had hoped, but SO-65 photography frame numbers AS-9-26A-3726, Matagorda, Eagle Lake, Freeport, Texas area; AS-9-26A-3799, Salton Sea and Imperial Valley, Calif. and Mexico-Mexicali; and AS-9-26A-3808, Lubbock, Texas have been studied and found useful for soil survey and crop species identification (2, 3). Color enhancements of these same frames were supplied by NASA through Dr. Yost of Long Island University. Frame AS-9-26A-3799 has also been used for a multiemulsion (Kodak[3] Ektachrome infrared aero) versus multibase (black and white film exposed in the green, red, and photographic infrared separately) comparison of crop species discrimination (3).

NASA provided Bendix 9-channel scanner overflights of Weslaco test sites on April 13, May 8 and 9, June 6, and July 9 of this year. It is hoped the magnetically taped outputs will yield quantitative reflectance data over the 380 to 1000 nm wavelength interval. We will also cooperate closely with NASA and Bendix on a signature data processing study using the data from these flights. Part of the data have been delivered. A ground truth report is being compiled.

---

[3] Company and trade names are included for the benefit of the reader and do not infer recommendation or preferential treatment of the products mentioned by the U. S. Department of Agriculture.

PRESENTATION OF RESULTS

In order to interpret remote sensing data acquired from aircraft and spacecraft, the reflectance produced by features on the surface of the earth must be understood. The specific problem in agriculture is interpretation of reflectance produced by vegetation, usually superimposed upon a soil background. Plant leaves yield most of the signal measured by remote sensors in aircraft and spacecraft and are therefore of prime interest in characterizing vegetation.

Figure 1 presents the absolute reflectance, transmittance, and absorptance data for a single cotton plant leaf over the 500 to 2500 nm wavelength interval. (This wavelength range is useful because it encompasses the wavelengths over which earth objects reflect most strongly). The absolute data are achieved by careful calibration of the laboratory spectrophotometer (4). The reflectance and transmittance spectra are very similar in magnitude and pattern over the entire wavelength interval. In the interval 750 to 1350 nm, the leaves are essentially transparent as is apparent from their low absorptance. The light reflectance and transmittance of leaves are dominated by their cellular structure and pigment contents in the 500 to 1350 nm wavelength interval and by their water content in the 1350 to 2500 nm wavelength interval (5, 6, 7, 8, 9).

Figure 2 (8) demonstrates a phenomenon that may be useful in remote sensing applications, namely the rounding of the reflectance plateau in the wavelength interval 750 to 900 nm, caused by internal cellular discolorations within leaves under growth stress conditions (8, 10, 11, 12). This wavelength interval may become very useful in remote sensing for identifying nonvisual symptoms of plant leaf stresses caused by insects, viruses, diseases, frost, and atmospheric pollutants.

A series of theoretical analyses have been made of the interaction of light with a plant canopy (13, 14), compact leaves (9) such as corn, and noncompact leaves (4, 15) such as cotton and soybeans. A compact leaf has few and a noncompact leaf has many intercellular air spaces in the mesophyll (5, 9, 15). The understanding of the interaction of visible and near infrared radiation with plant leaves that has come from these studies contributes much to understanding the response of remote sensors aimed at crops and provides a basis for anticipating differences among crops.

For example, the experimentally measured increase in reflectance and decrease in transmittance of cotton leaves as they mature have been explained theoretically and histologically (5). Histologically most plant leaves are compact when they first unfold but as they grow intercellular air spaces develop and the leaf thickens. Theoretically the leaf can be regarded as a pile of N compact layers separated by air space. The void area index (VAI) which is roughly the average number of air cavities penetrated by a ray passing through the leaf is calculable.

Very recently the Duntley equations for propagation of specular light through a diffusing medium have been generalized and interpreted to account for the effect of sun angle on crop canopy irradiance (14). Applied to a corn canopy at Ithaca, New York, the equations fit the experimental results within 3.2% for a period from noon to sundown. When laboratory-measured optical constants were used, the equations fit the data within 3.7%.

The theoretical work also yields fundamental optical information. One of the most interesting quantities for remote sensing purposes is the infinite reflectance, R_∞ (4, 15). The reflectance of crops against a soil background increases as number of leaf layers in the plant canopy increases until a stable value of reflectance termed the infinite reflectance is reached. The single leaf and infinite reflectance of cotton leaves are shown in Figure 3 for the wavelength interval 500 to 2500 nm. In the visible and in the 1500 to 2500 nm wavelength intervals the infinite reflectance is reached by the time plants reach a leaf area index (LAI) of 2. (LAI is defined as the cumulative one-sided leaf area per unit ground area measured from the canopy top to a plane at a given distance above ground.) In the 750 to 1350 nm wavelength interval a LAI of about 8 is required to reach R_∞, because of the transparency of the leaves (See figure 1). As shown in Figure 3 a typical mature cotton leaf reflects 48% of the incident radiation in this region. It transmits about the same amount to leaves below it on the plant which, in turn, reflect about half and transmit about half the radiant energy. Multiple transmission and reflection from leaves in a plant canopy result in a reflection maximum of about 75% of the energy incident on a mature crop canopy in the 750 to 1350 nm wavelength interval.

The leaves of corn, squash, and sorghum grown in the greenhouse and of sorghum, wheat, mature corn, cotton, sugar beets, potatoes, young corn, tomatoes, cabbage, and onions collected from the field have been analyzed for discrimination signatures using infinite reflectance at 50 nm wavelength intervals over the spectral range 500 to 2500 nm as the discrimination criterion (4). The largest differences in R_∞ among species occur in the atmospheric windows 1500 to 1750 nm and 2000 to 2400 nm. Since the leaf area index necessary to yield the infinite reflectance occurs early enough in the growing season of most crops to make estimates of acreage and yield forecasts valuable, discrimination procedures using measurements of reflectance from space in these wavelength intervals show considerable promise.

Table I presents the number of observations representing wheat, cotton, potato, cabbage, and onion plants; how each was classified; and the percent correct recognition achieved using R_∞ as the discrimination criterion (4). The overall percent recognition for all plants was 85.5%.

The reflectance and transmittance spectra reduced to the Kubelka-Munk parameters suggest that over the wavelength interval 1400 to 2500 nm, the absorption spectra of leaves are not statistically different from that of pure liquid water. Thus the physical quantity indirectly sensed by measuring R_∞ is the extent to which the water in the leaf has been subdivided by the cellular structure typical of the plant genus or species. Figure 4 presents the absorption spectrum for a corn leaf (5). The open circles on the curve represent the cotton leaf; the closed circles on the curve are the published values for pure liquid water (16).

Two pattern recognition techniques, the "Minimum Distance to the Mean" (MDM)(17) and the "Statistical Pattern Recognition" (SPR) (17, 18, 19, 20, 21), were investigated for discrimination reliability and amount of computer usage. The MDM schemes involve considerably fewer formula steps, hence computer time, and are considered adequate for agricultural applications (4).

Another important aspect of the program at Weslaco is film analysis. In the beginning we tried to use optical density to obtain quantitative digital data from film transparencies for correlation with ground truth soil, crop, and ground cover conditions. Correlations were poor. We then discovered that the differences among the optical densities measured with various bandpass filters in the microdensitometer beam would minimize the frame-to-frame and flight-to-flight variability caused by exposure conditions, film batches, and differences in processing. Figure 5 illustrates how optical counts from the microdensitometer, which are linearly related to film optical density, form a pattern for various crop cover conditions. Notice, for example, that the patterns for the bare fields 4 and 71 are very similar in shape, but are displaced on the ordinate. The displacement on the ordinate is due to variations in film density, yet the pattern is the same, because the optical density differences among filters are the same.

Computer programs have been developed to recognize various crop, soil cover, and soil condition categories (2, 3). The results of one such analysis are illustrated in Figure 6. A standard signature for cotton, sorghum, and bare soil was developed from their optical density differences measured for a number of fields of each category. In the computer program a sum of squares of differences from the crop standards is accumulated for each unknown. The unknown is identified as belonging to the crop or soil condition from which its signature differs minimally. The same technique has been used on space photography of the Imperial Valley, California (2, 3).

The film analysis method has been extended by fitting the optical density differences to regression equations which encompass the encountered range of film density to white light. This technique permits greater latitude in film exposure conditions over which the imagery are useable and narrows the confidence band around each crop or soil condition category so that more categories can be included and still be unambiguously identified. The standards developed this summer from previous years' film will be used to identify crops, soil, and water conditions on imagery obtained this year.

FUTURE PLANS

Our plans for the near future include:

(1) Bridging the gap between the primarily laboratory and theoretical work by trying to apply the most useful concepts in our field work. Some useful data should come from the Bendix overflights and from the field spectrometer on order. Another aspect of this endeavor is determining and obtaining the most meaningful ground truth for interpreting aircraft and spacecraft data.

(2) Continuing photographic analyses to test and improve the procedures.

(3) Working intensively on the Bendix overflight data and cooperating with NASA and Bendix on the signature data processing study.

(4) (a) Requesting an RB-57 flight primarily to obtain imagery useful to the Soil Conservation Service for soil survey and mapping purposes. Our experience indicates that space photography would be useful in soil mapping (2); the high man-power requirement for ground-based surveys make the use of aerial and space photography very attractive.
(b) Working on the thermal data from the C130 flight which has been scheduled in January 1970 to coincide with highest likelihood of frost conditions.

(5) Continuing cooperation with sister agencies such as Statistical Reporting Service (crop condition and yield forecasts); Statistics Institute (statistical analysis of film lots, cameras, and altitude on film density) and Remote Sensing Institute (various projects) of Texas A&M University; Entomology Research Division, USDA (citrus insect surveys); and, Crops Research Division, USDA (nematode and vegetable disease incidence studies).

In conclusion we wish to acknowledge the cooperation, assistance, and helpfulness of the many individuals in the NASA Earth Resources Division with whom it is so pleasant to work.

LITERATURE CITED

(1) Remote Sensing Investigations Staff, Spectral Survey of Irrigated Region Crops and Soils, 1969 Annual Report to NASA, Oct. 1, 1968 to Sept. 30, 1969, USDA-ARS-SWC, Weslaco. 296 pp.

(2) Wiegand, C. L., R. W. Leamer, and A. H. Gerbermann. Crop Species and Soil Condition Discrimination on Ektachrome Infrared Apollo 9 Imagery and Interpretation of Agricultural Features on SO-65 Experiment Color Recombinations. Apollo 9 Science Report. 1969. 36 pp + 2 appendices.

(3) Wiegand, C. L., R. W. Leamer, D. A. Weber, and A. H. Gerbermann. Comparison of Multibase and Multiemulsion Photography for Identifying Crop and Soil Conditions from Space. (In preparation; for submission to Photog. Engin.)

(4) Richardson, A. J., W. A. Allen, and J. R. Thomas. Discrimination of Vegetation by Multispectral Reflectance Measurements. Proc. 6th Symp. on Remote Sensing of Environment, Univ. of Mich., Ann Arbor, 1969.

(5) Gausman, H. W., W. A. Allen, R. Cardenas, and A. J. Richardson. Relation of Light Reflectance to Cotton Leaf Maturity (Gossypium hirsutum L). Proc. 6th Symp. on Remote Sensing of Environment, Univ. of Mich., Ann Arbor, 1969.

(6) Gausman, H. W., and R. Cardenas. Effect of Soil Salinity on External Morphology of Cotton Leaves. Agron. J. 60:566-567. 1968.

(7) Gausman, H. W., W. A. Allen, and R. Cardenas. Reflectance of Cotton Leaves and Their Structure. Remote Sens. Environ. 1:19-22. 1969.

(8) Cardenas, R., H. W. Gausman, W. A. Allen, and M. Schupp. The Influence of Ammonia-induced Cellular Discoloration Within Cotton Leaves (Gossypium hirsutum L) on Light Reflectance, Transmittance, and Absorptance. Remote Sens. Environ. 1970. (In press).

(9) Allen, W. A., H. W. Gausman, A. J. Richardson, and J. R. Thomas. Interaction of Isotropic Light With a Compact Plant Leaf. J. Opt. Soc. Amer. (In press)

(10) Colwell, R. N. Determining the Prevalence of Certain Cereal Crop Diseases by Means of Aerial Photography. Hilgardia 26:223-286. 1956.

(11) Keegan, H. J., J. C. Schleter, W. A. Hall, Jr., and G. M. Haas. Spectrophotometric and Colorimetric Study of Diseased and Rust Resisting Cereal Crops. National Bureau of Standards Rpt. 4591. 1956.

(12) Hart, W. G., S. Ingle, and V. I. Myers. Detection of Arthropod Activity on Citrus Foliage With Aerial Infrared Color Photography. Proc. Workshop on Aerial Color Photography in the Plant Sciences, Gainesville, Fla. Mar. 5-7, 1969. (In press).

(13) Allen, W. A., and A. J. Richardson. Interaction of Light With a Plant Canopy. J. Opt. Soc. Am. 58:1023-1028. 1968.

(14) Allen, W. A., T. V. Gayle, and A. J. Richardson. Plant Canopy Irradiance Specified by the Duntley Equations. Submitted to J. Opt. Soc. Am. for publication consideration.

(15) Allen, W. A., H. W. Gausman, and A. J. Richardson. Mean Effective Optical Constants of Cotton Leaves. Prepared for J. Opt. Soc. Am.; under review.
(16) Curcio, J. A., and C. C. Petty. The near infrared absorption of liquid water. J. Opt. Soc. Am. 41:302-304. 1951.
(17) Fu, K. S., and G. P. Cardillo. Optimum Finite Sequential Pattern Recognition. Lab. Applications Remote Sensing, Purdue, LARS Information Note 070767. 1968.
(18) Rosenfeld, A. Automatic Recognition of Basic Terrain Types From Aerial Photographs. Photo. Eng. 28:115-132. 1962.
(19) Kashyap, R. L. Recursive Algorithms for Pattern Classification Using Misclassified Samples. Presented at 7th Adaptive Symp., Los Angeles, Calif. 1968.
(20) Landgrebe, D. A., P. J. Min, P. H. Swain, and K. S. Fu. The Application of Pattern Recognition Techniques to a Remote Sensing Problem. Presented at 7th Adaptive Symp., Los Angeles, Calif. 1968.
(21) Freeze, Frank. Linear Regression Methods for Forest Research. U. S. Forest Service Research Paper, Forest Prod. Lab. Bul. 17. 1964.

Table I. Percent correct recognition using R_∞ for field-grown wheat (W), cotton (Co), potatoes (P), cabbage (Ca), and onions (O) using wavelengths 2.20, 2.15, 1.80, 1.75, 1.70, 1.65, 1.60, 1.30, 1.25, and 1.20 μ in a minimum distance to the mean pattern recognition technique.

Vegetation	Total number of observations	Samples classified into W	Co	P	Ca	O	Percent recognition
Wheat	21	21	0	0	0	0	100.00
Cotton	50	1	45	4	0	0	90.00
Potatoes	20	0	2	14	4	0	70.00
Cabbage	20	0	1	3	13	3	65.00
Onions	20	0	0	0	1	19	95.00
	Overall percent recognition						85.49

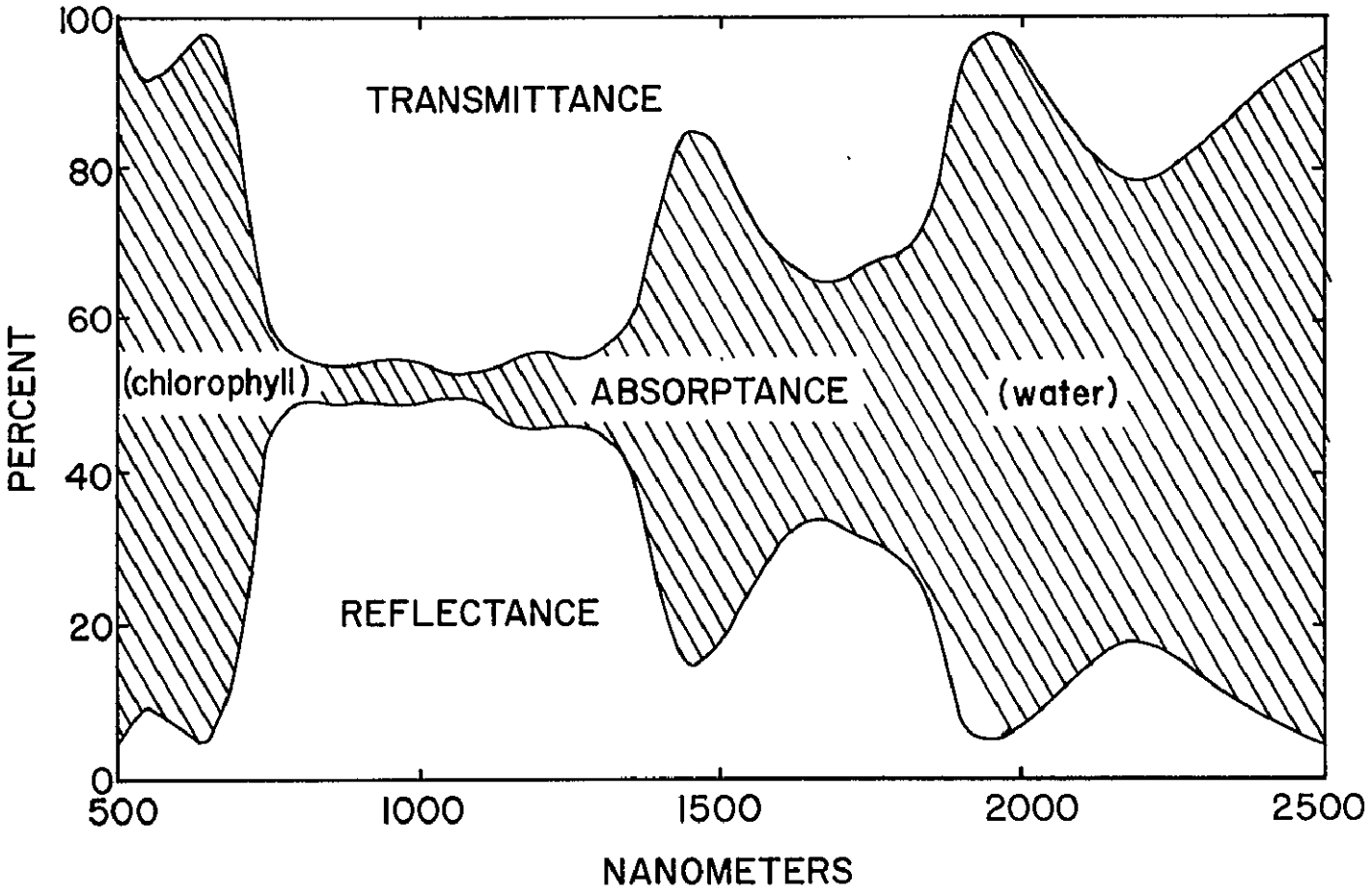

Figure 22-1.- Absolute reflectance, transmittance, and absorptance data for cotton plant leaves over the 500 to 2500 nm wavelength interval. Plant leaves yield most of the signal measured by remote sensors in aircraft and spacecraft that are viewing vegetation and are therefore of prime interest in characterizing vegetation. The reflectance and transmittance characteristics of leaves are dominated by their structure and pigment contents in the 500 to 1350 nm wavelength interval and by their water content in the 1350 to 2500 nm wavelength interval.

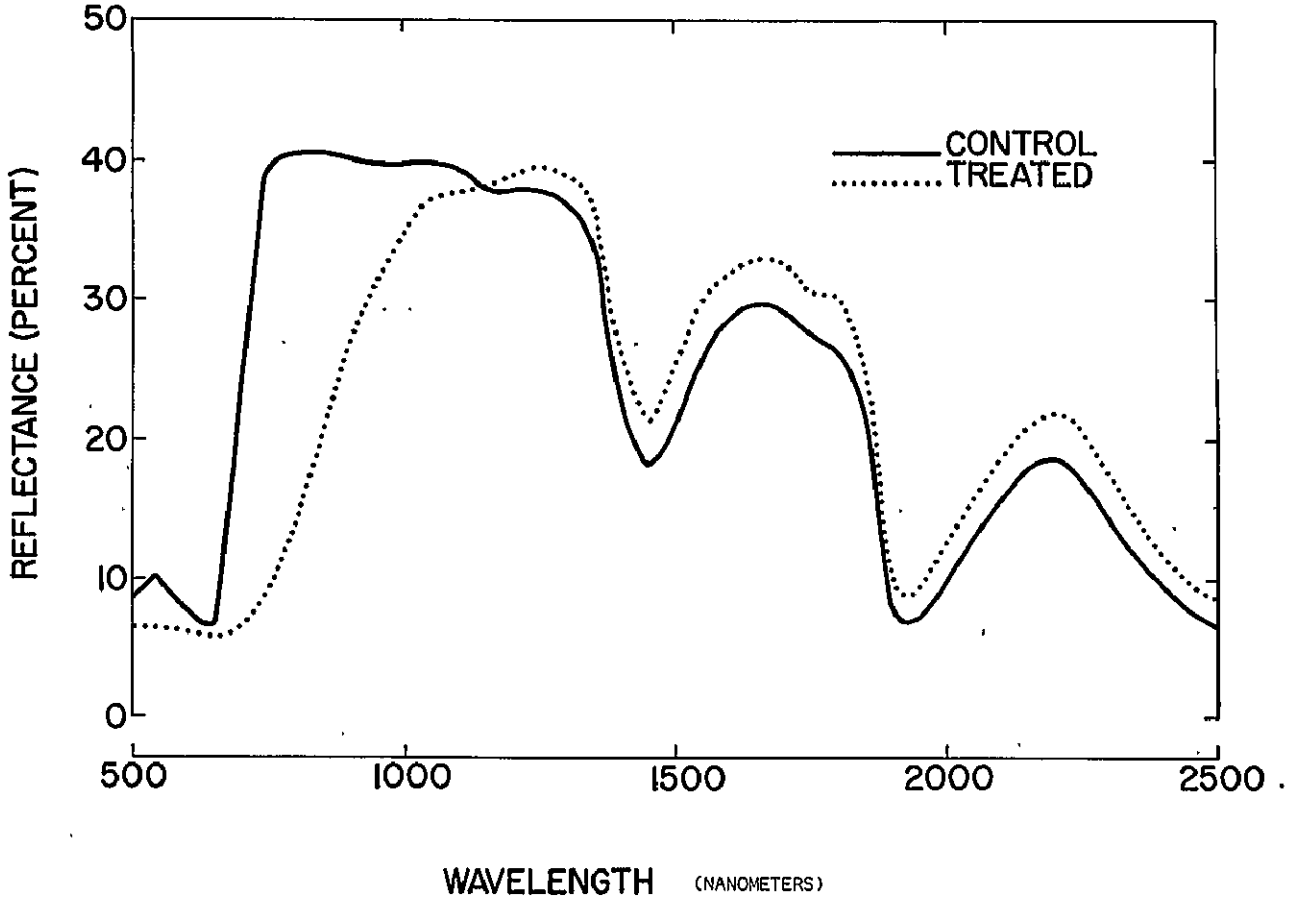

Figure 22-2.- Total light reflectance of the upper surfaces of cotton leaves exposed to ammonia vapor (treated) and unexposed (control) to ammonia. Growth stress conditions caused by insects, disease, viruses, frost and atmospheric pollutants cause a rounding of the reflectance plateau in the 750 to 900 nm wavelength interval. This wavelength may become very useful for identifying non-visual symptoms of plant growth stresses.

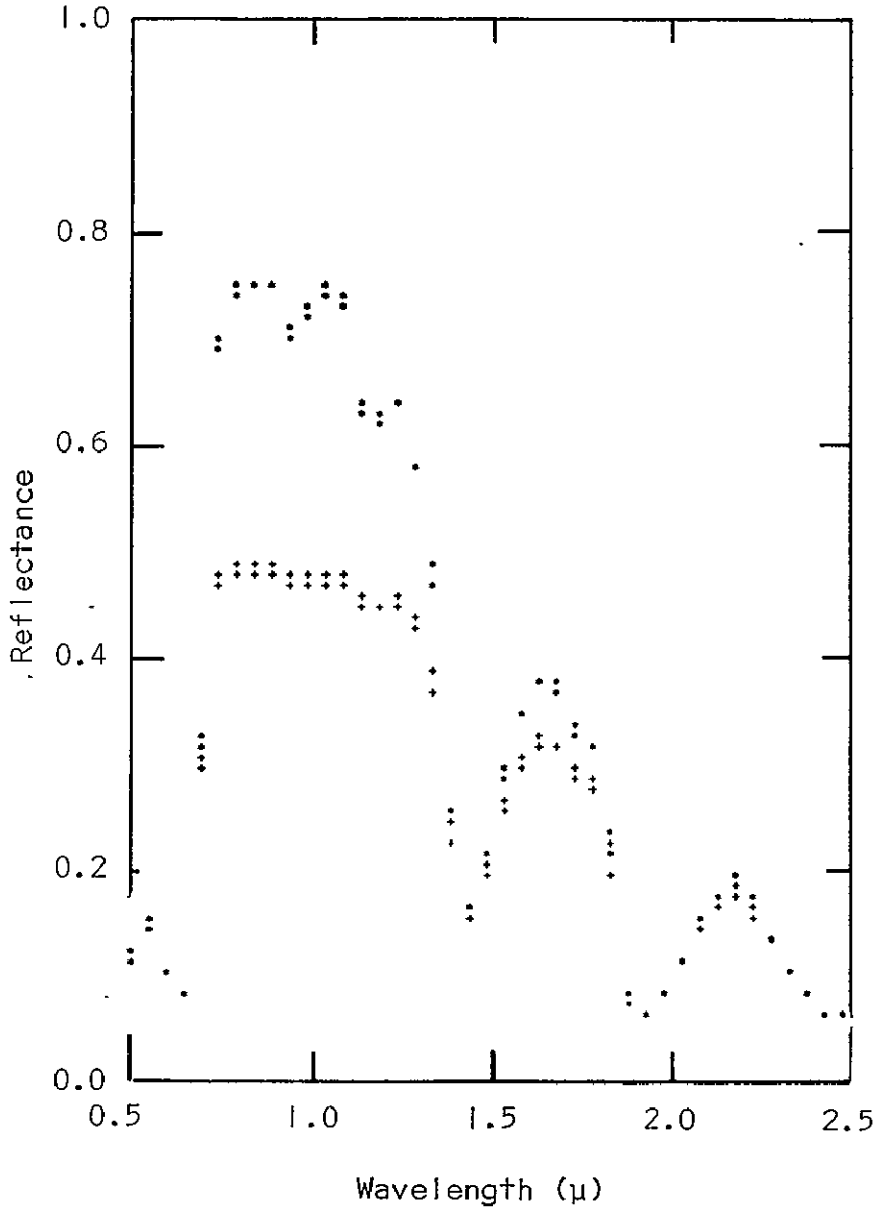

Figure 22-3.- The average diffuse reflectance of 50 single cotton leaves + and the average calculated infinite reflectance R_∞ of these leaves *. The reflectance of crops against a soil background increases as number of leaf layers in the plant canopy increases until a stable value of reflectance termed the infinite reflectance is reached. R_∞ is measurable from aircraft and spacecraft and has been found useful for crop species discrimination. (Note: $1\mu = 10^3$ nm.)

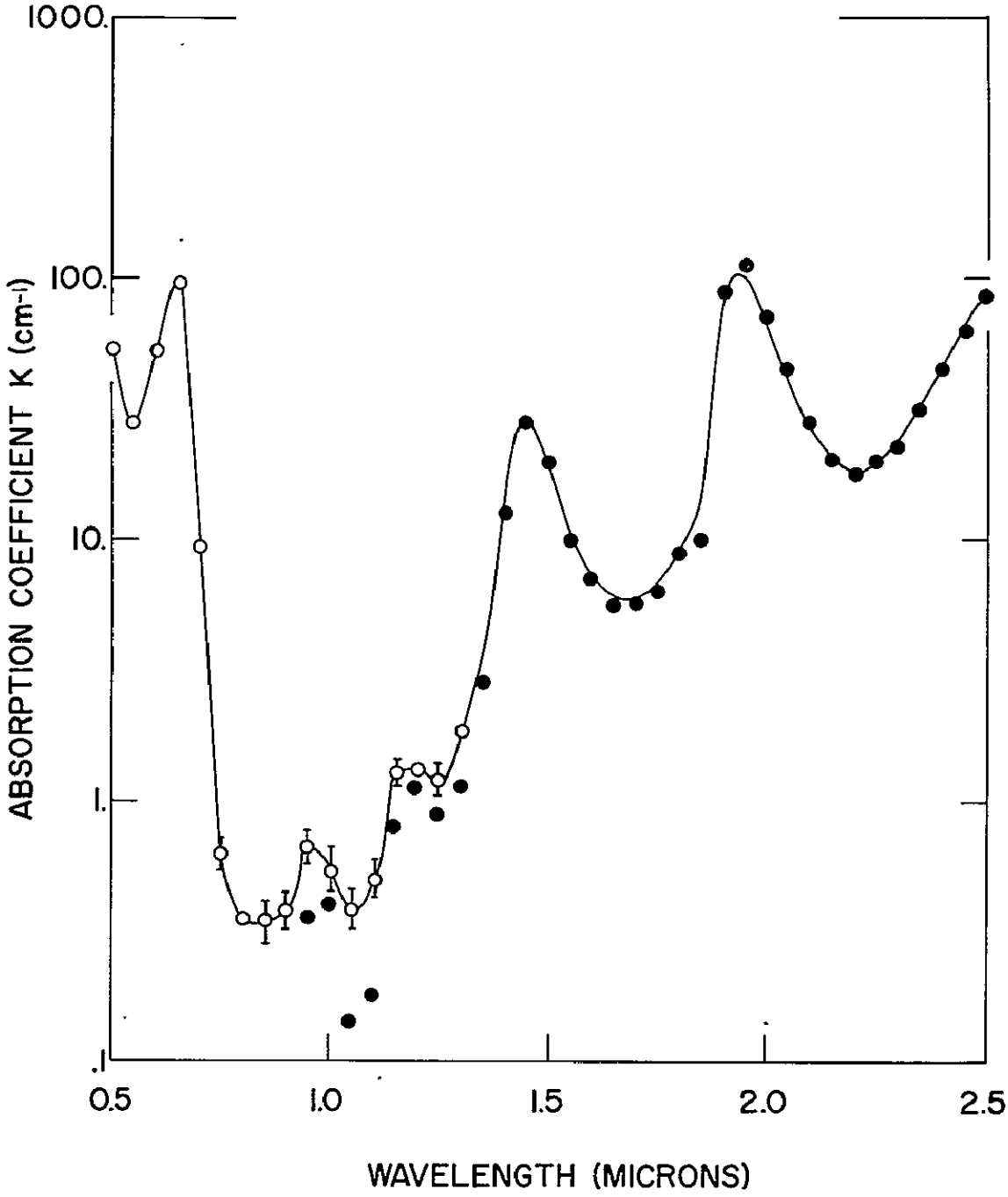

Figure 22-4.- Effective absorption curve of a maturing cotton leaf. Solid points are values for pure liquid water (Curcio and Petty, 1951). Leaf values and pure liquid water values are not significantly different statistically over the spectral range 1.4 to 2.5 μ. (Note: $1\mu = 10^3$ nm.)

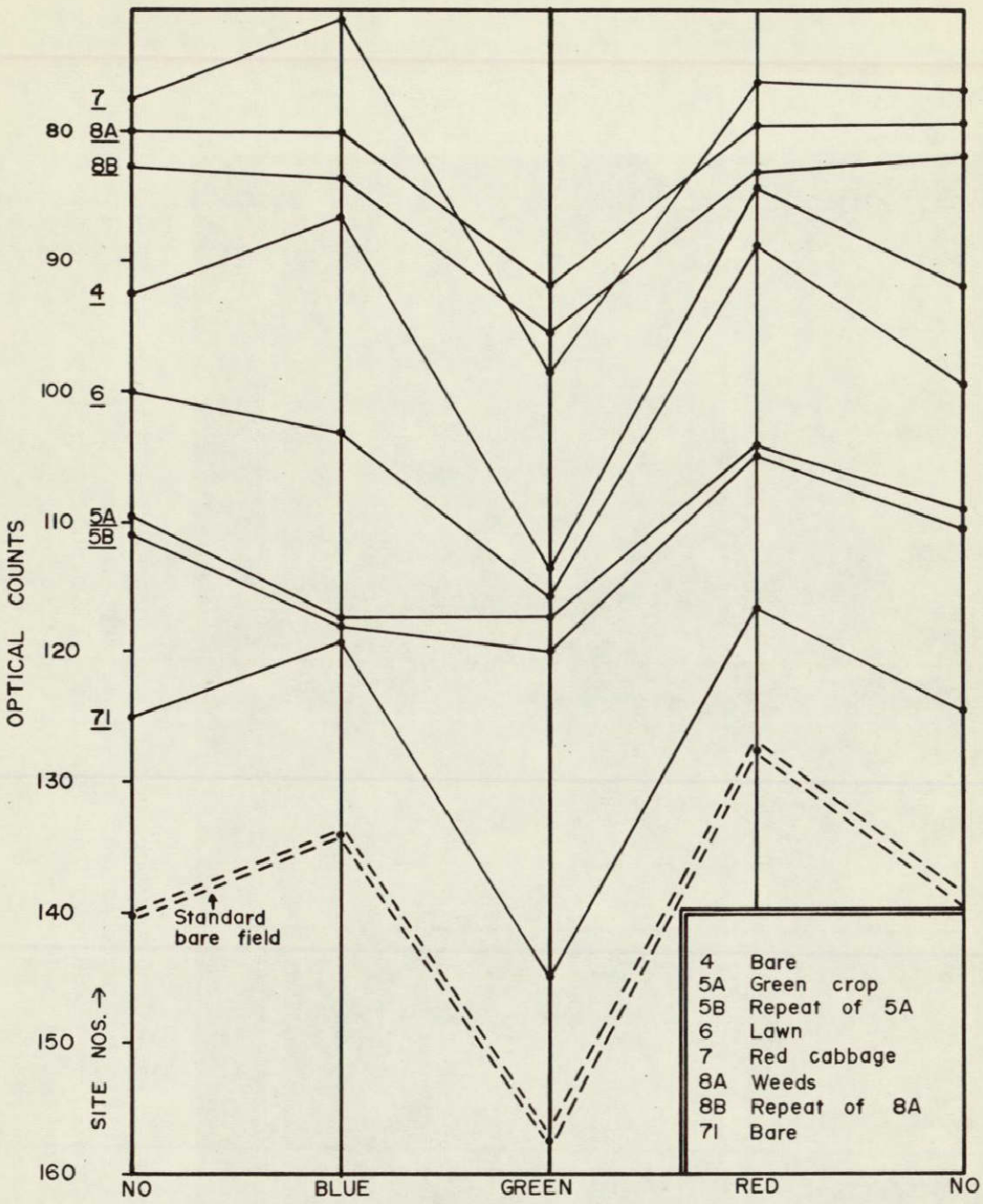

Figure 22-5.- Optical counts (linearly related to film optical density) versus color of filter in light beam for various crops and soil cover conditions. The optical density differences for a given cover condition form a pattern whereas optical densities per se are wild. Procedures have been developed and computerized for discriminating crop and soil conditions based on the optical density differences.

Figure 22-6.- Computer recognition of crops (C = cotton, B = bare soil, S = sorghum) superimposed on actual crop imagery taken July 27, 1968 from 1000 - 1200 hours at 1800 feet (Film 867). Letters appear just below the microdensitometer scan lines made on two adjacent frames across bare soil strips (green), cotton (red), and sorghum (brown) fields.

SECTION 23

APPLICATION OF AUTOMATIC RECOGNITION TECHNIQUES TO EARTH RESOURCES

R. B. MacDonald

Introduction

The National Aeronautics and Space Administration in cooperation with the United States Department of Agriculture and Purdue University continued to sponsor the Laboratory for Applications of Remote Sensing at Purdue throughout 1968/1969 to participate in the research and development of remote sensing techniques for application in agriculture.

LARS conducts a multidisciplinary program designed to explore critical problem areas in agriculture applications. Exemplary of these is the requirement for automatic processing capabilities. Automatic processing is essential to the design of information systems which adequately meet the needs of resource development planners and resource use managers. Thus, a key program area to LARS is devoted to developing a capability of automatically recognizing important earth resource features (Holmes and MacDonald, 1969; Fu, et.al., 1969).

A successful approach to this problem must include consideration of collection schemes which produce data which are generally amenable to automatic information extraction routines. Past research conducted at Purdue/LARS has established spectral radiance data to be of this nature (LARS Volume II, 1967; LARS Volume III, 1968). In 1968 and 1969 LARS continued to explore and to develop this approach in multiple investigations applied to situations involving the naturally occurring materials such as:

- vegetation
- soils
- water

In support of these investigations, LARS has organized programs in the following research areas:

- Biogeophysical
- Measurements
- Data Processing
- Requirements and Applications
- Aerospace Systems Analysis

Biogeophysical research programs are conducted by teams of application scientists. Teams have been organized to deal respectively with problems of vegetation, soils, and water. The primary objectives

of this research are the correlation of remotely sensed measurements to physical and chemical properties of radiating scenes.

The results of research at LARS to apply advanced remote sensing and processing techniques to agricultural situations are discussed in this paper.

Data Collection Missions

To meet the LARS 1968-69 objectives, data collection missions were scheduled over Tippecanoe County at particular times throughout the agricultural season. Data were to be collected over some 200 square miles along the five flight lines shown in the Purdue test sites (Figure 1). Each mission was scheduled at what was considered to be a cardinal point in the agricultural season in Indiana. Multispectral measurements together with multichannel photography were to be collected by the University of Michigan aircraft in April, June, August, October, and December. The aircraft was to collect data from altitudes of 3000 and 5000 feet and at various times of the day.

The data were fundamental inputs for LARS investigations of the 'automatic recognition' problem over larger geographical areas. Additionally, analysis of the data were to be performed to further delineate various features which could be identified and to quantify the results.

The larger quantities of data collected in each mission were essential for a more valid verification of performance accuracies.

Analysis of Soils Data

Major objectives of the April mission were to examine fields of winter wheat and areas of fresh tilled soil. In this period, fields are for the most part either in a freshly tilled condition or are in winter wheat. The April mission was unavoidably delayed until May. At the time of flight oats and other green vegetation were present in addition to winter wheat. However, a significant percentage of the area flown was in a tilled stage and much valuable data of the soils was collected. A principal objective of our soils scientists was to evaluate possibilities for soils properties mapping on the basis of spectral measurements. This project was based on previous work accomplished with data collected over central Indiana in the spring of 1967.

It is appropriate to discuss here for a moment some of the aspects of soils which the agriculturist is generally interested in. Principal components of soils are:

- minerals (clay, silt, sand)
- organic matter

- air
- water

Important characteristics of a particular soil include:

- areation
- water holding capacity
- supply of decomposing organic matter
- available plant nutrients

Elements essential to plant growth are shown in Table 1. Some of the minor elements are needed in very small amounts. Manganese deficiencies were found on soybeans in Tippecanoe County during July even though the plants needed less than 5 ppm of this element.

Table 1 Macro and Minor Elements Needed for Plant Growth

Macro Elements	Minor Elements
. Calcium	. Copper
. Magnesium	. Manganese
. Potassium	. Zinc
. Nitrogen	. Iron
. Phosphorus	. Boron
. Sulfur	. Molybdenum

Knowledge of the organic matter content of soils is of particular importance because it:

(1) indicates soil fertility and nutrient availability

(2) indicates soil drainage

(3) affects soils moisture

LARS soil scientists selected test regions along flight lines within the 500 square mile Tippecanoe County test site. Conventional soils maps were prepared for the selected regions to provide ground truth information (Figure 2). It should be noted that the soils maps are based on soil profiles as well as on surface conditions. Soils types, slopes, and state of erosion were identified. An area covering 60 acres and referred to as the Dieterle Farm (shown within the rectangle in Figure 2) was selected for more detailed ground truthing. Two hundred and four soil samples were

collected on a 100' x 100' grid (Figure 3) for detailed laboratory analysis. Chemical analysis defined such items as organic matter content, iron concentrations, mineral composition, etc. for each of the samples. Spectral data collected by the aircraft over this area in the May mission was subjected to computer aided analysis.

Investigators determined that the soils could be divided into many (10-20) categories on the basis of their spectral categories with soils characteristics of interest. The requirement and applications area, however, indicates that such a large number of categories is not practical for general use. It would appear that five to seven categories would be most practical for agricultural purposes.

Each of the 204 laboratory samples was given a 'Munsell' color designation. The samples fit into seven groups on the basis of their Munsell designations. Training samples were then selected from the spectral data for each of the seven groups. Statistics obtained from the spectral training sets were used to automatically classify all points of the Dieterle Farm (Figure 4). Typewriter symbols were selected to identify each group. Additionally the groups were colored to provide the reader with a clear delineation.

The results can be compared to the 'ground truth' map as shown in Figure 5. The reader will note that the computer-selected groups compare favorably with the soil types on the soil map. LARS investigators believe the computer derived map to be an excellent description of the color properties of the surface soils. Investigators are planning to develop a conventional soils map of an adjacent area with the aid of a computer derived spectral map of the surface soils. The results are to be evaluated on the basis of time savings and improved accuracy.

An attempt was also made to associate organic matter content of the surface soils with spectral characteristics after noting the variation of color of the surface soil samples. A soil collage was assembled from actual surface soils samples taken from the 204 points and compared to the soils map (Figure 6). Classification analysis was then conducted to separate the surface soils into one of five categories on the basis of organic matter content. The categories represented mean values 1.5%, 2%, 2.5%, 3.5%, and 5.0% organic matter. A sixth category was designated for the ditch plus 'spoil'. Analysis of training samples indicated that of the available spectral bands from 0.4 to 3 microns, the best four wavelength bands for classification were:

0.62 - 0.66 microns

1.00 - 1.40 microns

1.50 - 1.80 microns

2.00 - 2.60 microns

The classification results using a combination of these wavelength bands are shown in Figure 7. Classification accuracies as deduced from lab

analysis of the 204 sample points together with field checking were estimated to be in the neighborhood of 90 percent.

During these studies the effects of mis-registration on classification accuracies were noted. Channels of spectral data from 1 to 3 microns were not spatially registered with the channels from .4 to 1 microns. The effects of such mis-registration are indicated in Figure 8. The result of this was a spectral measure of the ditch material in one set of channels coupled to a spectral measure of the field in the second set. An 'adultrated' response was measured and mis-classifications resulted. The effects of this on classification results are illustrated in Figure 9. The area represented as ditch and spoil was clearly more accurately classified with the registered data on the left.

Soil scientists at LARS are currently investigating the effects of high iron content on organic matter delineations. Figure 10 shows a Brazilian soil which is high in iron compared to a high organic Indiana soil type. The objective of these efforts is to assess the effect of this and other conditions on the detection of organic matter in surface soils.

Vegetation Research

A second major effort at LARS is directed at developing a capability for the automatic recognition of floristic and physiognomic characteristics of natural and cultural vegetation, i.e., identification of species and of physical appearance of the vegetation of an area (Sinclair, 1968; Swain and Fu, 1968). A large number of activities can be served by vegetation maps. Application of vegetation maps include the following:

- scientific investigations
- geographical research
- climatic records
- pedology and geology
- agriculture
- forestry
- land management and planning
- commerical, engineering, and fiscal interests

While vegetation maps are used for a variety of purposes one should not conclude that there are as many types of vegetation maps as there are applications. Careful analysis of the various applications lead one to conclude that it is reasonable to standardize such maps in the future. As an example, one could decide on three basic map types (Kuchler, 1967): (1) a physiognomic type, (2) a floristic type, and (3) a physiognomic floristic combination.

Such maps are generally concerned with illustrating a characteristic of the cultural and natural vegetation of a region. In agriculture the user is primarily concerned with important species of cultural vegetation of an area. LARS has thus far concentrated efforts on developing a capability to recognize cultural species important to agriculture in the corn belt, i.e., corn, soybeans, and wheat and to discern important physical and chemical characteristics of the vegetation of these species.

It should be recalled that missions were flown in late June and July 1966 for similar purposes. Since data was collected over small areas (4-8 square miles) in 1966 a major objective of the 1969 missions was to work with data collected over much larger areas. Thus, LARS researchers planned to utilize the June 1969 mission data to reassess their capability to detect wheat over large areas prior to its harvest. LARS also wanted to reassess the capability to identify corn and soybeans in late June, July, and August over larger areas, i.e., Tippecanoe County. At this time only partial analysis of the data collected in these missions has been completed. Therefore, the results which can be reported herein must be considered to be of a preliminary nature. The analysis has thus far been hampered by the lack of color photography collected at the time of flight for use in analysis routines. LARS expects to be receiving these before long and will upon its receipt be able to improve results through better training sample selection and evaluation of classification results.

As an example of this, 1969 is known to be a year in which weeds have been especially numerous; wet weather early in the season prevented cultivation operations. In the case of mature wheat it is now believed that 5 to 10 percent of the remote sensing units will prove to have been correctly classified as green vegetation as opposed to mature wheat. LARS investigators observed that some 5-10% of the area within wheat fields were classified as green vegetation. If these are determined to be correct classifications, the accuracy of wheat recognition will increase by that amount. Analysis of color photography is to provide such answers in the near future. The reader should note that as new recognition schemes are developed, data from former missions are subjected to additional analysis and new results achieved (Huang, 1969).

The results of the analysis of June 1966 data and June 1969 data for identification of winter wheat is shown in Table 2.

Table 2 Automatic Identification of Winter Wheat in June for Two Different Years

Date	Wheat Resolution Samples	Wheat Samples Correctly Identified	Percent Accuracy
5-28-66	2736	2540	92.9
5-25-69	7859	6719	85.5

The results are encouraging. Good accuracies have been achieved over considerably larger areas in 1969. Further analysis described above is expected to improve the recognition accuracies above the 85 percent figure.

The results of analysis of 1966 and 1969 spectral data to identify corn and soybeans are shown in Table 3. The accuracy of the 1966 data was improved using a Per Field Classifier. The accuracy of the identification of corn was increased from 78 to 95 percent, for soybeans from 75 to 82%, and for row crops from 90 to 97%. With the Per Field Classifier use is made of the probability density function of the field based on spectral measurements of the remote sensing units (RSU's) within the field, the other analysis techniques used in this work are based spectral measurements obtained on a per point basis. It is expected that similar increases in accuracies will be realized with the 1969 data upon similar treatment. The reader should recall the analysis of the 1969 data is not complete and is only of a preliminary nature.

Table 3 Automatic Identification of Corn and Soybeans for Different Years

Crop	Total Fields Tested	Fields Correctly Classified 1/	Percent Correctly Classified	Total RSU's Tested	% RSU's Correctly Classified
		July 26, 1966			
Corn	55	43	78.0	11486	68.0
Soybeans	44	33	45.0	13781	69.0
Row Crops	99	90	90.0	-----	----
		June 25, 1969			
Corn	87	55	63.2	-----	----
Soybeans	66	28	42.4	-----	----
		August 5, 1969			
Corn	121	109	90.0	11507	84.7
Soybeans	78	64	82.0	6736	84.4

1/ Fields were termed correctly identified when more than 60 percent of the Remote Sensing Units (RSU's) were identified within each field.

Upon complete analysis of the data collected during 1969, LARS researchers hope to establish when and with what accuracy the major species can be identified during the growing seasons. Preliminary analysis of the late May data indicates that headed wheat may be discriminated from non-headed wheat. These first missions were scheduled in 1969 at what researchers estimated to be cardinal points for determining certain key factors. LARS expects that analysis of these data will provide valuable guidance for scheduling missions in 1970.

LARS investigators conducted a study to identify certain tree species and to detect beetle infested Ponderosa Pines. The results of these exploratory studies were promising and are to be pursued in future efforts. The principal investigator in this study was Joseph C. Bell, Jr. of the U. S. Forest Service while a special student at Purdue University under the direction and supervision of LARS.

The results of one study shows that conifers and deciduous trees could be separated and further grouped into light and dark categories (Figure 11).

Much of the analysis of the vegetation data being collected in 1969 remains to be done and is to be accomplished throughout the winter months.

Water Research

Research investigations of an exploratory nature were conducted to further evaluate the capability to automatically detect surface water bodies and to make water quality assessments.

As LARS has reported in the past, one of the simpler categories of natural materials to identify is surface water bodies (Figure 12). All areas covered by water have been accurately identified and mapped. LARS has customarily experienced recognition accuracies of better than 95%. Stream intersections where each stream has a varying sediment load (Figure 13) appear to be typical examples which can be detected by automatic mapping techniques. A portion of the White River in the vicinity of Indianapolis, Indiana (Figure 14) was automatically mapped. Computer aided analysis has delineated seven spectral categories of water. The original objectives of this particular data mission did not include this analysis and, consequently, ground truth was not collected to define existing water properties and meaning cannot be directly attached to the various categories which were discriminated in this case. LARS intends to pursue this in future studies.

Other Research

In addition to these efforts LARS has conducted exploratory research to assess the feasibility of accomplishing the following:

- Classification of certain engineering characteristics of soils in cooperation with the joint Highway Research Project at Purdue University.
- Identify certain geologic features with data collected in central Indiana.
- Categorization of natural materials in Yellowstone National Park in cooperation with U. S. Geological Survey.
- Classification of non-agricultural wildland resources for inventory purpose in cooperation with the Forestry Remote Sensing Laboratory.

The objectives of the engineering soils studies included:

- Investigation of variables influencing the radiation characteristics of natural materials in the spectral inverval from about 0.4 microns to 15 microns.
- Investigation of computer generated engineering soils maps based on digitized multispectral radiance measurements.

Data was collected in the spring of 1967 by the University of Michigan aircraft over a 70 mile long test site extending from Indianapolis, Indiana to Bedford, Indiana. A portion of the test site was in a limestone quarry area (Figure 15) leaving various geologic and vegetative features. The principal investigator, M. G. Tanguay, was generally able to:

(1) Classify land surface strips in terms of vegetation, soils, and water. Maps were obtained that distinguished and automatically classified up to seven soil types utilizing multispectral measurements.

(2) Delineate unique soil conditions on individual graphic printout maps, thus emphasizing the distribution of adverse soil conditions.

(3) Illustrate, for the first time, a relationship between spectral response of a soil and its land form and parent material.

(4) Relate a type of soil and its source location which was about a quarter a mile away.

This research is to be carried on in future projects due to the successful results received to date.

Uses of automatic recognition schemes utilizing multispectral measurements were investigated with data collected over Yellowstone National Park. The project was conducted in cooperation with H. W. Smedes and K. L. Pierce of the U. S. Geological Survey, Denver, Colorado.

Objectives of the project included evaluation of these techniques to identify and map different natural terrain types, and analysis of aircraft collected data to study the effectiveness of the proposed Earth Resources Technology Satellite (ERTS) data channels. The investigation generally revealed that highly satisfactory terrain maps portraying geologic-geomorphic units and rock-soil-vegetation association units could be produced (Figure 16).

Although attempts were not made to simulate coarser resolution of the ERTS sensors, the computer-generated maps indicated a good overall performance that compared closely with a map compiled through use of four channels selected by the computer.

It suffices to say that the results of these exploratory studies were highly encouraging and in-depth investigations are to be conducted in these areas in the future.

REFERENCES

1. Fu, K. S., D. A. Landgrebe, T. L. Phillips, 1969, "Automatic Reduction of Remotely Sensed Earth Resource Data," IEEE Proceedings Volume 57, Number 4, April.

2. Holmes, R. A. and R. B. MacDonald, 1969, "The Physical Basis of System Design for Remote Sensing in Agriculture," IEEE Proceedings, Volume 57, Number 4, April.

3. Huang, T., 1969, "Per Field Classifier for Agricultural Applications," LARS Information Note 060569, Laboratory for Agricultural Remote Sensing.

4. Kuchler, A. W., 1967, Vegetation Mapping, Ronald Press Company, New York, New York.

5. Laboratory for Agricultural Remote Sensing (LARS), 1967 Remote Multispectral Sensing in Agriculture. Volume II (Annual Report), Purdue University Agricultural Experiment Station, Research Bulletin 832.

6. Laboratory for Agricultural Remote Sensing (LARS), 1968, Remote Multispectral Sensing in Agriculture. Volume III (Annual Report), Purdue University Agricultural Experiment Station, Research Bulletin 844.

7. Sinclair, T. R., 1968, "Pathway of Solar Radiation through Leaves," Master's Thesis, Purdue University.

8. Swain, P. H. and K. S. Fu, 1968, "On the Application of a Non-parametric Technique to Crop Classification Problems," Proceedings of the National Electronics Conference, Chicago, Illinois.

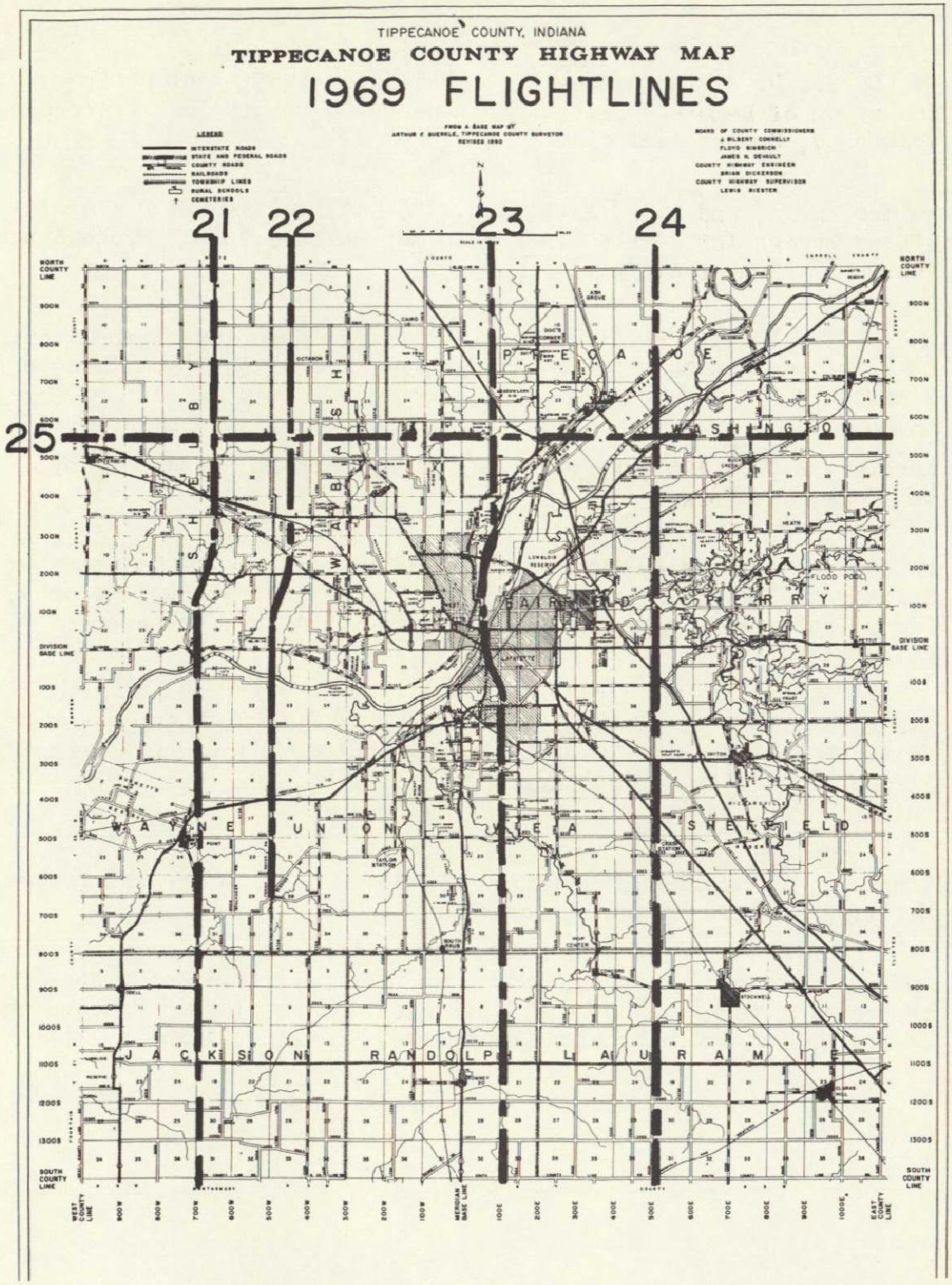

Figure 23-1.- 1969 flight lines over the Tippecanoe County Test Site.

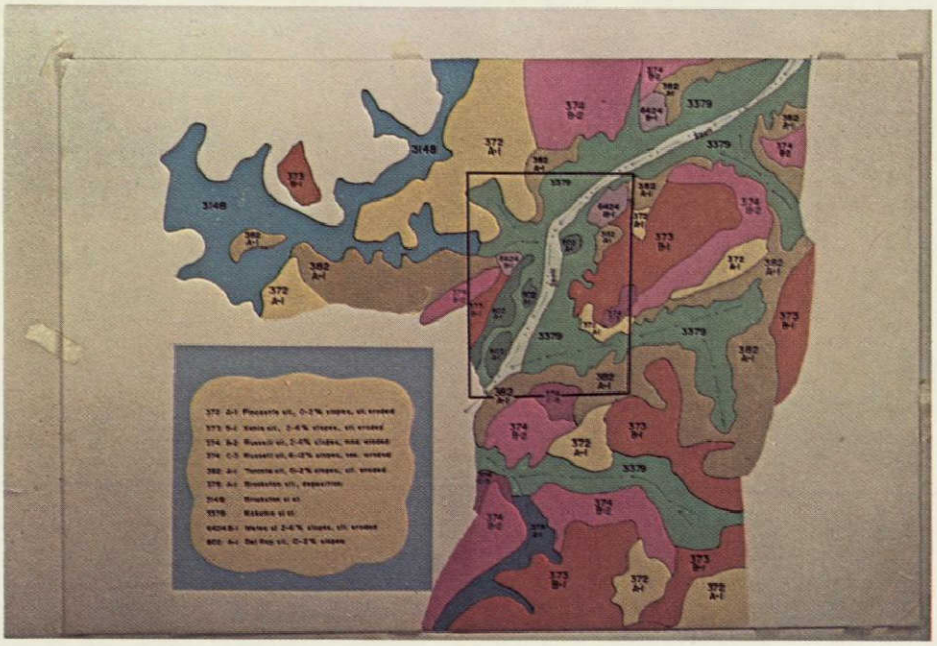

Figure 23-2.- Soils "ground truth" map of the Dieterle Farm and surrounding area.

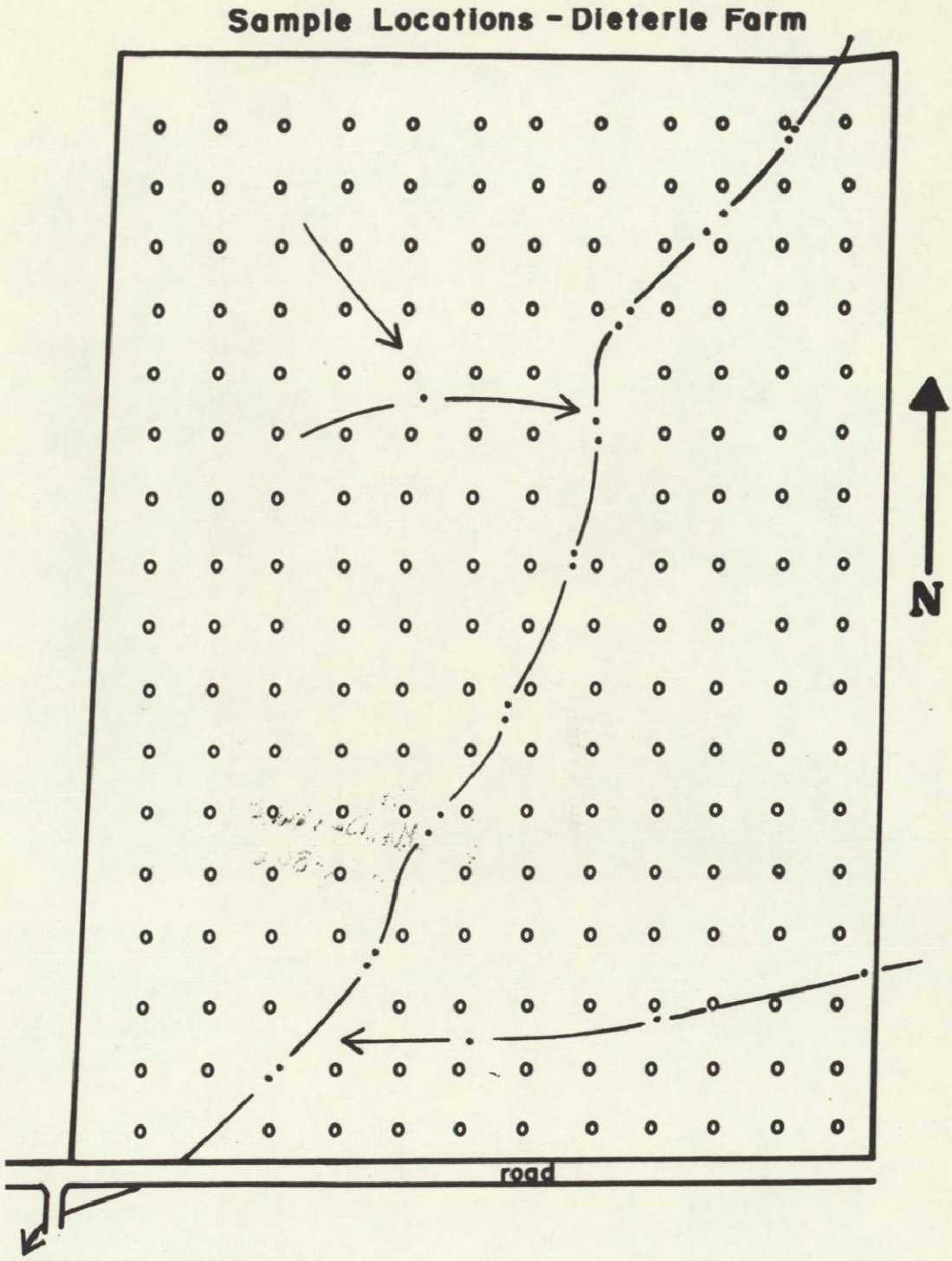

Figure 23-3.- Map of the Dieterle Farm showing locations where surface soil samples for laboratory analysis were obtained.

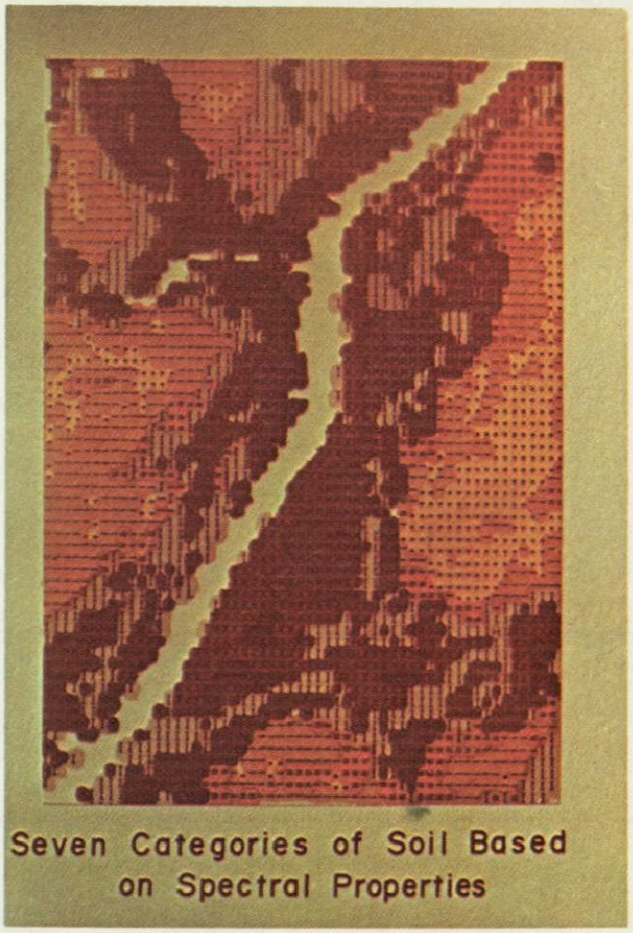

Figure 23-4.- Spectral Soils Map of the Dieterle Farm showing seven soil categories based on spectral properties measures by aircraft scanner.

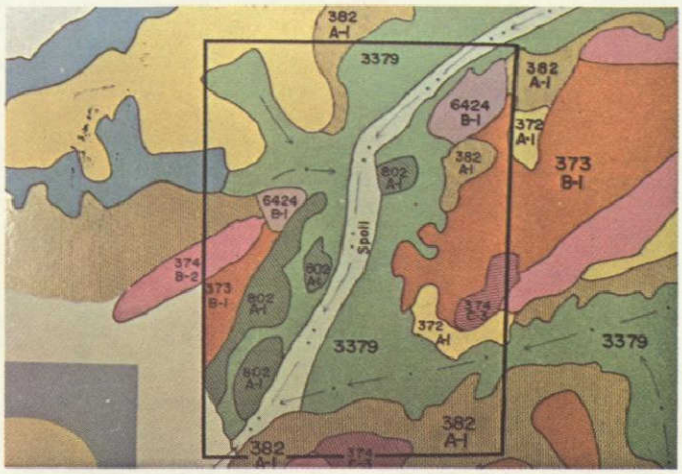

(a) Dieterle Farm area (rectangular field) showing detailed soils types as mapped in the field by a Soil Scientist.

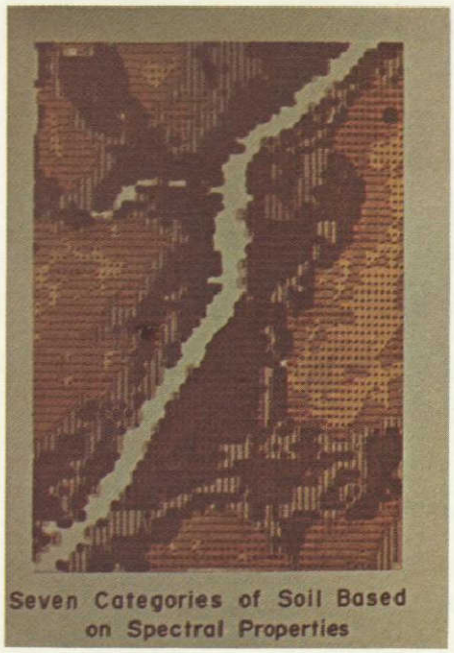

(b) Spectral soils map derived automatically by computer.

Figure 23-5.- Comparison of "ground truth" and "automatic" map.

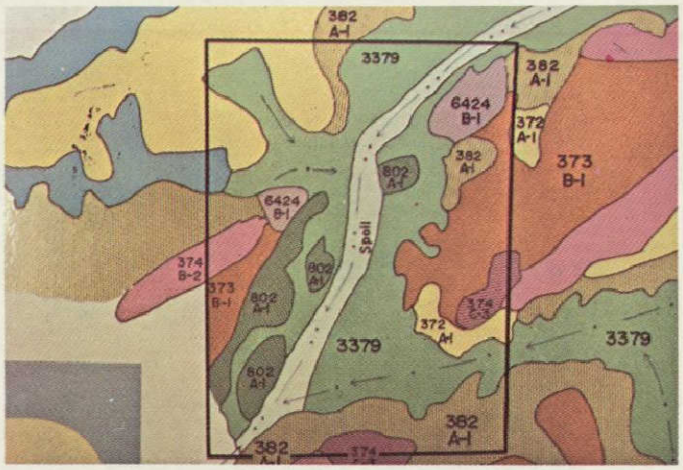

(a) Soils map of Dieterle Farm.

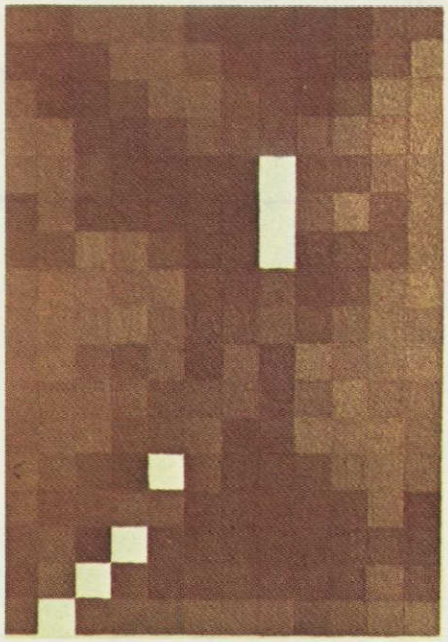

(b) Soil collage compiled from the 204 soil samples taken from the Dieterle Farm.

Figure 23-6.- Comparison of "ground truth" soils map and soil collage.

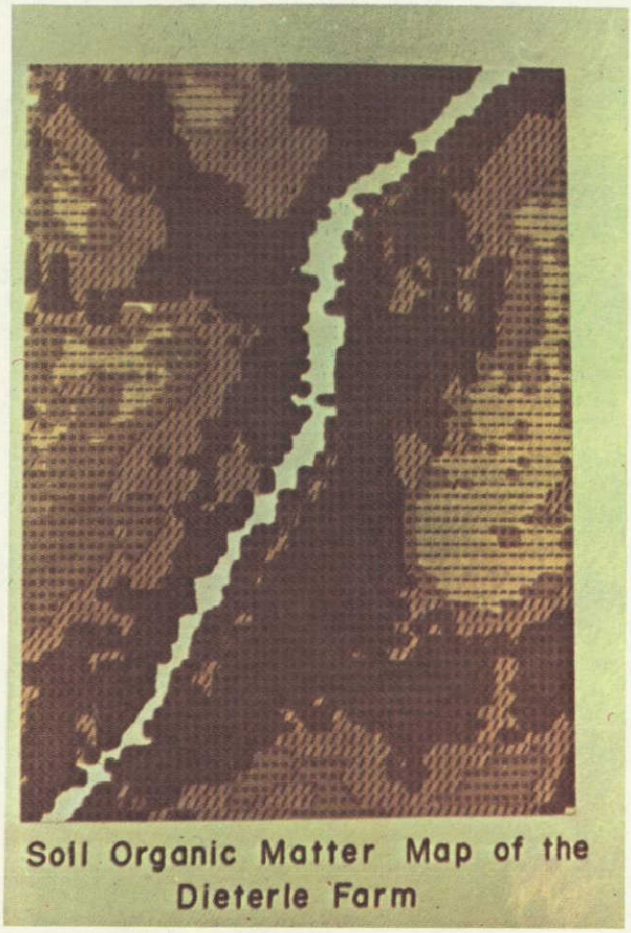

Figure 23-7.- Automatic map of organic matter content derived in conjunction with laboratory analysis of soil samples from the Dieterle Farm and spectral measurements near sample locations.

Effects of Mis-registration on Classification Accuracy

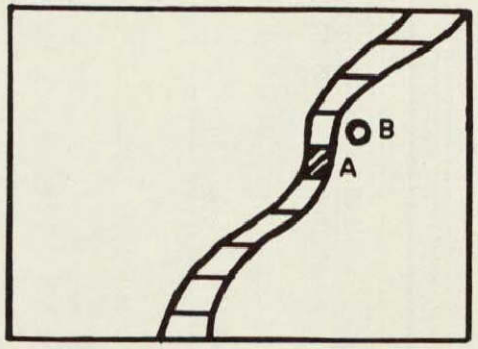

Properly Registered 0.4-5.0μ
Scanner Print

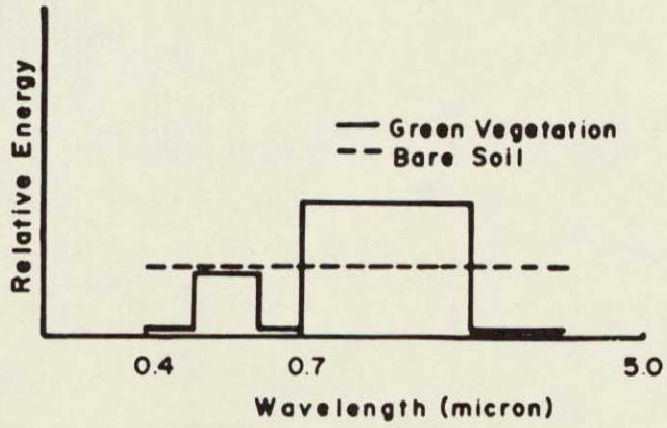

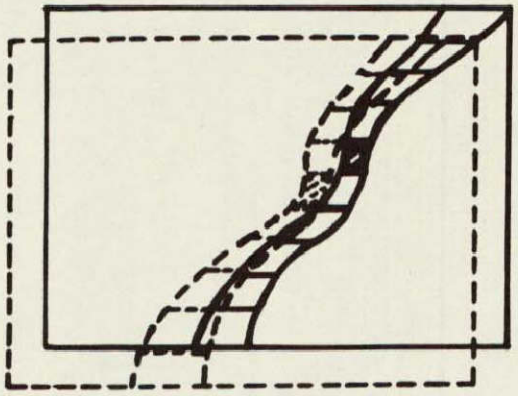

Mis-registered 0.4-0.7 and 0.7-5.0 μ
Scanner Print

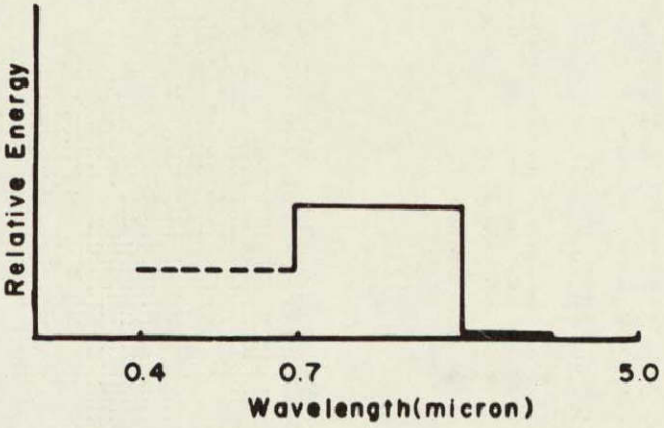

Relative Response Indicated by Utilizing Mis-registered Channels

Figure 23-8.- Conceptual diagram showing the difficulty in overlaying 0.4 to 1.0 micron data with data obtained at 1.0 to 2.5 micron wavelengths.

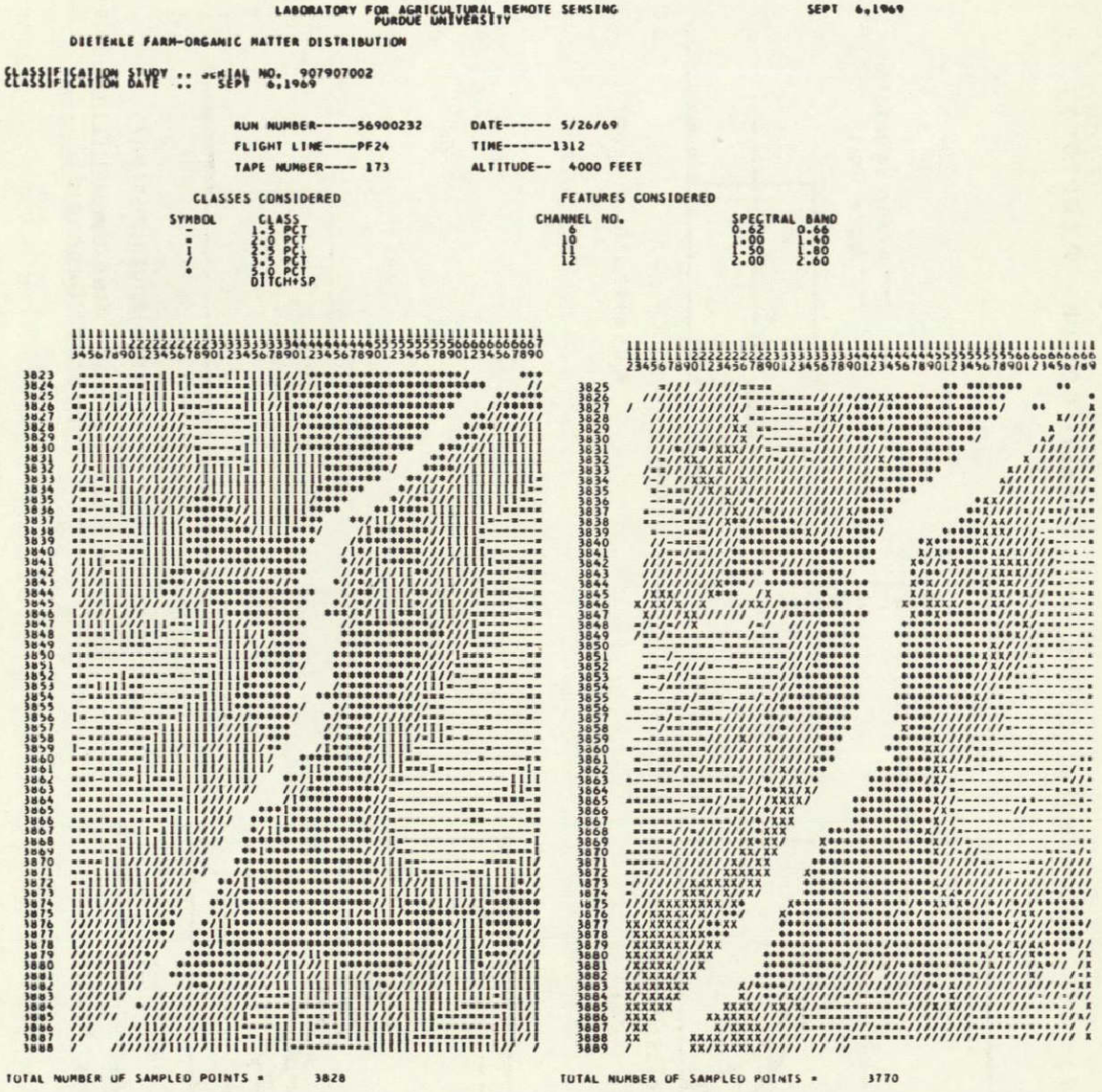

a. Properly registered printout. b. Improperly registered printout.

Figure 23-9.- Comparison of a properly and an improperly registered printout. (Note the width of the ditch area on the left printout compared to that on the right).

(a) Brazilian soils having high iron content.

(b) Indiana soils with a high percent of organic matter.

Figure 23-10.- Comparison of soils high in organic matter and soils which are high in iron.

Figure 23-11.- An aerial photograph and corresponding computer print-out over a forested area. Research has been successful in differentiating conifers and deciduous species into separate groupings.

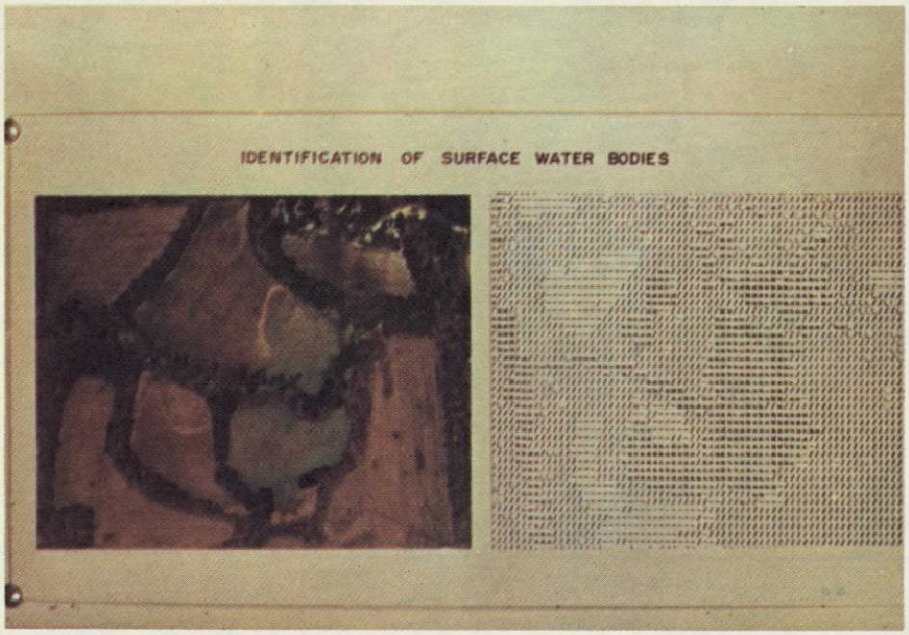

Figure 23-12.- An aerial photograph and computer print-out of an area in Southern Indiana, most of which is underwater. Experienced interpreters have difficulty in accurately mapping the water bodies on the photo. The computer, however, easily identifies water due to its spectrally different characteristics from surrounding soil and vegetation.

(a) Conventional color.

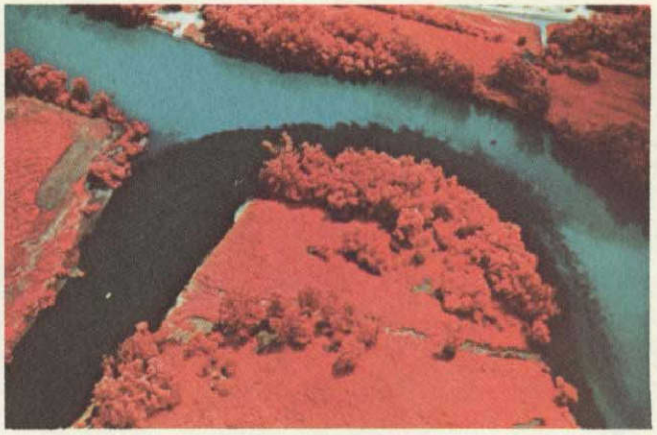

(b) Color infrared.

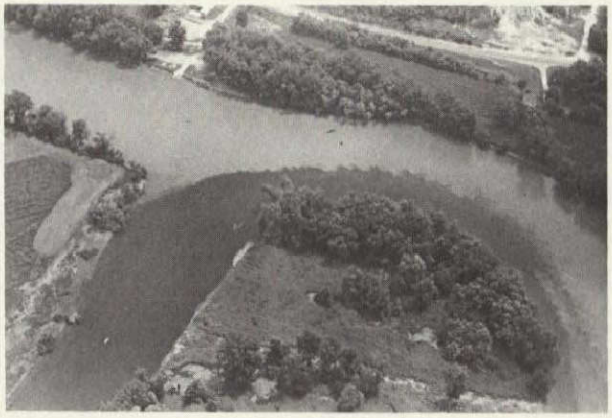

(c) Panchromatic black and white.

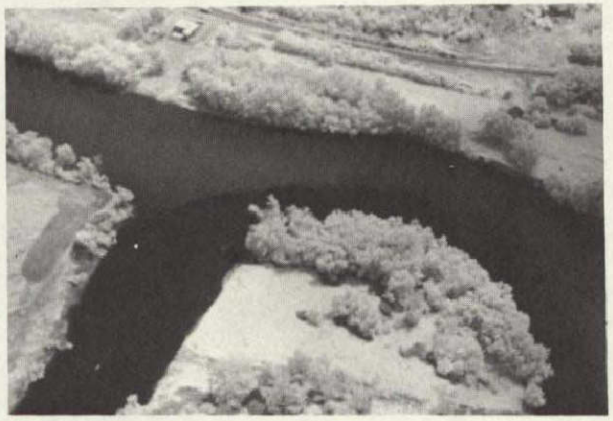

(d) Black and white infrared.

Figure 23-13.- Four film type comparison showing the junction area of two rivers.

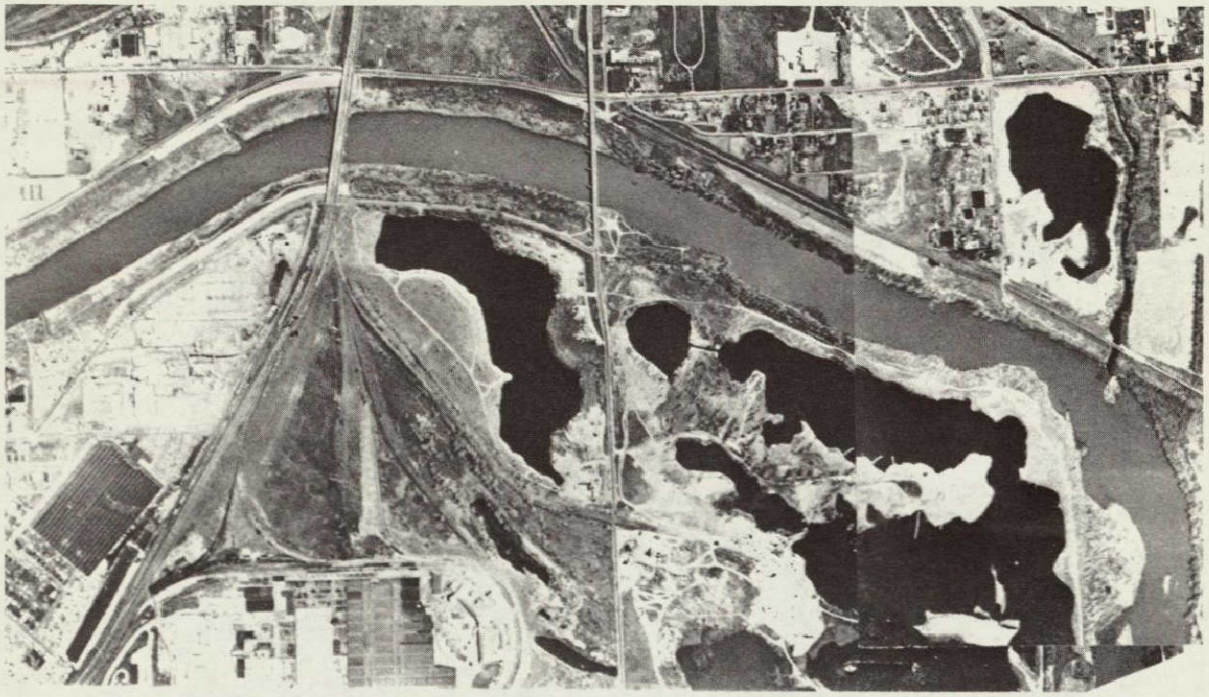

(a) Black and white panchromatic photograph taken near Indianapolis, Indiana, showing the White River and flooded quarry pits.

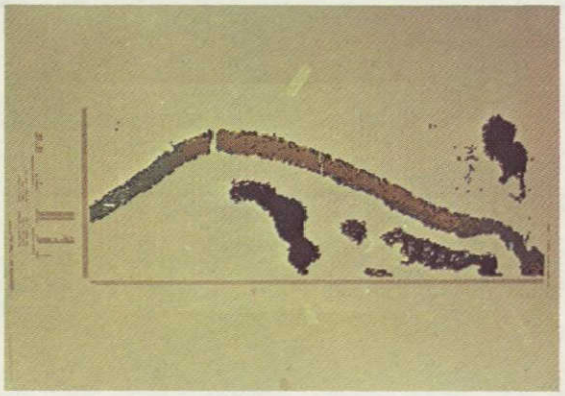

(b) Artificially enhanced computer printout of the same area showing the water areas. The computer separated the water into seven distinct categories.

Figure 23-14.- Comparison of aerial photography and computer printout for hydrologic purposes.

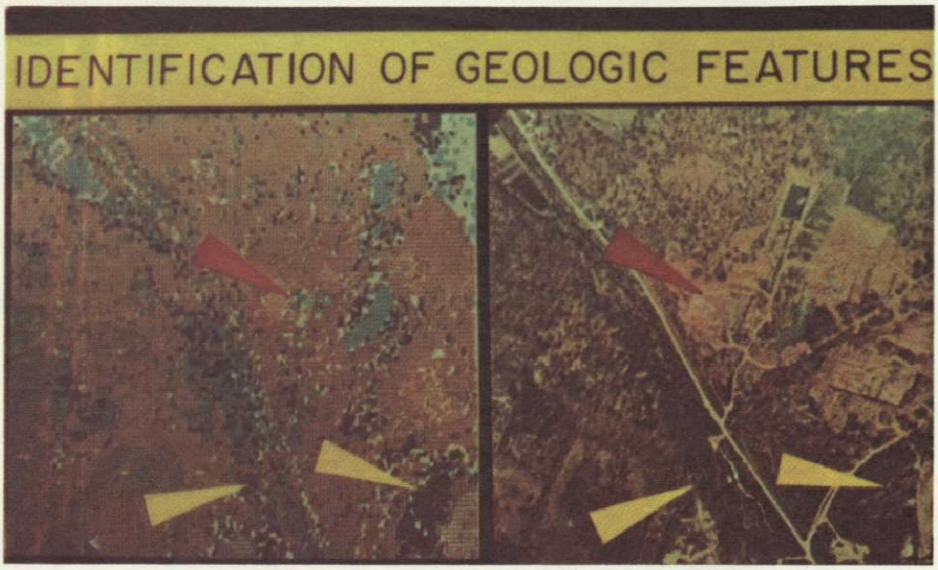

Figure 23-15.- Color aerial photograph and an artificially enhanced computer printout in Southern Indiana. Note how the computer identifies areas of standing water (red arrow), and limestone outcrops (yellow arrows).

Example Classification Results
from an Engineering Soils Study

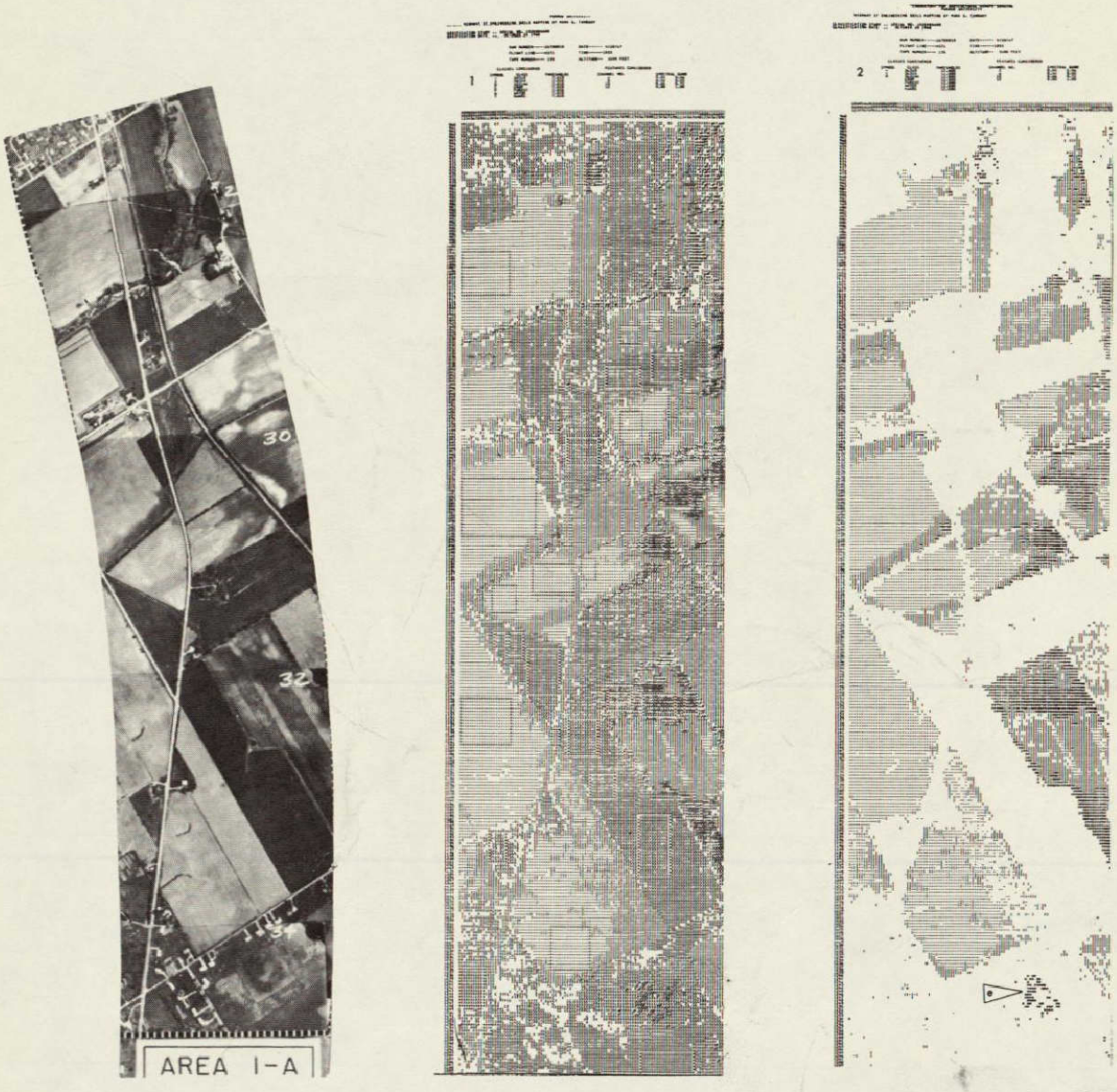

LARS/Purdue

Figure 23-16.- Geologists have been successful in using multispectral techniques in defining and classifying geologically interesting features as shown by the comparison of the aerial photograph and artificially enhanced computer printout of a portion of Yellowstone National Park.

SECTION 24

AUTOMATIC PROCESSING OF EARTH RESOURCE DATA

D. A. Landgrebe

Introduction

This presentation together with the one following by R. B. MacDonald constitute a report of work at the Purdue University Laboratory for Agricultural Remote Sensing (LARS) during the last year. The objective of LARS is to help develop knowledge and techniques necessary to design an earth resource system utilizing aerospace platforms. This objective is pursued through studies in instrumentation and measurement, data processing, basic studies regarding the nature of earth surface materials, and considerations regarding the specific need for and use of information which can be generated by such a system.

It was decided early to concentrate efforts in the data processing area at Purdue on techniques for those tasks involving such large quantities of data that machine processing would be required. Following this, an initial approach using spectral data was selected for study because this type of data appeared to permit processors of adequate speed and small size. These decisions resulted in the multispectral scanner being the prime data source and this is assumed hereafter.

Due to the quantity of data which such a system will produce, one must not only develop algorithms suitable for analyzing the data and reducing it to useful information but one must also develop new techniques in manipulating, formating, and interfacing with these data.

The remainder of this discussion is devoted to relating what progress has been made in data processing studies at LARS during the past year. It is broken into six segments covering the following: (1) Improvements in LARSYS, the LARS programming system, (2) Initiation of a System Parameter Sensitivity Study, (3) The Digital Image Display System, (4) Data Registration, (5) A new data classification scheme, and (6) A boundary-finding algorithm for multispectral data.

The LARSYS Programming System

At a meeting held here one year ago a computer programming system called LARSYS was first discussed. Figure 1 shows the general block diagram of this system. It is seen that the system contains segments for data handling operations of aircraft data, aircraft data analysis, ground truth processing, and several activities. Figure 2 shows a flow diagram of the manner in which this system is used in an aircraft data analysis task. It is seen that the system inputs are the aircraft multispectral scanner data and ground truth information. After appropriate processing by LARSYSAH and LARSYSGT respectively the data is available to the researcher. He is then in a position to carry out a dialogue with the portion of the system called LARSYSAA.

Figure 3 shows a more detailed diagram of LARSYSAA. The central portion of this system is a pattern recognition algorithm which permits the researcher to classify the data into one of several preestablished categories. There are several steps through which one must pass in utilizing this system. First, one must hypothesize the categories into which one wishes to divide the data. These categories may be plant species, soil types, geologic formations, or other type of earth surface cover of interest. The criteria for selecting the categories or classes are that they must be (a) of importance from an information value standpoint and (b) they must be statistically separable as a result of the data.

The second step is the selection of training samples or samples which typically describe each of the various classes. During the course of these two steps the statistics processor of LARSYSAA may be used to help. This processor can provide presentations of several statistics, histograms, and spectral plots of candidate classes of data.

Having tentatively established the classes and training for them one must decide upon what spectral bands are to be used in analyzing the data. The feature selection processor provides the researcher with an aid for this problem. Briefly, the feature selection processor implements an algorithm which determines the statistical distance between data sets in N-dimensional multispectral data space. Through calculations involving all possible N-tupples of spectral bands and all possible two-tupples of classes, one can decide not only upon the optimal set of spectral bands to be used but one can also get an initial determination of the degree of separatability of the classes.

The third processor, the classification processor, implements a maximum likelihood classification scheme and writes the result of the classification of each point on magnetic tape for further evaluation. This evaluation process is aided by the use of the fourth processor, the display processor which is capable of outputs giving both quantitative and qualitative information about the performance of the particular classification just carried out.

The general state of development of this whole technique can perhaps be summarized as follows. By the beginning of the 1969 crop year the system had been developed and demonstrated to the point of being able to adequately handle and classify data sets covering areas as large as a few square miles. The broad general objective for the 1969 crop year was to extend the size of area over which the system could be put to use to between tens and hundreds of square miles. The test site to be used for this development was Tippecanoe County in the State of Indiana, an area of 501 square miles. Flight lines were defined covering the length and breadth of the county and include a considerable percentage of the total land area of the county. Most of the flight lines are in excess of 20 miles in length. This is one to two orders of magnitude larger quantities of data then had been used previously and the question simply became can tecnhiques be determined for utilizing these methods successfully for quantities of data of that size.

As a result of this objective during the last year, a number of improvements have been incorporated into LARSYS. For example, an option was added to the feature selection processor such that in addition to using it to select the optimum feature set it can be used to group a large number of agricultural fields into those which are spectrally similar. This is useful in dealing with very large numbers of agricultural fields and in establishing the appropriate number of subcategories to use for a given crop type, for example.

In addition to modifications to the system for purpose of dealing with larger quantities of data, it was also recognized that the program needed to be made more general. At the time the programs were first written, the University of Michigan multispectral scanner system was the only system capable of supplying data for this type of algorithm. The programming had originally, therefore, been written specifically to process data from this scanner. The NASA scanner system placed under contract during the year has quite different and more general capabilities. Thus several modifications in the system were begun. Among these are the following:

*The system is being modified to handle any number of channels up to 30 and any number of samples per line.

*The calibration procedure used in the system is being considerably generalized so as to permit much more general tests and evaluation of calibration procedures.

*The system is being converted to work in terms of floating point numbers rather than fixed point numbers. This permits a more appropriate use of the dynamic range of the instruments among other things.

*Considerably more flexibility is provided to the user in that more functions can be performed and more parameters varied through the use of the control cards.

*The program has been rewritten to considerably ease modifications into the program.

One further comment may be in order about this programming system. The value of the system to the Earth Resources Program is considerably decreased if the system is only available to people carrying out research at Purdue University. As a result we have begun to give consideration to procedures by which the computer programs and the capability for data analysis which these programs make possible can be exported to other research centers. Since the programs exceed the equivalent of 15,000 Fortran cards, this is no small task. An initial step has been to temporarily fix the state of development of the system, document it at that stage, and transfer the computer programs to NASA/MSC. This has been completed in the last few weeks. I understand that NASA's purpose in this regard is to make sure that this type of capability is operationally available at MSC by the time the NASA scanner system is placed into operation.

In addition to the modifications indicated in the previous paragraphs this analysis system has been used extensively for data analysis purposes during the past year. Some of the results of these studies will be given by R. B. MacDonald in the next presentation. Further, LARS has recently been funded by NASA to determine the best way to apply these techniques to disciplines other than agriculture such as geology, hydrology, geography, etc.

System Parameter Study

Now that it seems clear pattern recognition techniques will be useful in the analysis of data in an operational earth resources system, there is a need to do a parametric study of the entire data stream to determine particular components of the system to which the analysis process is or may be particularly sensitive. Such a study would be beneficial in establishing adequately conservative but not overly restrictive (and therefore expensive) specifications for an operational system. One may reasonably ask questions such as the following:

What scanner sensor signal-to-noise ratio is really required?

What degrading effects occur in the processed data if the resolution of a single channel is considerably lower than other channels?

What are the effects of quantization noise on the analysis results?

In what manner do the analysis results degrade as the registration between spectral bands is degraded?

For the answers to most of these types of questions one can only speculate at this point as specific experimentation has not been carried out.

What we wish to do then is simply to indicate the need for such a parametric study and give some early results which have been obtained with regard to these questions.

First of all, consider the question of quantization precision. Data from the Michigan system is presently being quantized to 8 bit precision. This figure was selected based upon scanner signal-to-noise ratio considerations. During the year a data tape was constructed which contained 12 spectral bands as follows: ten spectral bands were recorded at 8 bit precision and two of the same 10 were also included but at a simulated 9 bit precision. In analyzing the data it was found that the feature selection algorithm favored these 9 bit bands over those of 8 bit precision from the same portion of the spectrum. The resulting classification accuracy was also slightly higher. Only a tentative conclusion should be drawn until these results are made more quantitative.

A question very often asked is how many spectral bands are required for a given classification? As one might expect, experimentation to date has shown that the answer to this question clearly depends upon what the

categories are. In addition, consider Figure 4. This figure shows some results reported previously for another purpose with regard to the feature selection algorithm being used in LARSYSAA. The figure, as can be seen, is a plot of the percentage error as a function of the number of spectral bands used. The particular study for which these results were obtained was designed to show that the procedures used for band selection did indeed indicate the best possible sets of bands of a given size. That is to say, if as was the case in this study, one has a total of 12 spectral bands available and one wishes to use only three of the bands, which three will produce the best results.

The perhaps unexpected results which are apparent here however, are that not only is one able to pick the best subset of bands but that a subset of bands may produce a lower over all error than using the complete set of spectral bands.

At least using hindsight one may suspect that this phenomenon should occur; as seen from Figure 4 it has now been seen experimentally. It is also of interest to know if it can be predicted on a theoretical basis. I wish to show briefly here some results derived from a theoretical viewpoint and reported by Hughes in the IEEE Transaction of Information Theory, January 1968. These results are summarized in the next three figures. Figure 5 shows a graph of accuracy versus what Hughes calls measurement complexity. The assumptions here are that one is using a Bayesian classifier in a two class problem and that one has an infinite number of training samples with which to train the classifier. Further, the data is assumed to be in discrete (i.e., digital) form and the results are averaged over the ensemble of all possible pattern recognition problems.

By measurement complexity is meant in our case, the product of the number of possible discrete values that data in a given spectral band can produce times the number of spectral bands available. This figure shows what one would expect, that is that as the measurement complexity (which, keep in mind, includes the number of spectral bands) as this complexity increases the accuracy continues to increase indefinitely. But of course after some point, the curve becomes reasonably flat.

However, the infinite training sample set assumption does not fit our conditions. Hughes has also derived the results for finite numbers of training samples. This is given in Figure 6. Shown here is the case where each of the two classes is equally probable. One sees immediately that the curve increases as the measurement complexity is increased for awhile. It then reaches a maximum and begins to decrease with increased complexity. On the basis of this curve then one would reasonably expect if he had not seen it experimentally before that there would be an optimum number of spectral bands for a given signal-to-noise ratio.

There is one further case for which Hughes has obtained results which are of interest to us. This is the case when the classes are not equally probable. Consider Figure 7. These are the results when one class has

a probability of occurence of .2. Since Hughes has assumed a two class situation the other class, therefore, has a probability of occurence of .8. Notice from this curve that there is not only a maximum but also a minimum indicating that other things being equal there is not only a best number of bands to use but there may also be a worst number of bands.

We do not wish to imply here that these results apply directly to any specific remote sensing problem and to the classification of multispectral data in the multi-class environment since the assumptions in Hughes work are somewhat different. Nevertheless, the two problems seem similar enough that a study of the effects of the data signal-to-noise ratio (we assume here that the data is digitized to a precision based upon its signal-to-noise ratio) as well as the number of spectral bands is indicated.

Digital Image Display System

Most of the discussions up to this point have been with regard to work in software systems. There has recently been completed however, the design for a major piece of hardware. I refer to the digital image display system on which work was begun some three years ago. At that time it was recognized that when interfacing with very large quantities of data one of the chief problems would be the matter of editing out those specific parts of the data with which one wished to be concerned. There appeared to be no suitable piece of hardware by which to achieve this capability and it was at that point that use of the now-familiar computer line printer printout technique as shown in Figure 8 was begun. This figure shows a conventional aerial photograph and a computer-line printer generated printout of a single channel of a multispectral data taken at the same time. The particular printout shown here happens to have 440 symbols per line, and 12 different symbols simulating a 12 step gray scale has been used. This kind of scheme can be used for data editing simply by locating the number of the scan line and the number of the sample within the scan line after viewing the printout.

This scheme works very well in many applications, particularly those where more limited quantities of data are involved. However, it does bog down when the quantity of data becomes very large simply because of the sheer amount of paper involved in the printout. Thus three years ago the design of the digital display system was begun as an answer to this problem.

Since that time it has become apparent that there are many more tasks besides simply data editing which require a human to be able to rapidly interface with a very large quantity of data. Thus the original design has been modified continually until it became essentially complete approximately a year ago. The acquisition for this equipment has been funded by NASA through the USDA and recently placed under contract for construction. Figure 9 shows a sketch of the display console itself. It consists of a display screen on which the imagery can be displayed

utilizing 768 sample points per line and a gray scale of 16 steps. There is also provided a light pen with which the operator can designate to a computer a particular data point of interest and a keyboard consisting of 32 keys and as many as 256 keyboard overlays by which the computer operator can control the computer processing and the display of the data. The keyboard overlays (see Figure 10) contain sensor elements shown at the upper edge such that when the overlay is placed in position on the keyboard the computer can automatically sense which overlay is present and therefore which computer programs are to be called by each of the keys.

Very briefly the complete display system consists of a CRT system similar to a TV monitor and a disc buffer system. On signal the data is transferred from the computer interface through a core buffer to the disc buffer system. The disc system permits the screen to be continually refreshed at a rate adequate to prevent flicker on the screen. A photo-copy unit is also provided to produce output in hard copy form.

Data Overlay

For several years now we have been pursing studies directed toward the precision overlay or registration of one scanner image upon another. The basic problem is illustrated in Figure 11. Here we have scanner images from two different scanners, in this case a visual and a thermal image. An airphoto is included for clairty. One wishes to bring the two images into registration or in other words overlay one image upon the other in such a way that corresponding points in the two are aligned in every case.

Last year at this meeting we reported a procedure which was used reasonably successfully for this purpose. This procedure is illustrated in Figure 12. The basic process necessary is to numerically correlate scan lines from the two images under the assumption that registration is correct when the correlation is maximized.

However, it has been found that particularly in the case of widely different parts of the spectrum correlation of the scanlines directly did not provide good results. The correlation between images from very different parts of the spectrum is not sufficiently peaked. This difficulty was overcome by first applying a simple border enhancement algorithm to both images, then correlating the result. The final step is the writing of a new data tape upon which the data from the separate tapes (i.e., images) has been merged and properly aligned.

Figure 13 shows the result of the border enhancement on the two images for a certain data set. The border enhancement scheme used was simply to take the magnitude of the first difference adjacent points.

During this last year several improvements have been incorporated into this system. First of all two deminsional correlation is now being used. In addition as would be expected, in using the system it became immediately

apparent that the effectiveness of the system is data, i.e., scene, dependent. Two pictures with a grid square pattern will be easier to correlate then, for example, two pictures of a smooth sea. One of the parameters available with regard to correlation difficulty is the data set size or window size used in the correlation. Too large a window unnecessarily slows the processing while one which is too small results in poor performance. In short what was needed was to make the system adaptive to the scene being processed.

This has been accomplished by defining and utilizing a "Picture Complexity Index" or PCI. The one used is defined in terms of the average number of border or boundary points in a cell of fixed size. To illustrate this consider Figure 14. This figure shows samples of three classes of imagery. The first class referred to as "Rectangular," would be relatively easy to correlate due to the number of distinct linear features. The second, referred to as "Natural" is relatively difficult to correlate and would require a larger correlation window due to the essential randomness of the structure. The third is intermediate to these two and is referred to as "Mixed."

Figure 15 shows border density histograms for these three scenes. This is merely a comparative plot of the number of 10 x 10 cells versus the number of border points per cell for each image. One would expect to find that a simple scene, in this case the one called "Rectangular," would have relatively more cells with a low number of border points and therefore the PCI which is the average number of border points per cell would be low. The opposite should be true for the "Natural" scene with the "Mixed" case intermediate. This indeed turned out to be the case. The resulting PCI's are given in the figure.

This "Picture Complexity Index" has now been incorporated into the overlay system as shown in Figure 16. As seen here after routine data handling operations, the border enhancement procedure is carried out and the PCI determined. This is used to set the range of a variable range correlation. This picture alignment operations complete the procedure. Ultimately, one of the most important uses of the overlay procedure will be in the overlay of the data gathered at different times of the day or year. This is a goal of the development.

Per Field Classification

The classification algorithm used in LARSYSAA utilized only spectral information and classifies points entirely without regard to the classification of neighboring points. As previously mentioned the reason behind this approach is the desirability of possible processing speed and simplicity. However, accuracy can certainly be increased by incorporating spatial information as well. Given that a certain point is a member of a certain class there is considerable likelihood that its neighbor is also.

With this in mind a new classification scheme, referred to as "Per Field Classification," has been proposed and is now being studied. Figure 17 shows an airphoto, gray scale printout of one band and a per point classification printout for the task wheat versus everything else. Suppose prior to classification one were to point to the second wheat field from the top of the gray scale printout and say, "I don't know to which of the classes this field belongs but whichever it is, all points in the field belong to the same class."

In this case one sees the possibility of a classification scheme which is fundamentally different than the per point classifier used in LARSYSAA. In the per point classifier one is comparing a single point with each of several conditional density functions (i.e., the class training samples) for membership likelihood. In the per field scheme one compares a point set or density function with the conditional densities. Intuitively one would expect the latter to be more accurate.

To see if this turns out to be the case three flight lines were selected from which data had been gathered during a time of the growing season for which analysis had proven difficult. Classes and training samples were chosen for each flight line. After choosing a set of spectral bands the flight lines were classified using LARSYSAA. Classification accuracies were determined in each case using sets of test fields which were as large as possible without using any of the training samples. Further, since these results were to be compared with the per field results, the accuracy was also tabulated by fields by assuming that if any field had 60 percent or more of its points assigned to a single class the entire field was considered correctly classified.

Following this the per field classification scheme was tested on the same data using the same training statistics, spectral bandsand test fields. The results are shown in the next three figures. Figure 18 shows the comparative results for a four class three band test of July 1966 flight line C-3. It is seen that the overall accuracy is increased from 77 percent to 91 percent using the per field scheme. A similar overall improvement resulted in July 1966 flight line C-4 data as seen in Figure 19. Figure 20 shows the results for September 1966 flight line C-2. We note by the way and in passing that though the term field might refer to an agricultural field, it need not; any set of points however defined which are presumed a priori to be from the same class can be classified by this scheme.

A Boundary-Finding Algorithm

As described above the per field classifier must be classed as a semi-automatic rather than a fully-automatic technique since it would apparently be necessary to manually delineate the field boundaries. One can imagine many circumstances under which it would be most useful as such. However, it can also be made fully-automatic if one can find a suitable method of automatically drawing boundaries between spectrally different surface cover types.

There are in remote sensing many other points at which a boundary-finding algorithm would be useful. We found the need to do this earlier in the overlay problem, for example. We have as a result begun to work on developing such a technique. At the outset this problem seemed to call for an unsupervised classification technique. A clustering algorithm was defind for this purpose and program logic suitable to image analysis of this type was established utilizing it. Basically the logic calls for the clustering of data in each cell of 9 x 9 points. Adjacent points which become assigned to different clusterpoints become delineated as boundary points.

Figure 21 shows an airphoto of a flight line, a gray scale printout and the result of using the boundary-finding algorithm on the same data. It is seen that a large number of the actual boundaries in the data are indeed located. There is in the algorithm logic an option to indicate the intensity of the boundary through control of a threshold. Figure 22 shows the result of changing the threshold so as to change the number of boundaries located.

This algorithm is very much in the early stages of its development and much work remains. For example for some applications it will be necessary to increase the sophistication of the program logic at least to the extent of being able to draw closed contours.

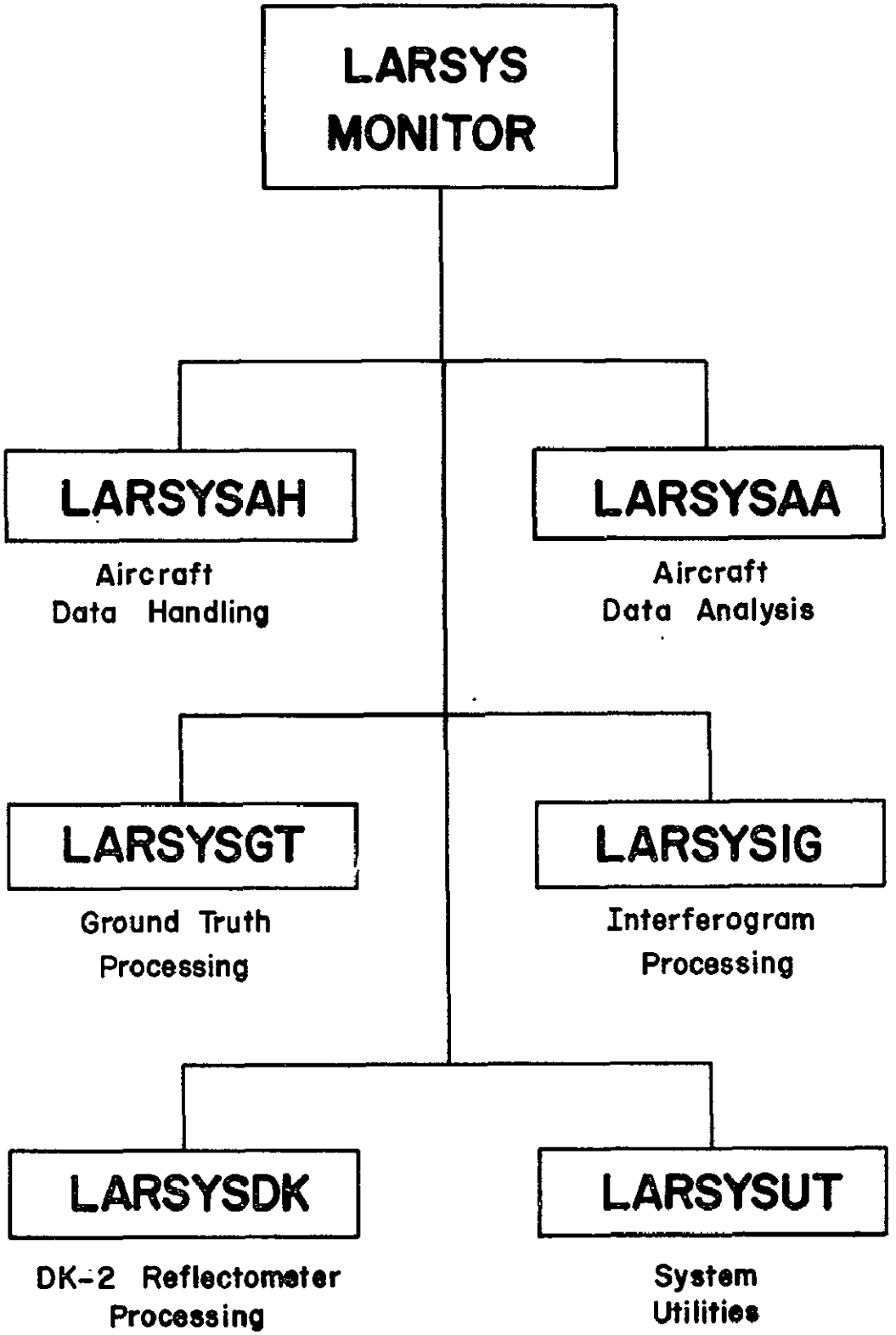

Figure 24-1.- Organization diagram of LARSYS programing system.

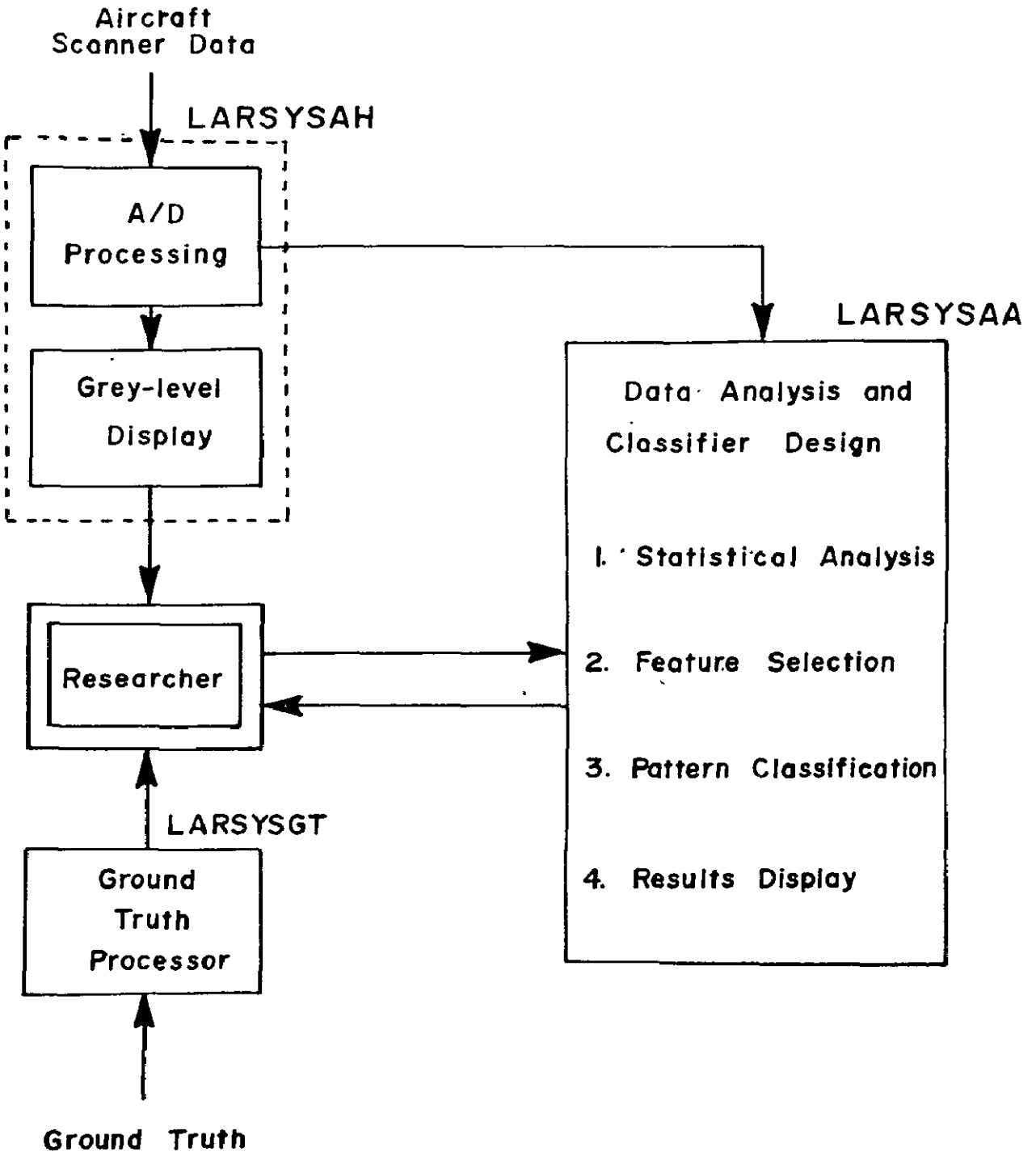

Figure 24-2.- Flow diagram of LARSYS system use for data classification studies.

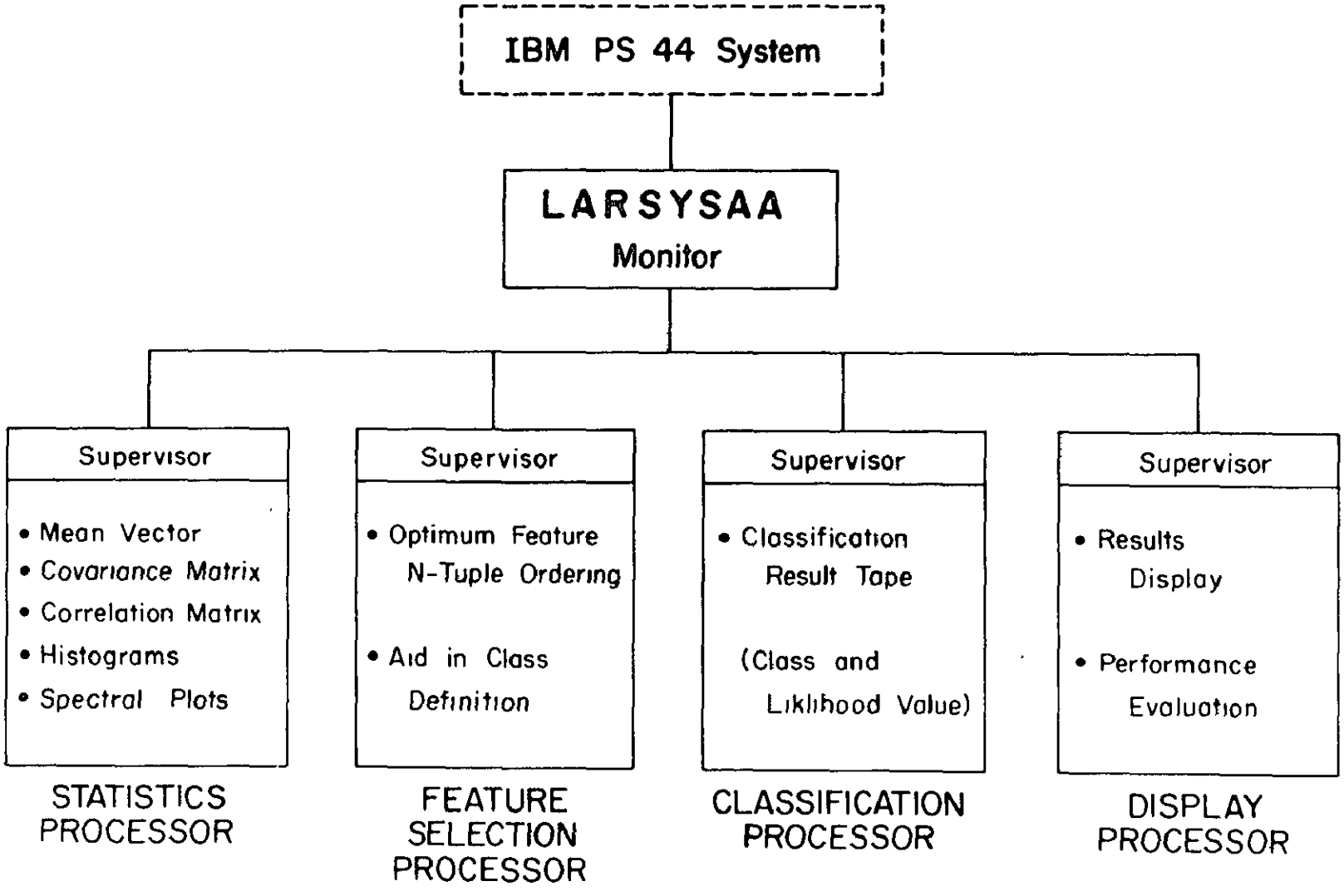

Figure 24-3.- Organizational diagram of LARSYSAA. This system enables the researcher to design and evaluate a pattern classifier.

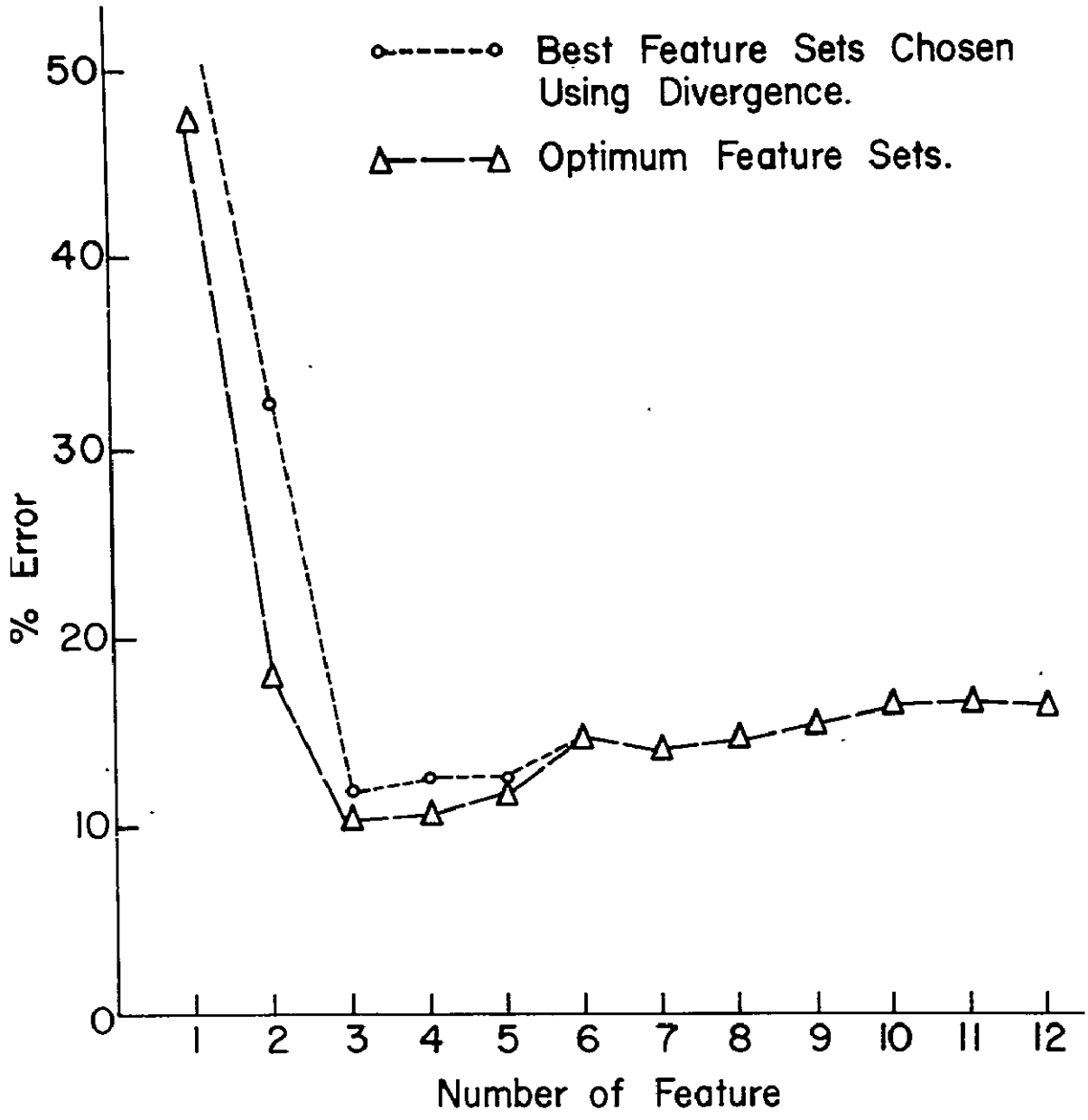

Figure 24-4.- Per cent error vs number of features (spectral bands) for a specific classification task. Note that better classification accuracy is obtained in this case using only three spectral bands than any other number.

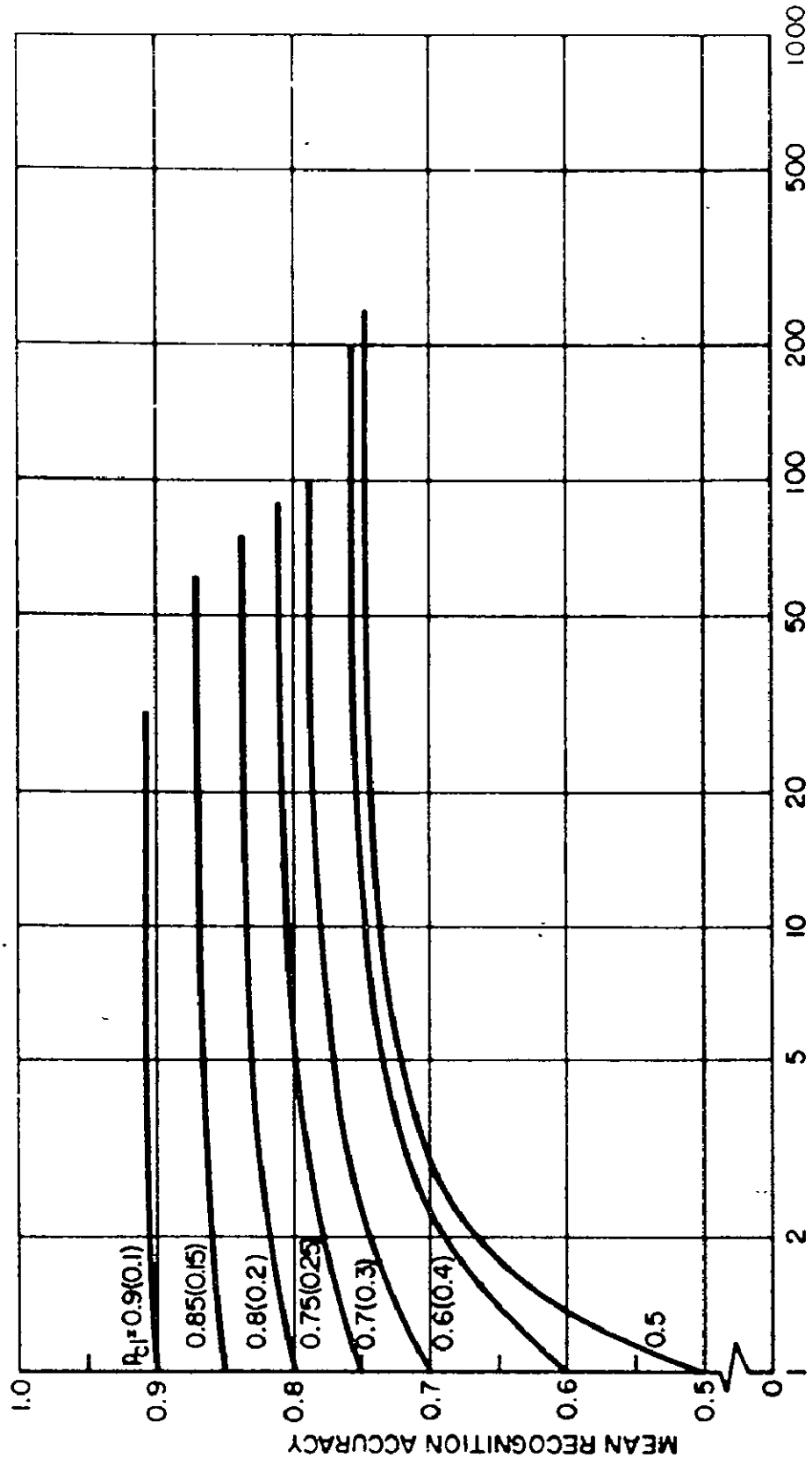

Figure 24-5.- Mean recognition accuracy vs measurement complexity for a training set infinite in size. The parameter of the graph is a priori class probability (Hughes, 1968).

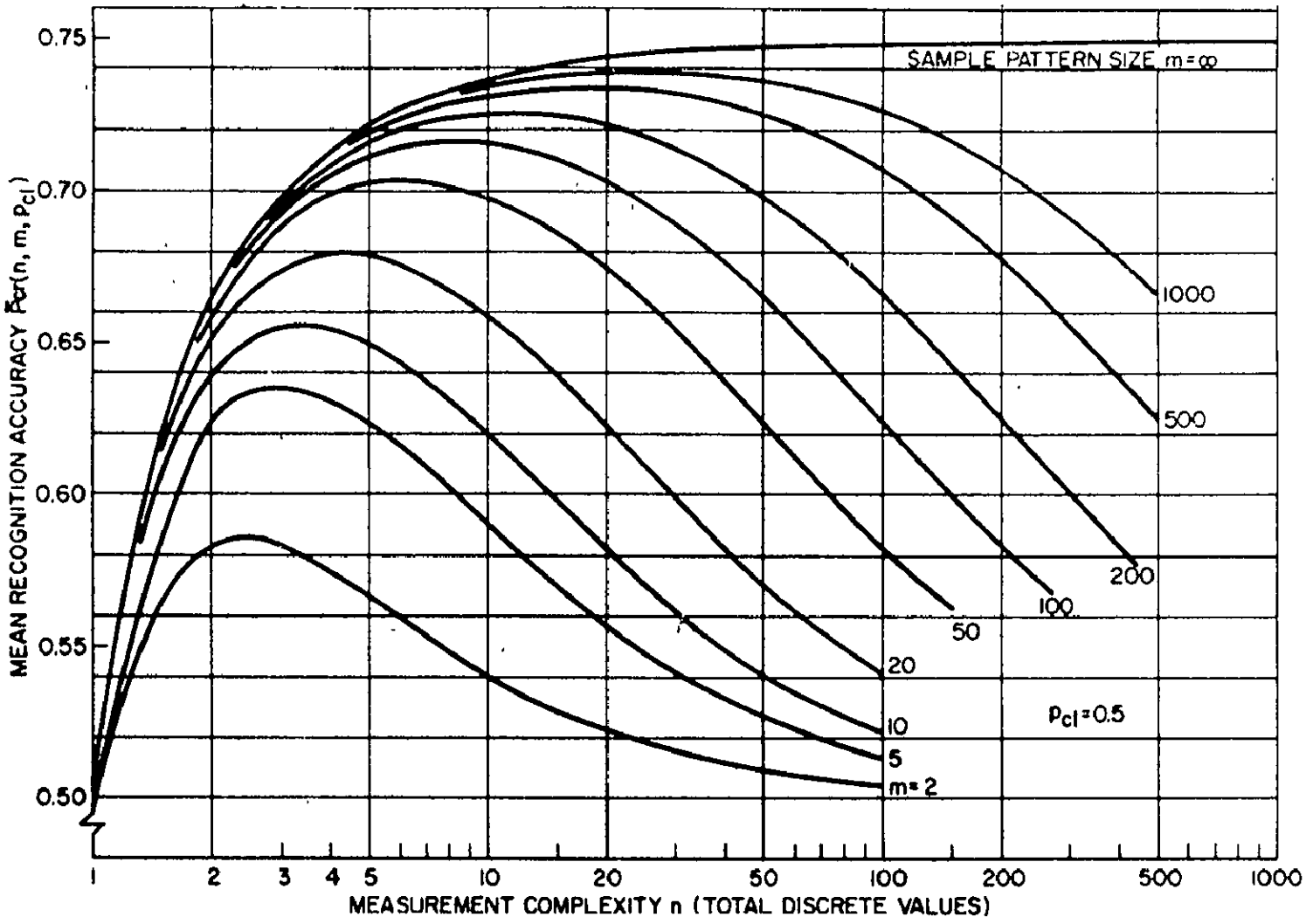

Figure 24-6.- Mean recognition accuracy vs measurement complexity for equal a priori class probability. The parameter m is the training set size (Hughes, 1968).

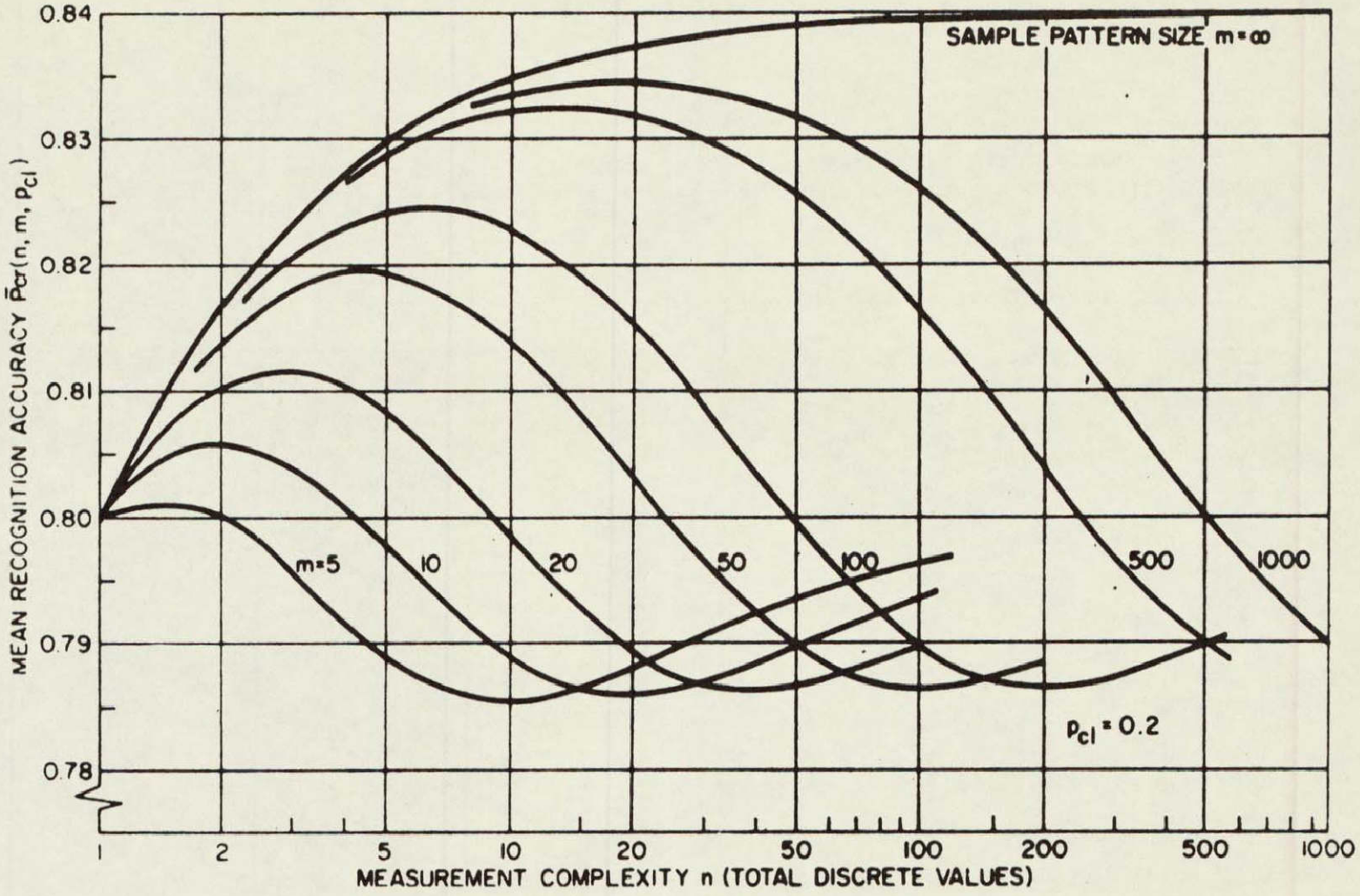

Figure 24-7.- Mean recognition accuracy vs measurement complexity for a priori class probability. The parameter m is the training set size (Hughes, 1968).

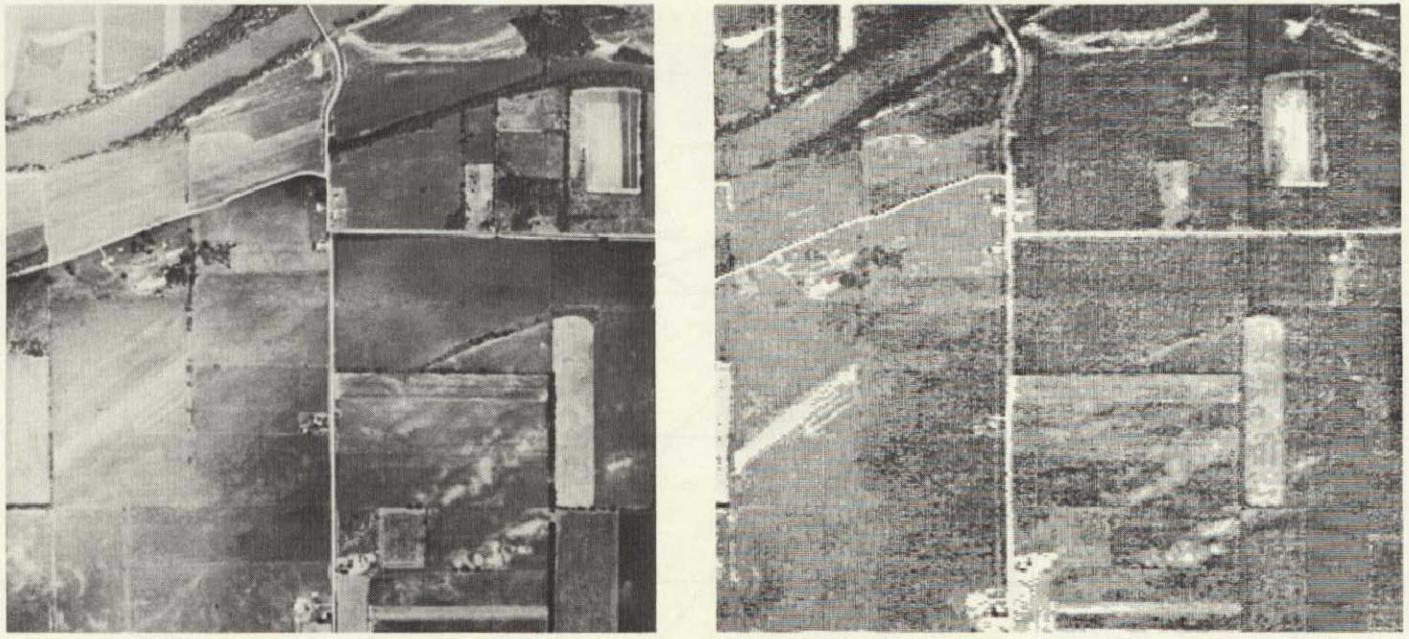

Panchromatic Aerial Photograph
(.4 - .7 micron)

Image Simulated on Line Printer

Figure 24-8.- Comparison of a panchromatic aerial photograph and computer line printer simulation of scanner image from the .62-.66 micromter band.

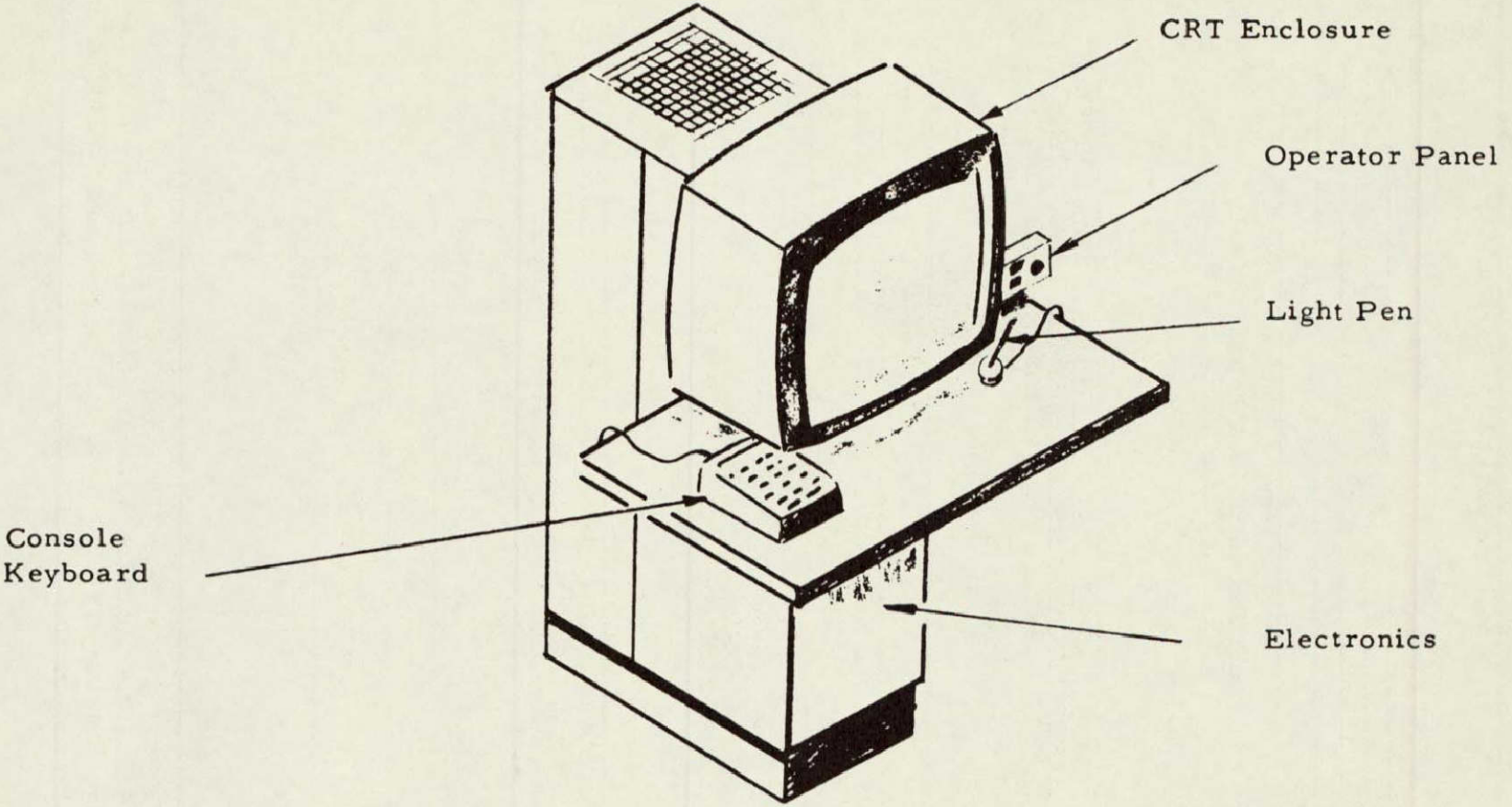

Figure 24-9.- Sketch of the Digital Image Display Edit Console.

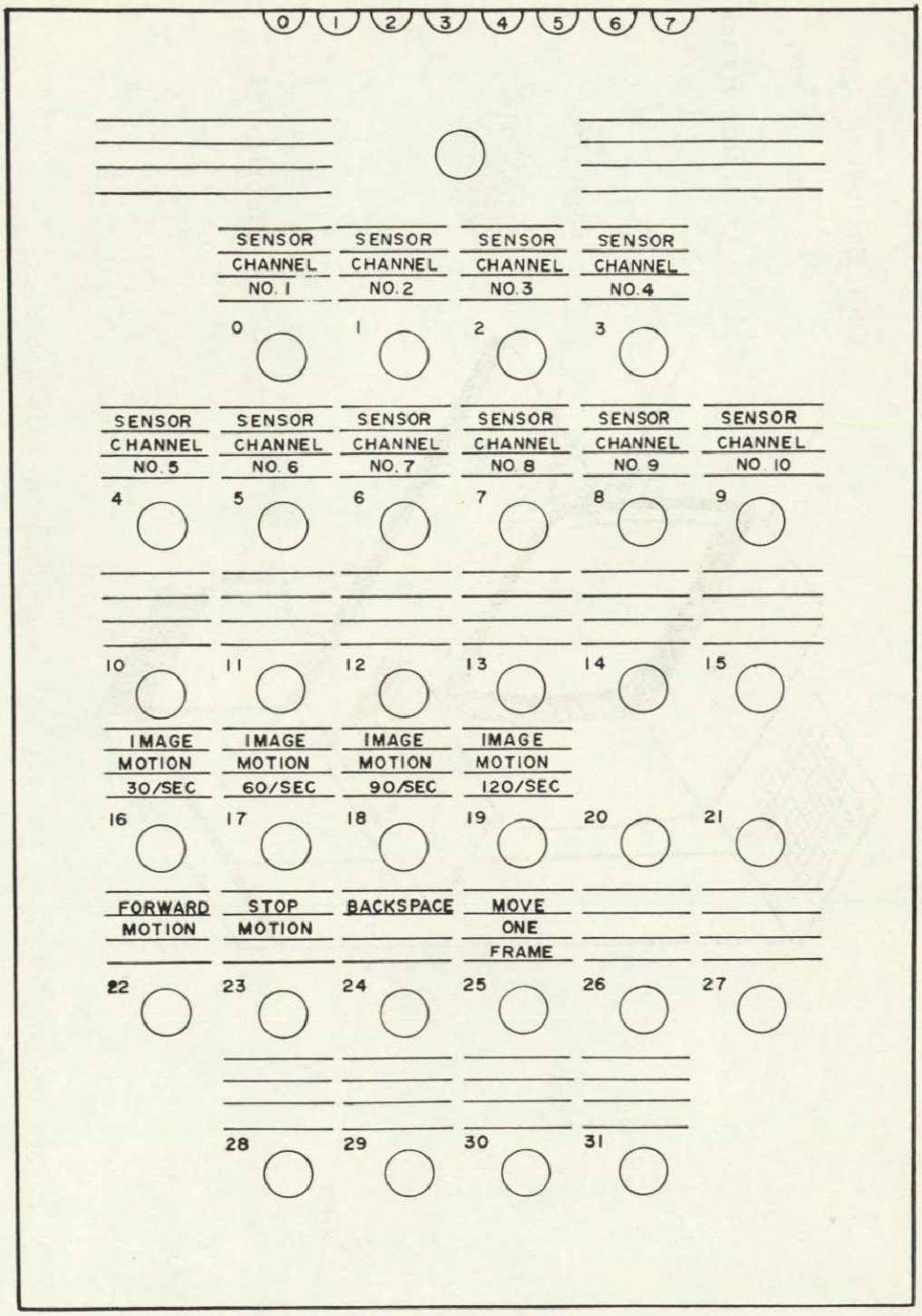

Figure 24-10.- Function keyboard overlay for the Digital Image Display System. Some sample keyboard functions are indicated on some of the keys.

Figure 24-11.- Scanner imagery from a visible (.62-.66μm) and a thermal (8-14μm) band. A panchromatic airphoto is shown on the left for comparison.

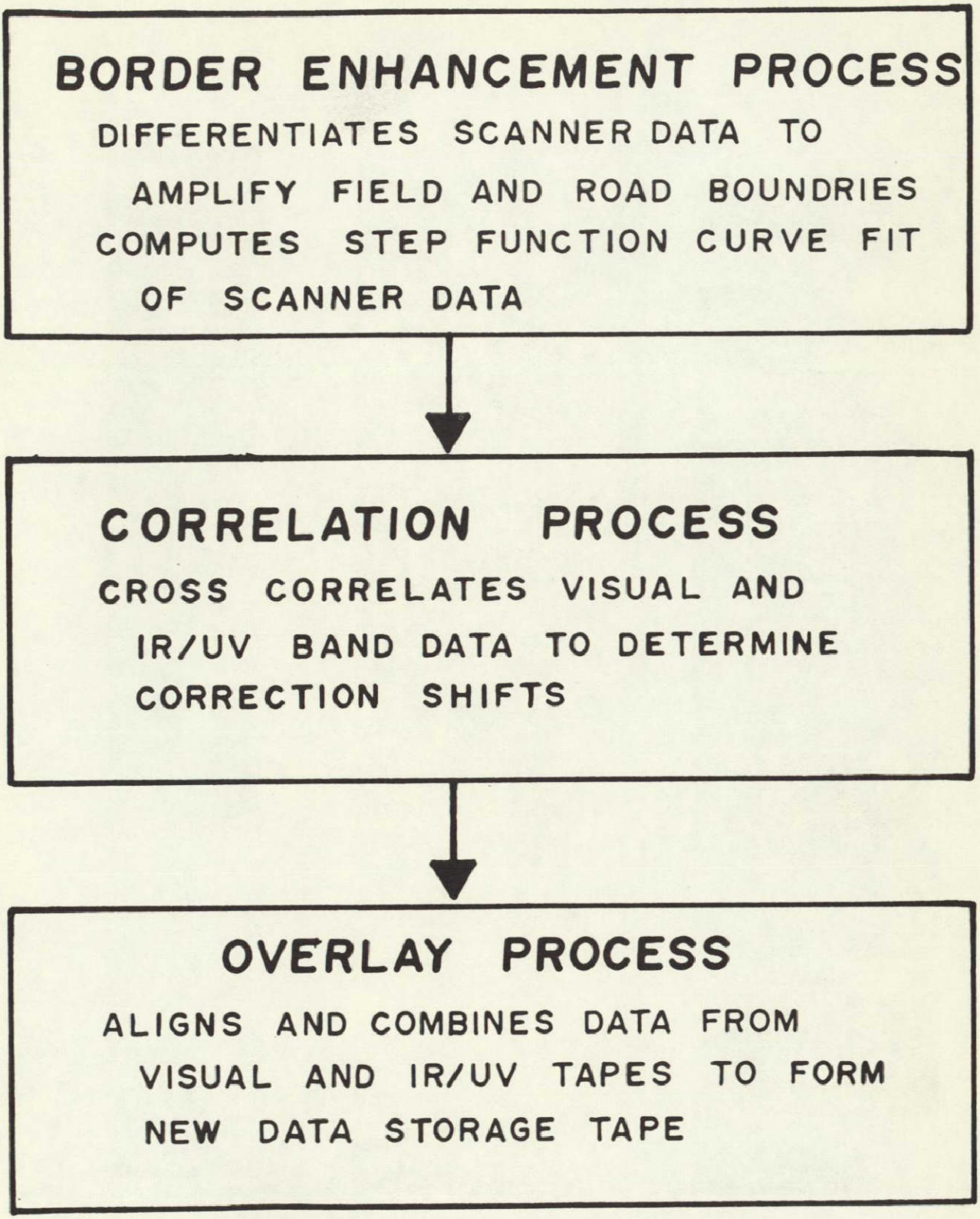

Figure 24-12.- Original organization of data overlay system.

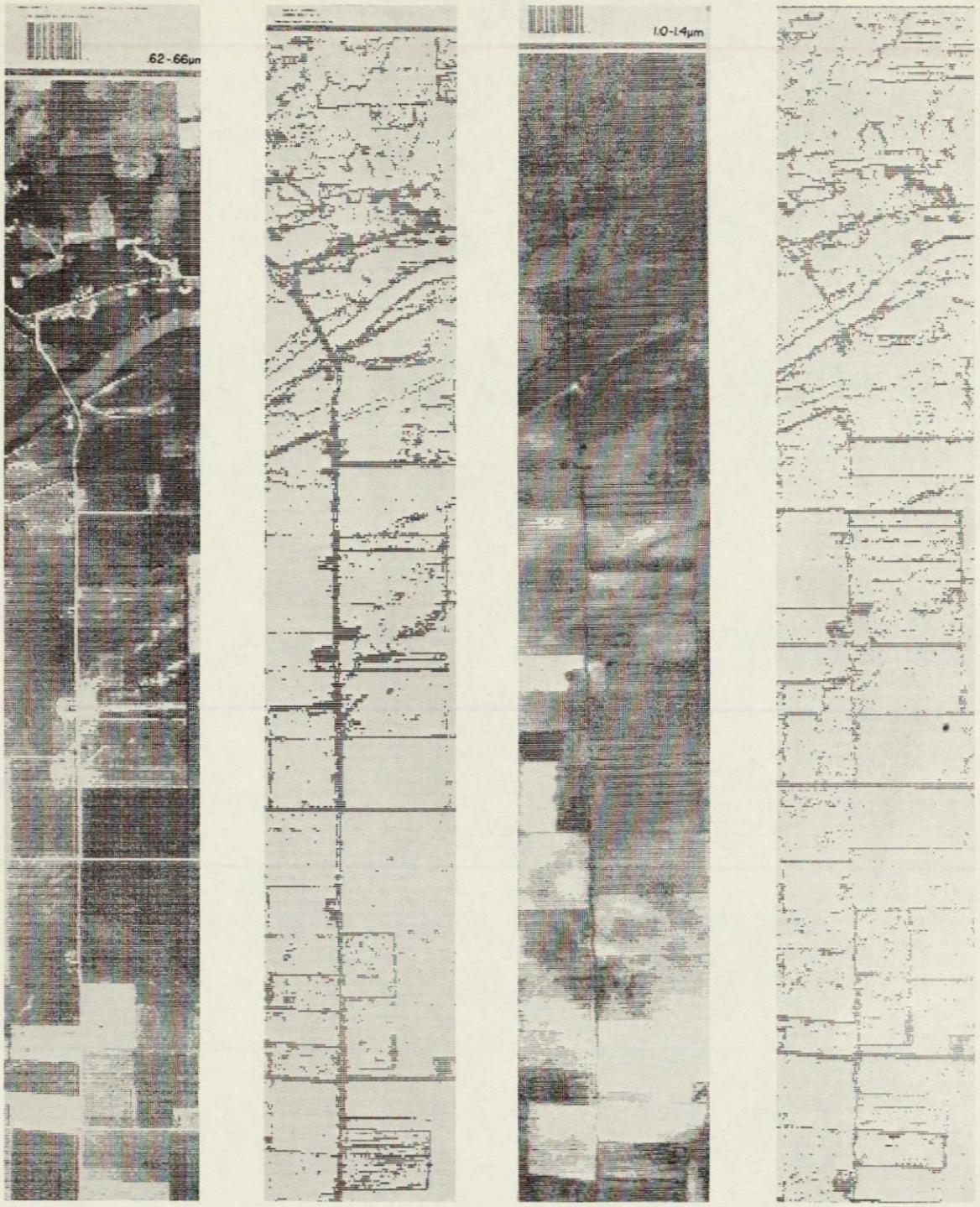

Figure 24-13.- Results of border enhancement on visable and thermal scanner images. A gray scale printout of each is also shown for comparison.

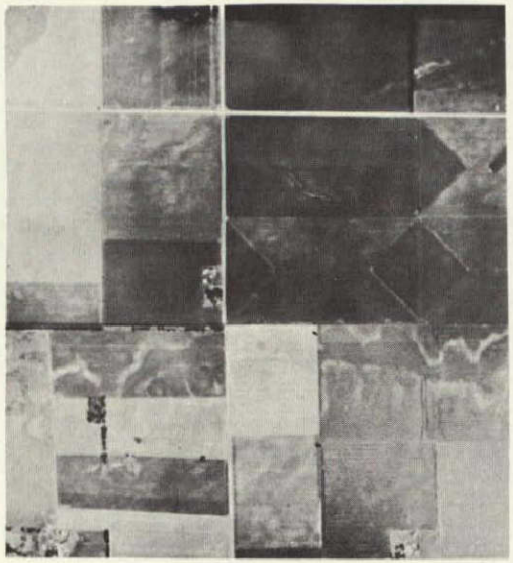

Class I- Rectangular plots such as agricultural fields in northern Indiana.

Class II- Natural areas such as forest, meadow or lake regions in Yellowstone National Park.

Class III- Mixed terrain cover such as hilly agricultural land in southern Indiana.

Figure 24-14.- Examples of three types of terrain cover.

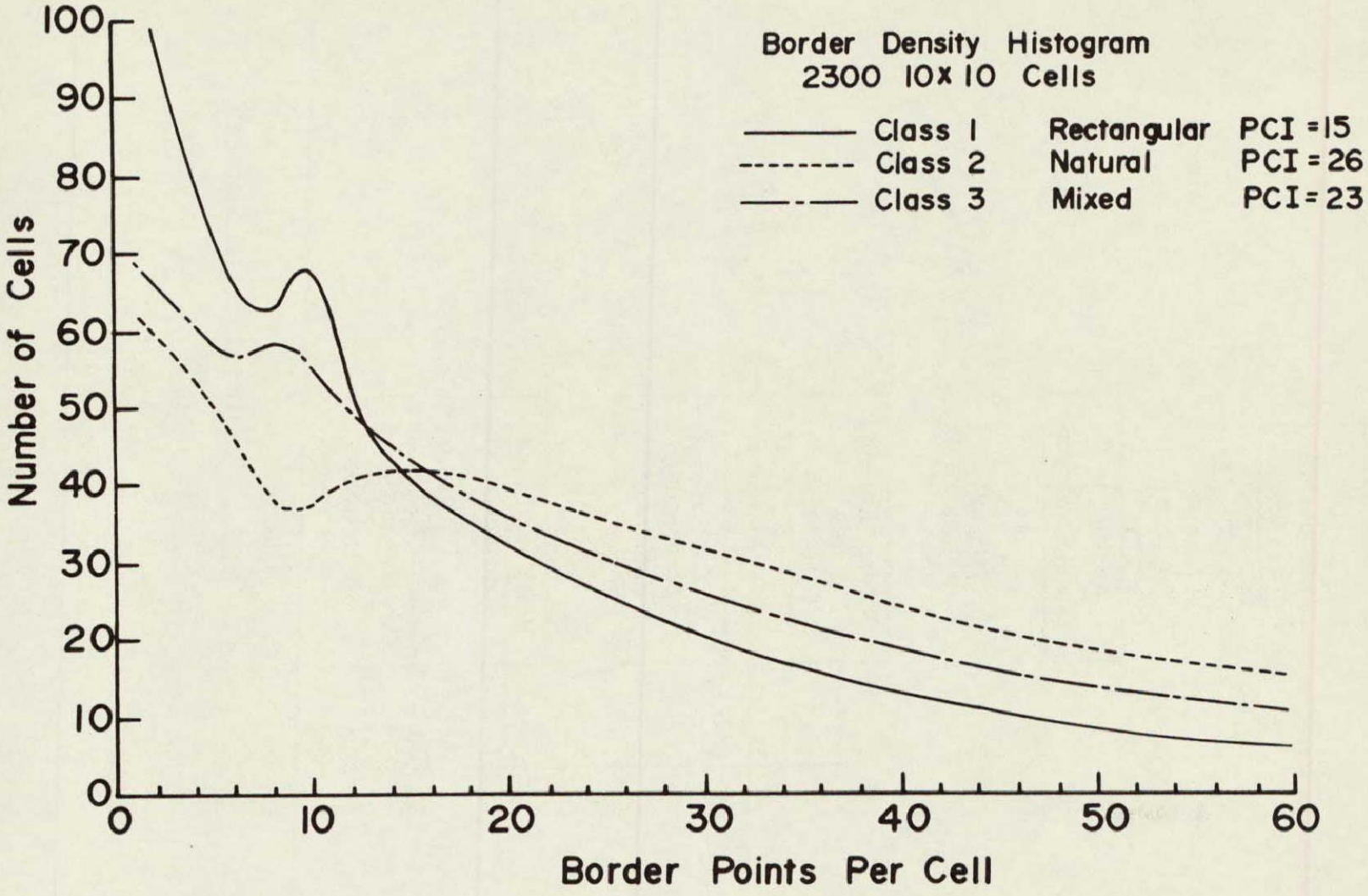

Figure 24-15.- Border density histograms for three classes of scenes.

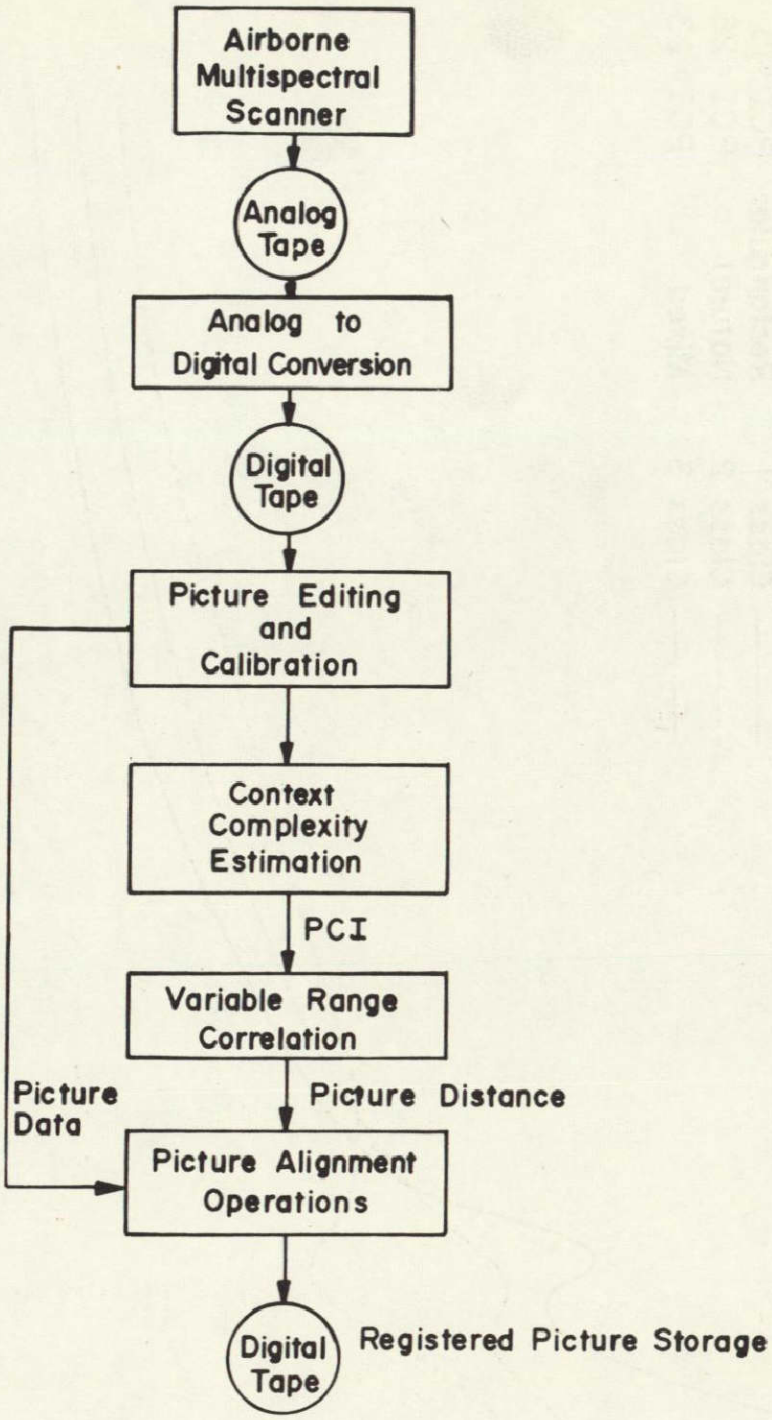

Figure 24-16.- Organization diagram of current data overlay system showing the adaptive feature using the picture complexity index.

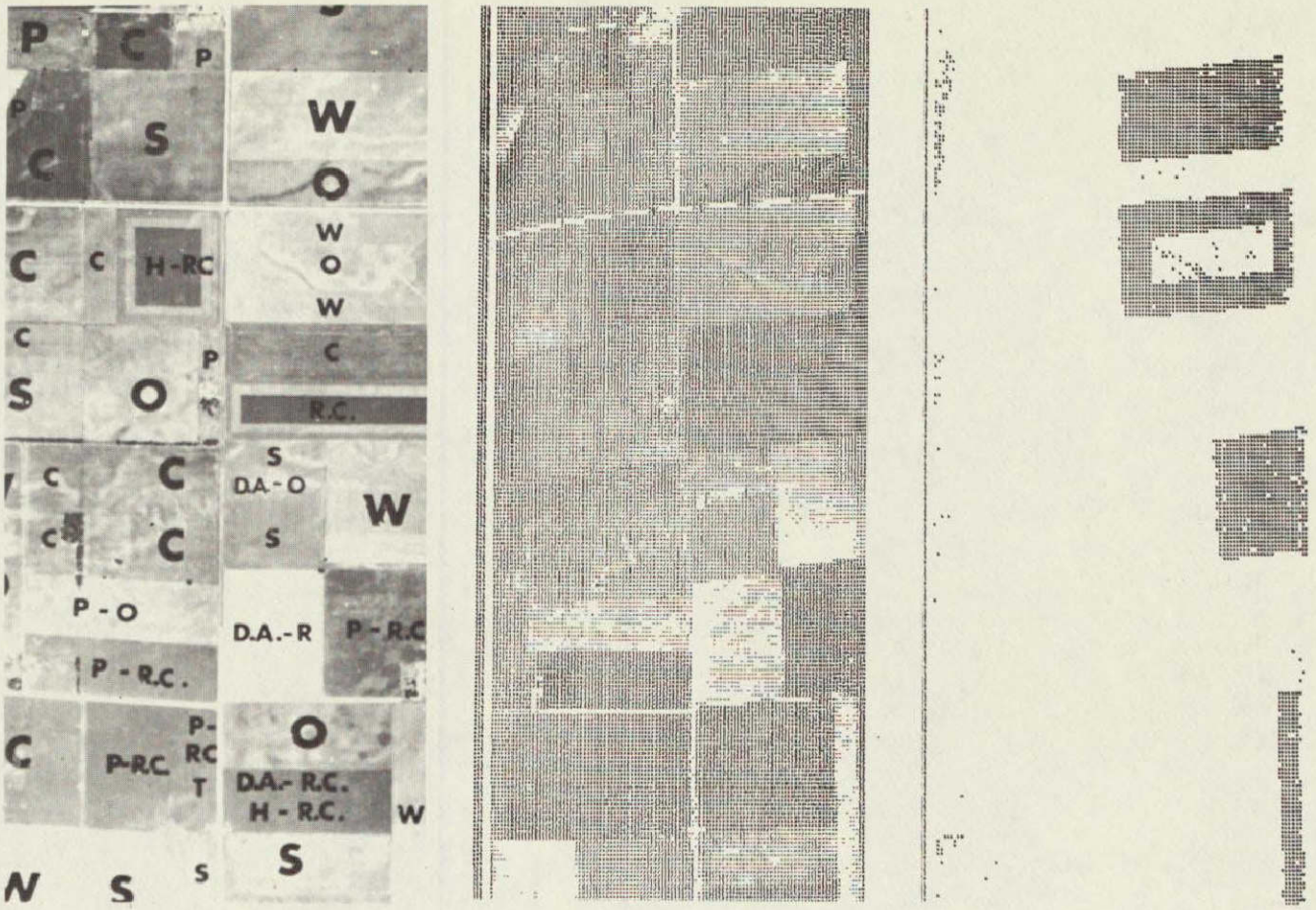

a. b. c.

Figure 24-17.- Airphoto (a) gray scale printout (b) and LARSYSAA classification result (c) of a section of data for the classes wheat and other. The ground truth is indicated on the airphoto by symbols as follows: W - wheat, S - soybeans, C - corn, O - oats, R.C. - red clover, R - rye, P - pasture, and D.A. - diverted acres.

PER POINT AND PER FIELD CLASSIFICATION RESULTS

Data from Purdue Area C-3 July 1966

Class	Per Point Classifier			Per Field Classifier	
	No. of Samples	Percent Correct	60% Classifier	No. of Fields	Percent Correct
Soybeans	2380	60.6	60.5	13	84.6
Corn	1188	72.0	70.0	10	90.0
Mixture	2725	91.7	94.4	18	94.4
Water	101	97.0	100.0	3	100.0
	6394	80.3	81.2	44	92.3
	Overall Performance = 76.6			Overall Performance = 90.9	

Figure 24-18.- Per point and per field classification results for July, 1966 Purdue Flight Line C-3. The same training and test fields and the same spectral bands were used for both types of classification.

PER POINT AND PER FIELD CLASSIFICATION RESULTS

Data from Purdue Area C-4 July 1966

Class	Per Point Classifier No. of Samples	Percent Correct	60% Classifier	Per Field Classifier No. of Fields	Percent Correct
Soybeans	5302	83.0	89.5	19	89.5
Corn	8875	79.6	83.8	31	96.8
Pasture	5233	75.7	77.8	18	100.0
Stubble	2943	81.2	84.6	13	76.9
	22353	79.9	82.0	81	90.6

Overall Performance = 79.7

Overall Performance = 92.6

Figure 24-19.- Per point and per field classification results for July 1966 Purdue Flight Line C-4.

PER POINT AND PER FIELD CLASSIFICATION RESULTS

Data from Purdue Area C-2 September 1966

Class	Per Point Classifier			Per Field Classifier	
	No. of Samples	Percent Correct	60% Classifier	No. of Fields	Percent Correct
Soybeans	3804	51.4	66.7	12	66.7
Corn	3718	80.0	78.6	14	92.8
Pasture	3608	78.9	76.9	13	100.0
Stubble	3692	57.4	45.4	11	81.8
Water	134	99.3	100.0	3	100.0
	14956	73.4	73.5	53	88.3
	Overall Performance = 67.0			Overall Performance = 86.8	

Figure 24-20.- Per point and per field classification results for September 1966 Purdue Flight Line C-2.

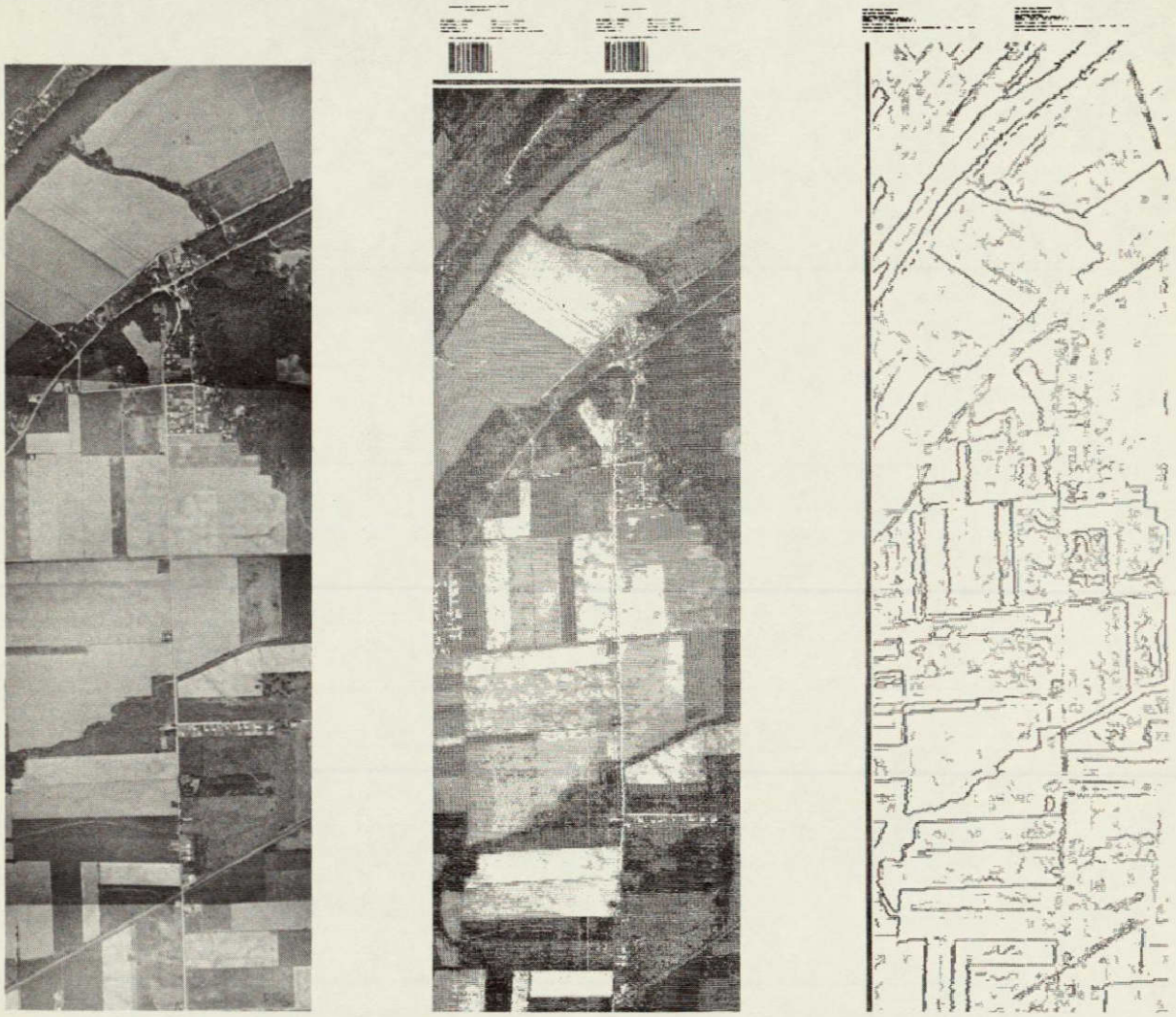

Figure 24-21.- Example output from the boundary-finding algorithm. An airphoto and line printer output are also given for comparison.

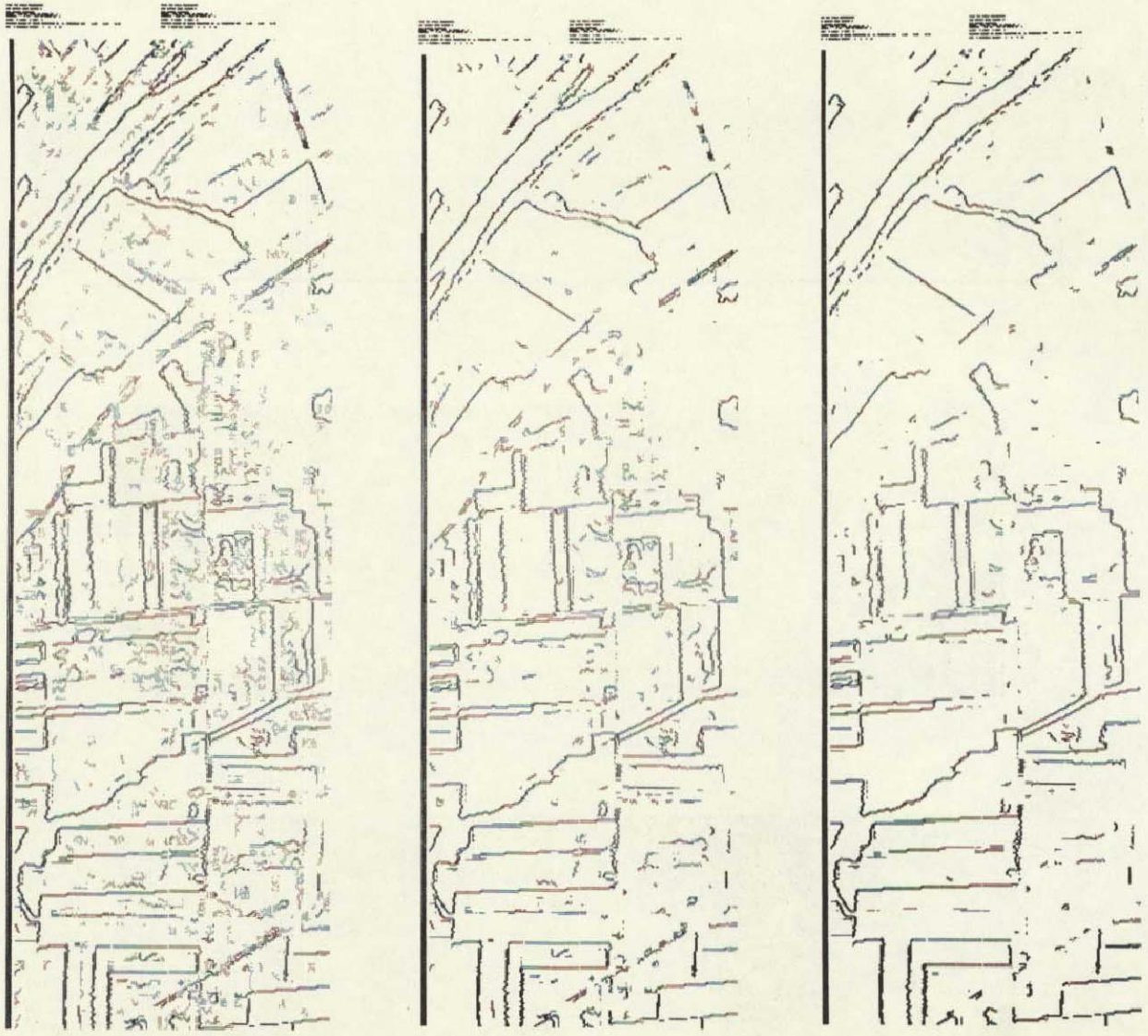

Figure 24-22.- Example results showing effects of varying the threshold of the boundary-finding algorithm.

SECTION 25

MULTISPECTRAL DATA COLLECTION AND INSTRUMENTATION STUDIES

D. S. Lowe

The University of Michigan
Willow Run Laboratories
Ann Arbor, Michigan

This paper reviews two programs sponsored by NASA/MSC. These programs are concerned with expanding and improving data collection with optical mechanical scanners. The multispectral data collection program, which is directed by Phil Hasell, will be discussed first. This will be followed by a review of the program of infrared instrumentation studies which is the responsibility of Jack Braithwaite.

The need for and uses of multispectral data has been discussed by many of the preceding speakers. Recognizing this need, NASA/MSC contracted with the University of Michigan to assure the availability of the multispectral data collection facility to the earth resources program. The capability of the Michigan C-47 multispectral aircraft has been described by a number of speakers and is reported elsewhere. [1] Suffice it to say, the main data collection ability is centered around optical mechanical scanners which allow simultaneous collection of imagery in as many as 19 wavelength bands. The scanners periodically view calibration sources, and the electronics have been modified to assure fidelity in signal handling and recording.

Photography is available in 70 mm and 9" formats and is gathered for interpretation purposes only. It should be emphasized that the outdated, GFE cameras have limited capability, and high quality photography cannot be assured. For example, proper exposure of the 74° FOV, 70 mm cameras can be obtained only under high illumination levels as the smallest f/no. is 4.8 and the longest shutter speed is 1/500 sec. Such minimal exposure settings hardly allow for special narrow band spectrozonal filtering frequently requested by users.

Since the aircraft has two 80" x 24" instrumentation wells, special sensors can be flown as requested. Under the NASA program, we have flown a PRT-5 radiometer in support of some missions.

Data collection is of a service nature, and one may ask why a University is involved in such an endeavor. The answer is simple. Multispectral data is vital to many of our programs. The equipment was developed to fulfill these needs as no other suitable source of data exists. Michigan

investigators request and receive data collection missions. Professor Holter's paper discusses some of the aspects and results of our multispectral program. Even though the equipment is far from ideal and can be considered to be the first experimental prototype of its kind, the type of data it produces is needed and wanted by non-Michigan earth resource investigators.

The results and status of this program can be presented best in tabular form. Table I summarizes the missions that have been flown and planned. As of 1 September 1969, Michigan has flown 12 missions and collected 4600 flight line miles of data. Sixteen missions for collecting 4855 miles of data are planned for the remainder of the contract period.

Each of the missions are planned and tailored to the user needs. Some of the variables among missions are multiple altitudes, multiple flight lines, multiple flights for varying observation times and conditions, various combinations of sensor channels, and various data formats. As for data formats, some users prefer duplicate tapes, others hard copy imagery. In the case of the Oregon Coast mission with data miles running into the thousands, thermal data of the ground track were recorded on a strip chart for immediate and convenient access. The video data from 11 channels were recorded on tape, but imagery processing can be performed at a later date if analysis of the strip chart recording indicates that imagery of selected areas is needed for more detailed inspection and analysis.

The strip chart recording was made by electronically gating out the video signal when the scanner views the ground track. Periodically the gate would be shifted a preset amount to sample the signal from the calibration sources or the ocean away from the nadir. Radiation from the known sources can be used to calibrate the instrument and the ocean observations through various slant paths can be used to correct for errors introduced by the intervening atmosphere.

The objective of the program on infrared instrumentation studies is to analyze the data requirements of users and conduct instrumentation and technique investigations necessary to assure that future data collection instrumentation will be capable of fulfilling the investigator's needs. The tasks can be classified as investigating short and long range problems associated with aircraft and spacecraft instrumentation. The tasks and results of these studies have been reported in the final report [2] and in special reports to the contract monitor. Two of these studies are of direct interest to the data users of the earth resource program and will be briefly summarized.

Recognizing that most users of thermal imagery desire semi-quantitative, if not quantitative, results; Michigan conducted a study to define what MSC

must do to make their RS-7 and Recon IV quantitative. The study provided detailed design of calibration sources, schematics of electronic modifications, and definition of installation modifications. Error analyses indicated that calibration with either extended sources or collimated point sources offered about the same degree of uncertainty. While the temperature of a small source can be measured more accurately than an extended source (because of variations over the extended source), optical surfaces needed to collimate the radiation from a point source introduces errors. The degree to which this error can be corrected is limited by the knowledge of the emissivity and temperature of the optical surfaces of the collimator. As a result, the error in predicting the apparent temperature of the calibration source is approximately the same for both extended or collimated point sources. Accuracies of the order of $\pm$ 0.5°C can be readily achieved with carefully designed sources of either type without undue engineering design or lengthy computational corrections.

A number of the tasks were concerned with analysis of problems associated with multispectral sensing from spacecraft. The results were incorporated into the design of a multispectral scanner to be flown in an early Apollo Application mission. The primary constraint in the design is that it incorporates only current state-of-the-art components and technology. As one knows, a sensor's performance cannot be optimized for multiple experiments. It can be designed, however, so that data utilization can be maximized. The performance specifications for a scanner which will be highly useful for many earth resources experiments are given in Table II. The remainder of this paper will discuss the design and trade-off relationships among vital parameters. These can be used to evaluate contemplated changes to the system whose performance is specified in Table II.

The scanner configuration and scan pattern are shown in Figures 1 and 2 respectively. The scan mirror is rotated about an axis which is tilted 2.5° from the normal. This results in a conical scan pattern having a half angle of 5°. In this scan pattern, the view angle is constant. The scan pattern on the ground is slightly oval; the major axis lying in the plane that contains the optical and scan mirror rotation axes. For the proposed design, the major axis is 9% longer than the minor axis. As shown in Figure 2, slightly less than one-third of the scan pattern is used with three detectors per channel. As will be seen later, the signals from the three detectors are stored and read out sequentially thereby making full use of the telemetry link. The three detectors remain almost parallel to the ground track throughout the nearly circular scan. Calculations show that the detector array does oscillate $\pm$ 1° from the direction of the ground track, but this effect is negligible. Figure 3 shows the scan pattern geometry.

Returning to Figure 1, radiation from the scan mirror is directed onto an f/2.5 off-axis parabola (which is a section of an f/1 parabola). The radiation is focused on a slit which serves as the field stop. Radiation

passing through the field-stop is split by a dichroic mirror. The long wavelength thermal emission is transmitted and refocused onto a three-element detector which is cooled by solid cryogenics. The short wavelength radiation, whose origin is reflected sunlight, is focused on the slit of a dispersing spectrometer. Six, three-element detector arrays are placed in the image plane of the dispersed radiation to give the spectral channels listed in Table II.

The performance specifications of the scanner are determined by the sensitivity desired, by the complexity one is willing to accept (size, weight, and number of detecting elements), and the acceptable data rate and volume. Assuming one wishes to telemeter the data in real time, the number of resolution elements scanned per second by each detector element is given by

$$n = \frac{2\pi \sin\theta}{\beta^2 \cdot p} \; V/h \qquad (1)$$

where θ is the scan half angle (5° is proposed)

V/h is the spacecraft velocity to height ratio

β is the angular resolution in radians

p is the number of detectors per channel (3 are proposed)

By using slightly less than 1/3 of the scan cycle for scanning the earth and the remainder of the 1/3 scan time to inject calibration signals, the entire scan process has a duty cycle of 33%. By data storing and sequential read-out of the three detectors per channel, a 100% duty cycle of the telemetry link can be achieved. The telemetry link is divided into 7 FM channels for transmission of the video from the seven spectral channels.

It can be shown that the signal to noise ratio, SNR, of each detector channel is given by

$$SNR = \frac{\sqrt{\pi}\, \beta^2\, L_\lambda\, \delta\lambda\, \tau(\lambda)\, D^*_\lambda\, D\, \sqrt{p\,\gamma}}{4\, F\, \sqrt{V/h \sin\theta}} \qquad (2)$$

where β is the angular resolution

$L_\lambda \delta\lambda$ is the radiance of terrain in the bandpass of operation

$\tau(\lambda)$ is the atmospheric and optical transmission in the bandpass of operation

D^*_λ is the detector detectivity in the bandpass of operation

D is the entrance aperture diameter

p is the number of detectors per channel

γ is the scan duty cycle (1/3)

F is the aperture ratio (f/no) of the optical system

V/h is the spacecraft velocity to height ratio

θ is the scan half angle

A more useful expression than SNR, is the Noise Equivalent Temperature Difference, NEΔT, or Noise Equivalent Reflectance Difference, NE$\Delta\rho$. The NEΔT is that temperature difference between two resolution elements of emissivity one which produces an SNR equal to 1. It can be shown that equation (2) can be written as

$$\frac{\sqrt{V/h \sin\theta}}{\beta^2 \quad NE\Delta T} = \frac{4 F}{C \pi(\lambda) D^*_\lambda D \sqrt{p\gamma}} \qquad (3)$$

where C is the radiance difference in the bandpass of operation per degree temperature change, i.e.,

$$\frac{\delta L_\lambda}{\delta T} \delta\lambda$$

The parameters on the left hand side of equation (3) are concerned with performance while those on the right hand side are determined by component constraints and design configuration. For the performance specifications given in Table II, the required entrance aperture diameter can be determined from equation (3).

The data rate of the scanner output is a product of the number of elements scanned per detector, the number of detectors per channel, and the number of channels. From equation (1), this product is given as

$$n\ p\ q = \frac{2\pi\ q \sin\theta\ V/h}{\beta^2}$$

where q is the number of spectral channels (7 are proposed). The available telemetry link and desired accuracies also determine the maximum data rate. The trade-off curves given in Figure 4 are based on the specifications given in Table II and the following telemetry capability and constraints

20 watt, S-band transmitter
omnidirectional antenna
40' receiver dish operating to within 8° of horizon

As seen from Figure 4, a ground resolution of 300 ft. can be achieved with a collector diameter of 12 inches. The total scan width would be 45 n. mi. (yielding a swath width of 35 n. mi.). The entire scanner system would weigh approximately 200 pounds. It is estimated that the volume would be 50" high, 25" long, and 18" wide.

To summarize the discussion on spacecraft scanner design, a seven channel multispectral scanner can be built for flight in an Apollo workshop which can meet the performance requirements for the earth resources program. The scanner would use only current state-of-the-art components and technology.

REFERENCES

1. P. G. Hasell, Jr. and L. M. Larsen, Calibration of An Airborne Multispectral Optical Sensor, Technical Report No. ECOM-00013-137, Institute of Science and Technology, The University of Michigan, Ann Arbor, September 1968.

2. J. Braithwaite, L. Larsen and E. Work, Further Infrared System Studies for the Earth Resources Program, Report No. 2122-14-F, Institute of Science and Technology, The University of Michigan, Ann Arbor (in publication).

Mission No.	Location	Application	P.I.	Data Miles	Schedule	Flown
1	San Diego	Ag./Geol./Ocean.	King/Eaton	170	3/8-10	3/8-12
2	Purdue	Agriculture	Hoffer	330	5/12-16	5/13-27
3	Purdue	Agriculture	Hoffer	330	6/23-27	6/25-26
4	Oregon Coast	Oceanography	Pearcy	2840	7/30-11	7/3-13
5	Wind River	Forestry	Wear	84	7/14-16	7/14-15
6	Bucks Lake	Forestry	Lent	40	7/17-18	7/16
7	Black Hills	Forestry	Heller	164	7/21-22	7/21-22
8	Missouri River	Geology	Crosby	160	7/23	7/23
9	Ann Arbor	Forestry	Olson	40	7/24-25	8/4
10	Purdue	Agriculture	Hoffer	350	8/4-8	8/5-6
11	Lake Michigan	Oceanography	Polcyn	50	8/8	8/11
12	Ann Arbor	Forestry	Olson	40	8/11-15	8/13
13	Washtenaw	Agriculture	King	80	8/11-15	9/3
14	Oregon Coast	Oceanography	Pearcy	3000	9/8-19	9/14-24
15	Wind River	Forestry	Wear	64	9/22-23	9/26
16	Moses Lake	Water Resources	Maierhofer	40	9/24	9/25
17	Bucks Lake	Forestry	Lent	20	9/25	
18	Mill Creek	Geology	Rowan	225	9/29-30	
19	Ann Arbor	Forestry	Olson	40	10/2-3	
20	Purdue	Agriculture	Hoffer	330	10/6-10	
21	Washtenaw	Agriculture	King	100	10/13-17	
22	Alafia/Pease	USGS	Coker	164	10/20-24	
23	Tampa Lakes	USGS		52	10/20-24	
24	Gulf Coast Springs	USGS		90	10/20-24	
25	Everglades	USGS	Higer	100	10/27-31	
26	Florida Keys	Oceanography	Polcyn	100	10/27-31	
27	Washtenaw	Agriculture	King	100	12/1-5	
28	Purdue	Agriculture	Hoffer	330	12/8-12	

TABLE I - MULTISPECTRAL DATA COLLECTION
MISSION SUMMARY

No. of channels:	7
Channel Placement: (tentative)	.5 - .6 μm
	.6 - .7 μm
	.7 - .8 μm
	.8 - 1.2 μm
	1.55- 1.75 μm
	2.1 - 2.4 μm
	10.5 - 12.5 μm
Ground resolution:	300' from 250 n. mi. orbit
Swath width:	35 n. mi.
Total scan width:	45 n. mi.
NEΔT:	1/2°C for 10.5-12.5 μm channel
NE$\Delta\rho$:	<1% for all reflective channels, clear sky, and sun elevation greater than 30°

TABLE II - MULTISPECTRAL PERFORMANCE SPECIFICATIONS

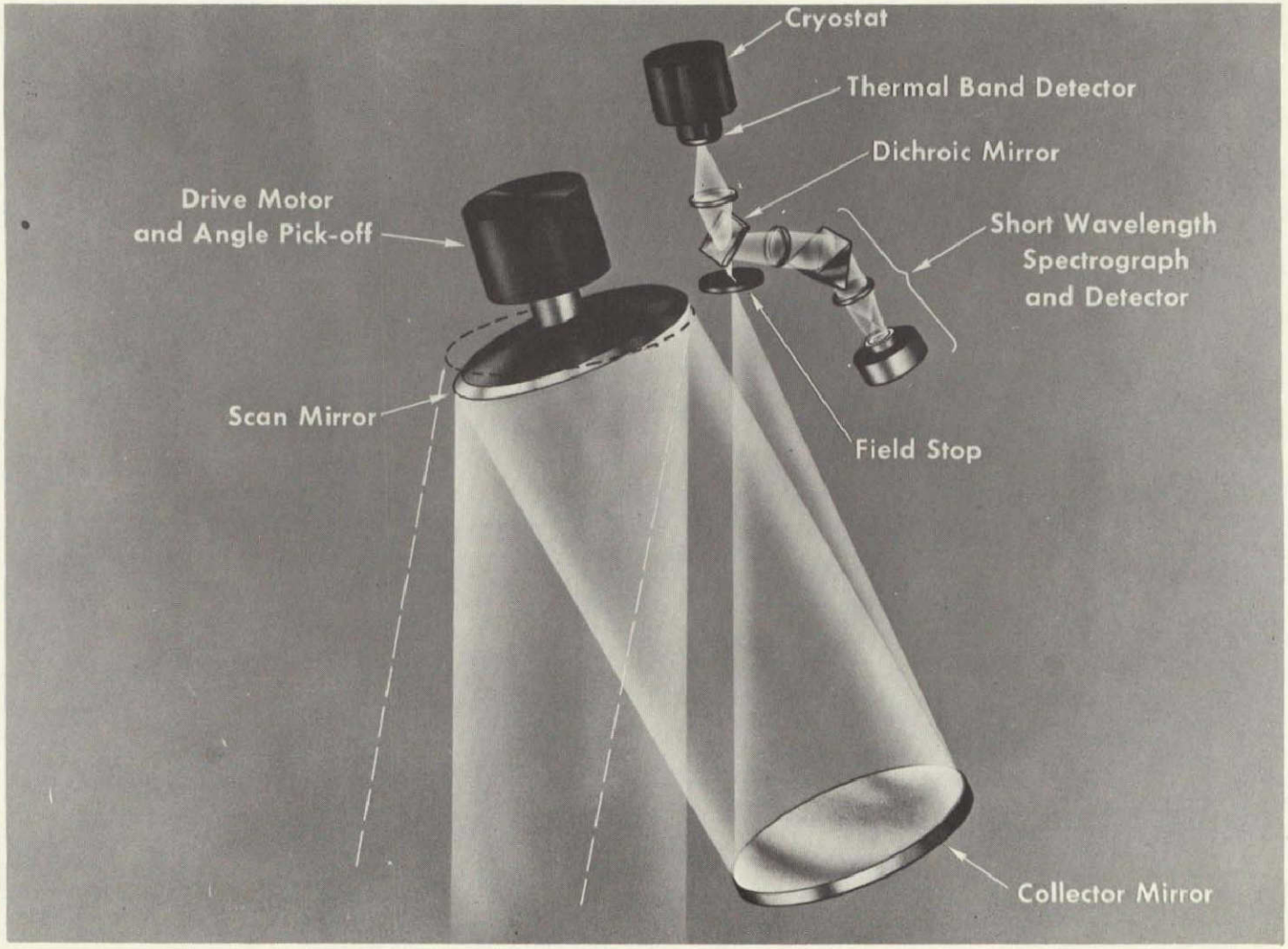

Figure 25-1.- Air-brush schematic of scanner layout.

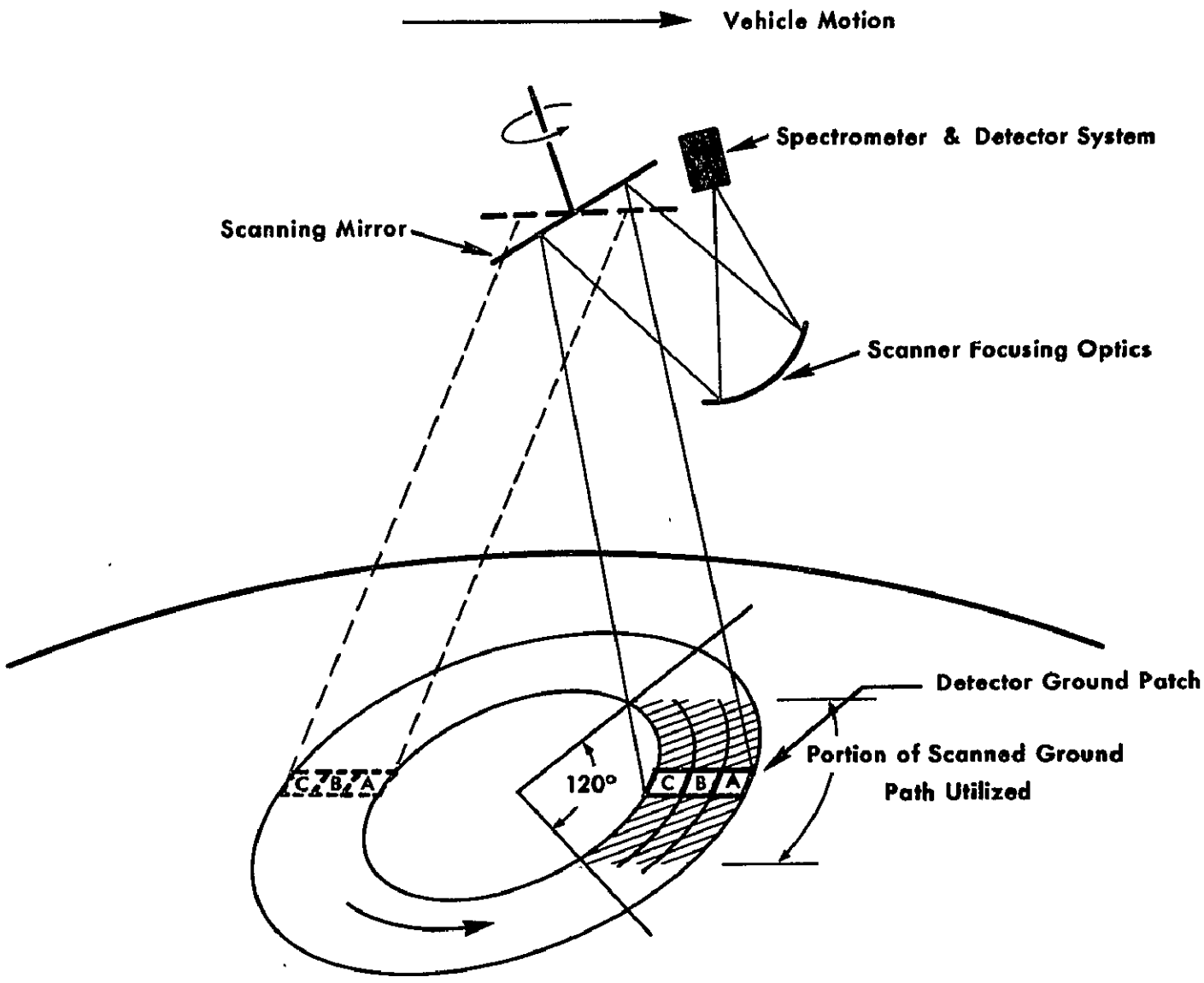

Figure 25-2.- Conical or small circle scanning technique.

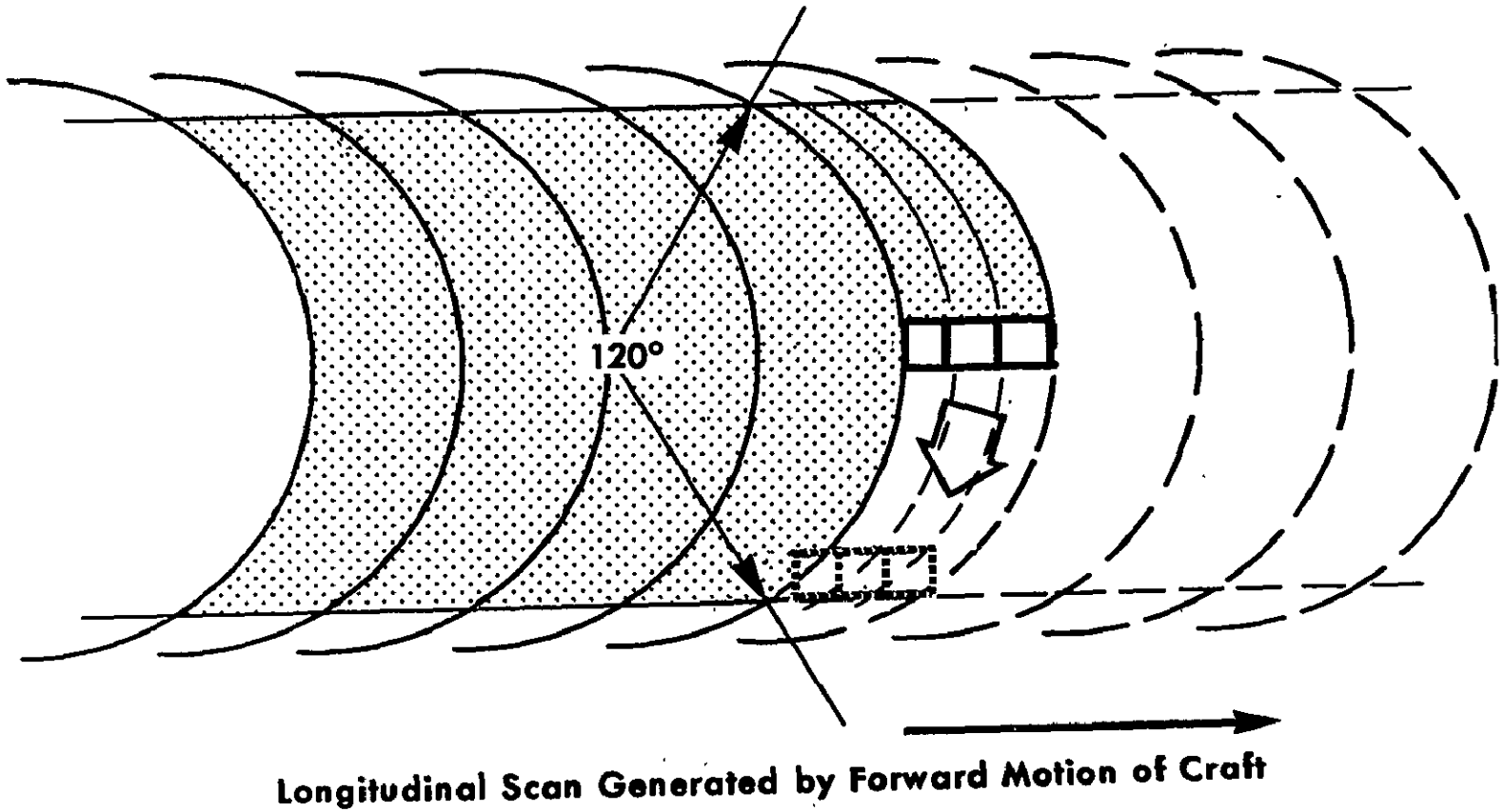

Figure 25-3.- Representation of scan pattern.

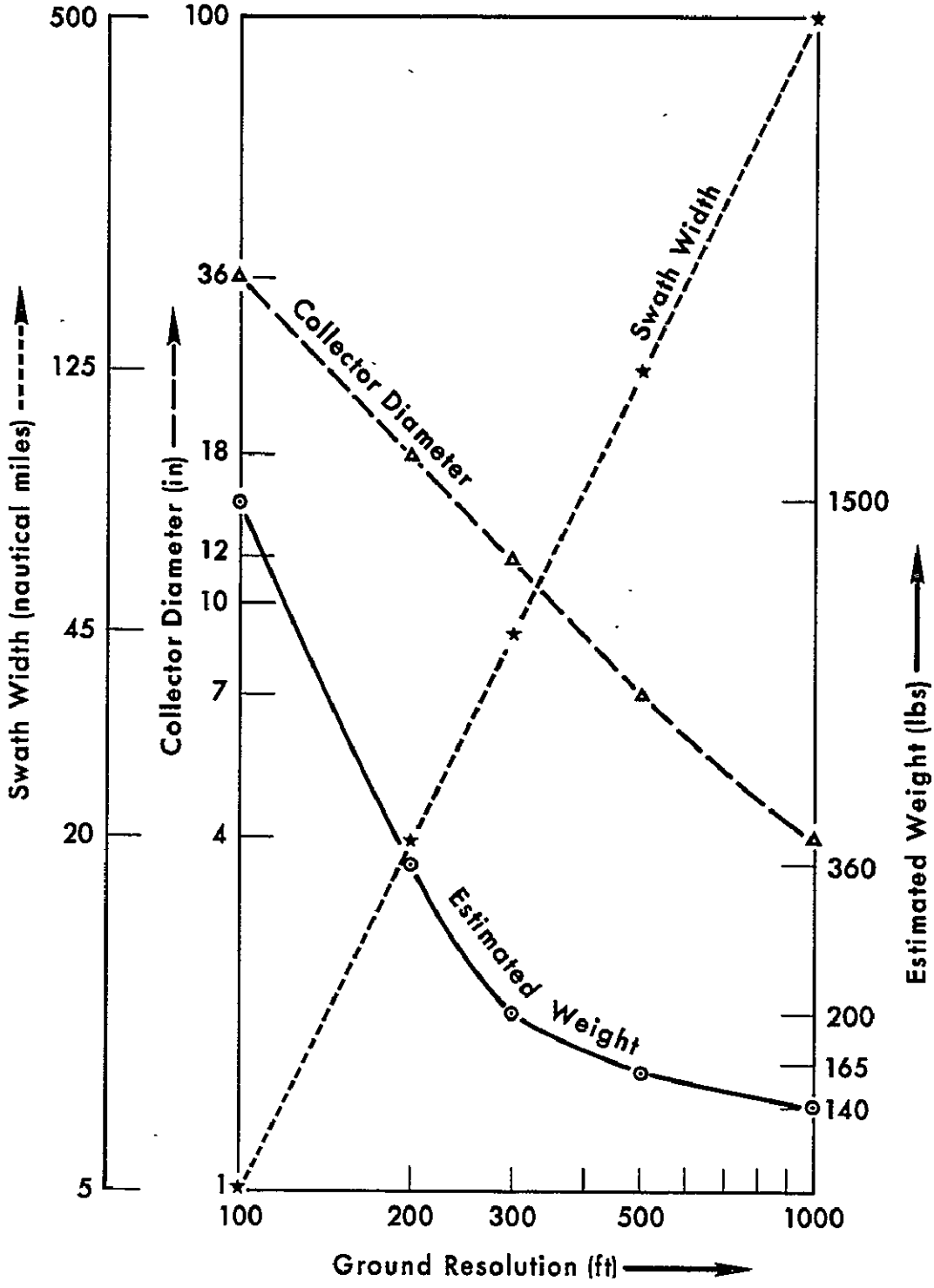

Figure 25-4.- Trade-offs for orbital MS scanner.

SECTION 26

AIRBORNE INFRARED STUDY OF IGNEOUS ROCKS IN SONORA PASS TEST SITE

by

I.A. Kilinc

Post-doctoral Research Associate

Stanford University

and

R.J.P. Lyon

Associate Professor

Stanford University

ACKNOWLEDGEMENTS

We would like to extend our sincere thanks to NASA-Earth Resources Program group for their cooperation in this project. Too many individuals to name here have directly or indirectly contributed to the infrared spectrometry project by maintaining the complex data receiving and recording systems in operational condition, by flying the instruments over the target areas and by reducing the data to our formats.

This study was supported by NASA Grant NAS9-7313 to R.J.P. Lyon of Stanford University.

AIRBORNE INFRARED SPECTRAL STUDY OF IGNEOUS ROCKS IN SONORA PASS TEST SITE

I. A. Kilinc and
R. J. P. Lyon

Mission 78 of NASA Earth Resources Program was flown over Sonora Pass and Mono Lake test sites during the period August 27-28, 1968. The aircraft was equipped with the infrared pallet, consisting of Lockheed airborne rapid scan IR spectrometer, Block IR radiometer, boresight camera (three-instrument IR pallet), PRT 5 radiometer and two RC8 cameras.

The purpose of the mission was (1) to obtain airborne infrared emission spectra in the 6.76-13.33 micron wavelength band, and; (2) by use of various data processing techniques to discriminate among rock types on the basis of their infrared emission spectra. Specifically, the primary objective of the mission was to test the feasibility of using a three-instrument IR pallet together with the data recording system and to identify the various rock types in selected geologic target areas.

In order to achieve this objective several target areas were selected within the high altitude granite terrain of Sierra Nevadas. Black Hawk mountain, one of the target areas within Sonora Pass test site, is located approximately 119° 42' W and 38° 12' N, and has an altitude of about 3200 meters above sea level. The rock exposed in the target area is predominantly the Topaz Lake quartz monzonite porphyry. At the top of the mountain andesite overlies the Topaz Lake quartz monzonite porphyry* in an area that measures about 1600 meters by 400 meters.

* Quartz monzonite porphyry and granitic rock will be used interchangeably throughout this paper.

The second target area, Brown Bear, is approximately 5000 meters east of Black Hawk mountain and consists of Topaz Lake quartz monzonite porphyry capped by basalt flows and small patches of rhyolite.

These two target areas were considered particularly suitable for this mission because of excellent soil-free exposures of unaltered andesite, basalt and granitic rocks, low atmospheric interference from water vapor due to altitude and almost total absence of vegetation.

The target areas were flown at absolute altitudes of 600, 700, 1000 and 2700 meters. Each run, where possible, started by crossing a lake and continued over the target area. The spectra obtained over the lake were used as blackbody spectra, as water in the 8-13 micron wavelength has an 0.98 emissivity.

During the flights, photographs as well as infrared spectral and thermal data were taken. The photographs were 23x23 cm black and white (B/W) RC8 photos, taken about every 4.23 seconds, and 35 mm boresight (B/S) photos taken by an electrically pulsed output from the spectrometer every 300 milliseconds. The precise time at which any B/S photo was taken was later obtained from computer-generated listings of the leading edge of these pulse times. Simultaneous with photography, spectral data in the wavelengths ranging from 6.76 to 13.33 microns were recorded with 0.07 micron increments, as a function of time, on an analog FM magnetic tape. A single spectrum starting at 13.33 microns and ending at 6.76 microns, corresponding to a rotation from 180° to 0° of the circular variable filter, was recorded in 150 milliseconds. The spectrometer used has a field of view of 0.4 degrees or seven milliradiants.

In order to define the geology along a flight line, the first step in the data processing was to determine the trace of the spectrometer field of view on the ground. Since both the spectrometer and the radiometer were boresighted with

the 35 mm camera to within five minutes of arc (92 cm at 600 meters), the photocenter of each B/S photo was assumed to be identical with the center of the field of view of the spectrometer. Easily identifiable features on the B/S photos were then matched with the same features on the corresponding RC8 photos, which are at the same scale, and the centers of the B/S photos were pricked through onto the B/W photos. The trace of the spectrometer was determined by connecting these marks on the B/W photos, as shown in Figure 1. Then, the contacts between different rock types were recorded as a function of time and keyed to known B/S shutter closure times by using either the computer-generated plots or tabulations, supplied by NASA on 35 mm microfilm.

Previous studies of individual spectra, as well as a group of spectra had shown that, in general, noise was present on the spectra (see Figure 1). The first step in noise reduction was the smoothing of the spectral emissivity curves. Among several smoothing procedures used, the 9-point, high-order smoothing program (Savitsky and Golay, 1964) was found superior to the others. This smoothing resulted in lowering the standard deviation at each wavelength without effecting the position of any characteristic emissivity peak. As a second step in noise reduction, the ratio of rock spectra to blackbody spectra was determined. To achieve this an average blackbody spectra was obtained from 10 or more spectra taken over a lake. Then, for each unknown rock spectrum the ratio of the emitted energy at a given wavelength to the emitted energy of the blackbody at the corresponding wavelength was determined. Theoretically, if the unknown rock spectra and the blackbody spectra are at the same temperature and comparable airpaths, the resultant curve would be the spectral emissivity. Furthermore, this ratio procedure also would eliminate the meteorologic information on the spectra, such as CO_2 or H_2O absorption bands. If a spectral departure from a horizontal line

appears at certain wavelengths, then identification of these characteristic wavelengths would define the target material or the rock type. The third and final step in noise reduction consisted of "normalizing" the spectral data by adjusting the mean to zero and the standard deviation to one. This step was found necessary to eliminate the effects of different rock surface temperatures on the spectra. Figure 2 shows what happens to average raw quartz monzonite training spectrum after these three steps.

Figure 3 shows the averages of the adjusted emissivity spectra from 10 Black Hawk andesite, 37 Brown Bear basalt and 49 Topaz Lake quartz monzonite porphyry. The average basalt and quartz monzonite porphyry spectra which were obtained a day after andesite spectra, are closely parallel in the 13.3-10.4 micron region, thus showing the similarity of their radiant temperature. Although the average andesite emissivity spectrum is parallel to the other two between 11.9 and 10.4 microns, it differs from them in the 13.3-11.9 micron region. Since there are CO_2 absorption bands in this wavelength interval, this deviation probably is due to different CO_2 content of the atmosphere in the two days that the spectra were obtained. In addition, all airborne spectra show a very sharp decrease in emissivity between 8.0 and 6.7 microns. This appears to be related to higher water vapor in the airpath over the rocks, even though all spectra are in reference to lake spectra which was assumed to represent a blackbody.

The emissivity spectra in the 8.0-10.4 micron range contains critical information for rock identification purposes. The spectra show two significant features in this range: (1) the expected emissivity differences for the three different rock types i.e., quartz monzonite porphyry has the lowest emissivity, andesite has the intermediate emissivity and basalt has the highest emissivity, and (2) the position of the characteristic emissivity peaks for different rock

types. Quartz monzonite porphyry shows an emissivity minima at 9.18 microns, andesite at 9.43 microns and basalt at 9.84 microns. Perhaps the most significant feature of these spectra is the departure in the position of the emissivity minima of various rock types which forms the basis for the identification of rocks from their infrared spectra.

The adjusted unknown emissivity spectra were analysed using BMD07M, Stepwise Discriminant Function Analysis program. Several groups of spectra, representing the known rock types, were established within the computer as "training" spectra. Each unknown spectrum was then compared with the known rock spectra and was identified as belonging to one of the training groups. Among the mission 78 data four flight lines were analysed following the procedure described above. An attempt has been made to evaluate the effect of the altitude and the complicated distribution pattern of rocks on the identification of rock types and the determination of their contacts.

The flight line for 15-01 was over the geologically simple Black Hawk target area at an absolute altitude of 600 meters. The flight starts over granitic rocks (Topaz Lake quartz monzonite porphyry), continues over andesite and a narrow band of snow, and terminates over the granitic rocks. The ground data and the computer rock identifications are shown on the bar-graph in Figure 4. The bar-graph shows that the rock types were identified and the contacts were determined with 83 percent accuracy. The area covered with snow was identified as granitic rock by the computer. This is because only two training spectra--one representing the granitic rocks and the other representing the andesite--were used to compare the unknown spectra.

Run 35-01 was flown at an absolute altitude of 700 meters over the Brown

and basalt flows as well as an outcrop of rhyolite covered with basalt debris (Figure 5). A comparison of the ground data with the computer rock identifications shows that all rocks were identified and the contacts were determined. In area A the rhyolite outcrop is covered with a thin layer of basalt debris. The rock in this zone however, was identified as basalt confirming the fact that emitted infrared energy gives information only about the surface layer material. In area B, granitic rocks are fractured and fractures are filled with basalt debris coming from adjacent basalt flows. In the computer evaluation of the spectral data, a zone consisting of granitic rocks and basalt was verified. Although this zone corresponds to the fractured granitic rock zone on the ground, the correspondence of individual spectra to ground data has not yet been proven because of the difficulties involved in the determination of very detailed geology of this zone from areal photographs. In area C, rhyolite crops out at the surface. Although this is not easily visible on the B/W photos, the presence of a granitic rock was concluded from the identification of four "granitic rock" spectra by the computer. A visual examination of Figure 5 shows that the rhyolite outcrop in this area has a very poor exposure relative to rhyolite outcrop in area A and yet it is identified as a granitic rock. The reason for this has not been understood and the problem requires further field checks. This run consisted of 123 unknown spectra, of which 111 were identified correctly, indicating that 90 percent of the rocks were identified accurately.

Run 16-01, which was flown 1000 meters above the Black Hawk mountain, is geologically complicated in the sense that the flight line crosses over interfingering granitic rocks and andesite as shown in Figure 6. Again, the rock types were identified and the contacts were determined from the spectral data.

Out of 48 spectra involved in the analysis of the data, 44 were identified correctly, corresponding to 92 percent of accuracy.

Run 14-01 was also flown over the Black Hawk mountain but at an absolute altitude of 2700 meters. The results shown in Figure 7 indicate that the spectral data gives information about the rock types along the flight line with an accuracy of 100 percent.

DISCUSSION OF RESULTS

It is appropriate to discuss the capabilities as well as the drawbacks of the technique, at this point, in order to evaluate its present status. The results indicate that certain types of igneous rocks in the Sonora Pass test site have been identified and the contacts between them have been determined with about 90 percent success. The airborne infrared emissivity study of a terrain, within the context discussed in this paper, appears to have three drawbacks: (1) high cost of data collection and data processing, (2) gathering information only along a given flight line, and (3) dependency of rock type identification on the training spectra taken from the area under study.

High cost of operation plus data analysis is the common drawback not only for this technique, but also for other airborne remote sensing techniques such as side looking radar and microwave. Furthermore, the cost should always be measured against the value of the information obtained, and there may be cases which warrant the use of these techniques. At present, however, the high cost of this particular technique severly limits its routine use for a variety of geological problems.

Although the identification of rock types only along a flight line somewhat

may result in rapid mapping of an area. This combination could be quite valuable particularly in volcanic areas where the identification of fine grained and/or glassy rocks on photographs is generally not possible. This should, however, be done only after documenting that various volcanic rock types in a given area, as well as in different areas, can be identified from their airborne emissivity spectra. In this regard, the results of this study provide encouraging data, but they are not conclusive.

Perhaps the most serious drawback of this technique is the method of identification of rock types. The stepwise discriminant function analysis program requires an average training spectrum for each and every rock type along the flight line. An alternative to this has been proposed by Lyon (1968): A "library" of spectra of known rock types is produced under simulated field conditions or obtained using a truck mounted spectrometer system. Spectra of unknown rocks are then compared statistically with the "library" spectra. In practice, this can be done if one assumes that a representative spectra for each rock type exists. Few emissivity data (Lyon, 1964) show considerable variation in the position of the emissivity minima for a given rock type. For example, among the basalt spectra listed, the major emissivity minima varies from 9.4 microns to 10.4 microns.* This presumably reflects the physical and/or chemical variations in basalts studied by Lyon. In other words, there is not a representative spectra for all basalts, another one for andesites etc., but each rock type may have several spectra showing an emissivity minima at a different wavelength. Thus, a "library" which can be used in any area seems to be impractical.

* A detailed study of the variation of major emissivity peaks as a function of wavelength is under study.

The BMD07M Stepwise Discriminant Function Analysis Program classifies the rocks by first comparing the training spectra of various rock types and then selecting a set of wavelengths at which these spectra can be differentiated and identified best. These wavelengths, however, do not necessarily correspond to the wavelength of the average major emissivity minima of the rock types under study. Since, theoretically the rocks should be identified according to characteristic wavelength at which major emissivity minima occur--this method of identification requires major modification of computer programs.

The variation in the position of the emissivity minima for a given rock type can possibly be used to search for a rock without identifying it. For example, if airborne emissivity spectra of a mineralized outcrop can be established within the memory of a computer aboard the aircraft, the computer can be programmed to give a signal when similar spectra are recorded during a flight in the adjacent areas. This, however, is only a speculation and its realization depends on experiments in the laboratory as well as in the field.

References

Lyon, R. J. P., 1964, Evaluation of Infrared Spectrophotometry for Compositional Analysis of Lunar and Planetary Soils, Part II: Stanford Research Institute Report, NASA CR-100.

Lyon, R. J. P., 1968, Field Analysis of Terrain: Final Report to NASA (November 1967-October 31, 1968).

Savitsky, A. and M. J. E. Golay, 1964, Smoothing and Differentiation of Data by Simplified Least Squares Procedures: Analytical Chemistry, v. 36, No. 8 pp. 1627-1639.

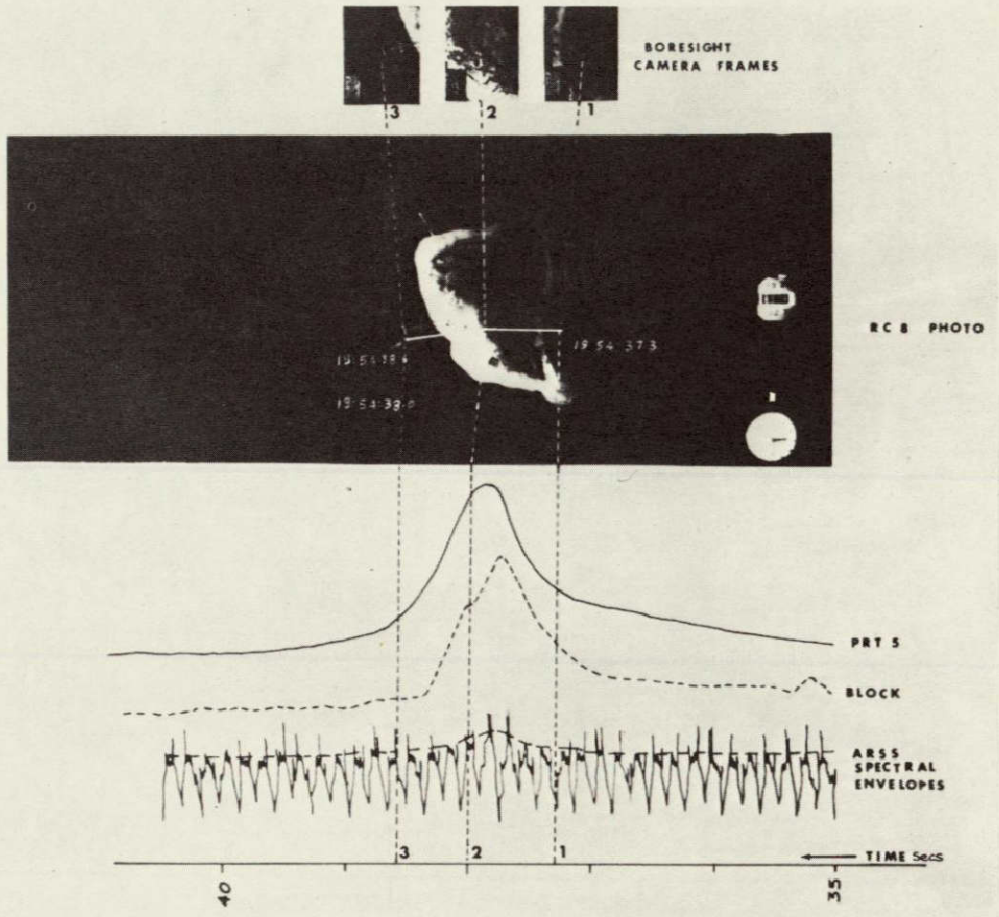

Figure 26-1.- Determination of the trace of the spectrometer field of view on the ground. Boresight camera shutter times for the three boresight photos are shown. The response of the Block and PRT-5 radiometers to temperature changes also are shown together with the raw infrared spectra taken in this run over Padre Island, Texas. Note the noise spikes on the spectra.

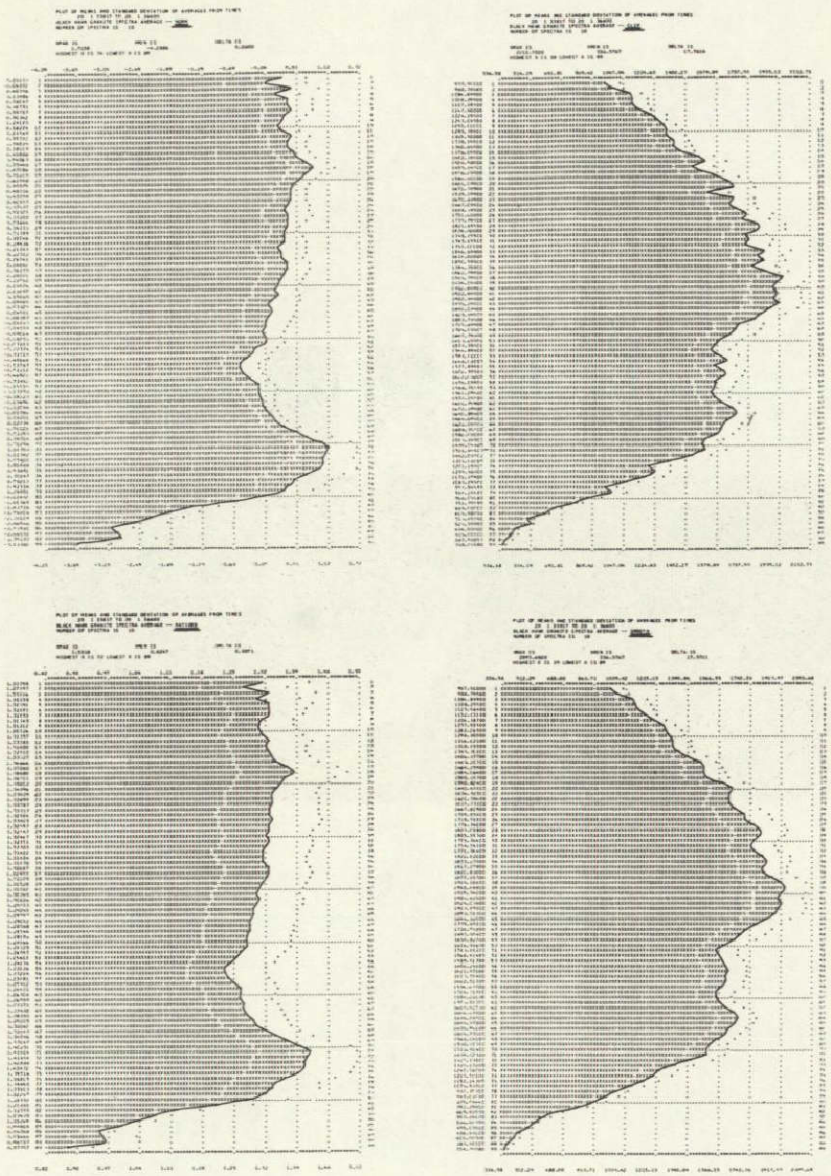

Figure 26-2.- Step by step data processing. The upper left hand diagram is the average of 10 quartz monzonite spectrum. The upper right hand diagram shows the same spectrum after smoothing. The lower right hand spectrum is the same smoothed spectrum after its ratio to an average black body spectrum is obtained. The lower right hand spectrum is again the same spectrum after it is "normalized".

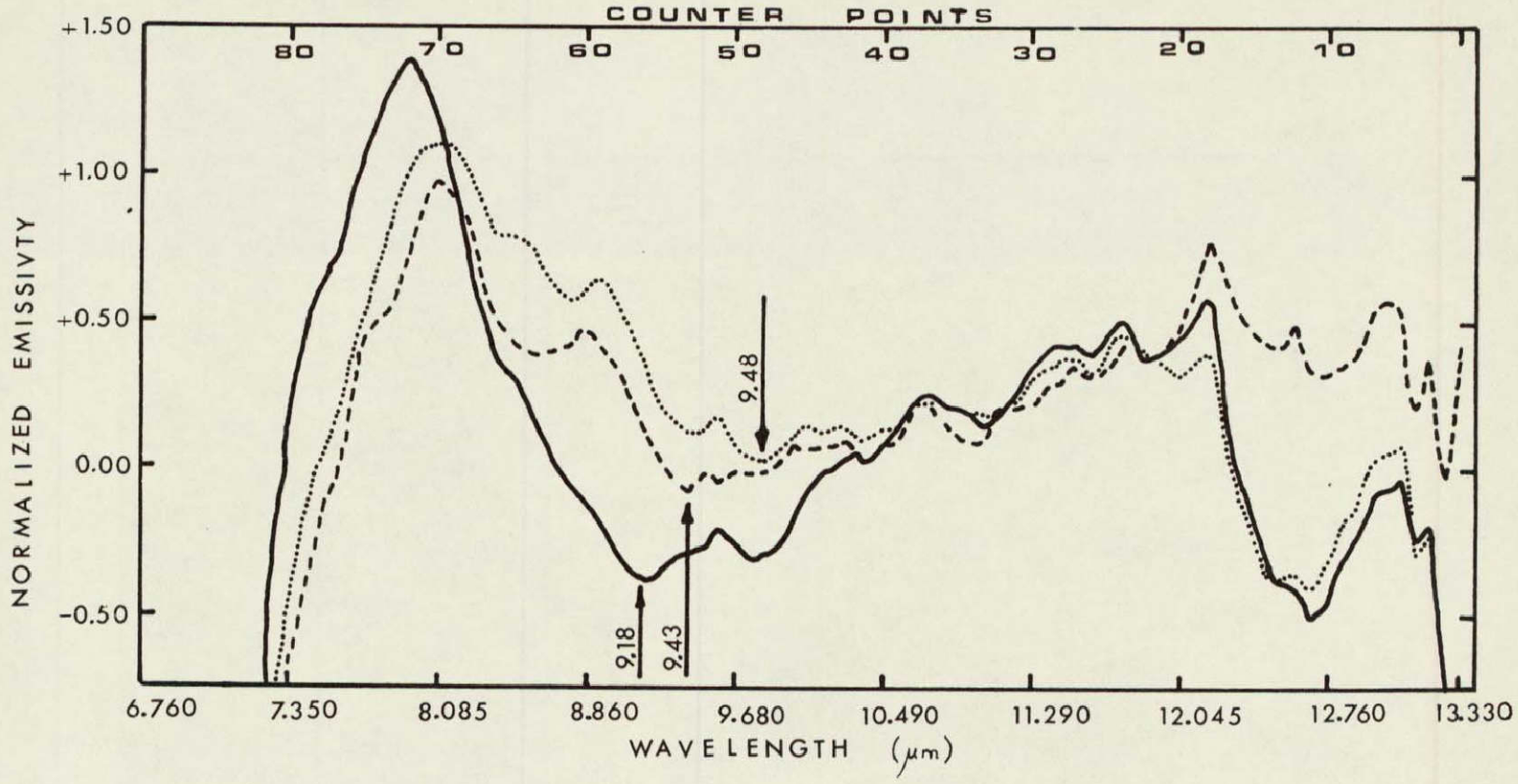

Figure 26-3.- The averages of quartz monzonite, andesite and basalt emissivity spectra in the 6.67-13.33 micron range. The vertical axis represents the "normalized emissivity" and the horizontal axis represents the wavelength. The characteristic emissivity minima for each rock type are shown. Solid curve represents the quartz monzonite, dashed curve represents the andesite and the dotted curve represents the basalt.

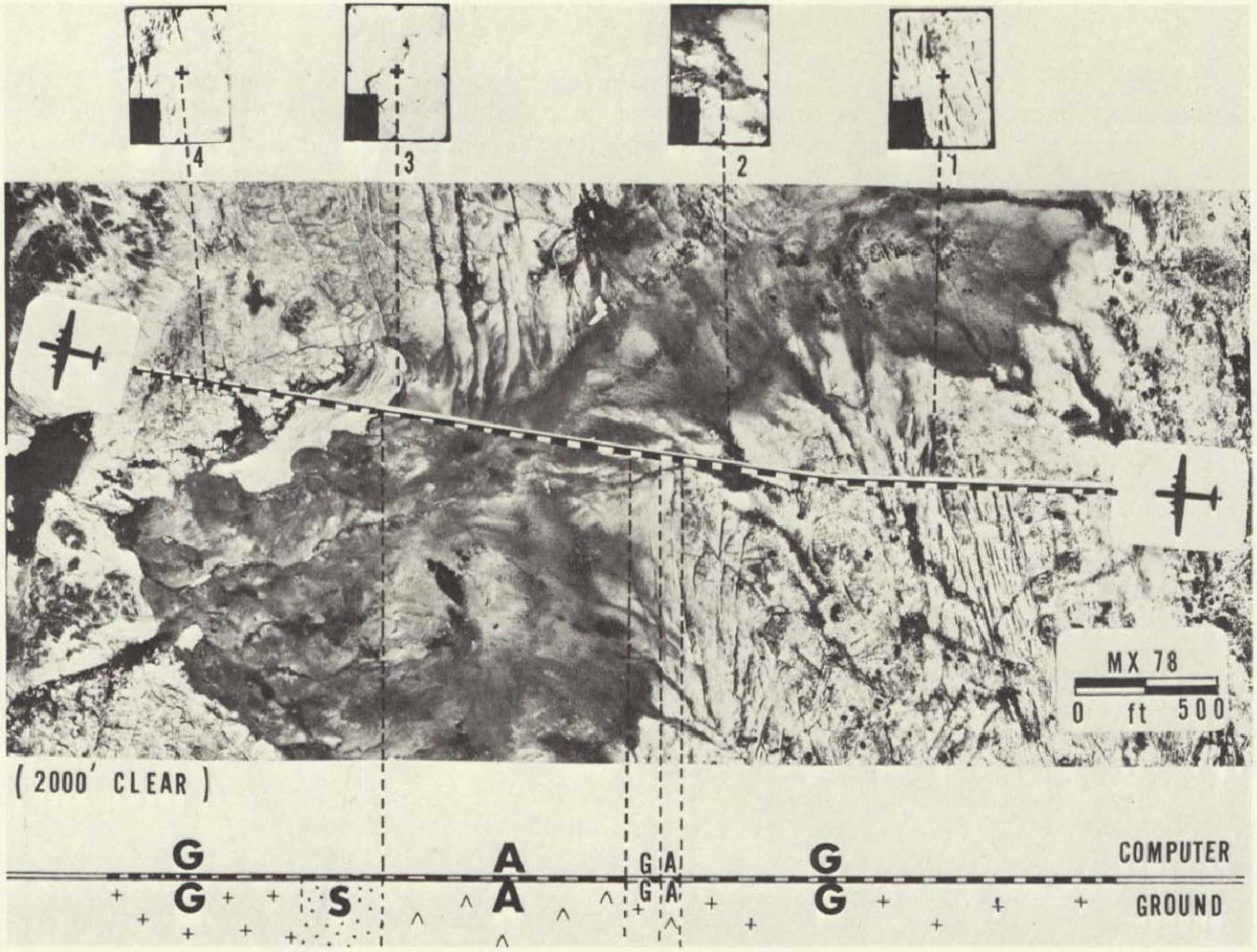

Figure 26-4.- Run 15-01. The trace of the spectrometer field of view is plotted on the photograph. The bar-graph shows the ground data and computer rock identifications.

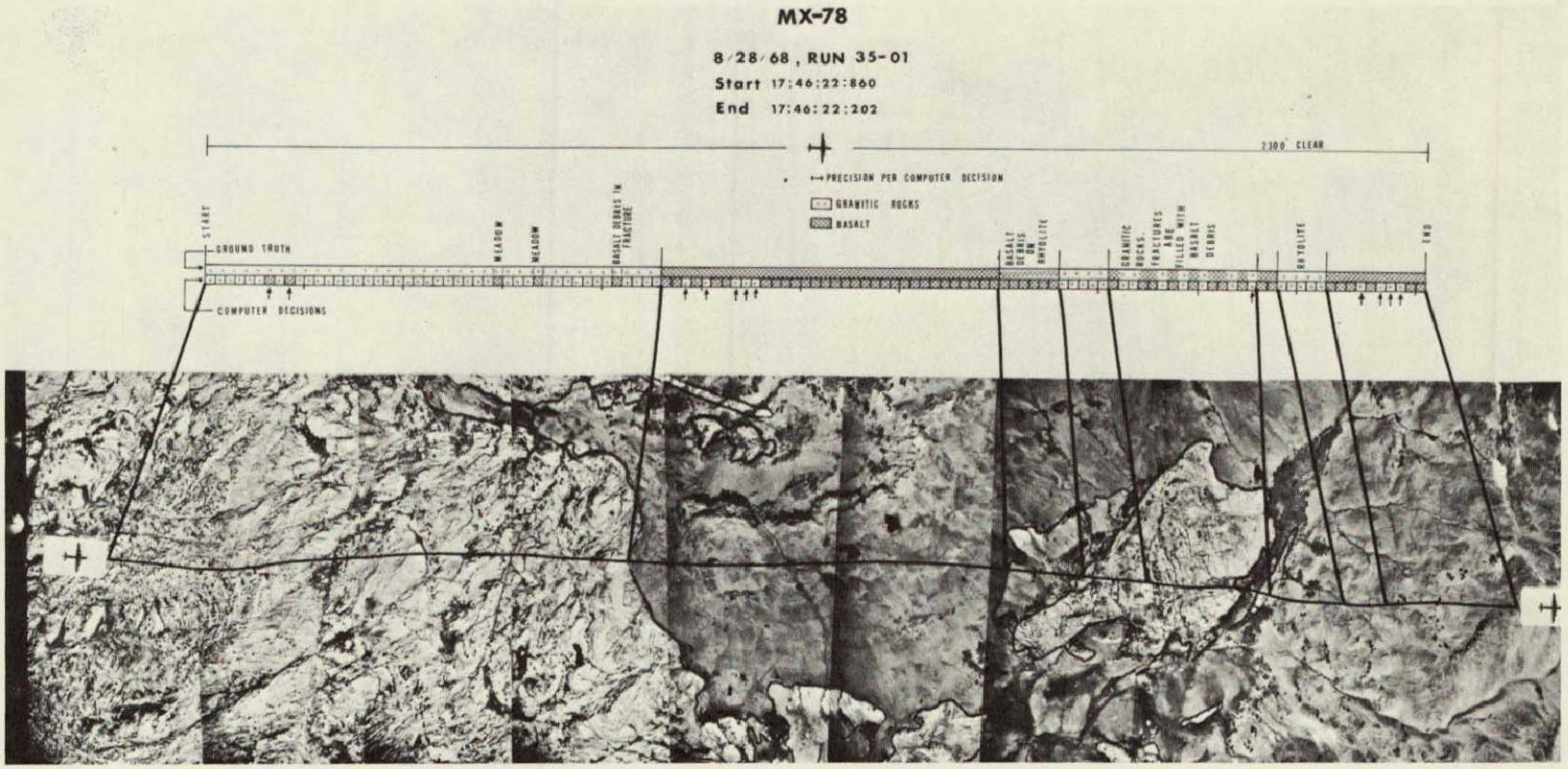

Figure 26-5.- Run 35-01 over Brown Bear target area. The solid line on the photograph represents the trace of the spectrometer field of view. Bar-graph shows the ground data and corresponding rock identifications.

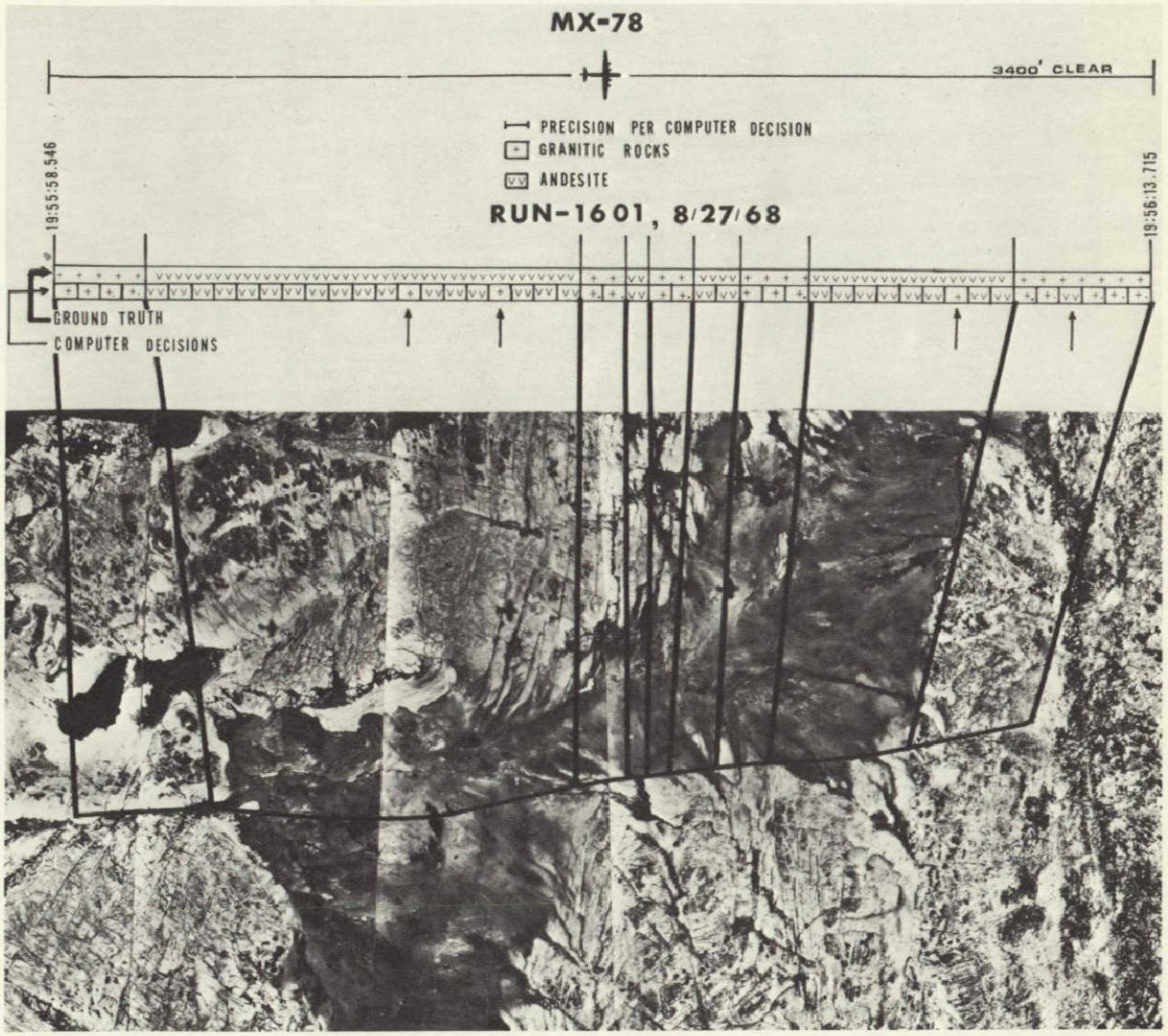

Figure 26-6.- Run 16-01 over Black Hawk target area. The trace of the spectrometer field of view and the contacts along this line are shown. Bar-graph shows the ground data and computer rock identifications.

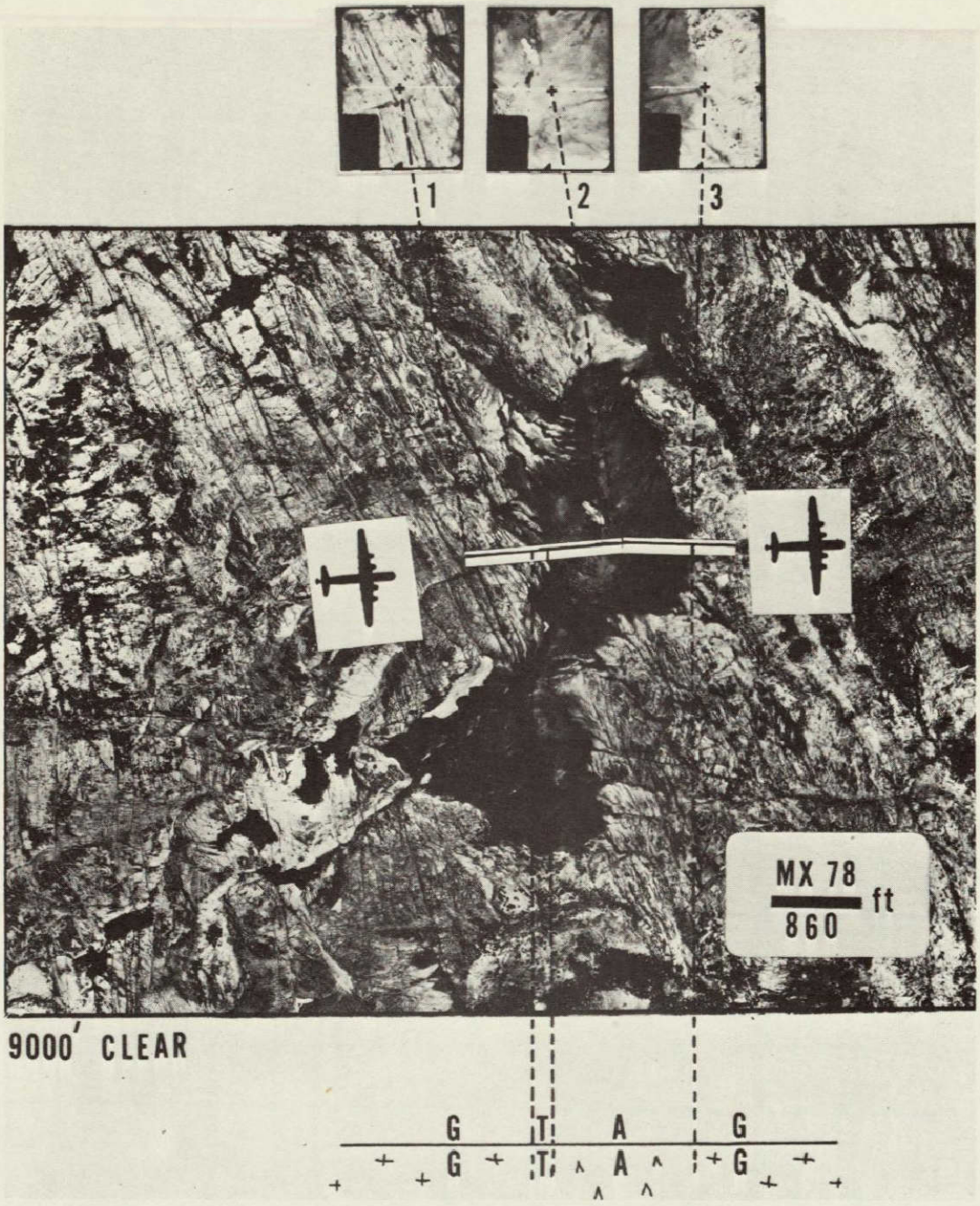

Figure 26-7.- Run 14-01 over Black Hawk target area. The contact along the ground trace of the spectrometer field of view are shown. The ground data and corresponding computer rock identifications are shown on the bar-graph.

SECTION 27
SEPTEMBER 1969 ANNUAL REPORT OF NASA SUPPORTED REMOTE SENSING ACTIVITIES AT THE UNIVERSITY OF MICHIGAN WILLOW RUN LABORATORIES

(Data Processing, Interpretation and Utilization Section)

By M. R. Holter

1. INTRODUCTION

Since 1946 there have been, at the University of Michigan, an average of 500 people engaged in all aspects of reconnaissance and remote sensing research and development. The total level of support is approximately $10 000 000.00 per year. Support is provided by many elements of the Department of Defense, the U.S. Department of Agriculture, the U.S. Department of the Interior, the U.S. Coast Guard, many commercial organizations, NASA and others. Last year the total NASA and NASA derived support was $500 000.00 or approximately 5% of the total. The NASA work is carried out in an environment containing a large amount of very closely related work supported by other sponsors and there is quite significant mutual sharing of results, equipment and personnel between the NASA supported programs and the programs supported by other sponsors. The technical scope of the work in the WRL includes techniques in the ultraviolet, visible, infrared, passive microwave, and radar parts of the spectrum as well as acoustic and seismic techniques. Work on the development and employment of components, sensors, data processing, interpretation, data utilization and systems studies including economic benefit analyses is currently in progress.

In 1960, under U.S. Army sponsorship, scientists at the University of Michigan originated the concept of coupling spectrometers to optical-mechanical scanners and joining these with digital and analog computers employing modern pattern recognition methods to produce semi-automatic sensing-interpretation systems. In 1964, when NASA became active in remote sensing, The University of Michigan began actively to transfer the concept and technology to NASA programs and to help many NASA supported individuals and organizations get started in research and development on these techniques.

This is a report of part of the University of Michigan work on data processing, interpretation, and utilization. Professor Donald S. Lowe, in an earlier paper in this document, has described the University of Michigan activities on instrument design and sensor data generating operations during the past year. Mr. Fabian Polcyn of the University of Michigan has previously reported on work done on oceanographic applications. The central focus of the University of Michigan work for NASA is on the data processing, interpretation and utilization rather than on instrument design. This is a report on only part of the data

processing, interpretation and utilization at the University of Michigan because some work has been carried out jointly with other organizations and the results of the University of Michigan contributions have already been included in the reports of other investigators and will not be repeated here. Table 1 illustrates the degree of involvement of the University of Michigan with other NASA supported investigators.

The work reported here was, for the most part, carried out under a contract from the U.S. Department of Agriculture with funds derived from NASA. However, the results are generally applicable to user disciplines other than agriculture. This is a progress report rather than a technical report. Furthermore, space does not permit commenting on all of the activities of the last year. Therefore, only a selected and representative subset of the total activities will be mentioned and the comments will be programmatic and indicative of progress rather than being complete technical descriptions of the type which would be appropriate in a technical report. Discussion of all the activities in full technical detail are contained in the formal, complete project annual report* which is obtainable from the U.S. Department of agriculture.

The annual report of the previous year, September 1968, by the University of Michigan contained results demonstrating that automatic spectral pattern recognition had been achieved in a number of instances for certain specific conditions, i.e., for a given sun angle, time of day, stage of crop growth, viewing angle, etc., etc. At the end of that September 1968 report, it was stated that the University of Michigan considered that the fact of achieving recognition under specific and limited conditions was established and that the work of 1969 should shift significantly in emphasis. The work of 1969, it was stated, would be concerned with investigating the many sources of signature variability which must be compensated for in order to extend the recognition capability to geographically distant locations, to accomplish recognition at widely different times, to accomplish recognition at several different stages of crop growth and health, etc. Attacking those problems is not so productive of dramatic pictorial results, but is vitally necessary if the recognition techniques are to be operationally useful in any practical sense.

---

*"Investigation of Multispectral Discrimination Techniques", R. F. Nalepka, The University of Michigan, Willow Run Laboratories, Report No. 2264-12-F, January 1970.

The sources of signature variability are sufficiently numerous that by no means could they all be studied during 1969. A number of those known to present difficulties were selected for investigation. While the results of the work are thus incomplete, it is fair to state that the sources of variability studied so far have yielded, at least partially, to practical methods of solution or compensation. Therefore, the prospects for developing generally useful recognition methods which are practical continue to appear good.

II. SPECTRAL RECOGNITION PROCESSING

One approach in investigating the effects of certain factors on the ability to automatically recognize objects of interest is simply to perform recognition processing of multispectral data gathered in the presence of those factors. Where the recognition results are not satisfactory, additional studies are necessary to define and test processing techniques which may improve recognition capability. The results of using this approach on two sets of data are discussed here along with a description of another set of data on which investigations of this sort should be completed.

Studies of Altitude and Time of Year Effects

Studies of the capability of recognizing wheat at two different times of the year at the same altitude and at two different altitudes for one time of year were made for wheat in the area near Lafayette, Indiana. Figure 1 shows the degree of recognition at two times of year and Figure 2 shows recognition at one time for two altitudes (the areas recognized are depicted as white). These pictorial presentations are shown for illustrative purposes only. The more meaningful results are contained in Table 2 which gives informations on the degree of correct recognition. The percent correct recognition figures in the table are probably lower than is in fact the case because of the method of computation. The figures represent the fractions of the fields known to have been planted with wheat which were recognized as wheat. Some of the parts of the fields planted with wheat but not recognized may have been areas that did not grow well and legitimately should not be recognized as wheat. This was not taken account of; it was assumed that all planted wheat grew well. Therefore, the percentage correct recognition figures are certainly minimums.

Reducing the Effects of Cloud Shadows by Preprocessing Techniques

At certain stages of growth soybeans and corn are one of the most difficult pairs of crops to differentiate by spectral pattern recognition.

When some fields can be partially or totally shadowed by clouds the problem is compounded. A study was conducted to determine whether corrective measures, in the form of processing steps carried out prior to the primary recognition processing could transform the data so that a single learning set taken from either the sunlit or shaded area could be employed to adequately recognize both areas. A discussion of the results of this study is given below.

Figure 3 shows unprocessed video data from one spectral channel taken over an agricultural area near Lafayette, Indiana. Here we see that fields of corn and soybeans were partially shadowed by clouds. Figures 4 and 5 illustrate the results of digital and analog recognition processing, respectively, to identify soybeans using a signature based on a training area containing only shaded samples. In neither the analog nor the digital case is the degree of correct classification very complete. The digital processing results shown here were carried out only for a portion of soybean field 32-5. Figures 6 and 7 are another pair showing digital and analog recognition respectively, but using two training areas, one having only sunlit plants and the other only shaded plants. The performance is obviously improved. Figure 8 depicts the results of digital recognition using the same training areas as above but with the addition of a preprocessing step. The preprocessing consisted essentially of deriving the ratios of the signals among pairs of bands and employing these ratios in the primary recognition processing. One can argue that the ratios are less sensitive to differences between sunlit and shaded conditions thereby providing signatures that are more characteristic of the objects being viewed and not the illumination conditions. Figures 9 and 10 show digital and analog processed results respectively using a single signature derived from shaded samples with the recognition preceded by ratio type preprocessing. The results shown here exhibit very little degradation in performance over the best recognition results which required training samples in both the sunlit and shaded areas. It is seen, therefore, that more universally useful signatures may be extracted by using the appropriate preprocessing transformation. A more detailed discussion and additional data for differing number of channels and for various decision thresholds are presented in the project technical report referred to above.

Both digital and analog recognition processing results were presented above. The question of whether digital or analog methods are better for such discrimination processing continues to be brought up by many in the remote sensing community. In that form, it is not a very meaningful question. As the above results indicate, it is possible to implement any decision process by either digital or analog means. Therefore, the type of processing methodology desired will, in itself, not dictate either analog or digital means. The decision should be based on other practical considerations such as speed and flexibility.

Analog processing has as one of its virtues the ability to easily parallel process the multichannel data resulting in very high speed. It can process at the same rate as sensors can generate data, i.e., in real time. It has, as its major drawback, the fact that analog machines are laborious to set up for any specific processing methodology. Digital techniques have as their major advantage the fact that programs can be changed very readily, i.e., set up is convenient and not time consuming. Digital means usually entail processing at a factor of approximately 30 slower rate than the sensors generate data, i.e., definitely not real time. Therefore, it appears optimum to employ analog techniques for large batch or production recognition runs not involving frequent changes in programs and to employ digital techniques for extraction of signatures from limited quantities of data and for small batch experimental work; i.e., ditigal computers should construct the programs which will be used for large batch recognition employing analog techniques. Conversation with many scientists in the so called user disciplines reveals a very common misconception. It appears to be assumed by them that all of the existing pictorial examples of digital recognition are the result of applying the recognition process to every resolution element. In most instances, that is not the case. The speed of A-D conversion and digital processing is sufficiently slow that a large fraction of the existing digital recognition pictures were obtained by working with, typically, only one out of five resolution elements along a scan line and with only one out of each fifteen scan lines. The results of such severe sampling are not well understood. Certainly the effective resolution of the recognition picture can no longer even closely approximate the quoted sensor resolution.

Imperial Valley, SO-65 Studies

During the past year, the University of Michigan participated in the SO-65 experiment in two major ways. First, Mrs. Norma Thomson and others at the University of Michigan coordinated the gathering of ground truth for the Imperial Valley, California site with the very extensive help of personnel from the U.S. Department of Agriculture. A ground truth report has been produced and distributed so no further discussion will be given here.

Second, as a U.S. Department of Agriculture Principal Investigator, the University of Michigan has begun a study of the data and recognition processing of the crops present. This work is not yet completed so few details can be presented at this time.

One feature of the Imperial Valley, SO-65 data does, however, merit comment and serious consideration. By a fortunate and fortuitous set of circumstances the SO-65 data over the Imperial Valley is, for certain

purpose, the best set of data which has been yet generated and is likely to be generated for sometime in the future. At the time of the mission the area was cloud free. Good ground truth is available. All the sensors in the University of Michigan aircraft, in several NASA aircraft at a number of altitudes and the spacecraft sensors functioned acceptably at the same time over the same area which is a somewhat unlikely event. Futhermore, the area is unusually rich in subject materials. The field sizes are large, there is an unusual diversity of crop types, many crop types are present simultaneously at different stages of growth and extensive repeat coverage subsequent to the spacecraft mission has been carried out. Therefore, the Imperial Valley data furnishes a suitable and unique data base for signature and modeling studies over many altitude regimes up to and including spacecraft altitudes and an unusually rich source of data for discrimination studies. In view of this, the resources which appear to have been allocated to study and interpretation of that data appear too small.

III. ANALYSIS

In order to develop practical methods of processing, pattern recognition and interpretation greatly increased understanding of the optical properties of the materials of interest and the atmosphere must be attained, the nature of the illumination must be better understood, calibration methods must be developed, etc. All of these must culimate in models which agree with experimental results before it is possible to be confident that the processes and data are understood. Therefore, during the past year the focus of the University of Michigan effort has been changed from merely producing individual (and possible unique) recognition results to activities aimed at gaining and understanding of the phenomena. This is necessary in order to learn how to extend the recognition methods in space and time. A few of these activities are reported on here and more completely discussed in the project report mentioned above.

Calibration

In order to meaningfully intercompare the signals from a number of different wavelength channels, it is necessary that the channels be calibrated. Otherwise unknow variations among the channel gains will produce apparent and unknown shifts in the electrical signals generated and in turn in the spectral signatures calculated for each material. Therefore internal instrument calibration is necessary to assure a knowledge of channel gains. Continuing efforts are being expended to improve and develop better methods of performing this type of calibration.

The internal instrument calibration, while necessary, is not sufficient. It will not reveal effects due to the changing character in the radiation illuminating the scene, shifts in atomspheric transmission nor elucidate spectral shifts due to changing illumination and viewing angles. Measured, standard reflectance panels located on the ground will provide information on these latter sources of variability. It has become common practice for the University of Michigan operating crew to employ, where possible such panels on the ground.

Studies were initiated to measure and model the behavior of the standard panels. The facilities of the University of Michigan — Air Force Target Signature Measurement Program were made available for this purpose.* Figures 11 and 12 show a precision gonioreflectometer system and field spectrometer which are representative of equipment from the facility used in the NASA study. Using the gonioreflectometer, measurements were made of the effects of varying illumination and viewing angles for the standard panels. Figure 13 shows the results for a single source location with varying viewing angles and combinations of source and receiver polarization as parameters. The angle off the normal of the viewing instrument is plotted on the horizontal axis. On the vertical axis is plotted the measured bidirectional reflectance divided by the cosine of the viewing angle. If the material were Lambertian and insensitive to polarization, the plots would have been straigth lines. Obviously the panels are not Lambertian. Figure 14 is a composite of plots similar of Figure 13 for a variety of illumination angles. For latitudes characteristic of the U.S. and for normal viewing, i.e., panels directly under the aircraft, the curves are reasonably flat so the Lambertian assumption which is made in using the panels to calibrate the data, is not too unreasonable for those conditions based on the limited amount of data presently available.

Under operational conditions it may be inconvenient or impossible to place standard reflectance panels on the ground at all desired locations. It is necessary, therefore, to determine whether other materials or instrumented outputs may serve as calibration standards in these cases. Materials occurring frequently on the ground and having sufficiently stable and uniform characteristics may serve in the role of secondary calibration standards, i.e., standards of opportunity. We have found that certain asphalt coated roofs and roads and concrete roads exhibit reasonably uniform and stable optical characteristics and could be used as secondary calibration standards. In the absence of such secondary standards, a device mounted in the aircraft which collects radiation from the entire upper hemisphere and directs it into the scanner, may be useful for calibration purposes. This device is called the "sun sensor".

---

*The AF supports, at the rate of approximately $500 000 per year a signatures program at the University of Michigan with extensive facilities.

Described below are some results of using the sun sensor and the secondary standards for calibration. Figures 15 and 16 show spectra of asphalt and concrete derived from scanner data on a number of dates. The data from June 27, August 23, and November 8, all in 1967, show spectra obtained using the sun sensor. The dashed curve is based on data from a March 3, 1967 flight where the primary standards, i.e., standard reflectance panels were used for calibration. In Figure 17 we see a comparison of calculated reflectance spectra for grass using both the sun sensor and the secondary standards.

These studies are preliminary in character but do indicate reasonable expectation that the sun sensor and the secondary standards of opportunity may be a practical means of providing information which can be employed to correct for some of the sources of signature variability.

Atmospheric Backscatter

Another source of signatures variability is often called atmospheric backscatter. The radiation entering the aperture of a remote sensor has three components; a) radiation from surface subjects within the geometrical field of view of the sensor, b) radiation scattered back towards the source and sensor by the atmosphere and aerosols, and c) radiation from ground objects not within the geometrical field of view of the sensor but scattered into the sensor collecting aperture by the atmosphere and aerosols. The effect of the two scattered components is to partially mask the spectral signatures of the ground objects in the sensor geometrical field of view. The magnitudes of these effects must be understood to adequately understand sensor performance and to optimize pattern recognition methods.

Simple theoretical calculations were carried out to determine the amount of backscattered radiation that might be expected under clear atmospheric conditions at several altitudes. For the purpose of the calculations, a solar zenith angle of 45 degrees was assumed and a continental atmosphere model was used. The results are shown in Figure 18.

The overall effect of the presence of scattered radiation is a reduction in apparent contrast between objects on the surface. A preliminary investigation of these effects was made by calculating a "Contrast Reduction Factor" (CRF) using the previously calculated backscattered radiance and assuming a background of 20 percent reflectance. The results are shown in Figure 18. Here we see that the effect on small targets, i.e., those just filling the instantateous geometrical field of view, is more serious than the effect on large targets. This is a result of more radiation being scattered into the sensor collecting aperture from objects outside the field of view than is scattered out of the aperture for those objects within the geometrical field of view.

Radiance Modeling

One of the objectives of the studies of calibration, atmospheric scattering, etc., in conjunction with understanding of target signature properties is a model of the radiance at the sensor aperture due to objects of interest under the normal range of practical operating conditions. Until such models have been formulated which agree with experimental results, there can be no great confidence that the data can be understood and interpreted and that proper or optimum choices during mission planning can be made! During the last year, personnel at the University of Michigan have begun constructing such radiance models and comparing them with experimental results. In addition to the results of studies of the types described above, data on the optical properties of materials of interest from the Air Force Target Signature Data Bank have been used in this modeling. The Air Force data bank contains thousands of such spectral curves and still is very incomplete. Figures 20 and 21 are illustrative of some of the types of information that can be extracted from the data bank by computer manipulation. All of the data in the bank is digitized and various computer programs are available for conducting analyses. It will be necessary for NASA, as part of its remote sensing programs, to institute complementary signature programs if the Earth Resources Program is to have available the needed information. The University of Michigan has proposed to initiate an effort of this sort during the coming year.

As an initial exploratory study of radiance modeling, the expected radiances for wheat in the multispectral scanner bands was calculated using a theoretical model and signature data from the Air Force data bank. The results of these calculations were then compared with some actual flight results from a flight on 25 July 1968 in the vicinity of Willow Run. These results are shown in Figure 22. As can be seen the degree of agreement between experiment and modeling results is quite good.

Choice of Spectral Bands

The question of the number and location of spectral bands required for various survey tasks continues to arise in the earth resources community so a few comments are in order here. The University of Michigan has been and still is involved in the study of this problem. Detection probabilities for varying numbers of bands and the optimal combination of band for the solution of particular problems have been calculated. If, however, we desire a general purpose sensor, i.e., one capable of detecting all possible surface materials, the following argument applies. As the number of objects of interest and number of background objects increases, the sensor must employ more and more spectral bands in order to effect discrimination. Therefore, the answer, in principal, to the number of bands in question is "as many as possible

for a general purpose instrument." This can be illustrated by a very simple example. Suppose a sensor having only two bands and capable of sensing only two levels in each band. Then the instrument will be capable of distinguishing only $2^2 = 4$ different conditions in the incoming radiation. If such an instrument is used to survey a world in which there are only five different surface materials only four of them can be discriminated unambiguously. The fifth will be indicated as one of the first four because the instrument has only four different distinguishable states.

Of course, if not all possible spectra actually occur in nature then some number of bands less than the maximum will suffice. Thus the proper method of resolving the question is revealed. It is a frequency of occurrence of spectra in nature question. This question cannot be resolved by a limited number of trial and error experiments but requires an understanding of the frequency of occurrence of spectra by type. As has happened in connection with other types of remote sensing questions, the central importance of a target and background signature activity is revealed.

In addition, this question cannot be best approached based on data from existing scanner spactral data because the existing scanner spectral bands are fairly broad and overlap in pairs.

There is evidence to show that for certain cases the thermal channels would significantly improve classification probabilities. These channels are not at present, completely synchronized with the visible and near infrared channels. Therefore, to employ these additional channels, it is necessary to bring them into synchronization or registry with the other channels. There are, conceptually, a number of different ways in which this might be attempted. Many of these methods depend upon correlating field boundaries as they appear in the channels. This may, on occasion help, but there is at least a partial logical contradiction in using such a technique. If the field boundaries are distinct enough to permit good spatial correlation then there must be sufficient contrast between the two fields so that there is some question whether the more powerful discrimination means may be necessary to identify the fields. Therefore, in the final analysis, it seems preferable to solve the registration by synchronizing the channels in the sensor rather than relying on post facto registration techniques of somewhat dubious character.

Another general question which continues to recur is that of whether spectral or spatial discrimination is better or best. The correct view is as follows: Neither spectral or spatial discrimination is likely to suffice alone. Spatial recognition requires some non-zero contrast among the various objects and improves with increasing contrast. Spectral methods can be used to enhance contrast. Therefore, it is apparent that

in some optimum sense spectral contrast enhancement followed by spatial recognition will provide maximum capability, i.e., spectral and spatial methods are complementary rather than competetive.

IV. CONCLUSIONS

This report has presented illustrative examples of the types of investigative tasks began during the past year. A significant change in direction has taken place in the University of Michigan work. The effort devoted to the production of additional individual recognition results has been very much reduced. The center of gravity of the activities has been shifted from the production of examples of pattern recognition to studies of calibration and the many sources of signature variability. This variability must be understood and compensated for if spectral pattern recognition is going to be placed on a practical footing. More complete descriptions of the work on these tasks is presented in the report referenced above. The problems attacked to date have all yielded, at least partially, to solution and this provides the motivation and encouragement to continue, i.e., there are reasons for being optimistic that it will be possible to develop practical operational methods.

Work on this class of problem reveals an important deficiency in the present manner of generating remote sensing data. In order to pursure studies of extending the partially automated interpretation of remote sensing data over time and space, it is essential to have synchronized multispectral data gathered repetitively over the same ground site so that there is sampling at frequent intervals during diurnal and seasonal cycles with more adequate ground truth and calibration. There is a very serious need for such data over at least one test site in the remote sensing program. Furthermore, with the ERTS satellite launch only two years away, it is important to have such intensive aircraft sensor coverage over at least one ground site which will be viewed by the ERTS sensors. Unless such experience over such a site with aircraft sensors for one or two years prior to ERTS operation is available judgements of the utility of the ERTS data may be seriously compromised.

TABLE 1

U of M EARTH RESOURCES DATA PROCESSING REPORT

9/1/68-8/31/69

PERIOD	SPONSOR	FUNDING
9/68-8/68	USN Oceanographic Office	48.4K
9/68-12/68	USGS – Hemphill	0.2K
9/68-8/69	NASA Houston	15.6K
10/68-8/69	USDA	85.0K
11/68-1/69	USDA	4.0K
11/68-8/69	USGS – Kilipinski	27.4K
12/68-1/69	USGS – SMEDES	1.5K
5/69-8/69	USGS – Anderson	5.5K
6/69-8/69	USGS – Johnston	7.8K
	TOTAL SUPPORT	195.4K

TABLE 2

WHEAT RECOGNITION PERFORMANCE OF THE ABSOLUTE VALUE PROCESSOR ON THREE DIFFERENT DATA SETS

(a) 5/6/66, 3500 feet, 1330 hours

Field	Acres	Acres recognition	Percent recognition
W1	10	13.7	80
W2	16	9.0	62
W3	26	23.1	89
W4	25	2.2	9
W17	80		95
W11	34		94
W12	58		92
W13	15		0

(b) 6/30/66, 3500 feet, 1400 hours

Field	Acres	Acres recognition	Percent recognition
W1	16	13.6	85
W2	16	14.1	88
W3	32	17.0	53
W4	25	20.5	81
W11	62	80.0	96
W12	58	52.2	90
W17	80	74.4	93
W13	15		0

(c) 6/30/66, 10 000 feet 1400 hours

Field	Acres	Acres recognition	Percent recognition
W1	16	13.6	85
W2	16	14.9	93
W3	35	28.4	81
W4	25	20.8	83
W5	15	10.5	70
W6	11	10.0	91
W7	13	13.0	100
W8	17	2.4	14
W9	33	1.0	3
W10	15		0
W11	62	56.4	91
W12	56		97

TABLE 2 — Concluded

Field	Acres	Acres recognition	Percent recognition
W13	15	10.5	70
W14	13	11.4	88
W15	15	1.5	10
W16	16	12.0	75
W17	80	77.6	97
W18	14		0
W19	11	0	0

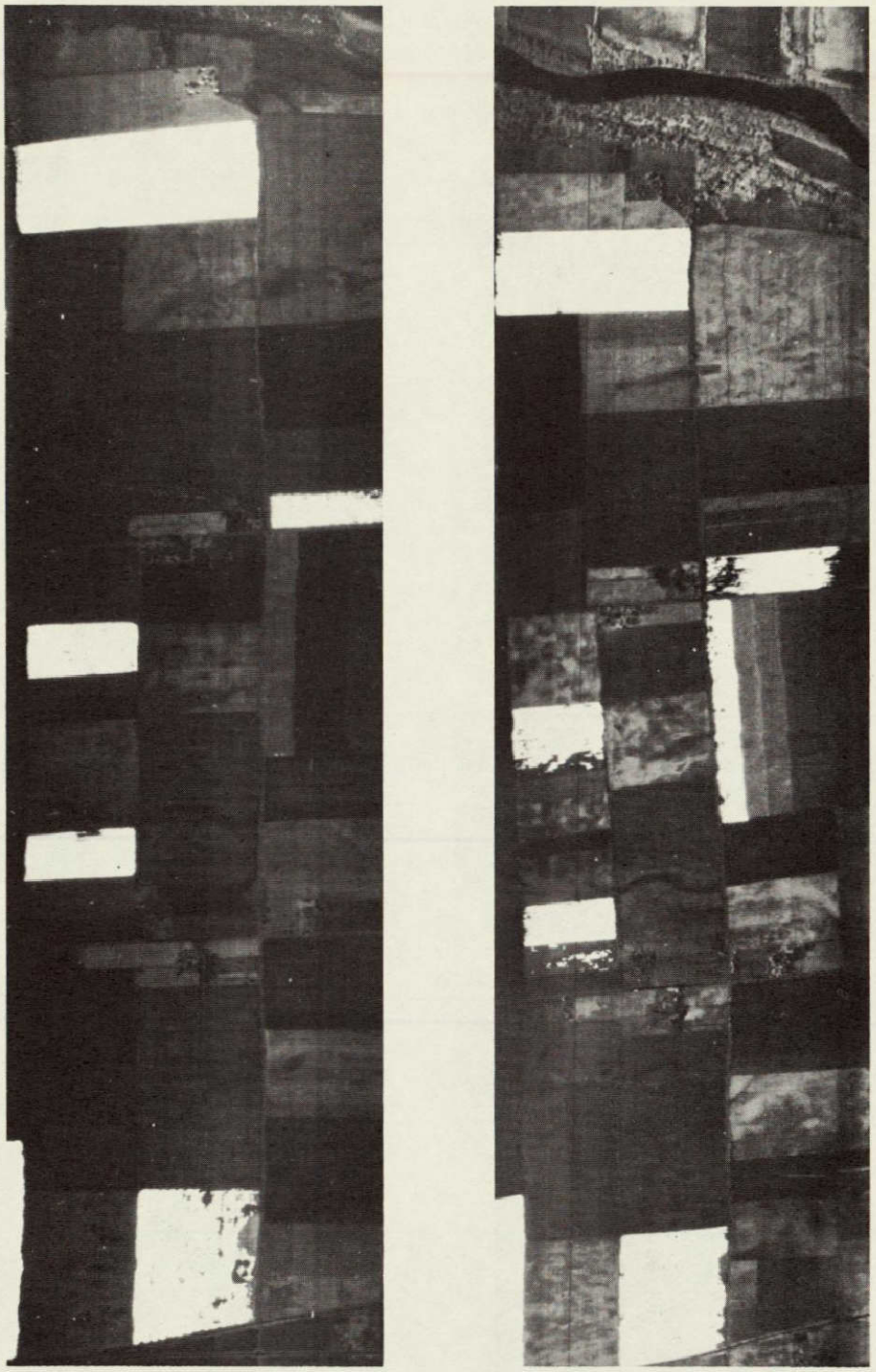

a. 5/6/66 at 1330 hrs.

b. 6/30/66 at 1400 hrs.

Figure 1.- Recognition of wheat near Lafayette, Indiana at two different times of year. Altitude – 3500 feet.

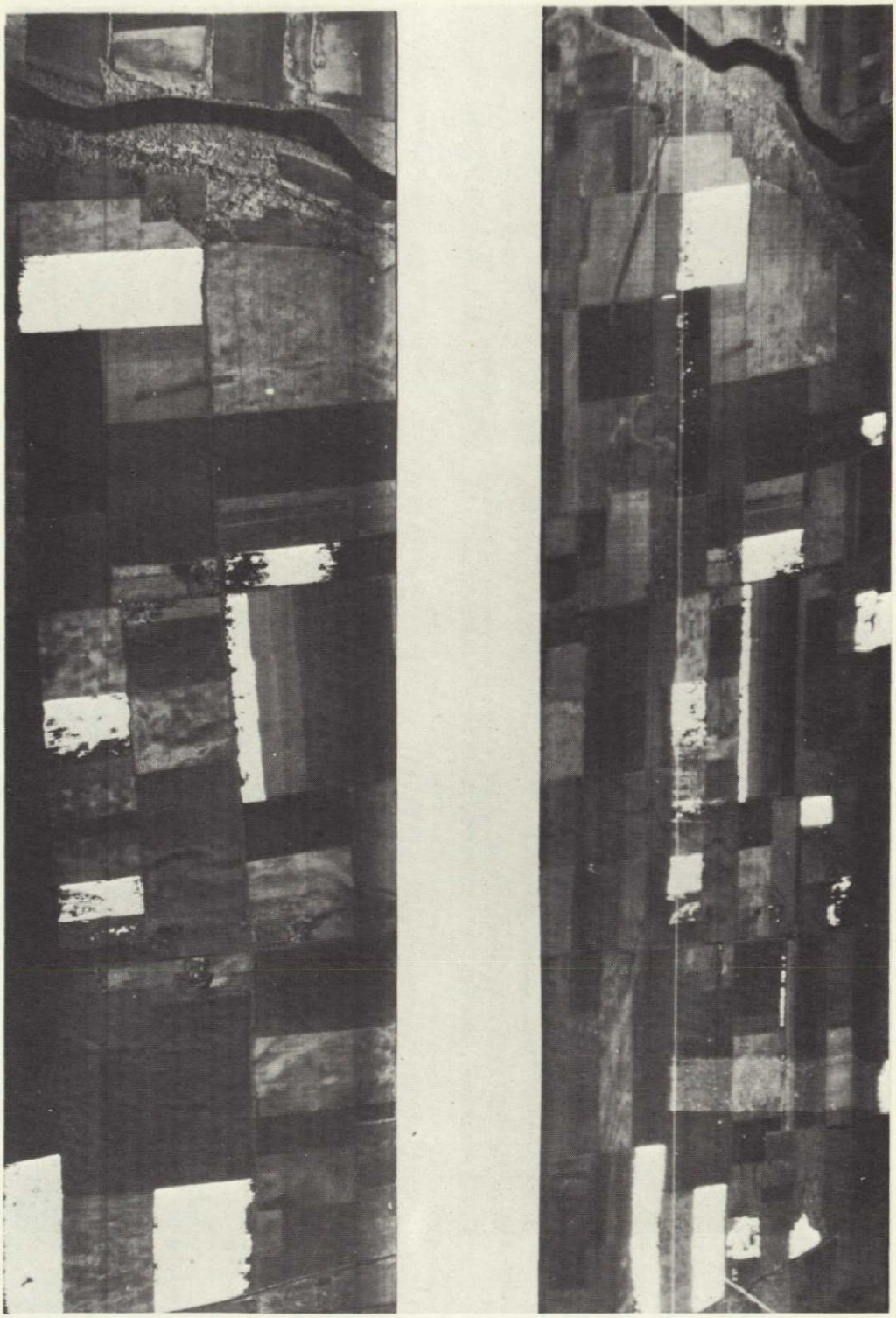

Figure 2.- Recognition of wheat near Lafayette, Indiana at two different altitudes on 6/30/66.

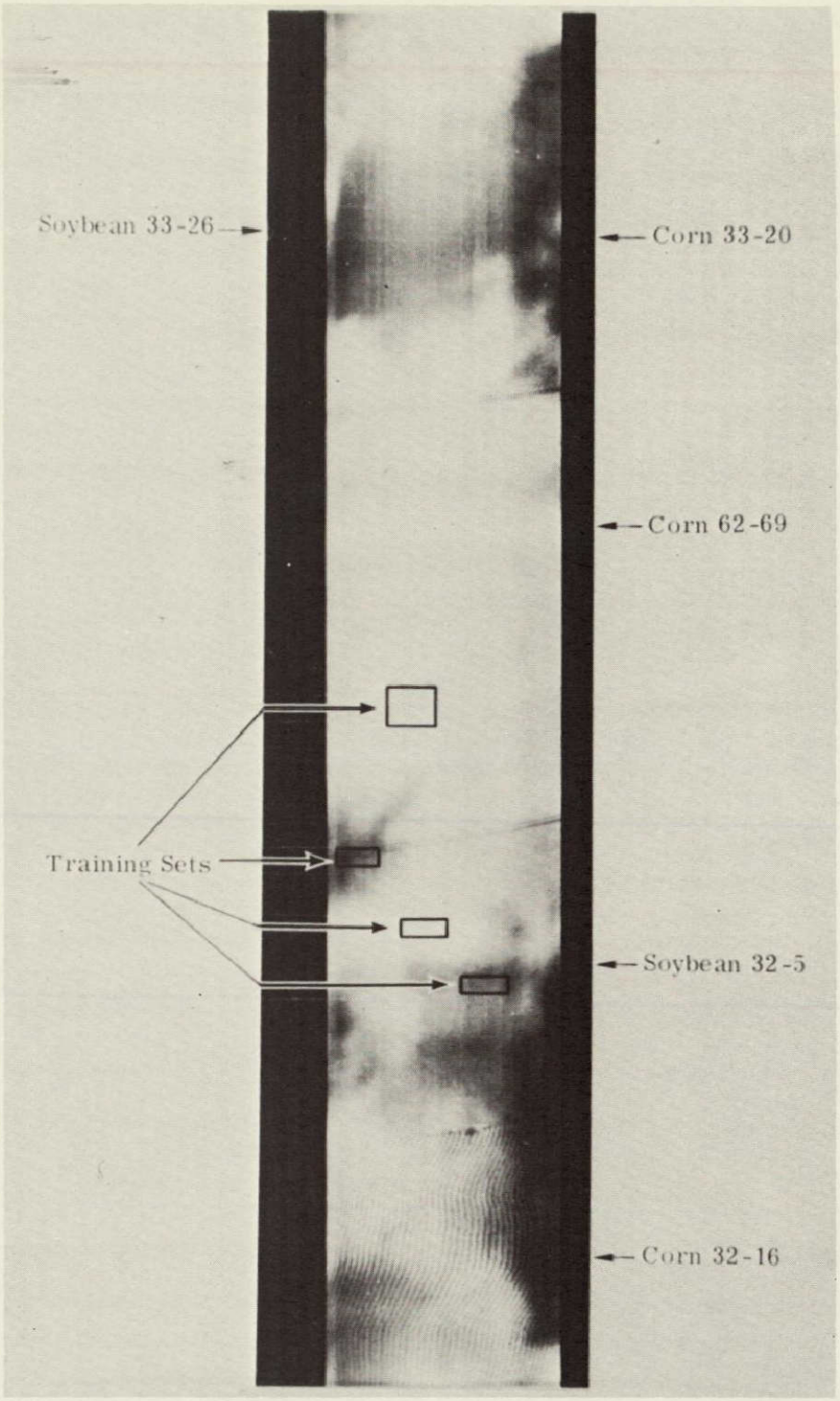

Figure 3.- Video Data for an agricultural area near Lafayette, Indiana, at 1000 hours and 700 ft. September 15, 1966: 0.8 to 1.0 μm wavelength band.

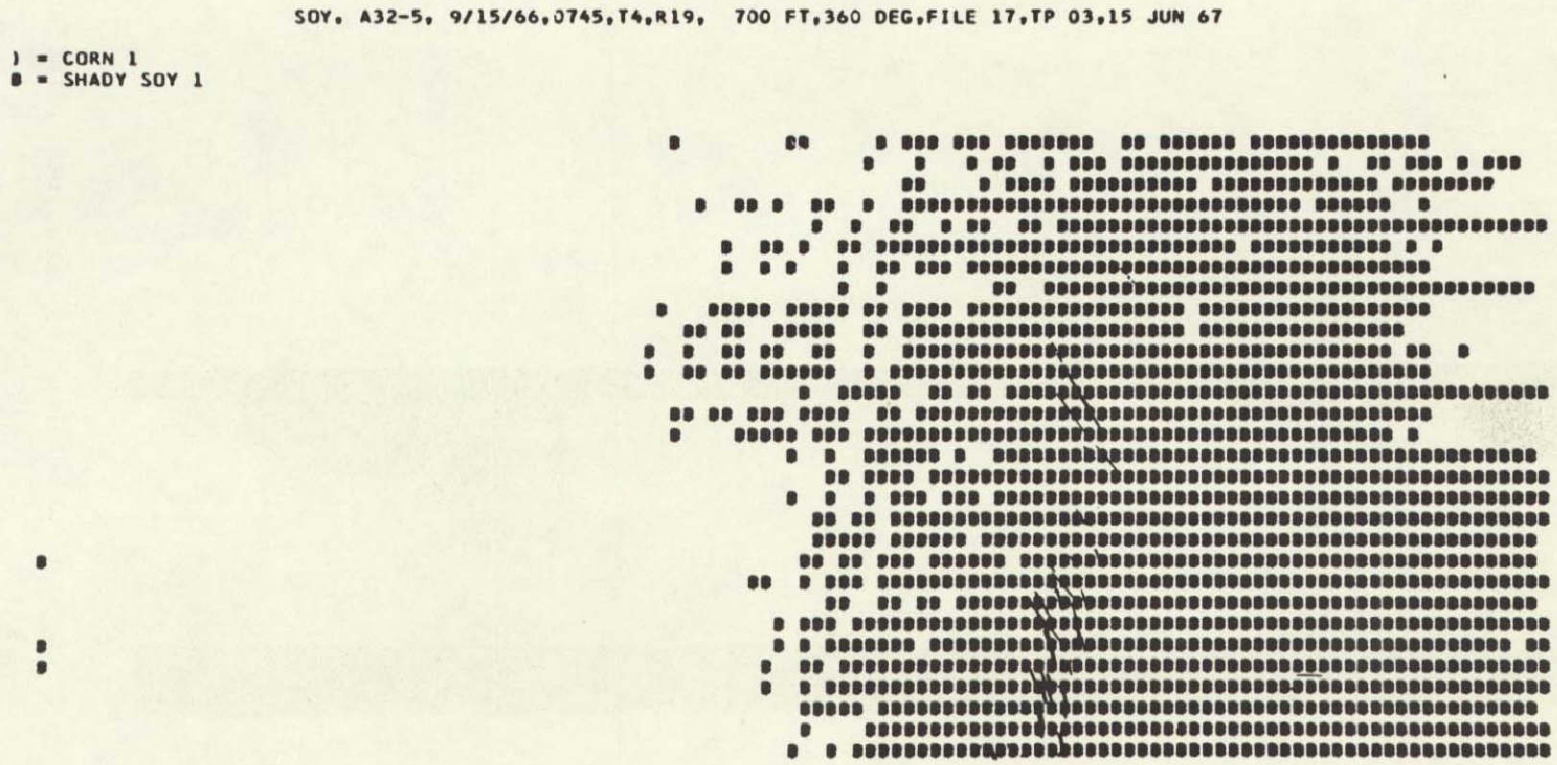

Figure 4.- Digital recognition map of a soybean field without preprocessing using shaded soybean signature

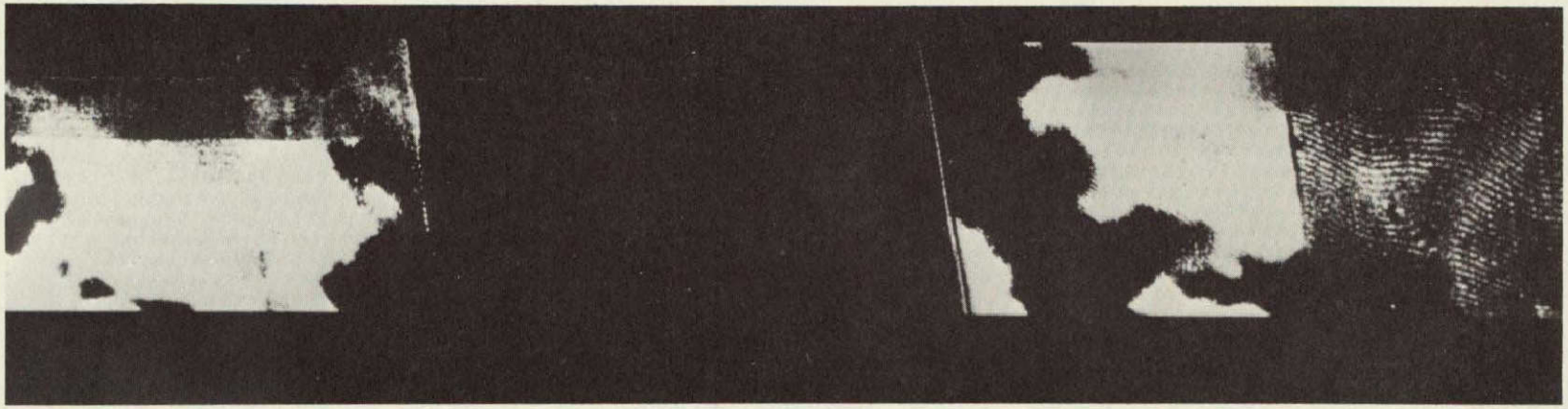

Figure 5.- Recognition map using a target signature derived from a shadowed area

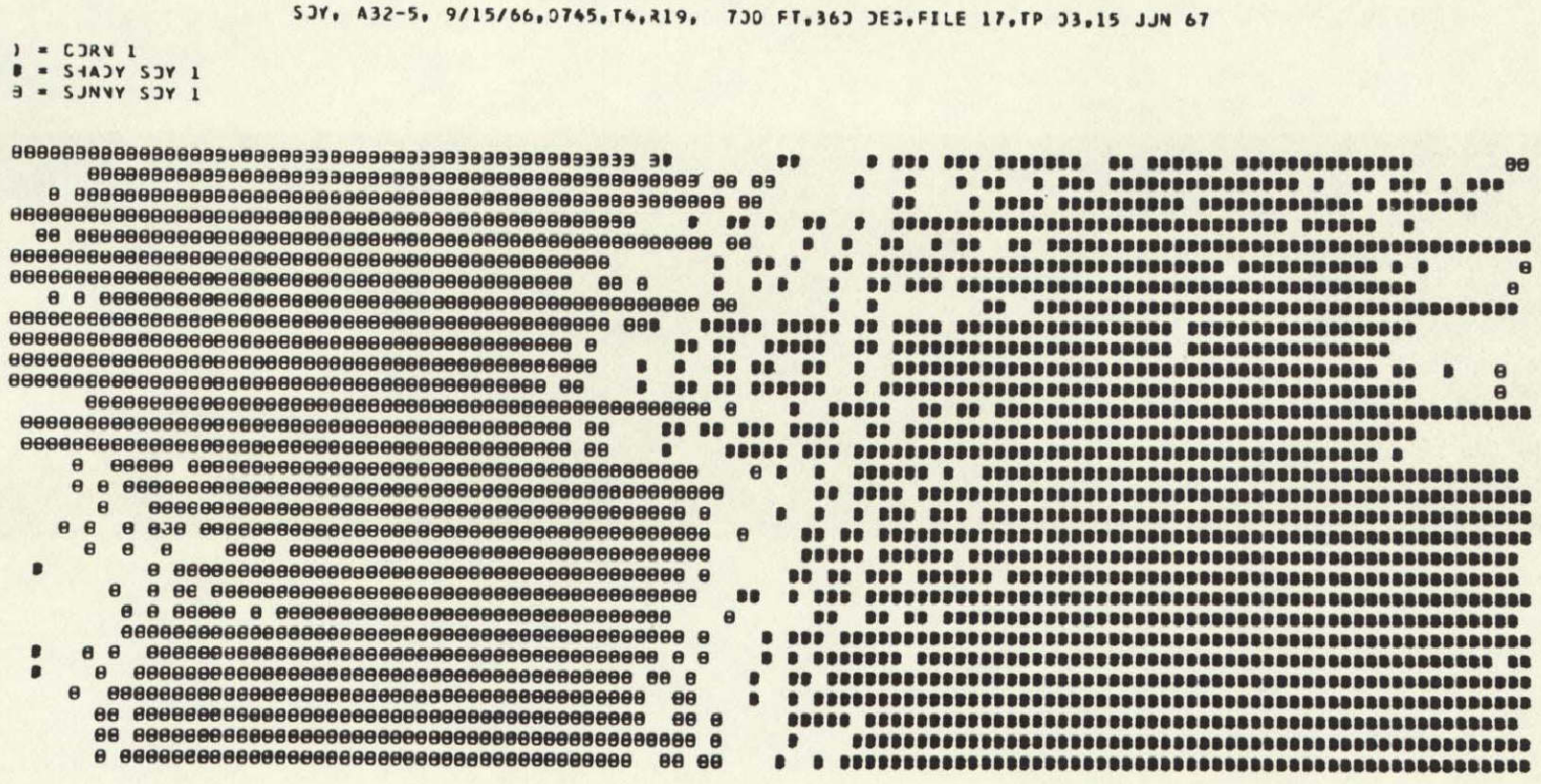

Figure 6.- Digital recognition map of soybean field without preprocessing using sunlit and shaded soybean signatures

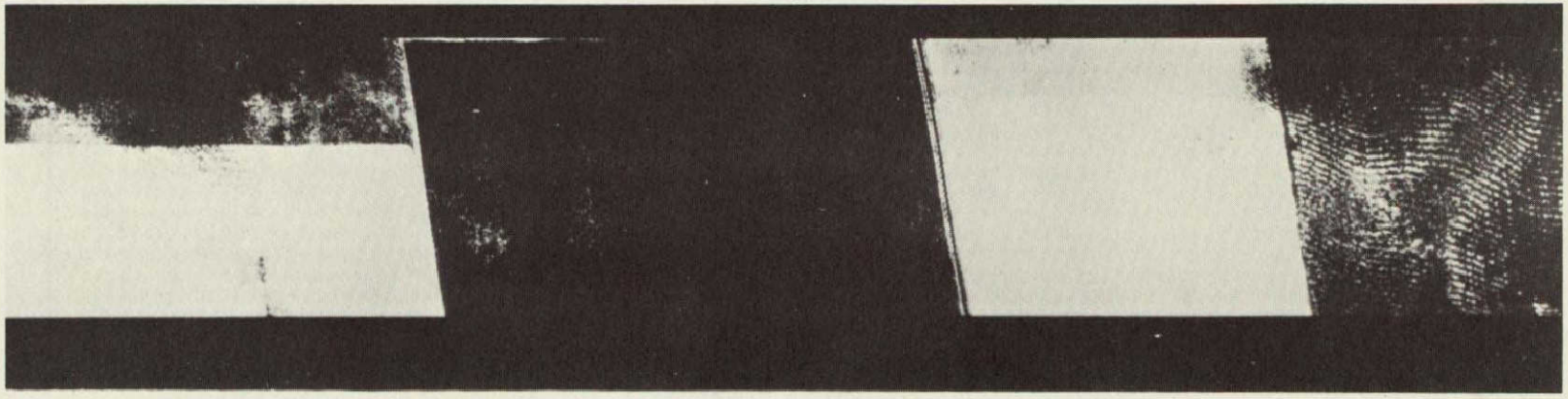

Soybean Recognition Without Preprocessing of Data

Figure 7.- Recognition map using a bimodal target signature map

SOY, A32-5, 9/15/66,0745,T4,R14, 700 FT,360 DEG,FILE 17,TP 03,15 JUN 67

) = CORN 2
8 = SHADY SOY 2
8 = SUNNY SOY 2

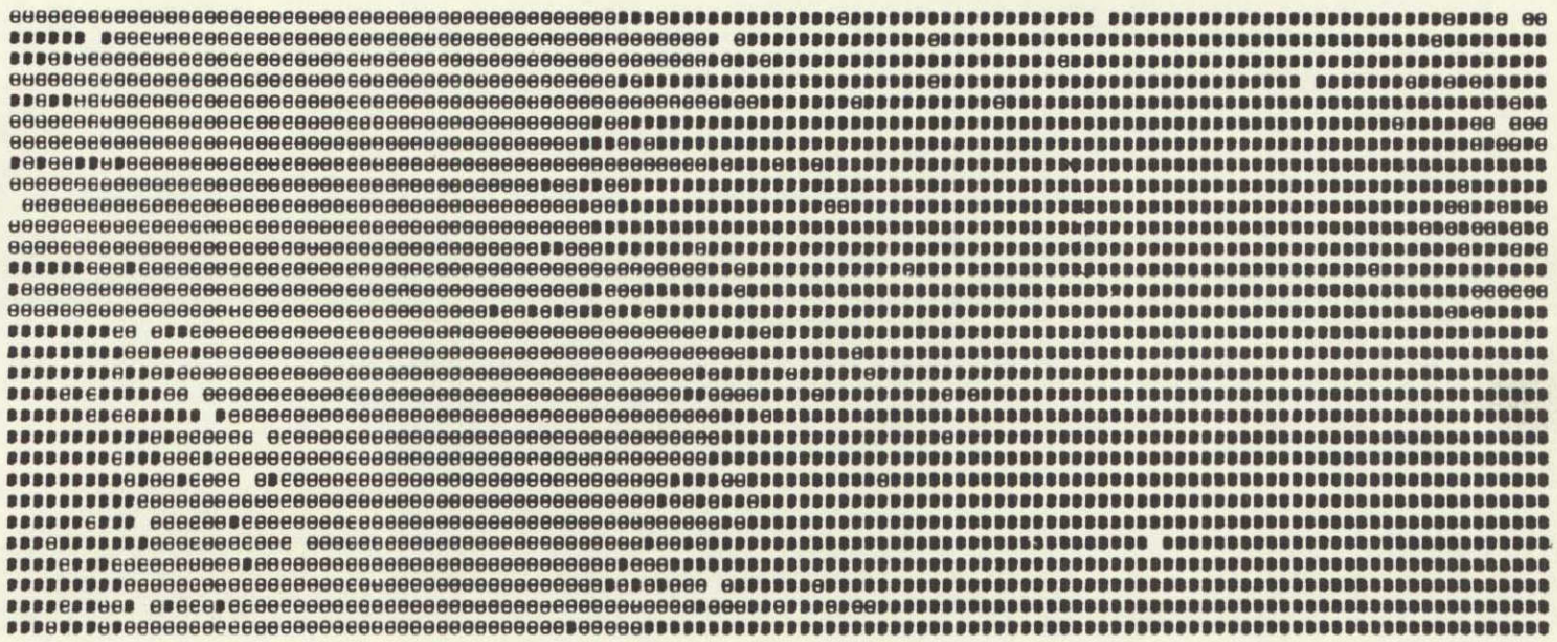

Figure 8.- Digital recognition map of a soybean field with preprocessing using sunlit and shaded soybean signatures

SOY, A32-5, 9/15/66,0745,T4,R19, 700 FT,360 DEG,FILE 17,TP 03,15 JUN 67

) = CORN 2
8 = SHADY SOY 2

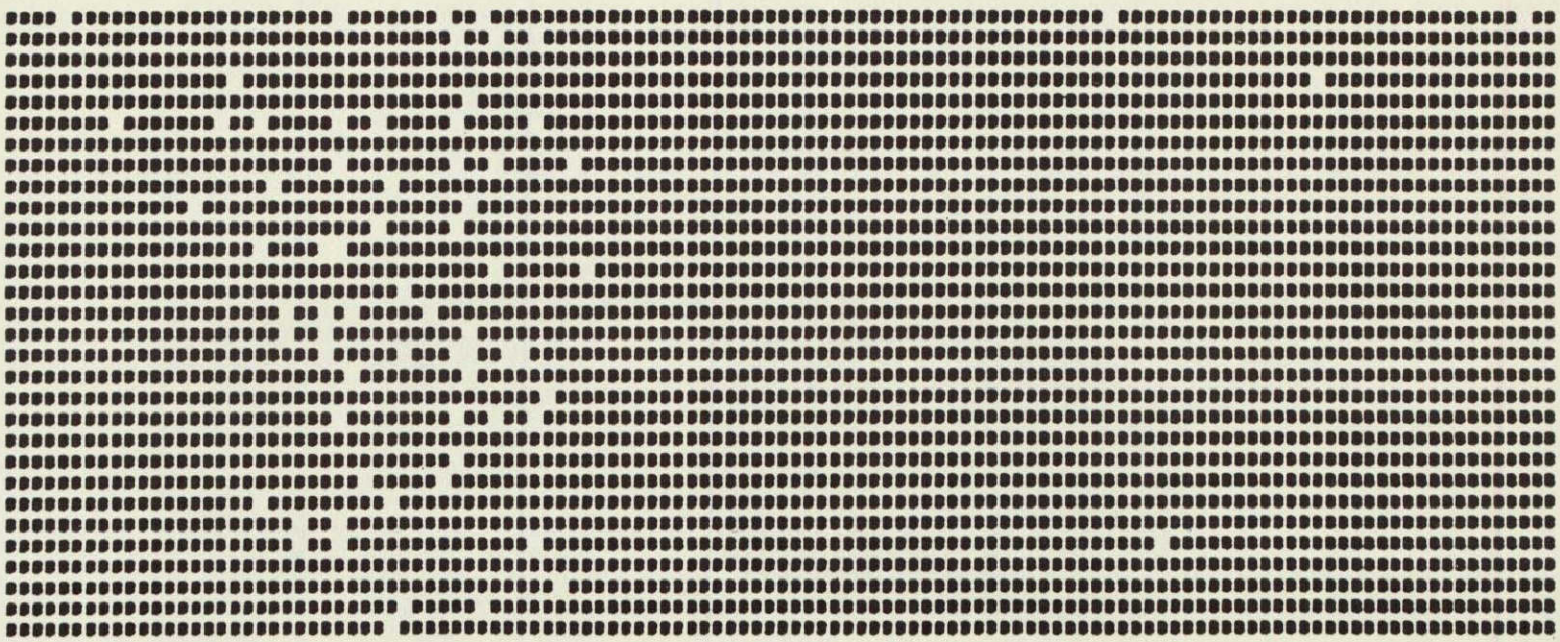

Figure 9.- Digital recognition map of a soybean field with preprocessing using shaded soybean signature

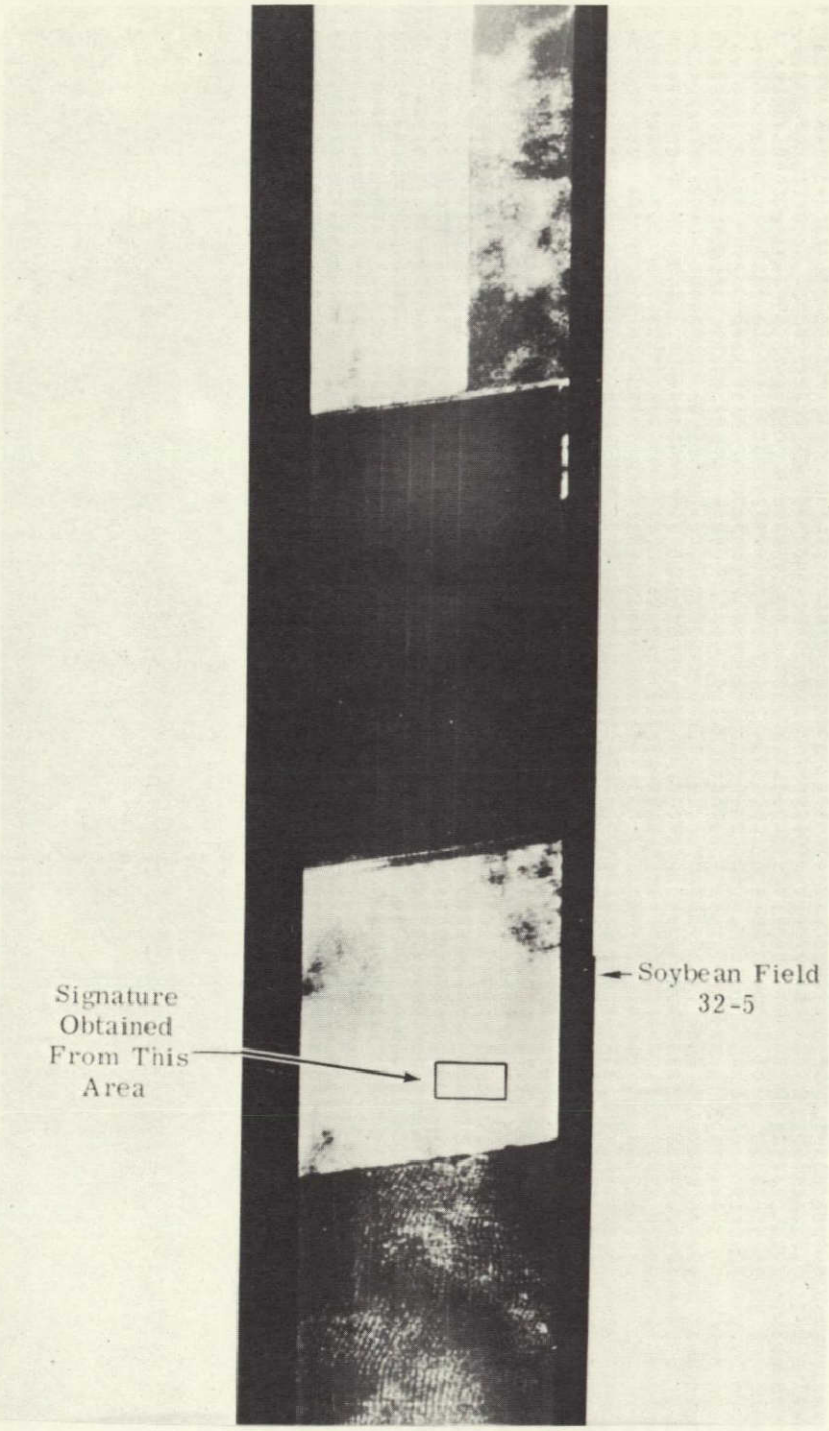

Figure 10.- Recognition map using a target signature derived from preprocessed data

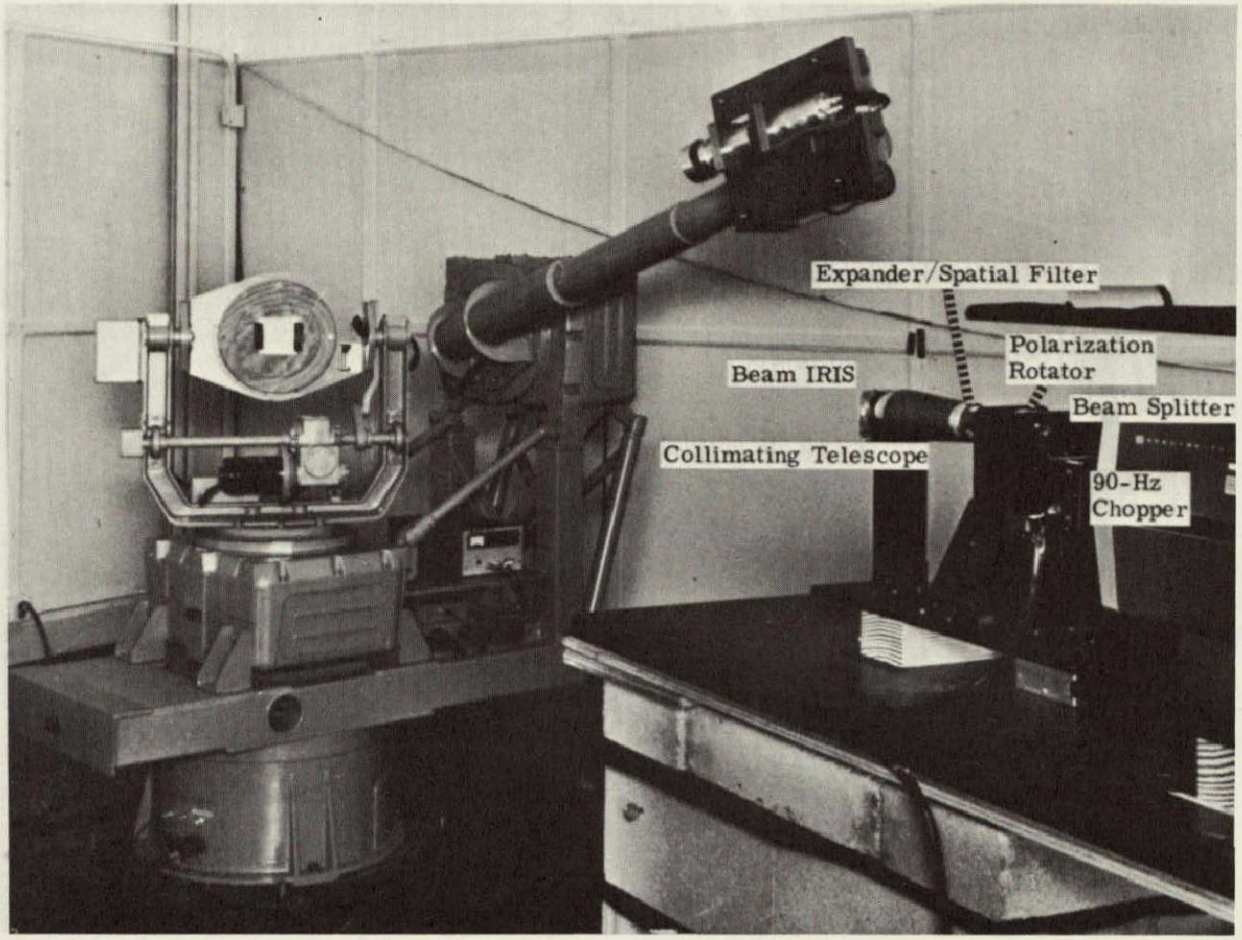

Figure 11.- Precision gonioreflectometer

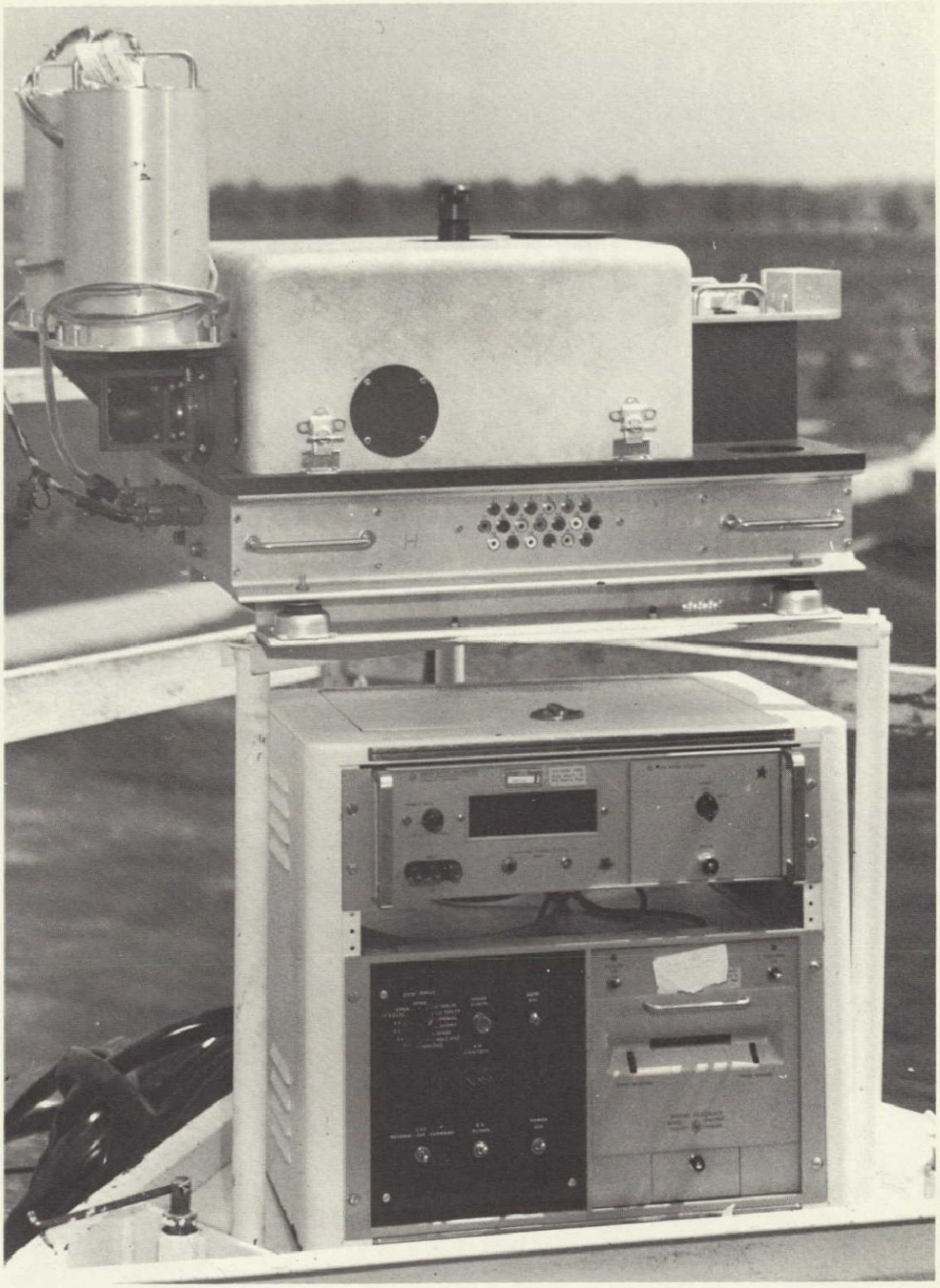

Figure 12.- Field infrared spectroradiometer

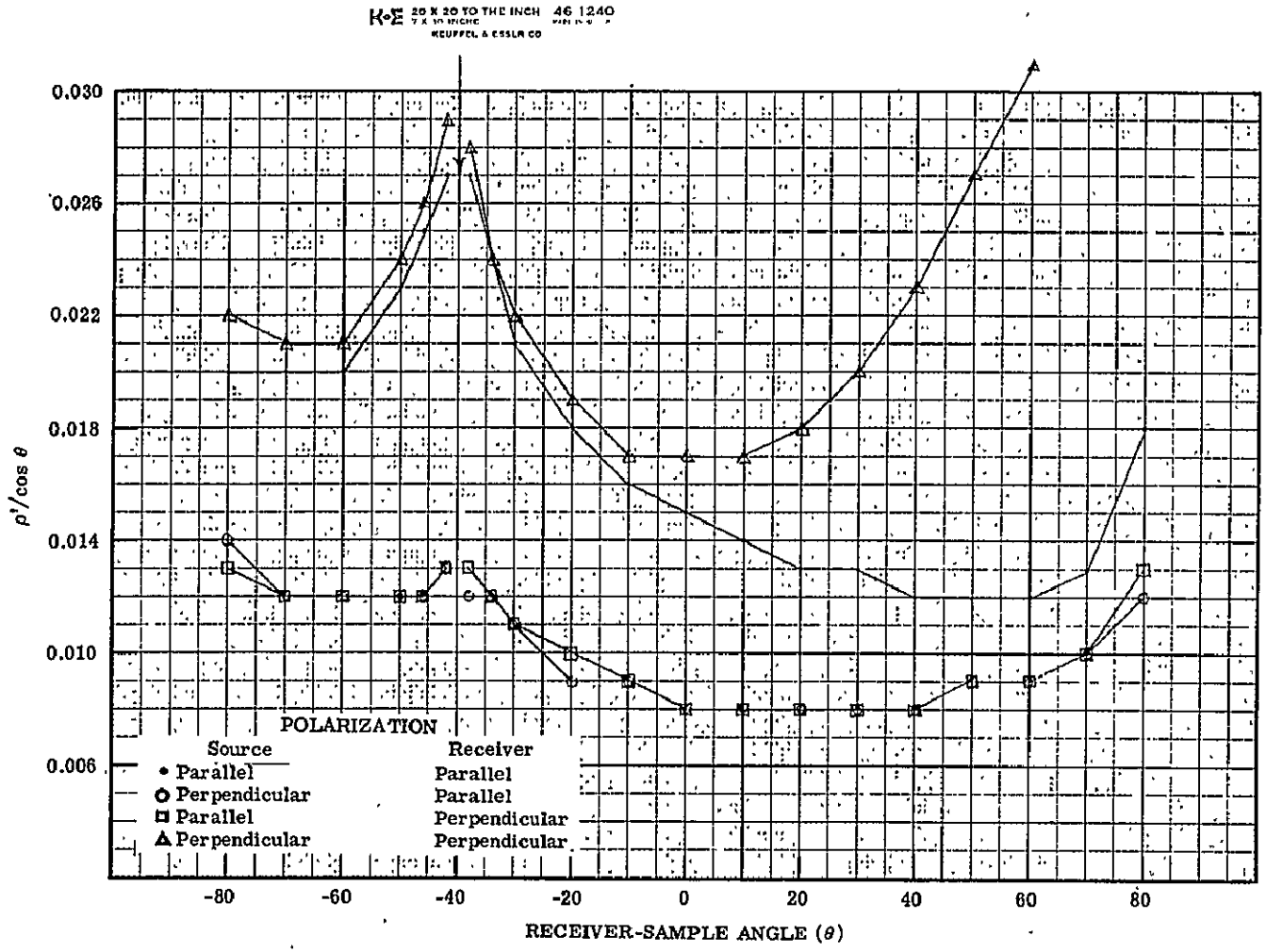

Figure 13.— Reflectance characteristics of a standard reflectance sample for polarized source incident at 40°.

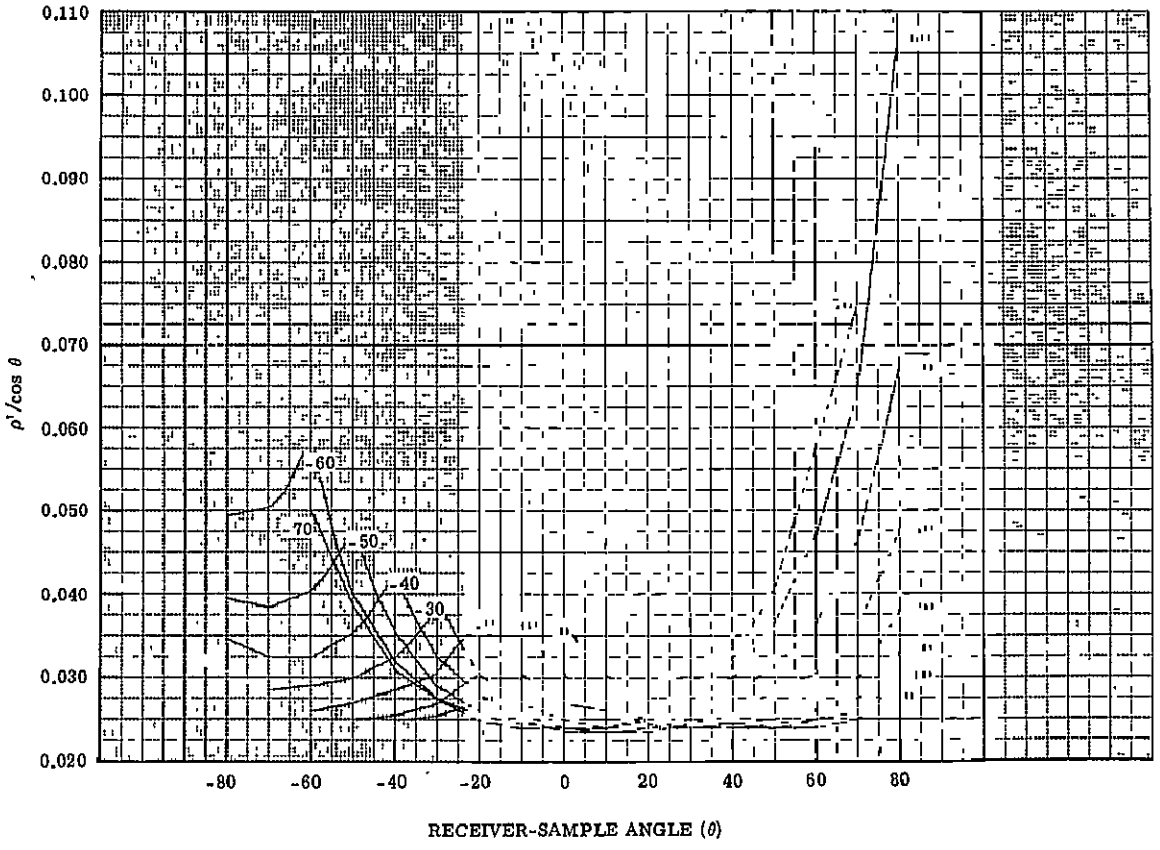

Figure 14.- Reflectance characteristics of a standard reflectance sample for an unpolarized source and receiver

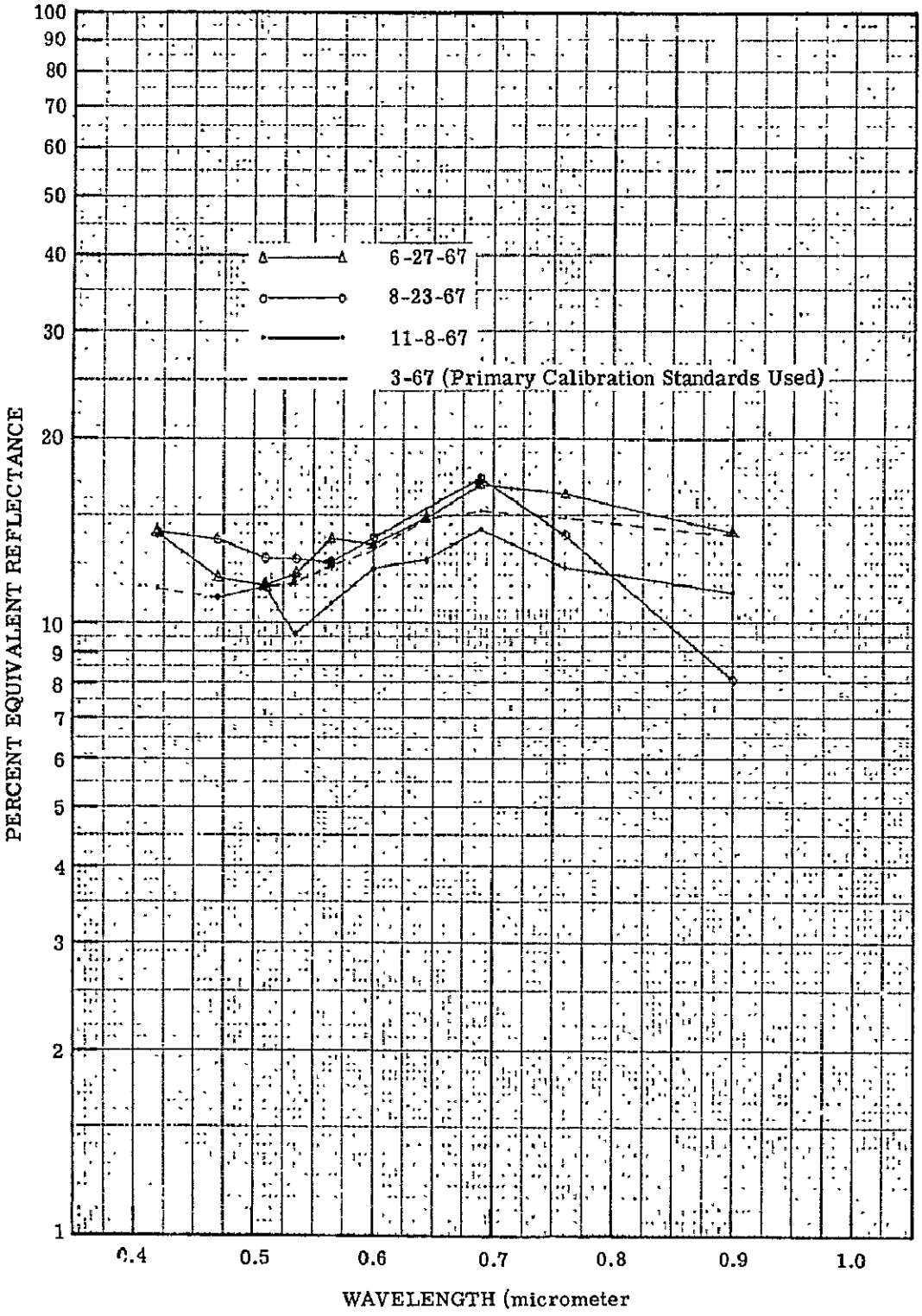

Figure 15.- ρ_e vs. λ for asphalt using sun sensor to calibrate

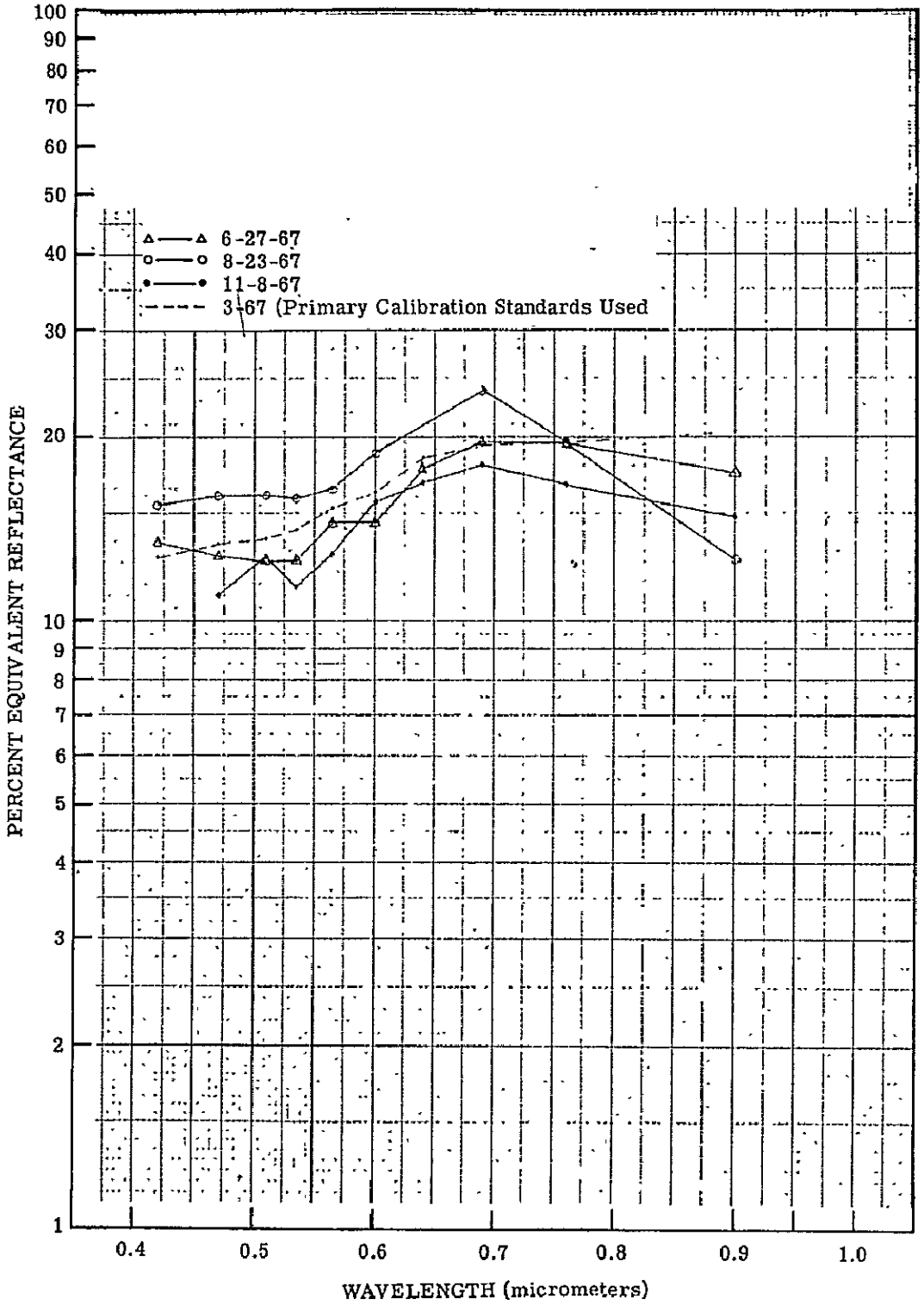

Figure 16.- ρ_e vs. λ for concrete using sun sensor to calibrate

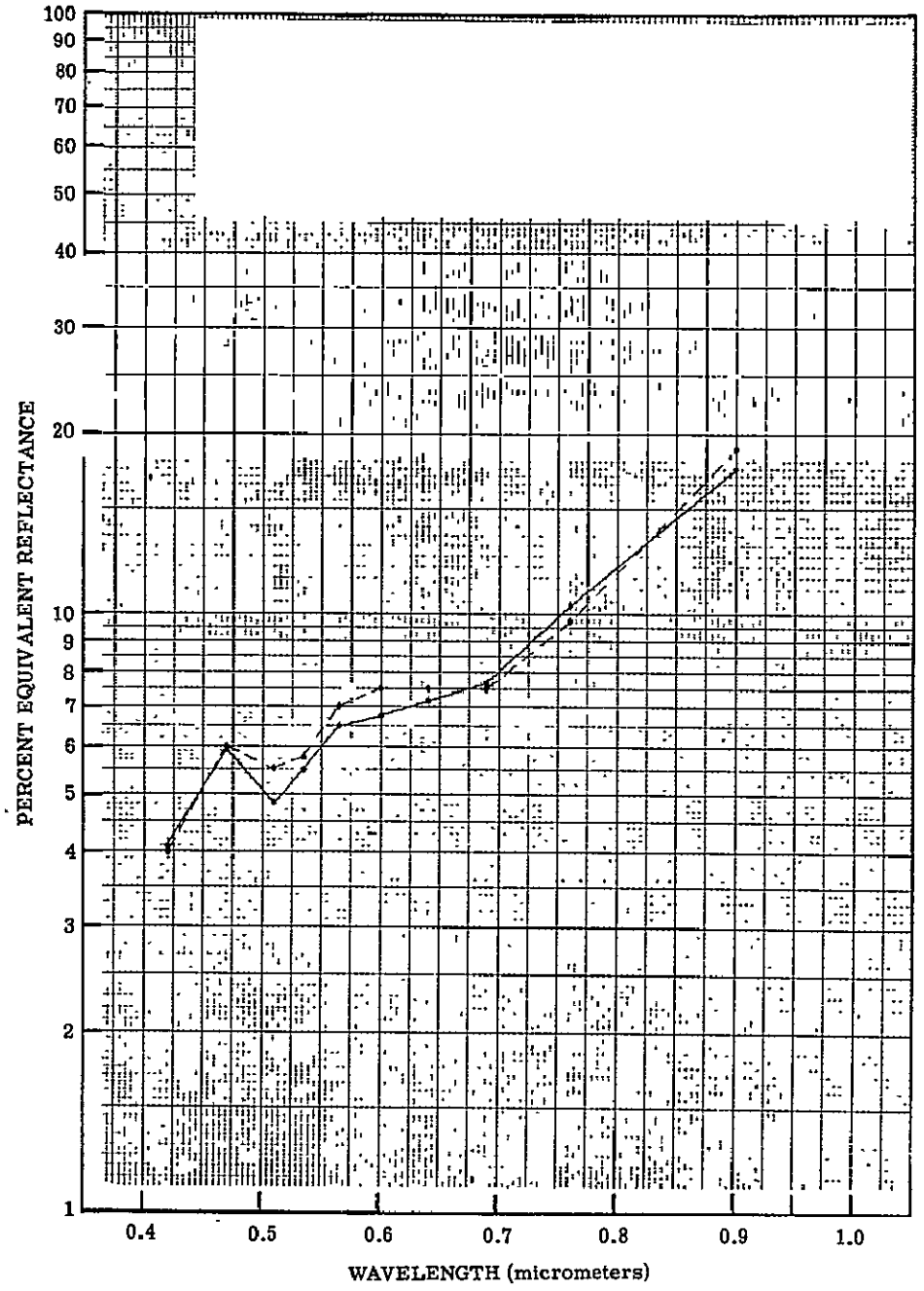

Figure 17.- ρ_e vs. λ for grass on 6-27-67 flight using sun sensor (·-----·) and secondary standards (·---·) to calibrate

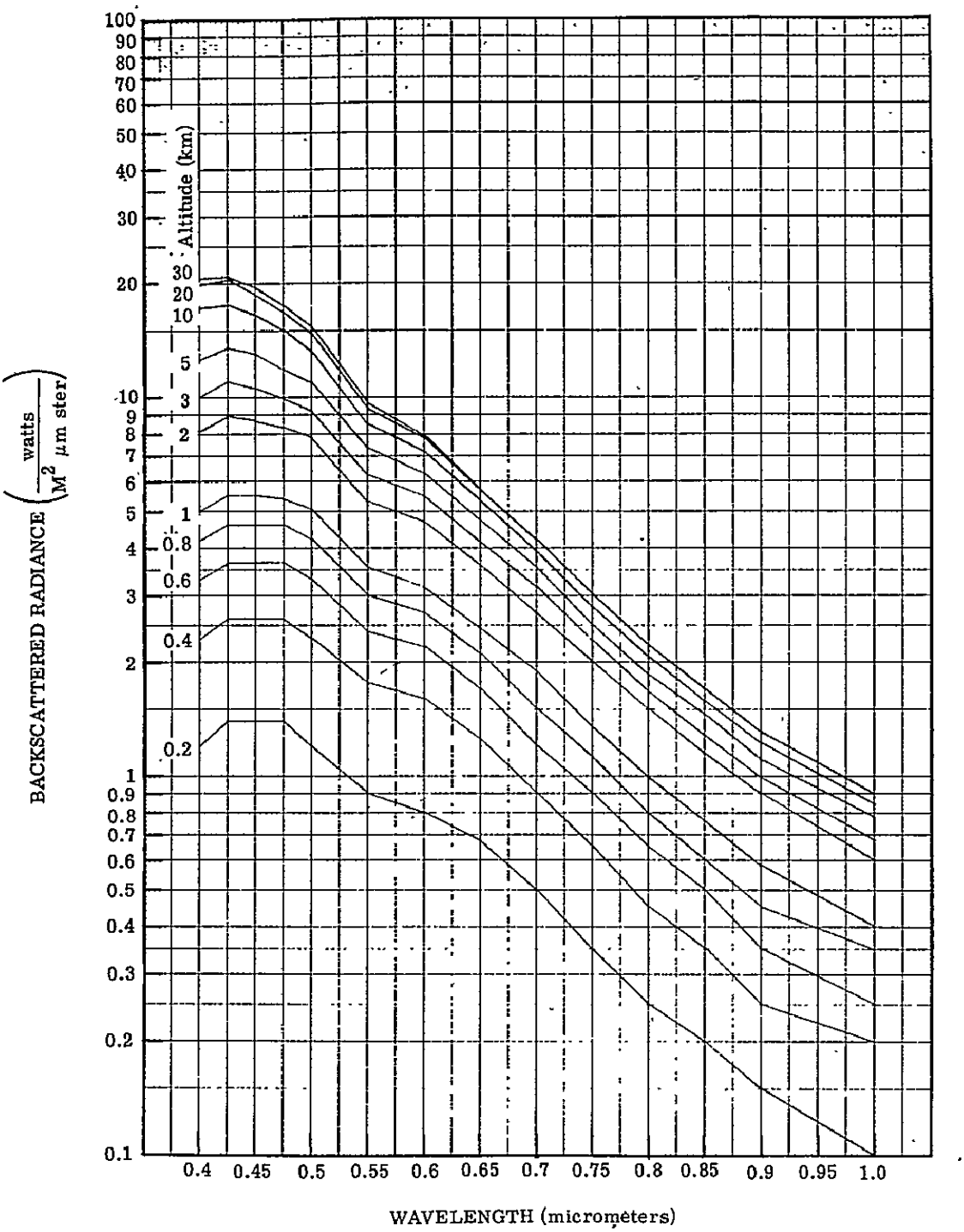

Figure 18.- Theoretical backscattered spectral radiance as a function of altitude

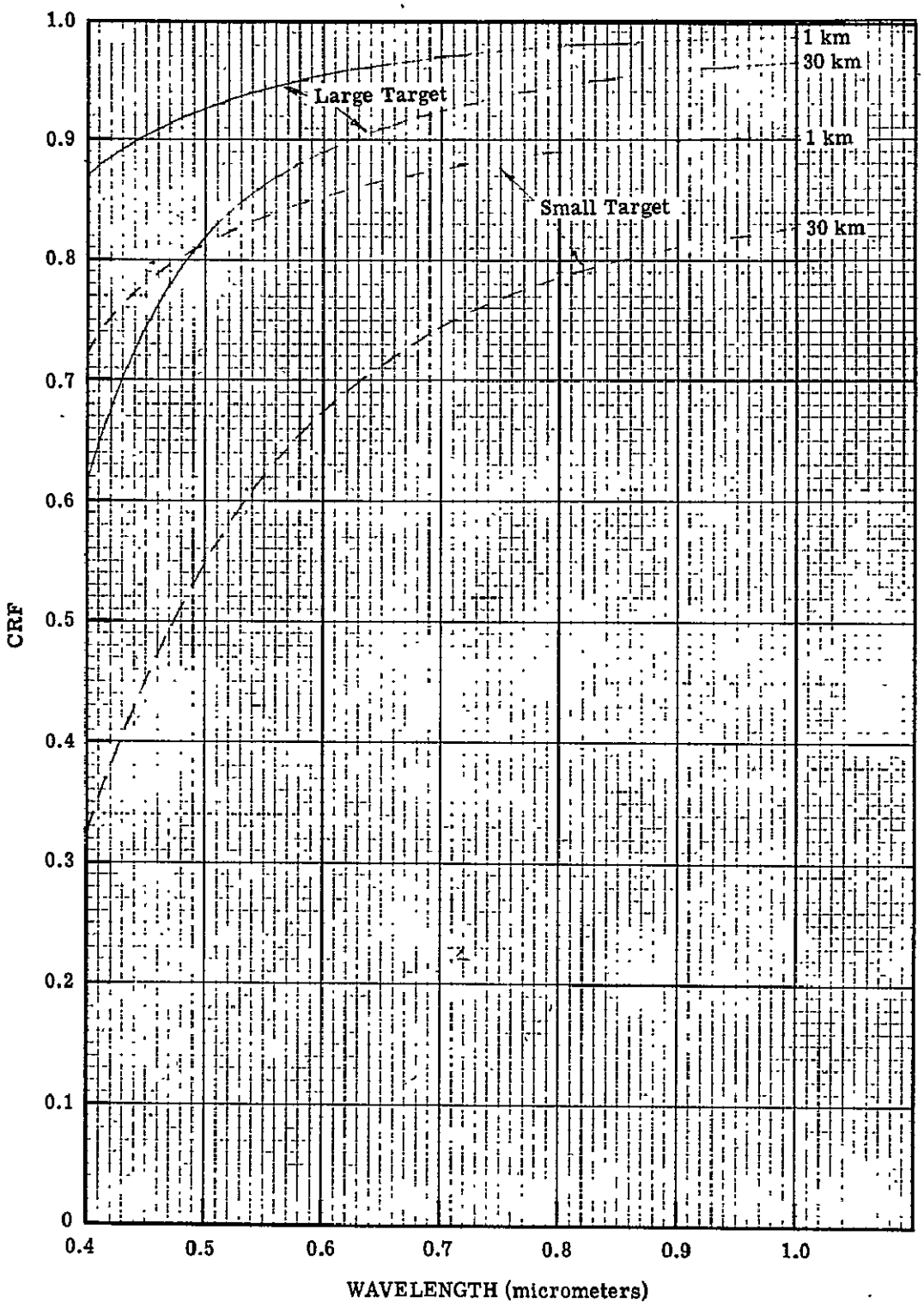

Figure 19.- Contrast reduction factor (CRF) for small and large targets at 1 km and 30 km

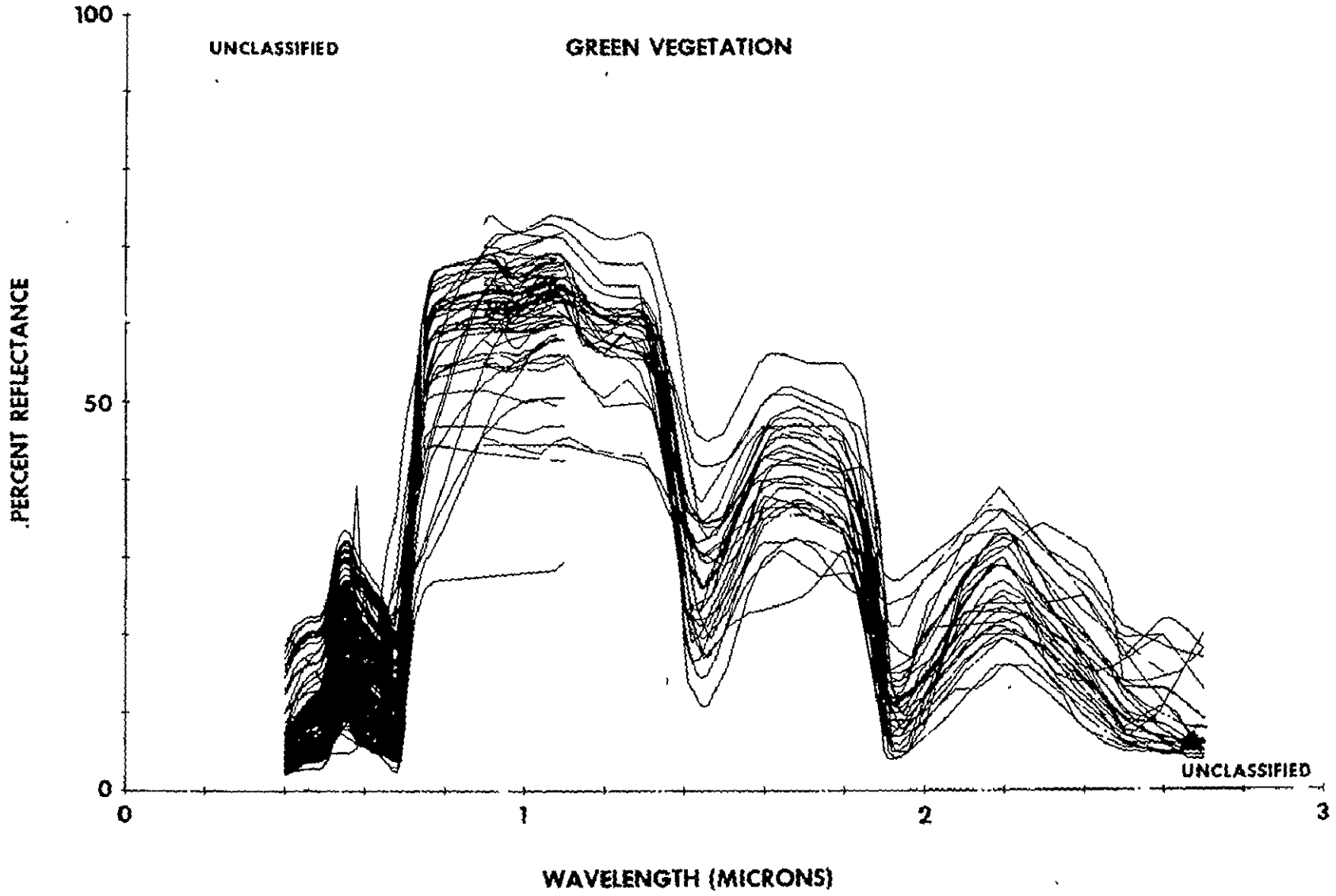

Figure 20.- Composite plot of 700 green vegetation spectra.

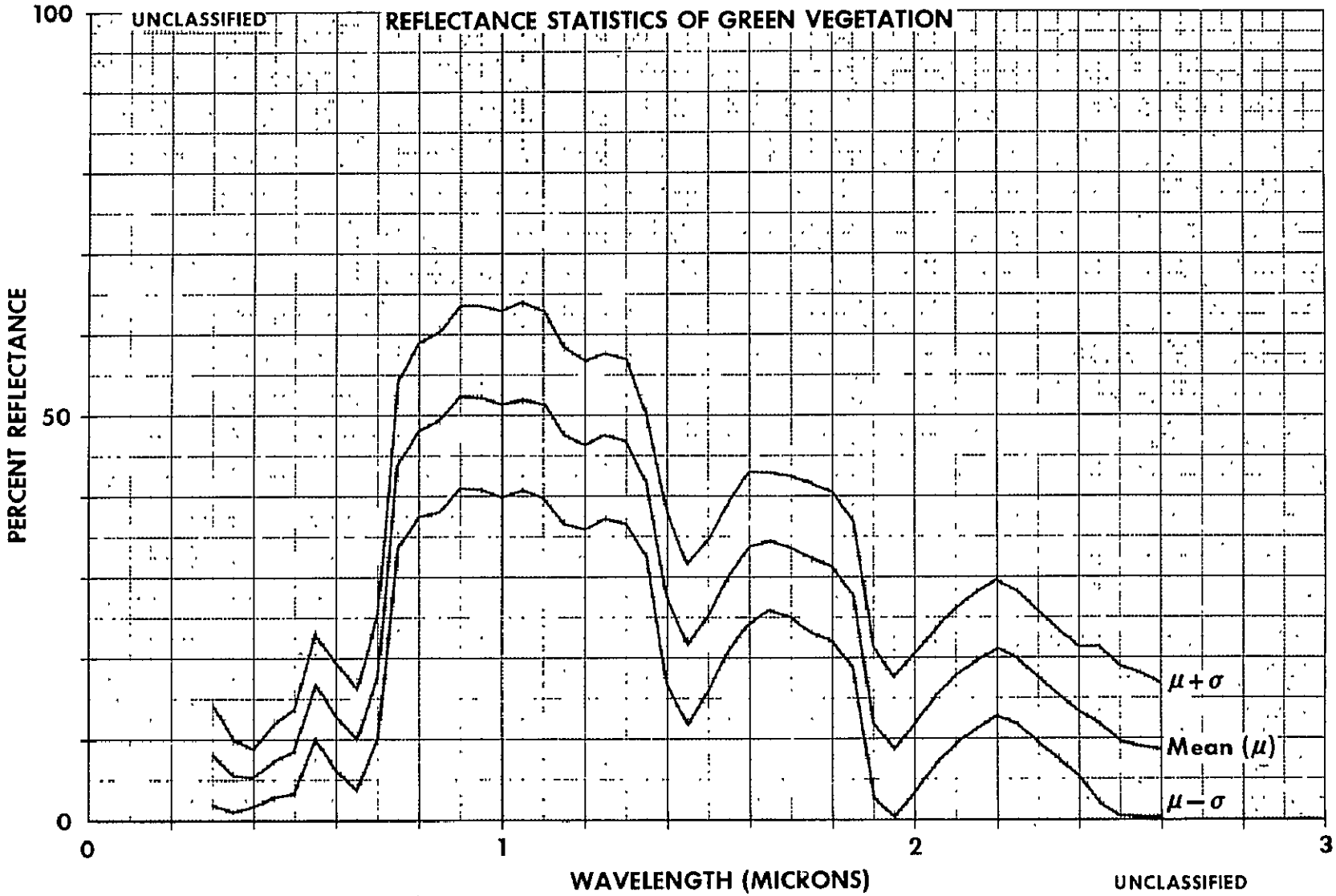

Figure 21.- Mean and standard deviation reflectance from 700 green spectra.

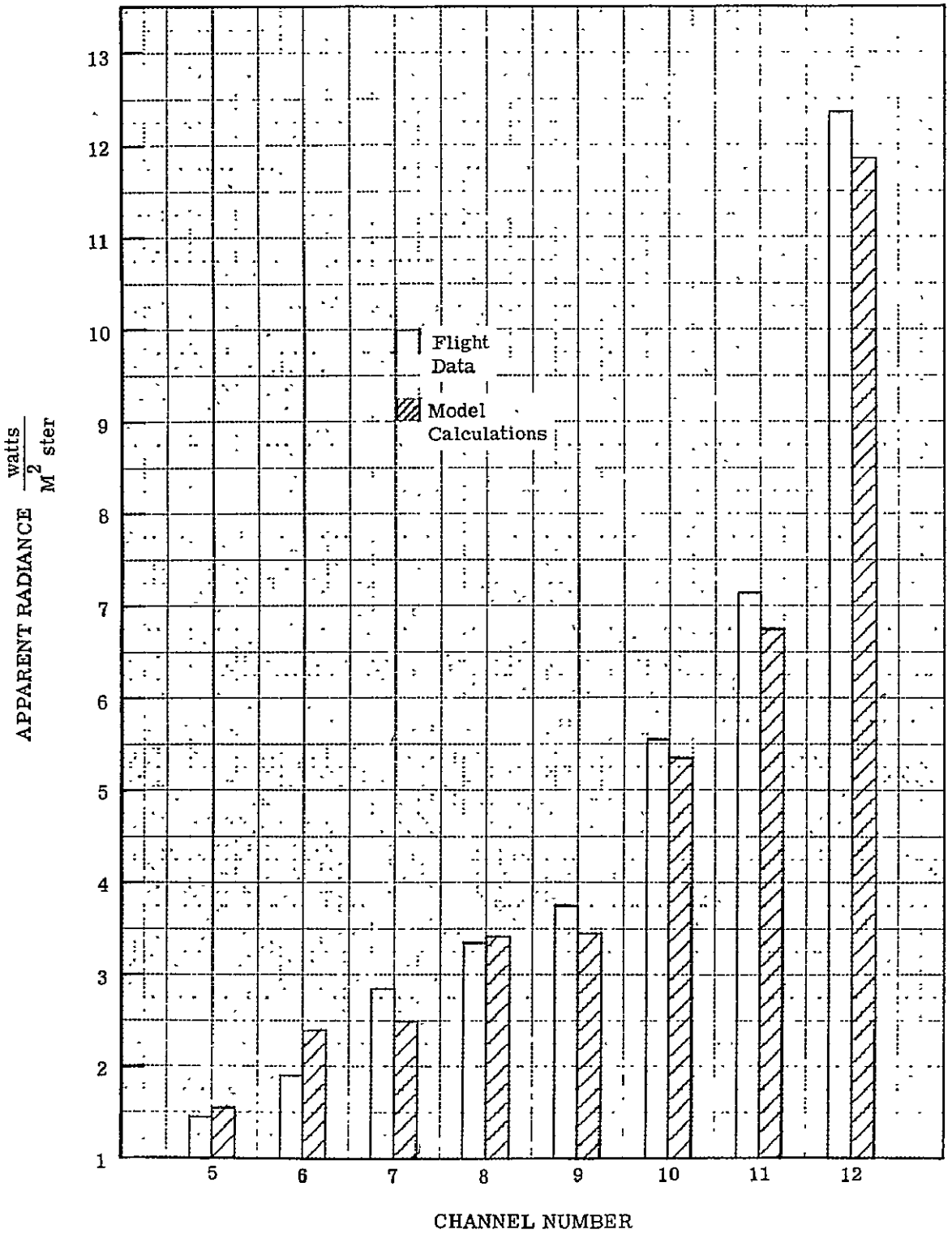

Figure 22.- Comparison of apparent radiance from ripe wheat as determined from flight data and predictive model calculations

SECTION 28

USE OF PASSBAND INTERFERENCE FILTERS IN MULTISPECTRAL PHOTOGRAPHY

Philip N. Slater and Dean B. McKenney*

Abstract: A new type of interference filter is described which can readily be designed for any central wavelength (400 to 900 nm) and any passband width (50 to 350 nm). These filters provide sharper cutoffs and greater efficiency than conventional absorption filters, and total transmittance in the required passbands is shown to be 2 or 3 times greater, resulting in shorter exposure times and consequently about a twofold increase in spatial resolving power for early space multiband photography experiments.

These passband interference filters deposited on flat glass plates can be used to replace conventional absorption filters for lenses of less than 40° field of view. For larger angular fields the passband changes in shape and wavelength position. However, by uniformly depositing the filter on a selected lens surface, we have shown that the changes in shape and wavelength position can be greatly reduced for some modern wide-angle aerial lenses.

1. Introduction

One of the outstanding problems in multispectral photography lies in the selection of the best set of filters for a particular study, say of agricultural areas. Another is the selection of filters for an orbital mission, for example when the same filter set has to be used for studies in such diverse subjects as agriculture, geology, and oceanography. Up to now, the worker in multispectral photography has been severely limited in the choice of filters available to him. The only suitable bandpass filters have been absorption filters of the Corning, Schott, and Wratten types. These can be obtained for only a few regions in the visible spectrum, and furthermore, the width of each is fixed. Besides these two basic limitations, which have hampered the search for an optimum filter set, absorption bandpass filters have two additional undesirable characteristics:

(1) Their efficiency is low; typically their peak transmittance is less than 0.60 (60%).
(2) The bandpass cutoffs are not steep. This is particularly true for the long-wavelength cutoffs, resulting in a bandpass which is far removed from the ideal rectangular shape.

Interference filters were considered for this application for three reasons:

(1) When made of dielectric thin films, they exhibit very small loss due to scattering and absorption.

*Optical Sciences Center, University of Arizona, Tucson, Arizona 85721

(2) They can be designed and built for any central wavelength in the visible and photographic infrared.
(3) The cutoffs can be made very steep.

Until now, however, interference filters have been rejected by those involved in multispectral work because--

(1) Filters of the width usually required in multispectral photography (≥100 nm) were unobtainable.
(2) The central wavelength and the shape of the passband change with angle of incidence. This effect becomes increasingly pronounced as the angle of incidence increases beyond about 10°.

For some years researchers neglected the problem of designing suitable interference filters to replace absorption passband filters in multispectral photography. This was because, with multispectral photography still in early development, other problems, such as multispectral photointerpretation, were more pressing and absorption passband filters were considered reasonably acceptable. Filters became a *major* problem only when consideration was given to multispectral photography of the earth from low earth orbit. Here the low efficiency of absorption passband filters (their high filter factor) means that little of the available energy is incident on the film plane. This necessitates long exposure times, which, coupled with the high angular velocity of the spacecraft, can cause substantial forward image motion. In the event that forward motion compensation (FMC) is unavailable* the amount of forward motion image blur can be reduced by a suitable choice of lens (high speed, short focal length) and film (high speed, low resolving power), but the result is inevitably a loss in ground resolution compared to the case when a lower filter factor is available. It was because of the low efficiency of absorption filters and the future possibilities of multispectral photography from orbit that the work described here was initiated.

2. Comparison of absorption filters and interference filter designs

Typical of the passbands in the visible spectrum suggested for multiband photography are 440 to 580 nm, 500 to 620 nm, and 580 to 680 nm. In attempting to isolate these passbands with Corning,† Schott, or Wratten filters we

* The first "Earth Resources" orbital multispectral cameras will have no provision for FMC.

† Corning filters cannot be used with a camera because they are not manufactured of optical grade glass. However, they can be used as part of the condensing system in a multiband projector or viewer.

find at once that only in one case does the passband of the filters available fall in the center of the required passband. In most cases the transmittance of the filters rises steeply at the short wavelength end of the passband and tails off slowly at the long wavelength end. These characteristics show up clearly in Figs. 1, 2, and 3, and it is also noticeable that the short wavelength end of the passband generally shows a much higher transmittance than the long wavelength end. We should also note that no high transmittance passband absorption filters exist in the red end of the spectrum. Thus, in the case of Fig. 3 we either have to ignore the requirement for the 680-nm cutoff or work with the very unsatisfactory filter shown as the dotted curve.

We may conclude that as a class, then, absorption filters isolate the required spectral passbands moderately well but not as well as desired.

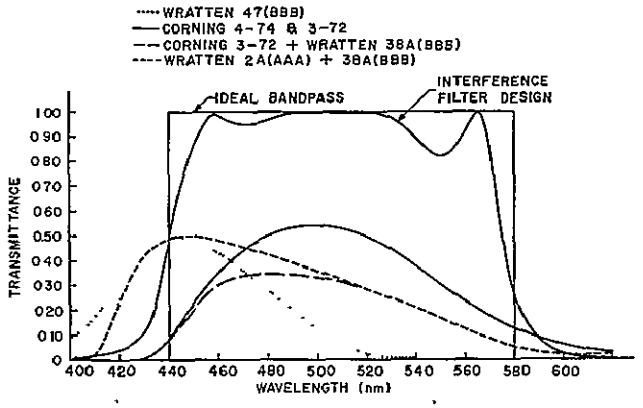

Fig. 1. Comparison of Wratten and Corning absorbing filters with interference filter design; required bandpass 440 to 580 nm.

Fig. 2. Comparison of Wratten absorbing filters with interference filter design; required bandpass 500 to 620 nm.

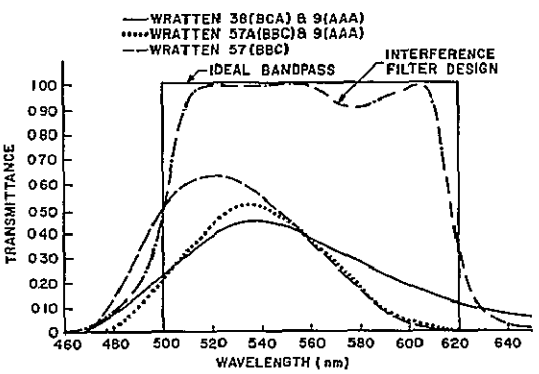

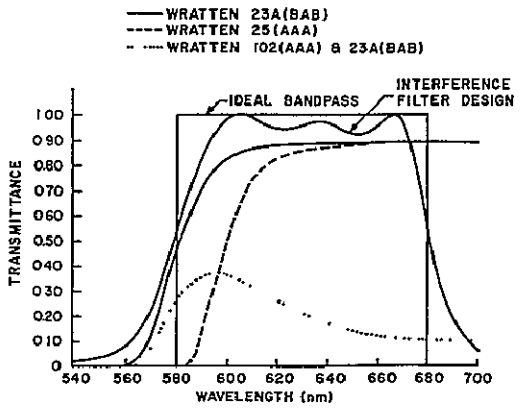

Fig. 3. Comparison of Wratten absorbing filters with interference filter design; required bandpass 580 to 680 nm.

A second serious drawback of absorption filters is their low over-all transmittance or high filter factor. This is also shown clearly in Figs. 1 and 2. A calculation for the dotted curve in Fig. 2 shows that the filter factor is about 9. In comparison, the interference filter designs (McKenney and Slater, 1968) show a maximum calculated transmittance greater than 0.9. If the fabricated filters were to show a transmittance of 0.8, then, for the design shown in Fig. 2, the filter factor would be about 3. Thus the gain in filter factor in this case, in using an interference rather than an absorption filter, is a substantial factor of 3.

To illustrate the importance of this decrease in filter factor, we take the specific case of a diffraction-limited f/5 lens of focal length 80 mm recording an object of contrast ratio 2:1 on Plus-X film. If the camera is stationary with respect to the object, the resolving power on film is about 56 cycles/mm. (These calculations were made with the aid of the Itek Photographic Slide Rule.) Now let us assume the camera is in a spacecraft orbiting the earth and the angular velocity of the camera with respect to the object is 50 mrad/sec. Let us also assume that the exposure time with a filter factor of 9 is 6 milliseconds. The image smear is then 24 μm and the resolving power is reduced to 30 cycles/mm. With a filter factor of 3, the exposure time will be reduced to 2 milliseconds and the smear to 8 μm. Under these conditions the resolving power will be 50 cycles/mm. As a percentage, the resolving power has dropped by 46% with the filter factor of 9 compared to 11% with the filter factor of 3.

Angular dependence of interference filters

The reluctance to use interference filters in multispectral photography has been partly due, understandably, to the unavoidable change in passband shape and position with angle of incidence. The designs shown in Figs. 1, 2,

and 3 show a shift that is roughly proportional to $\cos^{1/3}\theta$, where θ is the angle of incidence.

For angles of incidence (semifield angles) up to 20°, this $\cos^{1/3}\theta$ shift is a small factor, amounting to only 12 nm or 2%, as shown in Fig. 4. The change in shape, as we shall see later, is hardly discernible. In our opinion, both are negligibly small; however, we will have to await field experiments to check that this is true.

On the upper part of Fig. 4 we show how the fields of view differ, for equal areal coverage, in strip and frame photography. Strip cameras are now comparatively little-used; however, for several reasons (Slater, 1969) we think they should be considered for use as multispectral cameras.

One reason is that, for the same areal coverage, a smaller field of view is required than in frame photography. The gain is obvious from the 100% area line in Fig. 4. The field angles for the same areal coverage are 16° and 11° for frame and strip photography, respectively. The corresponding percentage shifts in the long-wavelength cutoff of the filter are 1.4% and 0.7%. Furthermore, it is clear that this gain will become more marked for larger semifield angles. For example, in the equivalent case of 27° semifield frame photography and 20° semifield strip photography, the percentage shifts are 5% and 1.4%, respectively.

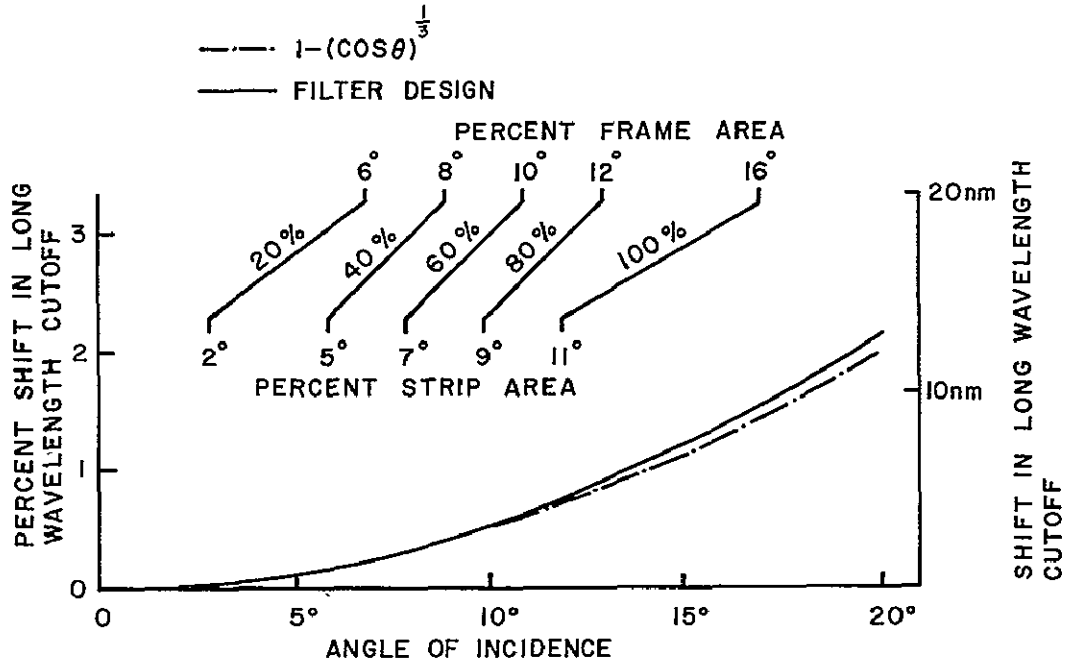

Fig. 4. Variation of cutoff shift with angle of incidence.

3. Use of interference passband filters with wide-angle lenses

The requirement for obtaining constant spectral content across the film plane can be met exactly if we can find a surface of the lens upon which the angles of incidence at full aperture are distributed identically for all field angles. The range of the distribution of angles will determine to what extent this requirement can be met.

In considering the coating of lens elements, we imposed several restrictions to avoid possible problems. First, so as not to change the lens system, we considered using only the available lens surfaces. An interference filter coated on such a surface is thin enough not to affect the imaging characteristics of the lens. Second, we considered only uniform coatings, which simplifies the theoretical problem, and we considered only concave surfaces, which are relatively easy to coat uniformly and thus simplify the fabrication problem later. Third, since interference filters are highly reflecting for wavelengths that are not transmitted, we considered locating the filter on one of the first two lens elements only, in order to reduce the chance that off-band stray light would be scattered or reflected back through the filter at a high angle of incidence.

We started this study by evaluating some of the older, readily available designs of cartographic lenses. (See, for example, Stavroudis and Sutton, 1965.) Ray tracing of these lenses quicly indicated a serious mechanical vignetting problem. Typically, an old f/6.3 cartographic lens, such as the 45° semifield angle Metrogon, will vignette a full-aperture pencil at semifield angles greater than 35°; or, at full field, the lens will vignette until reduced in speed to about f/10. When coupled with the decrease in illuminance roughly proportional to $\cos^4$ of the semifield angle, the total decrease can amount to about three stops. A filter factor of 4 (two stops) can be introduced by some of the absorption filters used in multispectral photography. Thus, the T-number of such a lens may be T/36, which is generally too high for aerial or space applications.

We then obtained design data sufficient for our purposes for three aerial camera lenses, all illustrated on the opposite page: the Geocon IV lens (courtesy of Kollsman Instrument Corporation), the Paxar lens (courtesy of Pacific Optical Division of Chicago Aerial Industries, Inc.), and the 125° Pleogon lens (courtesy of Carl Zeiss, Inc.).

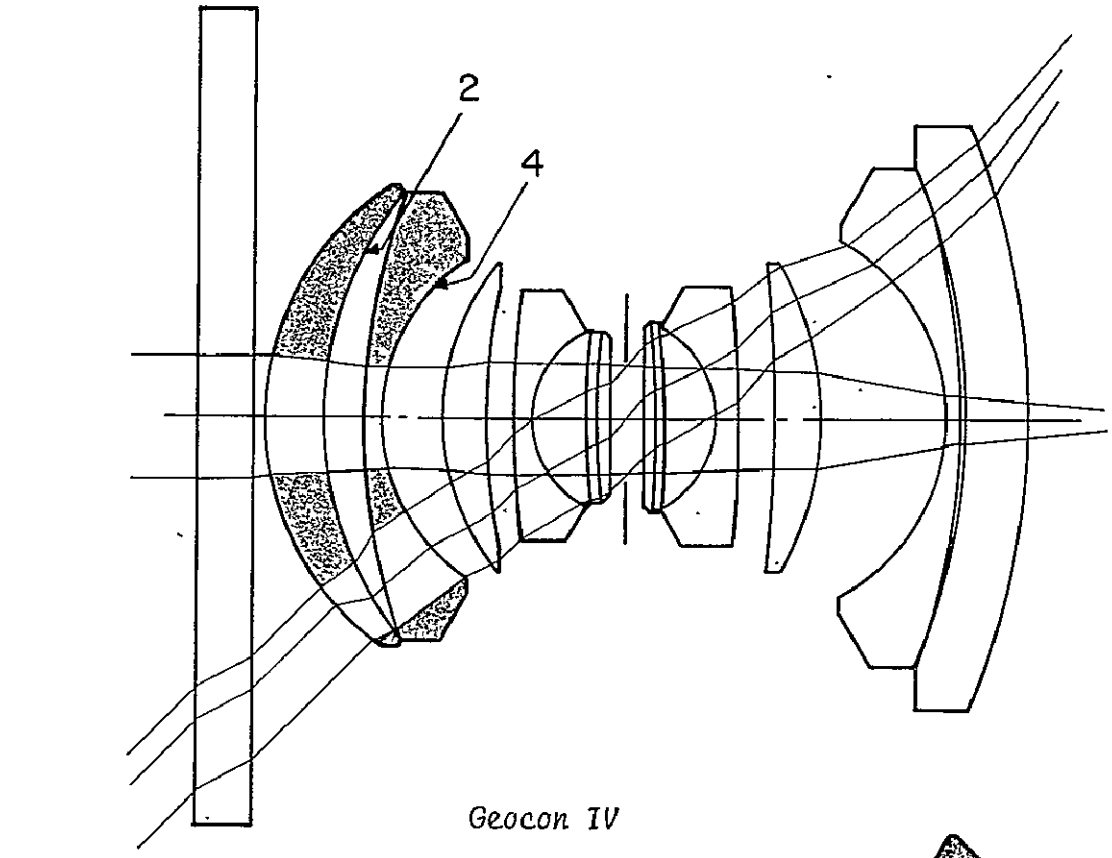

Geocon IV

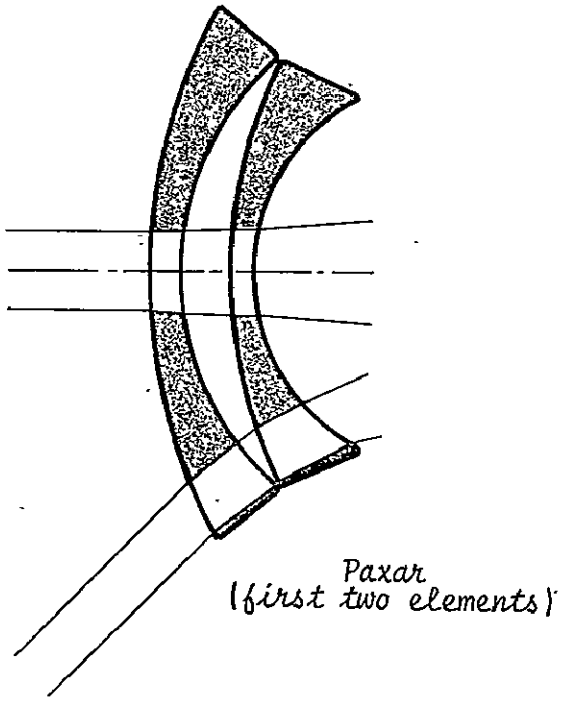

Paxar
(first two elements)

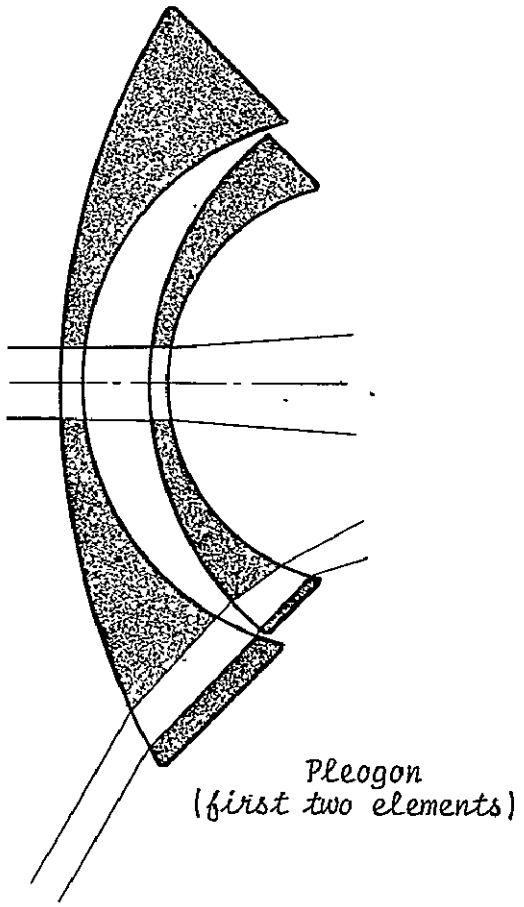

Pleogon
(first two elements)

Fig. 5. Three aerial camera lenses: the Geocon IV and the Paxar and Pleogon (first two elements only).

The Geocon IV and Pleogon are precision mapping lenses that have come onto the market during the past year, and the Paxar is a reconnaissance lens. Four Paxar lenses mounted in modified KA-62 cameras are being operated as a multiband camera in NASA's Earth Resources Aircraft Program. Specific characteristics of the lenses are listed below.

Lens characteristics

	Geocon IV	Paxar	Pleogon
F/number	5.0	4.5	4.0
Focal length	6 in. (152 mm)	3 in. (76 mm)	85 mm
Full-field angle	90°	90°	125°
Image format	9 × 9 in. (22.9 × 22.9 cm)	4.5 × 4.5 in. (11.4 × 11.4 cm)	9 × 9 in. (22.9 × 22.9 cm)

For each lens, the second and fourth surfaces meet the restrictions discussed above. Also, as shown in Fig. 1, we can see that angles of incidence encountered on these surfaces are not excessive for either the axial or the full-field ray pencils.

We want to calculate the spectral transmittance of the lens when an interference filter is located on one of the surfaces. The computation of the transmittance of multilayer filters is straightforward at any angle of incidence for plane waves incident on plane substrates. When the curvature of the wavefront is of the same order of magnitude as the curvature of the surface, the surface can be divided into a number of elemental "plane" surfaces, and the contributions from each surface element can be added up. The greater the number of surface elements, the greater will be the accuracy of the calculation. We found it most efficient to trace a number of rays through the lens surface in a specific order. Using a polynomial fitting technique, we then determined what percentage of the full-aperture pencil lay in a certain angle-of-incidence range. This percentage was used to determine the "distribution" of angles for computing the transmittance of the filter on the surface. The "transmittance" of the lens is defined as the ratio of the transmittance of the lens with a coating to the transmittance of the lens if the coated surface were perfectly transparent. McKenney (1969) presents a detailed description of the computational method.

We assumed that the light incident on the surface is unpolarized. This is necessary because we did not keep track of each ray to be able to determine the plane of incidence. The assumption of unpolarized light is probably valid even for the polarized case also since there will be, for any angle of incidence, an "average" plane of incidence making the transmittance appear at the image plane as if the light were unpolarized. Assuming that, under unusual circumstances, it might be possible to observe some polarization effects, we will discuss such effects later.

The rest of this report will be devoted to presenting and discussing the computed results of locating an accordion filter on the second or fourth surfaces of the Geocon IV, Paxar, and Pleogon lenses. We will examine how the shape and wavelength position of the passband change with field angle, then show to what extent polarization changes are introduced. We will show that a trace of two meridional rays defining the maximum extent of the full-aperture pencil at the extreme field angle gives an indication of the suitability of coating a given lens surface with an accordion filter.

Passband shape and position

Using the method described above, we calculated the spectral transmittance for each of the three lenses, at full aperture and for several field angles, with the accordion filter on the 2nd and then on the 4th surface. The results are plotted in Fig. 2 on the following pages. In the case of 0° field angle, the shape and position of the passband of the accordion filter on the 2nd or 4th lens surface are compared with the passband shape and position of the same filter on a flat substrate at normal incidence. For other field angles, the passband shape and position are compared with that for 0° field angle.

For purposes of multispectral photography we are primarily interested in finding the smallest change in passband shape and position over the image plane. Clearly, the second surface of the Paxar represents the best case although the second surfaces of the Geocon IV and the Pleogon could be acceptable depending on the application. It is interesting that for all three lenses the second surface is preferred to the fourth.

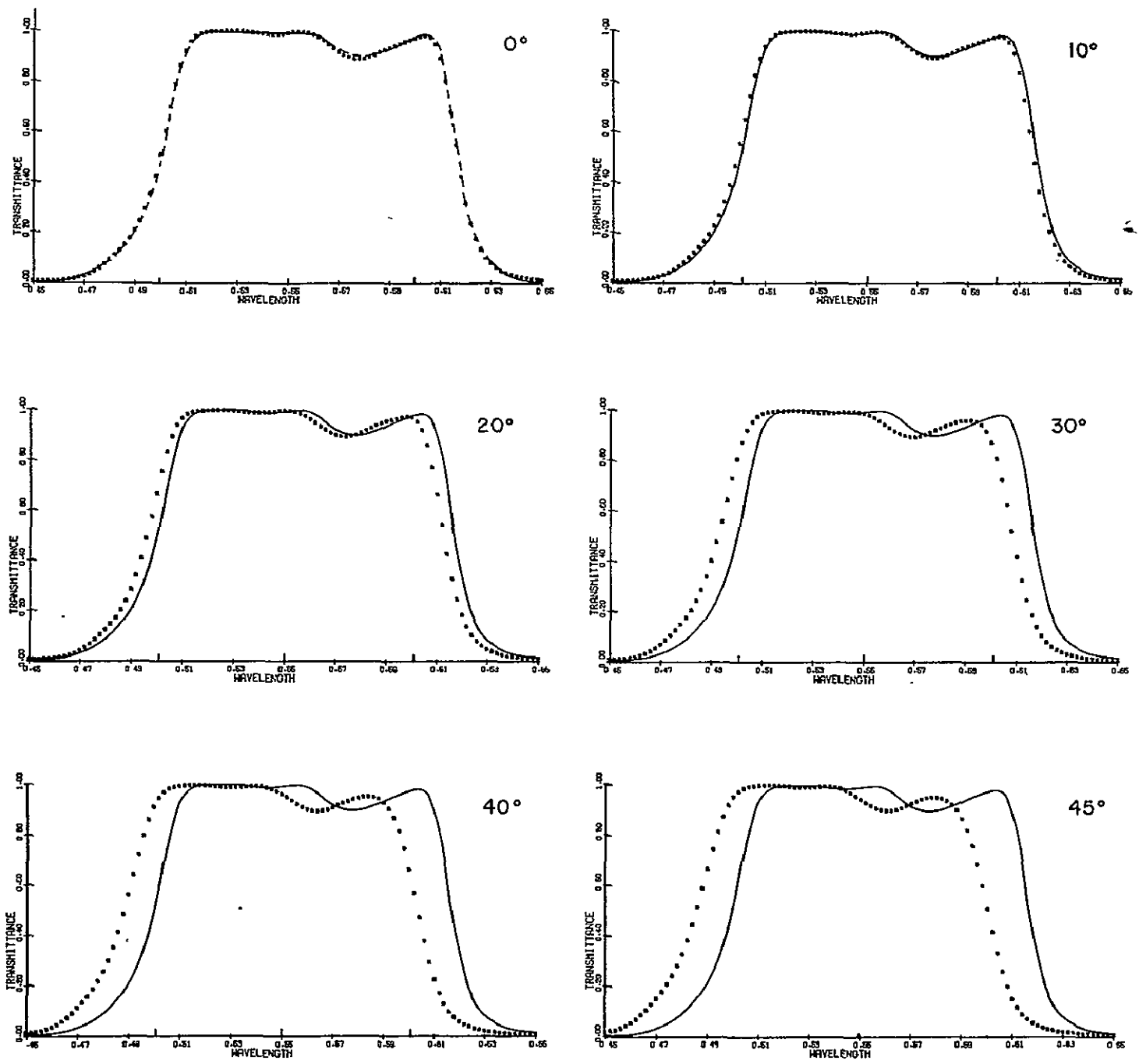

Fig. 6. These six pages show the spectral transmittance of an accordion filter located on the 2nd and on the 4th surfaces of the Geocon IV, Paxar, and Pleogon, for six semifield angles and for full aperture. (Wavelength scale is in μm.)

In the case of 0° field angle, the spectral transmittance of the filter on the lens surface (. . . . .) is compared with the transmittance that would result if the filter were on a flat surface (- - - - - - - -) at normal incidence.

GEOCON — SURFACE 4

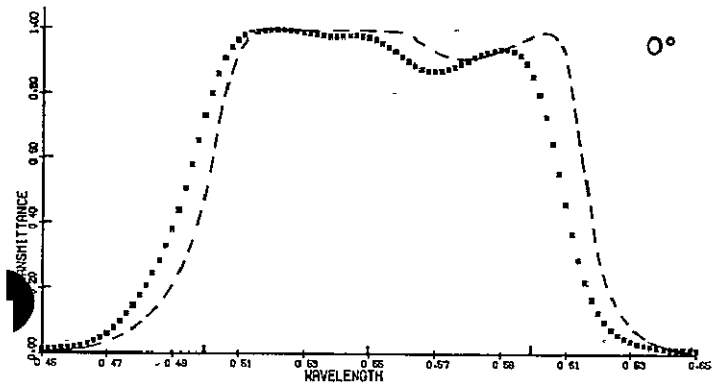

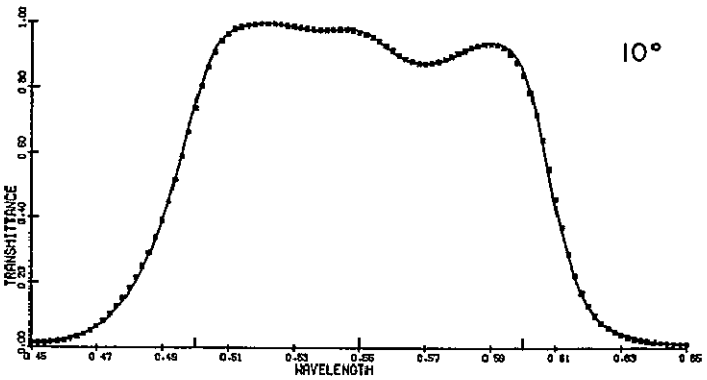

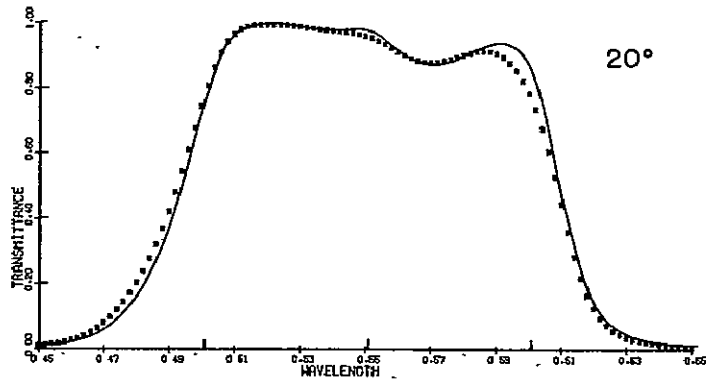

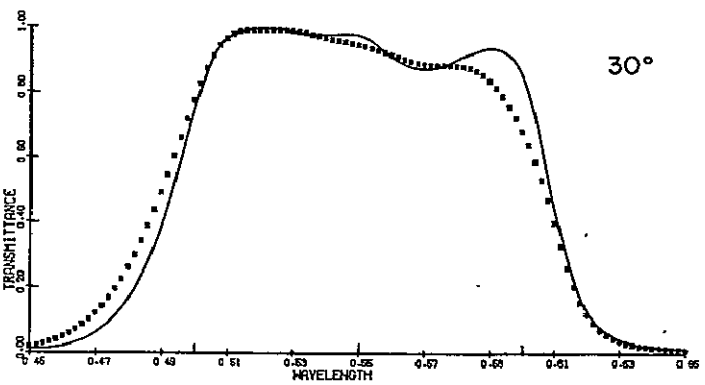

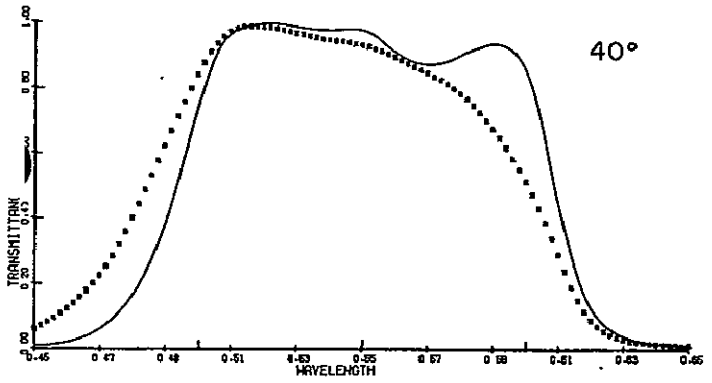

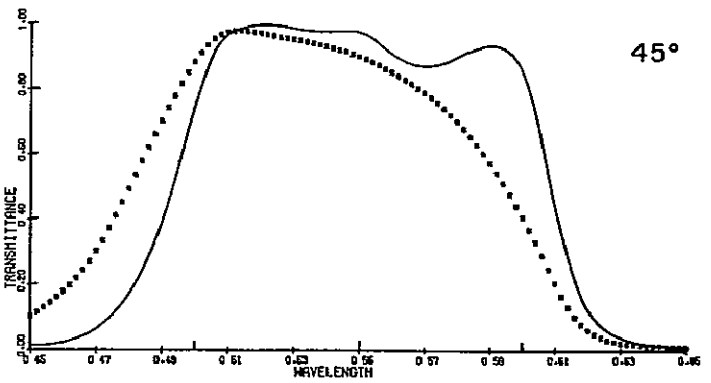

In the other five cases, the transmittance of the filter on the lens surface at the semifield angle indicated (- - - - - - - -) is compared with that at 0° (————————) to indicate the shift of the passband.

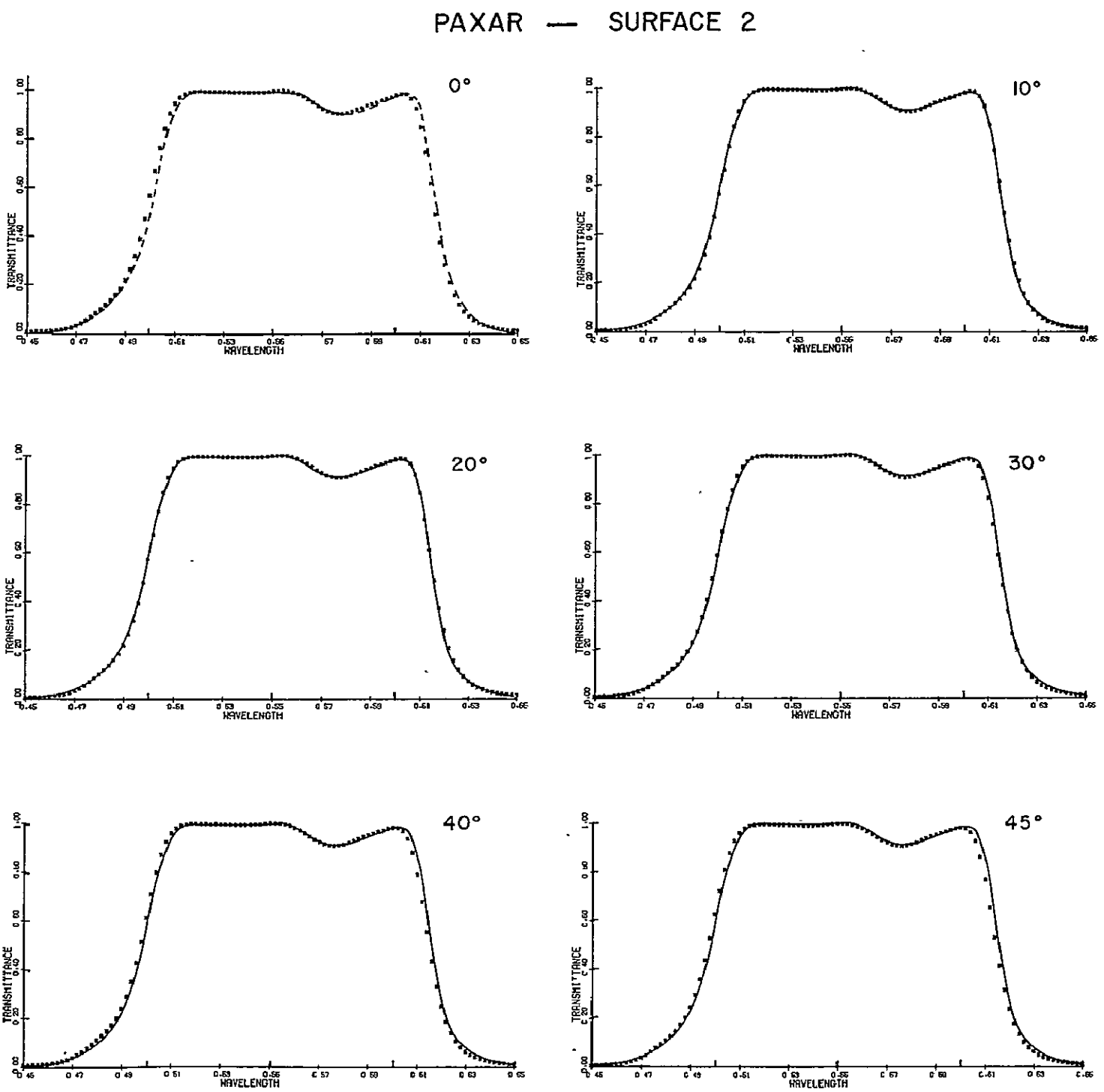

Fig. 6, continued

▪ ▪ ▪ ▪ ▪ ▪ Accordion filter on surface at semifield angle indicated

- - - - - - - - Accordion filter on flat surface, normal incidence

———— Accordion filter on surface at 0° field angle

PAXAR — SURFACE 4

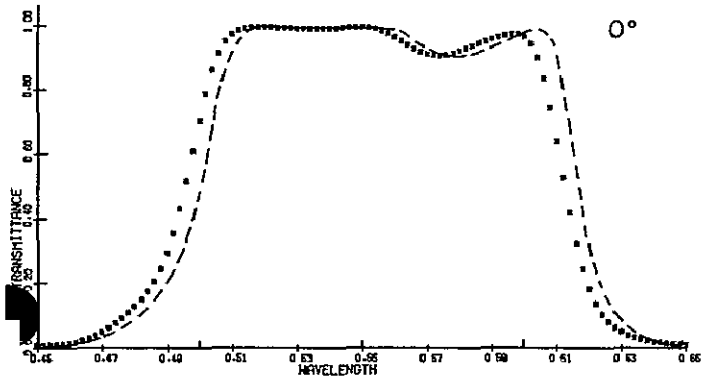

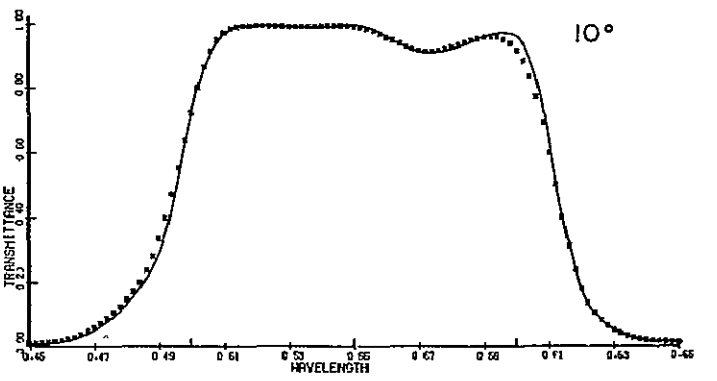

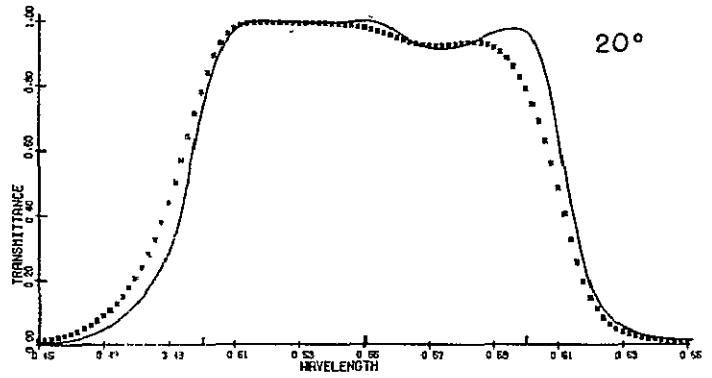

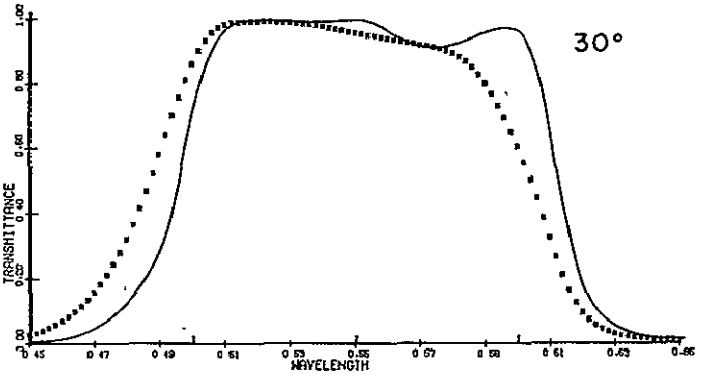

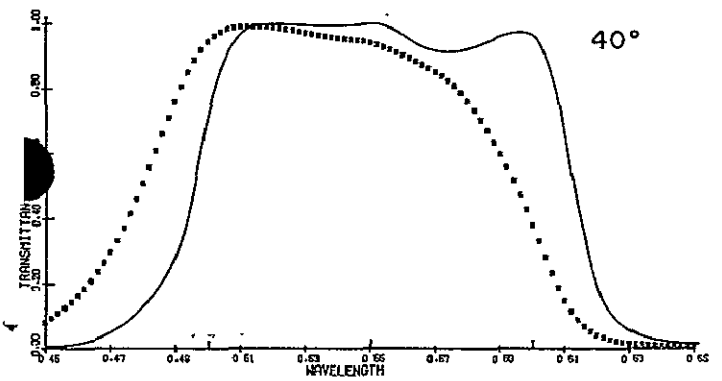

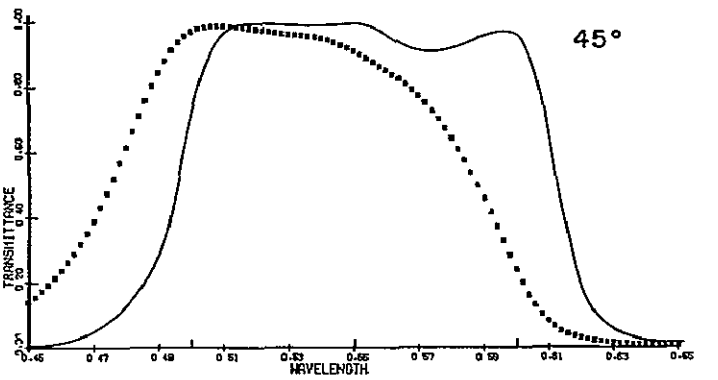

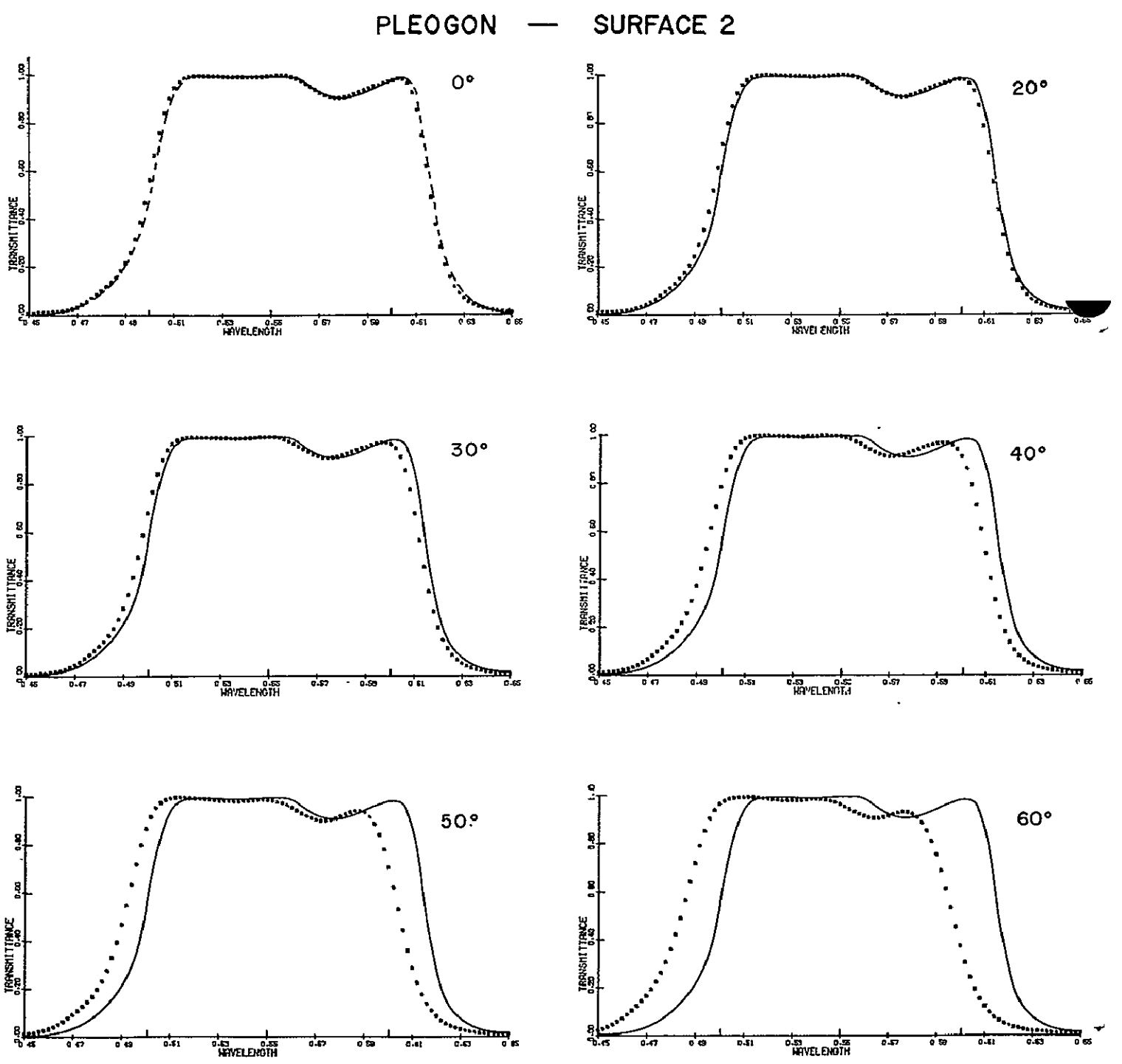

Fig. 6, continued

▪▪▪▪▪▪ Accordion filter on surface at semifield angle indicated

- - - - - - - - Accordion filter on flat surface, normal incidence

———— Accordion filter on surface at 0° field angle

PLEOGON — SURFACE 4

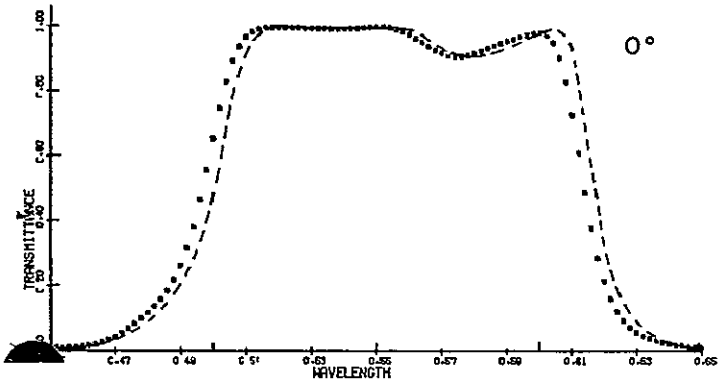

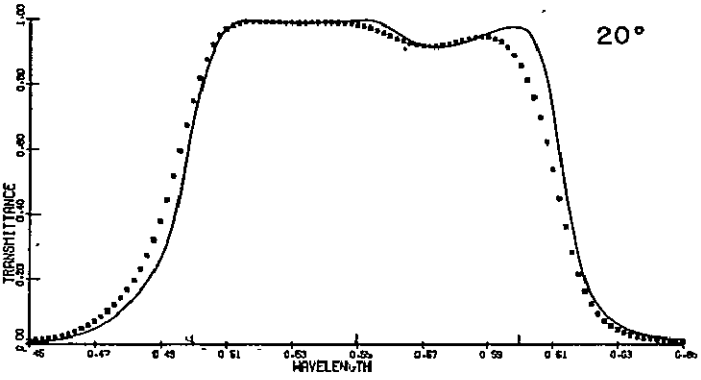

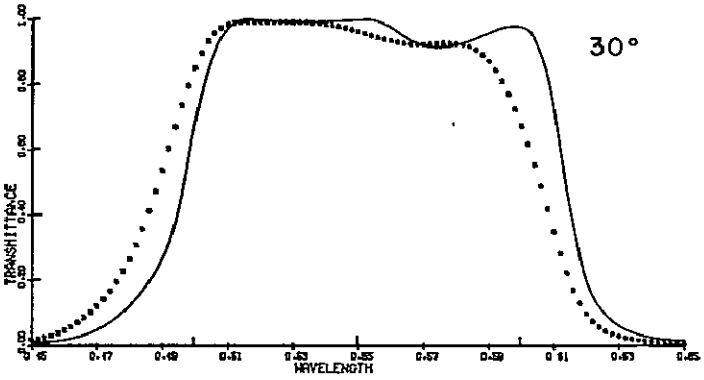

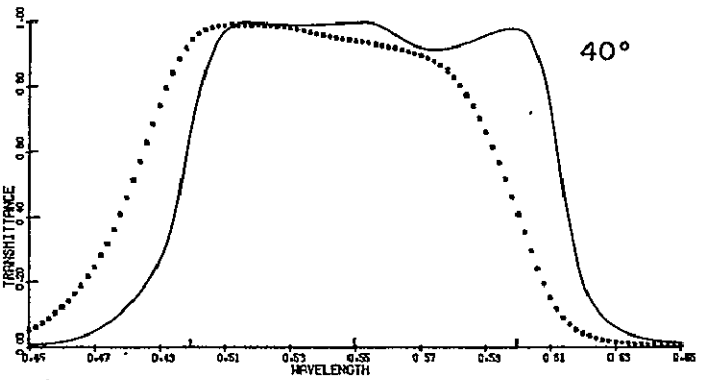

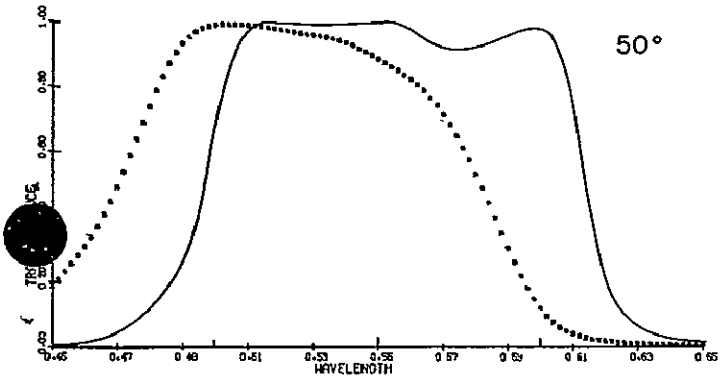

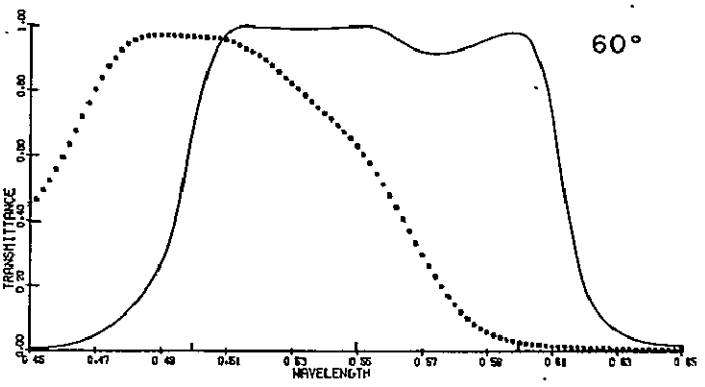

The graphs for the Geocon (pp. 6 and 7) indicate that the two surfaces modify the spectral transmittances in different ways. In the case of the second surface, the *shape* of the passband remains remarkably constant with change in semifield angle, while the passband *position* changes. In the case of the fourth surface, the *shape* of the passband changes noticeably, while up to 30° the change in *position* is small.

By reference to Fig. 3, below, we can quickly compare the shifts in the half-power points at the long wavelength cutoff of the filters. Again, the second surface of the Paxar is clearly the most suitable surface. The results for the Geocon illustrate an interesting point. Up to 30°, coating of the fourth surface is preferred to coating the second, but between 30° and 45°, coating of the second surface is preferred.

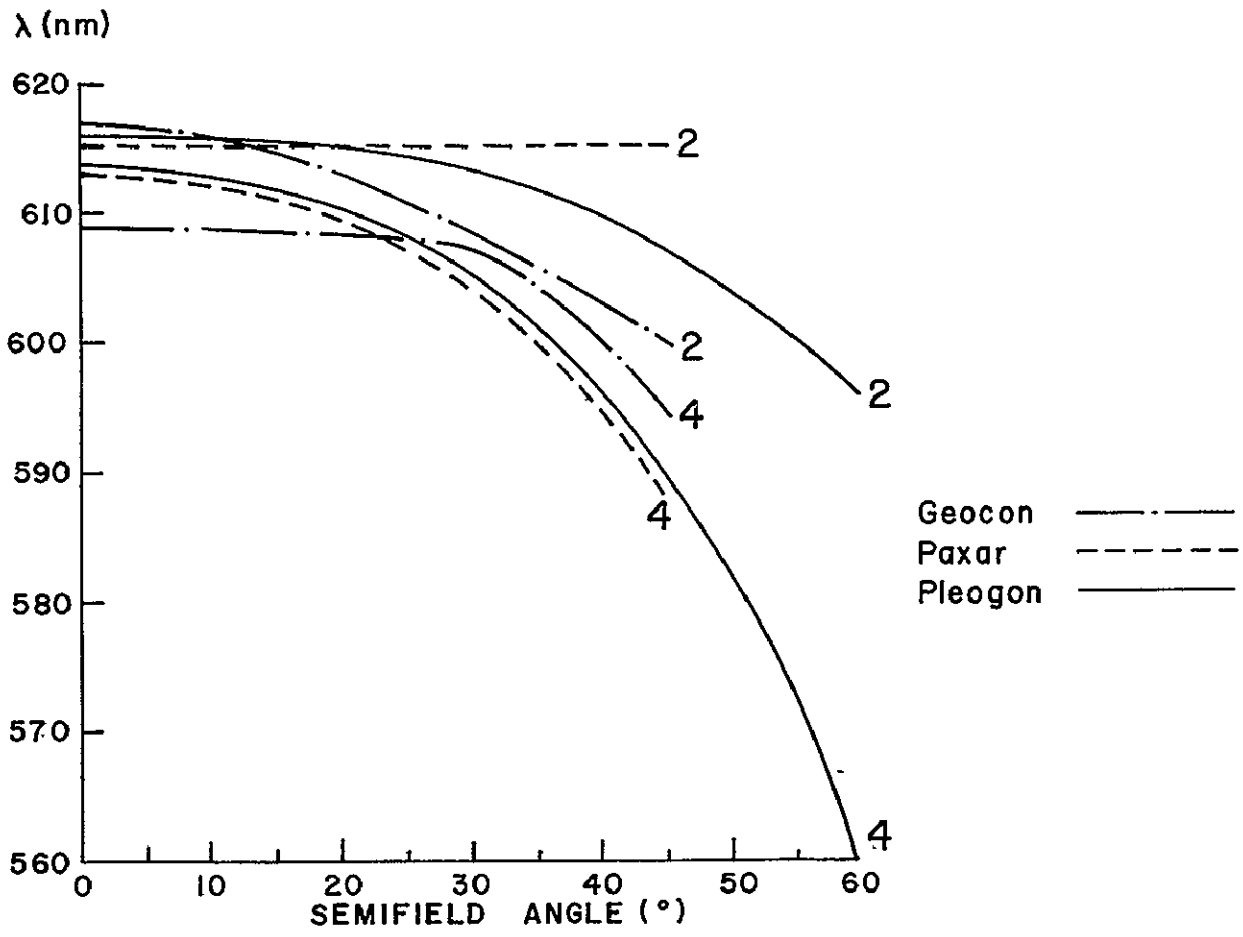

Fig. 7. Plots of λ against semifield angle for the 2nd and 4th surfaces of the three lenses; λ is the wavelength of the half-power point at the long-wavelength cutoff of the filter.

CONCLUSION

The results of this study indicate that some modern wide-angle aerial lenses can be used with wide passband interference filters if the filters are deposited uniformly on a selected lens surface. Of particular interest is the Paxar, four of which are being used with different Schott color filters in a multiband camera as part of NASA's Earth Resources Aircraft Program. It should be possible to improve the performance of this system, in terms of speed and spectral selectivity, by removing the Schott filters and coating each of the second surfaces with the appropriate accordion filter.

More generally, we believe that by tracing a meridional fan of seven rays across the full-aperture at the maximum field angle, we can select the best surface in a wide-angle lens for coating with an accordion-type filter. In the three cases examined in this study, we found that an upper and lower marginal ray trace was sufficient. The surface then selected is the one with the smallest value for its maximum angle of incidence.

REFERENCES

Badgley, P. C., A. P. Colvocoresses, and C. D. Centers, 1968, "NASA Earth-sensing space flight experiments," *Photogrammetric Engineering* 34(2):162-167.

McKenney, D. B., 1969, "Method for computing properties of interference filters on curved surfaces," *Optical Sciences Center Tech. Rept.* (in preparation).

McKenney, D. B., and P. N. Slater, 1968, "Interference filters for multispectral photography," *Optical Sciences Center Tech. Rept. 25*, 37 pp.

Slater, P. N., 1969, "Multiband camera monograph," *Optical Sciences Center Tech. Rept. 44*, 74 pp.

Stavroudis, O. N., and L. E. Sutton, 1965, "Spot diagrams for the prediction of lens performance from design data," *Nat. Bur. Standards Monograph 93*, 96 pp.

ACKNOWLEDGMENTS

The authors wish to acknowledge the assistance of Barbara A. Fell and G. W. Wilkerson in initial ray tracing and computer programming.

This work was supported mainly under contract NAS 9-7081 from the National Aeronautics and Space Administration. Mr. G. L. Kraus of the Manned Spacecraft Center, Houston, is the technical monitor. General support was provided from contract FO 4695-67-C-0197 from the U. S. Air Force.

SECTION 29

MULTISPECTRAL VIEWERS

Edward Yost
Long Island University
Greenvale, New York

INTRODUCTION

A multispectral viewer is an instrument for use in the intrepretation of multiband "black and white" photography. Using two or more spatially identical photos, the device produces a single color presentation by projecting the image of one photo on top of the other, using different color light sources. This technique of remote sensing permits a scientist to select a particular set of bands within the near ultraviolet-visible-near-infrared spectrum and interpret the results from a single color presentation. In addition, a multispectral viewer provides the scientist with the capability of altering the color of the presentation in order to enhance the particular relationships he may be seeking. Fundamentally, the multispectral technique allows the scientist to create a color film specifically for the purpose of his discipline and interests. [1-4]

There are three catagories of problems associated with multispectral photographic techniques which have been distinguished. These are:

1- The existance of instrumentation errors in multiband cameras which can seriously affect the accuracy of the image reconstituted by the multispectral viewer. The most important of these sources of error is lack of good quality image registration resulting from differential positioning of the same image on the set of multispectral positives used in projection. Such lack of good registration in the composite color image can be caused by: differences in focal length and differential distortion of the lenses in the multispectral camera array; angular variation of the optical axes of the cameras with respect to each other; differences in shutter actuation of the individual cameras when the camera platform is undergoing rapid angular motions.

2- There is an absence of accurate spectral reflectance data taken in situ correlated with the dynamic environmental variables such as variation in solar illumination, atmospheric scattering and absorption of radiation. As a consequence, it is difficult to predict if subtle chromatic differences will be exhibited in the

multispectral additive color image for the same earth resource phenomena photographed at different geographical locations at different times of the year.

3- There exist relationships in the processing and printing of photography such as: the dependence of image density on wavelength of radiation, variation in gamma and reciprocity failure which are not fully understood in relation to the resultant chromaticity of the additive color image. It also should not be overlooked, that in theory, while a unique reflectance spectra exhibited by an object will produce a unique color, the inverse is not true. Identical image colors may be produced by an infinite number of different reflectance spectra. Multispectral photographic techniques have been remarkably successful at circumventing this physical law of nature.

ADDITIVE COLOR TECHNIQUES

For the purposes of analysis of the operation of multispectral additive color viewers, let us assume that we have a set of four negatives taken in different bands of the spectrum; each negative being taken at the same instant by cameras having matched lenses, the optical axes of which were normal to the film plane producing four spatially identical negatives. Thus, all images will be in identical coordinate positions as measured from the principal point of each negative (the intersection of the optical axis with the film plane). When the film is processed and viewed on a light table, the set of spectral negatives will appear to be identical except that the densities of the same image may differ between them. This density difference is caused primarily by the selective spectral reflectance of ground objects, a fact which, in the visible spectrum, accounts for their apparent color.

Color is an effective means of discriminating density differences between similar images which appear on sets of multispectral negatives. This can be accomplished using additive color techniques first demonstrated by Clark Maxwell over 100 years ago. By projecting positives of each spectral negative on to a screen in such a fashion that one is registered upon the other (using a different colored primary light source for each), a composite color rendition of the scene is formed.

Conceptually, color may be defined as that conscious sensation which is exhibited when light of a specific spectral energy distribution enters the eye. It has been experimentally shown that differences in this energy distributior cause variations in the observed response of the eye and may be described in terms of three distinct psycophysical

variables. The first is hue which is basically that quality of color which leads to the definition of an object as being red, green, yellow, etc. As white light is dispersed by a prism, it is broken up into a multitude of hues each one of which may be related to a corresponding value of wavelength producing a so-called dominant wavelength which in turn enters the eye to produce the sensation of hue. Saturation, the second quality of color, is described as the amount of white in a given hue. It may be also considered as the concentration of the color. For instance, it is the difference between red and pink. As the amount of saturation in a color decreases, it approaches pure white. Brightness, which is the third variable of color, is described as the amount of visible energy contained in a certain hue which is saturated to a specific value. For example, the color royal blue, is identical to the color navy blue except that navy blue has a lower brightness value.

It has been estimated that the human eye can differentiate between 7,500,000 and 10,000,000 color differences over its sensitivity range.[5,6] For scientific purposes, it is impossible to use subjective terms for the unambiguous description of a color. The human eye is a relatively insensitive instrument when used to uniquely describe the appearence of an object with respect to its color. It is for this reason that a mathematical conception of the three variables defined above has been employed to describe that response (by the eye or any other recording instrument) to the stimulus known as color. We may envision these three variables of hue, brightness and saturation with the aid of a three dimensional color solid shown in Figure 1. It consists essentially of a solid cone standing on its apex with the hue positioned around the periphery of the solid, the saturation existing somewhere along the line connecting the center or white point with a particular hue and the brightness varying with position along the vertical axis. More precisely, the color solid is not a cone, but rather a rounded triangle. A horizontal slice through this solid, perpendicular to the brightness axes is known as a chromaticity diagram and is shown in Figure 2, in which certain colors have been identified. In order to pictorially describe the exact hue, brightness and saturation levels of a color, it is first necessary to determine the brightness level, place an orthogonal plane through the color solid at that level and determine the hue and saturation in this plane.

It should be emphasized that the mathematical study and description of color, which is known as colorimetry, only indicates the specific values of hue, brightness and saturation which are being measured and not the energy distribution of the color as a function of wavelength. The theory of colorimetry is based upon the concept that any color can be matched by some combination of three given colors or primaries. However, it has been demonstrated that there does not exist a single set of primary filters which can yield every color. In multispectral photography, a judicious choice of (camera) filters must be selected depending upon the spectral reflectance and the general domain of colors which are to be reproduced. For the reproduction of true color using additive methods, the primary colors shown in Figure 3, which are red, green and blue, have been selected for two distinct reasons. First, it is desirable to maximize the area of the inscribed triangle since only those colors within that triangle may be reproduced by a combination of the three primaries. Secondly,

the triangle is conventionally positioned so that one side lies close to the locus of the pure spectrum of the green-yellow-red colors since these colors appear in nature but the pure spectrum colors in the cyan portion of the chromaticity diagram do not.

The trichromatic system of color definition is a calculation of the faractional components of spectrally defined red and green primaries (referred to in colorimetry as the tristimulus values) for a given color. They are designated as x and y respectively and are known as trichromatic coefficients. These represent the percentage of standard red and green primaries required to produce a hue and saturation match to the color. A third value, Y, represents the luminance or brightness level of the color. The standard chromaticity diagram is a plot of the color in terms of x and y. The dominant wavelength of a color is determined by the intercept of the spectrum locus with the line which connects the illuminant point (the white point) and the color itself. The relative distance between the white point and the color and, the spectrum locus is the saturation.

When analyzing the image reproduction characteristics of a multispectral viewer, colorimetric measurement is a useful tool particularly in removing any anomalies associated with the visual response of the observer. The visual persceptibility of differences in the C.I. E. chromaticity diagram are shown in Figure 4. Generally, colors which appear identical on a viewer screen to an observer, will not exhibit the same energy distribution and may indeed be quite different spectrally. The advantage in using a trichromatic measurement of an image is that the resultant color measure is completely dependent upon the psyco-physics of the situation without any side effects of the human eye such as simultaneous contrast enhancement.

Often, the chromaticity of an image and the background in which it is embedded lie reasonably close when plotted in the color solid. When this is the case, it is often judicious to employ a set of color projection filters which bear no resemblence to the taking filters in the multispectral camera array, but which have the effect of increasing the apparent chromatic difference between the image and its background. This so-called false color space can be made as distinct as the image densities on the transparencies permit. The use of broadband filters in the camera which overlap along the wavelength scale, may make it impossible to chromatically separate an image from its background. Frequently in such cases, a set of narrow band filters in the multispectral camera array,which are spectrally non-overlapping,produce image densities of sufficient difference to give a marked color difference when reconstructed on a multispectral viewer.

LONG ISLAND UNIVERSITY VIEWER

The multispectral viewer shown in Figure 5 is a hardware embodi-

ment of these additive color principles. It is a console which displays a rear projection screen to the operator. Optically, the viewer is an analog of the multispectral camera array. The basic principle of this device is the utilization of preregistered sets of multispectral positives on a single roll of film. In this way registration is maintained as the operation proceeds from one multispectral presentation to the next. The four multispectral film images, each with its independent illumination system, are superimposed onto the viewer screen at a three times magnification and in precise registration, using the optical design shown in Figure 6. Misregistration of one image upon the other, when projected on the viewer screen, is not greater than .1 millimeter anywhere in the presentation, so that no blur will be discernable at a viewing distance of 18 inches. The fixed magnification projection system utilizes four, five inch focal length, f/4.5 lenses. These lenses are critically matched so that their equivalent back focus dimensions are within a few thousandths of an inch of each other. The differential distortion of the projection lens is matched in a unique way. As shown in Figure 6, a different part of the field angle of each viewer lens is used to project the image. This requires that the distortion of the lenses be different across their whole field but matched for all field angles associated with conjugate images.

Each of four images projected on to the viewing screen has its own dual illumination system which is also shown in Figure 6. This viewer utilizes 3200 degree Kelvin lamps which have the advantage of being quite bright with the appropriate filament configuration to best fill the apeture of the projection lens. The brightness illumination passes through a neutral density filter, a spectral filter, a beam splitter and a condensing lens to illuminate the positive spectral photo. The greatest loss in energy throughout the system occurs through the spectral (or color) filter. The second half of the illumination system is set at 90 degrees to the brightness lamp and is employed for purposes of desaturation. Its illumination is reflected from the beam splitter and is added to the brightness illumination as modified by the color filter. The filters associated with the brightness illumination system controls the hue and brightness while the addition of a desaturation selection provides the photo-interpreter with complete control over the displayed color.

Film flattening is provided by two optically polished glass plates, one of which is fixed to the viewer itself and is considered the focal plane or object plane of the viewer optical system. The other is mounted off the carriage through a spring loaded cam mechanism. This movable plate is raised off the fixed glass platen by means of a foot pedal during the transport of the film. This mechanism insures separation of the plates and avoids film scratching. A film guide is also provided to insure an even transport of the unitary film containing the four individual formats in the horizontal plane, thus maintaining the registration. The ability of the device to maintain registration of the imagery as the interpreter progresses from one multispectral image to the next, is completely dependent on preregistration of the set of associated multispectral photos on a single 9 1/2 inch roll of film.

Experience has indicated that the most satisfactory screen material for general rear projection viewing is a white Polacoat Lenscreen. Although other screens (such as the Kodak Dayview Screen) provide a somewhat brighter image, the falloff with incident obliquity is more pronounced and the resolution capability is somewhat less. It was noticed however, that with the type Lenscreen used, considerable color infidelity existed when photographic reproductions of the multispectral viewing screen were attempted. A recently developed type of plexiglass Lenscreen, which is designed specifically for exposing accurate color photographs of rear projected scenes has been used for photographic reproduction of the screen image.

The multispectral viewer projects four multiband images contained on a single piece of film (each one of which has a resolution of 45 line pairs per millimeter) at a magnification of 3 times, this results in a screen resolution of about 15 lines per millimeter. Since the average eye resolves seven lines per millimeter at a normal 18 inch viewing distance, a permissable misregistration which does not exceed .0056 inches has been specified and designed into the camera-viewer system. Each projection lens has its own birghtness lamp and filter set which illuminates one of the spectral records as well as a desaturation lamp. By placing various combinations of projection filters into the optical path and by linear transportation of a filter rack, the scene on the viewing screen appears in color. An important feature of the system is that it frequently enables, through proper choice of camera and viewing filtration, the detection, recognition and identification of objects by color differences which would not otherwise be visible.

THE EFFECTS OF PHOTO PROCESSING ON IMAGE COLOR CHARACTERISTICS

The chromatic characteristics of the multispectral image formed in additive color on the viewer screen are significantly affected by the photo processing techniques used. The relationship of exposure (or its radiometric equivalent) to density on both the negative film used in the camera and the positive transparency printed for projection in the viewer is a critical consideration. Also a significant parameter, often overlooked, is the maximum and minimum density of the duplicated positive image.

The fundamental relationships of the additive color image are examined in some detail in order to present to the reader the significance of photo processing and how errors associated with processing may be reduced or eliminated. Specific examples, experimentally obtained, are included to demonstrate salient points.

When a multiband negative is properly exposed and processed to a gamma of 1.0, a one to one correspondence will be created on the linear portion of the characteristic curve between the radiation reflected by an object and the corresponding density of the image on the film. Fre-

quently however, as will be demonstrated, a gamma considerably greater than unity is necessary to chromatically differentiate objects whose spectral signatures are nearly similar.

An ideal set of multiband negatives will reproduce a gray scale target having uniform spectral reflectance and which is illuminated by a uniformly distributed source of radiation so that the image density of each gray scale is the same on every one of the individual multiband negatives. This exact matching of exposure and gamma in the different spectral bands which are used is very difficult and frequently not possible.

The difficulty in exactly matching the exposure density relationship (the characteristic curve) is due partially to the effect of the wavelength of radiation which strikes the photographic emulsion. When one film type is used to expose all four spectral bands of distinctly different wavelengths, in general the characterisitic curve associated with each band will be different. This condition is unfortunately encountered even in panchromatic emulsions. This effect is shown in Figure 7, in which the characteristic curves for Infrared Aerographic film (5424) exposed with the filters transmitting blue (395 to 510nm), green (480 to 590nm), red (585 to 715nm) and infrared(700 to 900nm).

The so-called Aerial Exposure Index (or speed) of photographic emulsions used in multiband photography also varies depending on both the spectral sensitivity and the filtration used. The Aerial Exposure Index is defined as .5 divided by the exposure (meter candle seconds) at the point where the shape of the characteristic curve is .6 times the gamma (the tangent of the angle made by the linear part of the curve and x axis). Figure 8 shows the absolute relationship of the characteristic curves and the differences in photographic speed for Aerographic infrared film (5424) using filters similar to those used in the experiment.

The careful reader will note that exposure is measured in photometric units (meter candle seconds) and hence is defined only for the visible spectrum. The exposure of the infrared band contains no visible light and is really not capable of definition in terms of photometric exposure. It has been the practice in infrared and ultraviolet aerial photography to use the fiction that the exposure in this non-visible region consists of the meter candle seconds of a standard energy source (Luminant C) which has a predefined spectral distribution of both visible and infrared radiation. This practice has the effect of making exposure calculations for the infrared bands extremely difficult to determine because of deviations of the spectral distribution of solar radiation from this standard. Accurate and unambiguous exposure can be obtained in multiband photography by using absolute radiometric units (such as watts per centimeter squared) in each spectral band.

It should be noted that the intensity of the energy which forms the image on the photographic emulsion of an airborne multispectral camera

does not depend on the distance between the object and the lens of the sensor. That is, when an object is at sufficiently large distance with respect to the focal length of the camera, the intensity of the radiation which forms the image is:

$$I = \frac{B\,\pi}{4\,f^2}$$

Where: B = incident intensity of radiation times the reflectivity of the object.
f = f/number of the lens

In obtaining actual multispectral photographs, the experimenter must also include the actual lens and filter transmission characteristics in the above equation.

PHOTOGRAPHIC TONE REPRODUCTION

In order to accurately represent to the human eye the reflected light from a particular ground scene, there must exist a one to one mapping of the object luminance into the density on the positive. Assume that the negative has been well exposed and processed to a particular gamma. A tone reproduction curve may be constructed to represent the fidelity with which combination negative and positive transparencies reproduce the brightness of the original ground scene. A typical tone reproduction curve is shown in Figure 9, which represents the fidelity with which the red spectral band reproduced the five step gray scale under noon illumination at Davis, California on 31, July 1967. Quadrant I of this figure shows the characteristics curve of the spectral negative. The densities on the negative of the displayed gray scales in the scene were measured and the target brightness in relative units related to the photographic exposure on the negative film. The corresponding characteristic curve of the positive transparency was obtained through similar measurement of the gray scale densities of quadrant II. Vertical lines from several points connecting the negative and positive characteristic curves are made to intersect a 45 degree transfer line in quadrant III. By extending horizontal lines from quadrant III to intersect vertical lines from the original negative curve of quadrant I, and indication of reproduction process is obtained. Thus, the locus of all intersected points from the negative and positive characteristic curves yield the tone reproduction of quadrant IV. For exact reproduction, the curve in quadrant IV should appear as a straight line. An indication of the reproduced departures from this norm are made by comparing the curve A with the curve B.

HOW IMAGE DENSITY IS RELATED TO COLOR

In order to create an additive color presentation from a set of black and white multiband photos, each photograph must be projected by an optical system, each using a different colored light source, onto a screen in such a way that the images are accurately registered with respect to each other. A different proportion of light will be present in the screen image depending upon the densities of the image on each multiband photo which is projected.

In establishing the relationship between density of individual black and white images and the color characteristics of the corresponding recombined image that is projected on the screen, consider three primary taking filters, blue (395 to 510nm), green (480 to 590nm), and red (585 to 715nm). When each multiband negative is exposed through one of these filters and processed to obtain a specific characteristic curve, the slope being the gamma, a positive image is then made by exposing the negative onto duplicating film and processing to obtain a specific relationship between the brightness of the ground scene and the density of the image on this positive transparency.

By projecting each of these multiband positives using similar primary blue, green and red filters to form the additive color presentation on a viewing screen, a "true color" rendition of the ground scene is created. The fidelity of the colors of the image compared to the object is not perfect. In order for the image to be a perfect reproduction of the color of the object, it would be necessary to photograph the images exactly as would be recorded by the stimulation of the visual repsonse mechanism of the human eye, shown in Figure 10. To date, it has not been possible to construct with complete fidelity, filters whose transmission could be duplicated by the response of a photo sensitive material and the illuminant falling on the scene such that curves are exactly reproduced. Due to the necessity to create a less than zero exposure, it is usually assumed that it is theoretically impossible to obtain absolutely perfect photographic color reproduction. These facts not withstanding, a very close true color reproduction of a ground scene is possible with the primary blue, green and red filters noted above.

As discussed previously, not all colors can be reproduced using one particular set of filters due to the shape of the color triangle created within the chromaticity diagram (see Figure 3). No difficulty will be encountered in reproducing colors whose dominant wavelengths lie close to the transmission peaks of the taking filters. However, in order to reproduce the colors of objects which reflect only dominant wavelengths associated with secondary colors yellow, and cyan, it is necessary that there exist a wavelength overlap between the taking primaries as shown in Figure 11. That is, the overlap region between the red and the green filter will yield the yellows and in similar manner, the overlap region between the blue and green filter will yield cyan color. The amount of overlap (in nanometers) indicates the spectral re-

gion in which the secondary colors can be reproduced. Fortunately, for true color reproduction, most colors in nature are composed of broadband, which cover a considerable wavelength range extending into wavelengths where the primaries transmit considerable amounts of radiation.

The reproduction of such secondary colors is also dependent on the camera exposure. Since the region of overlap does not possess the amplitude of transmission which the primary colors do, too short an exposure will render only the primaries visible. As the exposure time is increased, the secondary colors will become apparent.

In view of the foregoing discussion, the image density on each of the multiband positives can now be related to the additive color image which they produce:

1 Where the densities on all the multiband positives are equal, a condition of zero saturation exists. The image is a shade of gray (achromatic). This is due to the fact that the human eye sees equal amounts of blue, green and red, which are combined in the image as being white. The brightness or luminosity of the white color which is perceived depends on the total energy combined in the image.

2 The color of the image is a function of the ratio of the three colors which are projected to form it. Since the densities on each multiband photo are a logarithmic relation of the image forming energy, the chromaticity obtained is the weighted average of the three densities.

3 The additive color image will faithfully reproduce the color of an object at a gamma of one. Increase in gamma above unity will increase the saturation of the image color above that of the object. Conversely, a gamma less than unity will decrease the saturation of the additive color image.

4 The magnitude of the minimum density multispectral image establishes the brightness of the additive color image.

EXPERIMENTAL RESULTS

The theoretical considerations discussed above were empirically

evaluated using the Long Island University multispectral viewer. A four color target was placed on the ground along with a five step gray scale. Multiband imagery was obtained at 1000 feet altitude at Davis, California at 1130 PDT, 31 July 1967. The spectral bands were blue (395 to 510nm), green (480 to 590nm) and red (585 to 715 nm).

Since a calibrated gray scale was used along with the color panels, it was possible to relate the density characteristics of the image directly to the brightness of the ground scene by comparing the image density on the positive with the reflection density of the gray scale. In this way the fourth quadrant of the tone reproduction diagram was produced directly without the necessity of using the individual negative and positive characteristic curves shown in quadrants I and II of Figure 9.

Four reproductions of the viewer screen additive color image are shown in Figure 12. Each rendition has been created by the addition of the blue, green and red spectral bands to form a "true color" reproduction of both the color targets and gray scale on the ground. Each of the sets of spectral positives was processed and projected on the viewer screen so that the gray scale target remained achromatic (without color). The characteristic curves of the multispectral photography associated with these photographs (and hence the gamma) are shown in Figure 13. Note that longitudinal displacement of the green spectral characteristic curve away from the red and blue is compensated by the adjustment of the brightness when the image is projected in the additive color viewer. Non-linearity of the characteristic curve of the red spectral band (graphs A and B of Figure 13) presents a more serious problem. In cases where the slope of the characteristic curve (gamma) of the blue, green and red spectral positives differ, the color of an object will vary with exposure. For instance, a gray scale such as that shown in Figure 16 might typically be bluish at the dark end, gray in the center and reddish at the bright end.

Color measurement of the chromaticity of the four color images and the lightest gray scale is shown in Figure 14. Note how the color becomes more saturated (moves away from the center of the chromaticity diagram) as the gamma is increased. In all cases the image of the lightest gray scale has been placed at the chromaticity coordinate (WH) in the diagram by manipulation of the multispectral viewer controls. In theory, all the points should lie on a line from the center of the diagram. The deviations from such a constant dominant wavelength is probably caused by variations in processing, particularly in the red band, as previously noted.

An often overlooked aspect of color reproduction is the effect of the maximum and minimum density on the color of the image produced. The effect of reduced brightness as the maximum density is increased while the gamma is kept constant is shown in Figure 15. Relatively dark objects such as the green target panel and grass areas lose color first while brighter objects such as the yellow target and soil still remain relatively bright to the eye.

CONCLUSIONS

Multispectral additive color viewing devices can provide a practical method for extracting meaningful information from sets of multiband photography. However, this photography must be of exceptional quality in that the spatial poisitioning of all images with respect to their principal points must be accurate. In addition, there must be a good correspondence between the image densities on all the multispectral photography and the quantity of radiation reflected by an object in that particular spectral band.

The significant advantages of multispectral color aerial photography to environmental scientists has been demonstrated by controlled experiments. The ability to control image density and thus the color of the image in a multispectral viewer presentation is most significant. It is now possible to eliminate many instrumentation errors which have heretofore plagued the multispectral photographic technology.

REFERENCES

1. E. Yost & S. Wenderoth, "Precision Multispectral Photographic Evaluation for Earth Resources Application" in the Manual of Multiband Photography, R. Colwell, editor, NASA Manned Spacecraft Center(In preparation).

2. E. Yost & S. Wenderoth, "Multispectral Color Aerial Photography", Photogrammetric Engineering, Vol.33, No.9, (1967).

3. E. Yost & S. Wenderoth, "Additive Color Aerial Photography" in Manual of Color Aerial Photography, K. Smith, editor, American Society of Photogrammetry, (1968).

4. E. Yost & S. Wenderoth, "Ecological Applications of Multispectral Color Aerial Photography" in Remote Sensing in Ecology, P. Johnson, editor, University of Georgia Press (1969).

5. D. Judd, Color in Business, Science and Industry, Wiley, (1952).

6. D. Nickerson and S. Newhall, "A Psychological Color Solid", Journal of the Optical Society of America, Vol. 33, pp.419-422, (1943).

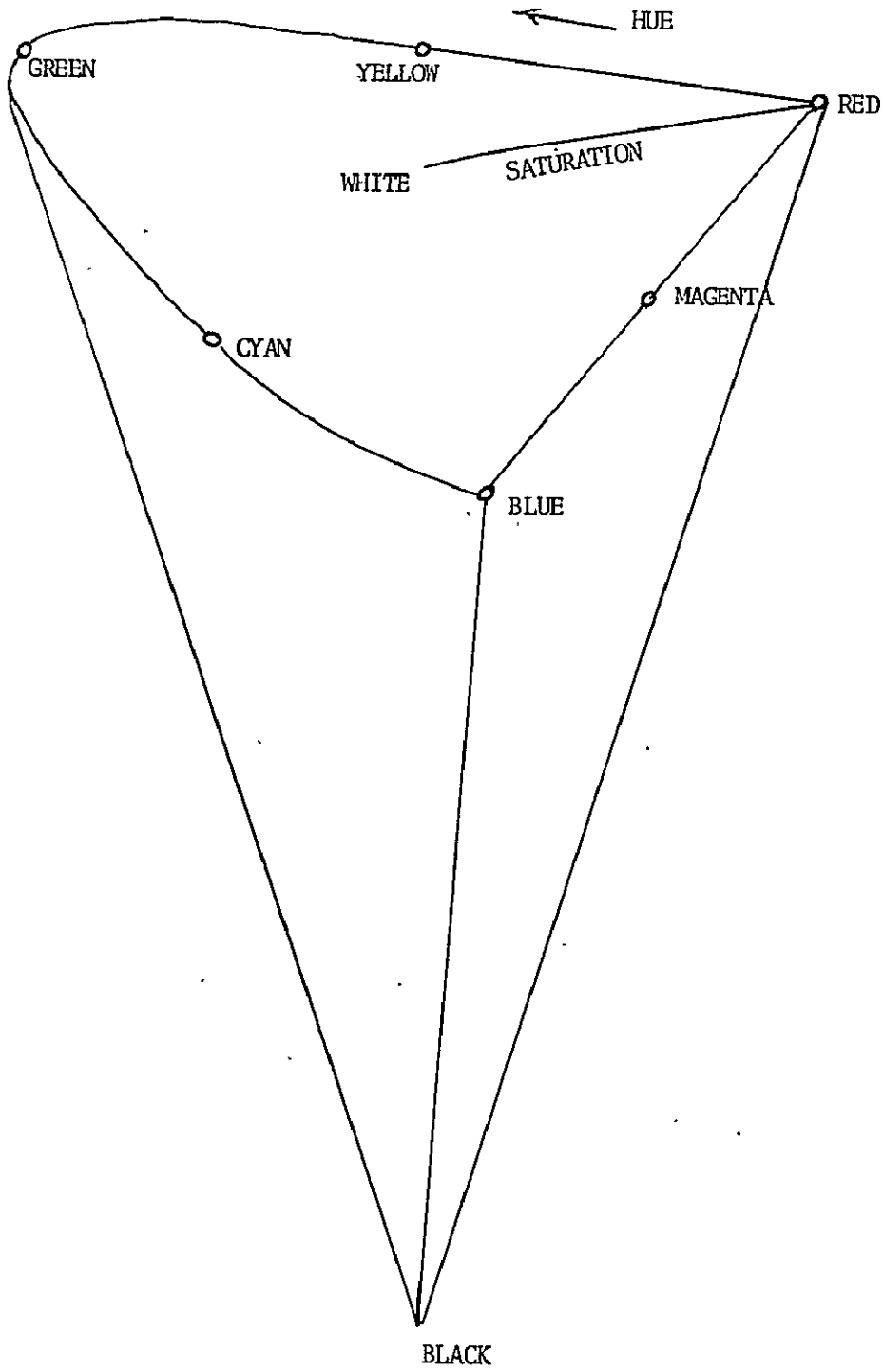

Figure 29-1.- Three dimensional color solid indicating the three variables of hue, brightness and saturation.

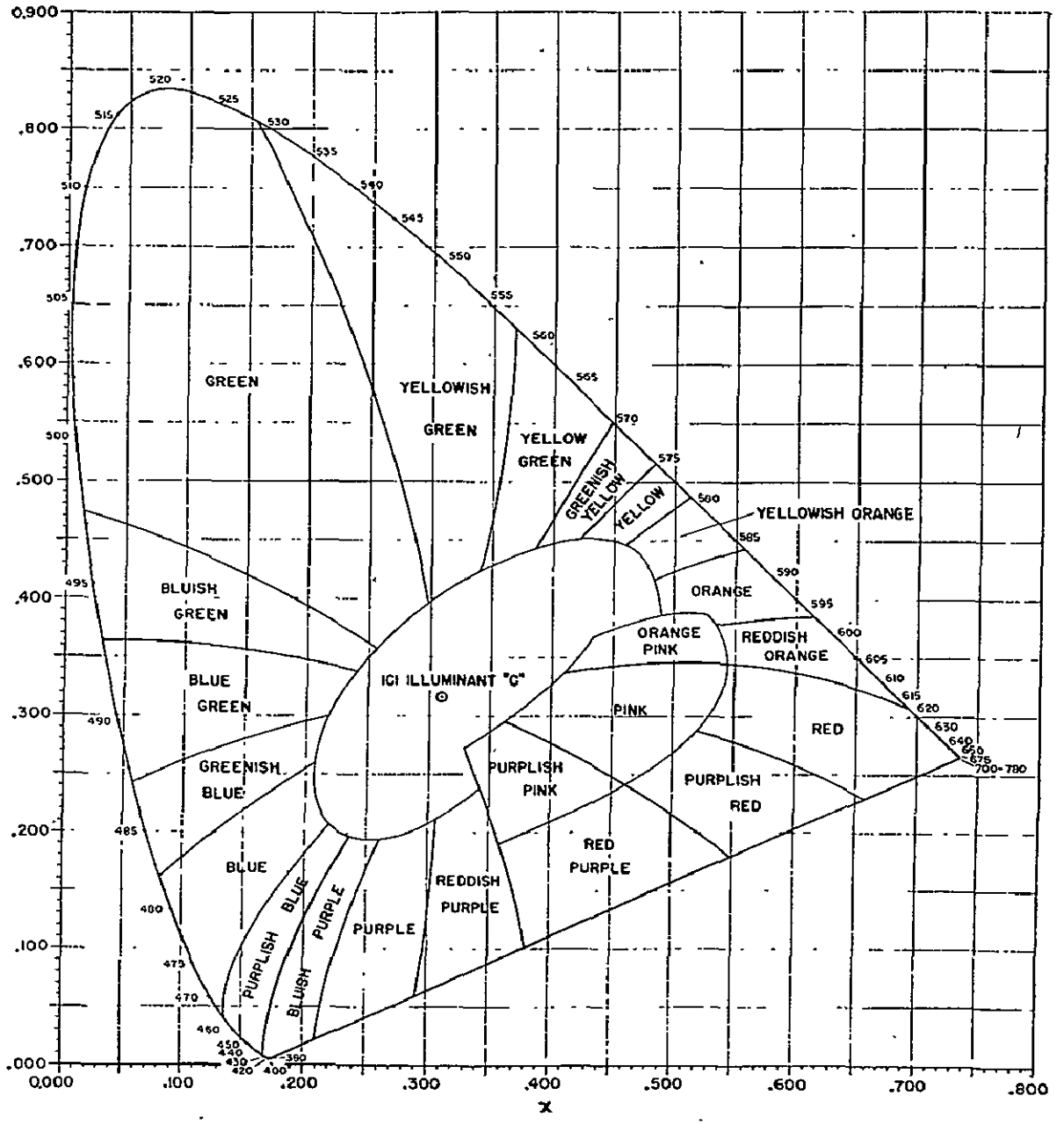

Figure 29-2.- The internation standard chromaticity diagram of the C.I.E. system.

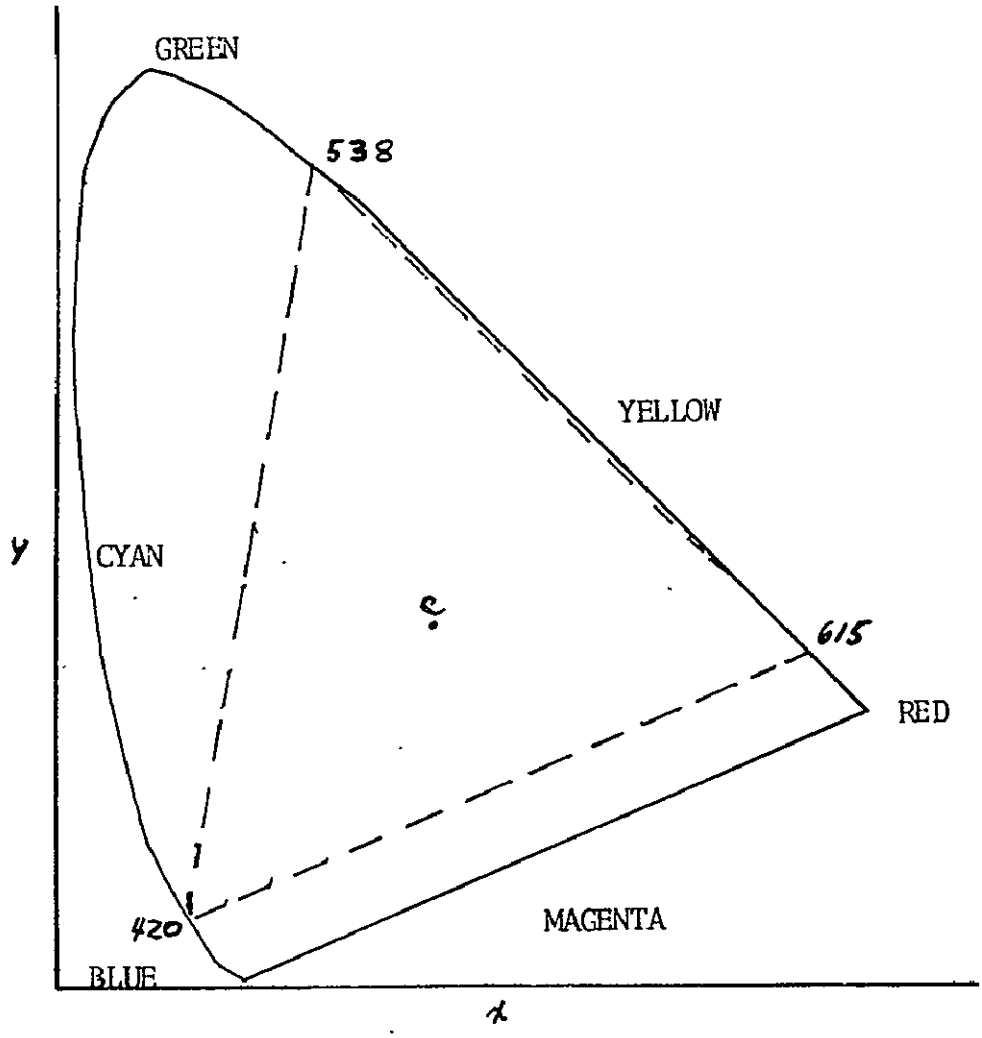

Figure 29-3.- Color triangle. All colors which lie on the border or inside the triangle can be reproduced by the primaries at its apices. Saturated cyan (to the left of the triangle) is rarely, if ever, encountered in nature.

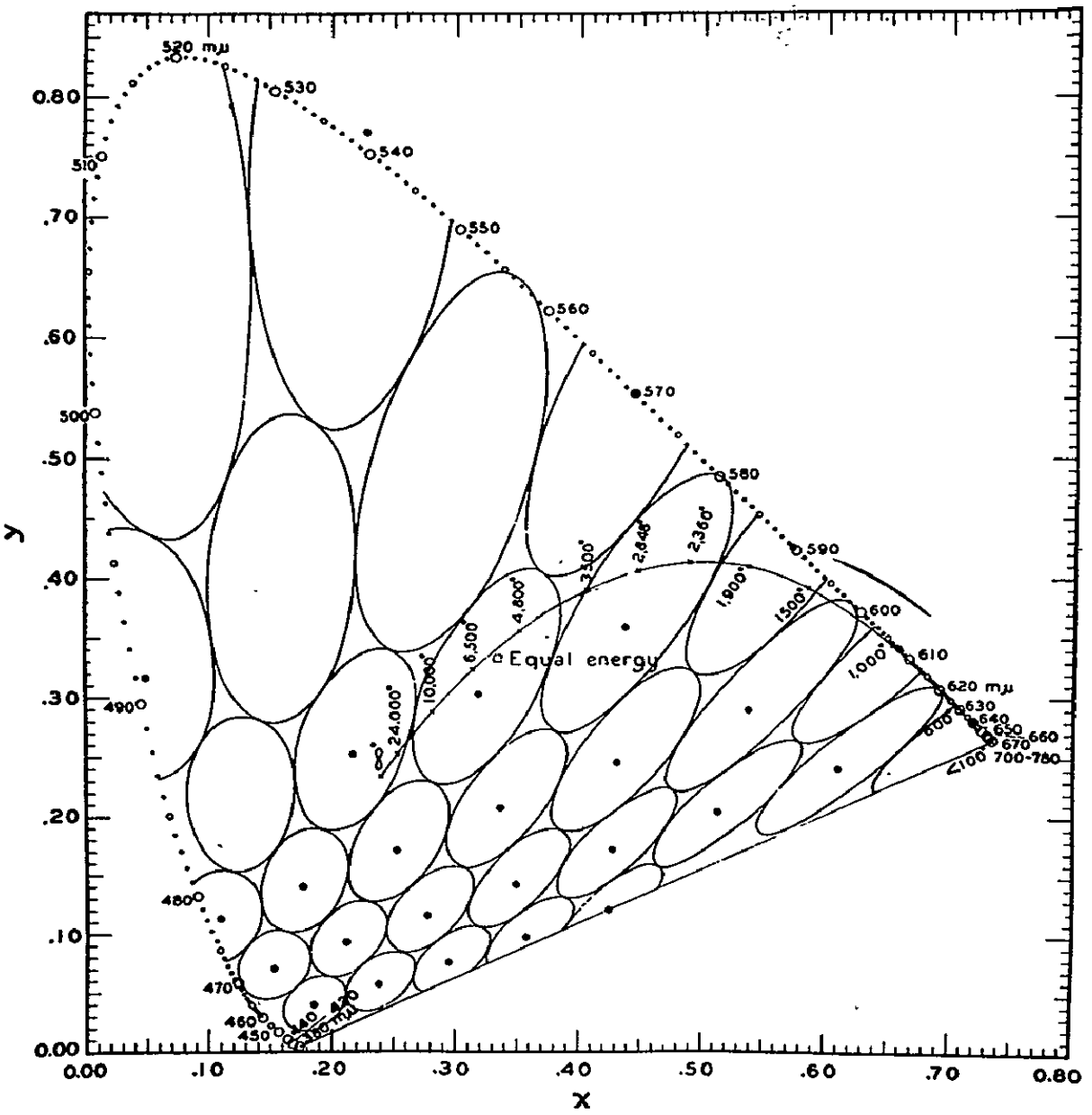

Figure 29-4.- Approximate perceptibility of chromaticity differences on the CIE chromaticity diagram. The distance from points on the boundary of each ellipse to the indicated point within it all correspond approximately to one hundred times the chromaticity difference just perceptible with certainty under moderately good observing conditions.

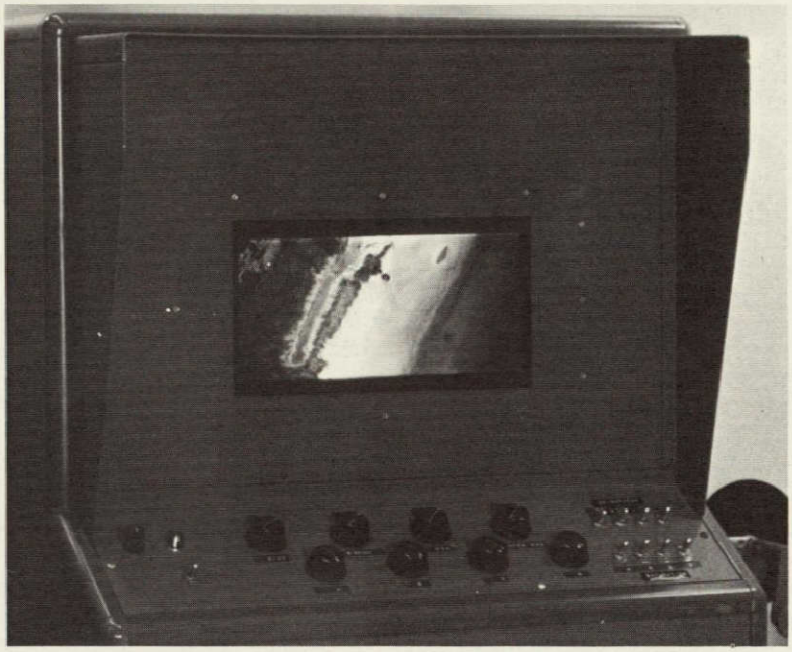

Figure 29-5.- Additive color viewer. Rear projection viewer superimposes four spectral photos taken by the camera creating a composite presentation in color.

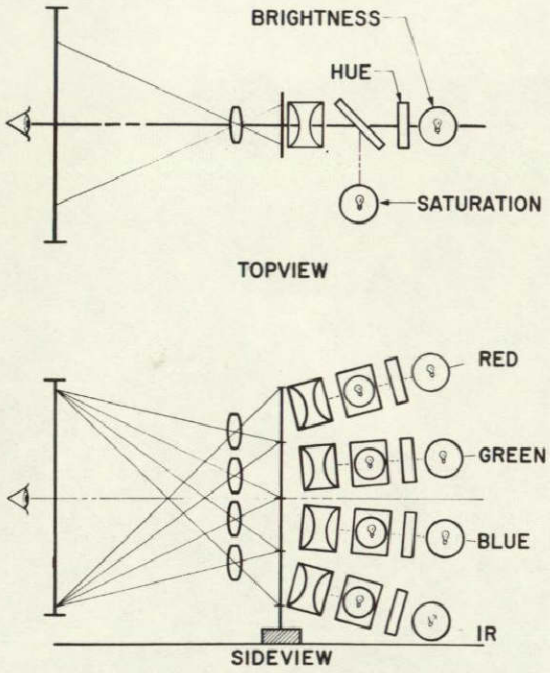

Figure 29-6.- Viewer optical system. The optical projection system of the viewer gives in registered superimposition all four spectral photographs on a rear projection screen. The illumination system allows the interpretor to control the brightness, hue and saturation of the image on the screen.

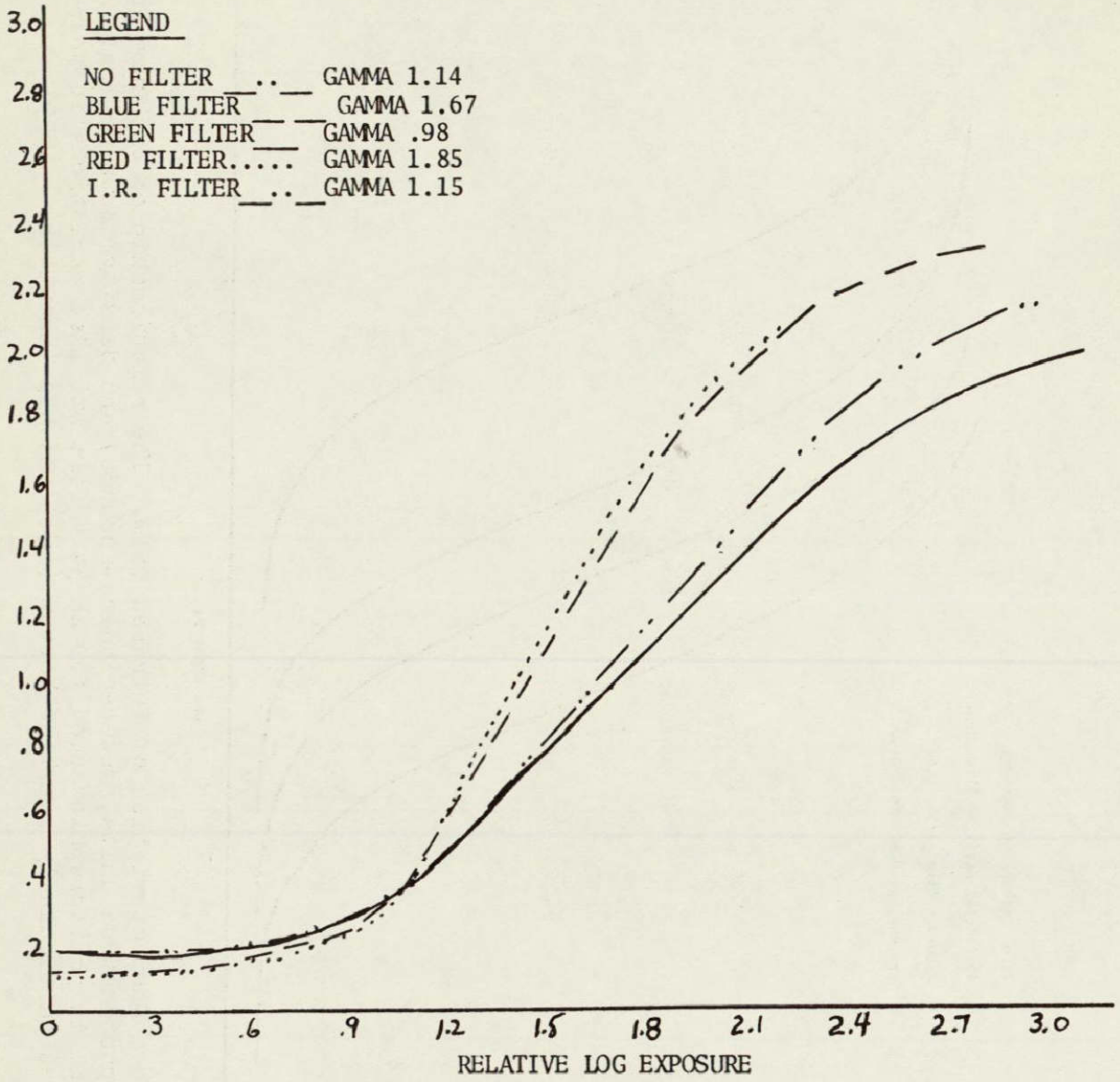

Figure 29-7.- Characteristic curves for infrared film (5424). Exposed with filters used in the experiment and matched at .6 Gamma.

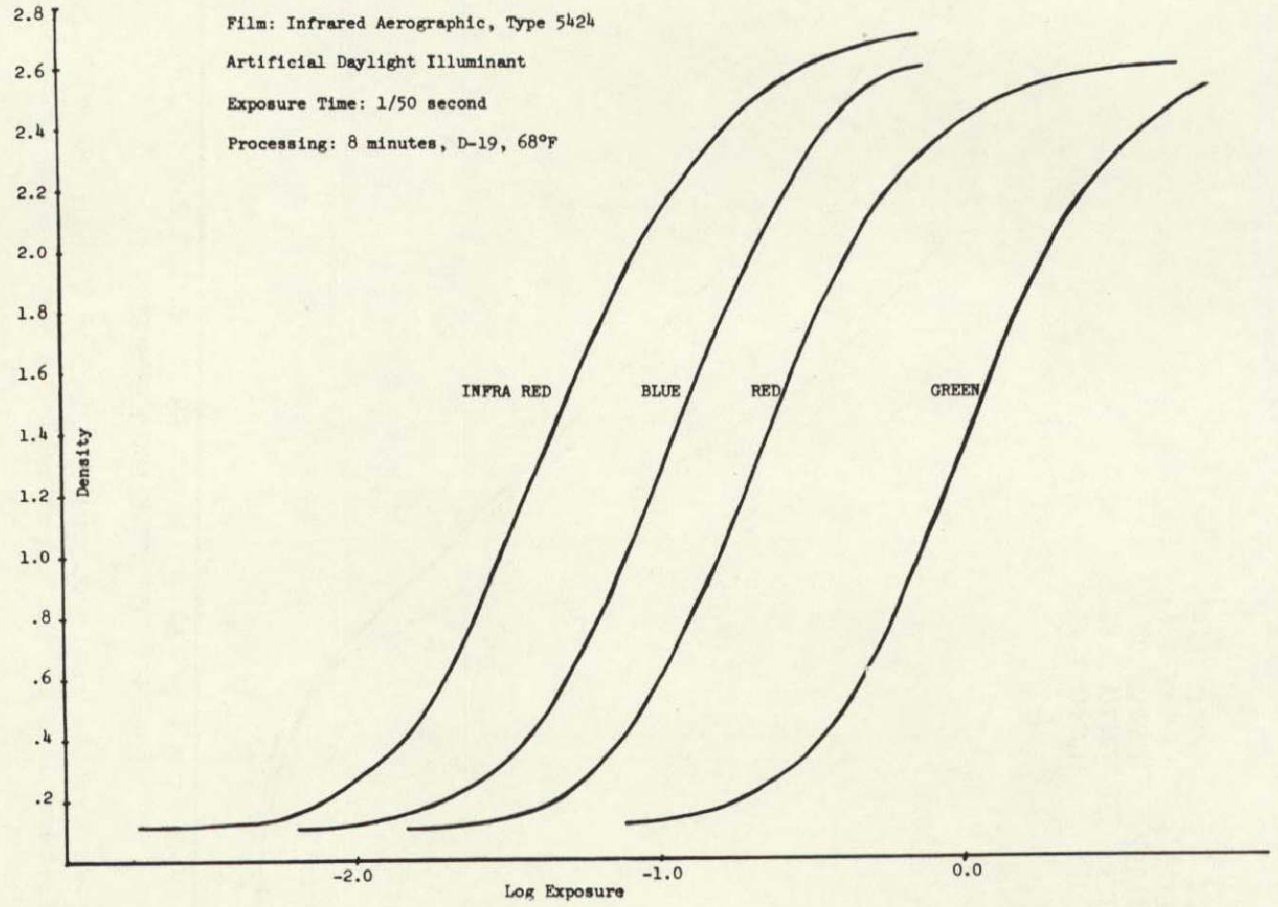

Figure 29-8.- Characteristics of infrared film. The relationship of exposure (measured in photometruc units, meter-candles-seconds) and density shows not only large variations in photographic speed for EK 5424 film but also variations in shape of the curves particularly near the bottom (toe) and top (shoulder).

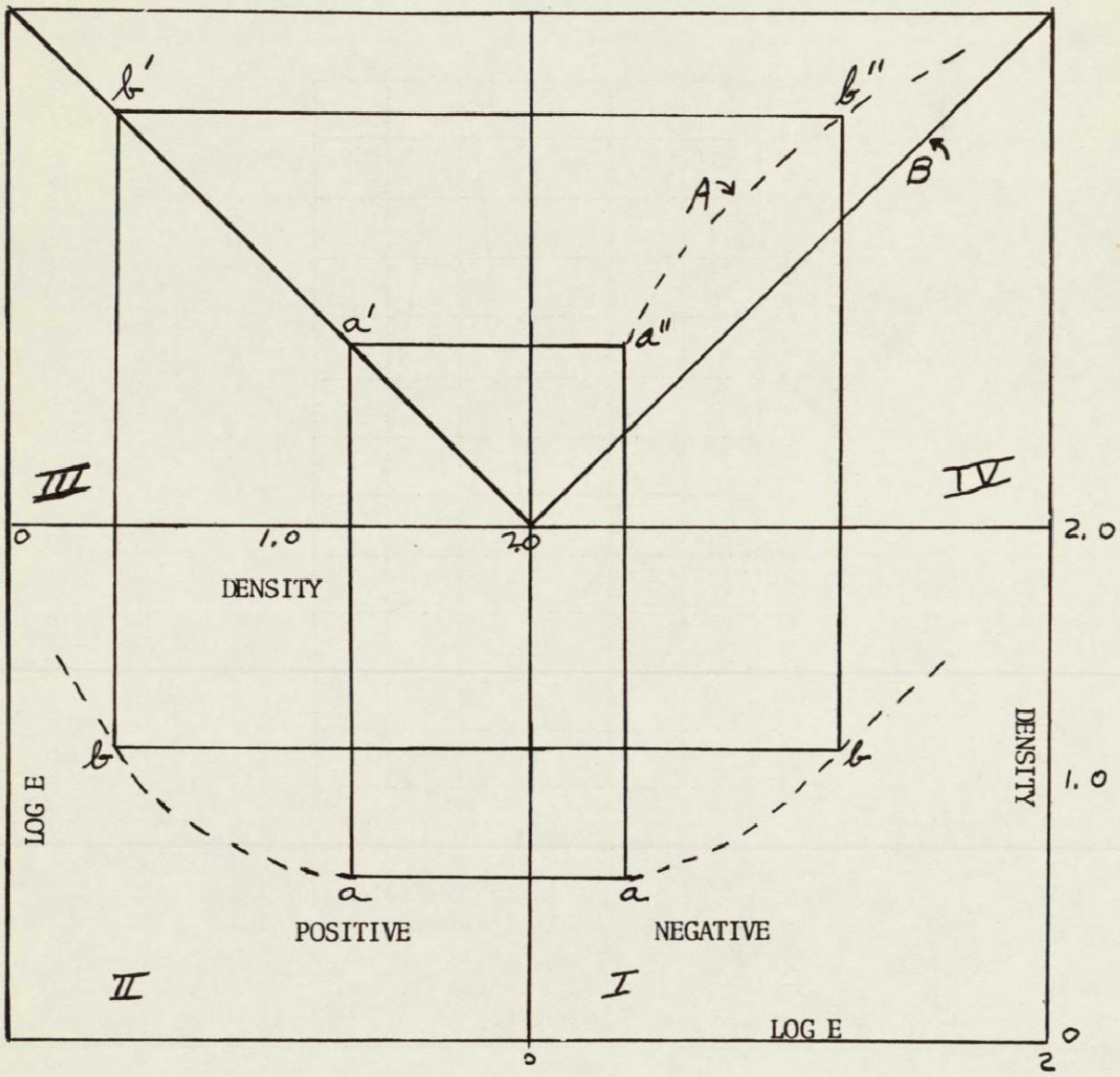

Figure 29-9.- Tone reproduction diagram. This diagram shows how well the red spectral negative and duplicated positive reproduced the original scene brightness.

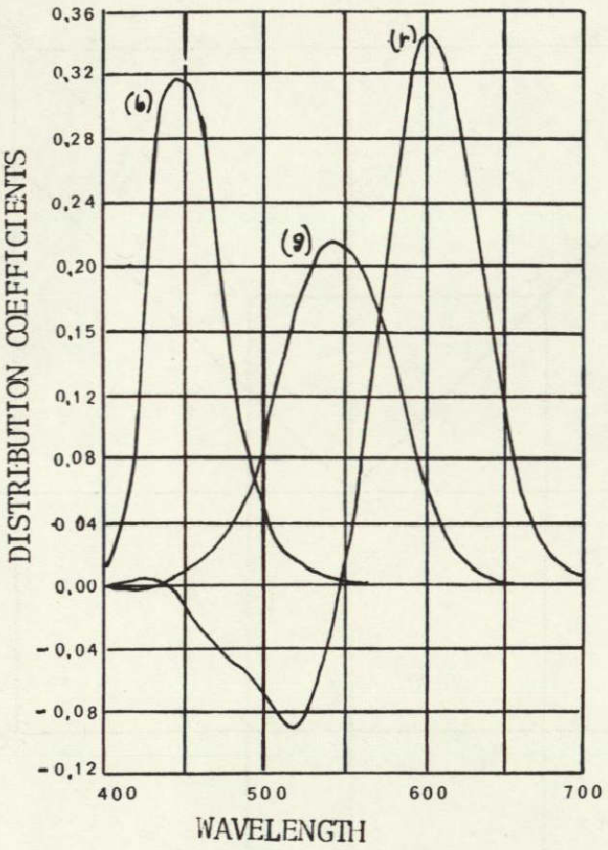

Figure 29-10.- Spectral distribution curves for the CIE "standard observer" and monochromatic primaries at the wavelength 700nm, 546.1nm, and 435.8nm.

FORM 3 BACK

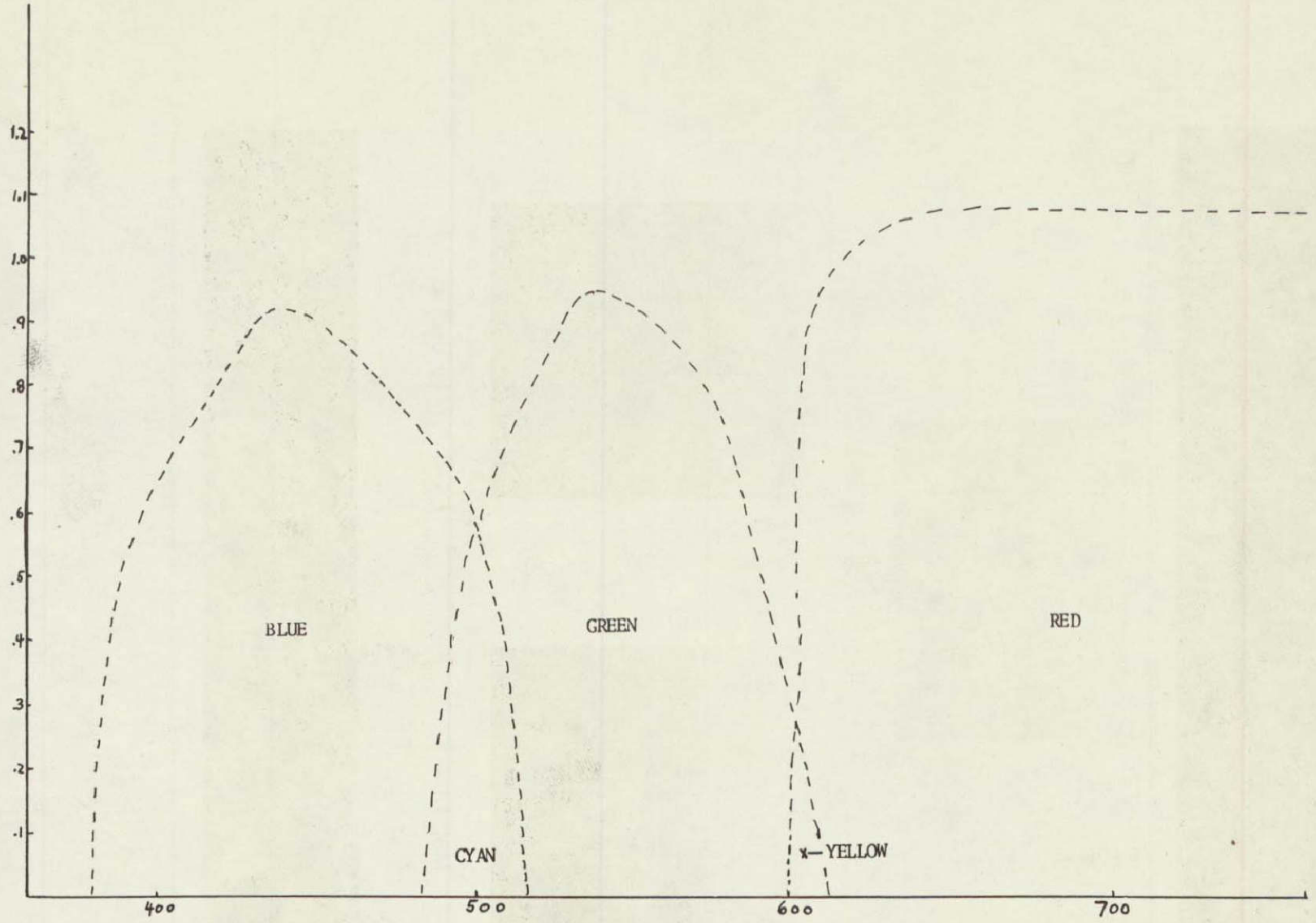

Figure 29-11.- Overlap in spectral taking filters to accurately reproduce secondary spectrum colors of cyan and yellow.

Map Units 5 & 6

Map Unit 7

Map Unit 8

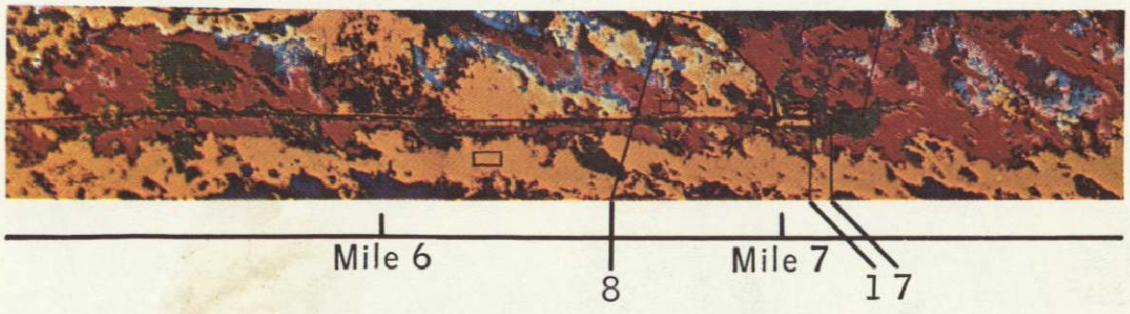

Figure 42-7.- Concluded.

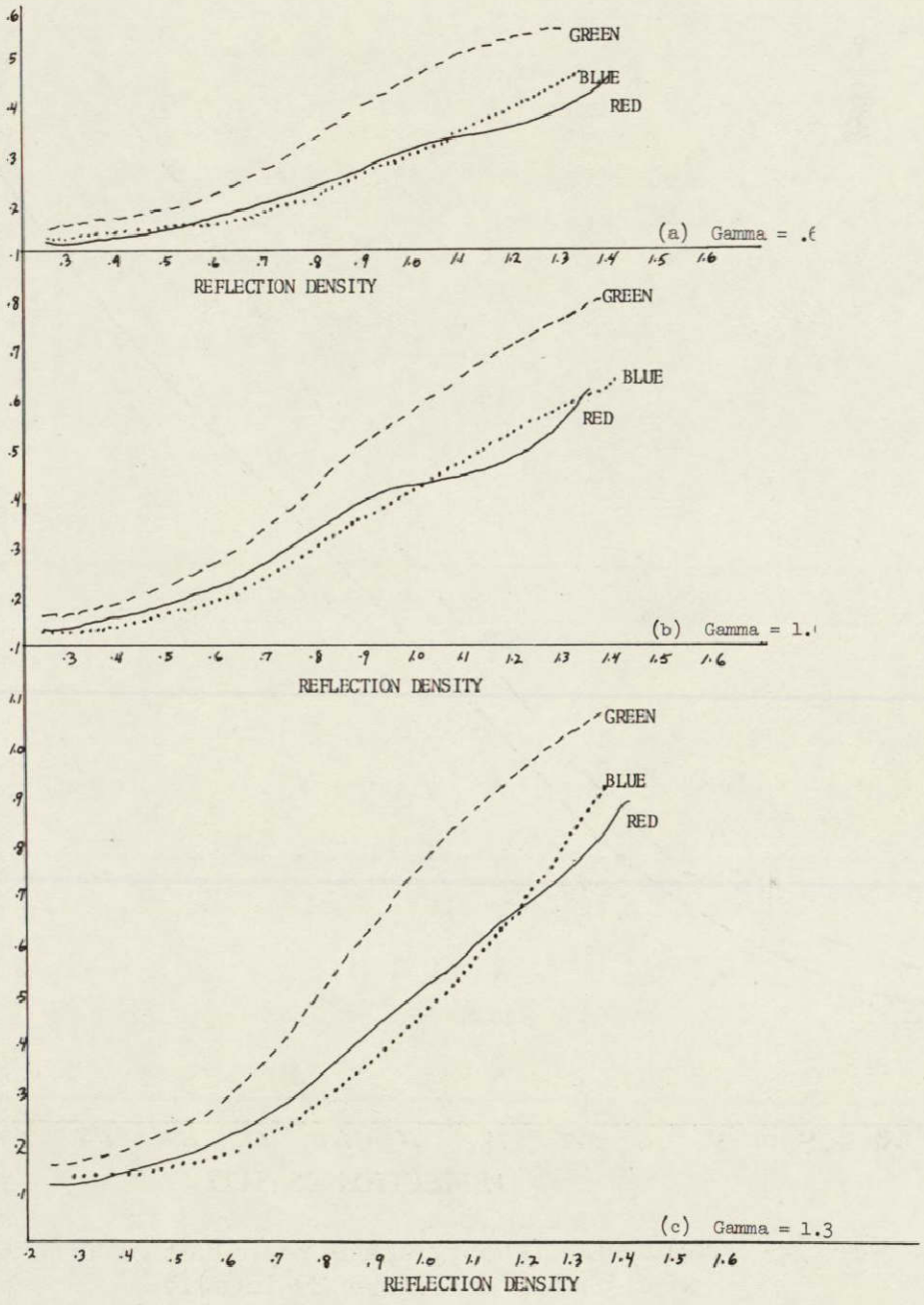

Figure 29-13.- Photographic reproduction data associated with photo, on figure 29-12(c).

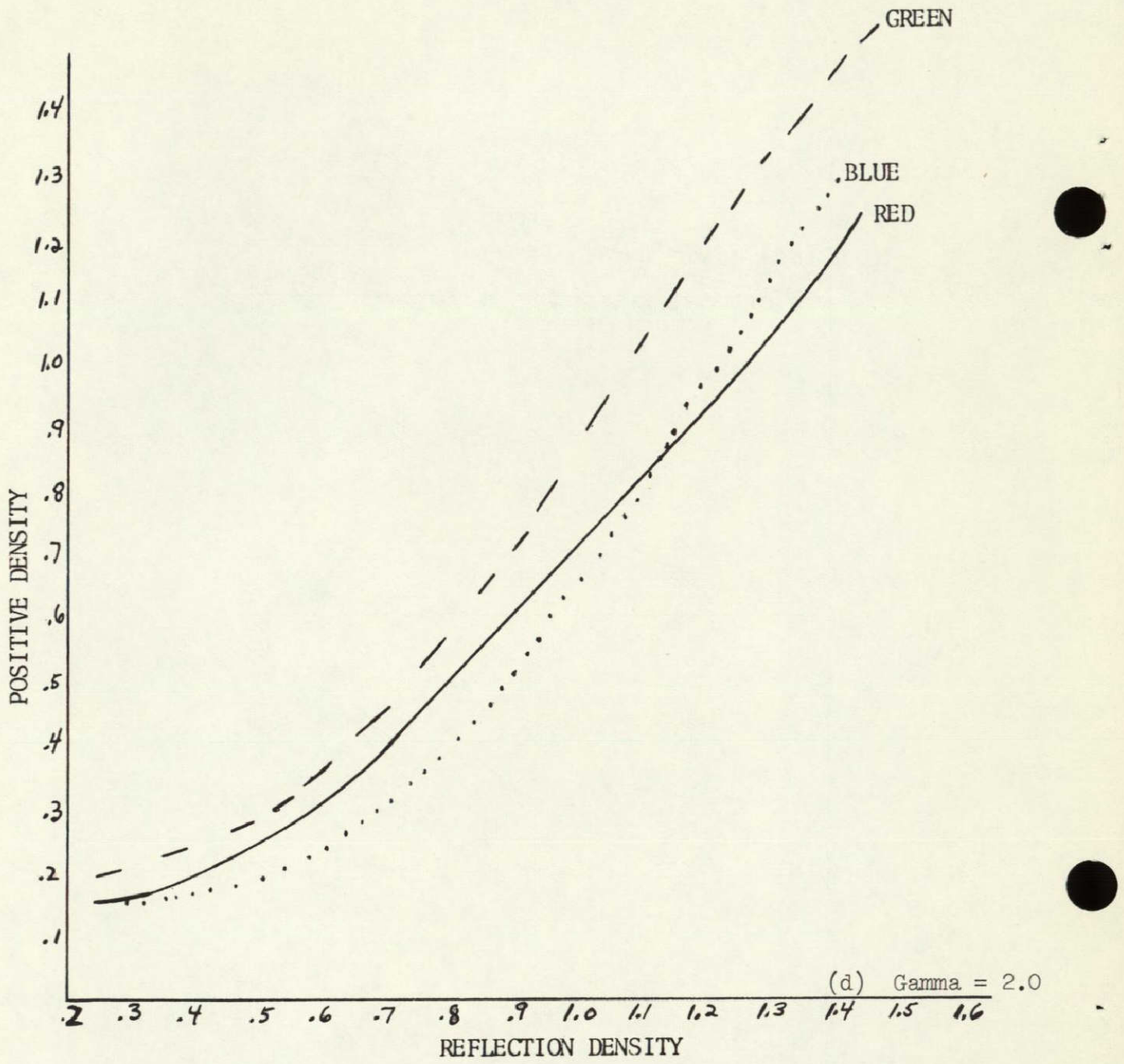

Figure 29-13.- Concluded. (Photographic reproduction data associated with photos on figure 29-12(d).)

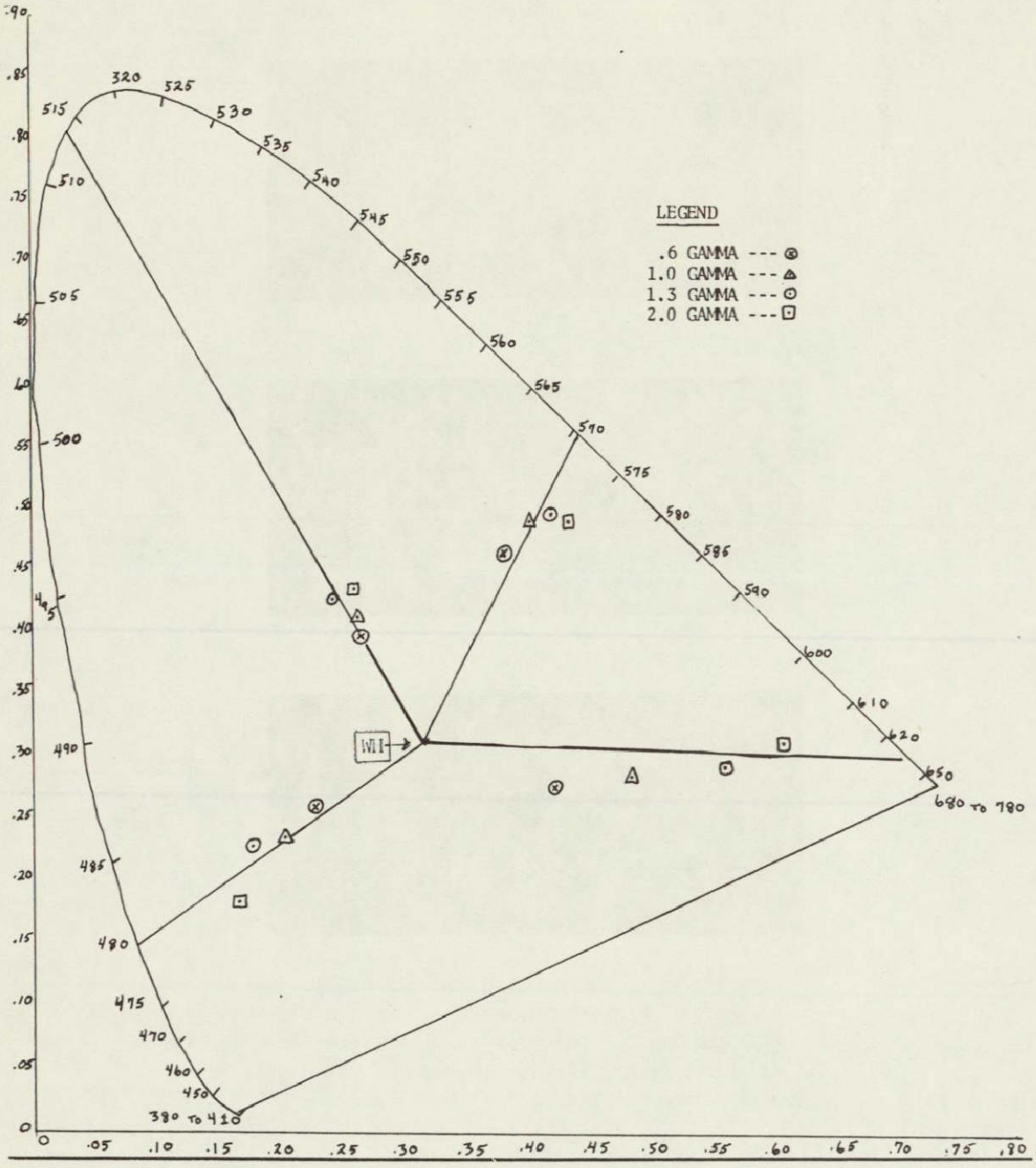

Figure 29-14.- Color measurement of the four color images shown in figure 29-12.

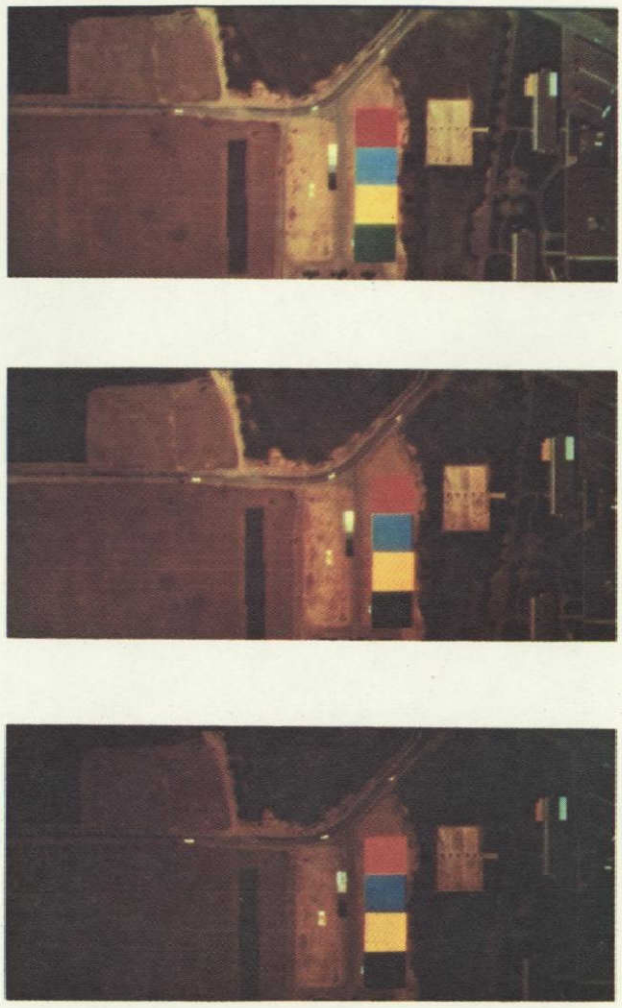

Figure 29-15.- Variations in brightness of target panel due to variations in the difference between maximum and minimum density.

SECTION 30

MICROWAVE STUDIES AND INSTRUMENTATION FOR THE EARTH RESOURCES PROGRAM

John C. Blinn III

Jet Propulsion Laboratory, Pasadena, California

I. INTRODUCTION

The Jet Propulsion Laboratory's efforts in microwave remote sensing encompass both the active (radar) and passive (radiometry) areas. Radar and radiometer groups have been involved in numerous projects relating to the application of microwave techniques, including development of radiometers for planetary measurements from fly-by spacecraft, prototypes for planetary radar systems, airborne imaging radar systems, radio astronomy instrumentation, radiometers for the Nimbus E Spacecraft and participation in the NASA Earth Resources Program. The goal of these groups' activities in the Earth Resources area is to further the understanding and application of microwave remote sensing techniques to the earth sciences. The pursuit of this goal takes the form of advanced planning through participation in the NASA Earth Resources Planning Panel and other ad hoc committees, proposing, designing and building advanced sensors, providing design and instrumentation support to NASA agencies and, particularly in view of manpower limitations, it takes the form of cooperative programs with various institutions which have included the University of Nevada, the USGS, MIT, and Kansas University among others.

In the past year, JPL has supported the Earth Resources in three areas: groundbased microwave radiometry, airborne microwave radiometry, and radar. These activities are summarized as follows.

II. GROUNDBASED MICROWAVE RADIOMETRY

A. 1968 Field Measurements Program

In the summer of 1968, a two-week field program was conducted utilizing a 9.3 GHz radiometer built by JPL, and 1.4, 13.7 and 37.0 GHz radiometers contracted from the Aerojet-General Corporation. This was a joint JPL/University of Nevada effort undertaken to:

1. obtain data for calibration of the aircraft microwave radiometers,
2. determine microwave penetration depth of various materials,
3. examine the effects of particle size on microwave emission,
4. examine the effects of water content on microwave emission.

The results of this measurement program are documented in two JPL reports which are scheduled for publication early in 1970.

Conel, J., "Determination of Microwave Penetration Depth from Buried Metal Plate Measurements"

Quade, J., Chapman, P., Brennan, P., Blinn, J., "Multispectral Remote Sensing of an Exposed Volcanic Province"

B. Previous Field Measurements Program

A contract was placed with R. Porter to reduce and analyze data gathered over water, salines, limestone and sand. This data was taken under a field measurement contract with the Raytheon Corporation. The final report on this work is scheduled for publication in December.

C. Ocean Roughness Measurements

A contract was placed with NRL to review the work done to date on ocean parameters in the passive microwave field and to perform a program of multifrequency radiometric measurements on the ocean in various conditions. This work has been completed and is being submitted to the Journal of Geophysical Research.

III. AIRBORNE MICROWAVE RADIOMETRY

A. 1968 Mount Lassen Mission

Four frequency microwave data from the CV 240A aircraft overflight of the Mount Lassen Test Site in 1969 was digitized, calibrated, and presented to the investigators. The results are discussed in the report by Quade, et al above.

B. Microwave Radiometer Calibration Facility

In order to accurately calibrate radiometer antennas and radomes, it is necessary to have a high altitude test facility above much of the atmospheric water vapor. Such a facility was constructed at the JPL Table Mountain site at 7500 feet elevation. It consists of a hard pad, reflective enclosure, and absorbing disks which are raised and lowered on three sixty-foot pole and pully systems. This facility was used for calibration of the NASA P3A Multifrequency Microwave Radiometer System during the period August 4 through August 12, 1969.

The purpose of the calibrations was to measure

1. Radome loss as a function of look angle.
2. Antenna loss.
3. Integrated energy distributions in the antenna patterns.

The results of these measurements are presented in the informal report:

"Table Mountain Calibration Data on P3A Multifrequency Microwave Radiometers and Radomes," J. Blinn, December 1969.

C. X-Band Microwave Imager Technical Specifications

The initial technical specifications for the X-Band Microwave Imager currently under procurement by MSC were conceived and written for MSC by JPL. This imager offers several advances over currently operational passive microwave radiometer imagers:

1. Conical scan for constant incidence angle over the scan.
2. Simultaneous dual polarization operation.

IV. RADAR

A. Radar-Radiometer

The radar-radiometer is to be a remote sensing instrument to obtain both active and passive information at the same time from identical areas. The polarization of the antenna beam will be electronically switched to permit studies of target signatures as a function of polarization. The components have been procured and tested. The assembly and test of the instrument has been started. It is expected to be ready for field tests in about three months.

B. Long-Wave Imaging Radar

Plans are being formulated to fly the JPL coherent radar on the MSC C-130 aircraft. Radar images at 25 cm wavelength have previously been obtained with this radar flying on the NASA 990 aircraft.

SECTION 31

GROUND TRUTH/SENSOR CORRELATION

By Peter Chapman, Jack Quade
and Peter Brennan
NASA Project Office University of Nevada

and John C. Blinn III
Jet Propulsion Laboratory, Calif. Inst. of Technology

ABSTRACT

In support of the Earth Resources Program, the Mount Lassen, California, test site (56) was overflown using the NASA 926 aircraft. The prime objective of the experiment was to examine remote-sensing applications on simple geologic features. This mission marked the second year of intense ground and airborne studies at a test site selected for its homogeneous surfaces, densities, lack of vegetation, and its similarity in composition and texture.

The overflights took place on July 18 and 19, 1968. Data were taken using the four-channel microwave radiometers as the prime instrument, supported by the radar scatterometers, thermal infrared imagers, and color infrared photography.

The preflight surface activities included albedo measurements (solar reflectivity), seismic experiments to determine the depth profiles of the various materials, thermal-diffusivity studies, and thermal-emissivity determinations. In addition, a joint venture with the microwave division of Jet Propulsion Laboratories and the microwave van team of Space General was conducted to study the penetration and diurnal heating effects on the microwave signal. The results of these studies in combination with the airborne sensor data from Mission 56 of the previous year led to the selection of two new flight lines.

During the overflight of Mission 76, intensive ground measurements of the thermal and physical characteristics of the materials at Mount Lassen were conducted. These measurements in connection with preflight studies greatly aided in subsequent data interpretation.

A discussion is included on the usefulness of various photographic techniques as an aid to the interpretation of long wavelength sensor data. Multifrequency microwave data indicates an ability to differentiate materials on the basis of their density, thermal characteristics, and surface roughness. The 13.3 GHz scatterometer demonstrated an ability to differentiate material on the basis of particle size and showed a sensitivity to surface geometry when the particulate material is small in relation to the Rayleigh scattering coefficient.

INTRODUCTION

The Mt. Lassen Test Site #56 was flown in mid-July, 1968 as part of Mission #76 of the Earth Resources program using the NASA 926 aircraft. The prime instruments for the experiment were the MR 62/64 microwave radiometers, the Reconofax IV thermal infrared imager, and two RC-8 metric cameras loaded with Black and White and Color Infrared film. The Ryan Redop Scatterometer was used as a secondary instrument. The report includes results from the mid-day and pre-dawn flights, special studies and subsequent data analysis.

The results from Mission #55 in 1967 led to the selection of two new flight lines, both of which originate at Butte Lake. The first line crosses the lava fields and flat lying cinder. Both lines cross materials of homogeneous chemistry, density, roughness and thermal characteristics.

Four ground stations were manned during the day and night flights to provide ground temperature and moisture measurements. These measurements were used in conjunction with preflight studies by the Jet Propulsion Laboratory and the Aerojet General microwave systems also present during the overflight. Data from the ground based systems were then used to calibrate the airborne microwave radiometers.

The results of the experiment demonstrate the effectiveness of a multisensor approach over a very specific geologic target when supported by ground based data.

Geology

The Mt. Lassen Test Site (#56) is part of a volcanic province which contains a well-exposed series of eruptive rocks and a well-formed cinder cone. The site lies about 10 miles east of Lassen Peak in the Mt. Lassen National Park (Figure 1). The cinder cone and lava flows were produced by several thousand years of sporadic eruptions (last active in 1851) separated by long periods of quiescence. The periods of cone building gave rise to basalt flows formed by the effusion of lava from the cone base.

The cinder fields are composed primarily of uncemented vesicular volcanic ejecta ranging in size from 1mm to 2cm. The altered cinder is the result of hydrothermal waters moving upward from the hot lava flows. Cinder which did not fall upon the hot lava shows little or no alteration and remains dark gray to black.

Geochemistry

Detailed studies of the rock chemistry indicate only small variation in the chemical makeup of the lava and cinder. The chemical consistency between cinder and lava eliminates the compositional parameter from effecting the sensor data.

Moisture

The cinder fields contain considerable moisture at depth; however, the first few feet are relatively dry due to the dehydrating effects of high daytime surface temperatures. Table 1 shows the average moisture of the cinder fields at the time of overflight.

Particle Size and Density

The lava consists of large blocks of material 30 to 60 centimeters in size. The cinder is composed of scoraceous pebble size material. Figure 2 shows the mean particle size distribution of a number of cinder samples.

The dense lava samples have a density of 2.59 gms/cm^3 which corresponds to a porosity of about 4%. Much of the basalt has a rather high density, though all gradations from very dense basalt to scoriaceous material exists.

The mean cinder density is 1.10 gms/cm^3; this corresponds to 57% porosity. The cinder density falls into a rather narrow range between .84 and 1.34 gms/cm^3.

Depth Probe Sensing

Shallow seismic work was conducted on both the basalt and cinder in order to determine the depths of discontinuities. These studies failed to show either bedrock or significant vertical change in any of the sampled areas to a depth of two or three feet in the cinder.

PHOTOGRAPHY

The black and white and the color infrared photography was taken with Wild RC-8 metric cameras, having 9" x 9" formats and 6" focal length lenses. The flight elevation of 2200 ft. above the terrain and an 8.5 second intervalometer setting, produced photographs with a scale of 1:4,500 with a 30% overlap.

Black and White Photography

The black and white photography was used to establish the actual flight tracks. Identification and mapping of lithologic units was done by combining observations of the overall albedo and the topographic overlap photographs from NASA Mission #55. An example of a detailed topographic map and stereoscopic pairs are shown in Figure 3.

A large portion of the incoming solar energy is concentrated in the visible and near infrared portion of the spectrum. The incoming radiation is either reflected or absorbed. The reflected energy is directly correlative with the photographic behavior of the target. Albedo is a measure of this reflectivity, and is the single lithologic parameter affecting the photographic systems. Table 3 shows the environmental variables which determine the albedo.

Curves produced by a spectrometer of the percent reflectivity of various units tended to be subparallel and infrequently cross in the visible spectrum. The visual albedos can be correlated directly with the shade of gray on black and white photographs.

Figure 4 shows the albedos of the three major lithologic types at the Mt. Lassen Test Site. These data were taken with an ISCO model SR spectroradiometer which measures light intensity at any desired wavelength.

Near Infrared Photography

The principle use of infrared film on Mission 76 was to photograph vegetation, and determine its density and vigor. For some sensors the presence of vegetation complicates the interpretation of geologic parameters, thus the screening effect of the vegetation must be known.

A vegetation density map was produced by plotting the estimated densities near the centers of photos on a 1:24,000 scale map. Each area supports its own characteristic botanical assemblage visible on the vegetation density map.

The color infrared photographs enhance the altered cinder area because of the cinders' low reflectivity in the violet, blue, and blue-green, with relatively high reflectivity in the yellow-green to infrared region. Three distinct tones may be seen on the color infrared film; 1) dark blue-green, 2) yellow-orange, and 3) white, where as only grays, tans and dull reds can be seen on normal color photography. The dark blue-green tone corresponds to areas of gray and olive cinder. Because of low overall albedo and its slight reflectance peak in the yellow-green, the gray cinder appears as a dark blue-green on the film. Yellow-orange response on the infrared photographs is actually deep red cinder which has the highest reflectivity in the far red almost at the response limit of the human eye and normal film. The white tone is produced by a varigated cinder which is composed of fragments of all colors of gray, green, orange, brown and red.

INFRARED IMAGERY

The Reconofax IV infrared imager records the thermal radiation of the surface at wavelengths between 8 and 14μ. The surface temperature is dependent on a number of physical and meteorological variables. During the daily heating period the surface temperature is regulated by the material's albedo and thermal diffusivity.

The thermal diffusivity, α, is equal to:

$$\alpha = \frac{K}{c\rho}$$

where K = thermal conductivity
c = specific heat
ρ = density

Thermal diffusivity controls material's ability to transfer heat, from the surface to subsurface areas, and from depth to the surface after the solar heating period. The thermal diffusivities of the basalt and cinder are summarized in Table 4, and the thermal diffusion is plotted graphically in Figure 5.

Albedo is the percent reflectivity of a material in the visible and near infrared portion of the spectrum, in which a majority of the incoming solar radiation is concentrated. Albedo for a given wavelength may be computed by:

$$\alpha_\lambda = \frac{R_\lambda}{I_\lambda}$$

where, α_λ = albedo
R_λ = reflected radiation flux
I_λ = incident or incoming radiation flux

By examining the three main lithologic units at the Mt. Lassen Site, the basalt flows, the gray cinder and the altered cinder, the relative contributions of albedo and thermal diffusivity, day and night may be seen. Table 4 summarizes the thermal parameters of the major lithologic units.

Thermal diffusivity dominantly influences pre-dawn temperatures. The eight hours of darkness prior to the flight eliminated any effect of dissimilar albedos.

Mid-day temperatures on the Mt. Lassen Site also show a strong dependence on thermal diffusivity, modified by dissimilar albedos.

A third variable, emissivity, controls the amount of energy emitted by the surface of a material. It is a measure of the relative contributions of radiance due to physical temperature and the reflected radiance from the sky and surrounding objects. The emittance characteristics of the lava and cinder were measured in the laboratory with an emissivity chamber, constructed at the University of Nevada. The instrument consists of a Barnes Portable Radiation Thermometer attached to a special environmental chamber. Table 5 shows the emissivity of major rock units at Mt. Lassen.

Infrared Data

The mid-day thermal imagery shown in Figure 6a indicates a high thermal contrast between water and cinder (the cinder at 60-63°C, and water at 15°C); the rock is at an intermediate temperatures. The water with its high thermal inertia remains relatively cold throughout the day and at a fairly constant temperature (day to night variation of about 2°C). The basalt flows with their relatively high thermal diffusivity remain cooler than the cinder (which has a higher albedo).

At the time the imagery was flown, there was an excellent thermal contrast between the ridges and valleys of the lava flows. This contrast enhances the flow structures of the lava and stress patterns created at the time that the flow surface cooled.

The day imagery shows a high amount of distortion, which may be due to turbulence which prevented the aircraft from maintaining level straight flight.

Figure 6b is the pre-dawn thermal imagery. There has been a complete thermal inversion, with the cinder now becoming the coldest and the water the warmest. The basalt remains warmer because of its ability to transfer stored subsurface energy to the surface. The compacted dirt roads in the campground c are now visible and are warmer due to their higher thermal diffusivities.

Larger particles on the sides and base of the cinder cone may be distinguished from fine cinder; the larger blocks being warmer due to their greater thermal capacity.

Several areas which are topographic lows on the cinder fields are colder due to settling of cold air. This phenomena is readily visible in the depressed center of the cinder cone.

The diurnal radiometric temperature shown in Figure 7 illustrates that the pre-dawn imagery generated at approximately 04:00 hours was flown at the time of maximum contrast between the principle units under study. If, however, one were trying to locate thermal anomalies such as hot springs, fumaroles, etc., the ideal time would be at 07:00 hours when all the principle units were at equilibrium. The diurnal measurements clearly demonstrate the advantage of prior field studies in selection of optimum flight times, if thermal properties are to be used in classifying rock units for geological interpretation.

AIRBORNE MICROWAVE RADIOMETRY

Calibration of Aircraft Data. Ground based water and cinder data were used as a two point calibration for the aircraft microwave radiometers (Figure 8). The ground based data at 9.3, 13.5 and 37.0GHz were used directly to calibrate the 8.6, 15.8 and 34.0 GHz airborne frequencies respectively.

The difference in emission between water and cinder provides a large brightness temperature differential for determination of radiometer gains. Due to logistic and experimental time constraints, ground based measurements of the lakes were not obtained. The theoretical values of brightness temperature for water used for calibration are listed in Table 6.

Since the cinder at the test site was inaccessible, data from diurnal runs at a nearby cinder pit were used for a second calibration point on the aircraft radiometer data. The values used for calibration of the aircraft data are listed in Table 7.

Aircraft Data. The microwave radiometers duplicated the results of the 1967 mission. However, diurnal temperature variations and seismic profile data permit more meaningful interpretation of the results. An example of the day-night multifrequency microwave responses over line two are shown in Figure 9. The 8.9 and 34.0 GHz responses at night show a definite delineation of the basalt and cinder. The day response of all frequencies is virtually featureless. The parameters which could effect the response are thermal properties and emissivity.

During the day flight (11:00 a.m.) the temperature difference between the units was relatively small. Hence, one would expect that the 34.0 GHz channel with its small penetration depth, would show approximately the same brightness temperature for the basalt and cinder. This is the case. Thus, at 34.0 GHz the emissivity differences between the basalt and cinder are small.

Considering the preflight 8.9 GHz penetration studies and thermistor probe measurements, the change in airborne data at 8.9 GHz from basalt to cinder is anomalous. This anomaly which may be explained by a higher emissivity for cinder than basalt, compensated for the temperature difference.

SCATTEROMETRY

The scatterometer is an active radar system which records radar reflections along the flight path of the aircraft. Data on radar scattering at a variety of illuminating and receiving angles may be sampled on a single flight. The data in this paper is presented as return versus distance (time) plots for each of a number of look angles.

The Ryan Scatterometer used on the Mt. Lassen site isolates individual resolution cells by combining a fan beam antenna with sampling at preset Doppler frequency shifts. Each angle has its own Doppler frequency as defined by:

$$D = \frac{2v}{\lambda} \sin \theta$$

where D = Doppler frequency
λ = wavelength
v = velocity
$\sin \theta$ = sine of the look angle

Figure 10 shows the shape of the fan beam and the size of the resolution cells for the Mt. Lassen Mission.

Roughness determinations

In order to differentiate the various surfaces at Mt. Lassen, the Rayleigh criterion of roughness can be applied to the resulting scatterometer data.

If ray a and ray b at grazing angle γ come in contact with a surface of irregularities of height h as in the example shown, the path difference (Δr) is:

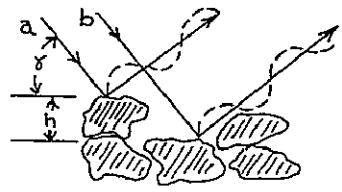

$\Delta r = 2h \sin \gamma$ hence, the phase difference is:

$$\Delta\phi = \frac{2\pi\Delta r}{\lambda} = \frac{4\pi h}{\lambda} \sin \gamma$$

at $\Delta\phi = \pi$ the rays come into phase opposition and cancel the surface is considered rough, $\Delta\phi = 0$ smooth and $\Delta\phi = \pi/2$ the intermediate.

Thus by the Rayleigh criterion a surface is considered smooth for

$$h < \frac{2}{8 \sin \gamma}$$

Using this criterion the "break" between specular and diffuse scatters can be seen in Table 8.

Since the lava blocks average 30 cm in diameter they are considered diffuse scatters regardless of grazing angle. The cinder size is at the dividing line between specular and diffuse while the lake surface on the day of the overflight remained specular at all angles. The forested areas, when the above criterion is applied, are extremely diffuse scatterers, but since vegetation has a greater absorbtivity than either the cinder or basalt, it must be considered as a special case.

Figure 11 is a smoothed diagram of the forebeam scatterometer data over line 2. The idealized portion of the diagram indicates the probable return if all the surface had the same absorbtivity.

Topographic variations

Topographic variations on the scale of 10's of feet can be observed on the Mt. Lassen scatterometer data. If a fixed transmission and reception point is considered, the "Rayleigh criterion" states: given two surfaces of equal roughness, the one with the more gentle hill-to-valley slopes should scatter less diffusely. The basalt flows, like the cinder, tend to form a rolling hill topography. However, since the basalt is such a diffuse scatterer the rolling hill topography is masked on the data and is only noticeable on the more specular reflecting cinder fields. This diffuse masking of slope should be considered when interpreting radar data, such as fault locations on radar imagery. Figure 12 shows the theoretical scattering diagrams of the three major surfaces (conifer forest excluded).

Large scale topographic variations are also observable on the data. The lava slopes gently toward the lake and the scatterometer returns show shrinking of the time lag between various look angles to the surface.

By producing time versus return plots such as in Figure 13 from data flown over areas with significantly large homogeneous lithologic units, much can be learned from the scatterometer. By considering the above mentioned limitations in planning flight lines, reliable information on roughness characteristics and topography can be expected over many geologic targets.

SUMMARY AND RECOMMENDATIONS

While the aim of the airborne sensors is to cover large areas in short periods of time and eliminate as much time consuming ground work as possible, it is equally important that costly aircraft data be well documented by ground-based measurements. As proficiency at interpretation and ground data collection become more sophistocated, vastly large areas of terrain may be sensed with confidence for only modest increases in ground calibration effort.

Photography

Metric photographs were flown primarily to establish ground track and to quantify the vegetation. The particular film-filter combination used on the

color infrared photographs differentiated the various colors of cinder very well, although if the cinder rather than the vegetation were the objective, a better filter might have been chosen. The following are recommended for simplifying and maximizing the potential of areal photographs:

1. Preflight spectral albedo studies on the major rock types to intelligently recommend the best film and filter combinations.

2. Separate photographic runs to produce scales which are directly comperable with other imaging sensors and with existing map coverage.

3. The establishment of a marked, surveyed grid to produce topographic maps in areas where detailed topographic coverage is not available.

Infrared Imagery

Because of the ability to measure thermal diffusivity and albedo quantitively, the dominant role of diffusivity in controlling infrared temperatures has become clear. With a modest ground truth effort at a few calibration points, it should be possible to infer diffusivity and albedo characteristics of materials from day and night IR imagery. The following steps are advised to realize the full potential from IR imagery:

1. Obtain albedos, thermal diffusivities and emissivities of representative units.

2. Preflight thermal radiometer measurements can be made to select the optimum flight times.

3. Take surface temperature measurements for calibrating the airborne data and collect rock and soil mositure data at the times of overflights.

Microwave Radiometry

Significant steps were made toward understanding the microwave emission from geologic targets. Through field studies, quantative measures of penetration depth were obtained for various materials. Also, a limited measure of the effect of water on penetration depth was obtained. A combination of ground based and theoretical radiometer data was used for calibration of the aircraft microwave radiometers.

This study points out clearly that a balanced effort between ground based and aircraft oriented studies are absolutely essential in relating microwave emission to geologic phenomena. Studies on penetration depth, the influence of water and roughness effects can only be accomplished with ground based sensors. On the other hand, airborne sensors are indispensible in obtaining rapid, synoptic coverage of an area, graphically demonstrating the differences or similarities between varying units at a particular point in time. It is the conclusion of this paper that ground based studies should be performed on a continuing basis and especially in concurrence with aircraft overflights.

The following criteria are listed as being desirable in obtaining ground based data for calibration or comparison with aircraft data:

1. Use identical radiometric systems.

2. View the same target.

3. View a large homogeneous area.

4. Arrange an identifiable point in the data or in time on the data.

5. Perform the measurements concurrently.

Scatterometry

The radar scatterometry can yield valuable information on surface roughness, particle size and topography. Because of the problems of data reduction, the full potential of this system has not yet been realized.

The following are recommendations for future scatterometry flights over geologic targets.

1. Provide for strict topographic control and bore sighting of the data if sigma curves are to be produced.

2. Fly scatterometry only when accompanied by 60% overlap metric photography for topographic control.

3. Collect particle size and roughness data on representative areas of terrain.

REFERENCES

Blinn, John C.; Chapman, Peter; Quade, Jack: Airborne Multifrequency Microwave Radiometric Sensing of an Exposed Volcanic Province. Jet Propulsion Laboratory Technical Memorandum 33-405, October, 1968.

Conel, J.E.; Loomis, A. A.; and Holstrom, G.B.: Determination of Microwave Penetration Depth From Plate Measurements. Jet Propulsion Laboratory Memorandum (in press).

Marandino, G. E.: Microwave Signatures from Various Terrain. B. S. Thesis Massachusetts Institute of Technology, Cambridge, Mass., May, 1967.

Table 1. Moisture Content of Cinder

Depth	Mid-day Avg. moisture	Pre-dawn Avg. moisture
0 - 1/2"	.05%	.16%
2"	.21%	.12%
6"	2.59%	2.24%
8-12"	5.24%	4.18%

Table 2. Aircraft Instrument Summary

Flight 4 11:25 - 12:30 PDT July 18, 1968 Altitude 2000' Line length 4 miles

Line	Run	Recon IV	MR62-64	13.3GHz Scatt	RC8 #1	RC8 #2	Comment
1	1	X	10V	X	Plus X all runs	Color IR all runs	
1	2	X	10H	X			
1	3	X	45V	X			
1	4	X	45H	X			
1	5	X	30V	X			
1	6	X	30H	X			
2	1	X	10V	X			
2	2	X	10H	X			
2	3	X	45V	X			Abort
2	4	X	45H	X			
2	5	X	30V	X			
2	6	X	30H	X			
2	7	X	10H	X			

Flight 5 03:00-04:30 PDT July 19, 1968 Altitude 2000' Line leng
4 miles

Line	Run	Recon IV	MR62-64	13.3GHz Scatt	RC8 #1	RC8 #2	Comment
1	1	X	10V	X			
1	2	X	10H	X			
1	3	X	45V	X			
1	4	X	45H	X			
1	5	X	30V	X			
1	6	X	30H	X			
1	1	X	10V	X			
1	2	X	10H	X			
1	3	X	45V	X			
1	4	X	45H	X			
1	5	X	30V	X			
1	6	X	30H	X			

Table 3. Surface characteristics of geologic targets affecting photographic characteristics.

Parameters Effecting Total Signal	Environmental Variables
Multispectral Albedo	Colors of dominant minerals (reflected light)
	Weathering characteristics of rock and soil
	Bulk iron and FeO/Fe_2O_3 ratio in surface skin
	Grain size distribution
	Surface roughness
	Vegetation cover (grass, lichen, etc.)
	Moisture - standing water and soil saturation

Table 4. Thermal Parameters of Major Units

Material	Density[1]	Porosity[2]	Thermal Diffusivity[3]	Specific Heat[4]	Thermal Conductivity[5]	Albedo	Mid-day Temp.	Pre-dawn Temp.
Basalt	2.59	4%	.085	.206	.045	.07	50°C	14°C
Basalt	2.18	19%	.070	.206	.031	.07	--	--
Basalt	.71	74%	.042	.206	.006	.07	--	--
Grey Cinder	1.09	60%	.030	.206	.007	.07	--	--
Grey Cinder	1.10	59%	----	.206	----	.07	63°C	4°C
Altered Cinder	1.10	59%	----	.206	----	.14	60°C	4°C

[1] In (gms/cm^3)
[2] Calculated assuming solid density of 2.7 gm/cm^3
[3] In (cm^2/sec)
[4] Computed using Kopp's rule from chemical data
[5] In (cal/cm sec C°)

Table 5. Infrared Emissivity (8 to 14μ) of Mt. Lassen Samples

Rock type	Emissivity (ε_λ)
Altered Cinder	.96
Altered Cinder	.95
Rough Lava	.95
Smooth Lava	.92

Table 6. Aircraft Calibration Data - Water (°K)

Look Angle		10°		30°		45°	
Polarization		H	V	H	V	H	V
Channels (GHz)	8.6	110.	113.	100.	125.	86.	144.
	15.8	116.	118.	106.	131.	92.	150.
	22.2	140.	142.	135.	154.	125.	176.
	34.0	139.	139.	127.	153.	114.	175.

Table 7. Aircraft Calibration Data - Cinder (°K)

Look Angle		10°		30°		45°	
Polarization		H	V	H	V	H	V
Channels (GHz)	8.6 day	293.2	294.3	291.6	296.2	280.0	297.6
	night	282.5	282.4	283.2	283.2	273.5	283.7
	15.8 day	293.4	293.4	293.3	295.4	288.8	294.0
	night	280.2	280.0	277.9	280.2	274.3	279.4
	22.2 day	288.8	288.8	287.5	288.8	283.5	286.4
	night	271.5	271.2	269.3	270.3	265.3	267.8
	34.0 day	284.3	284.2	281.8	282.2	278.1	278.8
	night	262.8	262.4	260.5	260.5	256.4	256.3

Table 8. 13.3 GHz dividing point between diffuse and specular surfaces.

grazing angle	scatterometer* angle	particle size
85°	5°	h = .282 cm
55°	35°	= .343 cm
45°	45°	= .398 cm
30°	60°	= .562 cm

*from nadir

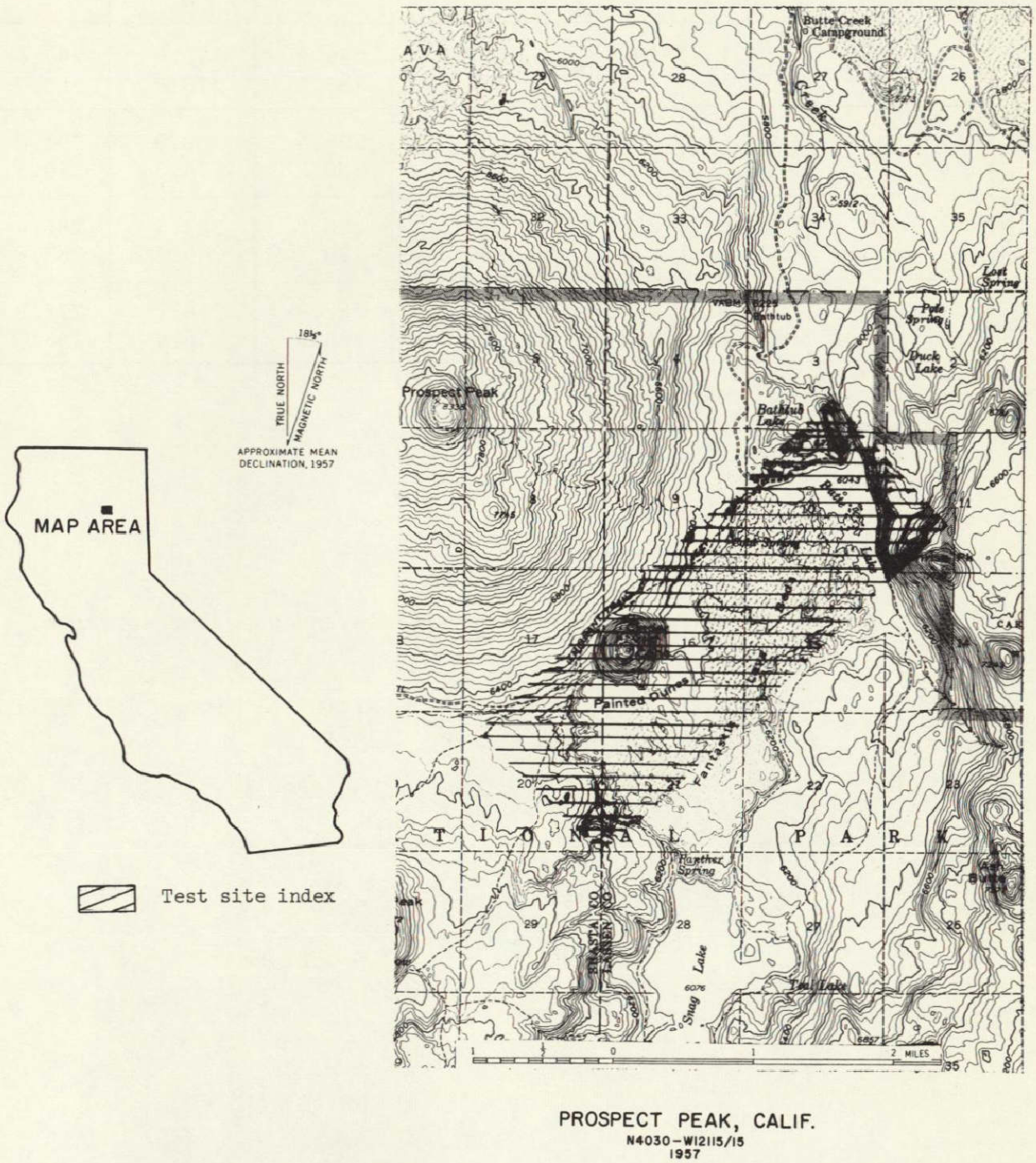

Figure 31-1.- Index map of the Mt. Lassen test site.

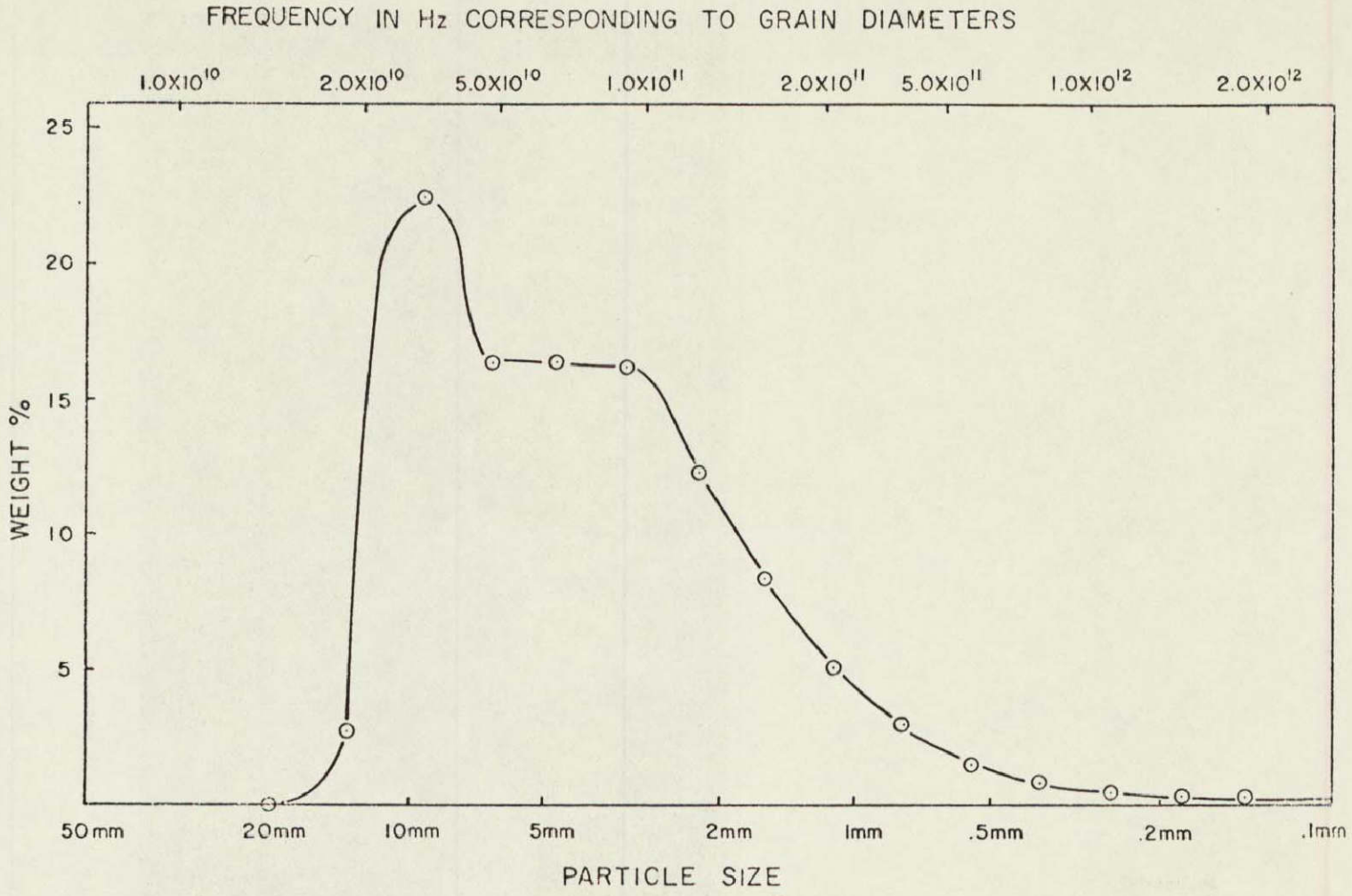

Figure 31-2.- Grain sized distribution of composite cinder sample.

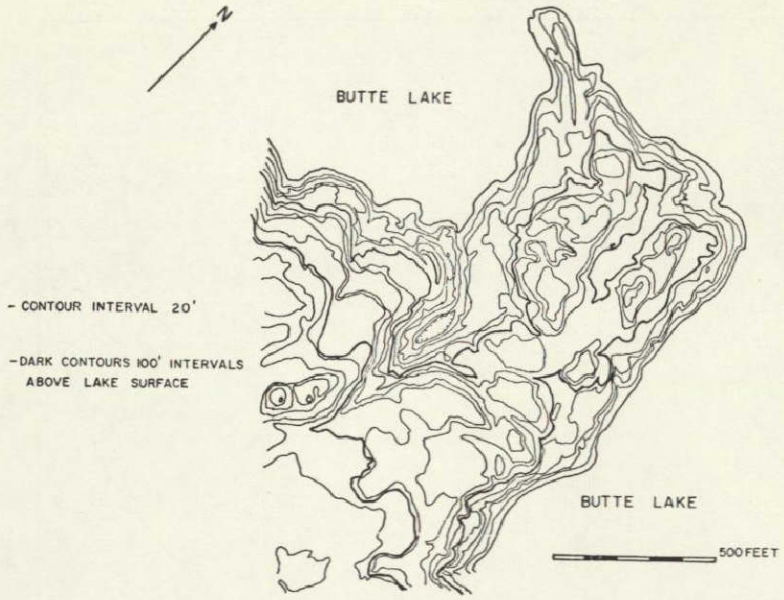

a. Topographic map made from metric airphotos.

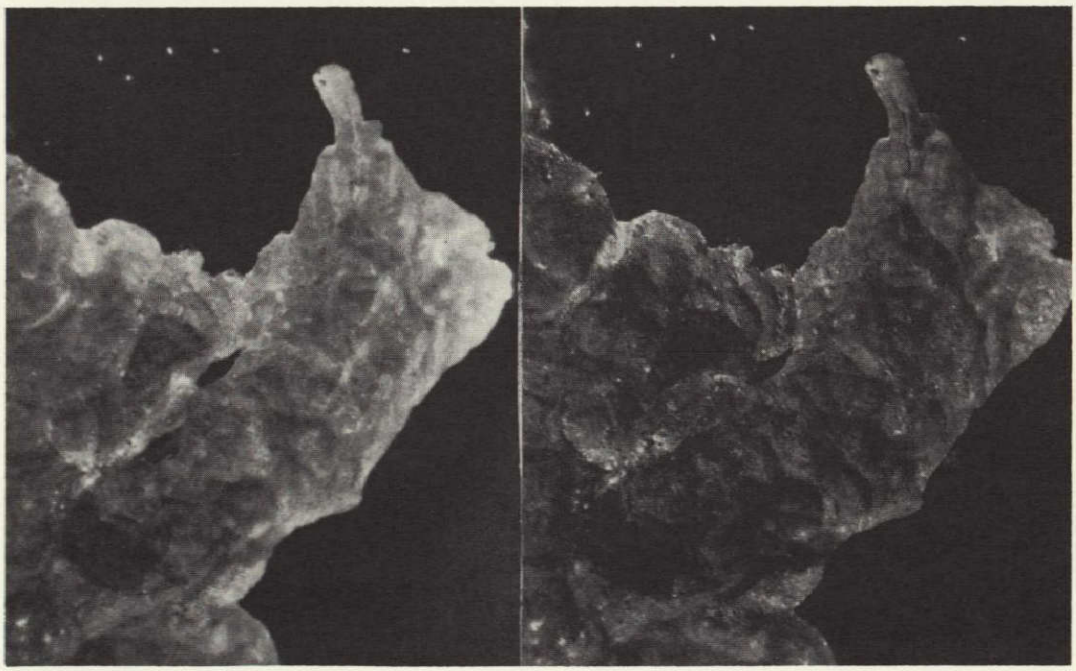

b. Stereoscopic pair of photographs (matches area in a.).

Figure 31-3.- An example of a detailed topographic map and the steroscopic photographic pairs from which it was constructed.

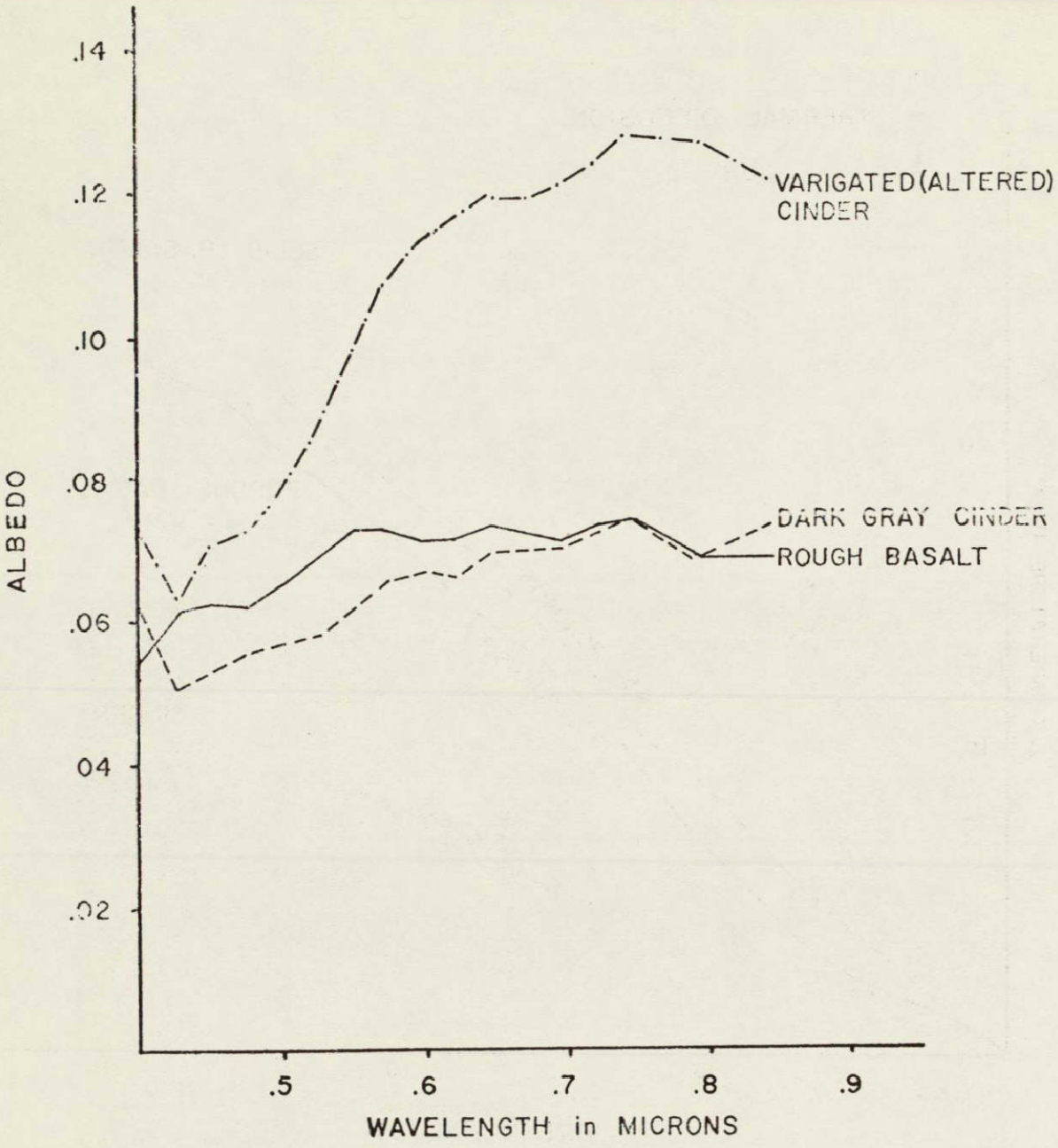

Figure 31-4.- Albedo curves of major lithologic units.

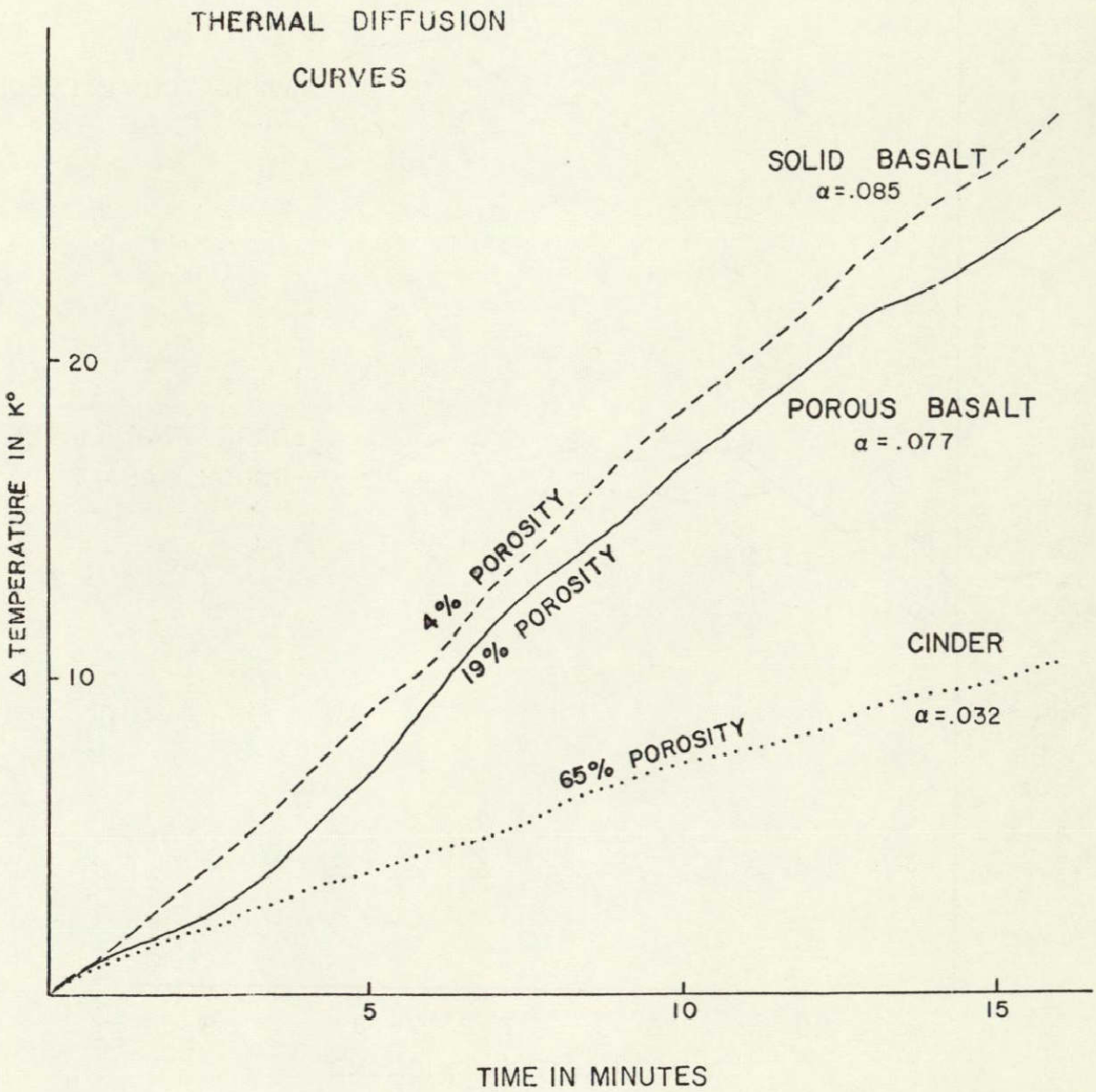

Figure 31-5.- Thermal diffusivity of basalt and cinder.

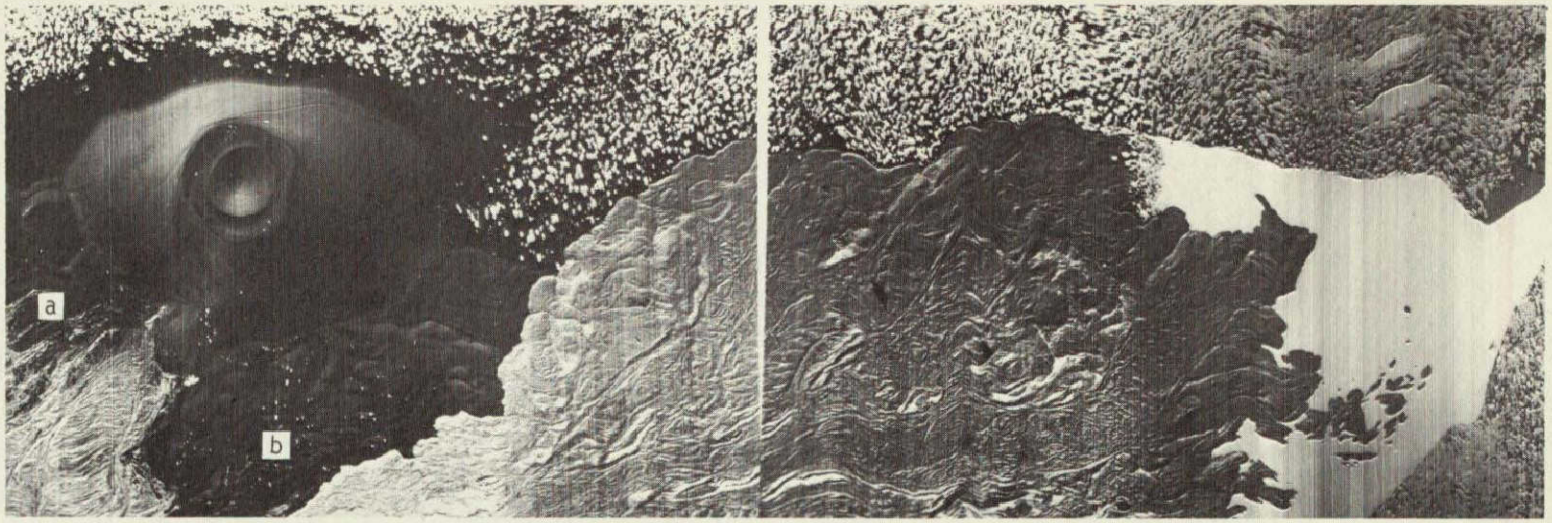

a. Mid-day thermal infrared imagery.

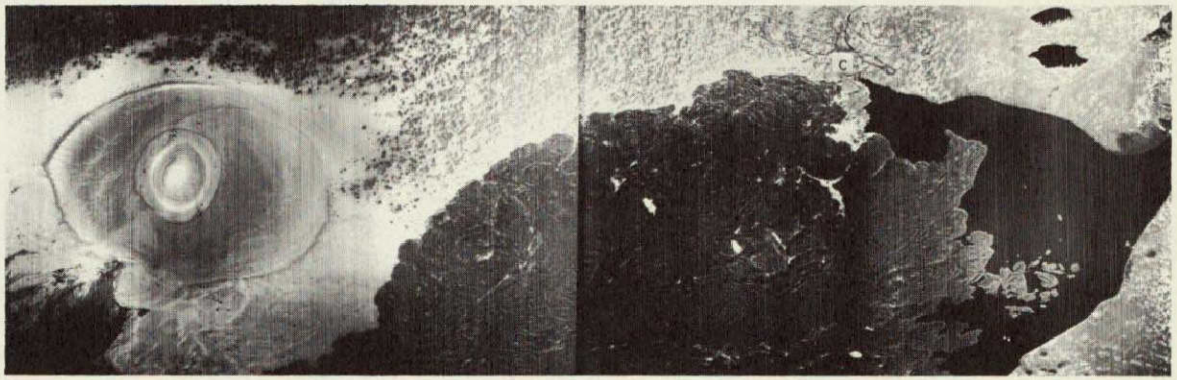

b. Pre-dawn thermal infrared imagery.

Figure 31-6.- Example of thermal emittence variation measured at mid-day and pre-dawn periods.
periods.

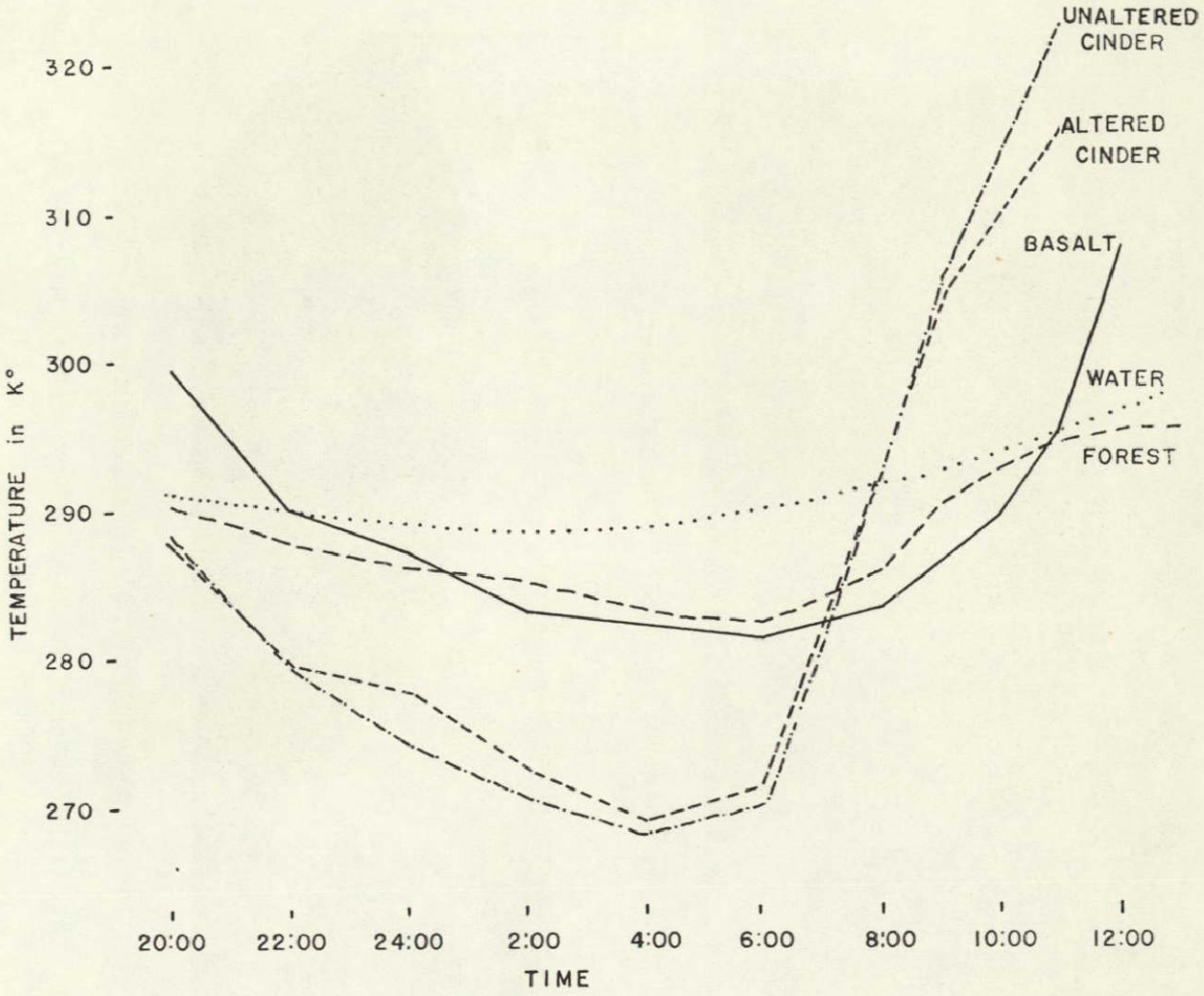

Figure 31-7.- Diurnal radiometric temperatures - July 24-25, 1968, Mt. Lassen cinder cone.

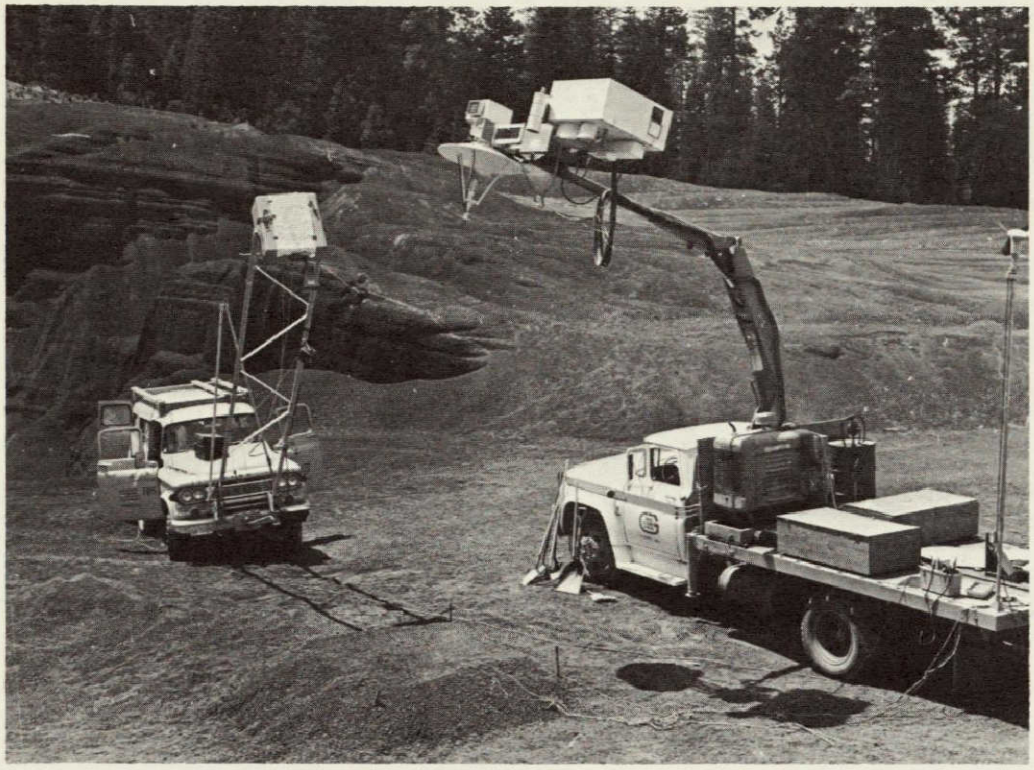

Figure 31-8.- J.P.L. and Aerojet-General Microwave vans at Poison Lake Cinder Pit.

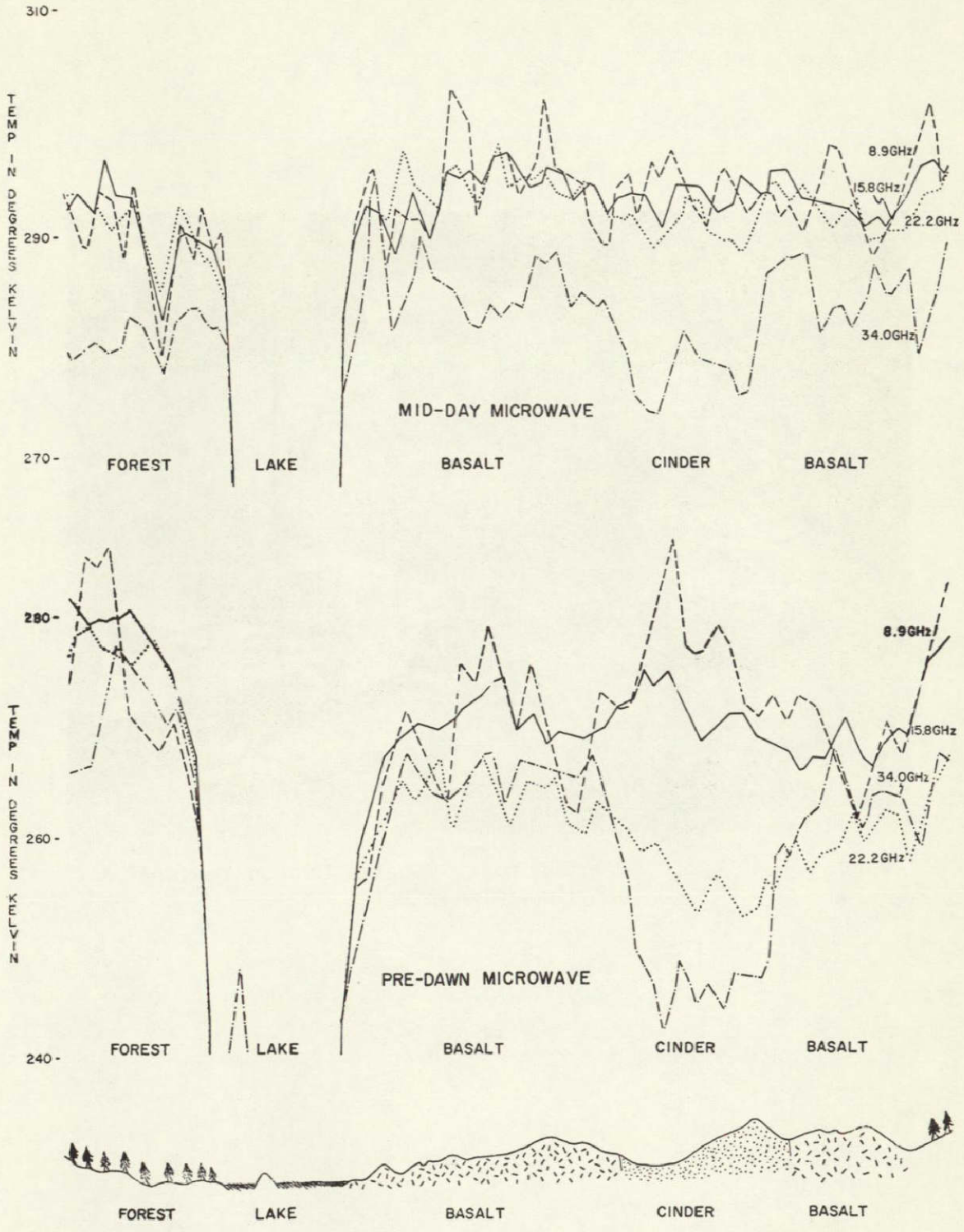

Figure 31-9.- Mid-day and pre-dawn microwave data.

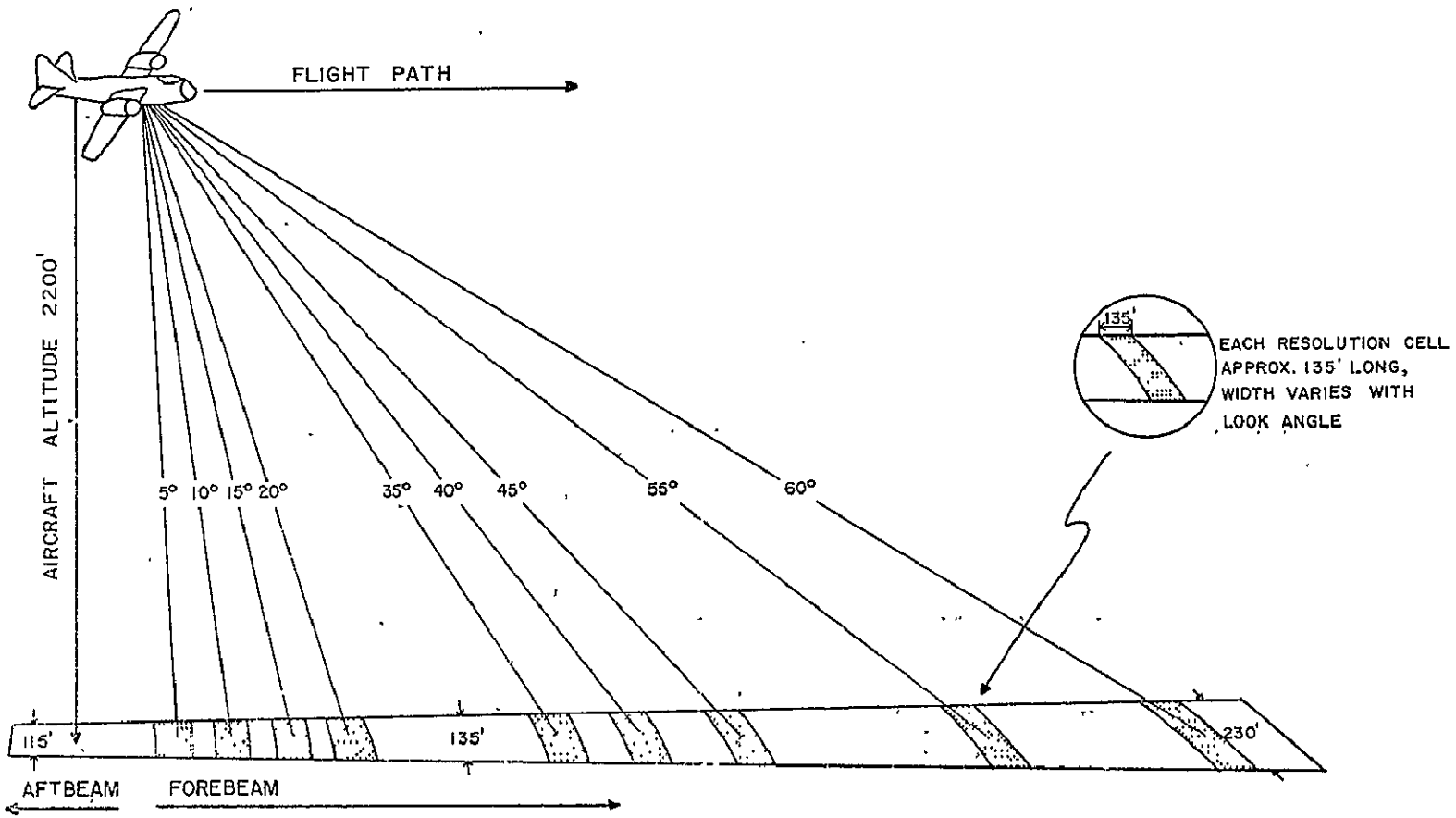

Figure 31-10.- Ryan scatterometer fan beam geometry.

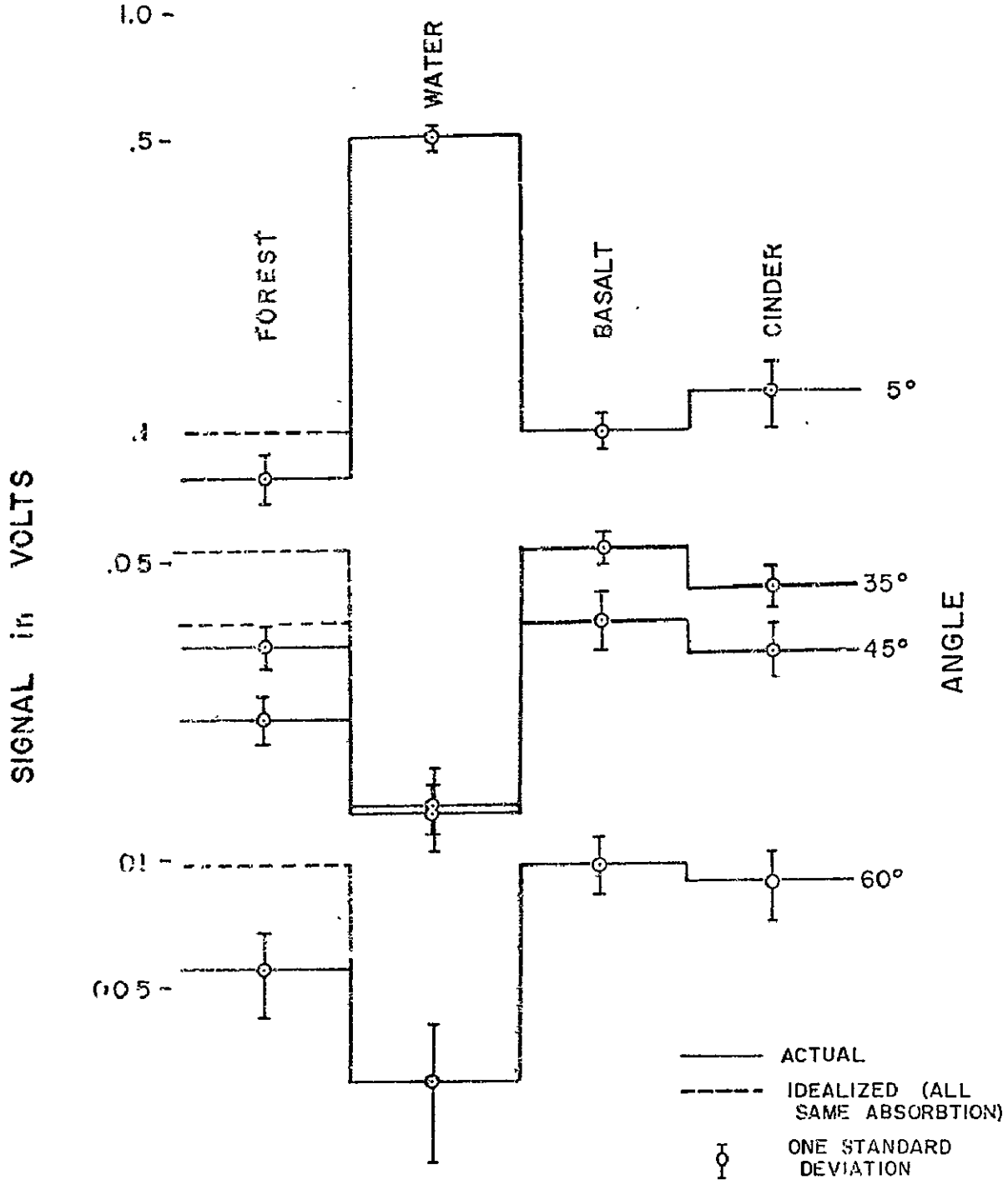

Figure 31-11.- Idealized scatterometer returns.

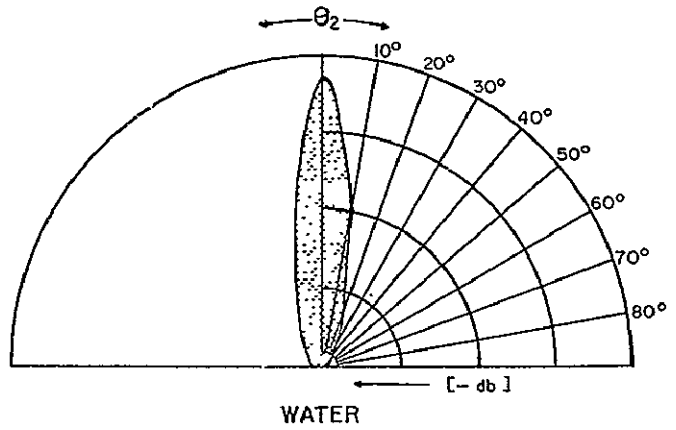

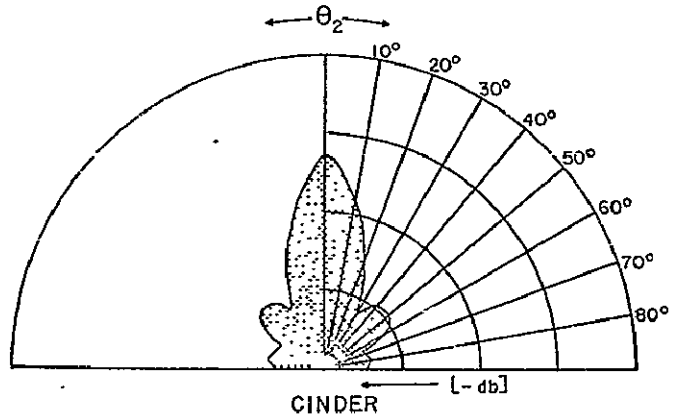

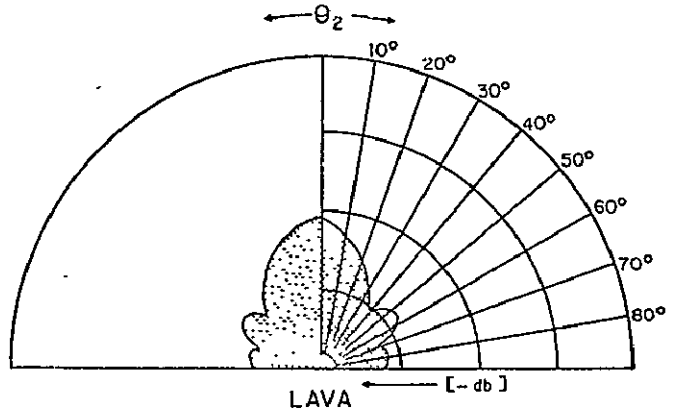

Figure 31-12.- Theoretical scattering diagrams of the three principle surfaces.

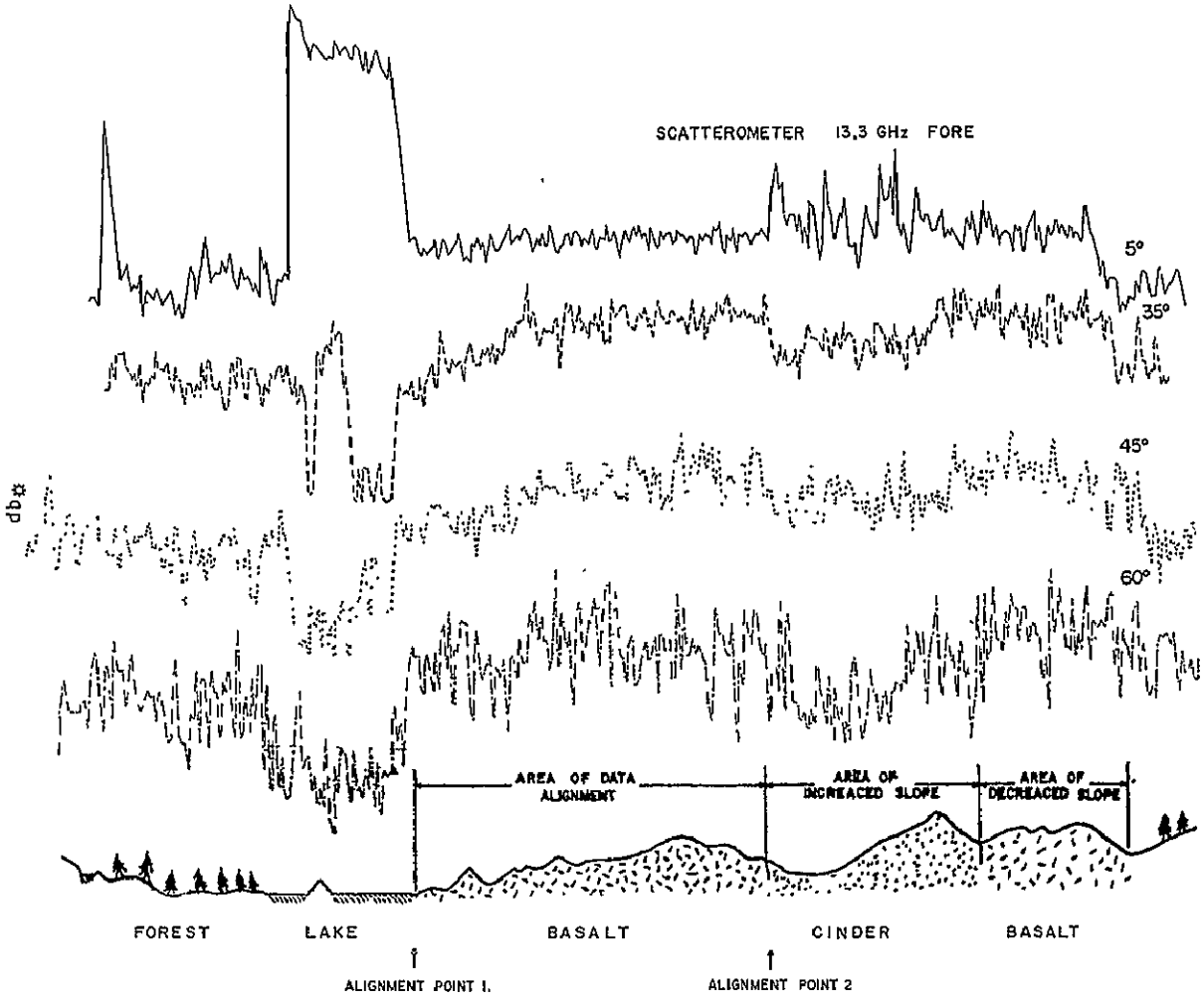

Figure 31-13. - Time delay shifts in scatterometer data due to topography.

SECTION 32

RADAR AND DATA PROCESSING

by

Richard K. Moore

The University of Kansas

University of Kansas research in radar and data processing continued during the past year toward the goals established in 1964 when we started working with NASA in this program. The overall goals of the study are: (1) to learn how to design the best space radars for earth resources application for different types of spacecraft, and (2) to develop means for automatically processing the tremendous quantity of multi-image data that will be produced by these radars and other sensing systems. The studies of spacecraft radars involve measurements with aircraft radars, development of radar systems and evaluation of trade-offs, and fundamental research to aid in understanding the way radars sense the quantities of interest to earth resource applications. The aircraft measurement program has two principal goals: (1) to determine what radar can do for the various earth resource disciplines, and (2) to determine the best radar parameters (frequencies or combinations of frequencies, look angles, polarizations, resolutions, etc.) for each of the identifiable earth resource applications. To make aircraft measurements that can answer these questions successfully, the University of Kansas continues to recommend radars to be used in the NASA Earth Resources Aircraft Program and experiments to be performed with these radars. In addition, we find it necessary to work closely with NASA/MSC personnel in validating the radars that have been procured for the program.

In our study of radar systems, we continued this year to evaluate the various possible spacecraft radars and trade-offs involved between the various parameters. More trade-offs are possible with radar systems than with any other type of sensor, so this is a complex task. In addition, we are continuing our research into the development of better radar techniques that will apply to the Earth Resources Aircraft and Spacecraft Programs.

To assist in understanding the empirically derived information from the aircraft measurements, we conduct a continuing study of the fundamentals of radar scatter from natural surfaces and simplified surface models. This is both theoretical research and experimental work under controlled conditions in the ultrasonic simulator and with our new broad spectrum radar.

Automation of parts of the data analysis for the spacecraft system will be indispensable. For example, a 40-kilometer-swath radar with 20 meter resolution and 32 gray scales produces information at a rate of about 3.5×10^6 bits per second. Yet, we believe that spacecraft radars will work with multiple frequencies and polarizations and, hopefully, with wider swaths, all of which will greatly increase the data rate. Because this was recognized in 1964, development was started at that time on a near-real-time analog processing system for multiple images, the IDECS (Image Discrimination Enhancement Combination System). The goal of this research is a system capable, where

feasible, of automatic classification of terrain uses and types, and of increasing the efficiency of human operators where automation is not feasible. Although we believe analog techniques are necessary for handling data in quantity, appropriate decision rules for the IDECS may best be developed by applying digital techniques to relatively small learning sets of the received images. Accordingly, an extensive system of digital multi-image pattern recognition and related programs has been developed since 1964, and its development continues. Within the past year this group of programs has been combined into KANDIDATS, the Kansas Ditital Image Data System, and most of it rewritten in a form making more efficient use of the GE 635 computer at the University of Kansas.

This paper is divided into five main sections: one dealing with the aircraft program, one with radar systems studies, one with fundamental studies, one with the IDECS, and one with the KANDIDATS.

AIRCRAFT PROGRAMS

Two types of radar are involved in the NASA Earth Resources Aircraft Program: scatterometers and imagers. The scatterometers have direct value over the sea from spacecraft altitudes, as detailed elsewhere in this meeting. Although scatterometers may be valuable in their own right at aircraft altitudes over land, we believe that neither scatterometers nor passive microwave systems have many direct spacecraft applications over land because of their poor resolution. For example, the scatterometer or passive microwave system must have an antenna 500 wavelengths long to achieve 2 milliradian resolution. Such an antenna would be 15 meters long at a wavelength of 3 cm for the scatterometer and 15 meters square for the passive microwave system. Even if a larger antenna could be built, it is doubtful if tolerances could be maintained to achieve much better resolution than 2 milliradians. For a low spacecraft altitude (200 statute miles) this represents a resolution of about 2,000 feet. As Simonett has pointed out,[1] the value of such resolution is quite limited, although it might be useful for determining such things as boundary of large regions of recent rainfall or of melting and freezing zones in the Arctic.

Because of this resolution problem, overland use of the scatterometer in the aircraft program should concentrate on obtaining quantitative data relating to optimum angles of incidence, frequency, and polarization to be used in spacecraft imaging systems. This is especially important because of a lack of well-calibrated aircraft imaging radars. Aircraft scatterometer missions flown with the 13.3 GHz system during the past year have apparently been subject to saturation and high noise levels which caused the measurements to be questionable at the angles of incidence most suitable for application to design of imaging radars. Apparently useful information was obtained within about 15^{o} of the vertical from three missions over Garden City (32, 61, and 80). This could be valuable for the design of a diffraction-limited downward looking radar for use at low altitudes where the diffraction limitation would not prohibit adequate resolution.

When the problems with the new 13.3 GHz scatterometer have been resolved, we will recommend flying it and the 0.4 GHz scatterometer simultaneously over land targets, as we believe much useful radar design information

will be obtained from this pair of systems.

During the past year, the 16.5 GHz SLAR was installed on the P-3 aircraft and initial test flights made. Users contemplating application of this system should be fully aware of the basis on which it was selected. A synthetic aperture system was desired that could be flown unclassified and would achieve resolutions roughly comparable with that for a first generation spacecraft radar. The system selected was the only one available that met these requirements. Its resolution is considerably poorer than desirable and it does not use any of the gray scale improvement techniques that one would desire in a system for earth resources application. Furthermore, it has only the most rudimentary motion compensation, achieved by coupling to sensors that are part of the aircraft system. Thus, results with this system may be disappointing to many users, particularly when it is flown in turbulent air.

A specially-designed experimental multipolarization antenna was procured for this system, rather than merely adding an antenna with vertical polarization to the existing horizontal polarization antenna. Ability of this newly designed antenna to separate the polarizations is considerably poorer than desirable. Whether it will be satisfactory remains to be determined upon analysis of images obtained from the system.

The initial functional check flight over the Houston area produced images that were quite disappointing. We understand that images obtained over Mexico and Brazil were equally disappointing. The strip of film from Brazil that I have personally examined appears to have been flown under turbulent conditions, so much of it is unsatisfactory.

The processor was recently adjusted before a flight to the Garden City, Kansas, area. Also a modification was made in the film development procedure for this mission. Preliminary examination of the film from this mission indicates that it is marginally acceptable for agricultural land use studies. Final conclusions about this application with the system in its present form must await detailed study of the imagery which has not yet been received at the University of Kansas.

Test imagery flown by Philco-Ford in the California area with the system operated in a real-aperture mode indicates that the gray scales for this mode are much more suitable for earth science applications than are those for the synthetic aperture mode although, of course, the along-track resolution is not as good. Modification of the system to permit use of this mode appears to be a relatively simple task involving installation of already existing logarithmic intermediate-frequency amplifiers in place of those used with the synthetic aperture mode. Recommendations have been made that a test installation of these amplifiers be completed as soon as possible. After the films obtained with the system in this configuration have been analyzed and compared with those obtained in the synthetic aperture configuration, final recommendations for the system will be made.

The present SLAR was designed about 1960. We have recommended that a more modern system constructed and flown by the University of Michigan be

flown over the same test sites at about the same time as this SLAR, so that comparisons can be made between a fine-resolution modern system and the system on the P-3.

The Naval Research Laboratory four-frequency radar aircraft was equipped to produce synthetic aperture images by NASA several years ago.* Problems have continued to plague this imaging system, but improvements are being made and it is expected that good synthetic aperture images at several frequencies will be made by this system during the forthcoming year.

RADAR SYSTEMS STUDIES

A computer study of trade-offs possible for imaging spacecraft radars is nearly complete. The effects of varying different parameters such as resolution, transmitter power, swath width and frequency are considered. A report on this study will be issued soon.

Imaging radar systems usually suffer from a "pepper and salt" effect because of insufficient averaging of the returns from the different resolution cells. If a resolution cell contains a large number of relatively equal scattering centers, the amplitude of the signal returned to the radar is determined by the Rayleigh distribution. In the Rayleigh distribution 90% of the returns are contained within a range of 18 dB. For adequate discrimination of different types of return, this spread must be reduced to, at most, a very few dB. The spread can be reduced by averaging many independent samples. In the scatterometer this can be achieved by making a long enough resolution cell so that as the radar passes the cell many elements of the fine structure of its scattering pattern are averaged; with the imaging radar this may not be possible because of the finer resolution. Real-aperture side-looking radars usually average several independent samples, hence the variation is much less than the 18 dB of the Rayleigh distribution. One way to achieve the same result with a synthetic aperture radar is to process for a finer resolution than ultimately will be used. The returns from each of the smaller resolution cells will be independent of the other so that several may be averaged to achieve a poorer resolution but better gray scale.

With optical sensors this "pepper and salt" effect is encountered only if very pure laser illumination is used. The reason is that averaging may be achieved in frequency when a sufficiently wide band is used. A radar that takes advantage of this technique is "panchromatic." If several broad band radars operating in different regions of the spectrum are combined together, we call the system polypanchromatic.[2,3]

A panchromatic/polypanchromatic test system operating over the frequency range from 4 to 8 GHz (wavelength 3.75 to 7.5 cm) has been constructed at the

---

* The University of Michigan provided the recorders used under a subcontract from the University of Kansas.

University of Kansas.[4] Most of the support for this system was provided by the Department of Defense,* but some has been received from the NASA progra The antenna for this system is truck-mounted on a boom. It is arranged so that either spectral signatures (scatterometer style) or panchromatic/polypanchroma PPI images can be produced. The system has been tested in the laboratory and its first truck test is expected about 10 October.

Figure 1 illustrates the advantage of the panchromatic system as found in an early test. Three images are shown, two with a narrow band system (40 MHz) and one with 160 MHz bandwidth. The targets shown are cars in a parking lot and buildings about a thousand feet from the radar. Clearly each of the narrow-band images shows some of the targets and misses others. The broad-band image shows every target contained in the narrow-band images plus some additional ones. No gray scale appears on this photograph because the radar was operated at ground level looking horizontally, and only vertical surfaces gave strong enough returns to be observed. Operation with the antenna elevated on a boom when the truck is parked on a high elevation should permit production of terrain images with suitable gray scales.

Clearly radar to be used for earth resources application should be panchromatic, at least to some degree, so that the 18 dB range of the Rayleigh distribution is reduced to a level permitting adequate discrimination between different types of terrain. Various averaging techniques, including the use of panchromatic radars, will be studied more in the near future and recommendatio made for their application to both the aircraft and spacecraft radar programs.

FUNDAMENTAL STUDIES

The effect on radar response of differences in polarization has been clearly demonstrated in studies with the Westinghouse radar system flown previously for NASA[5,6,7] and by other investigators such as NRL. Hence the National Science Foundation-sponsored research** at the University of Kansas into the theory of polarization dependence of radar returns is germane to the earth resources program.

Most natural surfaces are horizontally inhomogeneous within a resolutic cell. NSF sponsored research** on the effect of such inhomogeneities on the radar return are therefore also germane.

Radar return theory and controlled experiments in the past have always been based on the assumption that the return came from the rough boundary between the air and a homogeneous ground. Although this may be true for the ocean, it certainly is not true for most land surfaces. The soil usually comes i layers and the moisture content of the soil is also a function of depth. Accordingly, research has been conducted on the effect of scatter from boundaries beneath the surface on the scattering coefficient curves such as produced by a

---

* Contract DAAK02-C-0089, Project Themis, ARPA Work Order 1079 through U. S. Army Engineer Topographic Lab.
** Grants GP2259, GK1153.

scatterometer. The results are reported in a recent thesis by Dr. William E. Boles.[8]

Figure 2 illustrates the experimental equipment used by Boles. A layer of wax was used as a target in the ultrasonic tank. One surface was rough and the other smooth, and the roughness was accurately measured. Layers having the same surface statistics were molded with different thicknesses. The illustration shows a layer supported in the tank with the transducers (antennas) at the bottom looking up at the layer, which may be submerged completely or floated. The reflection coefficient between wax and water is about .05, whereas that between wax and air is 1.

Figure 3 shows the results for four different situations: rough surface to the front and both surfaces submerged (both reflection coefficients .05), rough surface to the front with the wax floating (back reflection coefficient 1), smooth surface to the front and both surfaces submerged (both reflection coefficients .05), and smooth surface to the front and the wax floating (reflection coefficient 1 at the back). Curves are shown for layers having different thicknesses and consequently different total attenuations. Clearly, when the attenuation is not too great, the scattering may be controlled by the back surface instead of the front surface, especially when the reflection coefficient is much larger at the back than at the front. This result may have important implications for the interpretation of radar returns from crops and layered soil and rock. Apparently just this sort of situation prevailed in the low frequency images obtained at Pisgah Crater with the NRL radar system.[9]

HIGH SPEED DATA PROCESSING (IDECS)

The necessity for rapid processing of multiple radar images was realized at the beginning of this program. Accordingly, a device was developed permitting the scanning of multiple images and performance of logic operations at the scan rate.[10] The output is on a color television set. Although this system was developed for multiple radar images, it is equally applicable to any kind of multispectral or multitime imagery that can be brought to congruence. The system developed at the University of Kansas was designed with the object of experimenting with new techniques and is not intended as an operational system. Accordingly, inexpensive flying spot scanners and a standard color television were used, with relatively poor resolution resulting. An ultimate system would use much better flying spot scanners (or obtain its data from magnetic tape) and would use a higher resolution display than obtainable with the ordinary color television set. Furthermore, an operational system for use with strip images such as those from the radar or the multispectral scanner would contain provisions for continuously moving and congruencing the various images so that a continuous output would be possible.

The IDECS has gone through several modifications. The form used during the summer of 1969 is shown in Figure 4, where Dr. Simonett is operating the equipment in a land-use mapping experiment. The four flying-spot scanners are shown at left, the control and monitor console in the center, and the color and black-and-white television displays at the right. Illustrated on the monitor oscilloscope is a three-dimensional plot representing microdensitometer type

traces for all the lines in the picture. The trace for an individual line can be brightened simultaneously both on the monitor and on the black and white displa and a cursor moved on the display to identify the particular point for which the density is observed. The counter shown in the upper hand corner of the monitor and control unit can, among other things, be used to determine the total area associated with a particular category selected by the controls.

Figure 5 shows the block diagram of the IDECS and indicates progress during the past year. Perhaps the most significant addition during the past year has been the digital disc recorder. This recorder was originally installed to serve as a buffer between the magnetic tape unit or the planned local digital computer and the television display. The technique is apparently similar to that being used in the Purdue display described by Landgrebe[11]---except that at Kansas we started with the display and will get the computer later, which is the reverse of the situation at Purdue.

Since the digital disc recorder became operational before the magnetic tape unit,* it has been used for other purposes than originally intended. This recorder contains 24 tracks, each of which can store one image, and it has made possible a considerable improvement in the use of the IDECS by its operators. For instance, a single category may be selected using the decision device** and black and white display and then stored on the recorder. The operator can then select another category, store it on the disc and repeat this up to 24 times. At the end of all of these separate selections, each channel on the disc may be assigned a different color on the color display so that a multicolor thematic map is automatically presented by playing back all the contents of the disc into the display. The texture generator will permit displaying various kinds of stippling or cross-hatching instead of colors.

The scanning densitometer will permit digitizing images with better resolution than possible with the flying spot scanners. Combining these units with the magnetic tape unit allows digitized images to be processed on the GE 635 digital computer at the Kansas University Computation Center and brough back for subsequent color display.

The local digital computer will be installed as a controller for the IDECS and a memory for decision rules; it will also be used for simpler digital processing tasks. This $40,000 computer is made possible by grants from the Nationa Science Foundation[X] and from the University of Kansas.

Tests of the value of a device such as this have been continued during th past year under an Army program[†12] and under the geography program of the USGS

---

* The magnetic tape unit was incorrectly shown as operational in the report presented last year (2). It should be operational about 1 November 1969.

** Also called spectrance selector and signature selector. A completely new version of this unit has been constructed during the year to overcome limitations in quantization and operator convenience with the old system.

X GK3738

† Contract DAAK02-67-0435

†† Contract 14-08-0001-10848

It has been used by USGS/Geography investigators from University of California, Riverside, and NASA/USDA investigators from Berkeley.

Figures 6 and 7 show an example of agricultural land use mapping with the IDECS. Figure 6 shows three mosaiced frames of aerial photography obtained over the Garden City area in a flight of the Earth Resources Aircraft Program. Figure 7 compares the land-use map for these photographs obtained from field and photo interpretation with the map produced by the IDECS. The IDECS map, of course, is based upon a point by point application of a decision rule to color separation black-and-white images made from the Ektachrome, and Ektachrome-IR photos. Errors in the mapping are primarily due to the fact that the decision rule simply could not achieve correct decisions at all points with the data presented to it.

Figures 8 and 9 illustrate the application of the disc memory to a set of multispectral SO-65 space photographs of the Imperial Valley. Figure 8 shows one of the images as it appeared on the black and white display, and Figure 9 shows the result of successively storing three categories on separate channels of the disc. In this case, red represents bare ground and and fields with minimum ground cover, blue represents rye and cut alfalfa, while green represents barley, sugar beets and uncut alfalfa. A slight signal delay in the early implementation of the disc memory causes displacement of some of the colors to the right.

Image texture is widely used by photo interpreters to discriminate between different kinds of surfaces. An experimental texture analyzer for the IDECS was constructed and tested during the year although final details of the data analysis are not yet complete.[14] Figure 10 shows the technique used. The normal flying spot linear motion is perturbed with a signal that would, in the absence of the scanning voltage, cause circular motion. Because of the simultaneous presence of the linear scan, this becomes a spiral motion. Thus, the intensity at the output corresponding to one loop of the spiral is an average of image densities in the vicinity of the center of the spiral, rather than the intensity for that particular spot. This technique involved determining the frequency content of the signal obtained by this type of scan for a particular part of the picture having a fixed texture. Presumably the spectrum of the scanner output in this case will have a shape determined by the texture.

In the implementation used, the output passed through a series of band pass filters, one for each of the harmonics of the rotation rate up through number 8. Thus the spectrum was sampled out to 8 times the rotation frequency. The output of the filter at the second harmonic of the scan rate produces an image in which edges are strongly enhanced, and this technique in itself is useful. Figure 11 shows such an edge enhancement for a photograph of a field pattern. Clearly the boundaries are all sharply delineated, along with some interesting structures in the uncultivated part of the image.

The same technique was tried with a radar image obtained in the Westinghouse flights for the Earth Resources Program. The image of the San Andreas Fault area and the harmonic output are shown in Figure 12. Although it is difficult for an unskilled interpreter to detect anything valuable from this line structure, the geologists who have been studying this area indicate that

the patterns of the harmonic display show valuable features that might otherwise be hard to detect. Further study of this technique will be conducted in the future

DIGITAL PROCESSING SYSTEMS

Although the computer memory required for handling the vast quantities of data expected in an Earth Resources Satellite would be too large to permit operational digital systems requiring image storage in the computer memory, such techniques may be extremely valuable in determining the proper algorithms to use for quantity data processing with a system like the IDECS. Numerous pattern recognition algorithms have been developed or applied to the multi-image problem at the University of Kansas since 1965.[15] During the past year these programs have been rewritten into a complete system, the KANDIDATS (Kansas Digital Image Data System). Although all programs were originally written in Fortran, they have been modified and a system monitor developed for use with the GE 635 computer in its assembly language GMAP. The language of the KANDIDATS system itself has been greatly simplified so that users may control input-output and the various processes with a simple set of code words. Most of the individual routines are complete and the system monitor program is presently being debugged.

Figure 13 shows the flow diagram for the KANDIDATS system. Across the top is a line representing digitizing of images. Of course, if the images were already on magnetic tape the microdensitometer would not be needed. After texture analysis, the various images are brought to congruence with each other by one or two programs involving different amounts of automation and also different amounts of computer time. A system with operator intervention can operate rather quickly in the computer; it simply interpolates between known points in the various images. On the other hand, an automatic system will take more computer time but does not require the operator intervention.

After the various points in the different images have been aligned the multi-image tape is subjected to a principal components analysis. This produces a new set of images that are linear combinations of the original ones. The first principal component contains the largest amount of variance possible from a linear combination of the inputs; the second component is orthogonal to the first and contains the next largest amount of variance, etc. Ordinarily the number of components needed to describe most of the variance is only four or five, even though many more images were brought in as original data.

The next step is quantization. Several possible quantizing techniques can be used. Most straightforward is a simple linear one; that is, if 32 quantum levels are to be used, the amplitudes are assigned to 32 equal-size ranges. Frequently, however, it is better to quantize with steps in one part of the amplitude range larger than those in another part. New ways of doing this are implemented in the different quantizing programs.

At this point the data may go either of two ways. If adequate ground truth is available, a Bayes decision program is selected. This compares the data in the training set of information with the ground truth and arrives at a decision rule. The decision rule may then be applied to the entire image or,

in fact, it can be applied to a machine like the IDECS which can implement it on a large quantity of data.

If insufficient ground truth is available, the data go from the quantizing program to the feature extraction and clustering programs where one of the three available may be selected. These programs attempt to locate natural boundaries in data space without reference to ground truth. After the natural boundaries have been located, detailed photo interpretation in a learning-region or dispatch of ground truth parties to sample points identified with each category will permit determining actual contents of the regions. These algorithms can also be used with the IDECS or a similar device once they are known. The structure analysis program will permit refining this technique, but is not yet written.

One of the clustering programs (believed to be unique) was applied to the Yellowstone Park University of Michigan multispectral scanner data obtained for H. Smedes of the USGS, with partial financial support from the USGS. Figures 14 and 15 are associated with this test.[16] In Figure 14, computer printouts of the first four principal components are shown. Figure 15 shows a feature map of the homogeneous regions identified in the data. The seven separate regions are tentatively identified on the basis of analysis of a single aerial photograph of the region. At the time of writing, it had not been possible to compare directly with ground truth. Note that the number of categories located was less than the number used in the Bayes decision program at Purdue.[11] Apparently there are two reasons for this: (1) clustering methods produce a map without ground truth while the Bayes program takes advantage of ground truth and can partition data space more finely than the clustering program since some clusters may indeed represent more than one category and can only be separated if the ground truth is available; and (2) the spatial resolution was considerably degraded prior to use of the clustering program to reduce the amount of computer time required. Thus the category "river" that appears in the Purdue data could not be detected here because the river was too small compared with the resolution cell used.

Further comparisons of the results obtained with clustering and Bayes' decision programs will be especially interesting, since the clustering technique can be used in regions where there is very little ground truth or where ground is to be gathered ex post facto---provided its identification is satisfactory.

CONCLUSIONS

Preliminary experiments indicate that the panchromatic radar technique and other averaging methods will be most important in earth resources radar imaging systems to improve gray scale rendition. Very soon we should have for the first time some continuous spectral signatures across an octave in the microwave region. This will give an indication of the expected value from a polypanchromatic system.

The 16.5 GHz SLAR on the MSC aircraft appears marginally acceptable pending further analysis for certain kinds of earth resources missions. However, we strongly recommend that a new polypanchromatic synthetic aperture system for the aircraft program be started as soon as possible, since spacecraft systems surely will ultimately use the polypanchromatic technique. Meanwhile use of

the 16.5 GHz SLAR, the University of Michigan SLAR and other SLAR's that may be available should be checked, and appropriate systems selected for continuing study of earth resources applications. Careful experiment design will permit quantitative answers to the many unresolved questions about the value of imaging radar. Furthermore, multifrequency scatterometry measurements over land made after the systems are fully checked out, should aid in determining the appropriate parameters for imaging systems.

By combining systems such as the KANDIDATS and the IDECS, an integrated real time or near-real time data processing system can be built. We believe such a system is an essential for handling the large quantities of pictorial information to be available from earth resources satellites. An operational IDECS would probably be less flexible but have much better resolution and image handling facilities than the experimental unit at the University of Kansas. Where appropriate, elements of the KANDIDATS and the LARSYS[17] should be combined to assist in establishing appropriate decision rules for the IDECS type machine.

References

1. Simonett, D. S., "Thematic Land-Use Mapping with Spacecraft Photography and Radar," Proceedings of Earth Resources Aircraft Program Status Review, September 16-18, 1969.

2. Moore, R. K., "Radar Progress in the NASA Earth Resources Aircraft Program," Proceedings of Earth Resources Aircraft Program Status Review, September 16-18, 1968, pp. 50-1 to 50-51.

3. Moore, R. K., J. W. Rouse, and W. P. Waite, "Panchromatic and Polypanchromatic Radar," Proceedings IEEE, vol. 57, no. 4, April 1969, pp. 590-593.

4. Shaw, P. D., " A Ground Based Polypanchromatic Radar," Master's Thesis, The University of Kansas, 1969.

5. Moore, R. K. and L. F. Dellwig, "Terrain Discrimination by Radar Image Polarization Comparison," Proceedings IEEE, vol. 54, no. 9, pp. 1212-1214.

6. Moore, R. K. and L. F. Dellwig, "The Geological Value of Simultaneously Produced Like and Cross Polarized Radar Imagery," Journal of Geophysical Research, vol. 71, no. 14, pp. 3597-3601.

7. Gillerman, E., "Investigation of Cross-Polarized Radar on Volcanic Rocks," CRES Report 61-25, 1967, 11 pp.

8. Boles, W. E., "Scattering of Waves from a Rough Layer," Ph.D. Dissertation, The University of Kansas, 1969, to be issued as CRES Report 118-19.

9. Dellwig, L. F., "An Evaluation of Multifrequency Radar Imagery of the Pisgah Crater Area, California, CRES Technical Report 118-6, September 1968.

10. Dalke, G. W., "Multi-Image Correlation Systems Study for MGI," Phase I, II, and Final Report Project 112, CRES, The University of Kansas, December 1967, June and December 1968.

11. Landgrebe, D. A., "Automatic Processing of Earth Resources Data," Proceedings of Earth Resources Aircraft Program Status Review, September 16-18, 1969.

12. Dalke, G. W. and J. E. Estes, "Multi-Image Correlation Systems Study for MGI, Final Report," CRES Technical Report 122-4, December 1968.

13. Simonett, D. S., "The Utility of Radar and Other Remote Sensors in Thematic Land Use Mapping from Spacecraft," Annual Report, CRES Technical Report 117-4, The University of Kansas, June 1969.

14. Nossaman, G. A., "Imaged Textural Analysis by a Circular Scanning Technique," CRES Technical Report 118-14, The University of Kansas, August 1969, to be published by NASA/MSC.

15. Haralick, R. M., "The Bayesian Approach to Identification of a Remotely Sensed Environment," CRES Technical Report 113-9, July 1969.

16. Haralick, R. M., "Multi-Image Pattern Recognition: Ideas and Results," Ph.D. Dissertation, The University of Kansas, 1969, to be issued as CRES Report 133-11.

17. Landgrebe, D. A., "Data Processing Programs at Lars-Purdue," Proceedings of Earth Resources Aircraft Program Status Review, September 16-18, 1968, vol. 2, pp. 33/1-24.

MONOCHROMATIC AND PANCHROMATIC IMAGES OF AREA SOUTH OF LEARNED HALL

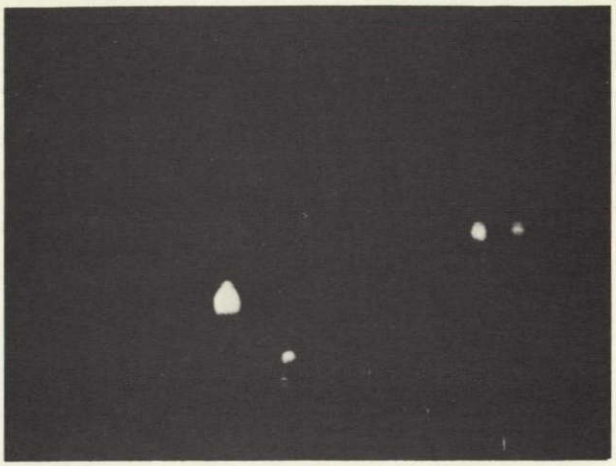

BANDWIDTH 40 MHz 1 SCAN

BANDWIDTH 40 MHz 2 SCANS

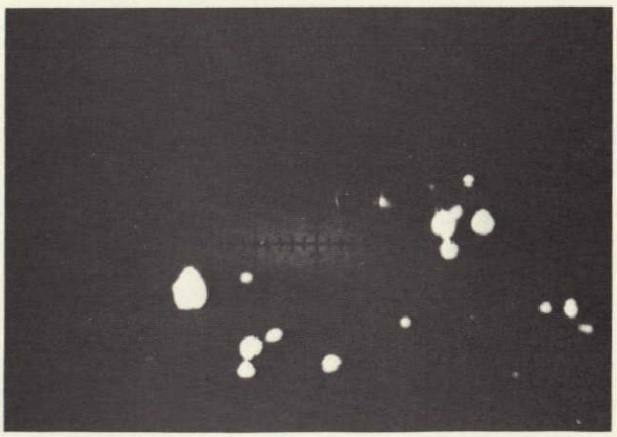

BANDWIDTH 160 MHz 1 SCAN

Figure 1. Illustration of the use of panchromatic (broad-band) radar imaging. High return targets only are shown due to location of radar.

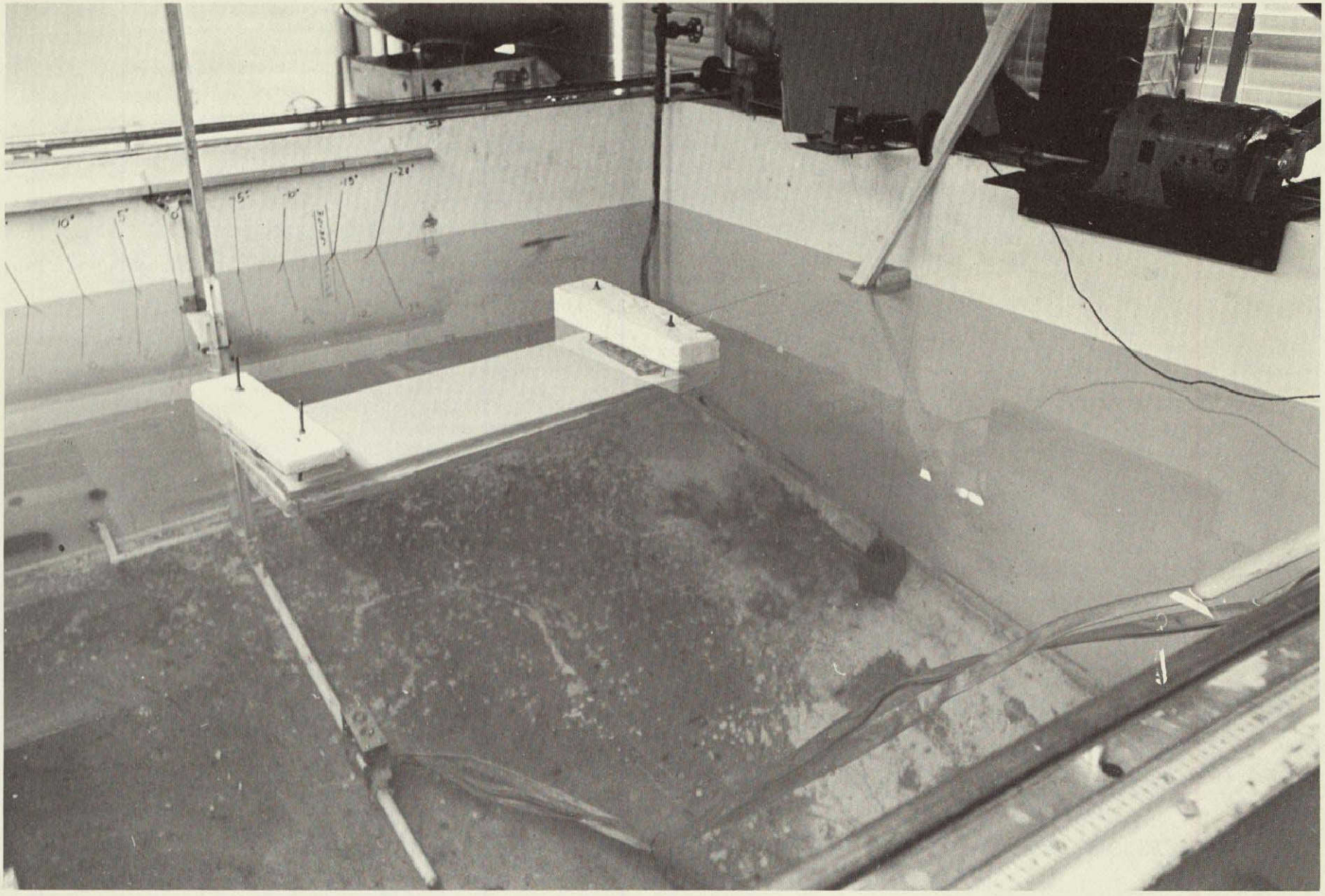

Figure 2. Experiment for ultrasonic measurement of scattering returns from a layer with controlled surfaces.

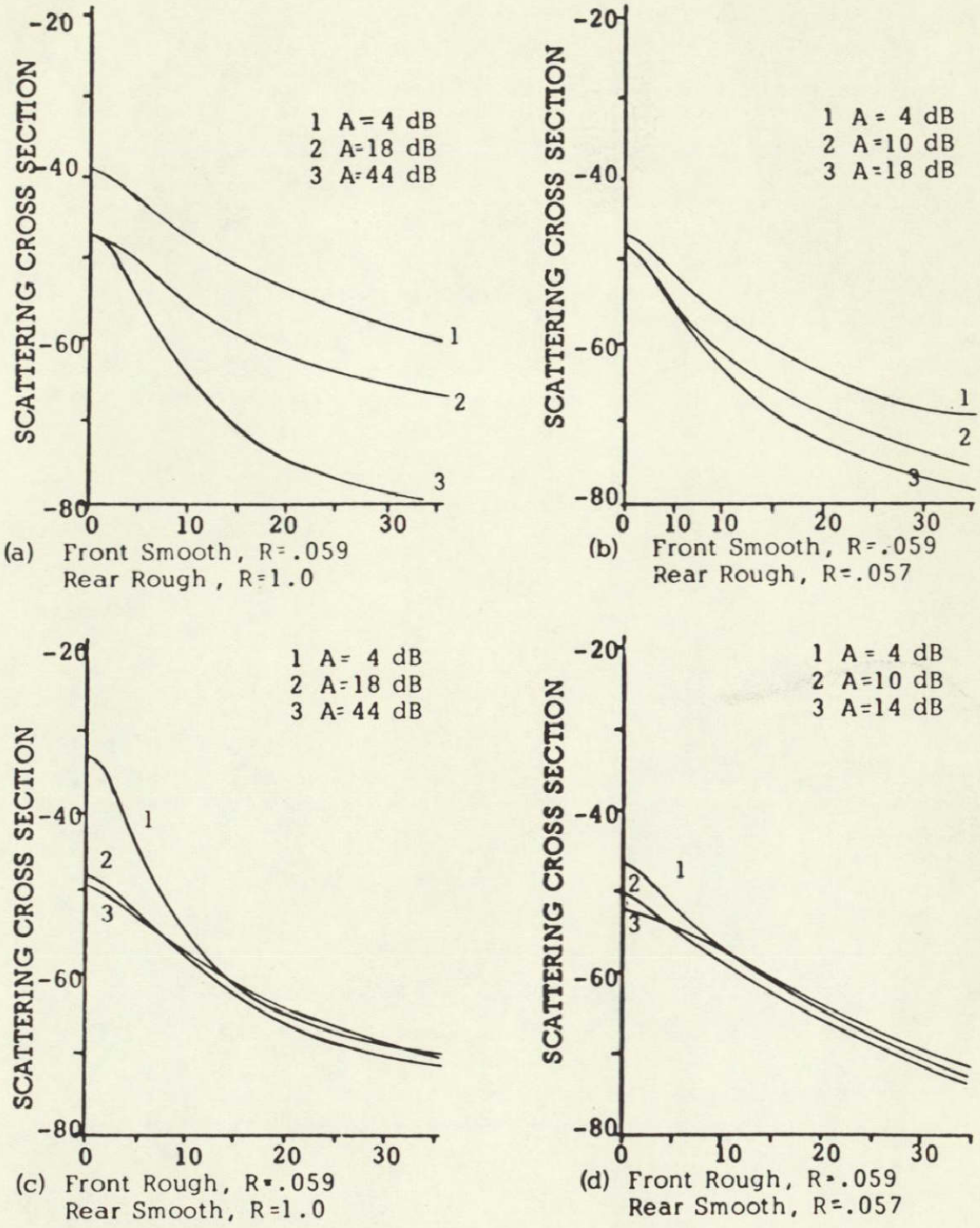

Figure 3. Results of layer-scatter measurements.
(R = reflection coefficient, A = attenuation)

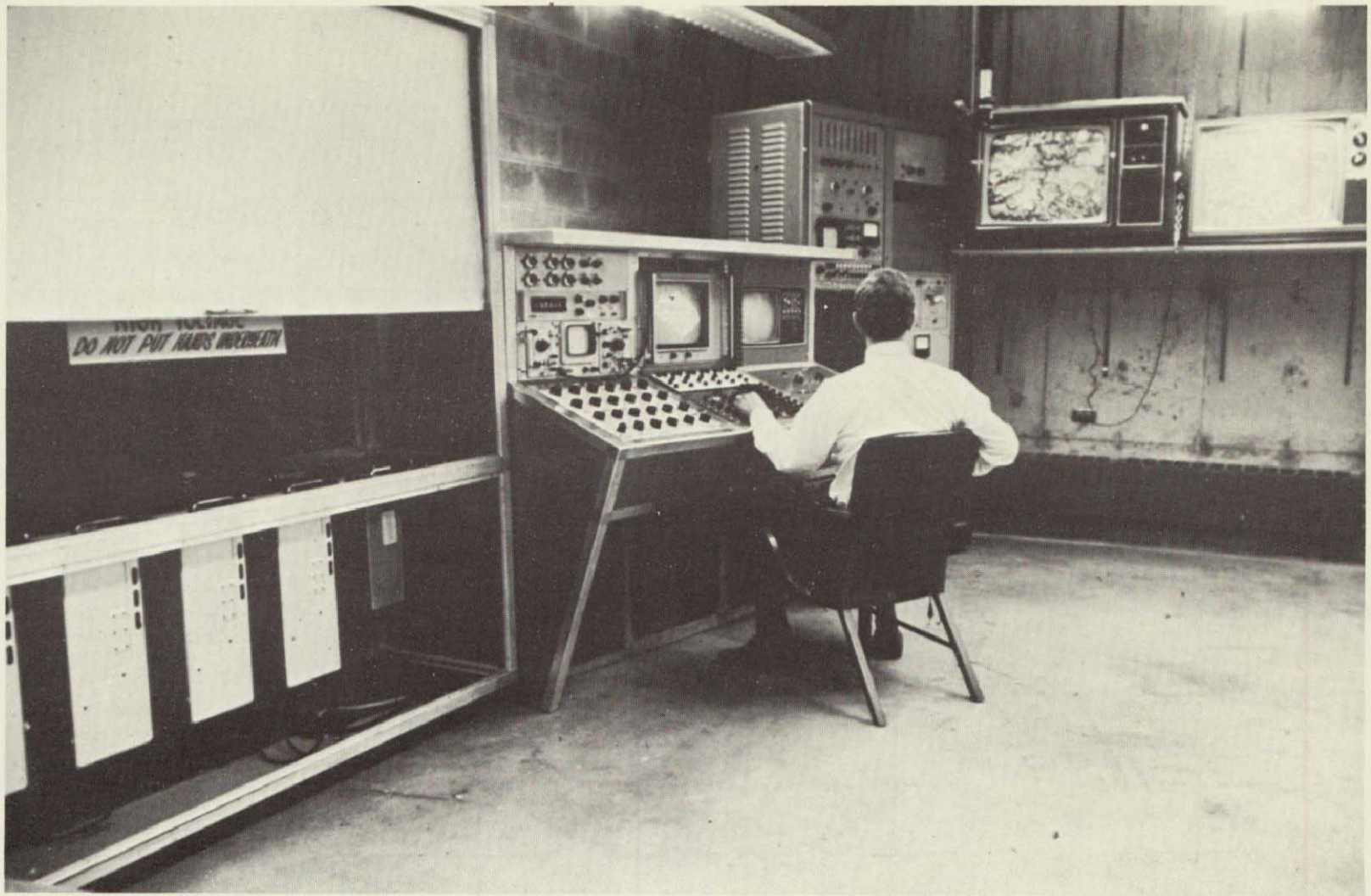

Figure 4. University of Kansas IDECS system used for rapid processing of multiple images (spring 1968).

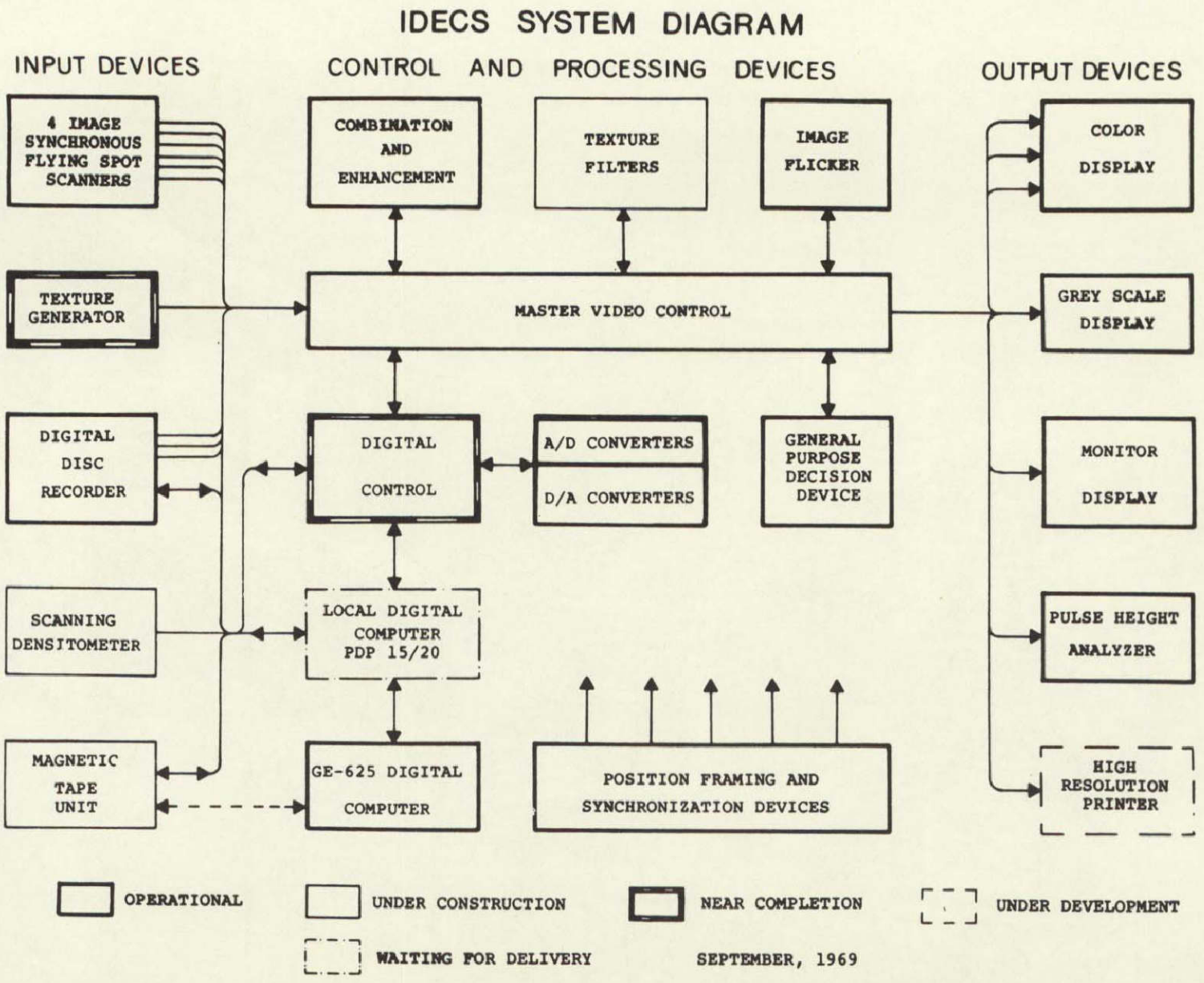

Figure 5. Block diagram of IDECS system.

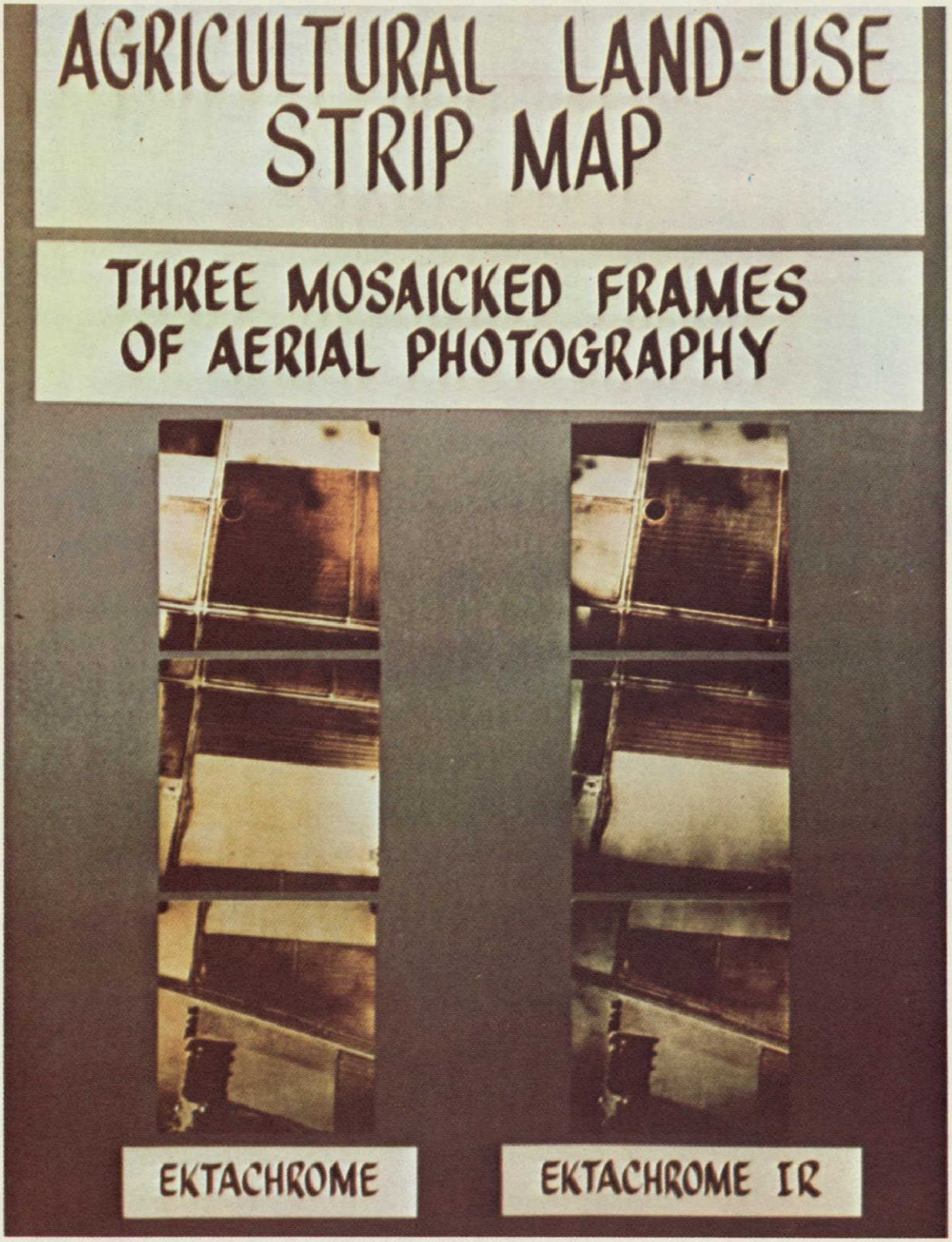

Figure 6. Agricultural land-use strip map (three mosaicked frames of aerial photography).

Figure 7. Agricultural land-use strip map (comparison of ground truth and IDECS interpretation).

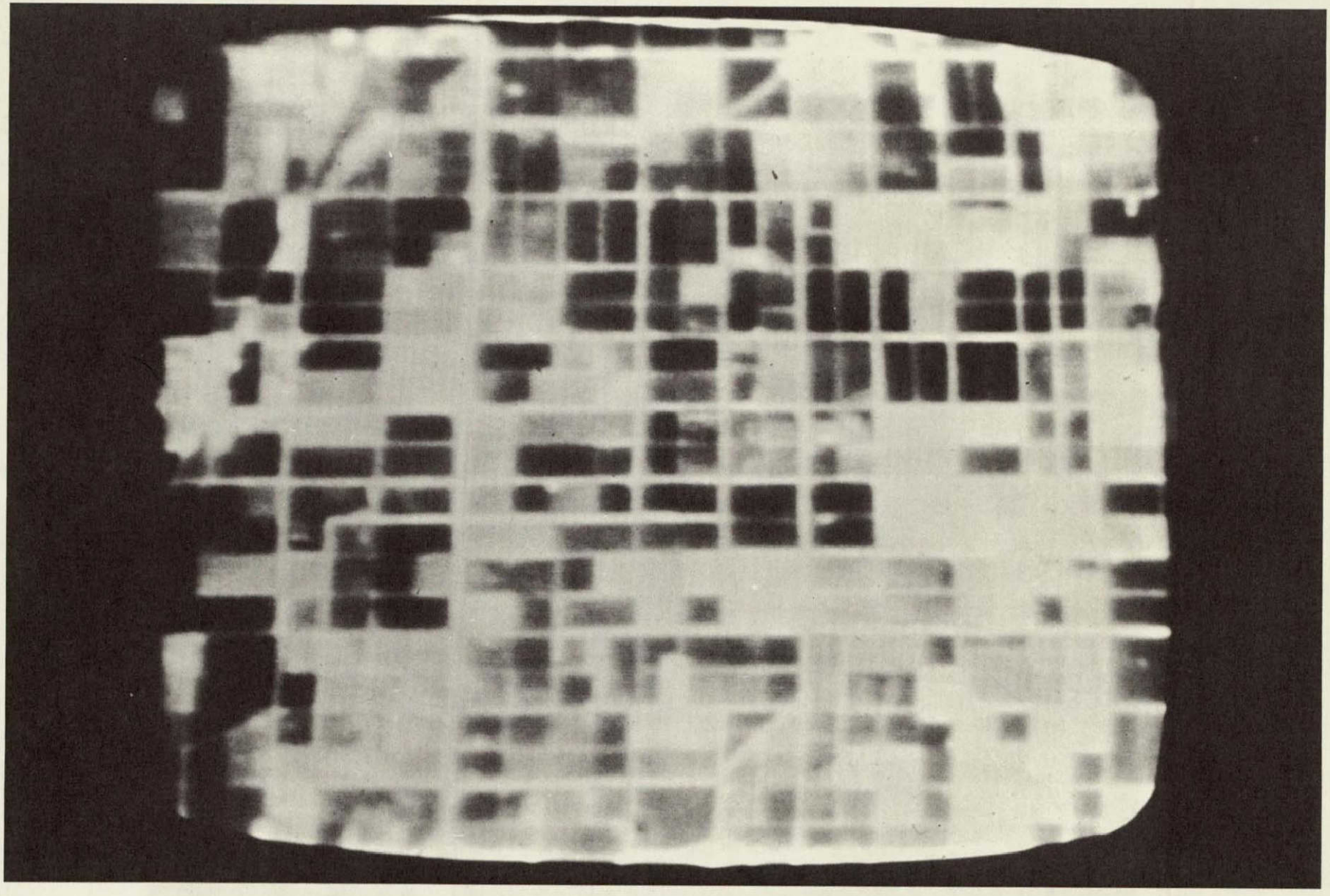

Figure 8. Space photograph of Imperial Valley, California, as displayed on the black-and-white IDECS monitor. This is one of the SO-65 multispectral images used in testing the IDECS disc memory discrimination.

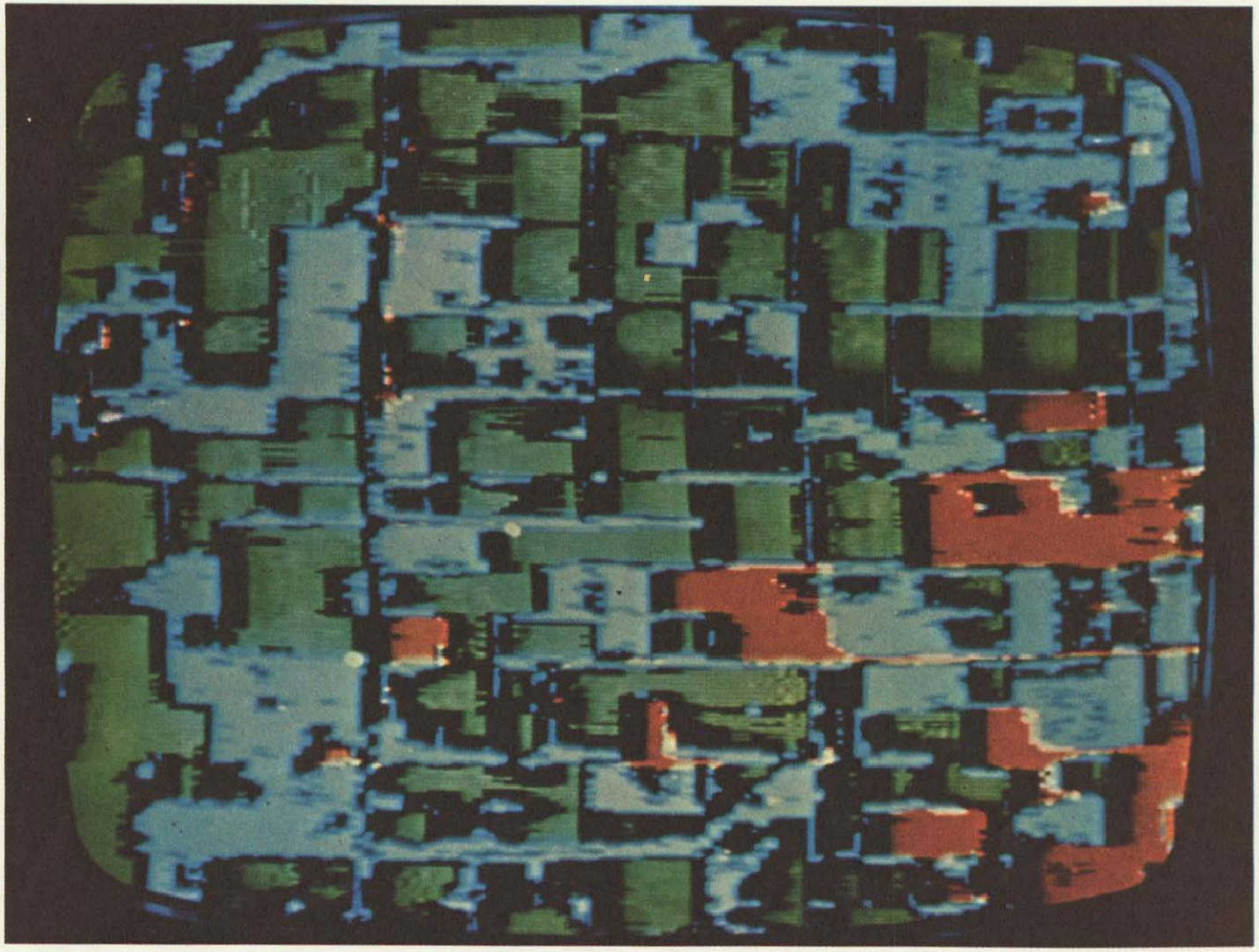

Figure 9. Vegetation categories discriminated by IDECS from S065 images of Imperial, California, during an early test of the disc memory. Red: bare ground and fields with minimum ground cover; blue: rye and cut alfalfa; and green: barley, sugar beets and uncut alfalfa.

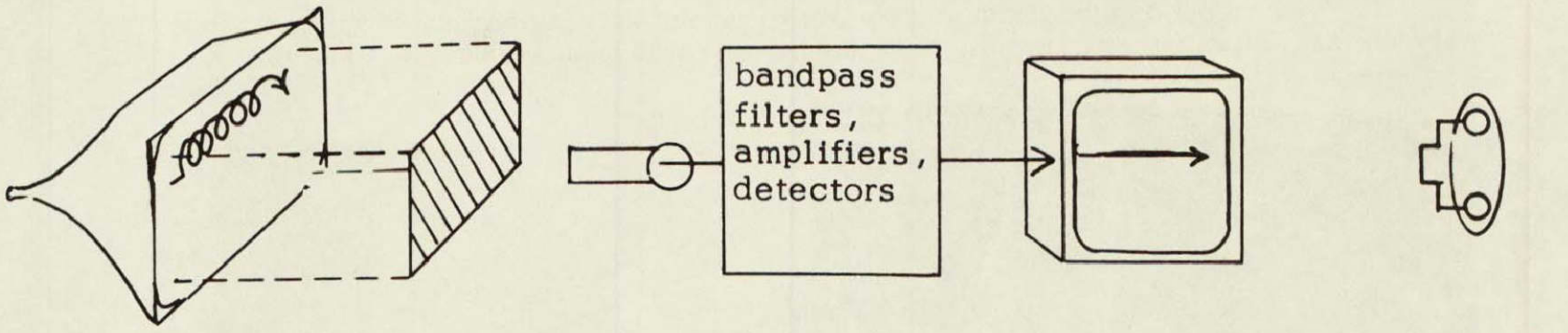

flying spot scanner (spiral trace)

Image

Photomultiplier

display (trace is intensity-modulated by filter outputs)

display recording

Figure 10. A circular scanning system used in IDECS experiments.

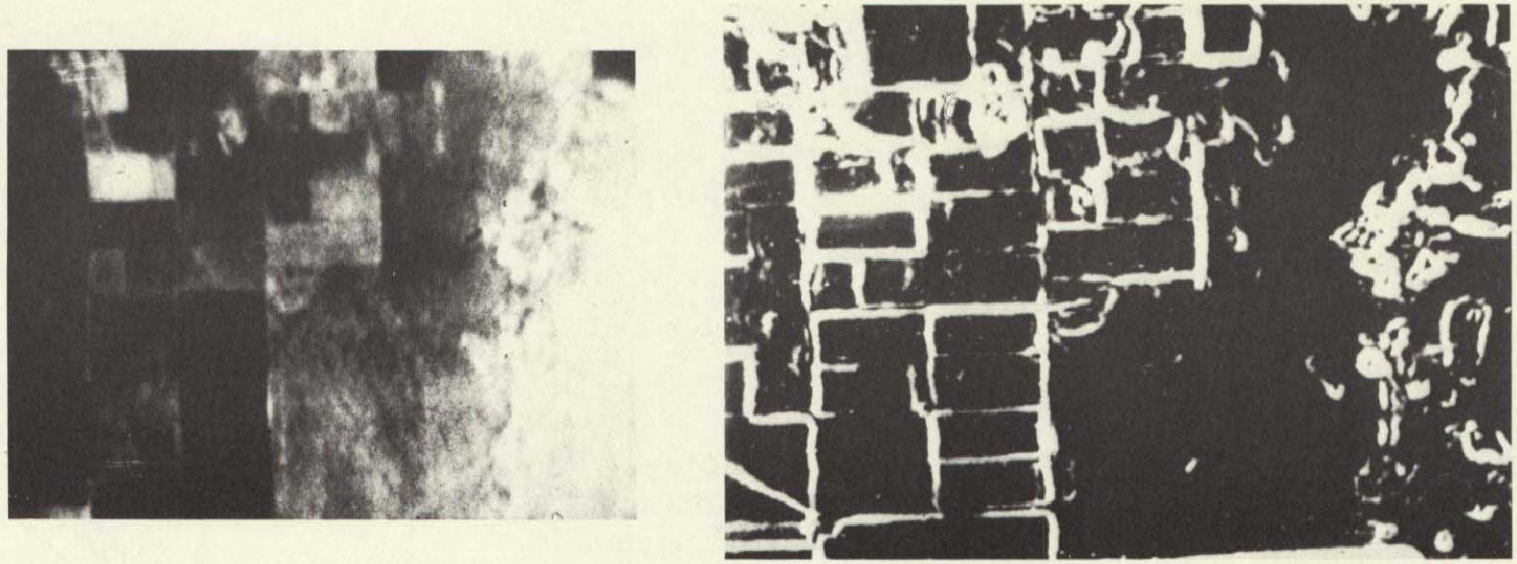

Figure 11. Example of edge enhancement with the circular scanning system used on IDECS. Photograph is shown to left and enhancement to right.

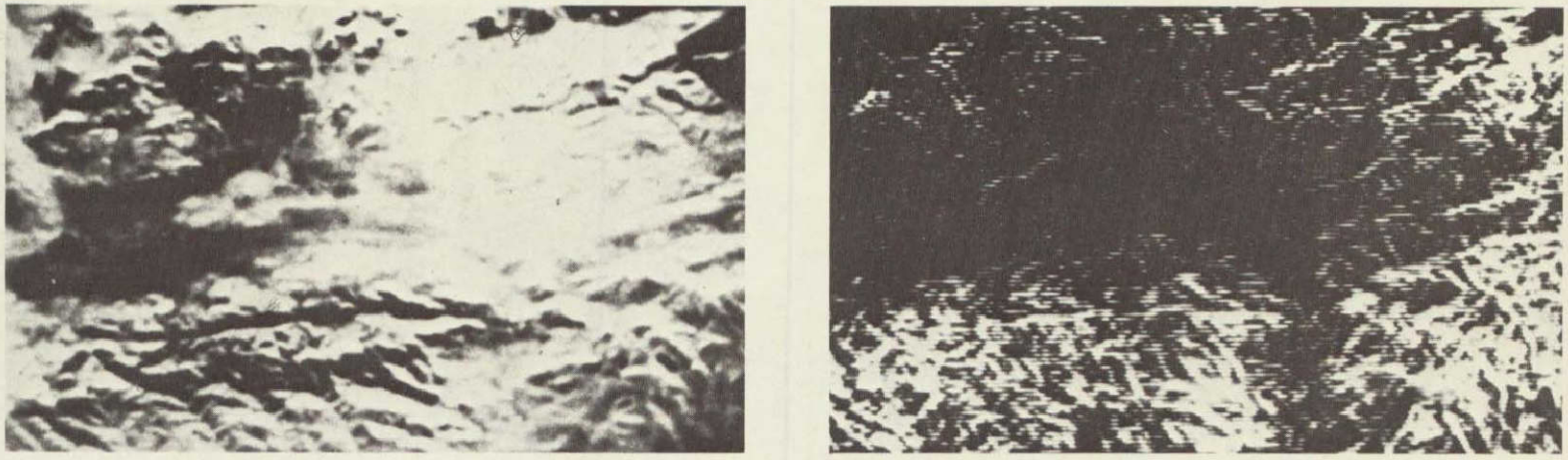

Input Output

Figure 12. Example of edge enhancement with the circular scanning system used on IDECS. Radar image is shown to left and enhancement to right.

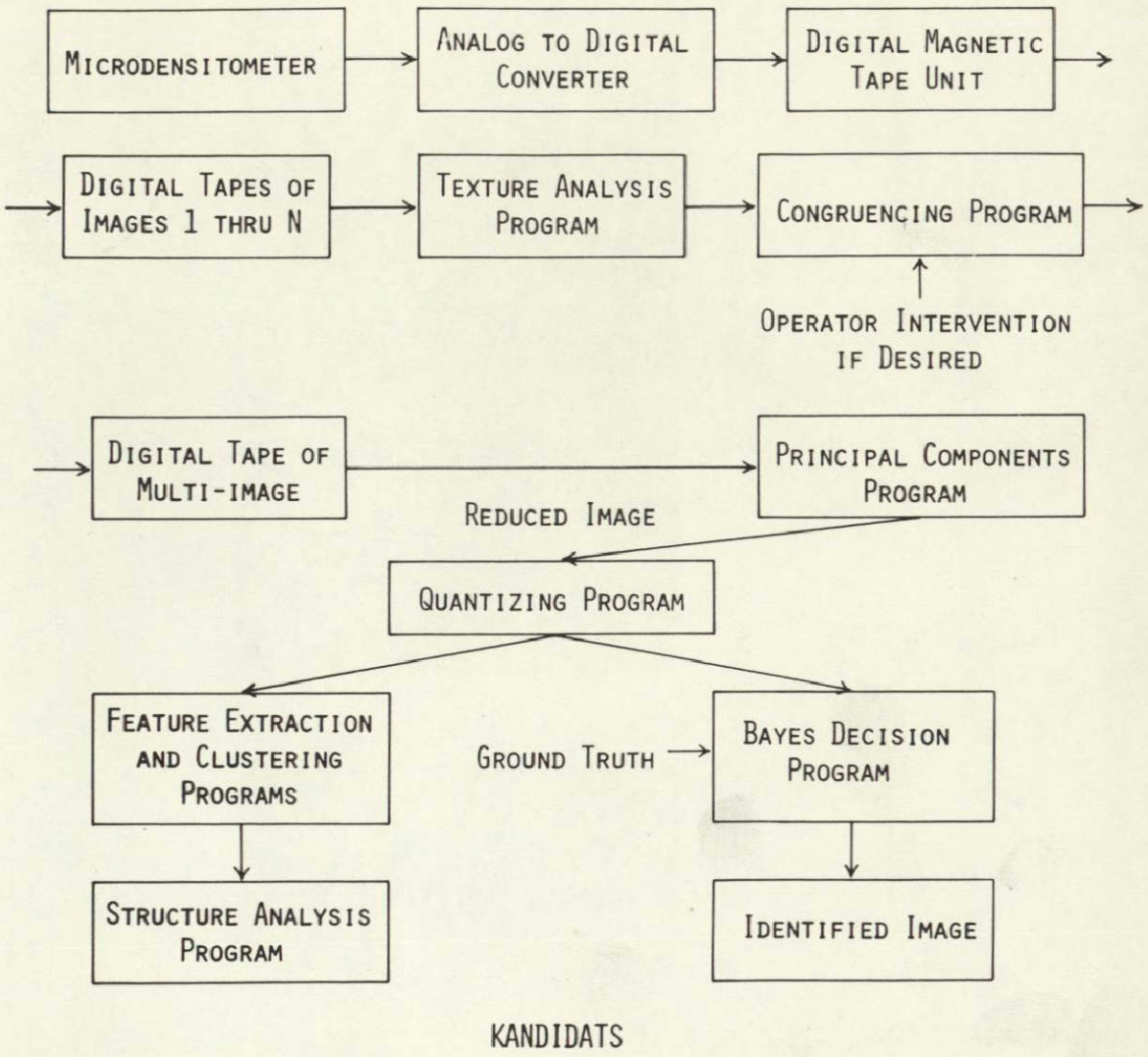

Figure 13. Flow diagram for the Kansas Digital Image Data System (KANDIDATS).

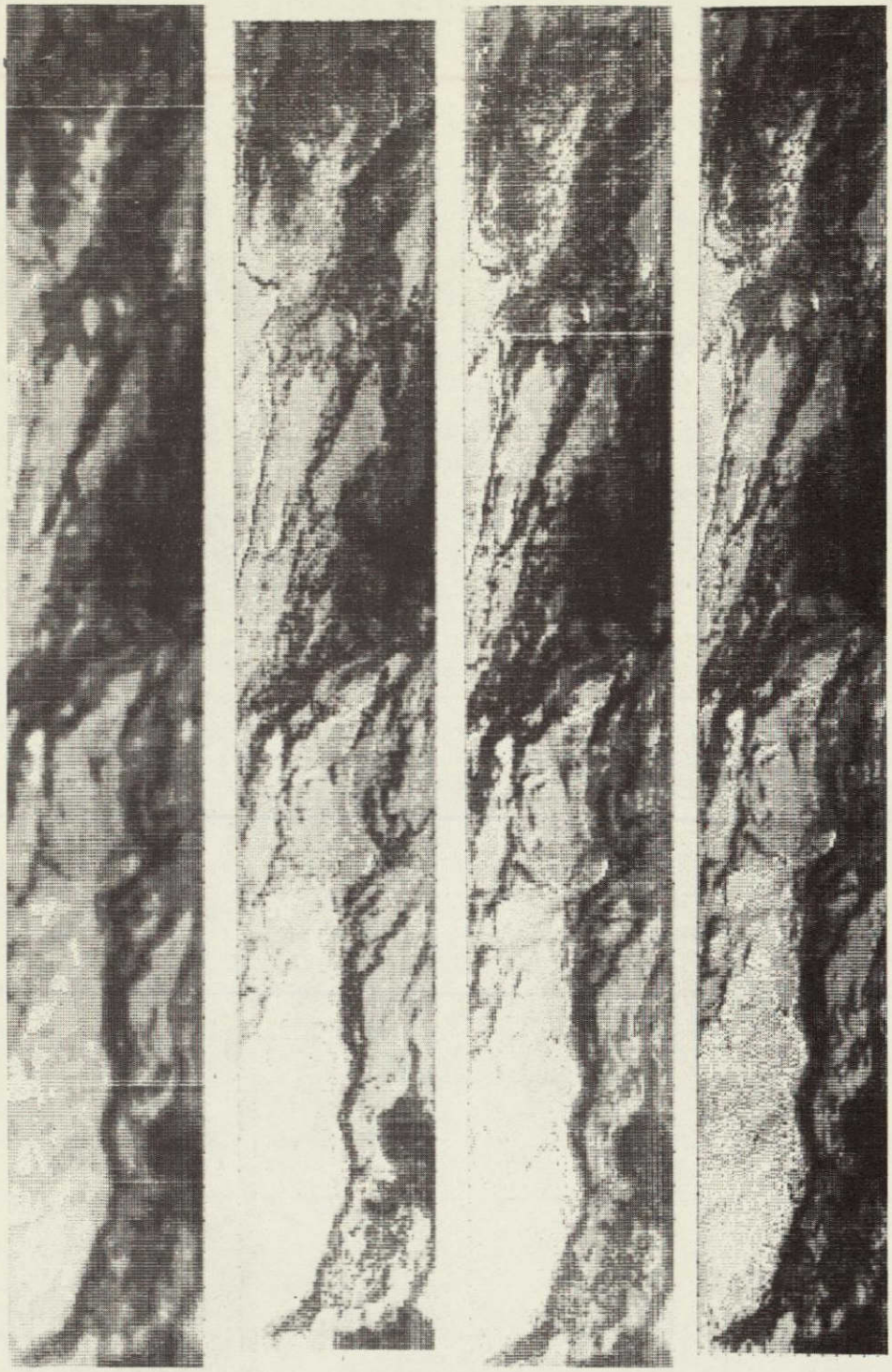

Figure 14. Digitized multi-spectral imagery of Yellowstone Park area. These are the first four principal components from the 12 channel imagery. (Original imagery courtesy H. Smedes, USGS.)

HOMOGENEOUS REGIONS PRODUCED BY THE SPATIAL CLUSTERING METHOD

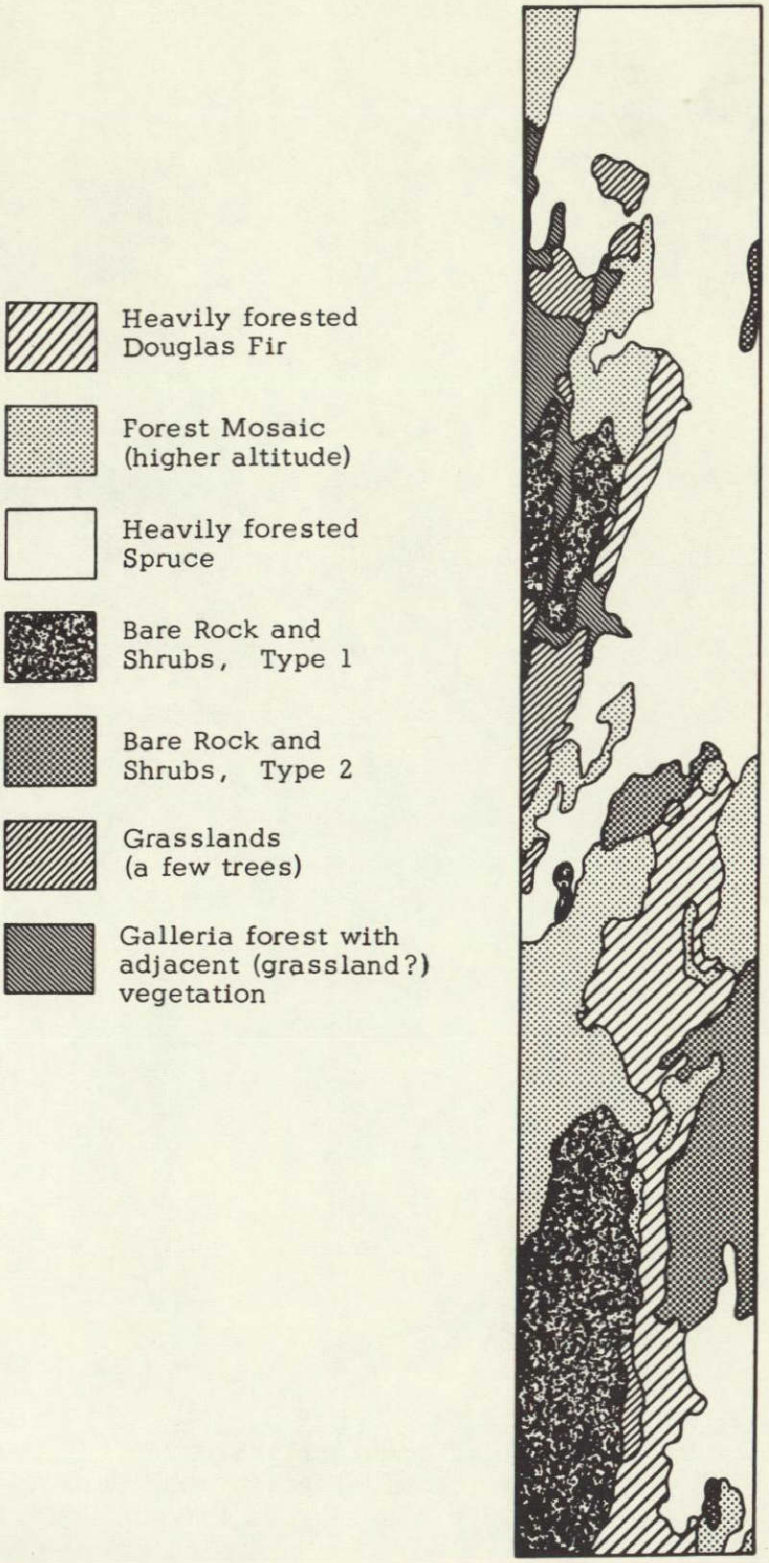

Figure 15. Example of categorization produced in terms of natural groupings of multispectral data without previous knowledge of ground truth at any point in the image or any other learning image. Indicated category identification made by tentative interpretation of aerial photography. Ground truth not available at time of writing.

SECTION 33

RECENT PROGRESS IN TANK, SHIPBOARD, AND HELICOPTER TESTS OF THE FRAUNHOFER LINE DISCRIMINATOR *

By George E. Stoertz and William R. Hemphill
United States Geological Survey
Washington, D.C.

ABSTRACT

The Fraunhofer line discriminator (FLD) is presently an experimental optical instrument for detecting substances that fluoresce near the sodium D_2 Fraunhofer line (5890 A). This unique instrument can continuously and quantitatively sense substances which fluoresce by solar stimulation. This fluorescent light is differentiated from ambient or background light, which is reflected and scattered sunlight of a similar wavelength.

From an airplane, the FLD functions as an airborne fluorometer, quantitatively measuring the concentration of substances in the water that fluoresce near 5890 A (yellow). The concentration of a substance is determined by using quantitative standards. Accurate quantitative measurements require ground-truth data: (1) the turbidity and temperature of the water column sensed by the FLD; and (2) the identity and approximate vertical distribution of the fluorescent substance.

Laboratory experiments using tap water show that 1 part per billion (ppb) of Rhodamine WT dye dissolved in 1/2 meter of water is detected. Shipboard and helicopter tests, in San Francisco Bay, indicate the dye can be monitored in concentrations less than 5 ppb. Helicopter tests over relatively clear water west of Golden Gate suggest that 0.5 ppb can be detected. Fluorometer analysis of water samples collected simultaneously indicate that the FLD is accurate to about 5 percent for the range 1 to 50 ppb.

---

* Publication authorized by the Director, U.S. Geological Survey.

INTRODUCTION

The luminescence emitted from a substance stimulated by sunlight can be differentiated from the reflected or scattered sunlight by using two narrow-band filters. The light passing one filter is the wavelength of a solar Fraunhofer line; light from the other filter differs by only a few angstroms. An instrument utilizing this filter system is called a Fraunhofer line discriminator (FLD). It is the only known instrument that permits quantitative remote sensing of solar-stimulated luminescence against background reflected and scattered sunlight.

Status of problem

An experimental FLD has been built and tested with Rhodamine WT in the laboratory and over open water bodies. Preliminary tests indicate that the FLD technique of sensing is applicable up to 5,000 ft. above the target.

In tank tests, the instrument can detect 1 part per billion (ppb), provided the vertical column of liquid illuminated by sunlight and viewed by the FLD is at least 1/2 meter in length. Shipboard and airborne field tests in San Francisco Bay and San Pablo Bay (Fig. 1) show that the FLD can monitor dye concentrations less than about 5 ppb, even if the water mass is turbid with suspended particles. Helicopter tests over less turbid coastal waters west of the Golden Gate (Fig. 1) suggest that 0.5 ppb can be detected. This paper briefly reviews the principle of the FLD, describes new apparatus and the methods of analysis that permit its use in airborne surveys, and discusses the preliminary laboratory and field results using FLD.

Scope of investigations

This study of solar-stimulated luminescence within visible and ultraviolet wavelengths is for the project: Ultraviolet absorption and luminescence studies, NASA Work Order No. T-80485C, Task 160-75-03-12-TA2511-TF41. This project began in November, 1965 and is jointly sponsored by the U.S. Geological Survey (USGS) and the National Aeronautics and Space Administration (NASA). Work prior to January 1968 has been summarized by Hemphill (1968a); subsequent work is summarized by Stoertz (1969a, b, c, and d).

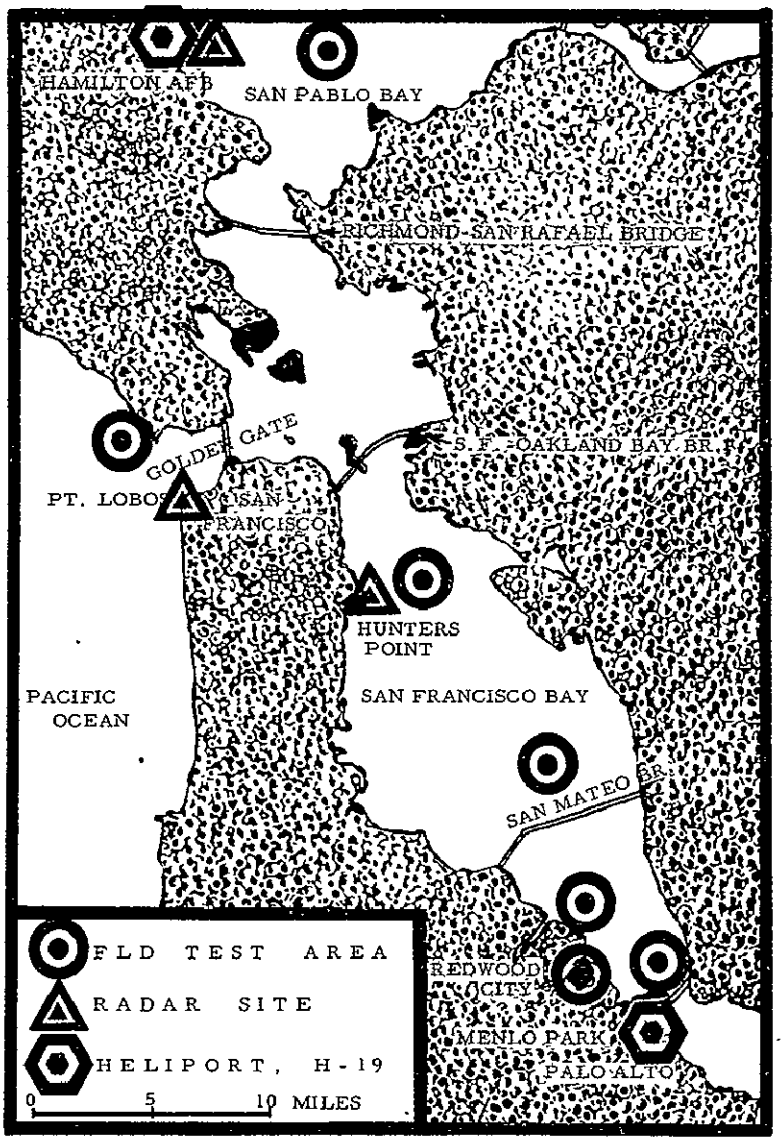

Figure 1.- Index map of FLD test areas and radar sites, May to August, 1969.

The ultimate goal of this and related solar-stimulated luminescence research is to develop sensing capabilities from aircraft and spacecraft. Sensing of luminescence stimulated in whole or in part by solar ultraviolet light is potentially a very useful technique. Present tests are limited to rhodamine dye solutions. The environment of outer space, however, favors solar-stimulated luminescence. For example, at extremely low temperatures a great variety of crystalline substances luminesce brightly. In addition, airborne FLD remote sensors

will be useful in dye dispersion studies, and in future development of imaging or active sensors for detecting either day or night luminescence. Future development of the instrument is expected to have a broad application in studies of outer space, and probably on earth in sensing over land surfaces.

Nature of fluorescence or luminescence

Fluorescence is the emission of light by substances within 10^{-8} seconds after being excited by the absorbed radiation. In this process a quantum of radiation is absorbed by an isolated atom or center. The atom achieves an excited energy state. Then, after a very brief interval, the atom may return to a more stable, unexcited state by direct emission of a photon of light.

Long wavelength ultraviolet light, which reaches the earth's surface in solar radiation, is effective in exciting luminescence in many materials in the visible part of the spectrum. Many natural substances fluoresce when exposed to ultraviolet or visible sunlight. However, this solar-stimulated fluorescence is small relative to the background reflection. The technique employed by the FLD to selectively sense the fluorescence has been described by Hemphill (1968b) and is briefly reviewed later in this paper.

Objectives of recent work

Airborne, shipboard, and laboratory tests of the FLD were conducted during April-May and July-August 1969 in the vicinity of Menlo Park, California. Test areas are shown on the index map (Figure 1). Objectives are:

1) To test the FLD for measuring the fluorescent dye concentration in natural water bodies having a wide range of turbidity.

2) To determine the smallest concentration of dye which is detected.

3) To use the airborne FLD to map dye concentration while the tracking radar automatically plots flight paths in real time.

4) To develop a water sampling procedure from a helicopter, in order to obtain samples that could be correlated with the FLD data.

5) To design and test a standard reference device which will permit an in-flight determination of FLD sensitivity to a luminescence signal.

6) To design and test equipment which will estimate (1) the total attenuation of the incident sunlight and (2) the emitted luminescence, by: a) the suspended sediment; b) the dissolved dye; and c) the water.

Significance of the results

The FLD appears to have an advantage over conventional dye sampling and fluorometer analysis because it adds the dimension of depth, and the greater mobility of aircraft operations.

Applications of the present instrument include monitoring of fluorescent dyes in studies of current dynamics, and measurement of the dispersion coefficient of water bodies. When used for sensing of rhodamine dye in turbid coastal waters and estuaries the present FLD is sensing in the spectral region permitting nearly maximum depth of light penetration. This is illustrated by Figure 2. It should be nearly

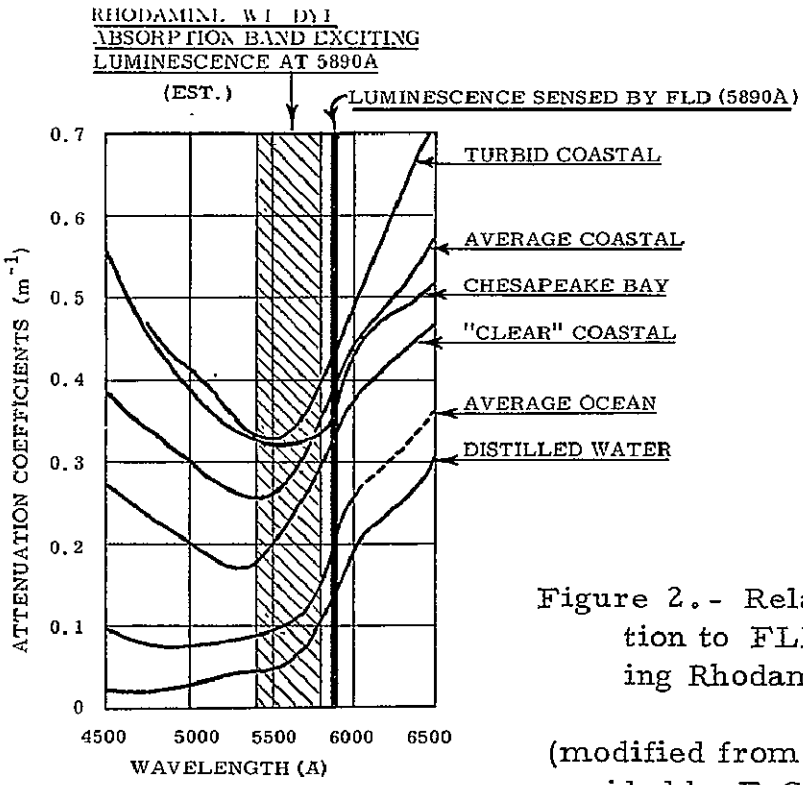

Figure 2.- Relation of light attenuation to FLD function when sensing Rhodamine WT dye in water.

(modified from an illustration provided by F.C. Polcyn and R.A. Rollin, 1969)

optimum for sensing in turbid estuaries such as Chesapeake Bay or San Francisco Bay.

The basic technique of sensing appears applicable to detection of oil spills and leakages, monitoring of certain fluorescent pollutants such as lignin sulfonates, and possibly monitoring of algal blooms in relation to pollution, by means of chlorophyll luminescence. Another possible application in the marine and estuarine environment is monitoring luminescent fish oils.

Acknowledgments

The work was cooperatively funded by the National Aeronautics and Space Administration (NASA) and the U. S. Geological Survey (USGS). Personnel of the USGS who participated in the work included Herbert Skibitzke, R. L. Howell, Wayne Lowry, F. A. Kilpatrick, John Lem, David McCulloch, Paul Carlson, James Trumbull, Vance Kennedy, and David Peterson. Valuable assistance was provided by David Markle and Hans Ludwig of the Perkin-Elmer Corporation, by David Minard of the Federal Water Pollution Control Administration, and by N. M. Hatcher of the NASA Manned Spacecraft Center. Spectral data on Rhodamine WT dye were provided through courtesy of G. K. Turner Associates. Aircraft operation was the responsibility of Arthur Zarkos, of A. E. Ferguson Associates.

DESCRIPTION OF APPARATUS

Background

The basic principle was used first by several astronomers who used a spectrometer to examine the Fraunhofer line profiles of light reflected from various parts of the lunar surface. Noteworthy results have been described by Kozyrev (1956), Dubois (1959), Grainger and Ring (1962), Spinrad (1964), Noxon and Goody (1965), Myronova (1965), and McCord (1967). This work has been summarized briefly by Hemphill (1968b). Construction of an FLD to perform the function automatically began in 1967 by the Perkin-Elmer Corporation. The purpose was to study the feasibility of remote sensing of luminescence by the Fraunhofer line-depth method.

A previous data-processing problem has been eliminated by an analog computer. The intrinsic luminosity of the target is calculated in a form suitable for direct strip-chart recording. The instrument has been briefly described by Hemphill (1968b) and more fully in unpublished reports by D.A. Markle, H. Ludwig, F.C. Gabriel, and G. Schlesinger (written communications, 1967-1968).

Key optical elements that have made the FLD practicable are two sensitive photomultipliers and two glass-spaced Fabry-Perot filters. A half-width of less than 1 angstrom was achieved in the filters, making possible the high spectral resolution required. Filters of this resolution should be capable of measuring intensities less than 50 percent of the intensity of the continuum in approximately 75 Fraunhofer lines between 3300 and 17,000 A (Minnaert and others, 1940; Mohler and others, 1950). Three of the broader lines are shown in Figure 3.

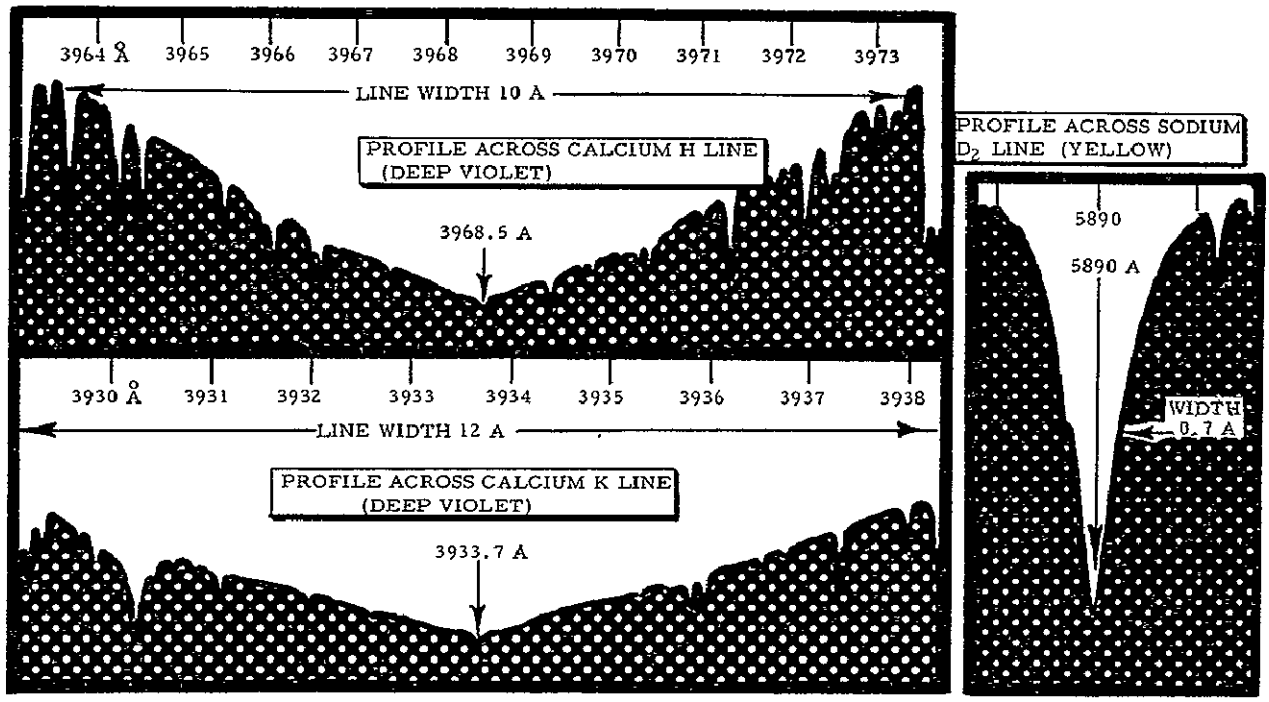

Figure 3.- Profiles across the sodium D_2, calcium H, and calcium K Fraunhofer lines.

A device for remote sensing of solar-stimulated luminescence is really an airborne fluorometer for daylight use. This FLD has many of the same advantages and disadvantages as a laboratory fluorometer. For example, a limitation of the FLD, common to most conventional fluorometers, is that the output is partly dependent on electronic factors, requiring frequent calibration with standards of known luminosity in order to maintain quantitative results.

Principle of operation of the FLD

The line-depth method for determining relative luminosities of substances requires the measurement of four components of light, as illustrated on Figure 4 (components A, B, C, and D). This is accomplished in the FLD by means of two Fabry-Perot filters centered at 5890 and 5892 A. Each filter covers an average half-width of less than 1 angstrom, represented diagrammatically by the vertical bars.

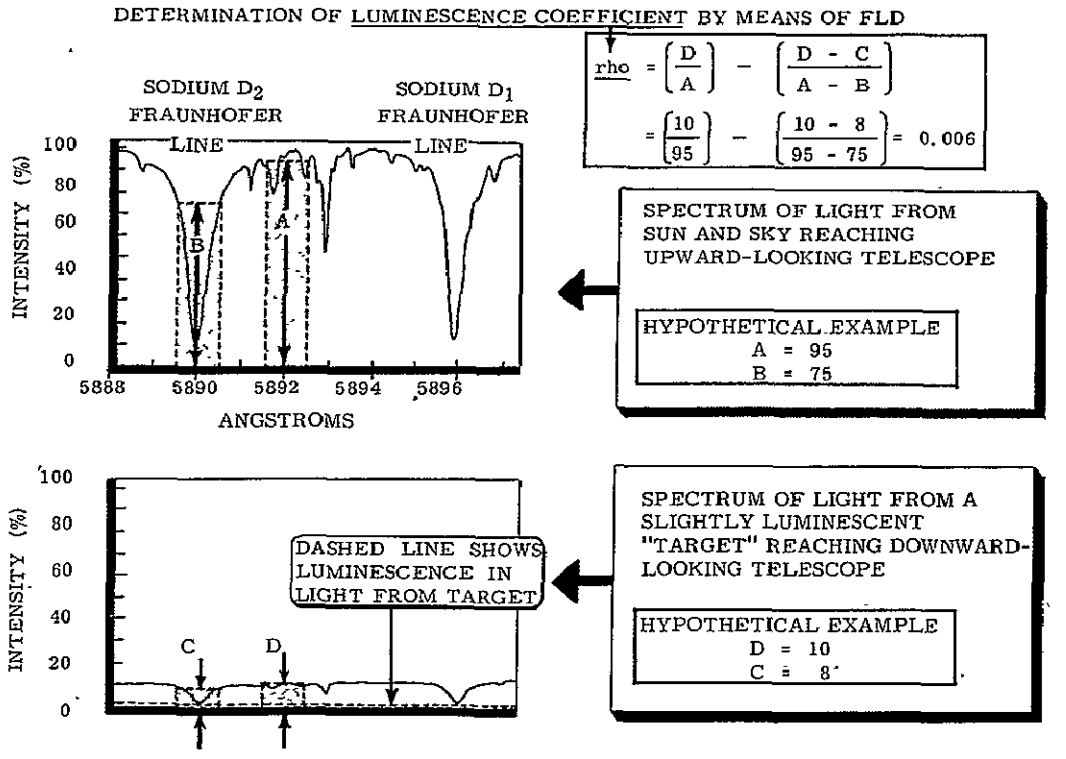

Figure 4.- Determination of luminescence coefficient by means of FLD.

The design of the instrument is such that light from the sun and sky enters an upward-looking telescope for comparison with light from the ground or water "target", which enters a downward-looking telescope. Light from both sources alternately passes through the two filters and its intensity is measured by photomultipliers. The four measured components are: (1) the background intensity of sunlight and skylight (designated "A"); (2) the intensity of sunlight and skylight within the Fraunhofer line (designated "B"); and (3) the corresponding intensities in light from the ground or water target (designated "C" and "D"). The hypothetical profiles on Figure 4 are intended to show that light from the target will be a subdued version of the solar profile. If the target were nonluminescent in the yellow part of the spectrum, the depth (i.e., intensity of light) of the reflected Fraunhofer-line profile at 5890 A would be proportional to its depth in the sunlight and skylight. If the target includes a substance that fluoresces in the yellow, however, the luminescence contribution (represented by horizontal dashed line in the diagram) will be superimposed on the subdued profile, elevating the overall intensity without modifying the detailed notched configuration of the reflected solar spectrum. The luminescence contribution can be represented by a horizontal line because luminescence emission spectra characteristically cover a broad band of several hundred angstrom units, the intensity being practically a horizontal line as seen in any very narrow region covering only a few angstroms (e.g., Figure 4).

By means of an analog computer in the instrument, a simple mathematical calculation is carried out approximately 20 times a second to convert the four measured light intensities (A, B, C, and D) into a signal that is proportional to the intrinsic luminosity of the target. The parameter calculated is designated rho, or luminescence coefficient. Rho is a measure of the intrinsic or potential luminescence of the target, arrived at by eliminating the effect of solar intensity on the luminescence level, and by eliminating the effect of variations in reflectivity of the target. In terms of the four light intensities measured by the instrument, rho is defined as: $\left[\frac{D}{A}\right] - \left[\frac{D - C}{A - B}\right]$. Thus, the proportion of incident light returned from the target as luminescence (rho) is equal to the total proportion of incident light returned from the target $\left[\frac{D}{A}\right]$ minus the proportion returned as reflectance and back-scatter: $\left[\frac{D - C}{A - B}\right]$.

New accessory apparatus

Accessories constructed recently to permit operational use of the FLD in airborne surveys of fluorescent dye are briefly described below:

Mounting the FLD.- The FLD is mounted on the starboard side of an H-19 helicopter approximately 10 feet behind the door, at the point where the fuselage narrows (Fig. 5). This is advantageous because a water-sampling device lowered from the door will fall along the same flight-line as the FLD field of view. When operated at a ground speed of 10 to 15 knots and at an altitude of 50 feet or less, it is possible to obtain a water sample close to the field of view. The mounting bracket (Fig. 6) is aluminum and is equipped with four shock-mounts (Fig. 7) which support the optical unit. The FLD is bolted to an aluminum frame (Fig. 8) and can be removed easily by four bolts at the shock mounts. An insulated jacket (Fig. 8) covers the optical unit to prevent heating from exposure to sunlight. The instrument is mounted at a height of 8 to 10 feet above the ground, allowing the light collector to be illuminated at practically all sun angles, plane angles and flight lines.

Figure 5.- Mounting the FLD on an H-19 helicopter.

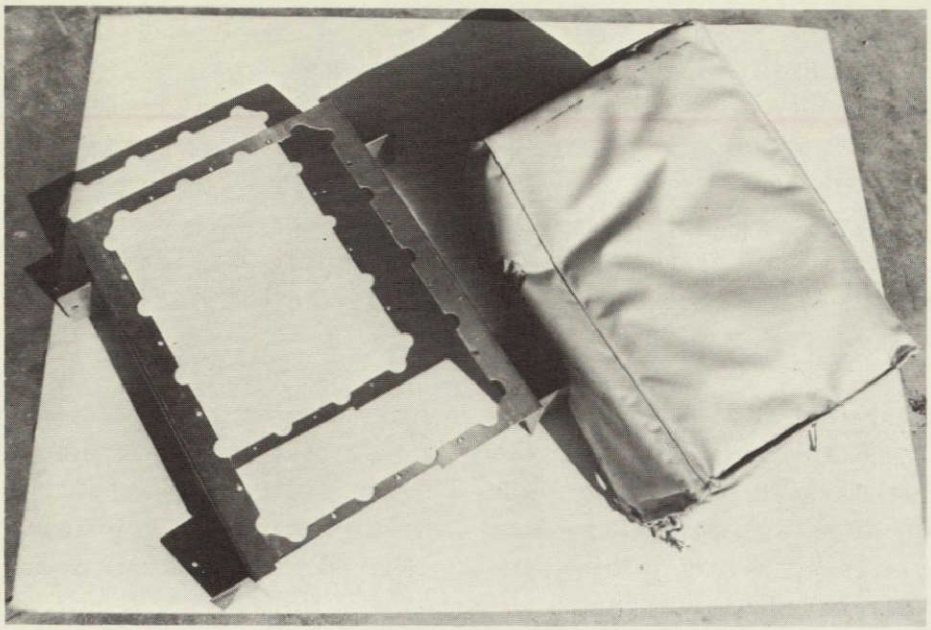

Figure 8.- Insulated jacket and aluminum frame.

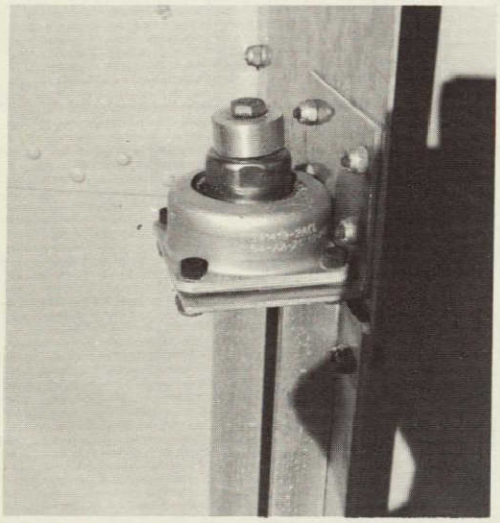

Figure 7.- Shock-mount.

Figure 6.- Mounting bracket for FLD.

Mounting the light collector. - The light collector gave the best results when mounted as shown in Figure 5. The horizontal white diffuser plate is elevated 10 inches above the upper portal and approximately 1 inch off-center with respect to the portal. It is off-center to compensate for a prism that blocks part of the field of view. The base of the mount is sealed against the optical unit with an "O" ring, which also prevents loosening from vibration. The diffuser-plate is placed sufficiently high so that reflection from the yellow side of the helicopter is not significant.

Standard target device. - An aluminum slide is about 18 inches beneath the FLD (Fig. 5). Standard fluorescent targets are fastened to a sheet of plexiglas and periodically moved in and out of the field of view during flight by means of an aluminum rod encased in BX-cable. The targets must be at least 2 inches in diameter in order to achieve reproducible luminescence coefficients (rho values). If fluorescent liquids are used it is necessary that the container be at least 4 inches wide and less than 1 inch deep so that the full column of liquid viewed by the FLD is illuminated by sunlight. Targets are shielded from sunlight by an aluminum cover when not in use to minimize heating. For reproducible results, the targets are viewed during straight and level flight. Liquid containers are leak-proof and free of bubbles. The most satisfactory target was an acrylic resin cylinder 1/2-inch deep filled with dilute Rhodamine WT dye solution.

Water samplers. - A suitable method for rapid water surface sampling from the air utilized the device shown in Figure 9. It is made from sections of standard plastic core liner (2 inches I.D.) and fastened with wire. The sampler holds a 6-ounce square widemouthed amber-glass bottle. The bottles will not drop out when the wire is squeezed closed at the top, and the bottles can be changed in a few seconds. A section of weighted pipe is placed in the bottom (Fig. 10) to decrease the cord angle when aircraft speeds or altitude cause the sampler to fall behind the FLD field of view. Amber glass is advantageous to retard deterioration of rhodamine dye in the sunlight. A 6-ounce sample is sufficient for measuring attenuation coefficients of light. During 20 hours of FLD operation in May, water samples were taken on an average of once every 6 minutes in order to calibrate the instrument. In certain locations, closely spaced samples were taken to establish an adequate profile across a single dye cloud. Single samples were obtained in as little as 18 seconds from the ship and as little as 25 seconds from the helicopter. During more recent tests in July and August the standard target device was used for calibration instead of water samples.

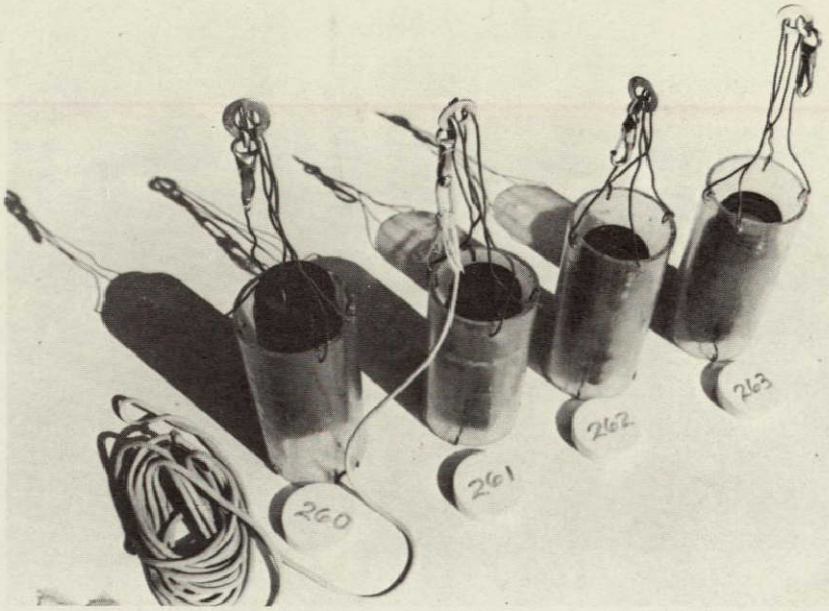

Figure 9.- Samplers holding 6-ounce amber-glass bottles.

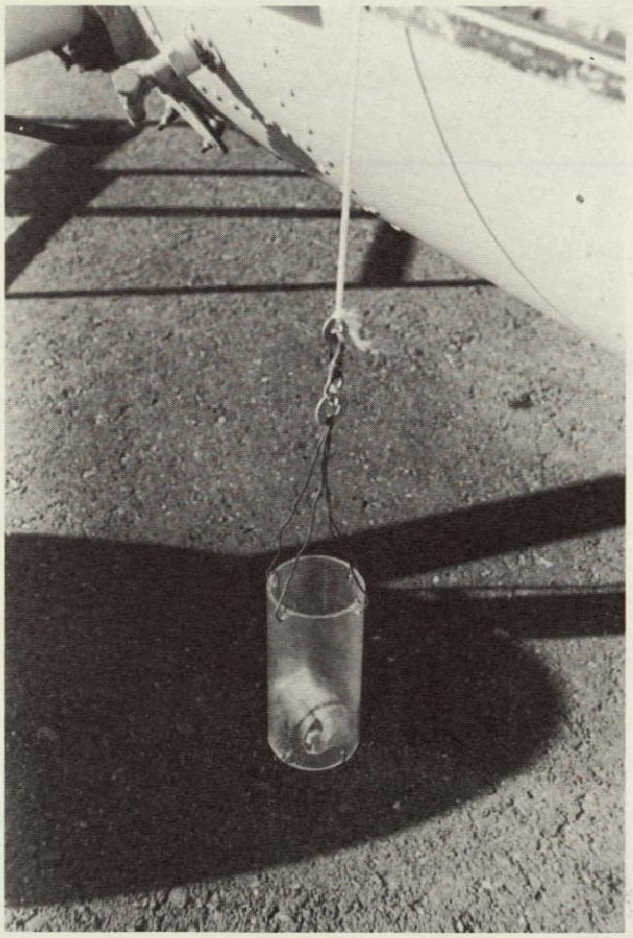

Figure 10.- Sampler weighted with pipe to adjust wire angle.

During shipboard tests some sampling was done with standard bottles for simultaneous sampling at pre-determined depths of 1, 2, and 4 meters. The apparatus is shown in use on Figure 11. Samples prior to and during FLD tests permit an estimate of the vertical distribution of turbidity and of fluorescent dye within the water column sensed by the FLD. It was not used from the air since light penetration was very shallow in most waters tested. In future tests over clearer water, however, subsurface sampling will be essential. A more simple and lighter device may be required for this purpose.

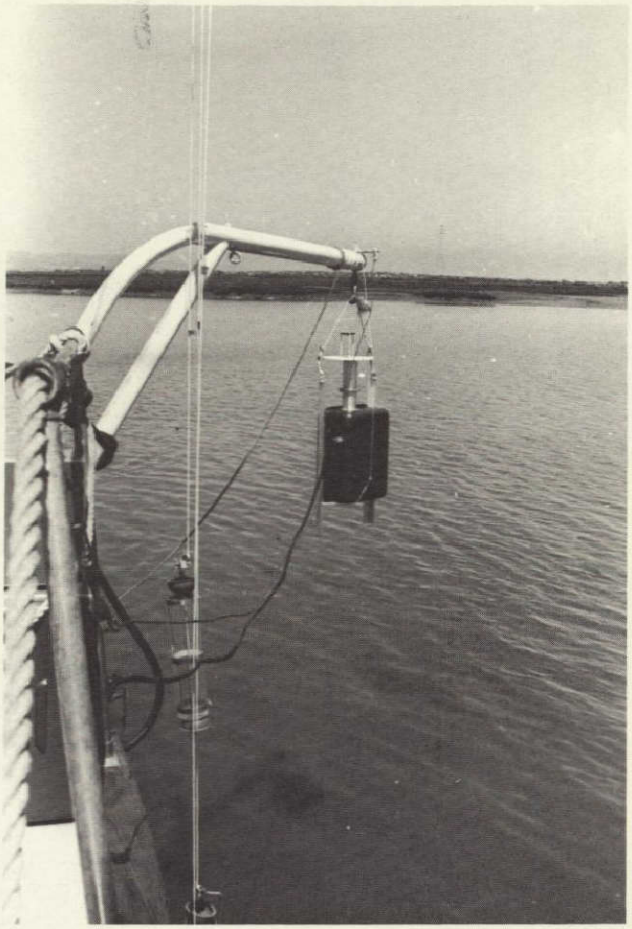

Figure 11.- Subsurface samplers used during shipboard tests of FLD.

Attenuation apparatus.- Apparatus which measures attenuation of emitted luminescence at 5890 A by passing artificial light through a water sample into the upper portal of the FLD is illustrated in Figure 12. Three alternate tubes of black acrylic resin and having clear bottoms are provided in order that the path-length of light can be varied from 8 to 20 inches, depending on sample size and water clarity. Use of the apparatus requires an average of five minutes per sample, including analysis of standards. Transmittance of light by the sample is compared with transmittance of distilled water and of rhodamine dye solutions. The relative values of component A or B give relative transmittance. The apparatus has the advantage that it can be used during cloudy weather or at night when other FLD tests are not possible. Since it utilizes the FLD optics it permits measurement of transmittance at a wavelength (5890 A) uniquely suited to this instrument, and provides results that are not possible using other methods.

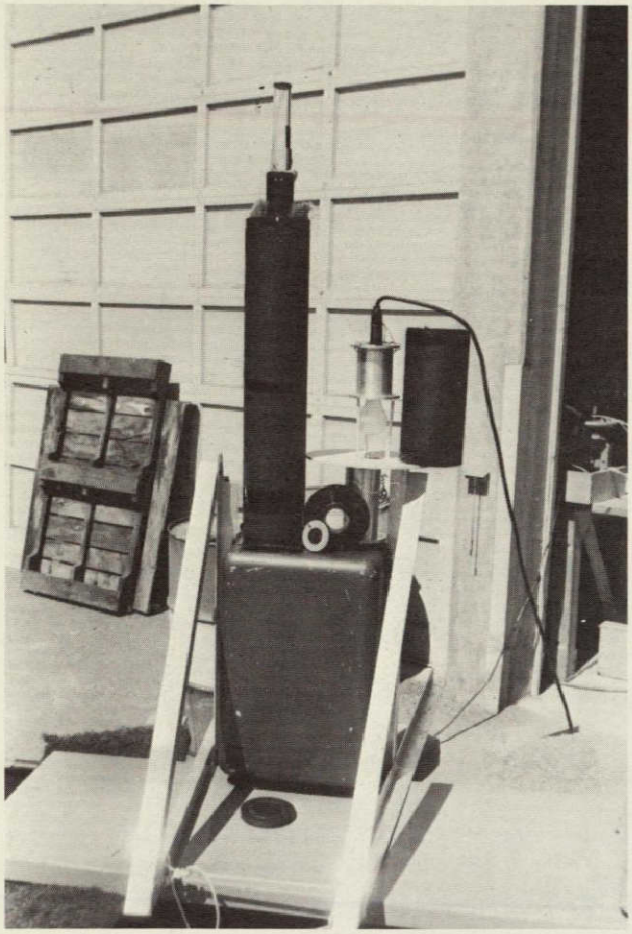

ATTENUATION
APPARATUS

Figure 12.- Apparatus for measuring attenuation of emitted luminescence at 5890 angstroms.

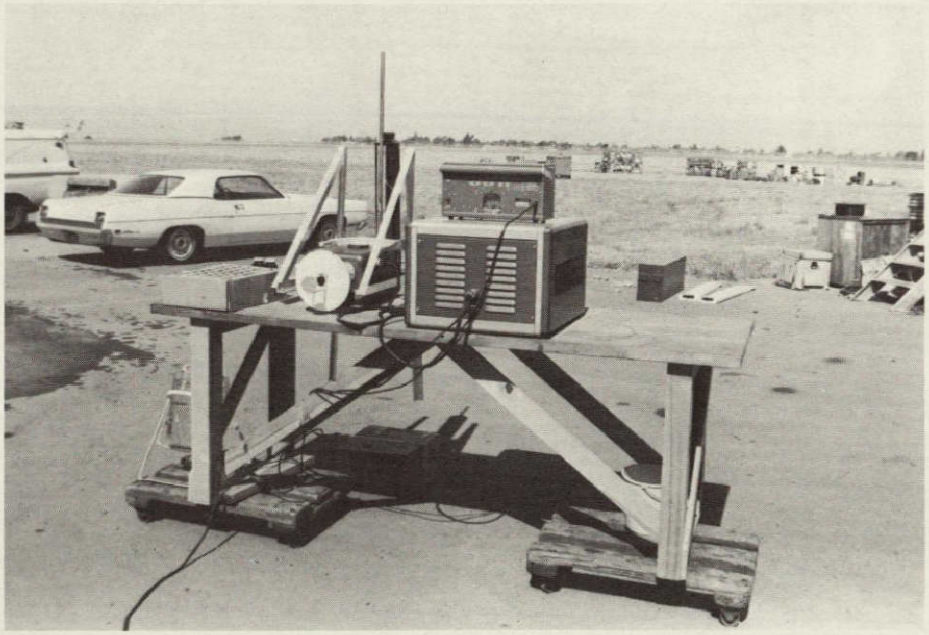

Figure 14.- Apparatus for measuring attenuation of sunlight that excites luminescence of dye at 5890 A.

A modification of the apparatus described above permits the measurement of attenuation of those wavelengths of incident sunlight that serve to excite yellow (5890 A) luminescence of Rhodamine WT dye. The spectral ranges of absorption and luminescence of the dye are illustrated by Figure 13. Absorption is chiefly in the green part

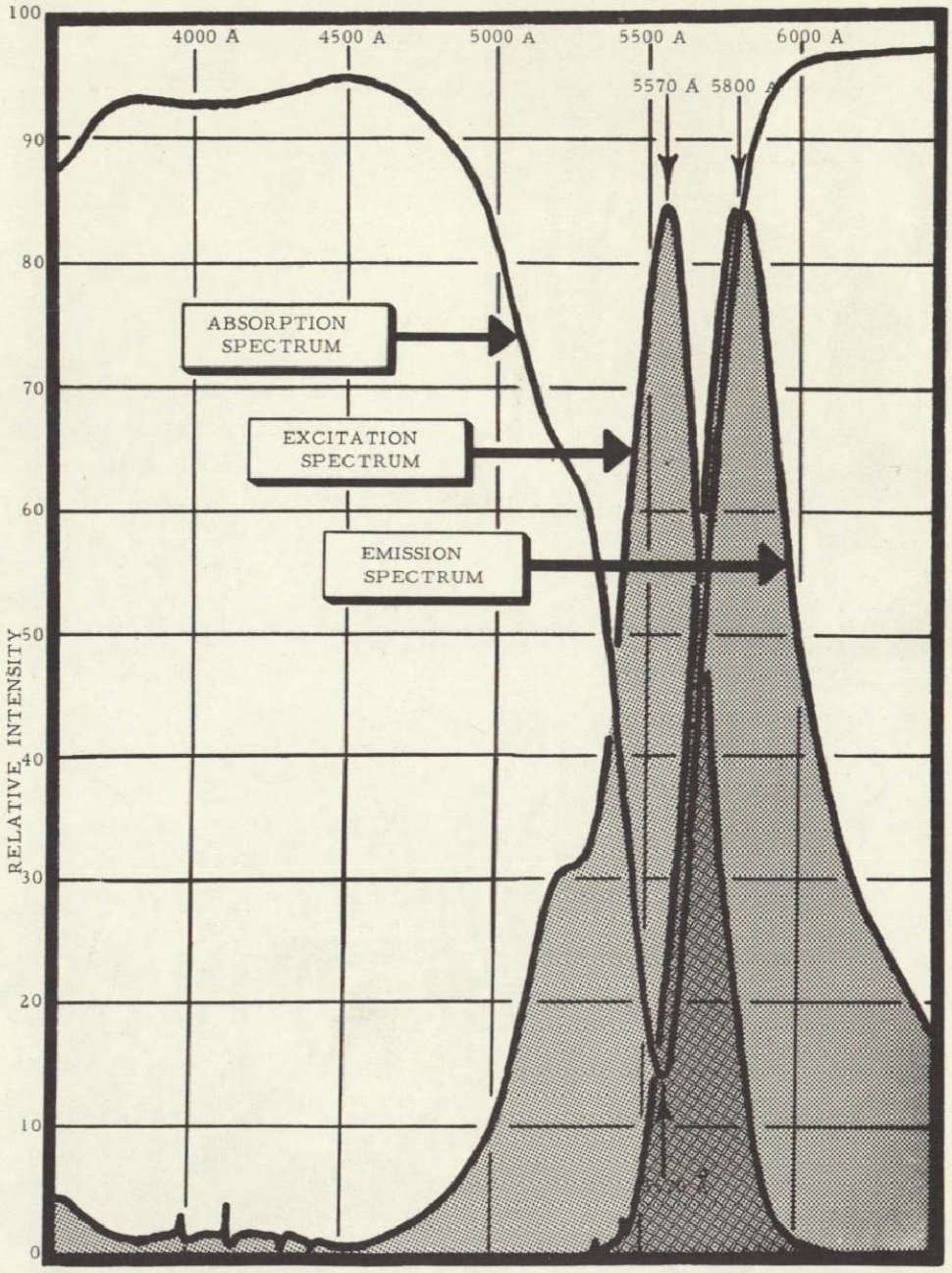

Figure 13.- Excitation, emission, and absorption spectra for aqueous solutions of Rhodamine WT dye (courtesy G.K. Turner Associates).

of the spectrum, the range of wavelengths probably varying somewhat with depth in the dye solution and with dye concentration. It is this uncertainty and the possible variability of this range that makes it desirable to use the FLD rather than a conventional instrument such as a spectrophotofluorometer. In the apparatus shown in Figure 14 (above), the incident sunlight is passed downward through a water sample with a hand-held mirror, the portion that is transmitted serving to excite luminescence in a small cylinder of Rhodamine WT dye that is being viewed at a right angle by the lower portal of the FLD. The upper portal monitors the solar intensity and solar line-depth ratio, as in conventional use, permitting computation of luminescence coefficient (rho) by the FLD. This is a measure of the attenuation, by the sample, of those wavelengths which cause the dye to luminesce.

PROCEDURES

Potentially useful products of the FLD will be contour maps showing areal distribution of fluorescent dye concentration in a water body during short time spans. Present work is developing suitable procedures for this. The procedures may be considered in four categories: (1) the airborne survey; (2) the ground radar; (3) the laboratory; and (4) the data compilation procedures. This report concerns chiefly the procedures in airborne surveying. The radar procedures have been described by Howell (1969). Data compilation procedures for both field data and laboratory data have been described in other reports (Stoertz, 1969b and 1969d). Accurate quantitative interpretation of FLD records depends on a correct mathematical analysis of FLD function as applied to sensing of fluorescent dye in solution. This has been attempted by G. E. Stoertz and D.A. Markle and will be described in a forthcoming report.

Method of obtaining data

The airborne survey party in the H-19 helicopter generally consisted of three persons: pilot, FLD operator, and water sampler. The latter two take notes, operate the standard target device, photograph, record time on chart, annotate chart with sample location and edge of visible dye, take water samples, drop dye, and measure water temperature.

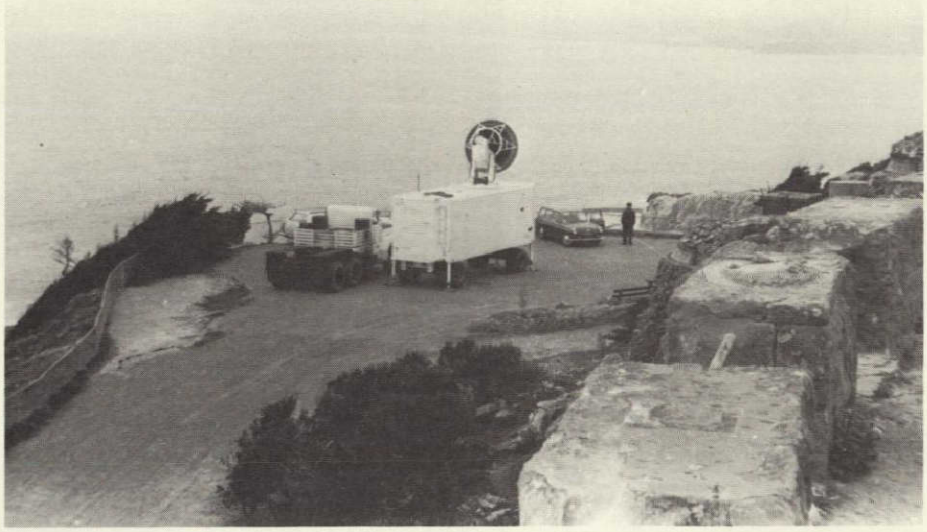

Figure 15.- Radar tracker at Point Lobos looking toward test site near Golden Gate.

The tracking radar (Fig. 15), a modified radar fire control system, was manned by one person, and all phases of this operation have been described by Howell (1969). Using this technique, the precise flight path of the H-19 is plotted on maps, the location of dye patches marked, the time of passage recorded to provide ground speed, and the aircraft directed to the dye when nearly invisible to the helicopter pilot. The three radar sites are shown on Figure 1, and the installation at Pt. Lobos on Figure 15. A survey with the FLD was made over the water in the background.

Fluorescent dye was commonly dropped in a string of uniformly spaced patches while flying at a uniform speed into the wind. Wind direction was indicated by a smoke signal from the Polaris' lifeboat when possible. The most suitable method of air-dropping any quantity of dye was found to be a double plastic bag of an appropriate size, released from a stiff widemouthed container. The bags are broken at the water surface by excluding all air and by dropping from 100 feet or higher. Dye was also dropped to mark flight lines for aerial photography from a Cessna 310 when the radar was not in use. Small spots of dye were dropped to mark the beginning and end of cross-traverses of a larger dye cloud so that the exact length of the traverse could be photographed from the Cessna. The locations of the marker patches were noted on the FLD strip chart. This will provide a means for determining aircraft ground speeds from aerial photographs.

The FLD was turned on at take-off and a continuous record of solar intensity (component A) and luminescence coefficient (rho) made on a Mosley dual-pen strip-chart recorder. A bandwidth of 2 Hz was used for both components throughout the tests. The recorder was generally set at a range of 1X for component A and at 10X for rho. Chart speed was generally 0.5 inch per minute until the dye survey started. Then the speed was increased to 0.1 inch per second. Flight paths plotted by the radar tracker were marked with ticks at uniform time intervals. Time checks were relayed from radar to the survey plane at frequent intervals by radio and noted on the FLD record to permit precise correlation of the two records for time and location.

The FLD was also operated as a shipboard fluorometer aboard the Geological Survey ship Polaris. The instrument was suspended from a davit on the starboard side (Fig. 16). It was supported by a 1/4-inch cable from an aluminum frame. Performance was successful, primarily because sampling at frequent intervals at a point only a few inches from the field of view was possible, permitting frequent calibration of sensitivity.

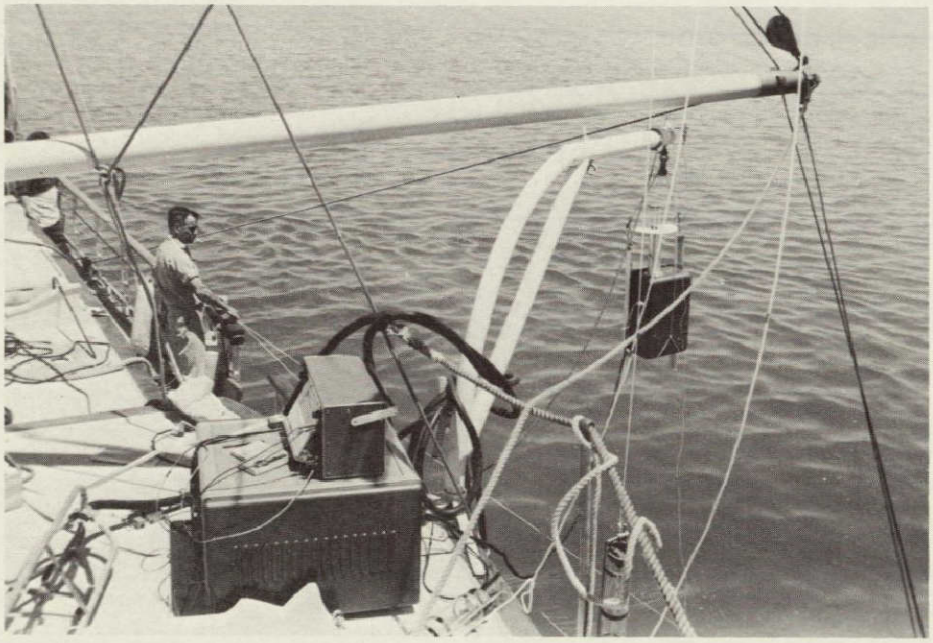

Figure 16.- Use of the FLD as shipboard fluorometer aboard Geological Survey ship Polaris.

Derivation of dye concentration from FLD readings

Initial tests of the FLD were made over aqueous solutions of fluorescent dye. Efforts to interpret FLD readings in terms of luminescence intensities or dye concentrations made it evident that a number of environmental variables influenced the recorded values of luminescence coefficient (rho). These values, in accord with the programmed computation in the instrument, are nearly equal to the intensity of luminescence emission reaching the water surface divided by the intensity of sunlight incident on the surface. A more meaningful definition of rho must consider the entire water column sensed by the FLD:- rho is the relative intensity of upward-trending luminescence reaching the water surface from the column sensed by the FLD, after being attenuated by absorption and scattering by all constituents of the column (suspended particles, the water itself, the dye itself, and other coloring matter.) Consequently rho is not equivalent to nor directly proportional to intrinsic luminosity, but is dependent on a

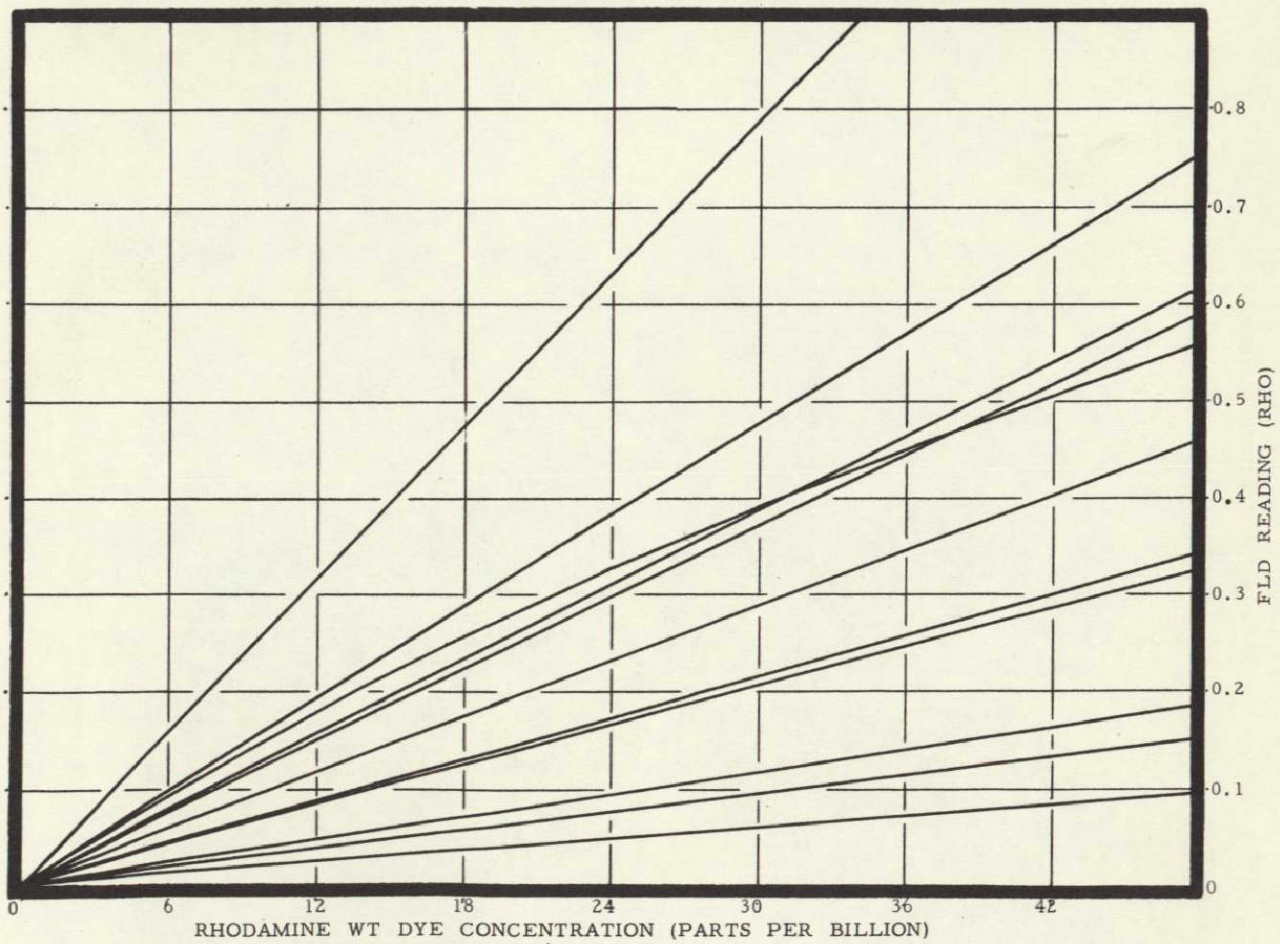

Figure 17.- Relation between dye concentration and FLD readings for short test periods.

number of environmental factors unrelated to intrinsic luminosity. It had been concluded previously (H. Ludwig and D.A. Markle, written commun., Apr. 18, 1968; Stoertz, 1969a) that rho is also dependent on instrumental factors, and is analogous to the dial reading of a fluorometer. Therefore rho might best be termed FLD reading, and interpretation of these readings in terms of luminescence intensities or dye concentrations requires that the pertinent environmental variables be considered.

Theoretical formulas have been derived (Stoertz, 1969b) relating several factors to rho, and pertinent constants have been tentatively evaluated. The principal factors are attenuation of light within the water column by all constituents, angle of the sun, temperature of the water column, and vertical distribution of the dye. Rho also depends in part on several indeterminate factors that cannot be separately evaluated. It was convenient to combine these into a sensitivity coefficient that can be evaluated periodically by means of standards, to relate instrumental sensitivity to increments of the fluorescent substance. Basically, this coefficient is the increment in rho produced by the luminescence from an infinitely small quantity of a luminescent solution divided by that quantity. The coefficient includes an error factor to compensate for the cumulative error from several indeterminate sources.

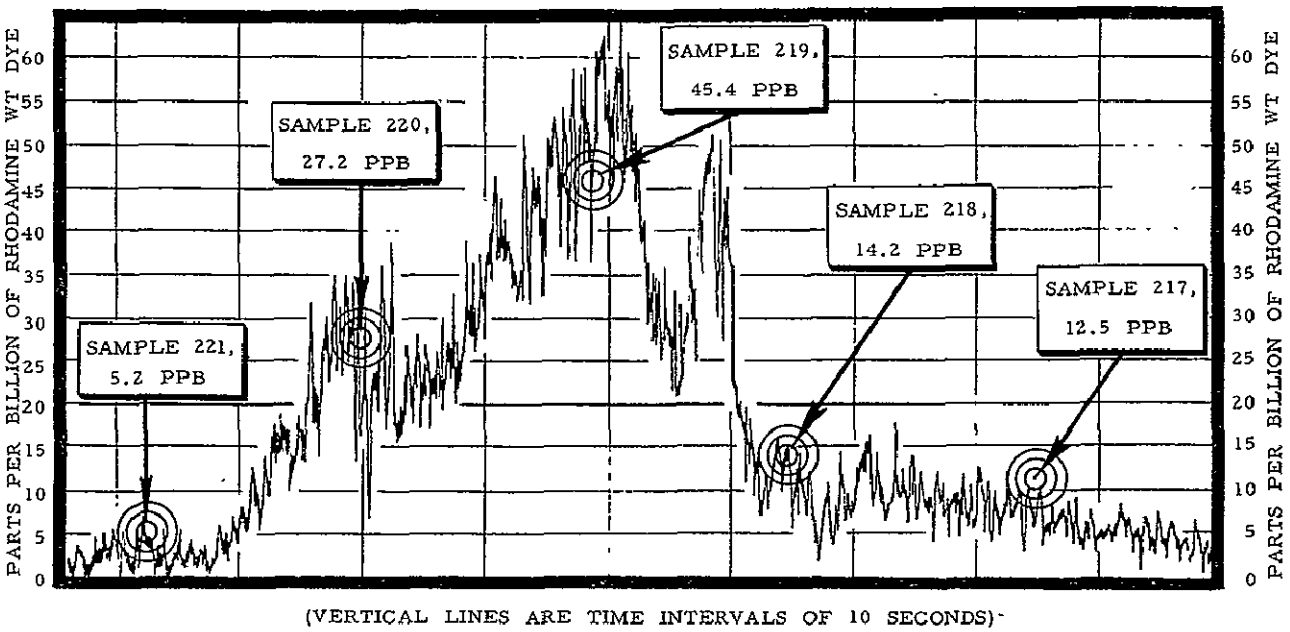

Figure 18.- Record from FLD used as shipboard fluorometer, San Francisco Bay, May 20, 1969.

In order to derive dye concentrations from FLD readings it is convenient to plot one against the other on a graph. Curves calculated for a number of short test periods during May are shown on Figure 17 (above). Most of the relations are nearly linear. These curves were used to scale the strip-chart records to read directly in terms of dye concentration. A typical FLD record showing the final scaling by horizontal ruled lines is illustrated in Figure 18 (above).

A segment of strip-chart record during a period of significantly lower sensitivity is illustrated by Figure 19, made during tests over Westpoint Slough (near Redwood City on Fig. 1). A period of significantly higher sensitivity is illustrated by a graph made during tests

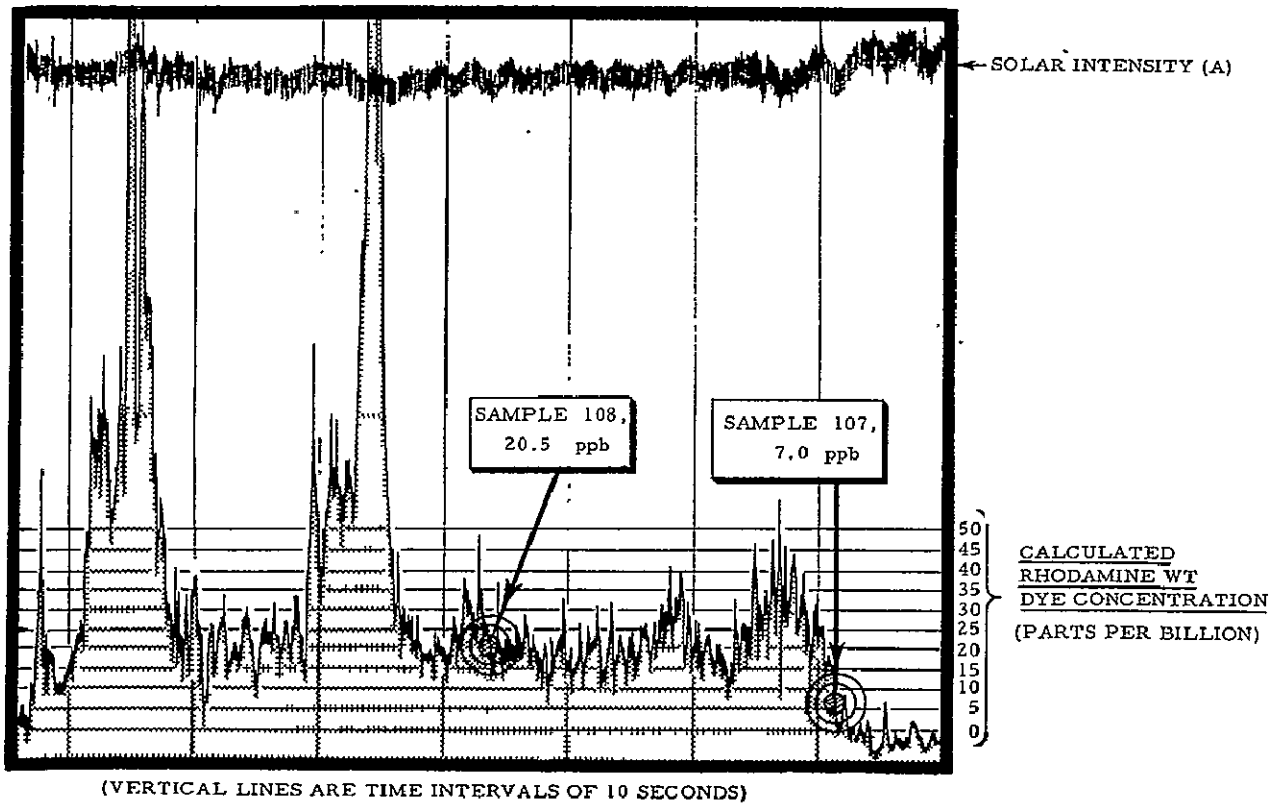

Figure 19.- Record from FLD used as airborne fluorometer, San Francisco Bay, May 13, 1969.

over San Francisco Bay north of San Mateo Bridge (Fig. 20). The latter graph also illustrates sufficiently rapid chart speed (1 inch per second) to show the limitation of pen response time. The uniform slope of all peaks apparently results from this limiting factor. A comparison of the spacing of horizontal lines on Figures 18, 19 and 20 shows that changes in sensitivity are appreciable from day to day and from place to place, and illustrates the necessity of frequent calibration by means of either standard targets or water samples.

A period of high sensitivity is illustrated in Figure 21, made during tests over the Pacific Ocean west of Golden Gate. The high sensitivity is attributable to the clarity of the water and possibly to the dispersal of dye with depth. The FLD readings could not be interpreted by formula because subsurface samples were not obtained and because the vertical column of water sensed by the FLD was probably much deeper than the lower limit of the dye. Surface samples analyzed by a laboratory fluorometer showed concentrations of 0.5 and 1.4 ppb. Locations of these samples as shown on Figure 21 are at the lowest possible levels of rho. This suggests that a sensitivity lower than 0.5 ppb was achieved.

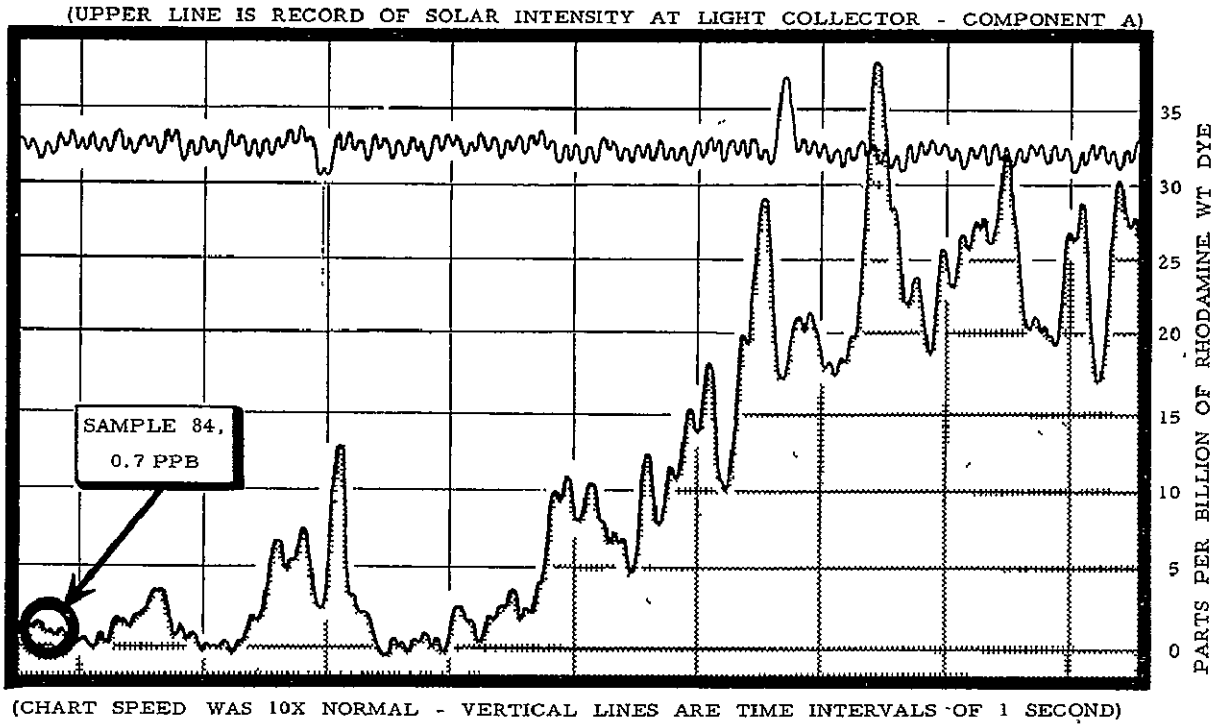

Figure 20.- Record from FLD used as airborne fluorometer, San Francisco Bay, May 8, 1969.

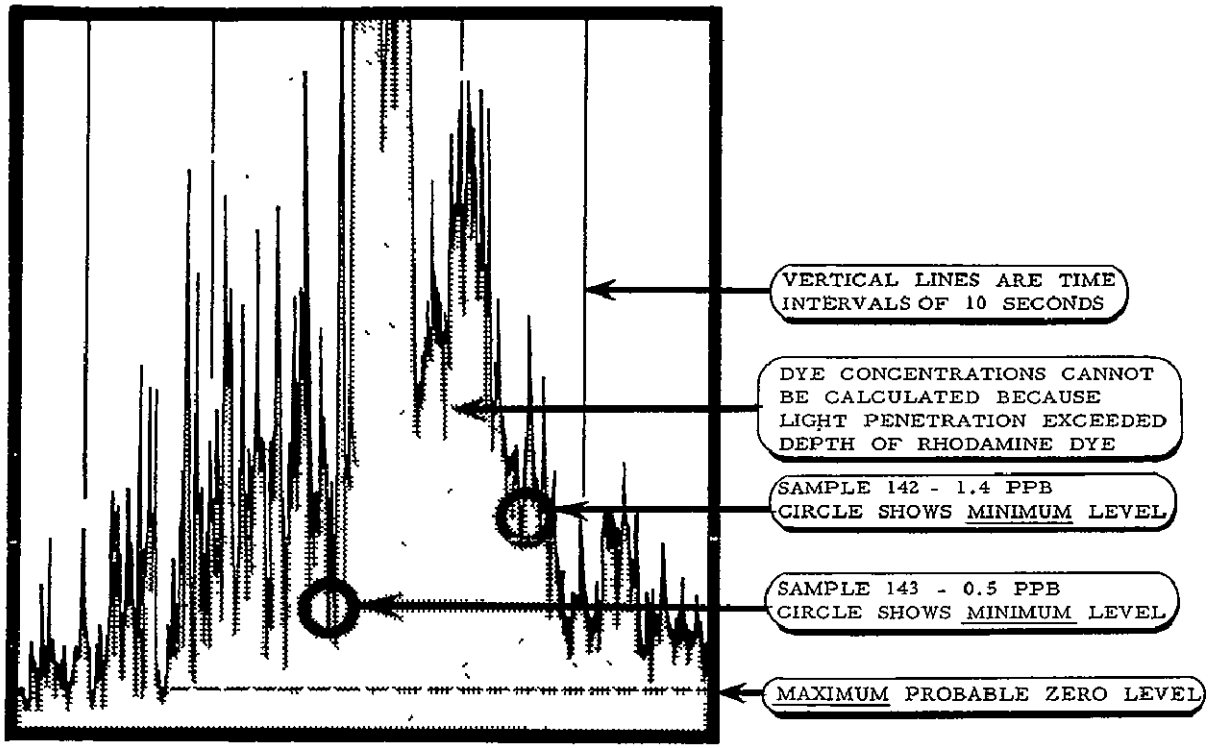

Figure 21.- Record from FLD used as airborne fluorometer, Pacific Ocean near Golden Gate, May 14, 1969.

RESULTS

1) Controlled experiments over tanks of Rhodamine WT dye in aqueous solutions showed that the smallest detectable increment of dye in 1/2-meter depths was approximately 1 ppb. During an experiment on November 2, 1968, between 11:23 and 11:52 a.m., 25 successive increments averaging 1.3 ppb were clearly differentiated, and the sensitivity of the FLD was such that rho averaged 0.053 per 1 ppb (Stoertz, 1969c). A typical strip-chart record made during such a test is illustrated on Figure 22. It can be inferred that increments considerably smaller than 1 ppb are detectable in depths considerably greater than 1/2 meter.

2) Tests showed that illumination of the dye column sensed by the FLD is more important in determining rho values than how much dye is in the column, although the two are interrelated. Therefore

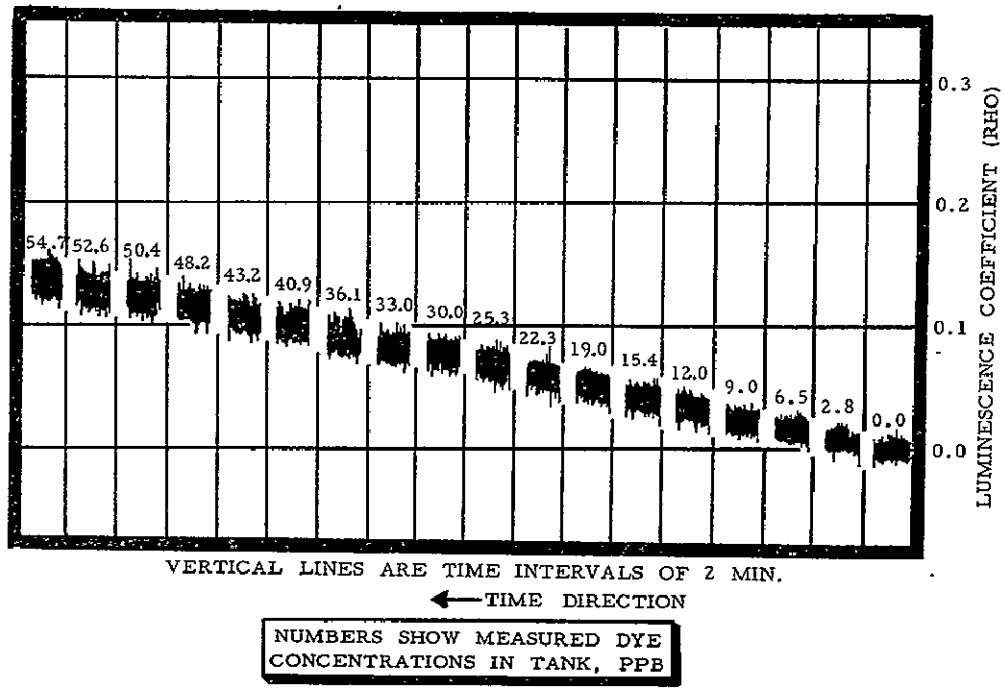

Figure 22.- FLD performance in controlled experiment over tank of fluorescent Rhodamine WT dye, October 29, 1968.

attenuation coefficients for light are the principal factors to be considered in interpreting FLD records.

3) Tank tests over dye dissolved in clear water in which attenuation of emitted light is isolated from that of incident light showed a nearly direct proportionality between rho values and emitted light intensity for varying depths. This indicated that only an insignificant amount of attenuation is attributable to that of emitted light, by the dye. Laboratory experiments with attenuation equipment on natural water samples also indicated that attenuation of yellow light by Rhodamine WT is slight relative to attenuation by suspended particles. Therefore, in most natural water bodies, self-absorption of luminescence by rhodamine dye appears to be negligible when compared to absorption by the suspended particles.

4) Absorption of green light by rhodamine dye appeared to be more significant than was the case for yellow light, a conclusion which might be inferred from the absorption or excitation spectrum for the dye (Fig. 13). However absorption of green light by suspended particles in the turbid waters of San Francisco Bay was many times greater than that of a 100-ppb dye solution. Therefore the most critical factor

to consider in interpretation of FLD records is generally turbidity of the water, and its effect on light attenuation.

5) Tests of temperature-dependence of fluorescence have shown that this factor is significant and cannot be overlooked in quantitative use of the FLD. If temperature variation with depth is known the average should be weighted to correspond to the average depth from which luminescence emanates.

6) Tests of the relation between reflectance of target materials and recorded rho values suggest that when reflectivity exceeds some critical limit the FLD computer cannot cope with the signal and a spurious rho value is recorded. This limit appears sufficiently high that reflectivity is generally not a problem during level flight over water. The critical limit appears to be exceeded only during low sun angles, high surface roughness, and when the aircraft banks toward the sun in turning.

7) Observations have established that the sky itself makes no appreciable contribution to the luminescence of rhodamine dye solutions, by comparison with direct sunlight.

8) Techniques were tested for using the FLD in remote measurement of fluorescent dye concentration in natural water bodies having a wide range of turbidity, and techniques for mapping the data were tested, using tracking radar that automatically plotted flight paths on maps in real time.

9) Water-sampling procedures for use during remote sensing by the FLD were devised and tested, the object being to obtain samples that could be correlated with an exact point in time and space as plotted on the FLD record. An apparatus was built to permit measurement of attenuation by these samples, of incident sunlight and of emitted luminescence.

10) Airborne tests up to an altitude of 5,000 feet were conducted over clouds of rhodamine dye. As altitude increased the highest peaks recorded by the FLD were flattened due to increasing size of the field of view, but the dye was clearly detectable at the highest altitude reached.

11) Sensing of rhodamine dye has proved successful at low sun angles, as late as 5:45 p.m. local time during August, or approximately 4-3/4 hours after sun's transit.

CONCLUSIONS AND RECOMMENDATIONS

1) The FLD appears to have a major advantage over conventional dye sampling and fluorometer analysis in hydrologic studies by adding, remotely from an aircraft, the dimension of depth. In such studies the FLD can be used effectively in conjunction with aerial photography. The present FLD appears to have the additional advantage, when used with rhodamine dye, that it is sensing in nearly the optimum part of the spectrum for penetration of turbid water by incident sunlight and emitted luminescence.

2) In order to improve accuracy of interpretation of FLD records, further work is needed on testing the optical and other properties of rhodamine dye in known concentrations, particularly any departures from direct proportionality to dye concentration. More data are needed to relate fluorescence of rhodamine dye to function of the FLD, particularly what specific wavelengths of absorbed light are effective in exciting luminescence at 5890 A, and how this varies with depth as certain wavelengths are attenuated more than others.

3) The possibility of computing dye concentration from FLD readings on an external computer should be explored, including conversion to digital output from the FLD. A computer program would be needed for compilation of large quantities of FLD data, and a future FLD should probably produce digital output. An assumption required without use of a computer is that there is a linear relation between dye concentration and sensitivity, but the relation is probably an exponential curve that closely approaches a linear approximation for low dye concentrations.

4) On clear sunny days the optimum time for sensing with the FLD is during the 6-hour period centering at midday. Since sensitivity is greatest at highest sun angles, the best time of year north of latitude 23-1/2°N. is near June 21 from the standpoint of sun angle alone. During spring and summer months at mid-latitudes the period suitable for sensing will probably average about 8 hours per day on clear sunny days.

5) During operational use there will be a need for more data on adsorption loss of rhodamine dye on suspended particles of various sizes. The greatest need will be for data on adsorption losses of Rhodamine WT in the concentration range from 0 to 10 ppb., in the time range from 0 to 24 hours, in the grain-size range of clay and

silt, and the turbidity range equivalent to attenuation coefficients from 0.10 to 1.0 m^{-1}. There may be a need for a coefficient of luminescence loss, expressed in percent per hour, to combine losses from adsorption, exposure to light, photochemical deterioration, and other causes.

6) Experimental or theoretical work is recommended to relate some of the following factors to FLD function: a) roughness of the water; b) dissolved salts in the water; c) scattering of light in the water; d) reflectivity of the bottom; e) absorption of luminescence in the air; f) viewing angle of the FLD; g) angle of the light collector diffuser plate; and h) differences between solar intensity at the instrument and at the target.

7) Exceptionally high sensitivity of the FLD occurred for relatively clear water during tests over the Pacific Ocean west of Golden Gate. In areas of well dispersed dye the sensitivity appeared to resolve 0.1 or 0.2 ppb of rhodamine dye. This finding is very encouraging but also indicates the necessity of sampling subsurface waters during use of the FLD. A limitation of the present method is the assumption that the dye is uniform throughout the water column sensed. Therefore an improved means for subsurface water sampling from a helicopter is needed.

8) No significant correlation was found between sensitivity of the FLD and solar intensity during periods of level flight. This is encouraging and suggests that records of solar intensity (A, B, or B/A) are not necessary in interpretation of dye concentration from FLD readings (rho). Such correlations were noted during banking of the aircraft, however, and probably limit useful data from the present instrument to periods of level flight.

9) A comparison of FLD records shows that significant changes in sensitivity occurred and illustrates the necessity of repeated calibration by viewing standards of known luminosity during flight. This is a limitation common to most conventional fluorometers, in that the output is partly dependent on electronic variables. This also may impose the limitation that for remote sensing of concentration it must be known in advance what substance is the source of the luminescence emission. A new design for a future FLD, having only one photomultiplier, should essentially eliminate problems of varying sensitivity and eliminate the need for monitoring standard targets (D.A. Markle, personal communication, August 1969).

10) Alternatively, the FLD could be modified to operate at a different Fraunhofer line, such as the hydrogen F line (4861 A) in the blue part of the spectrum. That line falls near the luminescence emission peak of oil from the Santa Barbara leak. The present FLD, at 5890 angstroms, failed to detect the oil in a series of tests. The instrument might also be modified to operate at a line in the red, for detection of chlorophyll luminescence. These modifications could convert the present FLD into a versatile sensor suitable for such practical applications as monitoring oil spills and leakages, algal blooms in water bodies as an indicator of pollution, or dispersion studies based on fluorescent dye.

REFERENCES

1. Hemphill, W.R., 1968a, Ultraviolet absorption and luminescence studies, progress report for the period April to December 1967: U.S. Geol. Survey open-file report, 47 p.

2. Stoertz, G. E., 1969a, The Fraunhofer line discriminator, an airborne fluorometer: U.S. Geol. Survey open-file report, 30 p.

3. _____, 1969b, Fraunhofer line-depth sensing applied to water: U.S. Geol. Survey open-file report, 43 p.

4. _____, 1969c, Testing the Fraunhofer line discriminator by sensing fluorescent dye: U.S. Geol. Survey open-file report, 40 p.

5. _____, 1969d, Test of data compilation procedures for Fraunhofer line discriminator: U.S. Geol. Survey open-file report, 35 p.

6. Hemphill, W. R., 1968b, Remote detection of solar stimulated luminescence, in 19th Congress of the International Astronautical Federation: Paris, Internat. Astronautical Federation, 6 p.

7. Kozyrev, N.A., 1956, The luminescence of the lunar surface and intensity of the solar corpuscular radiation: Izvestia Krymskoi Astroizitcheskoy Observatorye, v. 16, p. 148-161.

8. Dubois, J., 1959, Contribution a l'etude de la luminescence lunaire: Ceskoslovenske Akademie Ved, Rozpravy, v. 69, pt. 6, 42 p.

9. Grainger, J.F., and Ring, J., 1962, Anomalous Fraunhofer line profiles: Nature, v. 193, p. 762.

10. Spinrad, H., 1964, Lunar luminescence in the near ultraviolet: Icarus, v. 3, p. 500-501.

11. Noxon, J., and Goody, R.M., 1965, Noncoherent scattering of skylight: Akad. Nauk SSSR, Izvestiya, Atmospheric and Oceanic Physics Series, v. 1, no. 3, p. 275-281.

12. Myronova, M.M., 1965, Luminescence in the crater Aristarchus: Akad. Nauk Ukrainskoi SSR, Main Astronomical Observatory, no. 4, p. 455-459.

13. McCord, T.B., 1967, Observational study of lunar visible emission: Jour. Geophys. Research, v. 72, no. 8, p. 2087-2097.

14. Minnaert, M., Mulders, G.F.W., and Houtgast, J., 1940, Photometric atlas of the solar spectrum from λ3612 to λ8771: Amsterdam, D. Schnabel, Kampert and Helm.

15. Mohler, O.C., Pierce, A.K., McMath, R.R., and Goldberg, L., 1950, Photometric atlas of the near infrared solar spectrum, λ8465 to λ25,242: Ann Arbor, Michigan, Univ. of Michigan Press.

N71-11993

SECTION 34

EXPERIMENTAL RESULTS IN THE REMOTE SENSING OF GASES FROM HIGH ALTITUDES

By A. R. Barringer and J. H. Davies
Barringer Research Limited

ABSTRACT

A brief history of correlation spectroscopy is provided. The continuing progress made in the experimental and theoretical development of techniques for remote sensing of trace gases by optical correlation methods is reviewed. The concept of correlation spectrometry has been improved by the use of computer techniques for correlation mask optimization, and the problems of atmospheric scattering have been investigated in some detail. Theoretical work has been matched against various types of remote-sensing measurements, including long horizontal-path measurements using active light sources and passive remote sensing from aircraft flying above the inversion layer. Good results have been obtained in terms of monitoring patterns of pollution and tracking plumes, and methods are being developed for improving the absolute accuracy of measurements. A number of test airborne surveys of pollution have been carried out over cities with both NASA and HEW support, and a high altitude balloon experiment has occured. In this experiment, a combination of spectral and spatial scanning techniques were used to demonstrate the feasibility of detecting and monitoring the distribution of atmospheric pollution through the ozonosphere from either balloons or satellites. The gondola design includes a sun-orientation sensor, and the two downward-looking scanning spectrometers maintained at constant sun orientation. The preliminary results of this experiment are given.

Prospects are reviewed for the ultimate development of scanning multigas monitors for satellite platforms and their potential role in measuring the buildup of atmospheric pollution on a worldwide scale. Experiments are also described which relate to the feasibility of remote gas detection in trace amounts as an aid to natural resources exploration and survey.

INTRODUCTION

This paper outlines the progress being made in the experimental and theoretical development of techniques for remote sensing of trace gases by optical correlation methods. Work at Barringer Research has centered on trace gas and vapour detection for use in mineral exploration, natural resource inventory, and air pollution measurements. This work has been active for many years, and recently culminated in a successful high altitude balloon experiment. The purpose of the balloon experiment was to test the

validity of correlation spectrometric techniques for measuring gaseous SO_2 and NO_2 above the earths atmosphere. The results from the balloon flight proved conclusively that such measurements could indeed be made above the ozonosphere.

The concept of remote sensing trace gases, and the development of correlation spectrometric methods, goes back many years. Initial work centered around the detection of mercury vapour associated with soils. The anomolous high occurance of mercury with metallic mineralization is now well established. Figure 1 clearly shows the concentration of mercury in the Aljustrel Pyritic deposit in Portugal, the level approaching 4000 ppb. Because of this, initial work at Barringer Research concentrated in the development of a mercury spectrometer for the detection of mercury vapour associated with such metallic mineralization. This was the initial foundation of the present program and we are still currently active in this field. An airborne mercury spectrometer is now currently under development for the United States Geological Survey.

Because the mercury vapour absorption spectrum occurs below 2800 Å, it can not be remotely detected since there is no solar radiation available at this wavelength; the small amount emitted being heavily absorbed by the ozonosphere. Attention was then directed towards other gases or vapours that were of significance from earth resource aspects. The halogens were investigated as likely candidate gases, and iodine vapour appeared to be particularly attractive. The table below gives the reported occurance of Iodine in soils.

TYPE	SOURCE LOCATION	CONTENT PPM
COPPER ORES	Light ores from several localities in New South Wales, Australia	100 - 1,300
CUPRITE	Fine samples in New South Wales, Australia	600 - 700
MALACHITE	Three samples in Germany	600 - 4,000
	One sample in New South Wales, Australia	1,500
ROCK PHOSPHATE	Two samples in Florida	92 and 95

As can be seen from the iodine spectrum shown in Figure 2, it has a most regular absorption spectrum in the visible region between 5200 and 6500 Å, and is an ideal target gas for the use of correlation spectrometric techniques. Consequently further development work was directed towards the laboratory fabrication of an iodine spectrometer.

However, it was at the suggestion of Dr. Morris Tepper of NASA Headquarters, Washington, that sulphur dioxide was considered as a likely gas of significance as an air pollutant as well as a gas of geophysical importance. Since SO_2 has a characteristic absorption spectra in the ultraviolet region between 2800 and 3100 Å, (see Figure 3) it is amenable to remote detection through the use of scattered solar ultraviolet radiation as the background source. As a result of this a research and development program was initiated by NASA, and is presently being pursued, under contract to Manned Spacecraft Center, Houston. The remainder of this paper outlines in greater detail the experiments and results obtained under this MCS support, particularly the work during the last year during which the high altitude balloon experiment was conducted.

CORRELATION SPECTROMETER

The principle of correlation spectroscopy involves the cross correlation of the incoming absorption spectra against a stored replica contained in the spectrometer; this correlation being performed in real time. Since a multiplicity of spectral lines are used within the mask, correlation can be achieved at photon levels with high signal-to-noise ratios ensuring great sensitivities and selectivity. Correlation spectroscopy is now well described in the literature and references are appended.[1-7]

The original development work for a remote sulphur dioxide sensor, was sponsored by the American Iron and Steel Institute. This instrument is shown in Figure 4, the basic engineering design of this spectrometer was used as the starting point for the NASA SO_2 and NO_2 spectrometers. Many improvements and modifications were embodied into the instrument to upgrade its performance. It is worth noting that the performance of the spectrometer has been increased greatly. Instrument improvement has resulted from many engineering developments and modifications, and also the use of computer techniques for optimizing the design of the correlation mask.

Figure 5 shows the absorption spectra of three gases currently under active investigation for NASA, MSC as remote gas targets. The upper trace shows the SO_2 band structure extending from 2850 Å to about 3150 Å. The set of bands illustrated above the trace (wavelengths longer than 3000 Å) are those used for passive remote sensing i.e. solar illumination. For active systems where energy is available at all wavelengths of interest, the mask may contain as many as 10 slits and be centered on the most intense

band. The absorption bands presently used for NO_2 and I_2 sensing are similarly shown. Here again the choice of spectral bands and design of the mask will depend on the light source characteristics. Mask optimization for a given application is an automated mathematical process, in which the response of a computerized model of the correlation spectrometer is examined over the full range of anticipated light source spectral characteristics, target gas concentration and possible interfering spectra for a given mask design. Experience to date has shown excellent agreement between theoretical performance predicted by computer modelling and actual performance from working prototypes.

The use of a spectrometer in the remote sensing role entailed the investigation of atmospheric scattering phenomena which is of particular importance at ultraviolet wavelengths. In the UV, mie and aerosol scattering is of greater importance than pure molecular scattering. Considerable mathematical modelling work has been performed to generate models which are truly representative of the phenomena taking place. The results of this work was the development of an airborne SO_2 correlation spectrometer suitable for installation in an aircraft. The airborne determination of the ground level gas concentration requires a knowledge of the absorption and scattering properties of the atmosphere, the spectral distribution of radiant energy, ground albedoes and vertical mixing ratios of the gas under investigation.

Figure 6 shows the Aero-Commander aircraft into which the $SO_2/NO_2/I_2$ correlation spectrometer was installed. Clearly visible in this illustration is the fuselage pod which enabled the spectrometer to view vertically downwards, and also vertically upwards (the latter being required for calibration purposes). Figure 7 shows the actual installation within the aircraft. The installation included the correlation spectrometer, its associated electronics, chart recorder, intervalometer, flight path recovery camera and closed circuit television system for pilot navigation purposes. Through the use of this aircraft, numerous airborne air pollution surveys were conducted in the United States and Canada. Apart from local trials over the Toronto metropolitan and Hamilton area, successful air pollution surveys over Washington, Los Angeles, Chattanooga and San Francisco have been obtained. This was all pioneering work in the field of airborne remote gas measurements; the work proved conclusively that airborne spectrometric techniques can be used to remotely sense track and map gaseous air pollutant species. A Mass balance survey around Washington was successively concluded, plume tracks and dispersions have been plotted from thermal power stations extending over many tens of miles, and synoptic surveys have been realized.

Figure 8 is typical of the profiles recorded on one such survey and shows typical NO_2 profiles obtained over Chattanooga, Tenn. in August of 1968. Figure 9 shows NO_2 line profiles obtained over Chattanooga during this survey. More recently I_2 surveys over the kelp beds off the State of

Maine have been successfuly undertaken. Figure 10 shows the I_2 search off the Coast of Maine over Mahnicus Island which recorded 16 ppm-m of I_2. This was the first time that I_2 was detected from the air. The iodine backgrounds are very low; therefore it is necessary for the spectrometer to look sideways to obtain adequate signal-to-noise ratios. However, through the use of the side looking long path measurements (pathlengths of several miles), we observed definite buildups of iodine over the coast of Maine.

Apart from its geological significance, iodine is concentrated in all marine life forms, and hence is of great biological significance. Iodine is also significant in relation to oil depositions. Figure 11 shows the iodine concentration in soils plotted over the Gobles Gas and Oil Field, Ontario. As can be seen from this Figure, the I_2 concentration in the soil displays a profile of anomolous concentration directly related to the oil deposit itself and the porphyrin derivatives. Our knowledge of the behaviour of iodine in the atmosphere has greatly increased in recent times. This has been aided in no small way by the windscale atomic accident that occured in the United Kingdom in 1959. Resulting from that accident, large amounts of radioactive iodine were released into the atmosphere and thereby enable significant work to be done on its dispersion and distribution. As a result of this several technical papers have resulted which greatly assist in our understanding of its movement and atmospheric behaviour.

Apart from the development work that has been undertaken for SO_2 NO_2 and I_2, attention has been directed towards other gases and vapours of significance to earth resource application. One such gas is methane, its near infrared spectrum between 2.1μ and 2.8μ being depicted in Figure 12. This Figure shows that like SO_2 and NO_2, methane has its own characteristic absorption spectra in the near IR. Sufficient reflected sunlight is available in the 2 to 3μ near infrared region to enable methane to be remotely detected by near infared correlated spectrometric techniques. Figure 13 shows methane gas and CO_2 in the soil, and has been taken from a recent German paper by V.W. Ernst.

DESCRIPTION OF APPARATUS

The basic technique of correlation spectroscopy has been previously cited.[1-7] A description of the correlation SO_2/NO_2 spectrometer developed under the NASA Manned Spacecraft Center program is given in technical report number 108.[8] Figure 14 illustrates the basic correlation spectrometer. The field defining fore-optics is comprized of M_1 and M_2, a cylindrical lens and the entrance slit. An Ebert-Fastie F/3.6 configuration of 0.25 meter focal length comprizes the spectrometer with a stationary correlation mask. The incoming light is spatially modulated relative to the fixed mask by quartz refractor plates, fork driven at 100 hertz. A high-gain photomultiplier tube detects the mask/spectrum correlation function

and is followed by a FET pre-amplifier, the output of which is a series of uni-directional pulses produced by the spectrum moving in square wave fashion from one discrete position to a second discrete position and back again. Considering only one slit in position 1 and the slit moving relative to the spectrum to position 2, then the modulation ratio is:

$$M = \frac{I_o e^{-a_1 cL} - I_o e^{-a_2 cL}}{I_o e^{-a_1 cL}} \qquad (1)$$

where

I_o = incident light

a_1 = average minimum absorption coefficient across the slit

a_2 = average maximum absorption coefficient across the slit

c = concentration

L = pathlength

and

$$M = 1 - \frac{e^{-a_2 cL}}{e^{-a_1 cL}} \qquad (2)$$

or

$$M = 1 - e^{-(a_2 - a_1)cL} \qquad (3)$$

From equation (2) we see that the instrument simply measures the ratio of energy contained in the spectrum viewed by the slit. The above is of course a very simplified treatment and the full analyses is given in reference 5. For near real-time detection purposes however, a single slit would suffer from low energy throughput and low specificity. The number of slits therefore varies from 5 to more than 10 depending on the application.

If now the spectrum is made to move in one direction while the slit is oscillating back and forth between positions 1 and 2, the modulation ratio will swing through positive and negative values in a periodic fashion. This is the basis of the instrument operation as used in the Balloon flight.

BALLOON EXPERIMENT

Of considerable importance in detecting SO_2 in the ultraviolet region through the earth's atmosphere, are the effects of ozone absorption and atmospheric scattering. The ozone absorption occurs primarily in the upper layer between 20 and 30 km, as shown in Figure 15. This figure shows that an airborne instrument system would never be above most of the earth's ozone layer. As a consequence to this it was decided to fly the SO_2 spectrometer

on-board a high altitude balloon thereby placing the instrument above the major portion of the ozonosphere, as can be seen from the ozone concentration profile shown in Figure 16.

The current MSC contract involved a balloon flight over Chicago of two correlation spectrometers to satisfy the above requirements. One correlation spectrometer was optimized for the measurement of NO_2; the second was optimized for the measurement of SO_2. The two spectrometers together with a radiometer, batteries and telemetry equipment, were mounted onto a gondola package for suspension beneath the balloon.

The launch was actually made on September 3, 1969 from Dowagiac, Michigan and achieved the desired float altitude of 114,000 ft. (35 km). Figure 17 shows the balloon system; the ladder cable was constructed of 3/16" cable with 18" aluminum spacers to provide stiff coupling to the balloon. Because of errors that could arise by changes in polarization resulting from changing solar heading caused if the balloon was allowed to enter free azimuthal rotation, a sun tracking orientation system was installed.

The gondola payload is shown in Figure 18. This figure illustrates the SO_2 and NO_2 spectrometers, radiometer, telemetry interface, sun tracker electronics, NiCd battery pack and scanning mirror. The scanning mirror allowed both spectrometers to scan the ground through a common mirror assembly driven by a solenoid in bi-stable fashion. The scan went from Nadir to 24° on the anti-solar side. This resulted in gas sampling over two parallel ground tracks separated by about 10 miles. The anti-solar side was selected because of reduced backscatter in the anti-solar direction. The spectrometers spatial resolution was 1°, equivalent to 1/2 mile at the ground. The spectrometer settings were:

	SO_2	NO_2
Center Wavelength -	3075 Å	4400 Å
Spectral bandwidth -	150 Å	200 Å
Grating scan range -	6.2 Å	25 Å
Grating scan rate -	0.7 hz	0.9 hz

A solenoid-driven diffuser plate and quartz iodine light source were provided for calibration purposes. The radiometer is a Barringer Research development and designed to measure contrast ratios of the terrain at wavelengths of 3100 Å and 6000 Å. It scanned a small cone around the nadir and generated a high frequency output corresponding to the changes in reflectance plus a larger low frequency and DC component due to atmospheric backscatter. By using the average value of the signal to control an AGC loop, the high frequency output can be made proportional to the apparent

contrast changes in the terrain. Then given the average values and variations in reflectance at the two wavelengths, the ratio of apparent and actual contrasts show how the target signal is diluted by backscatter.

We also measured the SO_2 burden in the atmosphere over Chicago from the ground coincident with the balloon overflight measurements. The mobile ground spectrometer was adjusted to scan the spectral range identical to that of the balloon unit. By comparing the balloon measurements of SO_2 with that of the ground vehicle, with due consideration of the balloon results, the best possible measure of dilution can be arrived at. The ground runs made by this vehicle were intended to follow as closely as possible the balloons ground track. Simultaneous with the ground measurements and the balloon flight, was an airborne SO_2 pollution measurement. This was undertaken by the Aero-Commander aircraft. Again, the flight path of the Aero-Commander aircraft was selected to be as close as possible to the predicted ground track of the balloon.

DATA MANAGEMENT

The original calibration technique used in the Aero-Commander aircraft installation was not suitable for use in the balloon system. Calibration in the airborne system simply involved flying above the inversion layer, rotating a mirror within the wing tip pod to allow the spectrometers field of view to look vertically upwards. If the aircraft was flying above the inversion layer, it could be safely assumed that no gas of interest lay above the instrument, and thus a true zero reading could be obtained. This however, would be unworkable in the balloon system, since at 114,000 ft. the sky is essentially black, because no atmospheric scattering can take place. This resulted in the design of calibration cells which could be inserted into the spectrometers line of sight, and which were relay operated by command control. All signal channels and house keeping data were FM/FM telemetered back to ground receiving station.

A detailed description of the method obtaining the data and its subsequent analysis can be found in reference 9. For the sake of completeness, this report will outline the range of variables measured. The following signals were telemetered to the base station:

(1) SO_2 signal
(2) NO_2 signal
(3) UV radiometer
(4) Visible radiometer
(5) SO_2 AGC
(6) NO_2 AGC
(7) Sun track azimuth
(8) Housekeeping

An accurate record of the balloons ground track was to have been obtained from a high altitude balloon camera, which was supplied by the National Center for Atmospheric Research, Boulder, Colorado. This camera was triggered at a predetermined rate to ensure overlapping mosaic coverage of the ground beneath the balloon. From the mosaic, and graticules within the camera's field-of-view, it would have been possible to plot the balloon ground track. Unfortunately the high altitude camera failed to trigger and no photographic record of the balloons trajectory is available. However, radar tracking was obtained from the ground station and this coupled with observations of the balloon made from the ground and from tracking aircraft, enable a fairly accurate representation of the balloon track to be obtained.

All the data was handled in analog form. The incoming analog signals received at the ground telemetry station was converted into analog strip chart records for subsequent data analysis. It would have been most rewarding to relate the high altitude balloon camera mosaics against the analog chart records, so that representative correlations between the data and physical ground locations could result. Another benefit that would have resulted from the high altitude photo mosaics would have been the association of signal to areas free of cloud cover and the significant changes in signal return contributed by clouds within the instruments field of view.

RESULTS

The balloon flight originally called for an east-to-west or west-to-east trajectory over Chicago at an altitude of 37 Kcm (≃ 120,000 ft.) arriving over the city as close as possible to 1200 Noon solar time. To take advantage of the high sun altitude and the higher probability of favourable weather conditions as compared with later in the year, an August launch was scheduled. Towards the end of August however, the upper level winds at Chicago entered the turn-around phase and their speed and direction became less predictable. A launch site was selected at Dowagiac, Michigan and subsequent computed trajectories by NCAR's Palastine computer facility confirmed the choice as being the most suitable for a late August launch. With an accumulation of minor delays in the program however, the launch date slipped to Sept. 3, 1969. On Sept. 2nd, NCAR's studies showed the upper level easterlies were still holding although getting weaker and more variable and that surface conditions over Chicago should be favourable for a launch the following day. The launch took place at 3:55 CST Sept. 3/69. Figure 19 shows the actual balloon trajectory. The dotted track is the station wagon route. The circuitous track of the balloon was completely unexpected although the south-westerly and north-westerly position of the trajectory were anticipated. Unfortunately, heavy cloud covered the early portion of the track but by 10:15 CST this had given way to scattered

cumulous. Under the influence of a light (7 knot) easterly wind and strong inversion conditions the ground level SO_2 levels were somewhat higher than usual as shown by the ground station readings obtained from the automated pollution monitoring network of the City of Chicago. The station wagon followed a route which approximated the predicted balloon trajectory as far as Joliet and then returned immediately to the center of Chicago when advised of the balloon's change in direction.

Disregarding dilution, the amount of SO_2 present in the sensors field-of-view, relative to that in the background was determined by measuring the increase in peak-to-peak amplitude at the grating reversal points, that is at the mid-point of the +ve and -ve swings. The incremental sensitivity of the instrument is given by the increase in the peak-to-peak value using a reference cell of known SO_2 content.

The results of this balloon experiment are shown in Figures 19 for SO_2 and 20 for NO_2. It should be remembered that the data has only been partially reduced.

CONCLUSIONS

It can be concluded from this experiment that adequate measurements of SO_2 and NO_2 air pollution can be made through the Earth's ozonosphere even allowing for the dilutions caused by atmospheric backscatter in the ultraviolet regions.

The significance of the experiment is that it validates the concept of global synoptic air pollution monitoring from satellite platforms. Figure 21 depicts the effects of SO_2 exposure upon our health. The seriousness of air pollution is now well recognized. That the air we breath is of prime importance as a natural earth resource is beyond question. We can realistically foresee the time when second generation correlation spectrometric instruments with far greater threshold sensitivities can monitor SO_2 as a precusor of an earth resource; for example SO_2 emissions from geothermal sources and Volcanoes. Similarly the use of other gases such as I_2 and CH_4 are only the beginnings of gaseous remote sensing which must now be considered in its infancy.

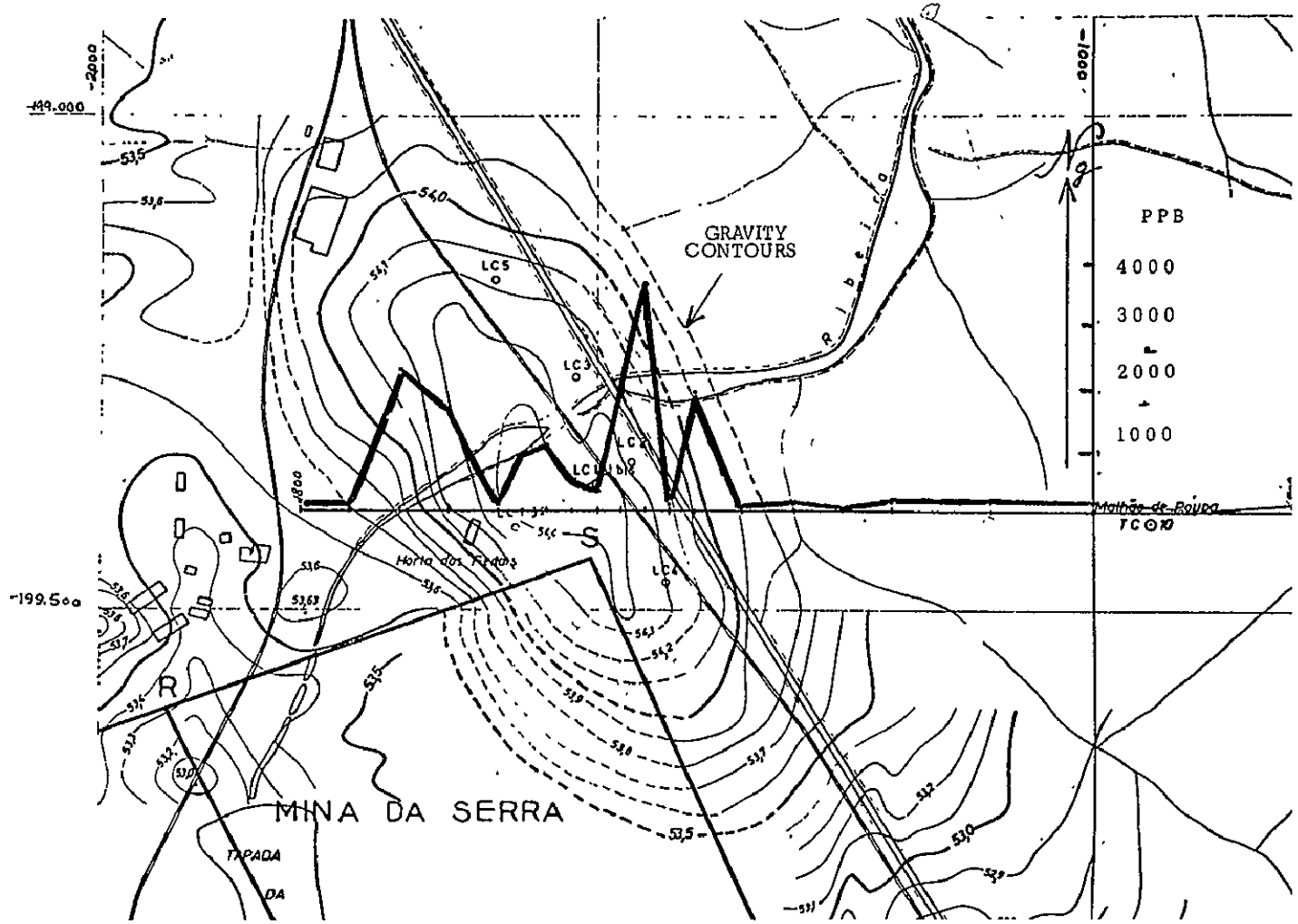

Figure 34-1.- Mercury concentration in the soils, Aljustrel pyritic deposit, Portugal.

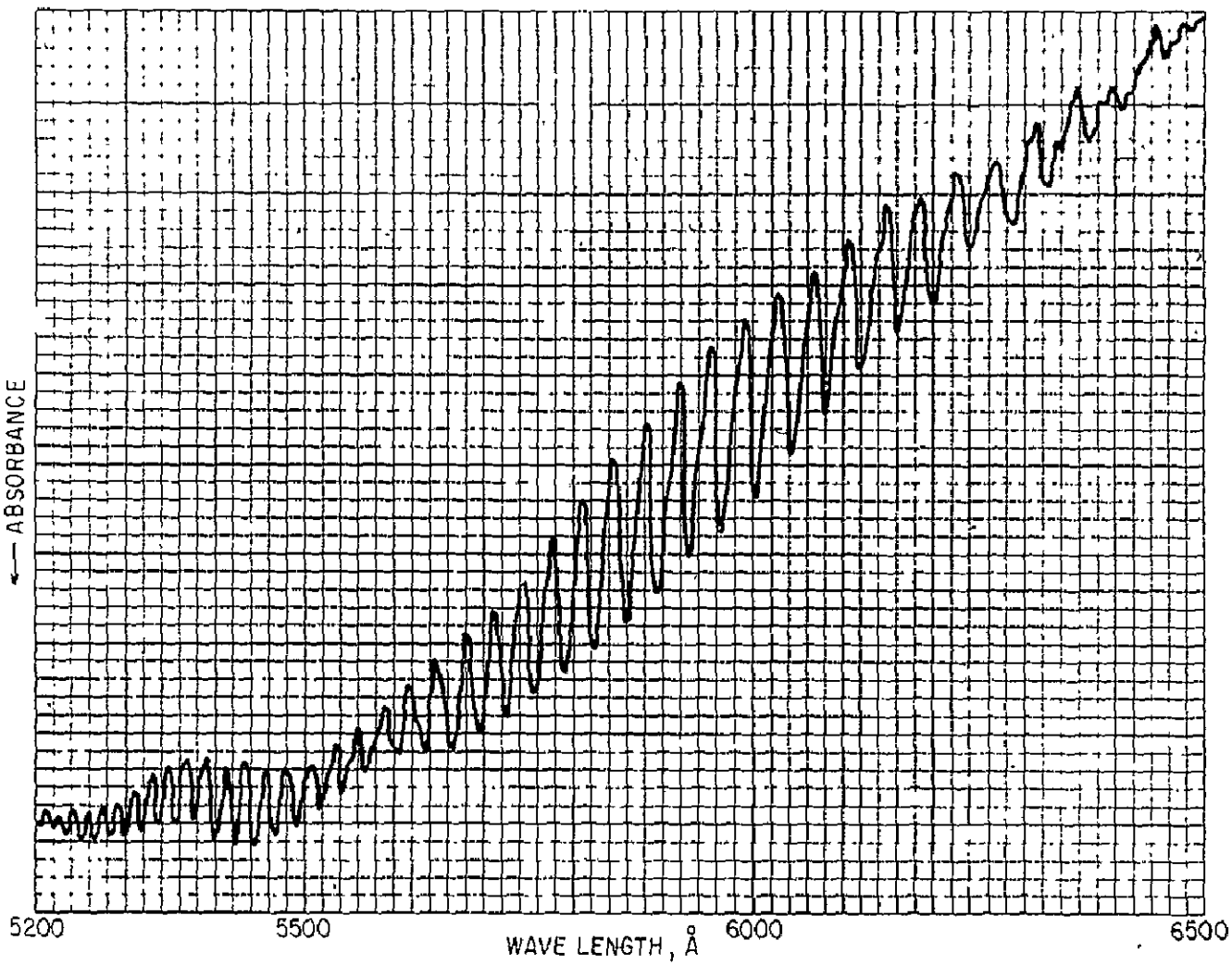

Figure 34-2.- Portion of the Iodine vapor spectrum.

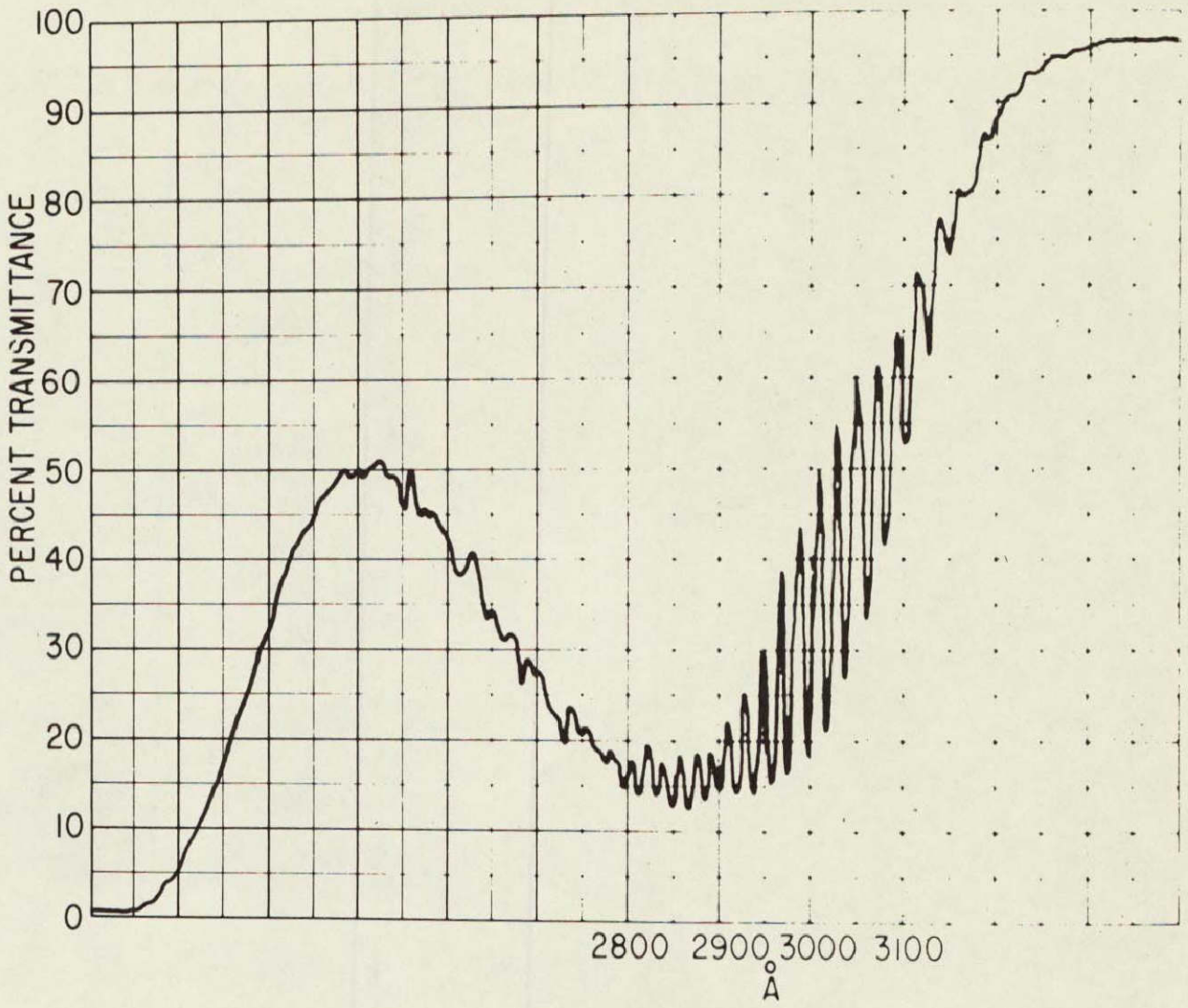

Figure 34-3.- Absorption spectra of SO_2 in the 3000 Å region.

Figure 34-4.- Correlation spectrometer used to monitor SO_2.

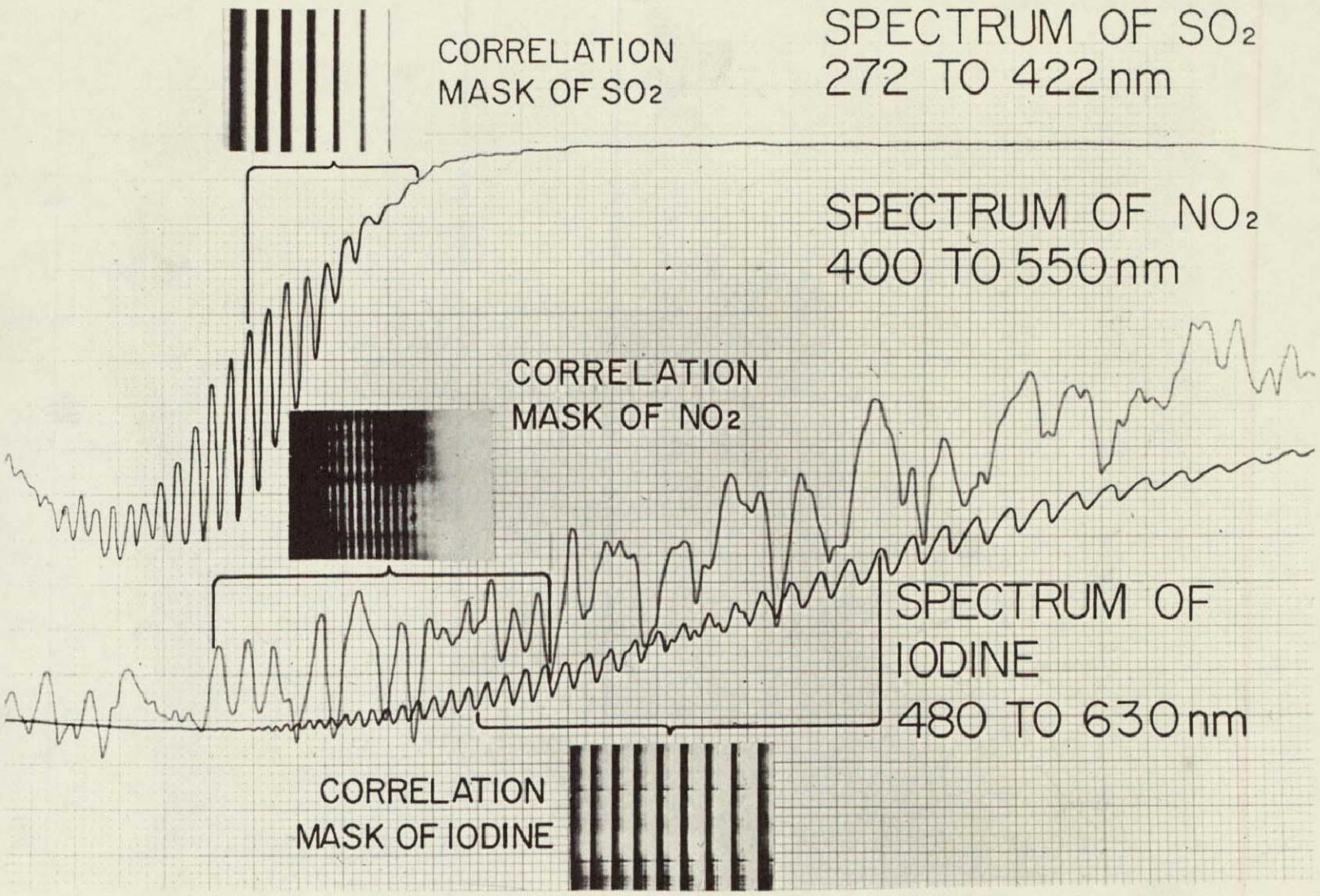

Figure 34-5.- Absorption spectra of SO_2, NO_2, and Iodine.

Figure 34-6.- View of aircraft into which the $SO_2/NO_2/I_2$ correlation spectrometer is installed.

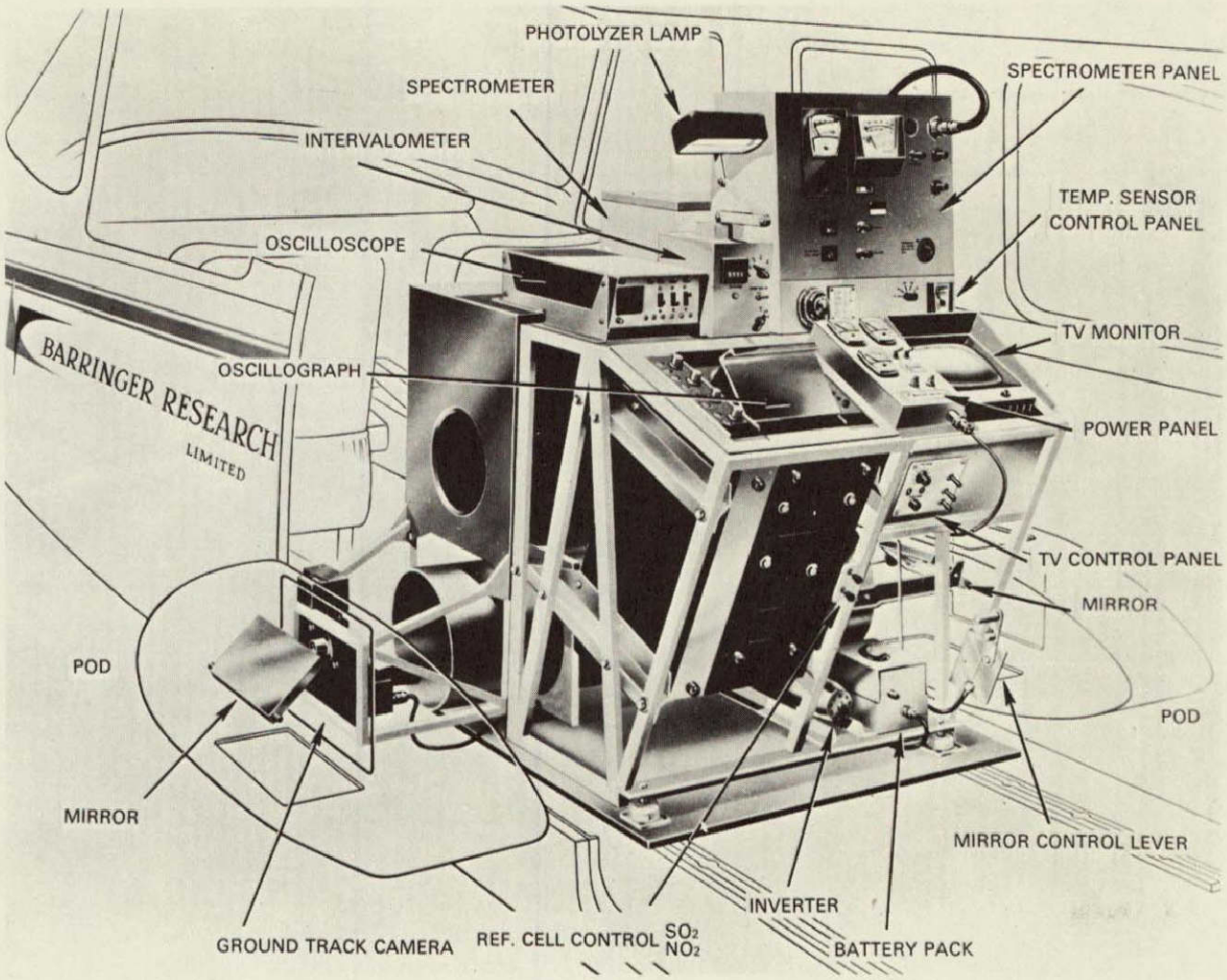

Figure 34-7.- Cut-a-way view of aircraft showing the actual installation of the correlation spectrometer.

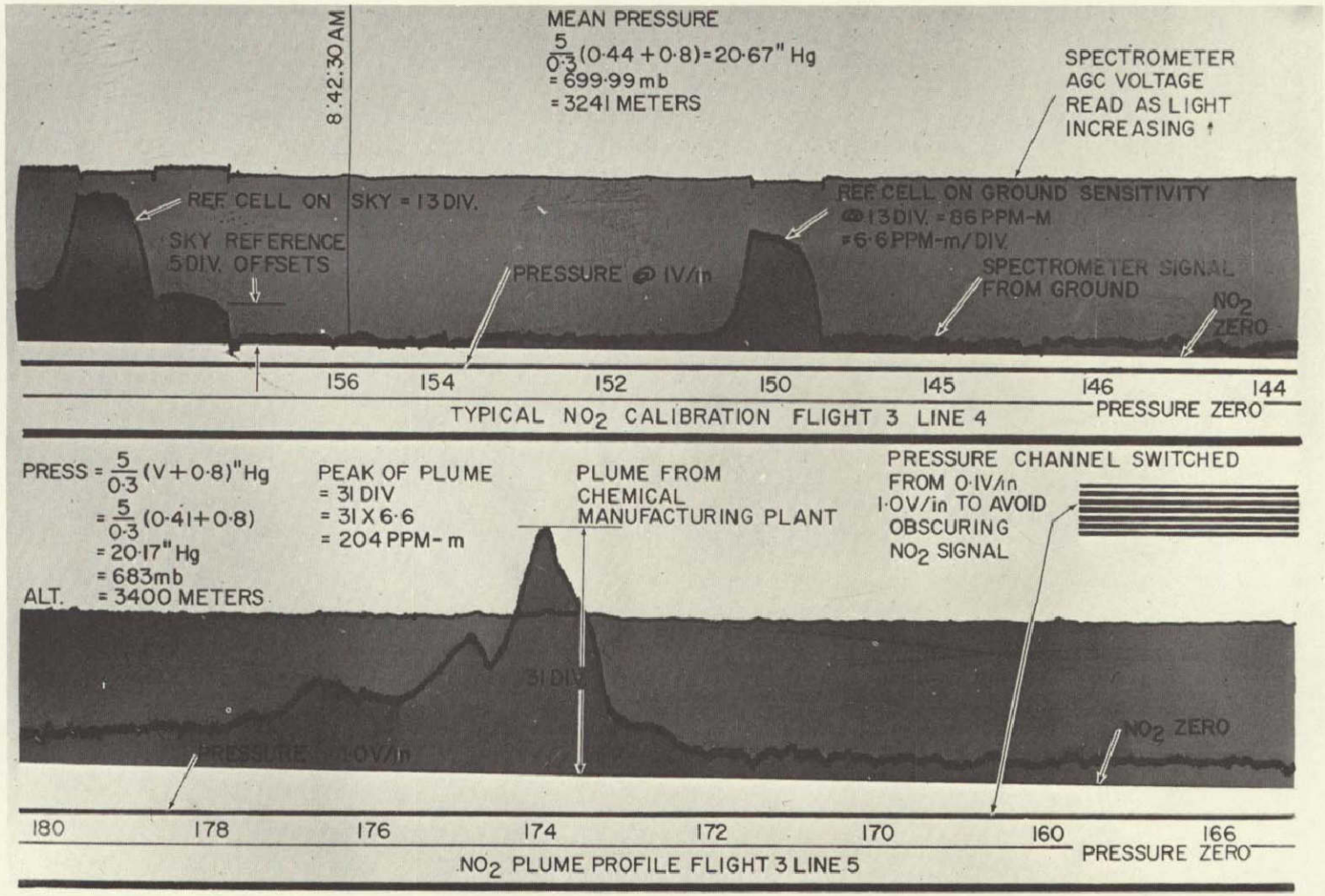

Figure 34-8.- Typical NO_2 profiles, Chattanooga, Tennessee, August, 1968.

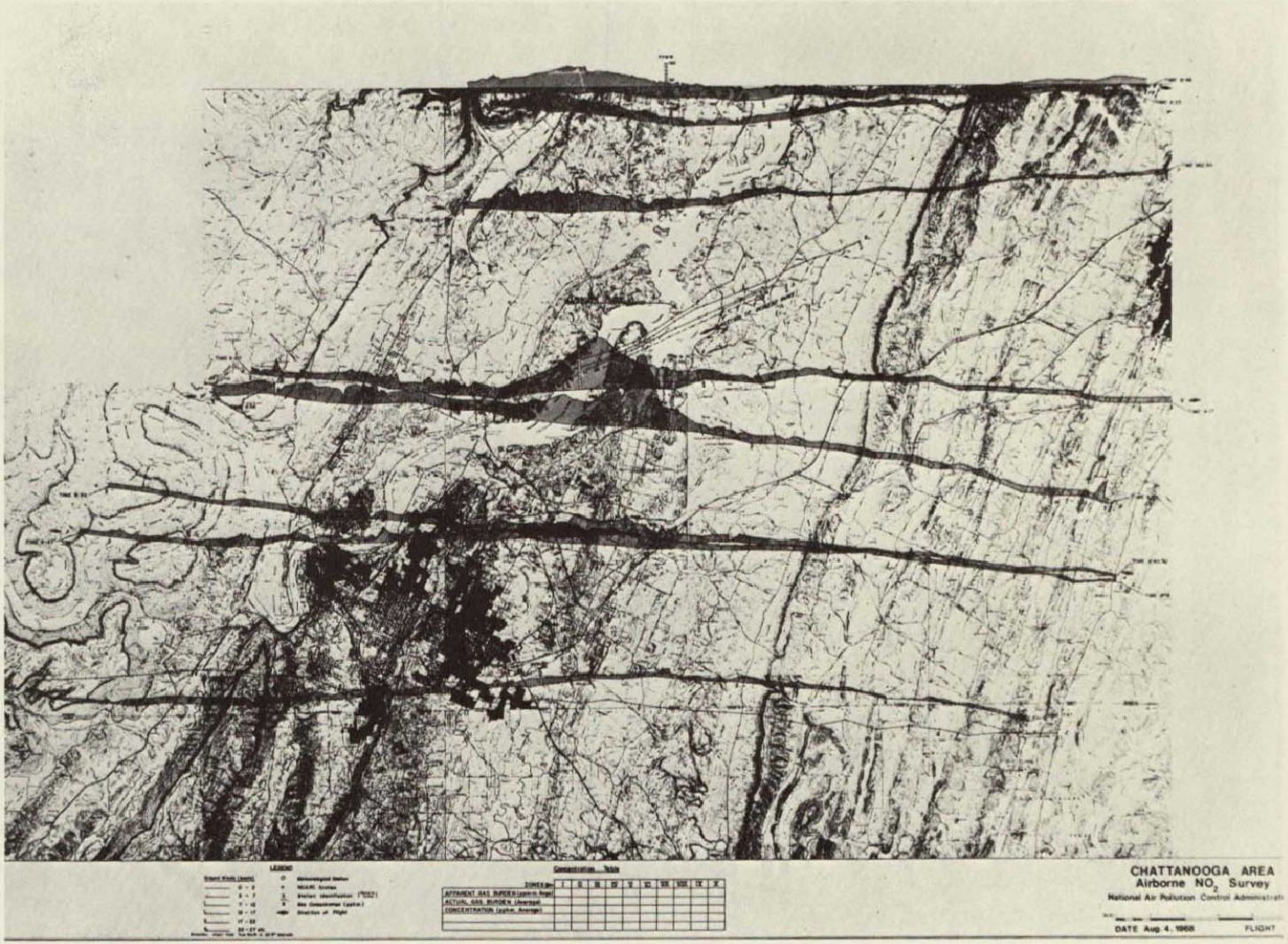

Figure 34-9.- Airborne NO_2 survey profiles Chattanooga, August, 1968.

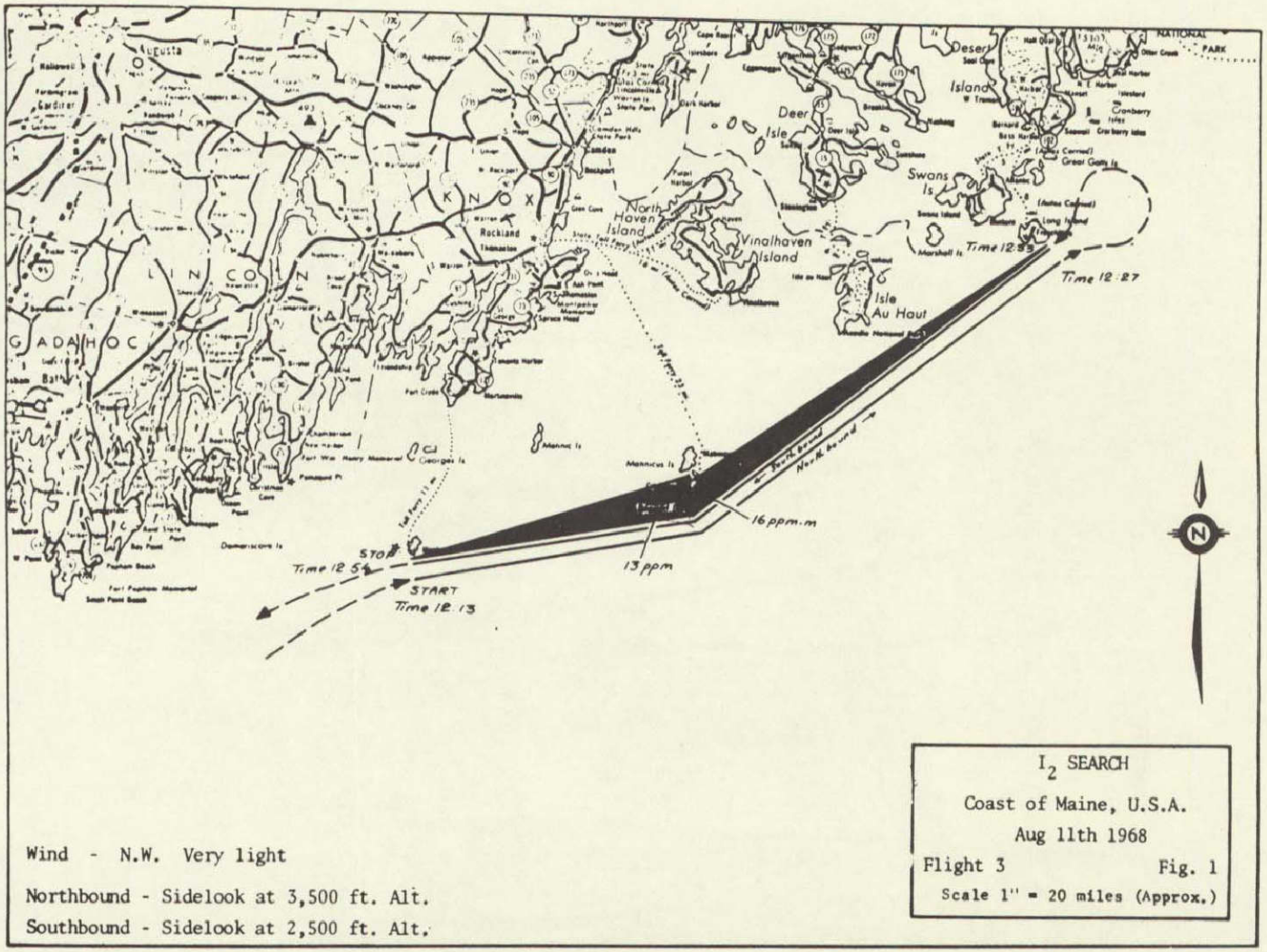

Figure 34-10.- Iodine search off the coast of Maine, August 11, 1968.

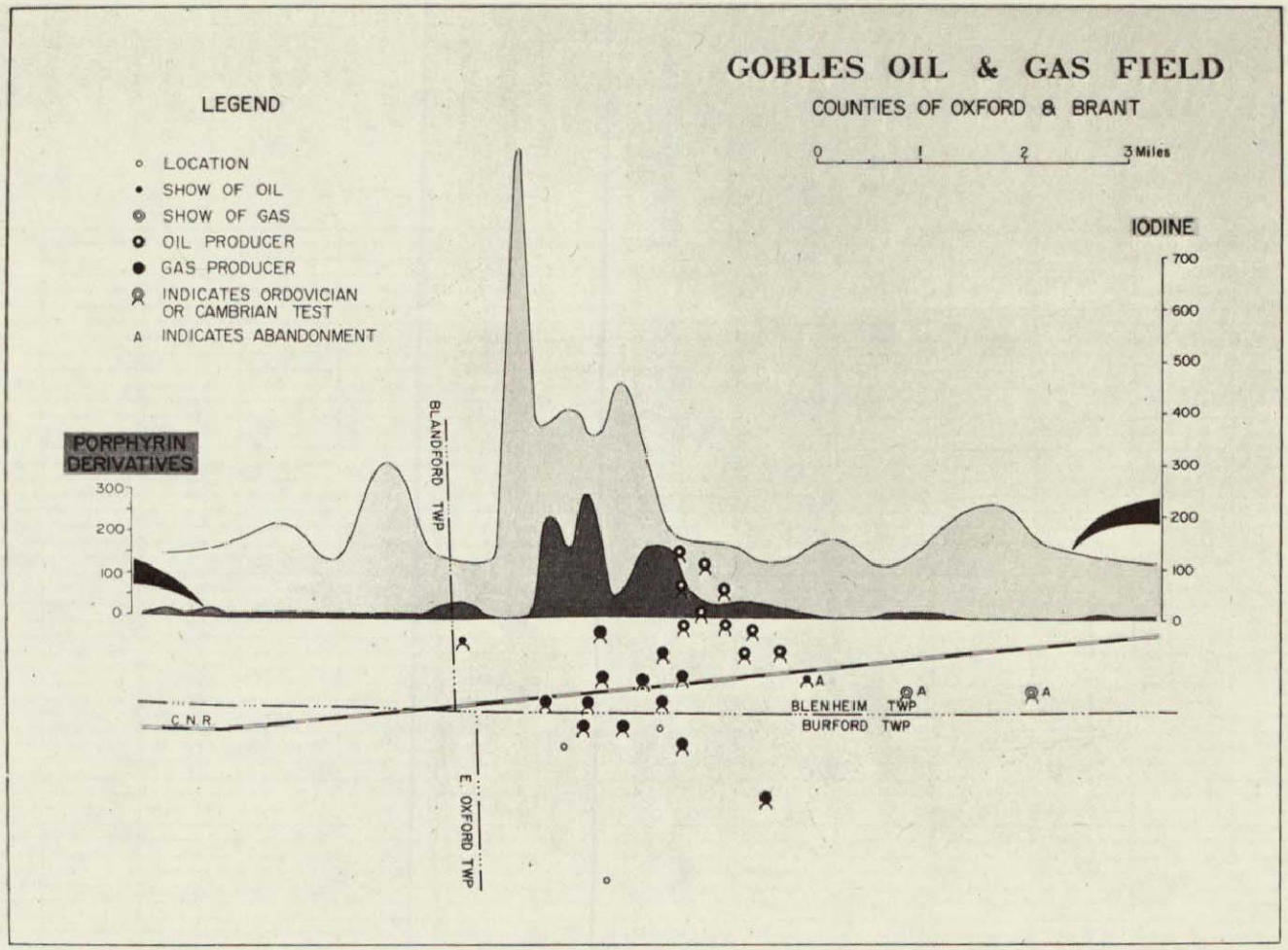

Figure 34-11.- Iodine concentration is soils over the Gobles oil and gas field, Ontario, Canada.

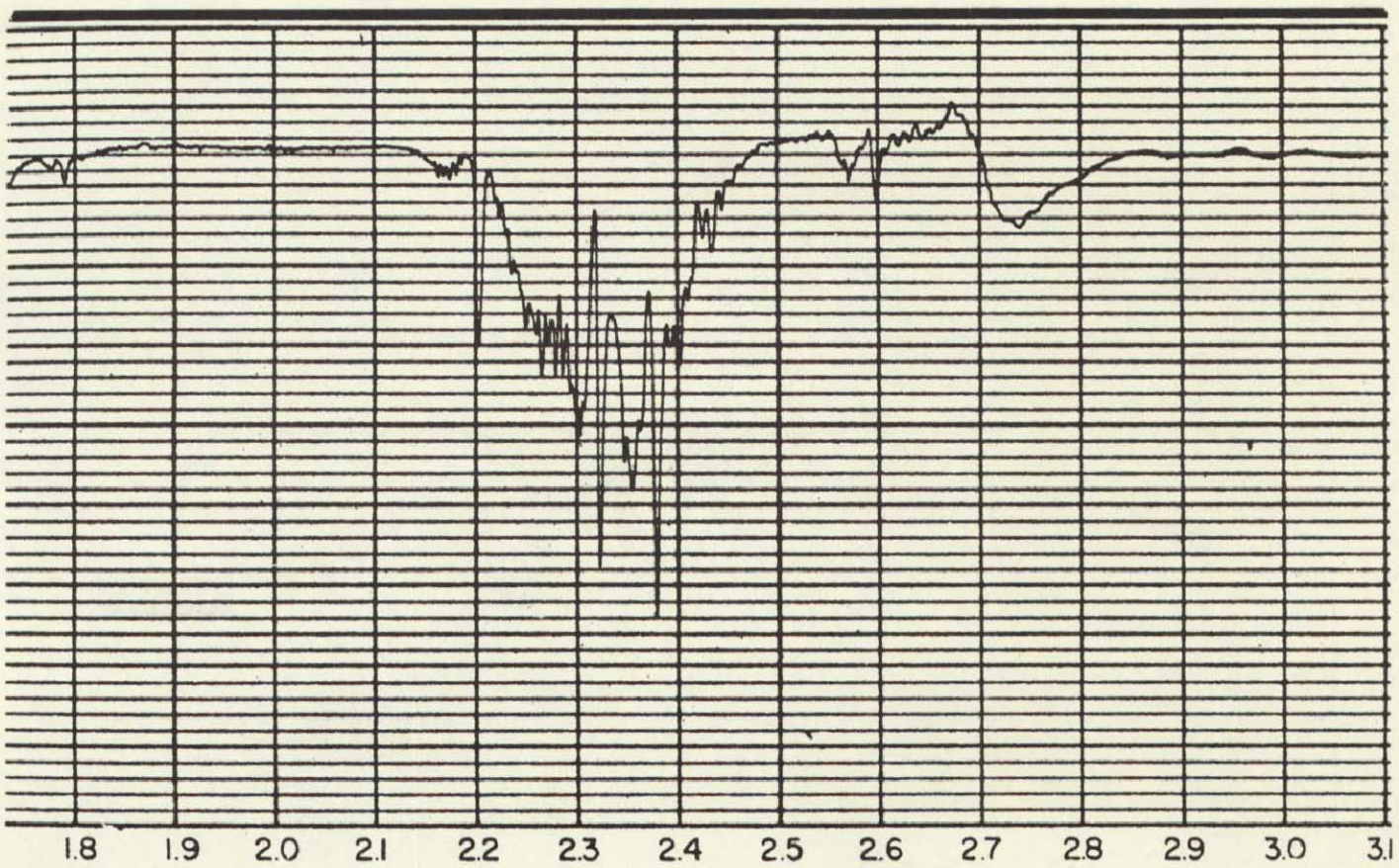

Figure 34-12.- Near IR spectrum of methane gas between 2.1 to 2.8 micron.

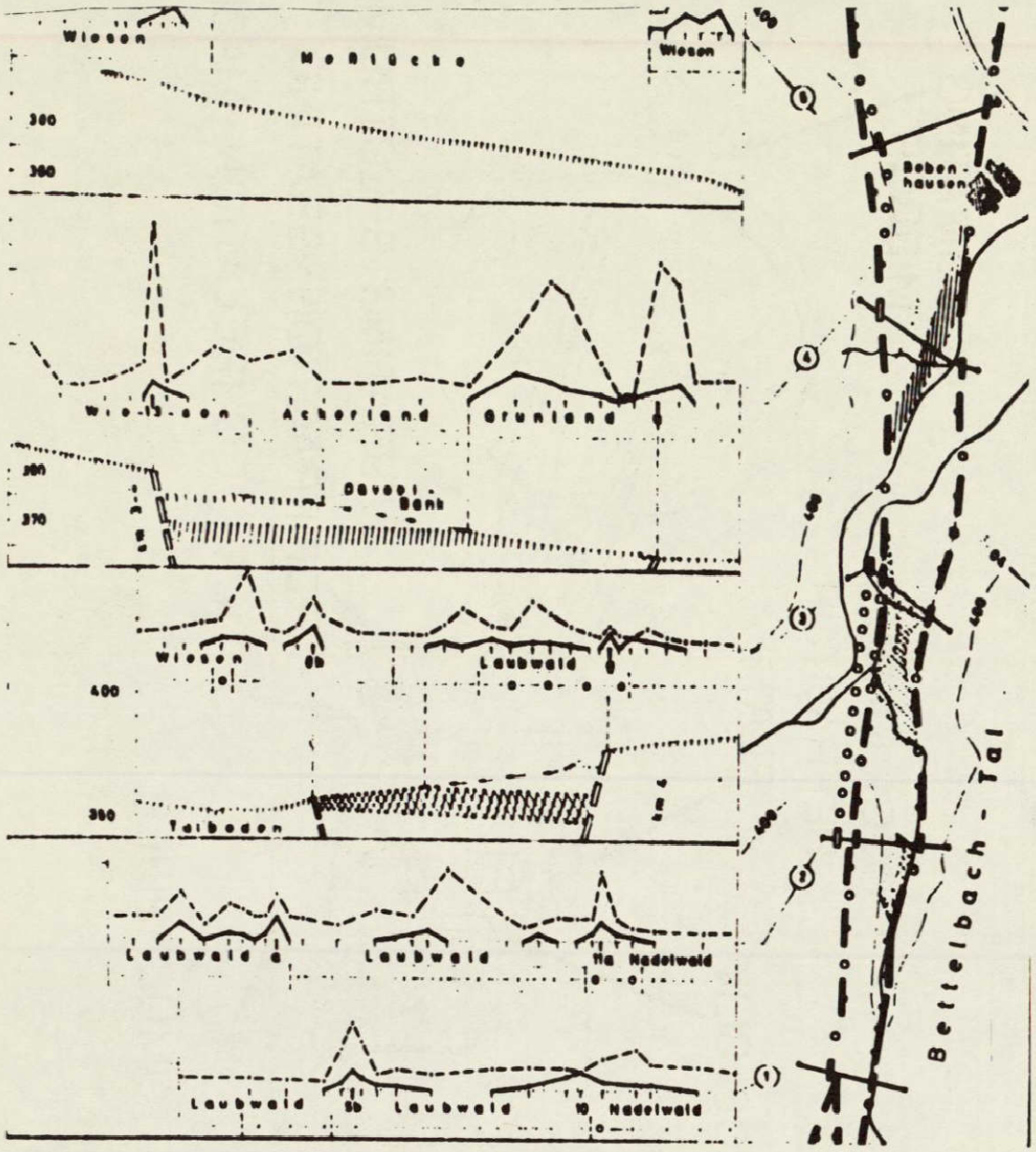

Abb. 1

CH_4 und CO_2 in den Böden des Bebenhausener Lias-Grabens bei Tübingen

AFTER V. W. ERNST

ERDÖL AND KOHLE-ERDGAS-PETROCHEMIE

Figure 34-13.- Methane gas and CO_2 in the soil of the Bedenhausen graben, Germany.

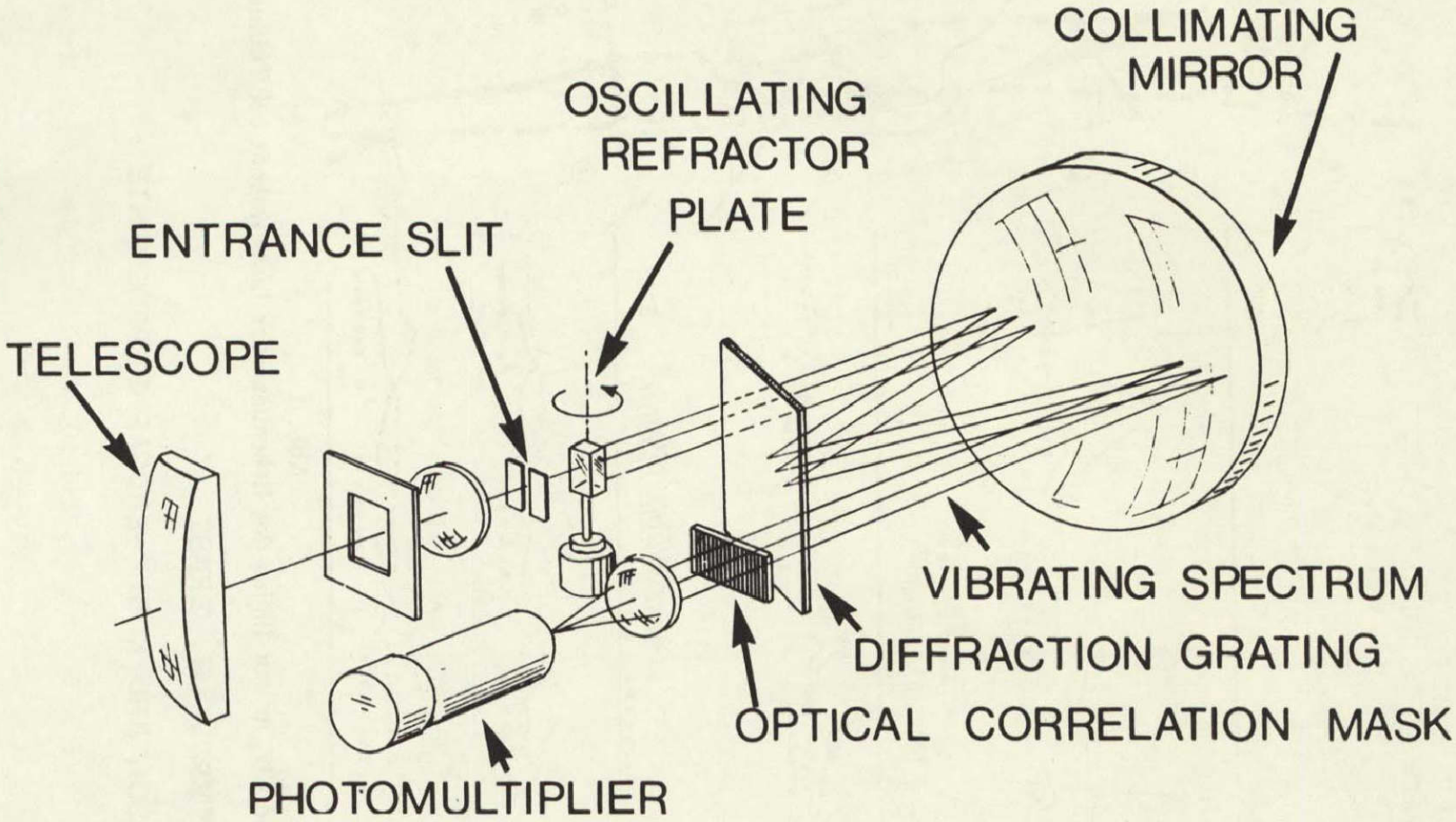

Figure 34-14.- Schematic view of the correlation spectrometer illustrating the basic elements.

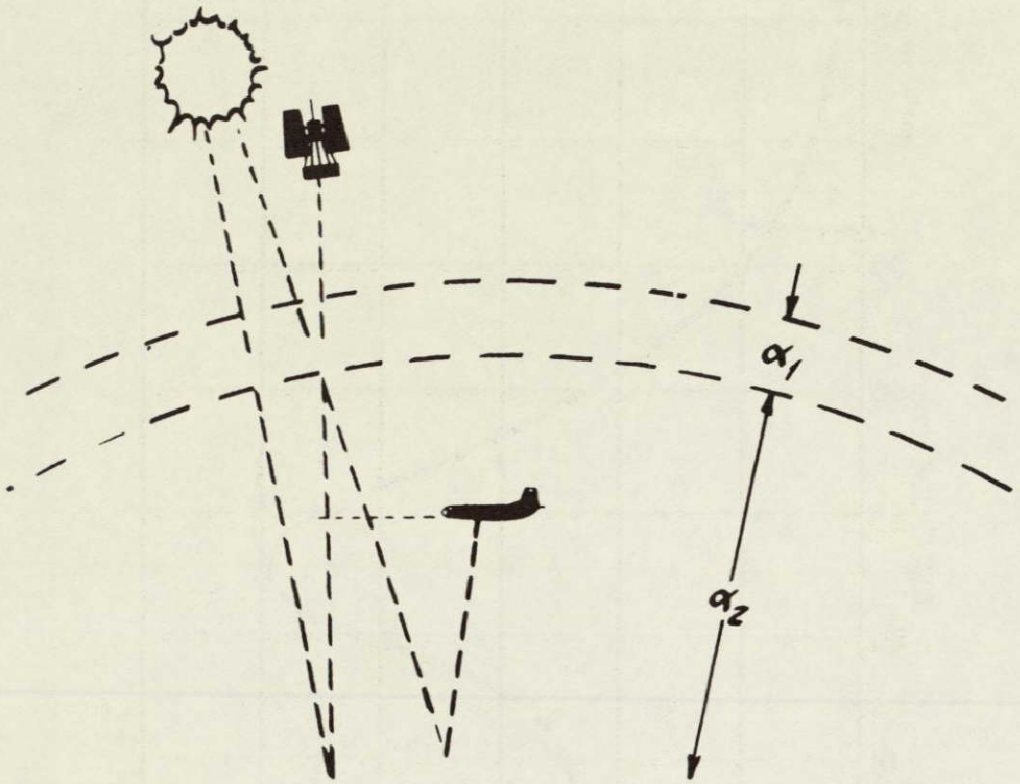

α_1 - ABSORPTION OF O_3 LAYER

α_2 - ABSORPTION OF REMAINDER OF ATMOSPHERE

$$\begin{bmatrix} S/C = 2\alpha_1 + 2\alpha_2 \\ A/C = 1\alpha_1 + 1.9\alpha_2 \end{bmatrix}$$

Figure 34-15.- Aircraft application data versus satellite application.

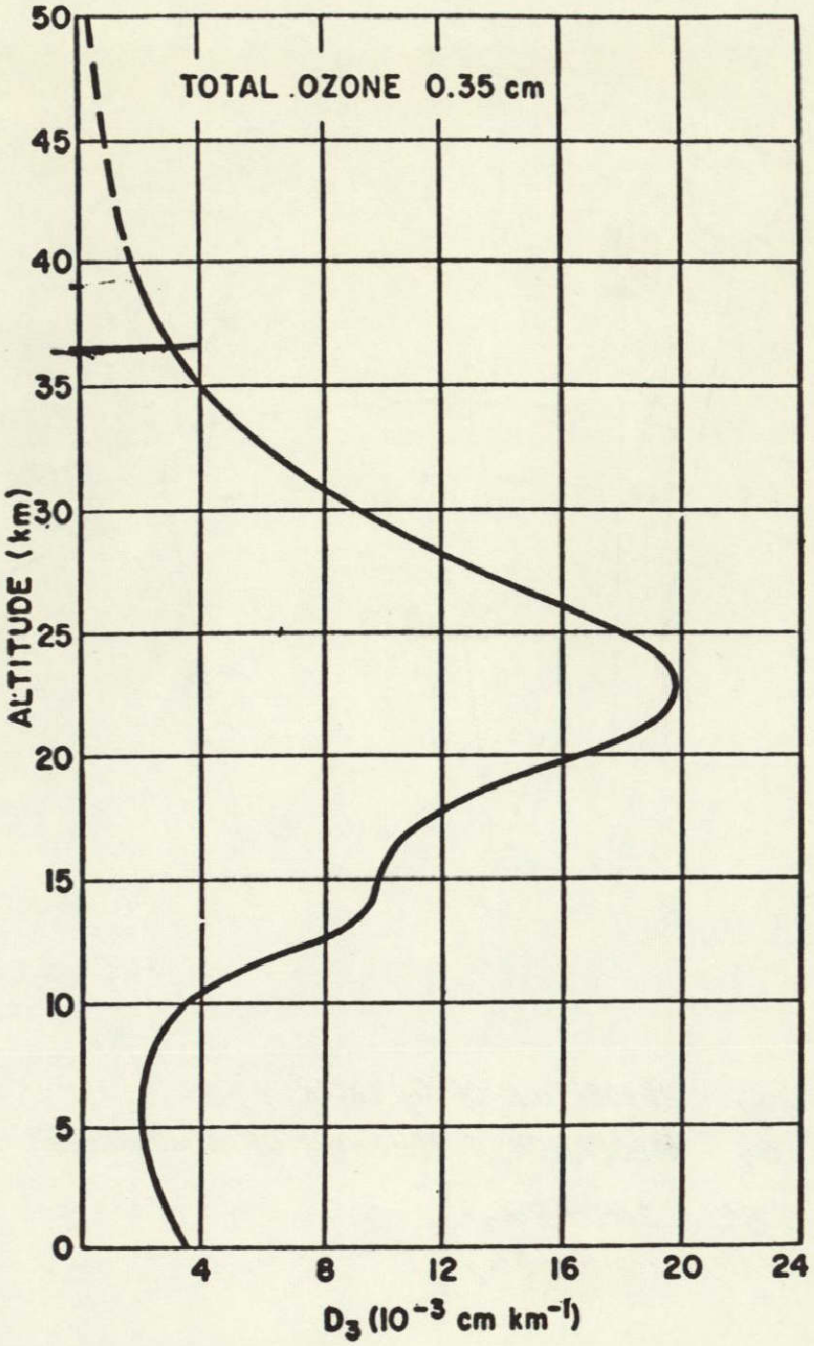

Figure 34-16.- Representative ozone concentration profile. Solid curve developed from ozone sonde network data, dashed curve from chemical equilibrium theory.

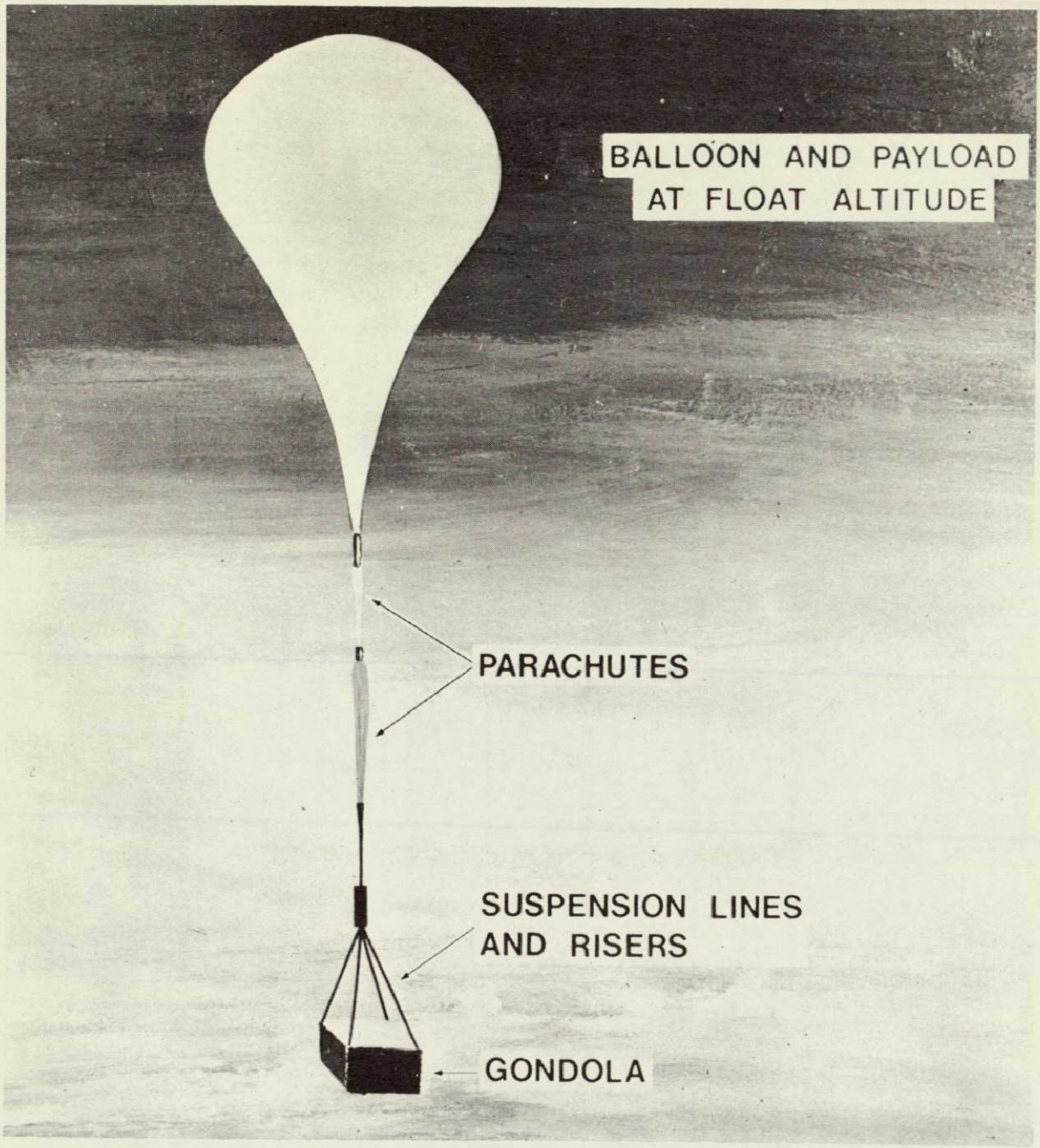

Figure 34-17.- Balloon and payload at float altitude.

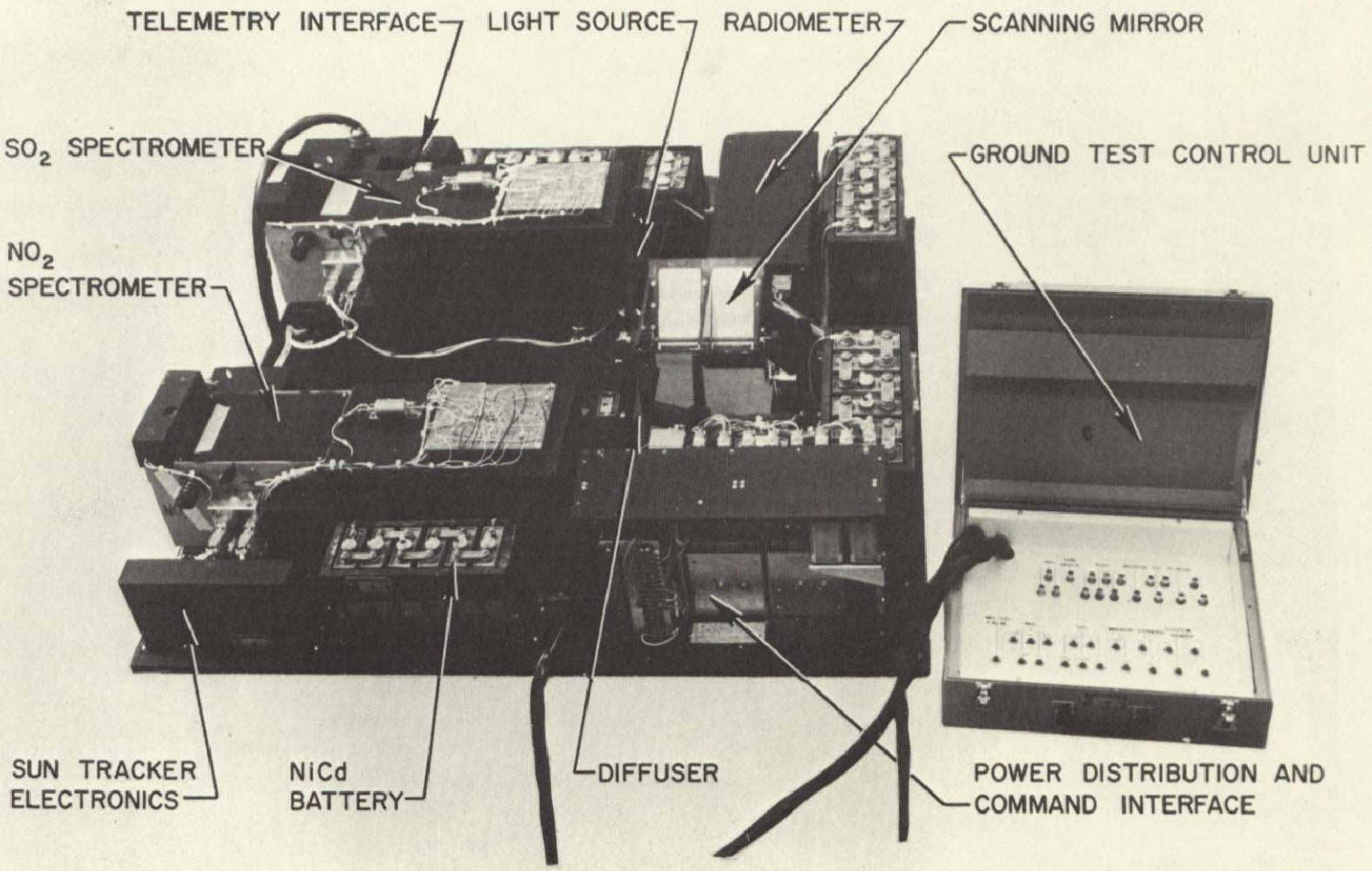

Figure 34-18.- Scientific payload for high altitude balloon measurements of air pollution.

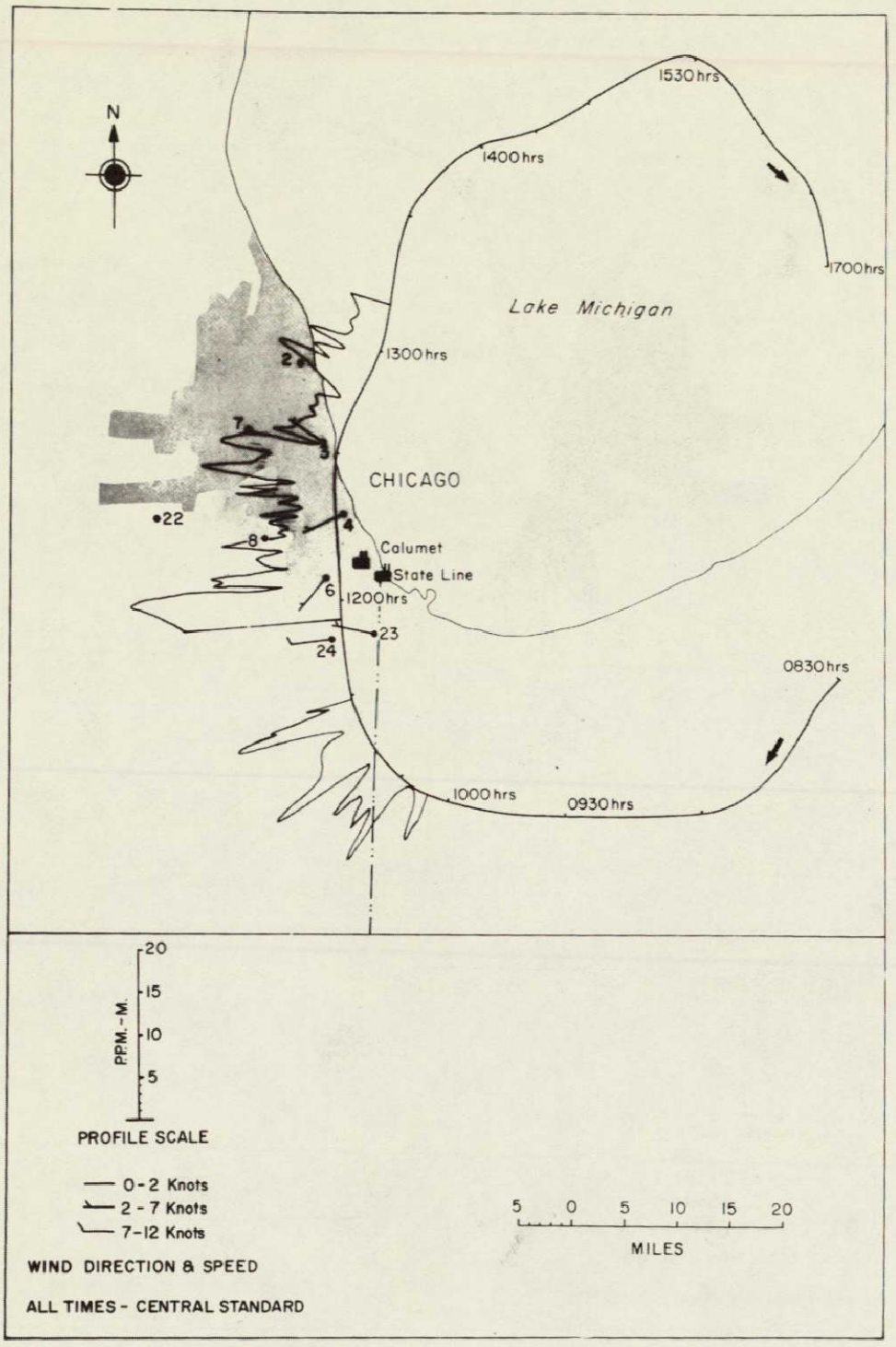

Figure 34-19.- Balloon flight SO_2 profile, Chicago area, September 1969.

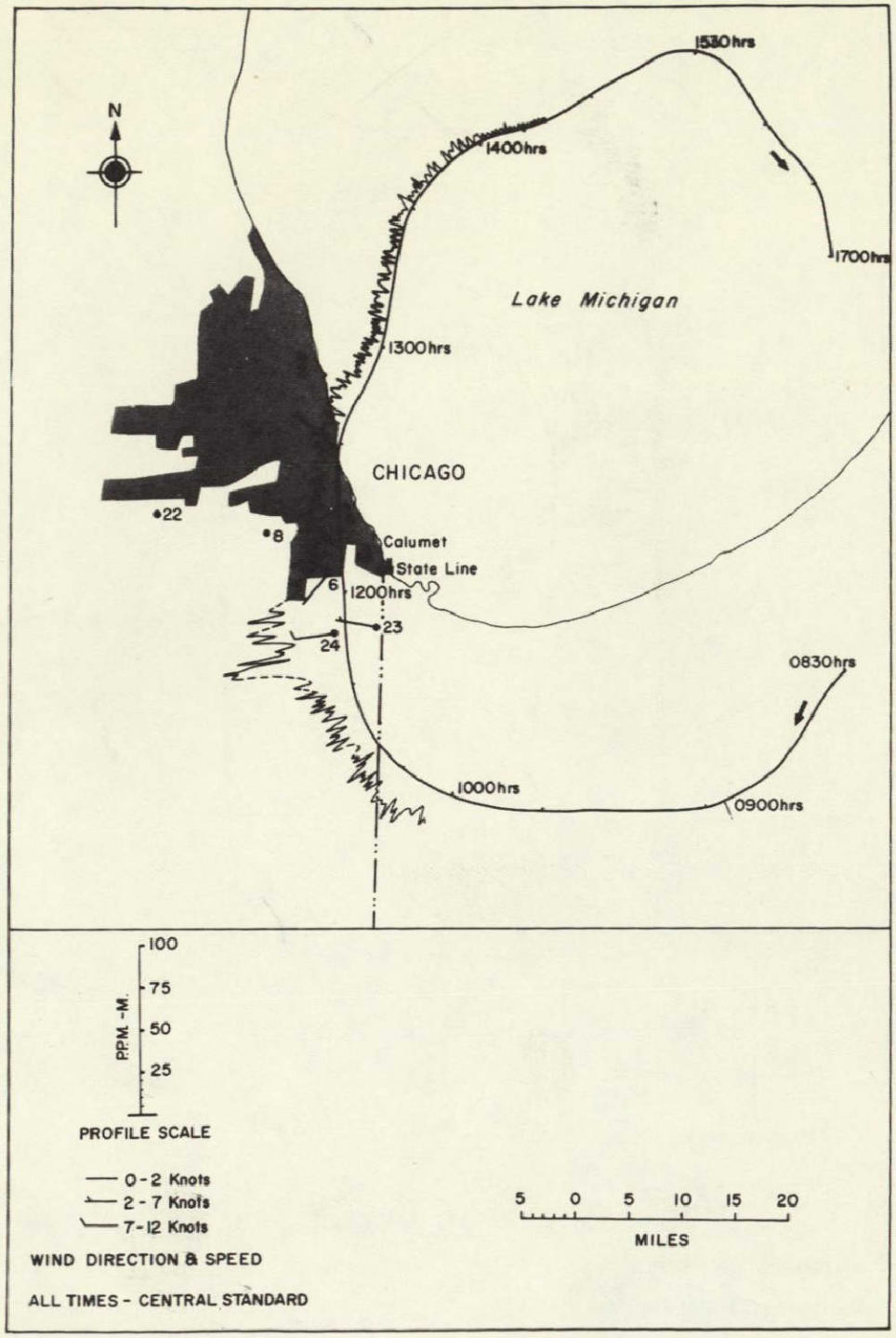

Figure 34-20.- Balloon flight NO_2 profile, Chicago area, September 1969.

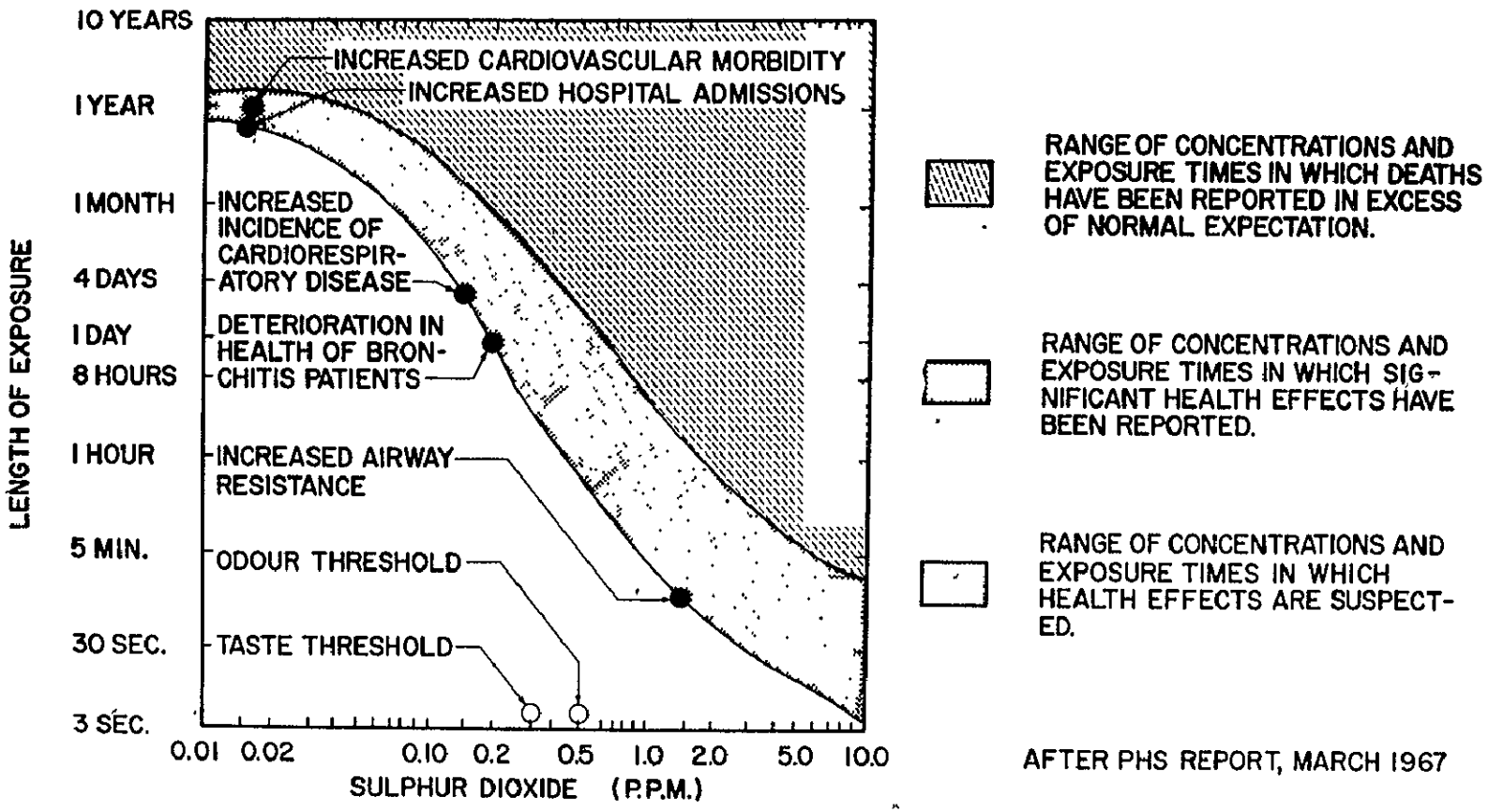

Figure 34-21.- Health effects of SO_2 pollution.